Assessment and modulation of gliosis in inherited eye disease and its impact on cell replacement therapy

Anna Barbara GRACA

Research degree: Institute of Ophthalmology [RRDOPHSING01]

Degree of Doctor in Philosophy

University College London (UCL)

Declaration

I, Anna Barbara Graca, confirm that the work presented in this thesis is my own. Where information has been derived from other sources, I confirm that this has been indicated in the thesis.

Abstract

In most inherited retinal degenerations such as age-related macular degeneration, death of photoreceptors leads to irreversible vision impairment. As the retina starts to degenerate, the retinal environment begins to remodel. While variations in the timing and magnitude of retinal response have been reported by various studies looking at different initiating insults, there has been no comparative assessment of the diseased retinae across time in multiple models of retinal degeneration. Here, the process of gliosis, outer nuclear layer cytoarchitecture and integrity of the outer limiting membrane (OLM) were examined in seven different mouse models of inherited retinal degeneration. Findings from this study demonstrated that each of the examined mutants manifests a unique pattern of alterations occurring in the retinal microenvironment, including significant changes to OLM junctions. Moreover, these animals showed that the type of the Müller glial response and its magnitude are not correlated with disease severity. Having identified marked but varied changes in the expression of GFAP, Vimentin and chondroitin sulphate proteoglycas (CSPGs) between different models, further work investigated whether it is possible to prevent or manipulate these changes. By knocking down expression of GFAP and Vimentin by with RNA interference (RNAi), the role of these proteins both in the development of degeneration-associated glial hypertrophy and in influencing photoreceptor transplantation outcome was assessed. Consistent with the idea that CSPGs deposition in the subretinal space represents a barrier to therapeutic interventions, an enzymatic approach was used to effectively digest these molecules in a diseased mouse retina. In the last instance, RNAi-mediated knockdown of CRB1, one of the key regulators of AJs, was used to introduce disruption of OLM integrity. The overall aim of this thesis was to provide a better understanding of the barriers in a diseased retinal environment and how they can be manipulated to ease in a future some of the therapeutic strategies to help to restore lost vision.

Acknowledgements

Every successful individual knows that his or her achievement depends on a work and support of other people. My PhD would not have been possible without all the help, assistance, guidance, motivation and love of many incredible people who I want to dedicate this work to.

Firstly, I would like to thank both Professor Rachael Pearson and Professor Robin Ali for giving me the opportunity to do my PhD project in their research group. I would like to express my special appreciation to my supervisor Professor Rachael Pearson, you have been a real teacher for me. I would like to thank you for encouraging my work and for allowing me to grow as a scientist. Your advice on both research as well as on my career plans have been priceless. I would like to thank my secondary supervisor Professor Robin Ali who has provided support and advice throughout my time in the lab. The lab he has built is full of amazing and awfully talented people whom I have had the pleasure to work and have fun with. I would like to thank Dr Alexander (Sander) Smith whose knowledge was invalauble in designing my experimental work and analysing the data.

I would like to express my whole-hearted gratitude and indebtedness to Dr Claire Hippert for being such a great mentor and lab partner. Your work on the gliosis project and viral vectors helped me to complete this PhD. We did it together, Claire!

I would like to thank Dr Tassos Georgiadis for always being there for my molecular biology and AAV questions, and Dr Emma West who taught me all the EM secrets and her invaluable advice on the OLM work. Here I have to thank Ms Joanna Ribeiro for doing a tremendous work by cutting my EM samples and helping with the cryo-sectioning. You are a star!

None of the viral injections and the cell transplant work would have been possible without help from Ms Yanni Duran, Professor James Bainbridge and Mr Manjit Mehat.

A special thanks goes to Dr Matt Hayes for helping me with 3*D* reconstructions and Peter Munro for all the support with EM. I would also like to thank Dr Ayad Eddaoudi and Mr Rob Sampson for giving me the absolute access to the FACSorter and the technical assistance. I have to say big thank you to Paul, Dom, Sam, Martha, Katerina and Debbie for being wonderful friends, work colleagues and people I could count on whenever I had a last minute lab emergency. The same goes to Xun, Davor, Andrianos and Steph, my PhD comrades and amazing friends.

I would also like to thank Dr Mark Basche, one of the most amazing people I met during my time in the lab. His support as a scientist and a friend cannot be measured in any units. Thank you Mark, for being you and for being my true coffee buddy!

The biggest gratitude I owe to my family. Words cannot express how grateful I am to my mum and dad for all of the sacrifices that they have made for me.

I have to thank all my friends in the UK, Poland, USA and Belgium, and my volleyball team for being understanding and not excluding me from their lives. Without you I would have gone insane. I love you ALL!!!!!

Last but not least goes to my supervisors and work colleagues at the Research Executive Agency in Brussels for their support and motivation during my writing months.

Thanks to ALL of you for helping me to achieve this GOAL!

Table of contents

List of Figures

List of Tables

List of Abbreviations

AA - antibiotic/antimycotic

AAV – Adeno-associated virus

AJ – adherens junction

AMD – Age-macular degeneration

aPKC - atypical protein C

BDNF – Brain-derived neurotrophic factor

BS – blocking solution

BSA – bovine saline albinum

CBA - cytomegalovirus/chicken β-actin promoter

CD - Cone dystrophy

CD42 - Cell division control 42

CDR - Cone-rod dystrophy

ChABC - Chondroitinase ABC

CMZ - ciliary marginal zone

CNF - cytotoxic necrotising factor family

CRB – Crumbs

CSNB - congenital stationary night blindness

CSPG - chondroitin sulphate proteoglycan

CMV – cytomegalovirus promoter

DNA - deoxyribonucleic acid

DMEM - Dulbecco's Modified Eagle medium

DR - Diabetic retinopathy

E - embryonic day

EBSS - Earle's Balanced Salt Solution

ECM – extracellular matrix

EGF - Epithelial growth factor

ERG – electroretinography

ESCs - embryonic stem cells

FACS - fluorescence-activated cell sorting

FCS - Foetal Calf Serum

FGF - Fibroblast growth factor

FPLC - Fast protein liquid chromatography

G - G-protein

GABA - Gamma-aminobutyric acid

GAG – glycosaminoglycan chain

GAP - GTPase Activating Protein

GCAPs - guanylate cyclase activating proteins

GCL – Ganglion cell layer

GFAP - Glial fibrillary acidic protein

GFP- green fluorescence protein

H2B - Histone 2B

HRP - Horseradish peroxide

HSPGs - heparin sulphate proteoglycans

ICAM-1 - Intercellular Adhesion Molecule 1

ICH- immunocytochemistry

IF – intermediate filament

IHC – immunohistochemistry

IL - Interleukin

INL – Inner nuclear layer

IPL – Inner plexiform layer

iPSCs - induced pluripotent stem cells

IS- inner segment

IS/OS – Inner /outer segment region

JAMs - junction adhesion molecules

LB - lysogeny broth

LCA – Leber's congenital amaurosis

MD - Macular degeneration

MG – Müller glia

mGluR - metabotropic glutamate receptors

MPP5 - Membrane protein palmitoylated 5

N - number

NL-68 – neurofilament-68

NSC – neuronal stem cell

OCT - ocular coherence tomography

OLM – Outer limiting membrane

OMI - ovomucoid inhibitor albumin

o/n - overnight

ONL – Outer nuclear layer

OPL – Outer plexiform layer

OS – outer segment

P – postnatal

PAR - portioning defective complex

PBS – phosphate buffer saline

PBST - phosphate buffer saline with Tween-20

PFA – paraformaldehyde

PG - Proteoglycan

PR – photoreceptor

PALS1- Protein associated with Lin Seven 1

PATJ - PALS1-associated tight junction protein

PDE - phosphodiesterase

R - Rhodopsin molecule

RCS – Royal College of Surgeons rat strain

RFP – red fluorescence protein

RNA - Ribonucleic acid

ROI – region of interest

ROS - reactive oxygen species

RP – Retinitis pigmentosa

RPC - retinal progenitor cells

RPE – Retinal pigmented epithelium

RT – room temperature

QRT-PCR - Real-time quantitative polymerase chain reaction

SAR – subapical region

SEM – standard error margin

Sh – small harpin

SHH - Sonic hedgehog

Si – small interfering

SOC - super optimal catabolite medium

TJ- tight junction

TNF-α - Tumor necrosis factor α

TR – transfection reagent

U – unit

VEGF - Vascular endothelial growth factor

v/v – volume per volume

WB – Western Blot

Wnt – wingless signalling pathway

w/v – weight per volume

w/w – weight per weight

ZO-1 – Zonula occludens 1

List of publications

Athanasiou D, Aguila M, Opefi CA, South K, Bellingham J, Bevilacqua D, Munro PM, Kanuga N, Mackenzie FE, Dubis AM, Georgiadis A, **Graca AB**, Pearson RA, Ali RR, Sakami S, Palczewski K, Sherman MY, Reeves PJ, and Cheetham ME (2016). Rescue of mutant rhodopsin traffic by AMPK activation accelerates photoreceptor degeneration. *Human Molecular Genetics*, ddw387.

Hippert C, **Graca AB**, and Pearson RA (2016). Gliosis can impede integration following photoreceptor transplantation into the diseased retina. Review. *Advances in Experimental Medicine and Biology 854:579-85.*

Graca AB, Hippert C, Barber A, West EL, Ali RR, and Pearson RA (2015). Müller glia activation in response to inherited retinal degeneration is highly varied and disease-specific. *PLOS One 10 (3).*

Pearson RA, Hippert C, **Graca AB,** and Barber A (2014). Photoreceptor replacement therapy: challenges presented by the diseased recipient retinal environment. *Visual Neuroscience 31, Special Issue 4-5, 333-344*.

Most people say that it is the intellect which makes a great scientist. They are wrong: it is character.

Albert Einstein

CHAPTER 1

Introduction

1.1 Thesis overview

Vision is often considered to be the most important of all the human senses as it enables human beings to interact with their surrounding environment. The sense of sight is a result of sequential activity, which begins with the reflection of the light from an object to the lens, which is embedded within the eye. The lens focuses this light onto a layer of tissue that lines the back of the eye, called the retina. The retina is packed with neurons, including the light-sensitive cells, the photoreceptors, which absorb photons of light and convert them into an electrical signal, which is passed to second and third order neurons for further processing, before travelling along the optic nerve fibres to the brain where it is decoded. The retina, therefore, is one of the most important players in the process of vision as it helps to decode the light stimulus and transfer it into a biological message that can be read by our brain.

Retinal diseases that lead to death of the photosensitive photoreceptor cells within the retina leave patients partially or completely blind. Inherited retinal dystrophies, typically grouped under the umbrella of retinitis pigmentosa (RP), affect 1 in 3,000 of the population, and age-related macular degeneration (AMD) affects 1 in 10 people over 60 years, a figure that is rising in Western societies as the society ages (Minassian et al., 2011; Owen et al., 2012). In the majority of cases, existing treatment options at best slow disease progression and do so only in a minority of cases. To restore vision in these cases, various alternative therapeutic approaches have been proposed and tested, both pre-clinically and clinically (reviewed in (Sabel, 2008; Pearson et al., 2014; Lewis et al., 2015)). Intraocular injection of soluble growth factors such as acidic and basic fibroblast growth factor (FGF) or brain-derived neurotrophic factor (BDNF) has been able to slow down progression of retinal degeneration, by promoting survival of remaining retinal cells (Faktorovich et al., 1990; LaVail et al., 1992; Chaum, 2002). Clinical and pre-clinical studies on gene replacement therapy with the use of viral vectors have shown the proof of concept in reintroduction of a normal gene product (Bainbridge et al., 2008; Maguire et al., 2008; Palfi et al., 2010; Mookherjee et al., 2015) with some patients reporting restoration of vision (Bainbridge et al., 2015; Edwards et al., 2016). Rescue of visual function following the transplantation of immature photoreceptors has also been reported to be successful with major advances in the generation of competent donor cells from different sources including patient derived stem cells (Gouras et al., 1994; Gouras and Tanabe, 2003; Seiler and Aramant, 2012). However, all of the mentioned strategies have their limitations mainly due to environmental and morphological changes that occur in the diseased eye that have a significant impact on the outcome of a clinical treatment (reviewed in (Colella and Auricchio, 2012; Hippert et al., 2016; Zarbin, 2016)). It is well known that during

disease progression, the retina undergoes structural remodelling, such as changes in retinal glia (reactive gliosis) or rupture of the outer limiting membrane (OLM) thus creating a different environment that can influence the outcome of a cell transplant. For these reasons, understanding the retinal remodelling and the processes behind glial scar formation may help us to develop more effective strategies to treat a wide range of retinal dystrophies. In Chapter 3, a variety of murine models of retinal dystrophies were examined to provide a detailed characterisation of the diseased environment at different stages of retinal disease. A comprehensive comparison was performed to investigate whether the aetiology arising from different underlying genetic causes of retinal degeneration leads to a unique pattern of retinal alterations and structural remodelling. In Chapter 4, the impact of preventing the upregulation of the intermediate filament (IF) proteins, Glial fibrillary acidic protein, GFAP, and Vimentin, which play a key role in gliosis, was studied in a model of RP. Specifically, their role with respect to glial hypertrophy and its impact on cell replacement therapy was investigated. Numerous studies have reported an upregulation of different proteoglycans, a class of inhibitory extracellular matrix (ECM) molecules, in a wide range of retinal retinopathies (Inatani et al., 2001; Zhang et al., 2003b; Singhal et al., 2008). Chapter 5 assessed the expression pattern of one of the main proteoglycans, Aggrecan and its receptor in two models of inherited RP. The last two will focus on the OLM integrity during retinal degeneration (Hippert et al., 2015) and its role as a third retinal barrier. In Chapter 6, a detailed characterisation of the OLM remodelling was performed over a time course of disease progression in different models of retinal degeneration. Consistent with the idea that OLM may represent a barrier to therapeutic strategies (Pearson et al., 2010; Barber et al., 2013), an attempt to disrupt it using RNAi strategy was made to knock down one of its junctional proteins, CRB1. The overall aim of this study was to provide a better understanding of the diseased environment and how it can be manipulated to ease some of therapeutic strategies.

1.2 Gross anatomy and function of the eye

The eye has evolved as a highly specialized organ with a common structure shared by all the vertebrates. It is organised into three distinct layers, which together allow the external stimulus encoded in a form of light to travel to the brain resulting in visual perception of the external world.

The eye (Figure 1.1) is protected from the outside by a relatively tough layer, the sclera. This layer minimises the risk of trauma and functions as a barrier to environmental pathogens. In the area protected by the eyelids, the sclera is covered by a thin, transparent membrane (conjunctiva), which runs to the edge of the cornea. The

cornea, together with the sclera, helps to shield the eye from the outside. This avascular structure also aids the light stimulus to be focused on the retina located at the back of the eye, therefore making it the first component of the visual process. The cornea is divided into specialised layers consisting of the epithelium, the stroma and the endothelium. The epithelium is constantly being regenerated by the stem cells found at the limbus of the cornea to ensure that the oxygen supply is efficiently maintained. The next layer, the stroma is made of collagen fibres, which allow the cornea to maintain its transparency. The last layer, the corneal endothelium is responsible for hydration of the stroma.

After passing through the cornea, light travels through the intermediate layer divided into the anterior components: the pupil, the iris, the ciliary body, and the lens, and the posterior part, the choroid. The pupil, which appears as a black dot in the middle of the eye, constantly enlarges and constricts itself like the lens of a photographic camera lens depending on the changes in the amount of light in the immediate proximity. The size of the pupil is controlled by the action of the pupillary sphincter muscle and dilator muscle. A coloured area surrounding the pupil, the iris, controls the amount of light that enters the eye allowing more light to enter when the environment is dark and less light when it is bright. The iris attaches to the sclera at its outer anterior edge, so-called the ciliary margin, which is also connected to the ciliary body. The ciliary body, which comprises of the ciliary muscles, is vital to proper functioning of the eye. This two-layer structure is divided into two regions, the pars plicata where the ciliary processes extend from and produce the aqueous humour in the anterior chamber, and the pars plana located more posteriorly, that secretes and releases components of the vitreous into the vitreous cavity. The vitrous humour is a watery substance that fills the eye allowing the eye to maintain its shape. This liquid is drained through the Schlemm canal so that any build-up in the eye can be removed. The ciliary body also extends the zonular fibers that act as an anchorage for the lens, allowing it to be positioned. The lens, that is located behind the iris, changes its shape and focuses light onto the retina. Through the action of the ciliary muscles, the lens is able to fine tune light refraction, a process known as accommodation, by becoming thicker to focus on nearby objects and thinner to focus on distant objects.

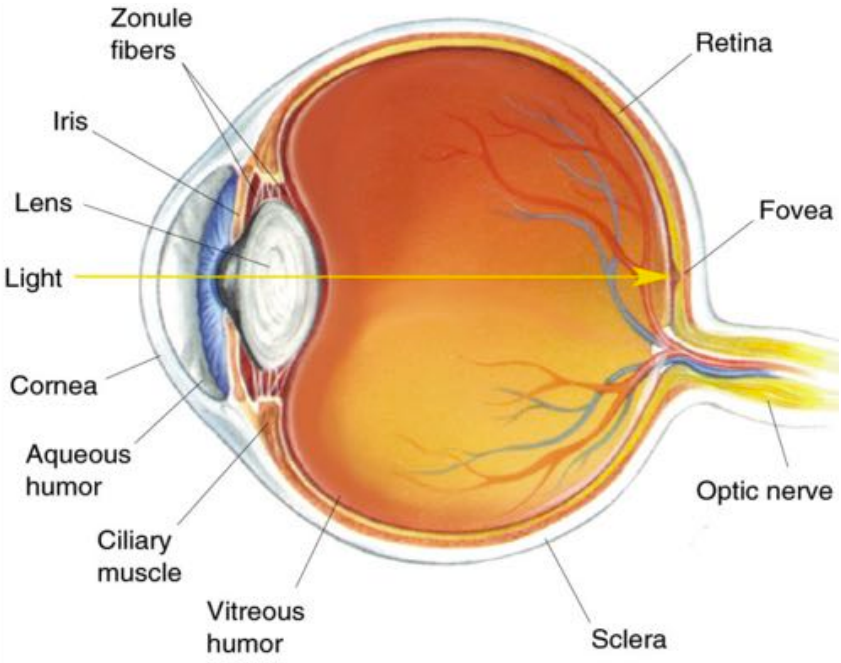

Figure 1.1 Gross anatomy of the human eye.

Copyright note: Image of the eye was taken from http://www.ehealthideas.com/2013/10/eye-diagram-fovea.html*. Accessed online on 20.05.2016.*

After the light passes through the lens, it is projected onto the retina (Figure 1.2A). The retina is made of photosensitive cells, rod and cone photoreceptors, which are responsible for converting the light stimulus into chemical and electrical signals. These cells are also responsible for 'seeing' colours. The electrical pulses generated by the photoreceptors, then travel along the fibres of different neuronal cell types connected to the optic nerve. It is the optic nerve that transmits these signals along its axons to the brain where the retinal images are being interpreted by the visual centres (Figure 1.2B). At the centre of the retina, there is a region called the optic disc, which serves as an exit point for the optic nerve and an entry point for several major incoming blood vessels that supply retina. No light sensitive tissue is found in the optic disc, causing a break in the visual field, more commonly known as the blind spot. Adjacent to the optic disc, in humans, lays a region, which is specialised for high acuity, the macula (Figure 1.2C). Together with its central part, the fovea, the macula helps to increase the details of the images to a perceivable point. The fovea, which is enriched in cone cells, is enclosed by the parafovea and in turn by the perifovea. The macula is the only place in the retina, where cones dominate over rods, as beyond it, the rod photoreceptor is more abundant responsible for highly compressed, low-resolution information.

Beneath the neurosensory retina, lies a single layer of retinal pigmented epithelium (RPE). It is an additional layer lying just underneath the photoreceptors and is responsible for creating a barrier between the retina and blood supply coming from the choroid (Figure 1.2C). Connected by a series of tight junctions, the RPE offers photoreceptors a trophic support, plays essential role in the maintenance of the retinal homeostasis and shields the retina from the blood supply coming from the choroid. The choroid, located between the retina and the sclera, is often referred to as the vascular layer, as it supports a dense network of blood vessels delivering all the vital nutrients and oxygen to various parts of the eye.

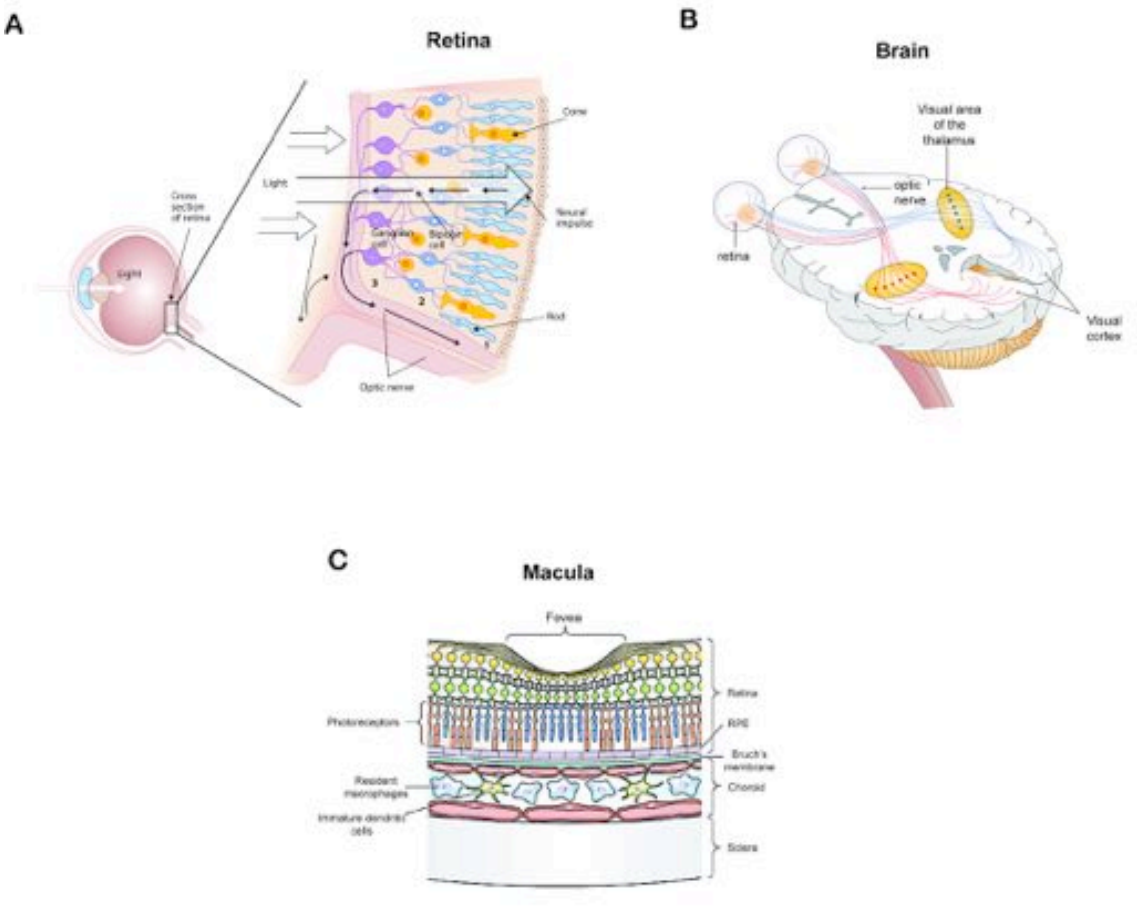

Figure 1.2 From the retina to the brain: the route of the light stimulus.

A) The light travels through the eye towards the outer part of the neuroretina, composed of photosensitive cells, rods and cones. After the light photon is converted into the electrical impulse, it travels to the bipolar and ganglion cells, and eventually to the optic nerve. **B)** In the next instance, the sensory information via the optic never fibres is sent to through the thalamus to corresponding areas in the visual cortex. Interestingly, the left and right eye sends information to both the left and the right hemisphere, and the visual cortex processes each of the cues separately and in parallel. This is an adaptational advantage to an organism that loses sight in one eye, because even if only one eye is functional, both hemispheres will still receive input from it. **C)** The macula together with its central region, the fovea, is very dense in cone photoreceptors. Below photoreceptors is the RPE, which is separated by a specialised membrane, the Bruch's membrane, from the vascular choroid, which is enriched in resident macrophages and dendritic cells.

Copyright note: Images A and B were copied from Stangor (2012) http://2012books.lardbucket.org/books/beginning-psychology/s08-02-seeing.html*. Accessed online on 20.05.2016. Image C was reprinted by permission from Nature Publishing Group:* (Forrester, 2003)*, Nature Medicine.*

1.3 The retina

The retina is a complex structure generated from the neuroectoderm, which also gives rise to other parts of the central nervous system (CNS) during embryogenesis. There are six major types of neuronal cells in the retina born at different stages during eye development. These cells assemble themselves into three distinct layers that are separated by the areas of synaptic contacts (Figure 1.3). This type of laminar organisation allows the retina to perform its unique functions including perception, integration and transmission of visual information. As in the CNS, the retinal neurons are provided with a support by glial cells, with Müller glia playing a major role in neuronal function and survival.

1.3.1 Development of a retina

In a mouse, development of the retina begins around embryonic day (E) 11 from the optic vesicles (Carter-Dawson et al., 1978; Young, 1985). Findings from numerous studies have shown that retinogenesis is highly conserved across vertebrates and it can be broadly categorised into several phases, including the initial proliferation of retinal progenitor cells (RPCs); restriction in the multipotent competence of RPCs; and commitment towards specific cell type by expression of cell-specific genes essential for maturation, specialisation and function of the differentiated cells. All of these stages are tightly regulated by a number of different transcription factors and extrinsic regulators (reviewed in (Swaroop et al., 2010)).

The process of retinogenesis starts when the optic vesicles, and later the optic cup, undergo a series of changes due to intrinsic and extrinsic factors (Figure 1.3A). This allows for generation of neuroepithelium, made of multipotent RPCs. In the early stages of retinogenesis RPCs undergo rapid symmetric proliferation to expand the progenitor pool (Figure 1.3.B). Several growth factors, including Sonic hedgehog (SHH), FGF and Epithelial growth factor (EGF) are active during the patterning of the neural tube to ensure the expansion and maintenance of the progenitor pool (Anchan et al., 1991). As development progresses, RPCs start to shift towards asymmetric division, allowing a subset of RPCs to exit the cell cycle in a strict order and differentiate into subsequent retinal cell types (Turner and Cepko, 1987; Wetts and Fraser, 1988). As illustrated in Figure 1.3, one of the first cell types to be generated are ganglion and horizontal cells, followed by cone photoreceptors and amacrine cells. In the second wave of retinogenesis, RPCs differentiate into rod photoreceptors, bipolar cells and finally Müller glia cells (Figure 1.3C). A large array of transcription factors, mostly basic Helix-loop-helix (bHLH) and homeodomain factors, expressed by subsets of RPCs or their post-mitotic progeny, together with extrinsic factors from the

environment induce and regulate the differentiation of the specific cell types within the neural retina (Jadhav et al., 2006; Yaron et al., 2006). One of early transcription factors involved in the development of different retinal cell types is Orthodenticle homeobox 2 (Otx2) (Nishida et al., 2003; Akagi et al., 2004). *Otx2* was found to be expressed in the cells that give rise to the RPE and post-mitotic RPCs that later form ganglion cells, bipolar cells and photoreceptors (Bovolenta et al., 1997; Baas et al., 2000). *Otx2* gene was demonstrated to be one of the key regulators of photoreceptor cell fate as it modulates the expression of Cone-rod homeobox protein (Crx) in photoreceptor precursor cells (Furukawa et al., 1997). Crx, is the principle transcription factor that directs rod and cone photoreceptor cell differentiation. Together with Otx2, Crx orchestrates the transcription of many photoreceptor-specific transcription factors which direct retinal precursors towards specific cell fate (Furukawa et al., 1999). One of the key regulators of the photoreceptor cell fate is a neuronal retina leucine zipper transcription factor (Nrl). Nrl is considered as one of the earliest rod-specific photoreceptor markers as it is preferentially expressed in rod precursors shortly after terminal mitosis (Mears et al., 2001). Nrl mediates a rod lineage through multiple mechanisms including activation the Rhodopsin (Rho) promoter as well as regulation of Nuclear Receptor Subfamily 2 Group E Member 3 (Nr2e3), which promotes rod photoreceptor genesis and, in parallel, represses cone-specific genes (Oh et al., 2008). The peak of Nrl expression overlaps with rod differentiation, with a subsequent decline in expression in later stages, but with the expression maintained in mature rod photoreceptors, suggesting that Nrl is required for both rod differentiation and maintenance (reviewed in (Montana et al., 2011)). While the commitment towards a rod fate is well characterised, much less is known about cone photoreceptor fate specialisation. A number of genes have been implicated in this process, though, including the retinoid-related orphan receptor (Rrb), which synergises with Crx transcription factor to positively regulate the S-opsin gene expression (reviewed in (Mansergh et al., 2015)).

The formation of synaptic connections between different neuronal cells in the retina happens in distinct stages (reviewed in (Reese, 2011)). First to be established are the lateral connections between ganglion and amacrine cells followed by connections between photoreceptors. Since bipolar cells are last to differentiate during retinogenesis, the vertical networks are not formed until early postnatal stages.

1.3.2 Retinal structure

1.3.2.1 Photoreceptor layer

There are nine layers in the retina with three distinctive layers of neuronal cells (Figure 1.3A) (Kolb et al., 2001). First, the photoreceptor layer, which is located directly above the RPE and consists of photosensitive rods and cones, designed to capture light quanta, or photons, that hit the eye. Photoreceptors are organized in four distinct regions: the cell body, which includes the nucleus, located in the outer nuclear layer (ONL); the inner segment (IS); the outer segment (OS); and the synaptic region (Figure 1.3B). The IS region houses the photoreceptor's metabolic machinery, which provides the energy in the form of ATP, which is produced by the numerous mitochondria and is required to power the sodium-potassium pumps necessary for stabilizing the resting potential. This segment is connected via a non-motile cilium to the photosensitive OS, which includes hundreds of stacked membranous discs transporting the proteins associated with phototransduction, including the visual pigment (Opsin). It has been estimated that each day approximately 10% of the OS discs at the distal end are shed and phagocytised by underlying RPE due to the light damage (reviewed in (Kevany and Palczewski, 2010)). All the shed discs are replaced with new ones, which are added at the proximal end, to allow photoreceptors for carrying the phototransduction process. The rate of formation and disposal of the discs are roughly equal so that a constant OS length is maintained in the adult retina (Young and Bok, 1969; Jonnal et al., 2010).

Different subtypes of photoreceptors can be classified based on the expression of a unique type of Opsin. In the human retina, three subtypes of cone photoreceptors have been isolated according to their opsin that defines the cell's light sensitivity including L-opsin (long, 564 nm), M-opsin (medium, 533 nm) and S-opsin (short, 437 nm). These different cone types help mediate colour vision, as well as high visual acuity under brighter light conditions. As mentioned in Section 1.2, the human retina has a region called the fovea, which is tightly packed with cones but only of the M and L type. S-opsin cones account for only 10% of the overall cone population and are absent from the fovea (Curcio et al., 1990; Cornish et al., 2004). By contrast, the murine dichromatic retina has only two types of cones: M-cones, located mainly in the superior region, and S-cones, mostly found in the inferior part of the retina (Applebury et al., 2000). In contrast to cones, only one type of rod cell has been found in the retina of all the vertebrates including both mice and humans. Rod photoreceptors express rhodopsin, which is a special type of opsin that enables for a vision in dim light conditions. In the retina of most mammals, rods greatly outnumber cones, even in species that are largely diurnal. Human retina has approximately six million cones,

which accounts for only 3% of the overall number of all the photoreceptor cells present in the retina (Sawides et al., 2016).

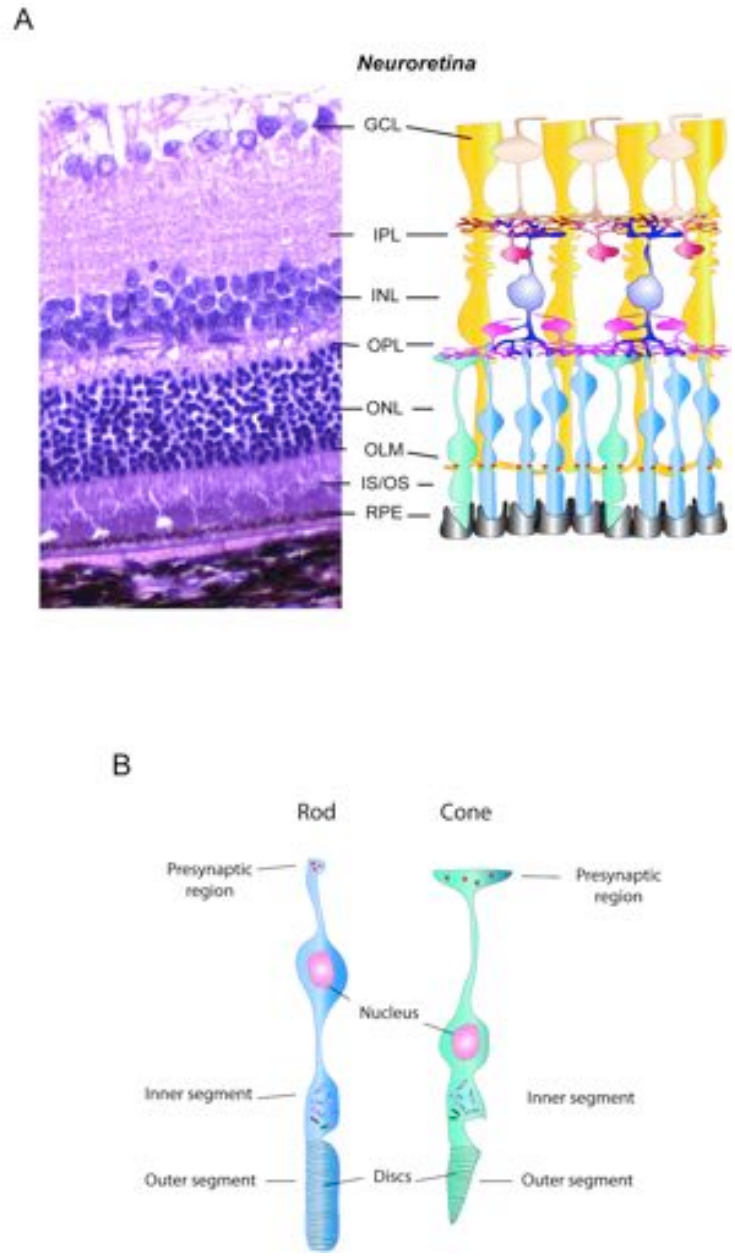

Figure 1.3 The retinal structure.

A) Histological section of the human retina with a schematic diagram illustrating different layers of the retina. The outer nuclear layer (ONL) contains photoreceptor cell bodies, from which the inner segment (IS) and outer segment (OS) extend towards the RPE. The inner nuclear layer (INL) includes amacrine, bipolar and horizontal neurons, whereas ganglion cells, axons of which form the optic nerve, reside in the ganglion cell layer (GCL). Outer and inner plexiform layers (OPL and IPL, respectively) contain synaptic regions. **B)** A schematic diagram illustrating the morphology of the cone and rod cell. The OS is made of hundreds of membranous discs that contain components of the phototransduction machinery, whereas the IS it contains hundreds of mitochondria and serves as the energy supplier of the photoreceptor cell. The visual proteins are transported to the outer segment via a connecting cilium. The nucleus is contained in

the cell body, and the presynaptic region includes one or more ribbon-like structures for docking of synaptic vesicles.

1.3.2.2 Inner nuclear layer

The inner nuclear layer (INL) comprises of different neuronal cell types, which propagate the electric signals received from photoreceptors to the brain.

1.3.2.2.1 Horizontal cells

Immediately above the photoreceptor nuclei, at the most apical side of the INL, reside the horizontal cells (reviewed in (Jeon et al., 1998)). These cells form synaptic connections with rods and cones and take part in a lateral inhibition circuit where they modulate multiple photoreceptor inputs projecting towards bipolar cells. One horizontal cell is connected to many neighbouring photoreceptors, which helps to modulate the magnitude of the bipolar cell activation. This helps the eye regulate the vision under different light settings.

1.3.2.2.2 Bipolar cells

Also located within the INL are the bipolar cells, which are excitatory glutaminergic interneurons and the predominant interneuron of the retina (reviewed in (Lauritzen et al., 2016)). The bipolar cells are connected to photoreceptor terminals via their dendrites and on the other side their axons form synapses with the ganglion cells. These cells are highly specialised and they are assigned only to rods or cones, but not to both as in case with the horizontal cells. There is only one type of a bipolar cell receiving the electrical inputs from rods, the rod ON-bipolar cell and at least 13 subtypes of the cone bipolar cells, both ON and OFF. The distinction between ON and OFF types depends on the response of the bipolar cell to photoreceptor activation and changes in their glutamate release.

1.3.2.2.3 Amacrine cells

Amacrine cells are the inhibitory interneurons that are located within the INL and GCL whose primary function is thought to moderate signals received from the bipolar cells and project them further to the cells located in the GCL (reviewed in (Baden and Euler, 2016)). There are many different subtypes of amacrine cells that can be distinguished based on the neurotransmitter they release and the type of connection they make, with type II being the most abundant.

1.3.2.3 Ganglion cell layer

Ganglion cells are the last neuronal cell type that is found in the retina. These cells are located in the inner most layer, the ganglion cell layer (GCL), where they collect inputs from bipolar and amacrine cells and project them to the brain via axonal projections that form the optic nerve (reviewed in (Sanes and Masland, 2015)). These cells constitute a large family, with different cell subtypes being responsible for encoding a

specific type of visual information. These distinctive subclasses can be distinguished into five major types due to their morphology, type of projections, and function they serve. The first three classes of ganglion cell, Midget, parasol and bistratified ganglion cells, project to different regions of the lateral geniculate nucleus (LGN) in the brain. The type 4 is unusual in its photosensitive properties, due to its expression of the visual photopigment, Melanopsin. Melanopsin enables ganglion cells to respond directly to light stimulus in the absence of rods and cones, for example in the pathological conditions. The projections of these ganglion cells end up in the suprachiasmatic nucleus (SCN) and help to maintain the circadian rhythm. The last class of ganglion cells, type 5, extends its fibres to the superior colliculus and accessory optical system where they allow for navigation of the eyes towards the regions of interest as well as they enable to keep the gaze when we move.

1.3.2.4 Synaptic layers

There are two distinct synaptic layers found in the retina, the outer plexiform layer (OPL) and the inner plexiform layer (IPL). The OPL is situated between the ONL and INL and contains the synaptic connections established between photoreceptor cells and the dendrites of the bipolar cells, as well as synaptic formations of the horizontal cells with photoreceptors and bipolar cells. The IPL holds synaptic connections between bipolar and ganglion cells, the bipolar and amacrine cells, and between the amacrine and ganglion cells.

1.3.2.5 Retinal glial cells

In the mouse retina there are two types of the glial cells, macro- and microglia.

Müller cells are the predominant macroglia type with their nuclei embedded within the INL, from where they project one process towards the vitreous surface and the inner limiting membrane (ILM), and the second towards the outer edge of the ONL and OLM. Müller glia cells surround blood vessels and neuronal cells in the retina providing a support for neuronal function and survival (reviewed in (Bringmann et al., 2006)). They deliver nutrients and trophic factors to the neurons, as well as removing metabolic waste (Bringmann et al., 2009b). By regulating transcellular ion, water and bicarbonate transport, Müller glia modulate the extracellular fluid and, in turn, keep the homeostatic balance of the retina. These cells are also involved in the regulation of synaptic activity in the retina as they are equipped with cellular machineries for the uptake and exchange of various neurotransmitters, including glutamate, released by neurons, particularly the photoreceptors (reviewed in (Bringmann et al., 2006)). By spanning the entire thickness of the retina, Müller glial processes act as optical fibres guiding the light towards photoreceptors in order to minimise the amount of photons being scattered across the inner retina. Previously, it has been thought that there was only one type of Müller glial cell; however recent studies have revealed that this glial population is more heterogeneous than previously thought, with individual Müller cells responding differently to a pathological insult (Luna et al., 2010). Moreover, it has been reported that although Müller glia in all vertebrates share similar morphological properties, there are some differences between different species (Dreher et al., 1992; Sarthy and Ripps, 2001). For example, in the feline retina, the Müller glia processes that lie adjacent to vitreous cavity have a club-like shape; whereas in many other species these processes are highly branched (Dreher et al., 1992).

The other macroglial cells of the retina are retinal astrocytes, which typically exhibit a stellate morphology. Astrocytes do not develop from the retinal neuroepithelium, but migrate from the outside of the neural retina along the optic nerve (Fernández-Sánchez et al., 2015). These cells primarily reside within the GCL, where their processes follow the fibres of ganglion cells towards the optic nerve forming rows with vitreal surface.

There are also two forms of microglia found throughout the retina: resident microglia and infiltrating microglia. These cells have a close relationship with neurons, where they protect them from the invading microbes, clearing cellular debris and enforcing programmed cell death (reviewed in (Rock et al., 2004)). They also release a number of factors including brain-derived neurotrophic factor (BDNF), as well as various anti-inflammatory cytokines that sustain and support neuronal survival. However, these cells may also release proinflammatory and pro-angiogenic factors in diseases such as

AMD leading to pathological neovascularization and further retinal damage (Lewis et al., 2005).

1.3.2.6 Inner and outer membranes

1.3.2.6.1 Outer limiting membrane

At the apical edge of the ONL, Müller glia and photoreceptor ISs are connected via a series of tightly arranged adherens junctions, which are formed from cadherin-catenin transmembrane protein complexes. These junctions contribute to the maintenance of the retinal structure, as they are linked to the actin cytoskeleton within the cell cytoplasm, via essential adapter proteins (reviewed in (Alves et al., 2014b)). The OLM structure, apart from providing mechanical strength, also functions as a permeability barrier to any molecules coming from the choroid and the phototransduction process, thereby protecting the neuroretina from toxicity.

1.3.2.6.2 Inner limiting membrane

On the side of the vitreous, Müller cells, together with astrocytes, form a very thin and transparent coating, the ILM. Its primary function is believed to act as a diffusion barrier between the neural retina and vitreous humour at the inner surface of the retina.

1.3.2.7 Interphotoreceptor matrix

The interphotoreceptor matrix (IPM) is a highly organized structure with interconnected domains surrounding cone and rod photoreceptor cells, which extends into the subretinal space. This subretinal region, located between the ONL and RPE, is highly enriched in proteins belonging to the proteoglycan family, which have an ability to bind to many ECM molecules and growth factors. Based on known roles of the ECM in other tissues, the IPM is thought to have several prominent functions including serving as a cell adhesion and migration substrate, regulating retinoid transport, participating in cytoskeletal organization in surrounding cells, and regulation of oxygen and nutrient transport (reviewed in (Ishikawa et al., 2015)). In addition, a number of studies suggest that the IPM may also play a significant role in the aetiology of retinal degenerative disorders (LaVail et al., 1981; Bridges, 1985; Mieziewska et al., 1993).

1.4 Process of phototransduction

The phototransduction cascade refers to a biological process that transforms a light stimulus in a form of photon into an electrical signal, with photorecepotors being the main players in this process. As previously mentioned, rods and cones possess outer segments, which contain the biochemical machinery needed for visual transduction. All the necessary components of the phototransduction cascade are packed into discs that in rods are surrounded by the plasma membrane of the outer segment (Figure 1.5), whereas in cones these discs are an extension of the plasma membrane, arranged into a series of infoldings. These open discs in cones allow for faster fluxes of molecules between the cell exterior and interior, such as chromophore transfer for pigment regeneration and fast calcium dynamics during light adaptation. Rods are able to detect single photons hitting the retina, which is attributed to three factors: high quantum efficiency of photoactivation, low intrinsic noise, and a powerful signal amplification cascade. The dense stack of discs of the OS allows for every photon traveling axially to be detected and transmitted to the inner retina.

1.4.1 Dark condition

In the inactive state, most neurons maintain a membrane potential of about -60 to -70 mV. When the neuronal cell becomes activated, the cation channels become open which causes influx of sodium (Na^+) cations inside the cell making it more positive. This results in cell depolarisation and opening of the voltage-gated calcium (Ca^{2+}) channels at the synaptic terminal. The influx of the Ca^{2+} cations stimulates fusion of synaptic vesicles with the plasma membrane and the release of neurotransmitter into the synaptic cleft. The process is terminated by a hyperpolarisation caused by the efflux of the positively charged cations from the cell, leading to restoration of the resting membrane potential. In rod and cone cells this process works “backwards”. In the dark, or at ‘rest’, the photoreceptors are depolarized to -35 to -45 mV, because the Na^+ gated channels located at the OS surface are open due to binding of guanosin 3’,5’ cyclic monophosphate (cGMP). To maintain this depolarisation state, potassium (K^+) selective channels in the IS pump out potassium cations K^+, which balances the influx of cations at the OS, completing an electrical circuit, referred to as the “dark” or circulating current. This results in photoreceptors depolarisation, which allows for the voltage gated Ca^{2+} channel located in the photoreceptor synaptic terminals to stay open. As Ca^{2+} ions flow inside the terminals, the synaptic vesicles fuse with the cell membrane and release the neurotransmitter glutamate into the extracellular space between photoreceptors and terminals of inner- neurons. When rods and cones receive light, the channels in the OS close and the membrane hyperpolarises towards the equilibrium potential for K^+.

1.4.2 Light detection

In a mouse retina, there are two type of cones S- and M-type, and only one type of rods. This distinction between different photoreceptor types depends on the expression of different Opsins, which belong to the super family of G-protein coupled receptors. Mouse retina is unusual in the sense that individual cones express both S- and M-cone pigments, but as the levels of the M-pigment start to decrease in a gradient manner from dorsal to ventral retina (Applebury et al., 2000). The activation of Opsins is the first step in the photodetection cascade with phototransduction occurring in rods being one of the best-characterised signalling pathways in the retina (Figure 1.4).

When the light is being detected, the light photon is being absorbed by the visual pigment Rho, which is embedded within the discs of the photoreceptor OS. Rho is a divided into two parts: the chromophore 11-*cis* retinal and one of the opsin molecules. First identified by George Wald in 1934, 11-*cis*-retinal cannot be made *de novo* by the body as it is derived from vitamin A (Wald, 1934). Deficiency of vitamin A in a diet lowers sensitivity of rod cells as fewer functional Rho molecules are produced, which leads to the development of night blindness (Goodman, 1984; Jacobson et al., 1995). The photon absorption results in 11-*cis* retinal chromophore photoisomerisation and its structural change converting it into the all-*trans* retinal isomer. This change forces the Rho molecule (R) to expand resulting in its activation (R*), which leads to activation of the next visual component located on the surface of OS disc membrane, transducin. Transducin is the most stable G-protein (G) known and it consists of three subunits: α, β and γ. Rods and cones have different isoforms of transducin, being $G\alpha t_1 G\beta_1\gamma_1$ in rods and $G\alpha t_2 G\beta_3\gamma_8$ in cones. In the dark, the α-subunit (Gα) normally binds GDP nucleotide. Upon Rho activation, the Gα subunit aligns with R* and GDP is being replaced with GTP. In turn, transducin becomes activated (G*) with the Gα-GTP separating R* molecules as well as the other two subunits (Figure 1.5b). In the next instance, the activated Gα-GTP* binds to cGMP phosphodiesterase (PDE) to carry the signal forward. Released R* is free to activate additional transducin molecules. Transducin is tenfold less abundant than rhodopsin pigment, but its activation by R* represents the first amplification step in the phototransduction cascade.

PDE represents the third component in the phototransduction process and the second amplification step with a density at roughly 1-2% of Rho. PDE is a tetrameric protein consisting of two equally active catalytic subunits, α and β, and two identical γ subunits. In the dark, the two PDEγ subunits bind to the two catalytic subunits. In the light, Gα-GTP* encounters PDEγ subunits causing a sterical displacement of the PDEα and PDEβ subunits and as a consequence PDE activation (PDE*). PDE* then hydrolyses the diffusible messenger cGMP present in a cytoplasm to 5'-GMP reducing its

concentration and leading to the closure of the cGMP-gated channels on the plasma membrane. The cGMP-gated channel belongs to the family of cyclic-nucleotide-gated (CNG) channels, which are non-selective cation channels. This channel closure leads to localised reduction in the influx of Na^+ cations into the OS, which results in membrane hyperpolarisation and cessation of glutamate release at the synaptic terminals. For the channel to respond to changes in cGMP concentration, it must revert to the closed state, thereby allowing cGMP to dissociate from the channel. This happens only if the concentration of cGMP reaches a certain level. If the concentration of cGMP remains low, the channel will stay closed since there will be fewer nucleotides around. Thus 'channel chatter' ensures that the response to a decrease in cGMP levels will be quick. The rod photoreceptor possesses a vast number of cGMP-gated channels, but only a small percentage is normally open in darkness. Here, the activity of PDE serves as an important regulator of photoreceptor function, as the rod photoreceptor possesses a vast number of cGMP-gated channels but only a small percentage is normally opened in darkness. As cGMP is constantly synthesised in the cytoplasm, the lack of activated PDE would lead to cGMP cytoplasmic accumulation and in turn activation of a greater number of cGMP-gated channels resulting in a permanent depolarisation of the photoreceptor. The lowering in the concentration of cGMP leads to closure the Na^+ channels which in turn causes photoreceptor hyperpolarisation and subsequent closure of voltage-gated Ca^{2+} channels. As the level of intracellular Ca^{2+} falls, the release of glutamate ceases, leading to depolarization of ON-bipolar cells and hyperpolarization of cone OFF- bipolars. The hyperpolarisation of the photoreceptor becomes the first step in the termination of phototransduction process.

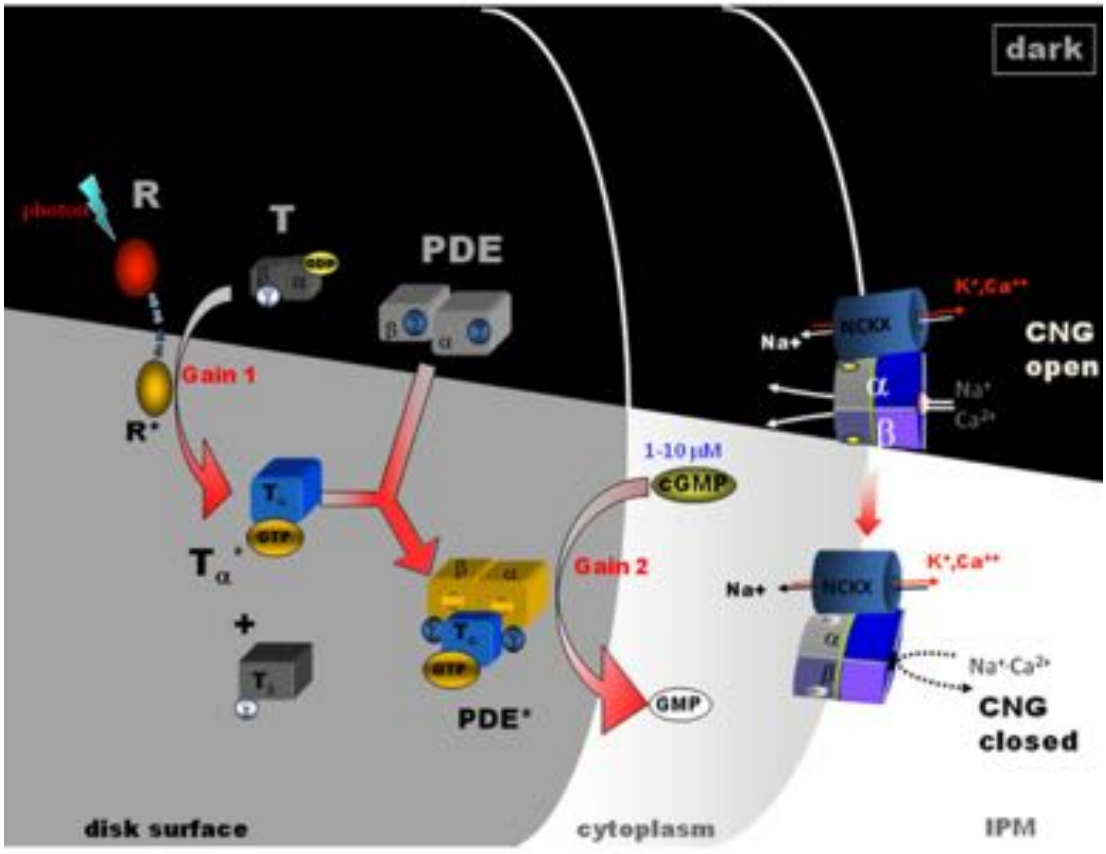

Figure 1.4 Phototransduction cascade.

Activation of rod phototransduction cascade in the OS results in the closure of cGMP-gated channels on the plasma membrane (from dark to light state). R, Rho (inactive); R*, Rho (active); T, transducin; PDE, phosphodiesterase (inactive); PDE*, phosphodiesterase (active); NCKX, Na/Ca,K exchanger. IPM, interphotoreceptor matrix.

Copyright note: Image taken from http://webvision.med.utah.edu/*, and it is a courtesy of Dr Wolfgang Baehr. Accessed online on 20.5.2016.*

Following light activation, a timely recovery of the photoreceptor is essential so that it can respond to subsequent light stimulus, hence the efficient inactivation of each of the activated components, R*, G*, and PDE*, as well as the efficient regeneration of Rho and the rapid restoration of the cGMP concentration, are needed. One hallmark of rod phototransduction is the reproducibility of its single-photon response in both amplitude and kinetics. First, Rho kinase (GRK1) phosphorylates serine and threonine residues at the C-terminus of R*. Phosphorylation of R* alone decreases is activity and allows for binding of arrestin. Arrestin is a very large protein, whose sheer bulk prevents any transducins from getting close enough to bind to R*. Arrestin remains bound to the Rho molecule until the all-*trans* chromophore is removed, diffused into the cytosol of the OS and transported out of the segment into the RPE. In the RPE the chromophore is reduced by appropriate enzymes to all-*trans* retinol, and ultimately converted into 11-*cis* retinal. In this form, the chromophore is transported across the IPM enveloped by 11-*cis* retinal binding protein back to the photoreceptor OS. Here, phosphatase dephosphorylates the deactivated Rho molecule allowing 11-*cis* retinal to re-bind to the opsin thus restore the inactive visual pigment.

G* is inactivated by hydrolysis of GTP to GDP via activity of GTPase, which is accelerated by the GTPase Activating Protein (GAP) complex. Upon hydrolysis of GTP to GDP, Gα* subunit releases the PDEγ* subunits allowing them to re-bind to the PDE catalytic subunits, α and β. Gα subunit eventually re-joins with the other two subunits to reconstitute the inactive transducin heterotrimer. To ensure that Gα* does not inactivate before triggering activation of PDE, Gα* transducin and the GAP complex have a low affinity for each other, until transducin Gα*-GTP binds to PDEγ.

Full recovery following the photoresponse requires that the cytoplasmic cGMP levels get restored to the dark-adapted concentration. As noted above, cGMP is synthesised continuously from GTP by a membrane-associated enzyme, guanylate cyclase (GC). Retinal GC is a transmembrane protein that exists as homodimer, whose activity is kept low by the action of guanylate cyclase activating proteins (GCAPs), which bind calcium ions. As levels of calcium start to fall as a result of Na+/K+, Ca2+ exchanger machinery, GCAP dissociates itself from its bound Ca^{2+} and activates GC leading to transformation of GTP back to cGMP. This allows for restoration of the intracellular cGMP levels to high concentrations, which cause the Na^{+} cation channels to re-open and restore the cell's depolarisation state.

1.5 Retinal degenerative diseases and their genetics

Vision is a primary sense that allows for normal interactions with the external environment; its loss has tremendous consequences on quality of life, especially for humans. The impairment of sight can be caused by an obstruction preventing light getting to photosensitive cells, as in the case of cataracts, or by the inability of the neuroretina to detect light or to transmit the received stimulus to the visual centres in the brain. The latter are usually a consequence of photoreceptor dysfunction or their complete loss due to degeneration. During the last decades, studies on retinal degenerative diseases identified over 1500 entries of inherited retinal dysfunctions associated with over 250 different causative genes (https://sph.uth.edu/retnet/). This genetic heterogeneity in retinal degenerations is further complicated by the fact that, very often, there is no clear one-to-one genotype-phenotype correlation. For example, mutations in the same gene can result in a spectrum of different phenotypes, whereas defect in one of many different genes can manifest itself in a similar manner (reviewed in (Boon et al., 2008)). As a consequence, hereditary retinal retinopathies are currently thought to be the most genetically heterogeneous group of diseases in humans.

1.5.1 Classification of retinal degeneration phenotypes

Recent advances in technology and medical equipment facilitated development of better methods for non-invasive assessment of the structure, physiology as well as function of the eye and the retina. Examination of the ocular fundus by ocular coherence tomography (OCT) is commonly used in clinics to examine the structure of the retina, whereas electroretinography (ERG) allows for studying of retinal function. On the other hand, next-generation sequencing is helping to identify numerous defected genes and/or loci associated with loss of vision in patients suffering from a retinal degeneration. These assessments allow clinicians for making correct diagnosis and classify patients according to different pathological phenotypes (Figure 1.6).

With regard to inherited disorders, depending on the disease type, rods and cones can be differently affected. Commonly, the clinical phenotypes of inherited retinal diseases are usually divided into rod degenerative RP and cone or cone-rod dystrophy (CD or CRD, respectively). Primary RP comes in many forms and consists of large numbers of genetic mutations affecting rods directly. Typically, in the early stages of the disease, the rods of the peripheral retina begin to degenerate, leading to gradual development of night blindness. As the disease progresses, patients start to lose visual field and visual acuity due to subsequent cone impairment. A typical pathological characteristic of RP is the occurrence of black pigment in the peripheral retina coupled with thinning of blood vessels at the optic nerve head (reviewed in (Parmeggiani, 2011)).

In contrast to RP, in primary CD, a dysfunction or loss of cone photoreceptors might not necessarily lead to secondary degeneration of rods; however, when rods are involved in CD, the disease is referred to as CRD. A typical clinical phenotype of CD manifests itself first with the loss of visual acuity, impairment of colour vision and photosensitivity (light aversion). In CRD, as the disease progresses and severe retinal degeneration has developed, rod photoreceptors start to follow the fate of cones (reviewed in (Hamel, 2007)).

Of all the retinal degenerations, Leber's congenital amaurosis (LCA) is one of the most severe, accounting for approximately 5% of all retinal dystrophies and 20% of paediatric patients. There are at least 20 known different gene mutations associated with this condition causing severe and early visual impairment, sluggish or near-absent pupillary responses, and severely subnormal or non-detectable ERG responses (reviewed in (Chacon-Camacho and Zenteno, 2015)).

Since the photoreceptor OS is a modified primary cilia, mutations in genes affecting cilia biogenesis or function often result in retinal degeneration, in addition to the dysfunction of ciliated cells in other organs. These so-called syndromic ciliopathies may affect vision, as well as hearing (Usher syndrome), renal function (Senior-Loken syndrome), or proper brain development (Joubert syndrome) (reviewed in (Rachel et al., 2012)).

In addition to primary mutations in photoreceptor genes, genetic defects in RPE, which takes part in the maintenance of photoreceptor homeostasis, are also found to be associated with retinal degenerations (reviewed in (Travis et al., 2007)).

Macular degeneration (MD) is a specific form of retinal degeneration where both rods and cones are affected but only within the macular region. This condition manifests itself by a loss of the central vision enabling us to read or see fine details. The most common monogenic MD is Stargardt disease, a condition that has an early age onset. AMD is a form of MD, with many genetic and environmental factors being involved, and with symptoms not present until affected individuals are much older. In this condition, the macular area and fovea become compromised due to the pigment epithelium behind the retina degenerating and forming drusen (yellow spots) leading to 'dry' AMD or abnormal neovascularisation and eventual leakage of fluid behind the fovea ('wet' phenotype) (reviewed in (Fritsche et al., 2014)).

Another retinal degenerative disease associated with ageing is glaucoma. This condition manifests itself by elevation in the intraocular pressure due to dysfunction in fluid exchange within the anterior chamber. As the pressure within the vitreous chamber gradually rises, the blood vessels of the optic nerve head become compromised leading to damage of the ganglion cells axons and their subsequent

death. Apart from this mechanical dysfunction, glutamate intoxication has also been associated with the progression of neuronal degeneration observed in glaucoma (reviewed in (Schumer and Podos, 1994)).

The last retinal condition worth mentioning with respect to the work described in this thesis is diabetic retinopathy (DR). In contrast to the previously mentioned diseases, loss of vision is a side effect of diabetes where the vital blood vessels of the eye become distorted and start to proliferate in uncontrollable manner. Among the symptoms experienced by diabetic patients are elevated blood sugar levels, blurred vision, dark spots and sudden loss of vision. In more advanced stages of DR, development of glaucoma, retinal detachment or macular edema are also accompany the above mentioned pathological changes (reviewed in (Cai and McGinnis, 2016)).

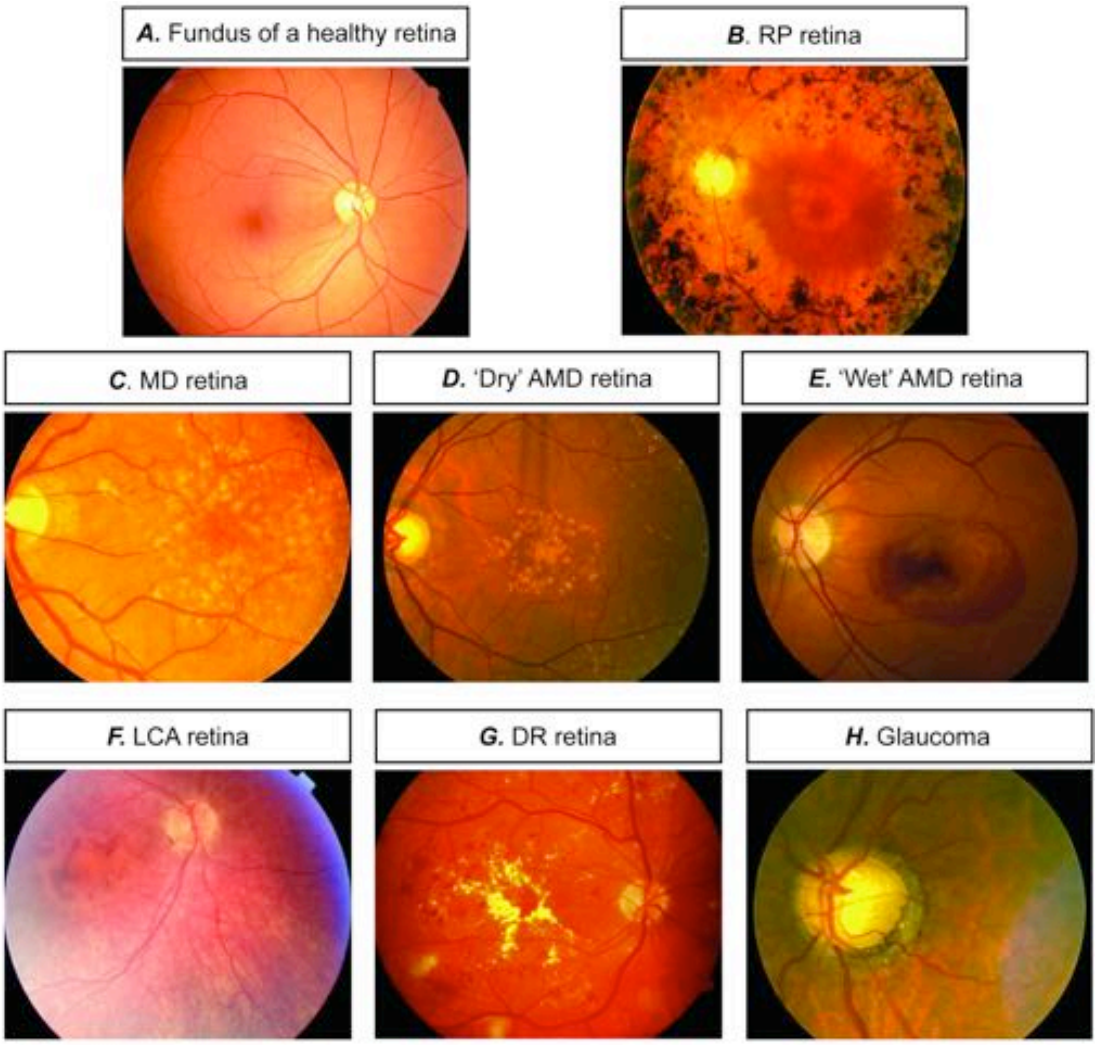

Figure 1.5 Characterisation of retinal diseases in human patients.

Fundus images of **A)** healthy retina, **B)** RP retina, C) MD retina, D) 'Dry' AMD retina, E) 'wet' AMD retina, F) LCA retina, G) DR retina and H) retina with a glaucoma.

AMD; age-related macular degeneration; DR, diabetic retinopathy; LCA, Leber's congenital amaurosis; MD, macular degeneration; RP, retinitis pigmentosa.

Copyright note: Images taken from http://webvision.med.utah.edu/*. Accessed online 20.05.2016.*

1.5.2 Genetics of retinopathies

The majority of our understanding of retinopathies comes from studies on animal models. The use of model organisms has not only increased our knowledge of a normal retinal function, but has also allowed us to shed some light onto the mechanisms underlying retinal pathologies. Although *Drosophila* and zebrafish have been used as classical models for discovering the basic principles of visual pathways, it is the mouse that has become the most widely used model in pre-clinical translational eye research. Naturally occurring mutants, as well as genetically engineered mice, not only provided invaluable insights into disease pathology, and have been key in the development of clinically relevant therapies. Here, an evaluation of the most common retinopathies is presented with a reference to genetic mutation (Table 1.1), with particular reference to those models used in this thesis.

1.5.2.1 Retinal diseases caused by photoreceptor developmental defects

Transcription factors including CRX, NRL, and NR2E3 are crucial for the proper development of photoreceptors, as they orchestrate the expression of rod and cone-specific genes (Swaroop et al., 2010). Genetic mutations in the genes encoding for these factors have been found in patients with LCA, RP, CD, and CDR and can result in photoreceptor dysfunction and, in some cases, photoreceptor death (Berger et al., 2010; Khateb et al., 2016).

CRX has a key function in regulation of rod and cone specific genes and because of that defects in *CRX* gene can result in development of a number of different phenotypes in humans. Mouse knockout mutants are born blind, have no functional photoreceptors and show malformations in OS and synaptic terminals with the expression of phototransduction genes being compromised. The mutation ultimately leads to photoreceptor degeneration (Furukawa et al., 1999).

NRL transcription factor was shown to be responsible for determination of rod cell fate as *Nrl* knockout mouse lacks rod photoreceptors and rod specific genes (Mears et al., 2001). In humans, mutations in *Nrl* gene are associated with RP with both rods and cones being severely affected (DeAngelis et al., 2002). In the $Nrl^{-/-}$ retina, the expression of cone specific genes is elevated, however the cone cells that are present are more of a hybrid cell type and have been referred to as ‘cods’. A typical characteristic of $Nrl^{-/-}$ retina is the development of retinal folds commonly known as rosettes (Stuck et al., 2012). Studies of this genetic mutant provided invaluable information on rod development and function and helped to understand better the photoreceptor fate determination (Mears et al., 2001).

Mutations in NR2E3, which is downstream of NRL (Oh et al., 2008), are associated with retinal spots, which correlate with presumptive rosette formation, and progressive photoreceptor degeneration leading to visual impairment at later stages of disease progression (Haider et al., 2009). The retina of individuals with defects in *Nr2e3* gene lacks rods, but shows an increase in the number of S-cones (Haider et al., 2001). Studies on *Nr2e3*$^{-/-}$ mutant showed that the expression of this transcription factor is limited to post-mitotic rod cells indicating that NR2E3 promotes rod cell fate while at the same time inhibiting cone specific genes (Cheng et al., 2006).

A number of mutations are associated with the malformation of photoreceptor OSs, especially to their discs. Mutations in Peripherin (Prph), which is essential for the formation of the rod and cone OS during development and their postnatal renewal (Travis et al., 1991), are linked to a variety of retinal diseases including CRD (Nakazawa et al., 1996) and autosomal dominant RP (Keen and Inglehearn, 1996). Commonly referred to as the '*retinal degeneration slow'* (*rds*) transgenic mouse line carries a mutation in *Prph* gene and has shorter OSs (Travis et al., 1991; McNally et al., 2002) and early photoreceptor degeneration (Kedzierski et al., 1997).

1.5.2.2 Retinal degenerations associated with phototransduction process

The process of phototransduction depends on many different phototransduction proteins. Mutation to any the genes encoding for these molecules frequently results in vision impairment. As visual pigment is a major structural component of rods and cones, it is not surprising that genetic defects in Rho and cone Opsins not only affect the process of phototransduction, but also lead to photoreceptor dysfunction and subsequent death. In humans, defects in *RHO* gene lead to the development of a variety of different RP phenotypes depending on the type of mutation, but are usually associated with night blindness and progressive photoreceptor deterioration. The *Rho* knockout mutant mouse shows a malformation of rod OSs, with degeneration of rod cells starting as early as three weeks of age (Humphries et al., 1997).

In 1996, a mutation in *GNAT1* gene, which encodes α-subunit of G protein transducin in rods, was found in patients suffering from congenital stationary night blindness (CSNB) (Dryja et al., 1996; Naeem et al., 2012). A transgenic mouse model revealed that defects in *Gnat1* result in a decrease in activity of GTPase and impaired ability to activate PDE6 (Moussaif et al., 2006) leading to slow degeneration of rods over time (Calvert et al., 2000). On the other hand, defects in *GNAT2*, which controls the expression of cone α- transducin (Morris and Fong, 1993), result in a lack of functioning cones with the majority of individuals developing a complete achromatopsia (Kohl et al., 2002). The *Gnat2*$^{-/-}$ mouse resembles the human phenotype and shows

clear dysfunction of cone photoreceptors, mislocalisation of Opsin protein, remodelling of a retina and clear signs of progressive cone deterioration (Jobling et al., 2013).

Null or missense mutations in the gene encoding PDE protein, which is the third major component in the phototransduction cascade, can be associated with an autosomal recessive form of RP (McLaughlin et al., 1993; Dryja et al., 1999) or autosomal dominant CSNB (Gal et al., 1994). The *Pde6b*$^{rd10/rd10}$ mutant manifests a mild degenerative phenotype and is a widely used tool by researchers working on therapeutic interventions for RP (Chang et al., 2002). In contrast, *Pde6b*$^{rd1/rd1}$ mouse, commonly referred to as *rd1*, is the oldest mouse model used in RP research and manifests a very fast degeneration of photoreceptors with the majority of cells absent by the 2nd month of age (Caley et al., 1972; Sanyal and Bal, 1973). In a recent study by Nishiguchi, Carvalho *et al.,* the most commonly used strain of the *rd1* mutant, (C3H/HeN background), which is often used in preclinical studies, was found to harbour a second genetic mutation in the GPR179 gene, expressed in bipolar cells (Nishiguchi et al., 2015), which impairs further transmission of detected light stimulus towards the visual centres in the brain.

Mutations in different components of the phototransduction pathway may result in abnormal CNG channel activity, triggering photoreceptor cell death. Moreover, over 50 different genetic defects in the genes that encode CNG gated channels have been found in relation to channelopathies (https://sph.uth.edu/retnet/). Depending on the cell-type expression of mutant protein, rods and cones are affected differently, leading to distinct clinical symptoms. Mutations in CNGA1 or CNGB1 genes that encode CNG channels in rod photoreceptors lead to autosomal recessive RP (Dryja et al., 1995; Bareil et al., 2001), whereas mutations in the cone CNG channel gene CNGA3 and CNGB3 are the major cause of achromatopsia in humans (Kohl et al., 1998; Kaupp and Seifert, 2002). In mice, complete knock-out of *Cngb1* mimics retinal degeneration observed in human RP patients, with the loss of rods at birth followed by progressive degeneration of cones (Hüttl et al., 2005). *Cnga3*$^{-/-}$ mouse mutants lack functional CNG channels in the cone OS with progressive loss of cone photoreceptors over time (Biel et al., 1999).

Termination of phototransduction cascade is achieved by R9AP protein and G protein β5 deactivating the G*-PDE* complex, and GC with their activators GCAPs that transform GTP back to cGMP. *R9AP* mutations are responsible for a bradyopsia condition, where the eyes of affected individual adapt more slowly than usual to changing light levels (Nishiguchi et al., 2004). Defects in *GC1* gene expression leads to permanent closure of cGMP gated cation channels and development of in CD and LCA (Hanein et al., 2004); whereas *GCAP1* mutations have been linked to CRD (Baehr et

al., 2007) as they decrease the sensitivity to detect Ca2+ causing continuous stimulation of GC1 protein in dark conditions (Hanein et al., 2004).

RPE plays a crucial part in the visual cycle as it is responsible for recycling of the rod and cone visual pigments and mutations in several RPE specific genes are associated with retinal degeneration. Human LCA type 2 is associated with mutations in Retinal Pigment Epithelium-specific 65 kDa protein (RPE65) (Cideciyan, 2010). RPE65 is almost exclusively expressed in the RPE and functions as the retinoid isomerase responsible for converting *all-trans* retinoid to *11-cis* retinal during pigment regeneration (Moiseyev et al., 2005). Improper functioning or absence of RPE65 results in a lack of *11-cis* retinal production and an inability to efficiently form the visual pigments, Rho and Cone Opsin (Redmond et al., 1998; 2005). *Rpe65* mutant mouse suffers from severe visual impairment with progressive retinal degeneration probably due to constant activation of phototransduction cascade by the large amount of free visual pigment. A more mild form of retinal degeneration manifests *RPE65-R91W* transgenic mouse where the retina is able to produce some of 11-*cis*-retinal allowing for partial recovery of Rho pigment (Samardzija et al., 2007).

1.5.2.4 Other retinal degenerations

Mutations in the *Crumbs Homologue Protein 1* (*CRB1*) gene are associated with variable phenotypes of severe retinal dystrophies, ranging from LCA to CRD which may be accompanied by specific fundus features including Coats-like vasculopathy (reviewed in (Bujakowska et al., 2011). Retinae of CRB1 patients have altered laminar organisation and are usually much thicker than that of healthy individuals (Jacobson et al., 2003). Moreover, CRB1 mutations seem to present a phenotypic variability in patients which leads to differences in clinical diagnoses (for example, LCA, juvenile-onset RP, or autosomal recessive RP). Patients with CRB1 defects present an abnormal hyperreflective lesions of various sizes and retinal depths in regions of thickened, non-seeing retina. These hyperreflective lesions show some resemblance to the retinal folds observed in the $Crb1^{rd8/rd8}$ mutant mouse, which suffers from similar disruptions to OLM integrity (Mehalow et al., 2003). Previous studies of different *Crb1* mutants ($Crb1^{-/-}$, $Crb1^{c249wl}$ and $Crb1^{rd8/rd8}$) have shown the retinal abnormalities reported in these animals seem to be light-dependent and usually restricted to the inferior quadrant of the retina (van de Pavert et al., 2004). Recently, Alves et al. reported that the *Crb2* knockout mouse manifests a more similar disease phenotype to that observed in CRB1 patients (Alves et al., 2014a) indicating that the role of Crumbs proteins may vary between different species.

Interestingly, a recent study by Zhao, Andrieu-Soler et al., published in *The Journal of Neuroscience* characterized a recessively inherited retinal phenotype of the Brown

Norway rat strain from Janvier Breeding Centre (BN-J). A thorough analysis of the BN-J retinae showed that they display retinal abnormalities such as neuronal and vascular changes, focal alternations to retinal lamination and development of retinal cysts, all very similar to retinal pathology seen in Macular telangiectasia type 2 (MacTel 2) Genetic analysis showed that the BN-J rat has a mutation on the 6th exon of the *Crb1* gene, which results in the ablation of 14 nucleotides and insertion of 8 new one. This mutation was shown to lead to dislocalisation of CRB1 from the SAR in glial cells of the BN-J retina.

Stargardt disease is an autosomal recessive form of juvenile MD that severely impairs central vision. Mutations in *ABCA4* gene were one of the first to be associated with this condition (Allikmets et al., 1997). *ABCA4* gene encodes an ATP-binding cassette transporter (ABC) which actively transports all-*trans*-retinal (atRAL) from the internal membranes of retinal OS discs to the cytoplasm, where it is reduced to retinol (Kiser et al., 2012). In the generated *Abca4*$^{-/-}$*Rdh8*$^{-/-}$ transgenic mouse model, this process is impaired which results in the accumulation of the retinoid waste in the OS (Maeda et al., 2009).

Usher syndrome belongs to genetically heterogeneous group of RP diseases accompanied by a progressive loss of hearing and varying degrees of vestibular dysfunction. To date, 11 different genetic mutations have been found linked to three distinguished disease phenotypes. The most severe form of Usher condition, Type 1, is caused by genetic defects in *MYO7A* gene that encodes myosin motor protein expressed in embryonic RPE, photoreceptors, cochlear and vestibular neural epithelia (Weil et al., 1996).

Following activation by light, photoreceptors propagate the received stimulus towards inner retina via a graded decrease in glutamate release at the synaptic terminals. Mutations in the genes encoding for the voltage-gated calcium channels have been associated with X-linked CSNB (Strom et al., 1998), X-linked CRD (Huang et al., 2013) and autosomal recessive form of CRD (Wycisk et al., 2006b). In mouse, spontaneous mutation in *Cacna2d4* gene results in retinal degeneration with a characteristic malformation of a synaptic layer (Wycisk et al., 2006a).

Phenotype (disease)	Cell type affected	Mode of inheritance	Genes
Non-syndromic monogenic			
CSNB	Rods more than cones	Dominant Recessive X-linked	*GNAT1, PDE6B, RHO* *GNAT1,CABP4, GRK1, SAG* *CACNA1F*
LCA	Rods and cones	Dominant Recessive	*CRX* *CRX, APIL1, TULP1, CABP4, REP65, CEP290, CRB1*
RP	Rods more than cones and/or RPE	Dominant Recessive X-linked	*CRX, NRL, NR2E3, PRPH2, RHO, ROM1, RPE65* *ABCA4, MERTK, NRL, NR2E3, PDE6A, RHO, RPE65,SAG, TULP1* *RPGR, RP2*
CD-CDR	Cones more than rods	Dominant Recessive X-linked	*AIPL1, CRX, PRPH2* *ABCA4, CNGB3, RAB28* *CACNA1F, RPGR*
MD	Rods and cones	Dominant Recessive X-linked	*PRPH2, ELOV4* *ABCA4* *RPGR*
Synaptic diseases	Rods and cones	Dominant Recessive X-linked	*UNC119, RIMS1* *CACNA2D4* *CACNA1F, XLRS*
Syndromic			
Joubert syndrome	Rods and cones	Recessive	*CEP290*
Senior-Loken syndrome	Rods and cones	Recessive	*CEP290*
Usher syndrome	Rods and cones	Recessive	*MYO7A, USH2A*

Table 1.1 Genetics of some common human forms of retinal degenerations.

CSNB, Congenital stationary night blindness; CD or CRD Cone or Cone-rod; DR, Diabetic retinopathy; LCA, Leber's congenital amaurosis; MD, Macular degeneration; RP, Retinitis pigmentosa.

Copyright note: Table adapted from (Veleri et al., 2015).

1.6 Retinal remodelling in degenerative conditions

In retinal degenerations such as RP, AMD, or Usher Syndrome, death of photoreceptors, often triggered by rod degeneration, leads to irreversible vision impairment. As the retina starts to degenerate, the retinal structure and the environment begin to remodel, with a series of morphological, molecular and functional alterations in different retinal cells (Strettoi et al., 2002; Jones et al., 2003a; Jones and Marc, 2005; Sethi et al., 2005). This retinal remodelling is a complex pathophysiological process, but studying it may help to advance the research towards more efficient ocular therapies.

Retinal remodelling is usually divided into three different phases (Figure 1.6) (reviewed in (Cuenca et al., 2014)). Phase I is a pre-degeneration phase, indicated by early markers of cellular stress but with no major changes to retinal morphology or function (Figure 1.6A). In Phase II, photoreceptors start to deteriorate, with glial and RPE cells becoming involved (Figure 1.6B). Phase III is the ultimate phase where the retina undergoes major organisational alterations including neuritogenesis, cell migration, loss of distinct layer lamination, glial hypertrophy, metabolic changes of neurons and glia cells, synaptic rewiring and many more (Figure 1.6C). The progress of the remodelling is directly linked to a degree of retinal damage and speed of photoreceptor loss and it should be taken into account before any therapeutic intervention.

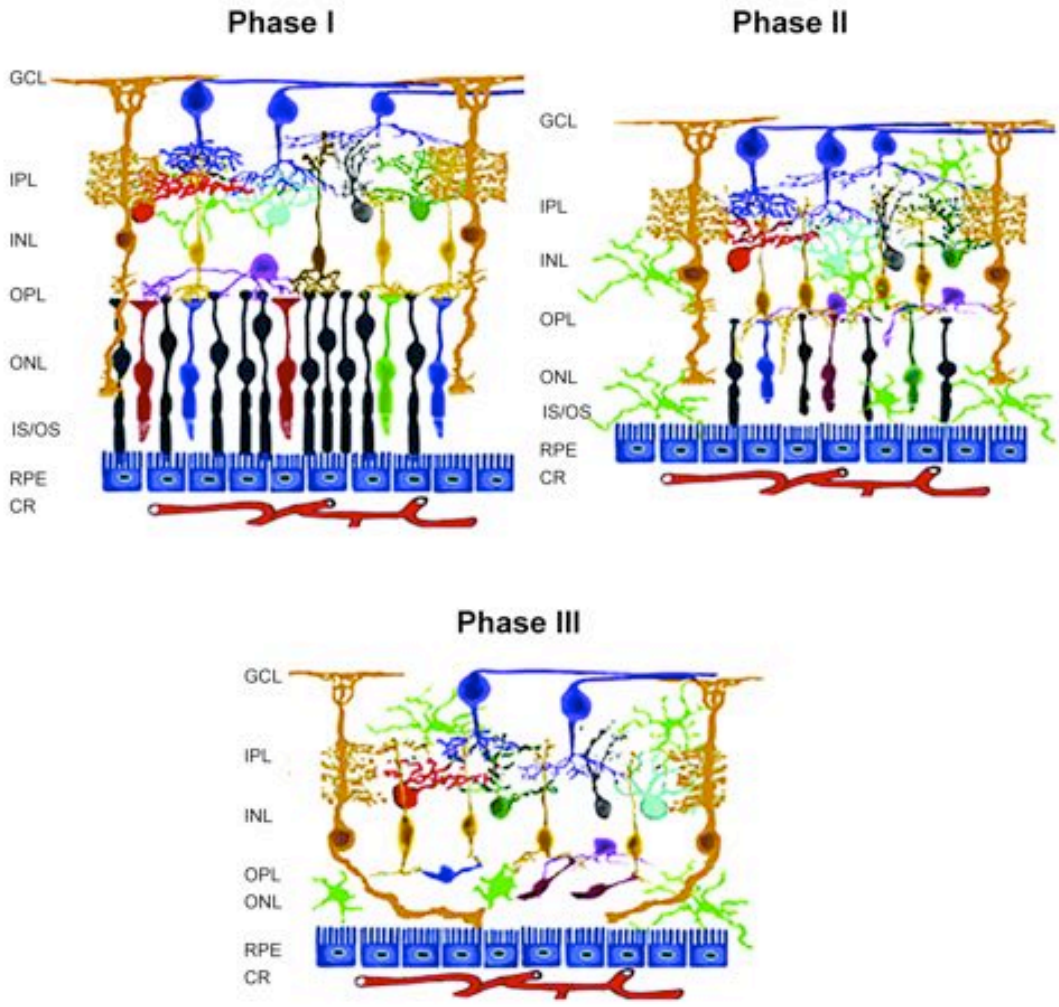

Figure 1.6 Retinal remodelling during degeneration.

Retinal degeneration leads to significant remodelling which can be classified into three different phases. **A)** Phase I is a pre-degeneration phase as indicated by early markers of cellular stress, but with no major changes to retinal morphology or function. **B)** In Phase II photoreceptors start to deteriorate, with glial and RPE cells becoming involved. **C)** Phase III is the ultimate phase where the retina undergoes major organisational alterations including neuritogenesis, cell migration, loss of distinct layer lamination, glial hypertrophy, metabolic changes of neurons and glia cells, synaptic rewiring and many more.

Copyright note: Figures A-C were reprinted by permission from Elsevier: (Cuenca et al., 2014)*, Progress in Retinal and Eye Research.*

1.6.1 Alterations of photoreceptor cells

Pathological insult induces photoreceptor stress leading to a cascade of events that culminates in molecular changes and eventual photoreceptor apoptosis. Two symptoms of photoreceptor malfunction typically occur in stressed rod and cone cells; anomalous delocalisation of visual pigments and anomalous restructuring of photoreceptor axons by sprouting and/or retraction. The period preceding rod death is often associated with a progressive shortening of rod OS and slow changes in the distribution of the Rho pigment (Roof et al., 1994). In healthy retina, Rho is mainly found in the OS of rods with small traces in the IS. In animal models of RP (Fariss et al., 1997; Fernández-Sánchez et al., 2011; Martinez-Navarrete et al., 2011) or in RP human retina (Fariss et al., 2000) Rho was found to relocate to rod photoreceptor cell bodies, axon processes and axon terminals. These changes are accompanied by disorganisation in the OS disc membranes, as reported by Cueneca et al. (Cuenca et al., 2013). In retinal diseases where cones degenerate secondarily to rods, the lack of trophic factors secreted by rods is thought to be responsible for cone deterioration (Léveillard et al., 2004). In this disease scenario, cones start to degenerate similar to rod cells, with prominent changes in the cytosolic macromolecule expression, notably decreased levels of calbindin and arrestin (John et al., 2000). The morphological profile of cone cells also changes, with swelling and shortening of the OS and IS taking place (García-Ayuso and Ortín-Martínez, 2013; Cuenca et al., 2014)The retinal changes associated with photoreceptor stress are also visible at the rod and cone synaptic connectivity. Studies on *rd1* mouse mutant (Fei, 2002) and human RP retina (H et al., 1998; Fariss et al., 2000) showed that in regions where the photoreceptors have significantly degenerated, the remaining rod photoreceptors extend their neurites beyond the INL and towards the IPL. Gupta et al. also observed these axonal extensions into the INL in human 'dry' AMD retina (Gupta et al., 2003). Interestingly, this pathological elongation of cone neurites was reported to be absent from the macula, at least in retinae suffering from LCA (reviewed in (Vugler, 2010)). As retinal degeneration progresses and the number of photoreceptor cells drastically falls, the ONL becomes noticeably thinner (Hippert et al., 2015). As a consequence, synaptic connections become lost and a range of rewiring events in the inner retina starts to take place (Sullivan et al., 2007).

1.6.2 Remodelling of the inner retina and re-wiring of the neuronal networks

Following the death of photoreceptor cells and loss of synaptic contacts with rod and cone terminals, the bipolar cells start to retract their unused dendrites from the OPL, which leads to remodelling of the synaptic connectivity (Cuenca et al., 2005). With the

old synapses disappearing, the functional bipolar cells begin to seek for new input contacts with remaining photoreceptor cells indicating that there is some degree of synaptic plasticity in the adult retina (Strettoi et al., 2003; Barhoum et al., 2008; Martinez-Navarrete et al., 2011). Surprisingly, this bipolar remodelling is not a characteristic common to all retinal degenerations. In the study on the Royal College of Surgeons (RCS) rat model of RP, no new sprouting of the bipolar dendritic processes was observed (Cuenca et al., 2004).

Alterations in the efferent terminals and morphological changes of the amacrine cells also accompany retinal remodelling in disease conditions. In the *rd1* mouse mutant, the synaptic ribbons, the protein structures surrounded by synaptic vesicles (Dowling and Boycott, 1966; Kolb et al., 2001), of the bipolar postsynaptic terminals manifested an abnormal shape similar to that observed in the immature retina (Strettoi et al., 2002). As degeneration progresses, changes to amacrine cell synaptic connections also become more apparent, with some reports showing neuronal sprouting and alterations in the signal propagations towards the GCL (Jones et al., 2012). In the animal model of DR, the loss of dopaminergic and cholinergic amacrine cells has been observed which lead to significant deficits in vision (Gastinger et al., 2006).

1.6.3 Müller glia reactivity and development of the glial scar

In the retina, Müller glia are the first indicators of any alterations to the retinal environment and almost any pathological insult causes their activation. As these glial cells span the entire thickness of the retina, they interact with all retinal cell types across all the layers. The number of physiological functions that Müller glia perform is countless and ranges from the maintenance of structural integrity of the retina to being the light-guiding fibres (reviewed in Bringmann 2006). In a healthy retina, these cells are key modulators of neurotransmitter levels preventing toxic accumulation of glycine, GABA and glutamate in the retina. Alterations in functioning of the neurotransmitter transporters have been found in many different retinopathies including retinal ischemia, diabetes and glaucoma (Naskar et al., 2000; Barnett et al., 2001; Holcombe et al., 2008). Following insult to the retina, these cells undergo activation and change of their function including a reduction of the glutamate transport, which results in the rise of extracellular glutamate to excitotoxic levels and consequent damage to the retinal neurons (Barnett and Pow, 2000). The composition of cytoskeleton of Müller glia also changes including the increase in the density of the IFs (Lu et al., 2011) that is accompanied by the hypertrophy of the glial processes throughout the retina and development of so–call glial scar (Lewis et al., 1989; Lewis and Fisher, 2003). Although, the precise role of gliosis is still to be determined, the extend of it is strictly driven by the size and nature of the neuronal damage, influencing how much cell

replacement is actually needed to fill up the injured space (Ridet et al., 1997; Wilhelmsson, 2008).

1.6.3.1 Upregulation of the intermediate filament proteins and glial hypertrophy

Glial scar is considered to be a hallmark of any CNS damage (Ridet et al., 1997; McGraw et al., 2001; Beattie et al., 2002; Myer et al., 2006). This scar is mainly formed by reactive glial cells that migrate to the site of the injury, where they start to proliferate and increase the complexity of their processes (Panickar and Norenberg, 2005; Pekny and Nilsson, 2005). The final outcome is a tightly packed, hyperfilamentous astrocytic tissue with limited extracellular space that is filled with glial processes high in IFs levels. This glial scar has been reported to have a negative impact not only on the spontaneous neuronal regeneration, but also on the therapeutic interventions including gene therapy (Grüter et al., 2005), cell replacement therapies (reviewed in (Pearson et al., 2014; Hippert et al., 2016) and the ability of implanted retinal grafts to contact the underlying retina (reviewed in (Zhang et al., 2004)).

Under normal conditions, Müller glial cells in a mouse retina maintain high levels of filamentous Vimentin (Kivelä et al., 1986). GFAP is less abundant in Müller cells and is usually restricted to inner end feet terminals and astrocytes (Dreher et al., 1992; Sarthy and Ripps, 2001; Lewis and Fisher, 2003). Following trauma to the retina such as retinal detachment, GFAP undergoes rapid upregulation in Müller glia (Guérin et al., 1990; Fisher and Lewis, 2003). Increased levels of GFAP have also been found after the introduction of retinal ischemia (Kim et al., 1998), hypoxia (Kaur et al., 2007) or experimental glaucoma (Xue et al., 2006). Similar response and upregulation of IFs were reported in astrocytes that invade the lesion site elsewhere in CNS (Petito et al., 1990; Schmidt-Kastner et al., 1990; Panickar and Norenberg, 2005). Several researchers claimed that this pronounced increase in IF proteins has several physiological and pathological functions in the modulation of the CNS damage. The Eng group (1998) was one of the first that created a transgenic mouse model that carried a full copy of a human GFAP gene. They have shown that GFAP overexpression prompted glial hypertrophy in the uninjured CNS which was also more severe and complex than that observed in normal wild-types (Eng et al., 1998). Studies on the knockout animals reported that following retinal detachment the absence of IFs results in fewer morphological alterations in the Müller cells with a marked decrease in the extend of reactive gliosis (Kinouchi et al., 2003; Lundkvist et al., 2004), suggesting that IFs play an important role in glial hypertrophy.

In a healthy retina, Müller cells are much softer than any other retinal cell type (Lu et al., 2006). This biomechanical property of the glial cells allows the retina to adapt to physical forces, such as traumatic injury or raised intraocular pressure. Following

retinal degeneration, Müller cells undergo structural changes, which make them much stiffer (Lundkvist et al., 2004). This increase in stiffness is a major factor that contributes to viscoelastic properties of the glial cells and is coupled with a remodelling of the glial network associated with changes in the retinal architecture, such as folding and shrinkage (Lu et al., 2011). Although the exact purpose of this rigidness still remains unknown, it is believed that stiffer glial cells help to stabilise the delicate retinal architecture after loss of photoreceptor cells. Moreover, Lundkvist et al. suggested that more rigid Müller cells may modulate neovascularisation with new blood vessels growing towards the vitreous rather than within retinal tissue (Lundkvist et al., 2004). Interestingly, this increase in stiffness is thought to be associated with the upregulation of IF proteins such as Nestin, Vimentin and GFAP (Lu et al., 2011) that also contribute to glial associated hypertrophy and formation of a glial scar at the edges of the neuroretina (Figure 1.7) (Lewis and Fisher, 2000).

1.6.3.2 Müller glia activation and neuronal regeneration

For many years, researchers have debated the role of Müller glia in the diseased retina, with both cytoprotective and cytotoxic roles being proposed. For example, Pease *at al.* study showed that in the animal model of glaucoma, these glial cells are invaluable producers of neurotrophic factors such as ciliary neurotrophic factor (CNTF), which has been shown to have potent neuroprotective effects on neuronal cells (Pease et al., 2009). On the other hand, Müller glia have an intimate relationship with cells from the immune system (reviewed in (Cuenca et al., 2014)). Molecules from inflammatory cells, platelets, and plasma may activate Müller cells, and these cells may express a wide variety of inflammation- and immune-response-related factors and enzymes such as Tumor necrosis factor α (TNF-α), Interleukins (IL), interferon, and Intercellular Adhesion Molecule 1 (ICAM-1) (Bringmann et al., 2009a). Müller cells were found to be propagators of neuronal cell death through their interactions with microglia and the synthesis and secretion of TNF-α (Lebrun-Julien et al., 2009). Wang et al. demonstrated that the cytokinesis released by reactive Müller glia lead to activation of the resident immune cells and their migration within the retina (Wang et al., 2011). In the healthy retina, microglia are located almost exclusively in the inner retinal layers up to the OPL. However, under the injured or diseased circumstances, microglial cells become activated and start to migrate in a radial direction across retinal lamina. Wang et al. suggested that Müller glia ease the migration of activated microglia cells by providing an adhesive cellular scaffold that guides the movement of microglia across various retinal layers (Wang et al., 2011).

In the studies on retinal detachment, the upregulation of IFs in Müller glia and the formation of a glial scar at the outer edge of the neuroretina was reported to impede tissue regeneration such as outgrowth of photoreceptor OS (Fisher and Lewis, 2003). It

has been demonstrated that a single Müller cell process lying between the reattached neuroretina and the RPE is sufficient to completely inhibit OS regeneration in that region (Anderson et al., 1986). Interestingly, there appears to be a special relationship between the formation of the glial scar and cone photoreceptors. Lewis and Fisher observed that if a Müller cell process grows beyond the OLM into the segment region that process inevitably occurs adjacent to a cone (Lewis and Fisher, 2000).

Müller cells mediated gliosis was also implicated in the failure of therapeutic intervention including cell transplants. Young *et al.* reported that hippocampus-derived neuronal progenitors integrate poorly in the adult retina of dystrophic rats, in comparison with a neonatal or mature animals (Young, 2000). Additionally, it has been found that reactive gliosis exacerbated the progression of some retinopathies including those observed in diabetes (Amin et al., 1997). Studies with transgenic animals lacking both GFAP and Vimentin in Müller cells have found that these animals create a more permissive environment for the grafted cells as demonstrated by better integration and differentiation of transplanted cells as well as a higher neurite outgrowth than in wild-type recipients (Kinouchi et al., 2003). Interestingly, when either GFAP or Vimentin alone was suppressed the migratory capacity of the transplanted cells was reduced (Kinouchi et al., 2003). The formation of glial scars was also implicated in the failure of visual recovery after subretinal implantation of microphotodiode arrays (Pardue et al., 2001) indicating that the scar tissue acts as a barrier between the implant and retinal neurons. Further support for the negative role of the IF proteins comes from the studies with viral vectors. Calame et al. study reported that the lentiviral cell transduction was affected by the extent of the reactive gliosis, showing that retinal environment may modify the tropism of the viral vectors (Calame et al., 2011). Moreover, glial hypertrophy and extension of Müller cell processes are also believed to support the immunological response to injury (Wang et al., 2011).

Although it is widely believed that the glial scar is a hindrance to retinal regeneration, some studies have shown a useful role of the glial scar during the acute phase of retinopathy. Glial hypertrophy is thought to help maintain the structural integrity of the retina by filling the space where photoreceptors die. Lee et al. found that glial processes of reactive Müller glia take part in the formation of “rings”, which contribute to the survival of remaining cone photoreceptors by releasing tropic factors (Lee et al., 2011). Additionally, the IFs upregulation could potentially have a beneficial role for the therapeutic outcome such as cell transplantation. In regions with increased levels of GFAP, the number of survived transplanted stem cells was found to be significantly higher in comparison with control, undamaged retinae (Nishida et al., 2000). These findings have led to a hypothesis that changes in the properties of Müller glia

cytoskeleton after injury may play a beneficial role in the migration and integration of transplanted cells.

1.6.4 Changes in the composition of the extracellular environment

The ECM is a complex network of scaffolding molecules that plays an important role in cell signalling, migration and tissue structure. Following a pathological insult, the composition of this matrix adapts to retinal needs, which results in the expression of both growth-inhibitory and growth-stimulatory factors (Jones and Marc, 2005).

Proteoglycans (PGs) are major components of the ECM in the CNS and consist of a protein core with one or more glycosaminoglycan (GAG) chains attached. GAGs are classified into four families: heparan sulphate (HS), chondroitin sulphate (CS), dermatan sulphate (DS) and keratan sulphate (KS). PGs are commonly classified according to their associated GAG chains (e.g. CSPGs) and also by the core protein properties. Neurocan, Versican, Brevican and Aggrecan, also called hyalectans, are the main PG core proteins found in the CNS.

During development, proteoglycans contribute to guidance of neurons and axonal pathfinding. After maturation of the CNS, CSPGs become concentrated in the perineuronal nets where they help to maintain the CNS structural organization (Carulli et al., 2005; Tsang et al., 2009). It has been hypothesized that these CSPGs -enriched perineuronal nets may be responsible for the loss of synaptic plasticity of the neuronal cells (reviewed in (Fawcett, 2009)). Following the CNS injury, these proteins are markedly upregulated in the reactive astrocytes within the glial scar which makes them one of the major contributors to a formation of barrier for regenerating neurons (Bradbury et al., 2002; Faulkner, 2004; Silver and Miller, 2004). Numerous studies found that CSPGs inhibit growth of sprouting axons, restrict plasticity and cause growth cone collapse both *in vitro* and *in vivo*. It has been shown that CSPGs inhibit binding of adhesive matrix molecules, such as laminin, to their transmembrane receptors which results in a blockage of their normal growth promoting function (Muir et al., 1989; Zhou, 2006). Therefore, it is believed that inhibition of CSPGs at the site of the insult could become an effective strategy for the CNS regeneration.

In the eye, CSPGs predominate in the neural retina, while HSPGs are expressed throughout the basement membranes (Inatani and Tanihara, 2002). As CSPGs interact with many different ECM proteins and growth factors, it makes them key players in a range of cellular and signalling processes. For example, during eye development, both CSPGs and HSPGs help to guide navigating axons (Ichijo, 2004). During pathological condition, CSPGs deposition changes within the ECM, as the neuronal structures start to remodel (Friedlander et al., 1994; Gilbert et al., 2005; Crespo et al., 2007). Currently,

our understanding of PG function in the diseased retina is very limited. As described in Chapter 3, a recently conducted extensive assessment of different models of retinal degenerations showed disease specific changes in the CSPGs expression (Hippert et al., 2015), which had previously been reported to correlate with good or poor outcomes following photoreceptor transplantation (Barber et al., 2013). Clinically, PGs have been implicated in the pathological deposits associated with AMD due to less efficient binding of the disease associated 402H variant of complement factor H to sulphated PGs in Bruch's membrane (Clark et al., 2010a; 2010b). In animal study, Chen *et al*. reported a marked increase in the levels of Aggrecan in the IPM in two rat models of retinal dystrophy (Chen et al., 2012a). In a recent study by the Cepko's lab, microarray analysis of individual Müller glial cells revealed CSPG5 (Neuroglycan) to be significantly upregulated in a mouse model of RP in comparison to wild-type controls (Roesch et al., 2012). Alterations in Neurocan expression have also been found to be associated with pathological insult to the retina (Inatani et al., 2000) and animal models of RP (Tucker et al., 2011). This increase in the CSPGs deposition may have detrimental impact on the elongation of neuronal processes, as demonstrated by Inatani *et al.* where the outgrowth of rat RGCs was inhibited on Neurocan-coated plates (Inatani et al., 2001). Moreover, they found that this inhibition persists even after removal of CS sugar chains from the core protein suggesting that the Neurocan protein itself is inhibitory. In a study by Li *et al.* β1-integrin mediated adhesion was impeded in the presence of Neurocan, which may stop the neurite outgrowth from retinal neuronal cells (Li et al., 2000). In studies of cell-based therapies, it has been reported that the upregulation of CSPGs in the diseased retina prevents the migration and integration of transplanted donor cells (Suzuki et al., 2007; Singhal et al., 2008; West et al., 2009; Ma et al., 2011; Barber et al., 2013). Moreover, therapeutic approaches such as cell transplants may also be impaired by the presence of specific CSPGs, as the increase of these molecules in the subretinal space may act as an inhibitory cue for the migration of the transplanted rod precursor cells towards the ONL (Barber et al., 2013). Indeed, treatment with chondroitinase ABC (ChABC) enzyme, which digests sugar chains from the core protein, increased the number of integrated cells in the mouse model of RP following transplantation of *Nrl* rod precursor cells (Barber et al., 2013).

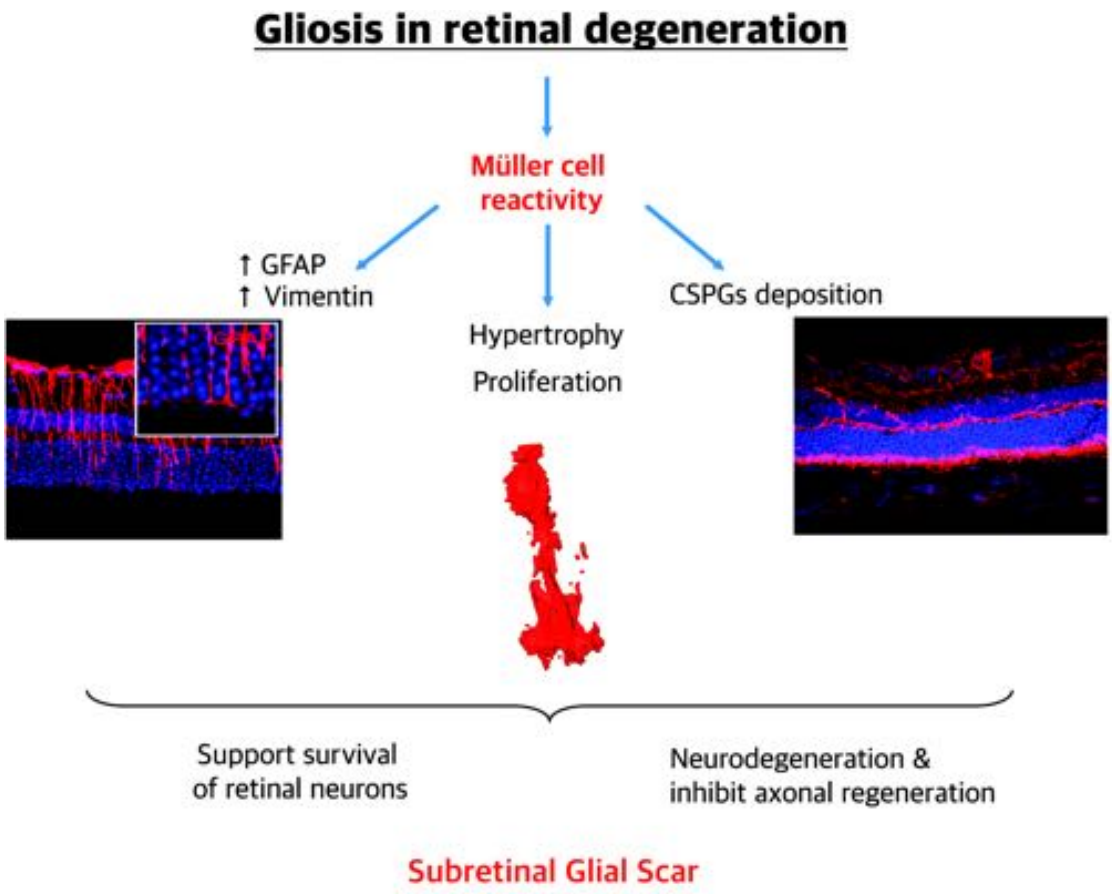

Figure 1.7 Gliosis in a retinal degeneration.

Retinal degeneration leads to significant changes in the retinal environment including development of gliosis. The retinal gliosis is associated with an increase in intermediate filament proteins, proliferation of Müller glia and hypertrophy of their processes, and upregulation of inhibitory ECM molecules such as CSPGs.

1.6.5 Remodelling of the outer limiting membrane

The OLM acts as a semipermeable diffusion barrier for extracellular components (Bunt-Milam et al., 1985). This could be of particular importance in diseased conditions as loss of photoreceptors leads to extend remodelling of the retinal structure including the OLM (Chen and Ma, 2007; Daniele et al., 2007; Stuck et al., 2012; Hippert et al., 2015). Hippert et al. reported that the OLM, which comprises of a number of adherens junctions, seems to be compromised in many models of retinal degenerations (Hippert et al., 2015). The *Nrl*$^{-/-}$ mouse mutant that shows an extensive disruptions to the OLM continuity, manifests aberrant photoreceptor packing, abnormal association between photoreceptors and RPE, retinal detachment, changed dendritic fields, vascular leakage, and ganglion cell death (Mears et al., 2001; DeAngelis et al., 2002). Loss of CRB1 protein was reported to lead to displaced photoreceptors and focal degeneration of all neural layers (Mehalow et al., 2003; van de Pavert et al., 2004). In humans, mutations in *CRB1* gene have been associated with a variety of autosomal recessive retinal dystrophies, including LCA, RP type 12, RP with Coats-like exudative vasculopathy and other early-onset forms of RP (Bujakowska et al., 2011; Pellissier et al., 2014; Zhao et al., 2015). Recently, mutations in CRB1 were also linked to development of the vascular leakage similar to that observed in MacTel2 patients (Zhao et al., 2015).

It is tempting to speculate that the disruption of the OLM could exacerbate the spread of retinal degeneration, as OLM integrity is critical for cell survival. The OLM has also been shown to act as a modulator of the size of the apical villi of Müller cells. It is also possible that loss of the OLM proteins results in a decrease in the strength of the adherens junctions and subsequent susceptibility to retinal detachment. Although the retina makes some successful attempts to restore the lost connections by forming new junctions between the remaining cells (Hippert et al., 2015), these junctions may not have the same properties as the ones in a normal retina as there are differences in the expression of the junctional proteins between different cell types. Omri *et al.* reported that in a rat animal model of diabetic retinopathy in which the number of S-cone photoreceptors decreases, the expression of Occludin and aPKC was found to be downregulated (Omri et al., 2013). Recently, the importance of the OLM continuity has been implicated in the clinics. Mitamura et al. reported that patients with a continuous OLM have a better visual acuity than those in which OLM is disrupted making them more prone to increased vascular leakage upon mechanical stress (Mitamura et al., 2013). Thus, the OLM appears to be an important element of retinal health and additional studies on OLM remodelling in degenerative disease could provide some invaluable insights on the pathological environment before therapeutic interventions.

1.6.6 Additional changes to the degenerative retina

Due to their function, photoreceptors are constantly exposed to light photons and they are the primary consumers of oxygen in the CNS. These two factors put rod and cone cells at a high risk of the damage due to reactive oxygen species (ROS) (Stone et al., 2008; Fernández-Sánchez et al., 2011). For example, the oxidative stress in the RPE leads to development of photoreceptor degeneration associated with AMD condition (Ardeljan and Chan, 2013). In the DR, high levels of glucose increase the metabolic rate of photoreceptors and as a consequence production of ROS (Du et al., 2003; Kowluru and Kanwar, 2007). El-Bab *et al.* demonstrated that the expression of several antioxidants in the DR retina is significantly reduced in comparison to healthy retina, resulting in even higher accumulation of ROS (El-Bab et al., 2013). As ganglion cells are highly susceptible to any changes in the concentration of ROS, this increase could induce ganglion cell apoptotic death in this pathological condition (Chrysostomou et al., 2013; Himori et al., 2013).

One of the hallmarks of retinal degeneration is the alteration in retinal protein expression. Studies on human post-mortem eyes, showed that AMD leads to region-specific changes in retinal protein levels with the majority of observed changes being restricted to macula and the periphery (Ethen et al., 2006). Recent research findings showed that following the pathological insult several cell cycle components in photoreceptors become reactivated. For example, in a dog model of early retinal degeneration caused by a mutation in *STK38L* gene encoding the cell cycle regulator, Berta *et al.* reported photoreceptors starting to express markers of the cell cycle (Berta et al., 2011). Immunohistochemistry of the canine retina showed PCNA and phosphor-PH-3 positive cells in the ONL, which was further confirmed by the RT-PCR analysis. Further studies of rodent models of RP, demonstrated that the levels of cyclin dependant kinases (CDK) are 4-5 times higher during neuronal apoptosis in comparison to healthy retina, indicating at Bmi1 as a key regulator of cell cycle proteins (Zencak et al., 2013).

1.7 Current therapeutic strategies

Advances in gene discovery and stem cell research have presented new opportunities for potential therapeutic interventions for many diseased conditions. The eye represents an ideal organ for testing the safety and efficiency of any of these novel treatments due to its accessibility, relative immune privilege, small size, compartmentalization, and the existence of a contralateral control (Figure 1.8). Here, a summary of some of the current therapeutic approaches to treat retinal degeneration

will be presented, with a particular focus on the treatments that are already in clinical trials or show the most promising potential for clinical application in the near future.

1.7.1 Drug therapy

Potential molecular targets for drug therapy are being identified for different retinal disorders. One of the main therapeutic strategies used to treat retinal degeneration associated with neovascularisation including DR and 'wet' form of AMD is anti-VEGF treatment. Vascular endothelial growth factor (VEGF) is a proangiogenic factor, which stimulates growth of (leaky) blood vessels in the eye leading to so-called vascular leakage (Adamis et al., 1995; Kvanta et al., 1996). Anti-VEGF drugs injected into the eye of a patient block VEGF protein, which in many cases leads to a very significant reduction in the formation of new blood vessels and can even reverse retinal damage such as edema, with many patients seeing an improvement in visual acuity (reviewed in (Ferrara and Adamis, 2016)). Unfortunately, despite its efficacy, targeting VEGF in the eye has presented several challenges, including the optimal route of administration, and the ocular and systemic safety of the anti-VEGF treatment, as patients require repeated intravitreal injections. VEGF mediates many signalling pathways and the retina needs it for normal functioning (Saint-Geniez et al., 2008; 2009); therefore blocking it completely may lead to secondary pathological events. Recent preclinical studies in mice have pointed towards a promising alternative to current anti-VEGF treatment. Westenskow *et al.* reported that inhibition of a specific signalling pathway, the Ras GTPase, which functions downstream of VEGF, by delivery of a chemically engineered oligonucleotide α-miR-132, can successfully prevent angiogenic sprouting (Westenskow et al., 2013). Importantly, however, approximately 40% of patients do not respond to VEGF treatment, suggesting that the pathological mechanisms responsible for neovascularisation may differ between different clinical presentations of AMD (Brown et al., 2006; Simó and Hernández, 2015; Usuelli and La Rocca, 2015; Holz et al., 2016).

1.7.2 Gene therapy

There are more than 250 gene mutations associated with retinal disorders and gene replacement represents an obvious therapeutic approach. The majority of inherited retinal diseases are caused by mutations in genes that affect photoreceptor function. Although there is currently no cure for RP, well-characterised animal models and a developed understanding of the genetic basis of the disease allow gene therapy to be a potentially viable therapeutic strategy. The first report of successful gene supplementation via the viral vectors was reported in 2000 by Ali *et al.*, who demonstrated rescue of photoreceptor structure and function in the *Prph*$^{rd2/rd2}$ mouse

(Ali et al., 2000). They showed that the injection of adeno-associated virus serotype 2 (AAV2) vector carrying the *Prph2* gene under the control of the Rho promoter targets rod cells, leading to expression of Prph2, increase in photoreceptor survival and rescue of function. However, greater improvements were seen when vector was delivered in early stages of retinal degeneration (Ali et al., 2000), than when injected in older mice (Sarra et al., 2001). These results illustrate a limitation of the gene supplementation approach, as it relies on sufficient numbers of endogenous cells being present at the time of treatment. This can be difficult since diagnosis is often not made until the patient has lost a significant proportion of their photoreceptors.

Gene supplementation/augmentation therapy was also tested to treat murine and canine models of achromatopsia. Alexander *et al.* used an AAV5 vector to deliver a wild-type version of *Gnat2* gene under the human M-opsin promoter into the retina of *Gnat2*^{cpfl3} mutant (Alexander et al., 2007). In 2010, a naturally occurring mutation in *CNGA3* gene was discovered in improved Awassi sheep (Reicher et al., 2010), providing an excellent large animal model for studying the human phenotype. Later Banin *et al.* used this model to test the efficacy of AAV5 vector carrying either the mouse or the human wild-type version of *CNGA3* gene under the control of the red/green opsin promoter (Banin et al., 2015). They reported a robust expression of *CNGA3* gene and significant improvements in the visual function in the treated *CNGA3*-mutant sheep in comparison to untreated animals.

The first gene to be targeted clinically was the *RPE65* gene mutations, which are associated with LCA. As mentioned previously, the enzyme encoded by *RPE65* is crucial for converting *all-trans* retinoid to *11-cis* retinal during visual pigment regeneration (Moiseyev et al., 2005) and without a functioning enzyme, the photoreceptors gradually deteriorate. The researchers hoped to halt this process by using a virus to shuttle a functional *RPE65* gene into the eye. First results published in 2001 described a successful attempt to use a recombinant (r)AAV2 to treat naturally occurring *Rpe65*$^{-/-}$ mutant in Briard dogs (Acland et al., 2001). Acland *et al.* reported that treatment with AAV2 vector carrying a wild-type canine *Rpe65* gene, under the control of the hybrid cytomegalovirus/chicken β-actin (CBA) promoter, led to substantial improvements in visual function. Further studies on a naturally occurring murine model of *Rpe65* LCA, the *rd12* mouse (Pang et al., 2005), confirmed the potential and efficiency of AAV use in treatment of LCA (Pang et al., 2006), which allowed for the first studies on human patients (Bainbridge et al., 2008; Maguire et al., 2008; Testa et al., 2013). Currently, there are a number of clinical trials, in different countries and at different phases, related to correcting the *RPE65* mutation. These differ in surgical protocols, DNA promoter types, vector preparation and volumes or patient characteristics. A phase I safety profile trial of rAAV2 carrying human (h) RPE65 is

currently underway in the United States with five cohorts of LCA patients which aims to test the safety of uniocular subretinal administration of rAAV2-CBSB-hRPE65 vector (Clinicaltrials. gov Identifier NCT00481546). The most advanced clinical trial focused on the retinal diseases was recently completed in the United States. In October 2015, Spark Therapeutics published the phase III results of the SPK-RPE65 gene replacement therapy showing that patients who received a viral treatment navigated significantly better in different lighting conditions than individuals from the untreated group (http://ir.sparktx.com/phoenix.zhtml?c=253900&p=irol-newsArticle&ID=2093863. Accessed February 20, 2016). This is the first to date gene therapy study conducted in humans that has reported a therapeutic benefit to patients.

As previously mentioned, formation of new blood vessels is mainly controlled via angiogenic factor VEGF, which can be clinically treated with the anti-VEGF agents. Numerous reports showed that ocular neovascularization can be inhibited after subretinal injection of AAV2 vector carrying the sequence for the expression of a soluble portion of the R1 VEGF receptor, sFlt1 (Lai et al., 2005; 2011). SFlt1 normally binds extracellular VEGF protein, which prevents it from binding to its cell surface vascular endothelial receptors FLT-1 and FLK. These data indicate that subretinal injection of AAV2.sFlt-1 vector can be a promising therapeutic strategy for the long-term treatment of neovascular diseases of the eye.

There is no doubt that gene therapy offers an attractive approach for treatment of a number of inherited retinal diseases. The evolution of gene editing technologies, such as the CRISPR/Cas9 system, will certainly allow for targeting a wider spectrum of retinopathies. However, one of the main issues with the use of gene therapy is a lack of genetic diagnosis in patients suffering from inherited vision loss, which is crucial in designing treatments based on use of the viral vectors.

1.7.3 Cell-based replacement therapy

An important feature in both animal models of many retinal diseases is the death of rod and cone cells. Interestingly, despite this progressive photoreceptor degeneration much of the inner retinal neuronal architecture, including the visual pathways and GCL remain largely intact (Mazzoni et al., 2008; Damiani et al., 2012). As mentioned previously, gene therapy relies on there being sufficient numbers of endogenous photoreceptor cells present at the time of treatment; restoring vision in cases of severe and/or very rapid degeneration, therefore, may only be possible by either replacing the missing sensory cells, or by providing visual information to the remaining neurons of the retina. In recent years, considerable progress has been made concerning the prospects for cell transplantation as a potential treatment for retinal degenerations. Considerable effort has been made in order to find the best method to replace lost

photoreceptor and RPE cells, including transplantation of whole retinal sheets, microaggregates of foetal neural retina and suspensions of stem cells and progenitor cells (reviewed in (da Cruz et al., 2007; Pearson, 2014; Pearson et al., 2014)). While there have been some reports of success in preserving visual function using these strategies (Radtke et al., 1999; 2008), there is still only limited evidence to suggest that these transplants can both integrate within and make functional connections to the host tissue (Gouras et al., 1994; Gouras and Tanabe, 2003; Seiler and Aramant, 2012).

In recent years, a number of different research groups have examined the transplantation potential of progenitor cells derived from immature retinae, which can differentiate into retinal neurons (Yang et al., 2002; Qiu et al., 2005; MacLaren et al., 2006). Sakaguchi, Young *et al.* demonstrated that transplantation was more effective when transplanting cells into immature recipients. They showed that cultured murine neural progenitor cells transplanted into the eyes of neonatal Brazilian Opossums, successfully migrated into the recipient retina following cell transplant, but instead of integrating within the ONL, transplanted cells were only found within the inner retina (Sakaguchi et al., 2004; 2005). Later studies showed that rod cell transplants into the adult mouse retina are achievable, but they rely on donor cells being isolated from a particular stage in their development, when rod photoreceptors are immature (Kwan et al., 1999; MacLaren et al., 2006; Bartsch et al., 2008; Pearson et al., 2012). Kwan *et al.* reported that retinal progenitor cells isolated from postnatal day 7 - 9 animals and transplanted subretinally into adult *rd1* mice were not only able to survive within the recipient retina but were also capable to extend their processes towards the outer nuclear layer (Kwan et al., 1999). In 2006, Ali and colleagues, used *Nrl* marked postmitotic rod cells (Akimoto et al., 2006; Eiraku et al., 2011) to transplant them into the adult retina (MacLaren et al., 2006). Their study showed that subretinal transplantation of post-mitotic receptor precursor cells led to the presence of reporter-labelled cells within the host retina that bore all the hallmarks of mature photoreceptors. Further research with the use of photoreceptor precursor cells confirmed these results (Bartsch et al., 2008; Lakowski et al., 2010; Eberle et al., 2012; Barber et al., 2013) and even showed that these cells were capable of responding to light stimulus when transplanted into a mouse model of stationary night blindness (Pearson et al., 2012). Although these results provide a proof of concept for cell replacement, a better source of donor cells for human application is needed. Advances in recent years in the use of embryonic stem cells (ESCs) and induced pluripotential stem cells (iPSCs) provide a promising stem cell source for the use in human trials. The ground-breaking 3*D* culture systems developed by Sasai and colleagues enabled to generate from ES cells the isolated optic cups with a continuous epithelial structures showing clear laminar stratification similar to the early postnatal retina (Eiraku et al.,

2011; Eiraku and Sasai, 2012). Further studies used this 3*D* system to develop rod precursor cells for cell transplantation that morphologically resembled normal photoreceptor cells of a mouse retina (Gonzalez-Cordero et al., 2013). With the development of methods to produce laminated retinal structures *in vitro*, an attempt to develop and transplant whole retinal sheets has been made by Takahashi's group. Their study showed that transplanted retinal sheets into the subretinal space of 6-8-week-old *rd1* mice can integrate and differentiate into laminated, mature retinal structure (Assawachananont et al., 2014). A variety of retinal differentiation protocols for mouse and human iPSCs has also been described (reviewed in (Jayakody et al., 2015)) and, after less than a decade from the first developed iPSCs protocol (Hirami et al., 2009) and further improvements of cell differentiation, the first transplants with human iPSCs are already on the way (Zhong et al., 2014). Moreover, patient-specific iPSCs are being developed for autologous cell transplantation and as a tool for modelling specific retinal diseases, testing gene therapies, and drug screening.

Because normal RPE physiology needs a polarized monolayer of tight junctions, post-cell suspension transplantation of the monolayer formation is the most important part for successful transplantation. Current research uses biodegradable substrates as retinal scaffolds to growth a polarized monolayered RPE (Lu et al., 2001; Kamao et al., 2014; Yao et al., 2015). After the monolayer is formed, the scaffold can be dissolved and the whole sheets can be used in RPE cell transplants. The first trials of hES-derived RPE cell transplants into patients with Stargardt disease are underway in the US and the UK (Schwartz et al., 2012). If shown to be safe, such studies set the stage for future clinical trials of ES-derived donor cells.

Studies of developing and injured retinae have shown that there are cells within the adult retina that possess neurogenic potential; thus opening new avenues for regenerative medicine. The retinal stem cell niche in the peripheral region, the ciliary marginal zone (CMZ) (Perron and Harris, 2000), has been extensively studied regarding its proliferation properties and signalling pathways (Johns, 1977; Wehman et al., 2005; Agathocleous and Harris, 2009); however, it was not until 2011 when the evidence for genuine stem cells in the CMZ was reported (Centanin et al., 2011). By using a chimeric approach with *Wimbledon*, a permanent and ubiquitously EGFP-expressing fish, Centanin *et al.* demonstrated that postembryonic cells in the CMZ are multipotent and can generate all cell types of the differentiated neural retina including neurons and glia. The other endogenous retinal cells with proliferating properties found in fish are the Müller glia, which are distributed all along the differentiated retina and were shown to be capable of generating different retinal cell types upon pathological insult (Johns and Fernald, 1981; Bernardos et al., 2007; Fimbel et al., 2007; Ramachandran et al., 2010). In the mammalian retina, the progenitor-like profile of

Müller glia was also described with Müller glia cells showing a significant transcriptome overlap with retinal progenitor cells (Blackshaw et al., 2004; Roesch et al., 2008; 2012). Since then, the identification of factors that could be used to recruit Müller cells and stimulate their regenerative potential is a subject of intense research. In 2004, Ooto *et al.* reported that in response to NMDA-induced excitotoxic retinal damage, Müller glia cells re-enter the cell cycle, de-differentiate and generate new bipolar and rod photoreceptor cells (Ooto et al., 2004). Further evidence coming from the *in vitro* studies revealed that rodent and human Müller cells are capable of producing both glial cells and neurons (Das et al., 2006; Lawrence et al., 2007; Zhao et al., 2014). In the study by Giannalli *et al.,* human Müller glial cells were found to differentiate toward rods four to six times faster than normal stem cells *in vitro* (Giannelli et al., 2011). Interestingly, when transplanted into a rat retina that lacks photoreceptor or ganglion cells, these Müller cell-derived neurons are able to migrate and integrate into the appropriate retinal layer (Singhal et al., 2012; Jayaram et al., 2014). These studies provide evidence that Müller cells could be a source of retinal neuronal cells within the adult mammalian retina used for treatment of retinopathies.

Until very recently, the primary method to treat cataract was an extraction of the damaged lens and replace it with an artificial intraocular lens (http://www.nhs.uk/Conditions/Cataract-surgery/Pages/Introduction.aspx). Two recent studies, published in 2016, demonstrated that there is an alternative to cataract surgery using the novel stem cells approach. Lin *et al.* study showed that in rabbits and macaques, as well as in human infants with cataracts, it is possible to remove the damaged parts of the lens without damaging the endogenous pool of lens epithelial stem cells, in order to promote lens regeneration (Lin et al., 2016). In the second study, Nishida's lab developed a protocol for *in vitro* generation of a self-formed ectodermal autonomous multi-zone (SEAM) from human iPS cells (Hayashi et al., 2016). The generated SEAM included distinct cell lineages from the ocular surface ectoderm, lens, neuroretina, and RPE and were shown to form a functional corneal epithelium when transplanted to a rabbit model of blindness. These reports further underlie the enormous potential of the stem cells for tissue regeneration and treatment of many pathological eye conditions.

1.7.4 Retinal prosthesis

Advances in microelectromechanical systems and computer science have allowed researchers to explore new avenues for future treatment options for the patients with a severe vision loss. Retinal prostheses have been designed to restore rudimentary form vision to patients with RP by replacing the function of lost photoreceptor cells through the stimulation of a relatively preserved inner neurosensory retina. The pioneer in this

field was a German Neurosurgeon, Otfrid Foerster, who demonstrated that electrical stimulation of the visual cortex in humans could lead to the perception of light spot (phosphene). Years of research led to the development of so-called bionic eyes, a small retinal implant that can be implanted within the human eye with an external device attached to the human body (reviewed in (Iezzi, 2016)). This bionic eye mimics the original functioning of the human eye by receiving a radio signal, which is then transferred to the brain via the optic nerve. Findings from the first studies in patients showed that following the implantation of a bionic eye, some individuals regain their ability to decipher outlines of objects and people improving patient's social interactions (Ho et al., 2015).

As discussed in this chapter, any of the presented retinopathies leads to different remodelling events within the retina, which involve a variety of cellular and signalling cascades. Therapeutic approaches are available, but none of them is sufficient to stop and/or reverse the detrimental effects of the disease. Based on the recent findings it seems reasonable to suggest that at least in advance stages of retinal degeneration a combined treatment strategy, which first aims at stopping the disease progression and then repairs the damaged tissue will be able to help patients to regain their lost sense of vision.

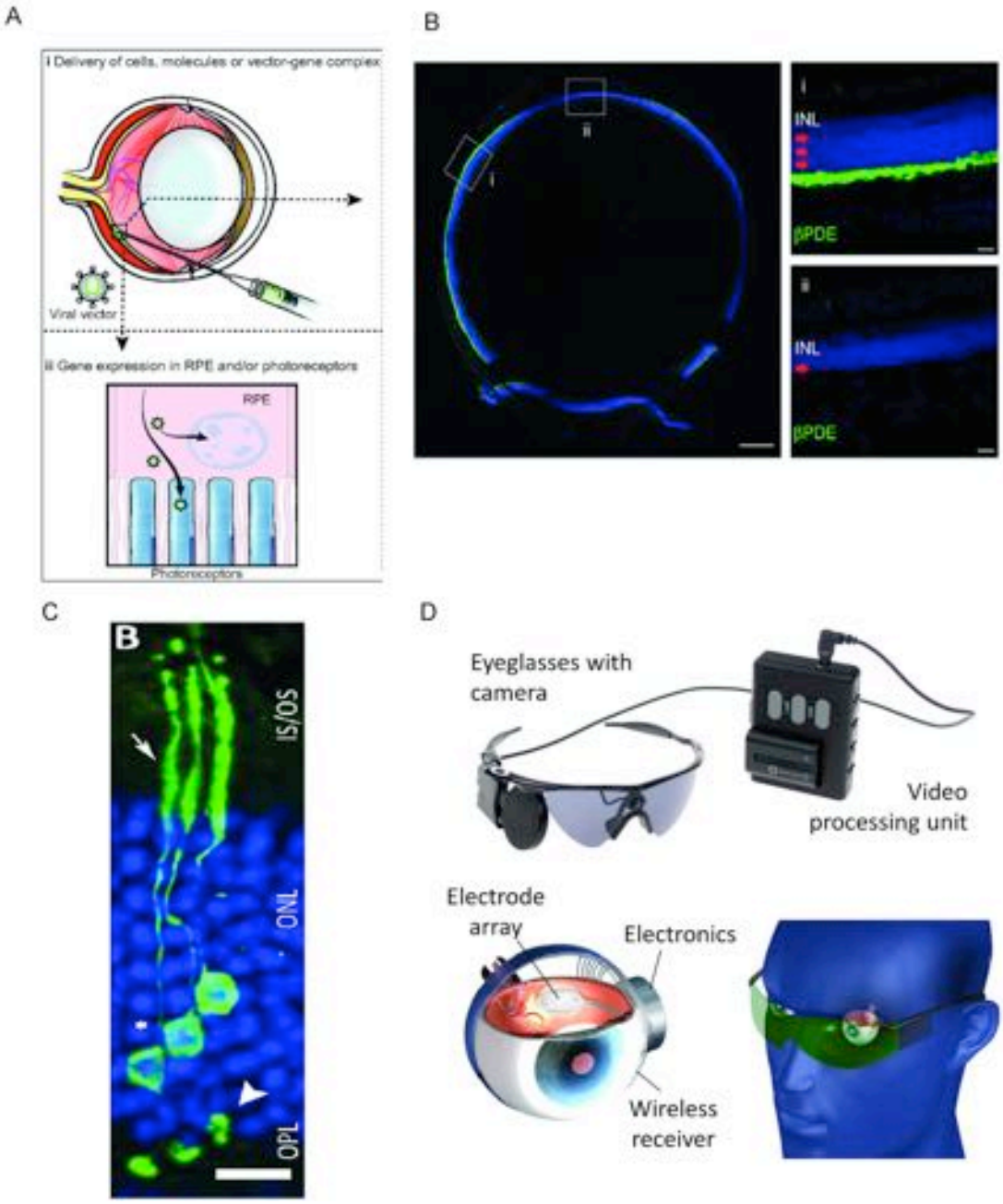

Figure 1.8 Ocular therapies for retinal disease: From drug delivery to retinal implants.

A) The accessibility of the eye and retina allows for delivery of appropriate drugs (e.g. neurotropic factors), gene therapy vectors (viral vectors used for specific gene replacement in recessive disease) and even cells using intravitreal or subretinal injections/ transplantation**. B)** *In vivo* images of the transplanted cells (green) in *rd1* mouse eye. **C)** Delivery of gene therapy vectors into photoreceptors or RPE cells can lead to widespread viral expression in order to facilitate rescue of function and phenotype. **D)** Components of the bionic eye, as designed in the Argus II system.

Copyright note: Figure A was taken from (Veleri et al., 2015)*. Image B was reprinted by permission from Nature Publishing Group:* (Pearson et al., 2012)*, Nature. Image C was reprinted by permission from*

Nature Publishing Group: (Nishiguchi et al., 2015)*, Nature Communications. Figure D was taken from* http://www.secondsight.com/*. Accessed online 20.05.2016.*

1.8 Experimental aims

As described above, different genetic defects can lead to profound structural and environmental remodelling, which can manifest as a unique degenerative phenotype. In turn, these changes may have positive or negative influences on the outcome of therapeutic strategies such as cell transplantation and implant devices. In 2013, Barber *et al.* performed rod - photoreceptor transplantation in different murine models of slow, moderate and fast photoreceptor degeneration (Barber et al., 2013). Their study showed that photoreceptor precursor transplantation is feasible in all examined animals; however, disease type has a significant impact on both the number of reporter-labelled cells and their morphology. Although gliosis is characteristic of many retinal disease models (Ekström et al., 1988; Sheedlo et al., 1995; Fan et al., 1996), no characterization and/or direct comparison between different RP models has been made. Given the apparent complexities of the gliotic process, more precise dissections of the links between glial reactivity and progressive neurodegeneration are needed. Moreover, understanding the processes behind glial scar formation and changes to retinal environment may help us to develop more effective strategies to treat a wide range of retinal dystrophies. This represents a major challenge to the advancement of the ocular therapies. This thesis addresses two main questions:

1) Is the process of retinal remodelling and development of gliosis equivalent across different forms of retinal degeneration?

Studying changes within the recipient microenvironment, especially how the gliotic process differs in different types of retinal degeneration, will help us to understand where, when and how much gliosis is present in a diseased retina at different times in the degenerative process and influence the timing of therapeutic intervention.

- A comprehensive assessment of the expression of IFs and ECM molecules, particularly the CSPGs, was performed in different animal models at early, mid and late time points and the retinae were examined in different regions to account for any local changes within the recipient environment.
- The examination of the OLM adherens junctions was performed in order to assess the extent of the retinal remodelling and any alterations to retinal integrity and permeability under pathological circumstances.

2) How can the glial scar be manipulated using molecular tools in models of retinal degeneration to improve therapeutic outcomes?

The second part of this thesis focused on developing molecular tools that aimed to manipulate or remove some of the potentially inhibitory aspects of retinal remodelling.

- The role of IF proteins in the development of glial scar was studied by suppressing GFAP and Vimentin expression in a model of chronic retinal degeneration.

- The CSPGs represent a large family of proteins and understanding the changes in their expression may be crucial in designing effective therapeutic strategies. In this study, for the first time, the spatio-temporal expression of the CSPG, Aggrecan, and the CSPG receptor LAR were assessed to determine their role in the diseased retina.

CHAPTER 2

Materials and Methods

2.1 Animals

Male and female *C57Bl/6J* (Harlan, UK), *Crb1*$^{rd8/rd8}$ (Mehalow et al., 2003), *Prph2*$^{+/\Delta 307}$ (McNally et al., 2002), *PDEβ6*$^{rd1/rd1}$ (Danciger et al., 1995), *Rho*$^{-/-}$ (Humphries et al., 1997), *Rlbp.*GFP$^{+/+}$ (Vázquez-Chona et al., 2009), *Prph2*$^{rd2/rd2}$ (Kedzierski et al., 1997), *R91W;Nrl*$^{-/-}$ (Samardzija et al., 2014), *Nrl*$^{-/-}$ (Mears et al., 2001) and *Nrl.*GFP$^{+/+}$ mice (Akimoto et al., 2006) were used in this project. All mice were maintained in the animal facility at University College London (UCL). All animal procedures have been performed under the Policies on the Use of Animals and Humans in Neuroscience Research (UK Home Office regulations, Scientific Procedure, Act of 1986). Mice were maintained under standard 12/12 hour light-dark cycle. Eyes were collected for each animal model at different ages specified in each relevant section. *C57Bl/6J* mice were used as wild-type controls.

2.2 Cell dissociation, FAC sorting and cell cultures

2.2.1 Müller glial cell cultures

Primary Müller glial cell cultures were established using an adapted version of previously published protocols (Sarthy, 1985; Hicks and Courtois, 1990; Kljavin and Reh, 1991). Retinae from postnatal (P) day 7-8 mice *Rlbp.*GFP$^{+/+}$ mice (GFP expressed in Müller cells under the control of the RLBP promoter) were dissected in Earle's Balanced Salt Solution (EBSS) (Sigma Aldrich, UK) + Antibiotic-Antimycotic (AA) (ThermoFisher Scientific, UK) and cells were dissociated using a papain-based dissociation kit (Worthington Biochemical, Lorne Laboratories, UK). All the reagents were made up according to manufacturer's instructions. Papain with 0.005% DNase, ovomucoid inhibitor albumin (OMI), DNase and sterile EBSS were preincubated at 37^{o}C. Dissected retinae were added to papain solution (7-8 retinae per 0.5 mL of papain) and incubated for 30 min at 37^{o}C in a humidified 5% CO_2 incubator. After incubation, dissociated retinae were passed through a cell strainer mesh (70 µm) (BD Biosciences, UK), washed with 200 µL of EBSS and spun down for 5 min at 200g. The supernatant was removed and cells were resuspended in 200 µL of papain inhibitor solution (900 µL EBSS with 5% DNase and 10% OMI) and incubated for 10 min in the incubator. After 10 min, cells were layered on the top of 500 µL of OMI in clean 1.5 mL eppendorf tube and spun down for 5 min at 100 G. The supernatant was then removed and 200 µL of resuspension solution (900 µL EBSS with 5% DNase) was added to cells. Live cells were counted using a haemocytometer before the fluorescence-activated cell sorting (FACS). For FACS procedure, cells were resuspended in 2 mL of EBSS medium with 1% Foetal Calf Serum (FCS), kept on ice and either taken to the Institute of Child Health or Institute of Ophthalmology (UCL) (see Section 2.2.2).

Following FACS, cells were resuspended in Dulbecco's Modified Eagle Medium (DMEM) containing 10% FCS and 1% AA and then seeded into eight-well imaging chamber plates (PAA, GE Healthcare, Austria) that were pre-coated with laminin (5 µg/mL, Sigma Aldrich, UK) at a density of 35,000 cells per well and incubated at 37^{o}C in a humidified 5% CO_2 incubator for 2 weeks. Separate *Rlbp.*GFP$^{+/+}$ cell preparations were used for each experimental repeat; therefore, *n* number indicates the number of independent cell preparations used per experiment.

2.2.2 Fluorescence-activated cell sorting (FACS)

FACS was carried out with either Cell Sorter MoFlo XDP (Beckman Coulter, UK) or BD Influx^{TM} (BD Biosciences, UK) fitted with a 200 mW 488 nm blue laser (adjusted to 150 nW) to excite GFP. GFP was collected using the 530/40 nm channel. The sort used sterile PBS and a sample pressure of 60 psi and a sheath pressure of 60.8 psi using a 70 or 100 nm nozzle. Viability of both the original and sorted sample was assessed using DRAQ7 (Biostatus, UK) to label dead and dying cells. GFP^{+} cells (*Rlbp.*GFP$^{+/+}$ and *Nrl.*GFP$^{+/+}$) were separated from the other retinal cells, and collected in 50% EBSS/50% FCS medium. The total number of collected and sorted cells and the efficiency of the sort were noted (Figure 2.1A). A normal non-GFP expressing retina was used as a negative control to set the GFP signal gate (Figure 2.1B). Following the sort, cells were spun down for 20 min at 200 G, the supernatant was removed and the cell pellet was resuspended in 200 µL of resuspension solution (EBSS with 5% DNase). GFP^{+} cells were counted and taken either for primary cell cultures (see Section 2.2.1) or cell transplantation experiments (see Section 2.3.5.2.3)

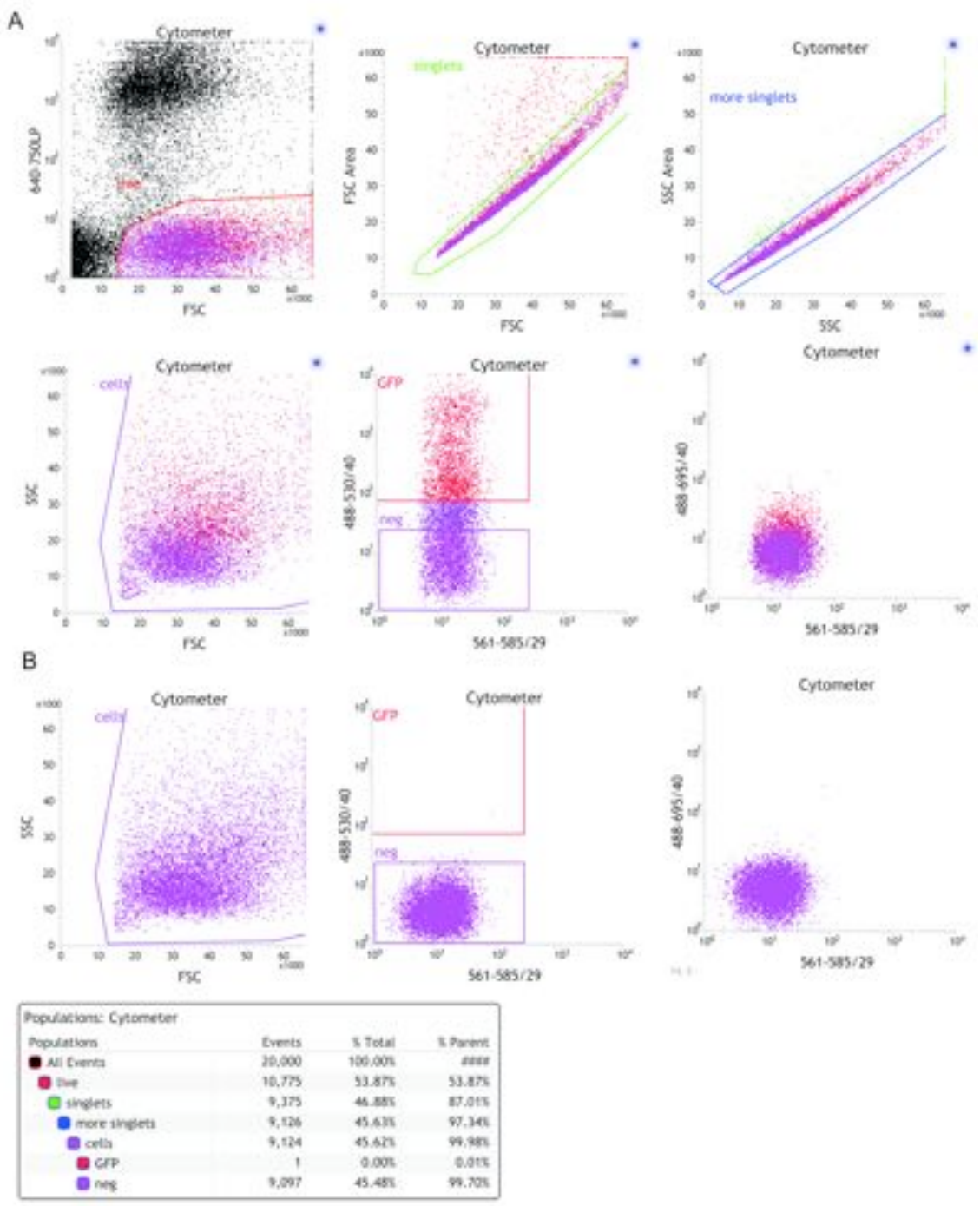

Figure 2.1 FACS analysis.

Representative FACS plots showing **A)** *Rlbp.*GFP$^{+/+}$ cells within the whole populations of retinal cells and **B)** the negative control taken from the retina which does not express GFP that was used to set the GFP^{+ve} signal gate.

2.2.3 Growth of Müller glial cell cultures in presence of a purified CSPG mixture

Two methods were chosen to assess effect of Chondroitin sulphate proteoglycans (CSPGs) on Müller glial cells. In the first experiment, the 8-well plates were coated with 10-20 µg/mL solution of purified CSPGs, a commercially available mixture containing Aggrecan, Neurocan, Phosphacan, and Versican (CC-117, Millipore, UK) at 37^{o}C in a humidified 5% CO_2 incubator for 3 hrs, followed by a rinsing with D-10 medium (Siebert and Osterhout, 2011). The control wells were coated with 5 µg/mL laminin. After FACS, *Rlbp.*GFP$^{+/+}$ cells were seeded at a density of 35,000 cells per well and incubated at 37^{o}C in a humidified 5% CO_2 incubator for 2 weeks. In the second experiment, *Rlbp.*GFP$^{+/+}$ cells were grown on 5 µg/mL laminin coated plates for 2 weeks at 37^{o}C in a humidified 5% CO_2 incubator and pre-assessed under a white-light microscope before the addition of CSPGs mix. Two concentrations were used of 50-100-µg/mL and added to cultures at intervals of 2 days for 1 week to account for any intrinsic degradation mechanisms. Cells were assessed for morphological changes 1 week post-treatment with immunocytochemistry (ICC) analysis.

To assess the effect of CSPGs on *Nrl.*GFP$^{+/+}$ cells neurite outgrowth, after first day of CSPGs treatment, FACS isolated *Nrl.*GFP$^{+/+}$ cells were added to *Rlbp.*GFP$^{+/+}$ cell cultures at a density of 10,000 cells per well and left in culture for 4 days. The cells were fixed with 4% paraformaldehyde (PFA) at 4 °C for 30 min before immunocytochemistry. The neurite number was counted per each cell and expressed as an average per experimental condition; therefore, *n* number indicates the number of independent cultures used.

2.3 Molecular Biology

2.3.1 Bacterial cloning and plasmid production

2.3.1.1 General cloning strategy

Cloning was achieved by excising the relevant insert fragment and opening the appropriate backbone vector with restriction enzymes that created mutually compatible 'sticky ends' to facilitate DNA ligation in the correct location. All cloning products were validated by both diagnostic restriction enzyme digests and DNA sequencing (Genomics, UK). Concentration of all DNA products was measured by photospectroscopy at 260 nm using a NanoDrop® ND-1000 Spectrophotometer (LabTech Int., UK).

2.3.1.2 Restriction digests

To characterize DNA plasmids or fragments, or to isolate fragments of interest, DNA was selectively cut using restriction enzymes (New England Biolabs, UK,).

Digestions were performed as follows:

(A) 0.5 – 1 µg of DNA

(B) 0.5 µL of each restriction enzyme (10 U/µL)

(C) 1.6 µL of appropriate 10x Buffer

(D) 1.6 µL of 10x BSA

(E) Sterile, deionized water added to a total volume of 16 µL

The mix was incubated for 4 hrs at 37°C.

2.3.1.3 DNA electrophoresis and gel extraction of DNA

DNA fragments resulting from restriction enzyme digests were separated by size using electrophoresis (BioRad, UK). Each DNA sample had 4 µL of a loading dye (Blue/Orange Loading Dye, 6x: Promega, UK) added to it before being loaded on to a 1% (w/v) agarose gel prepared in 1x TBE buffer containing SafeView Nucleic Acid Stain (NBS Biologicals Ltd., UK) 15 µL of 1 mL SaveView per 100 mL of gel).

For a 100 - 150 mL gel volume, a voltage of 170 V was applied across the gel for 60 - 120 min, according to the expected size of the DNA bands. Gels were photographed digitally on an ultraviolet transilluminator (BioRad, UK).

For further cloning, DNA fragments were excised from the gel and extracted using a silica gel based purification kit (QIAquick Gel Extraction Kit, Qiagen, UK) according to the manufacturer's instructions.

2.3.1.4 DNA ligation

Ligation of the gel purified DNA fragments into the appropriate vector backbone was performed using 1:5 molar ratio of backbone to insert. DNA was first heated to 45°C for 5 min to melt any annealed cohesive ends, and then rapidly cooled on ice.

Ligations were performed in a mix formulated as follows:

(A) 4 µL of DNA (insert and backbone in 1:5 ratio respectively)

(B) 5 µL of 2x Ligation Buffer (LigaFast: Promega, UK)

(C) 1 µL of T4 DNA Ligase (3 U/mL, LigaFast: Promega, UK)

Ligations were then incubated overnight (o/n) at 4°C after which the ligase was used to transform competent bacterial cells.

2.3.1.5 Transformation of bacteria and DNA amplification

All plasmids used contained the ampicillin antibiotic resistance gene as a selection marker for successfully transformed bacteria. For transformation, chemically competent DH5α™ cells (α-Select, Bioline, UK) were thawed on ice from -80°C. Cells were incubated with construct containing DNA clone for 30 min on ice, before heat-shock for 1 min at 42^{o}C and then incubated back on ice for 5 min. 60 µL of super optimal catabolite (SOC) medium (Thermo Fisher Scientific, UK) was added to cell mix and incubated for 1 h at 37^{o}C. After the incubation time, cells were spread on a lysogeny broth (LB) - agar plate containing 50 µg/mL ampicillin (Aldrich, UK). Plates were incubated at 37^{o}C o/n to allow resistant bacteria to grow. The following day, bacterial colonies were picked using a sterile pipette tip and DNA was amplified. Briefly, 5 mL of LB medium containing 100 µg/mL ampicillin was inoculated with a single bacterial colony and incubated at 37^{o}C o/n. For small scale preparations, plasmids were recovered using QIAGEN® Miniprep Kit (Qiagen, UK). The concentration of the eluted DNA was measured with a spectrophotometer. The isolated DNA was analysed by the appropriate restriction enzymes digests and subsequent gel electrophoresis. Plasmids were then sequence checked and clones containing the desired vector products were prepared as glycerol stocks for long term storage at -80°C. If needed, the correct clones were amplified using MEGA-prep kit (Thermo Fisher Scientific, UK) for further experimental use.

2.3.2 Plasmid constructs

2.3.2.1 pCMV.Crb1.GFP plasmid construct

pCMV6.Crb1.GFP vector plasmid containing the human cytomegalovirus (CMV) promoter was designed using the PrecisionShuttle vector system and made commercially (OriGene Technologies Inc., USA; Figure 2.2). The GFP-tagged plasmid was amplified using DH5α™ competent cells and sequenced to check for any possible mutations, as described in Section 2.3.1.5.

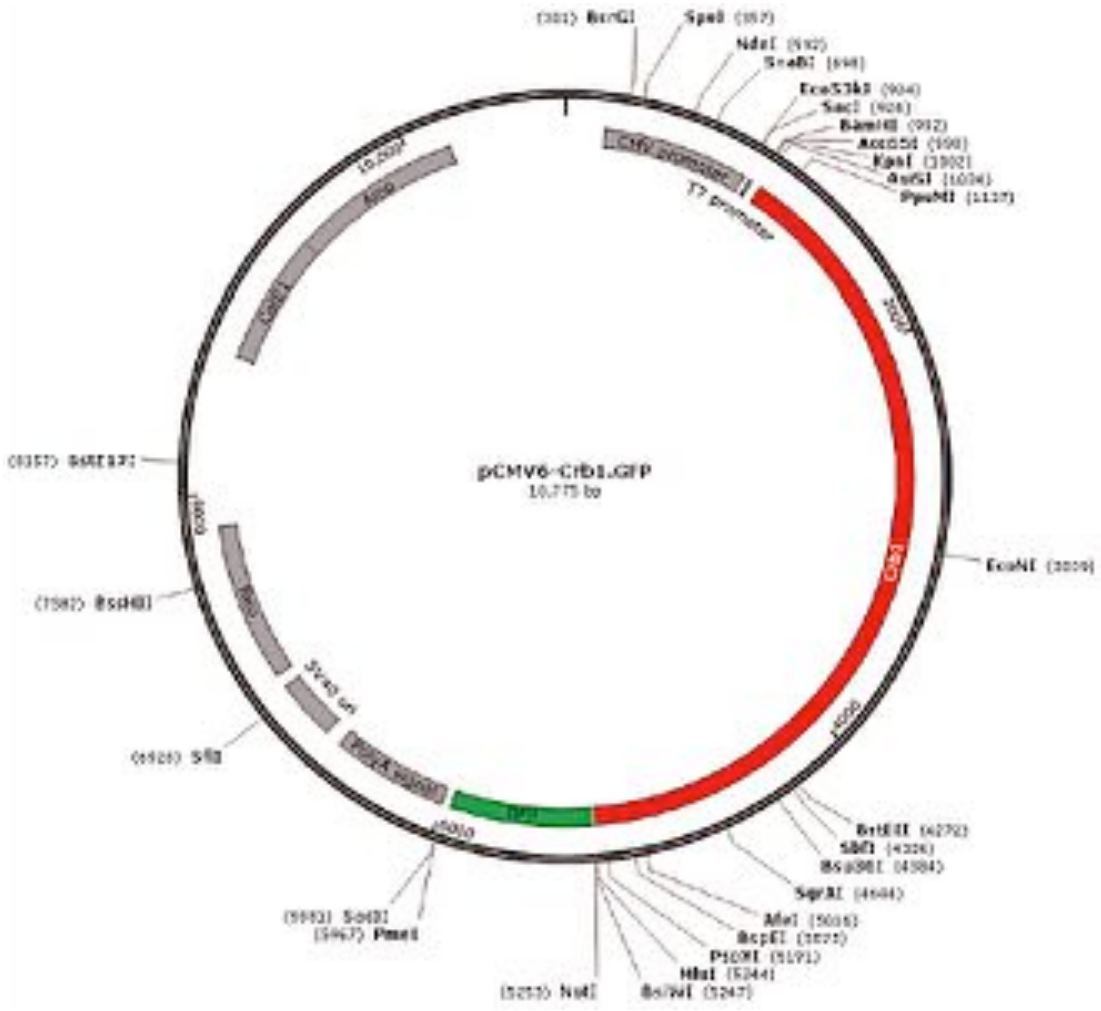

Figure 2.2 Plasmid map of pCMV6.Crb1.GFP construct.

The *Crb1* expression sequence with the GFP reports was placed downstream of the human cytomegalovirus (CMV) promoter. The construct's sequence was verified and tested *in vitro* for its efficiency.

2.3.2.2 pd10.MU6.RFP.shCrb1 and pd10.MU6.RFP.shControl vectors

CRB1 targeting sequences were generated by subcloning the target hairpins (shCrb1) into the mU6 promoter plasmid. The target hairpins were placed downstream of the U6 promoter to form an RNAi-expression cassette. The RNAi cassettes were excised and cloned into the AAV pD10.CBA/RFP backbone. The shCrb1 targets the *Crb1* sequence 5'-GGAAGTGGATGAATGTGTTTCTGAT-3' (position nt 718. NM_133239). ShCrb1 hairpin was designed using a standard shRNA motif of sense-loop-antisense in which the loop consisted of nine nucleotides. A non-targeting hairpin (sequence: 5'-GATCGGACACTCCTCATAA-3') was used as a control. The resulting constructs were named pD10.RFP.shCrb1 (Figure 2.3) and pD10.RFP.shControl respectively (Figure 2.4). Both constructs were verified by sequencing (Beckman Coulter Genomics, UK) and tested *in vitro* for their efficiency.

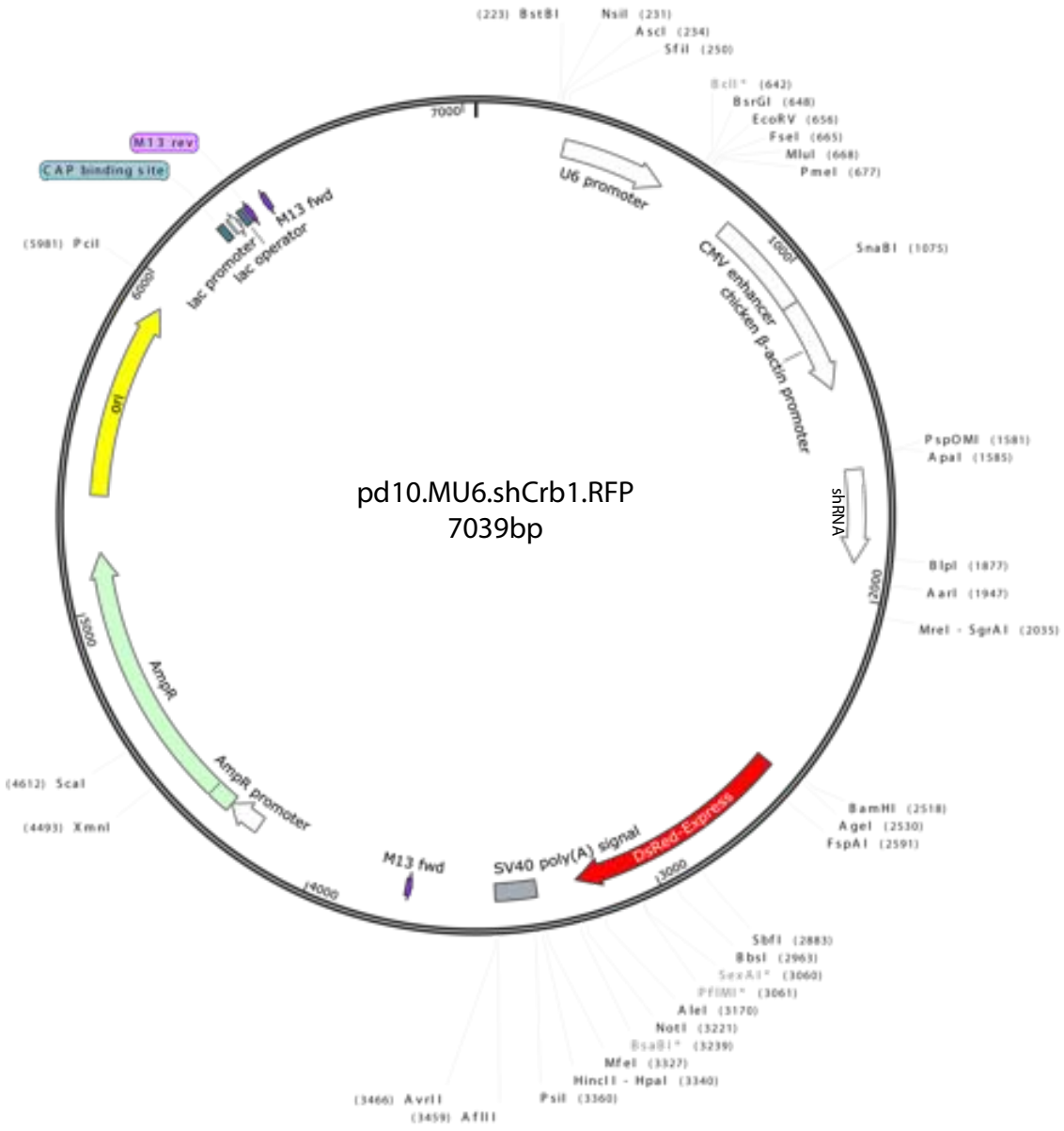

Figure 2.3 Plasmid map of pd10.MU6.shCrb1.RFP vector.

The target hairpin was placed downstream of the U6 promoter to form an RNAi-expression cassette. The RNAi cassettes were excised and cloned into the AAV pD10.CBA/RFP backbone. The shCrb1 targets the Crb1 sequence 5'-GGAAGTGGATGAATGTGTTTCTGAT-3' (position nt 718. NM_133239).

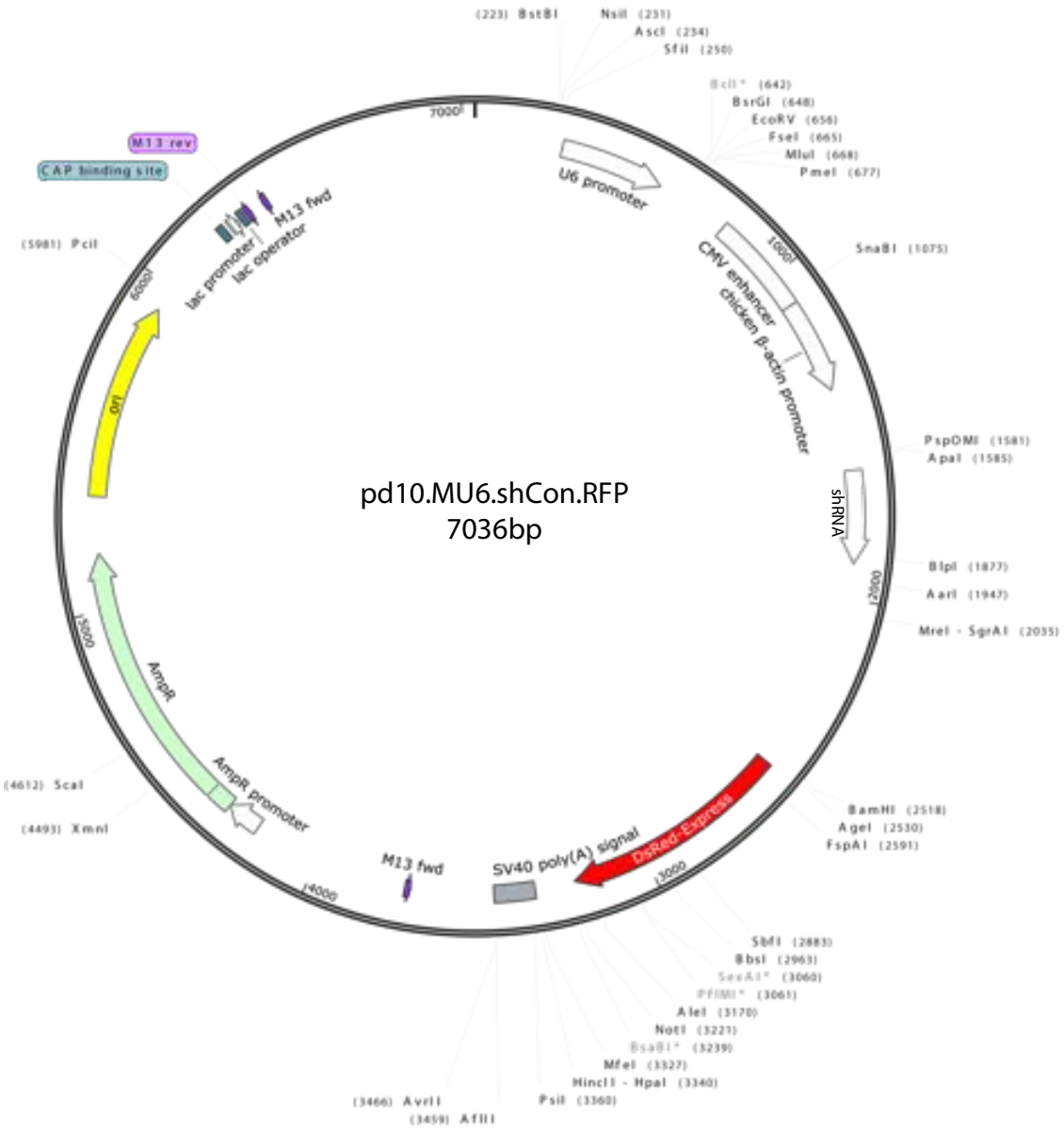

Figure 2.4 Plasmid map of pd10.MU6.shControl.RFP vector.

The on-targeting hairpin (sequence: 5'-GATCGGACACTCCTCATAA-3') was placed downstream of the U6 promoter to form an RNAi-expression cassette. The RNAi cassettes were excised and cloned into the AAV pD10.CBA/RFP backbone and was used as a control.

2.3.2.3 Targeting constructs for intermediate filament proteins

Generation of shGfap and shVimentin vectors was performed by Dr Claire Hippert and is briefly described here. Targeting constructs for *Gfap* and *Vimentin* were generated by subcloning the target hairpins (shGfap or shVimentin) into the mU6pro plasmid. The target hairpins were placed downstream of a U6 promoter to form an RNAi-expression cassette. The RNAi cassettes were excised and cloned into the AAV pD10.CBA/RFP backbone. The shGfap targets the *Gfap* sequence 5′-GCACGAAGCTAACGACTAT-3′ (position nt 911. NM_010277) and the shVimentin targets the *Vimentin* sequence 5'-GTGAGATGGAAGAGAATTT-3' (position nt 1155. NM_011701). ShGfap and shVimentin hairpins were designed using a standard shRNA motif of sense-loop-antisense in which the loop consisted of nine nucleotides. An additional long shRNA (lh) targeting both *Gfap* and *Vimentin* was designed using shGfap targeting sequence linked by 3 nucleotides (CAC) to the shVimentin and cloned into the mU6pro plasmid. As for the single RNAi constructs, the long RNAi cassette was excised and cloned into the AAV pD10.CBA /RFP backbone. A non-targeting hairpin was designed and used as a control and the sequence used for shControl was as follows: 5'-GATCGGACACTCCTCATAA-3'. The resulting constructs were named pD10.RFP.shGfap (Figure 2.5), pD10.RFP.shVimentin (Figure 2.6), and pD10.RFP.lh (Figure 2.7). All constructs were sequence verified and tested *in vitro* for their efficiency.

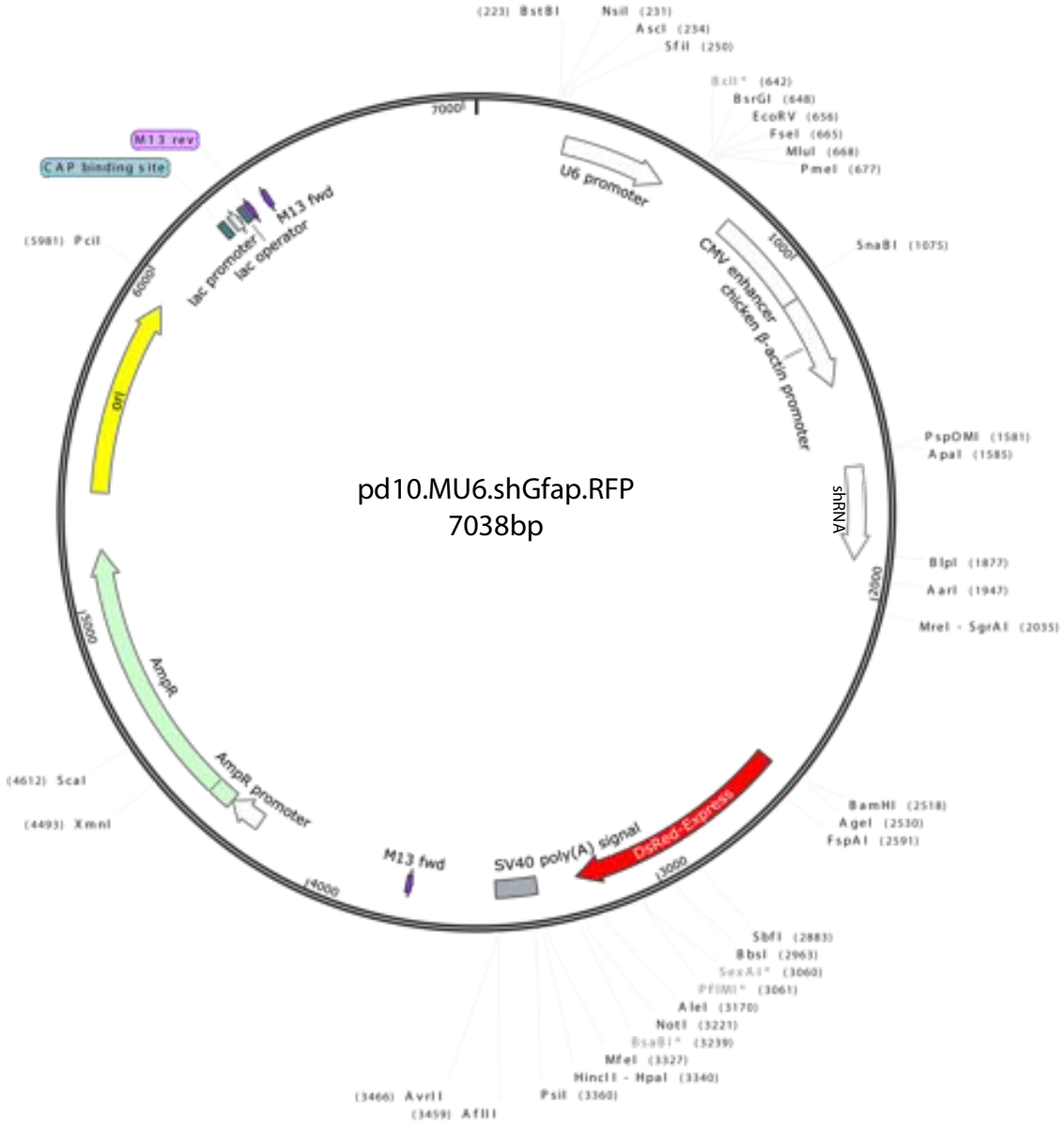

Figure 2.5 Plasmid map of pd10.MU6.shGfap.RFP vector.

The target hairpin was placed downstream of the U6 promoter to form an RNAi-expression cassette. The RNAi cassettes were excised and cloned into the AAV pD10.CBA/RFP backbone. The shGfap targets the Gfap sequence sequence 5′-GCACGAAGCTAACGACTAT-3′ (position nt 911. NM_010277).

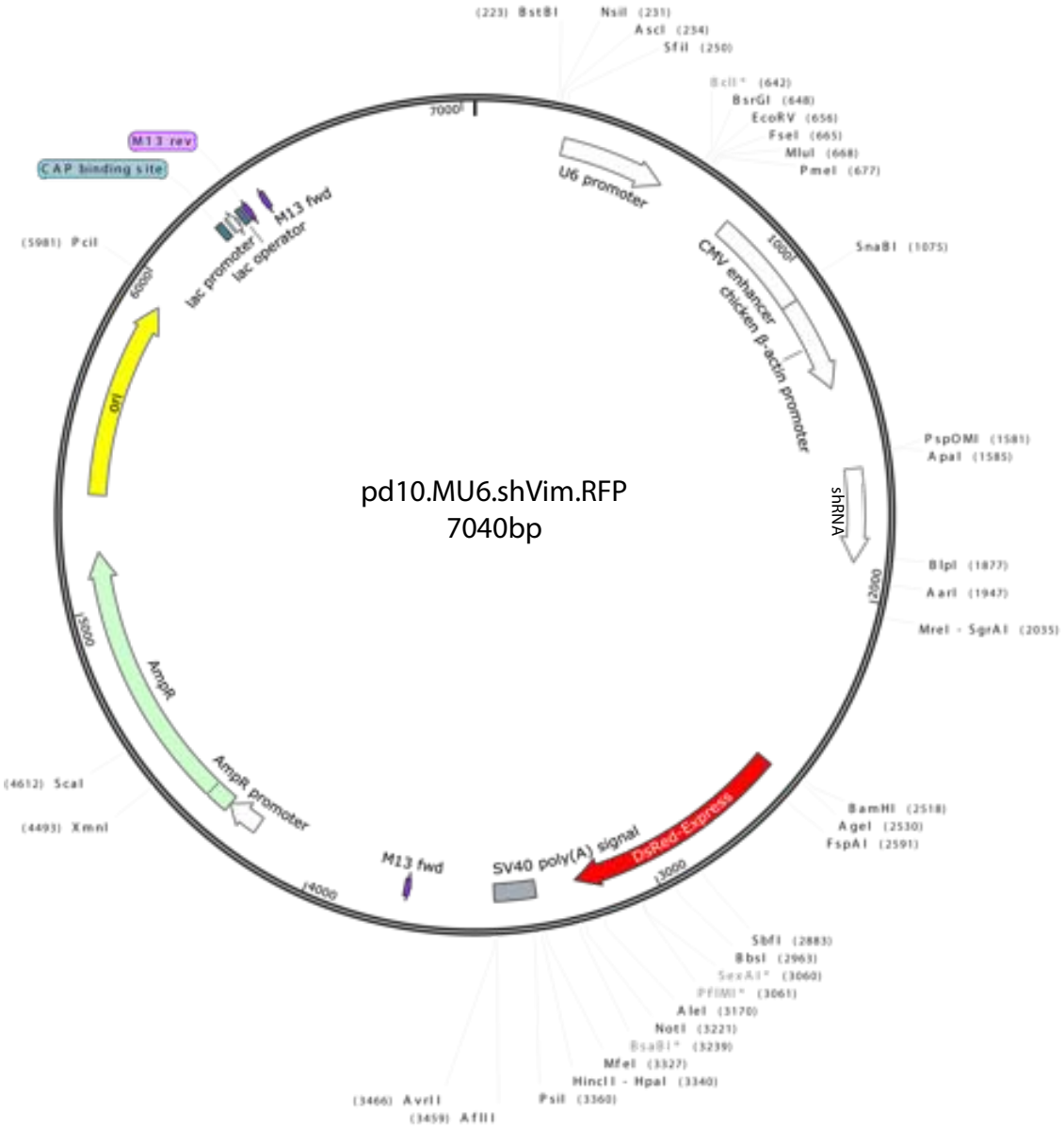

Figure 2.6 Plasmid map of pd10.MU6.shVim.RFP vector.

The target hairpin was placed downstream of the U6 promoter to form an RNAi-expression cassette. The RNAi cassettes were excised and cloned into the AAV pD10.CBA/RFP backbone. The shVimentin targets the Vimentin sequence 5'-GTGAGATGGAAGAGAATTT-3' (position nt 1155. NM_011701).

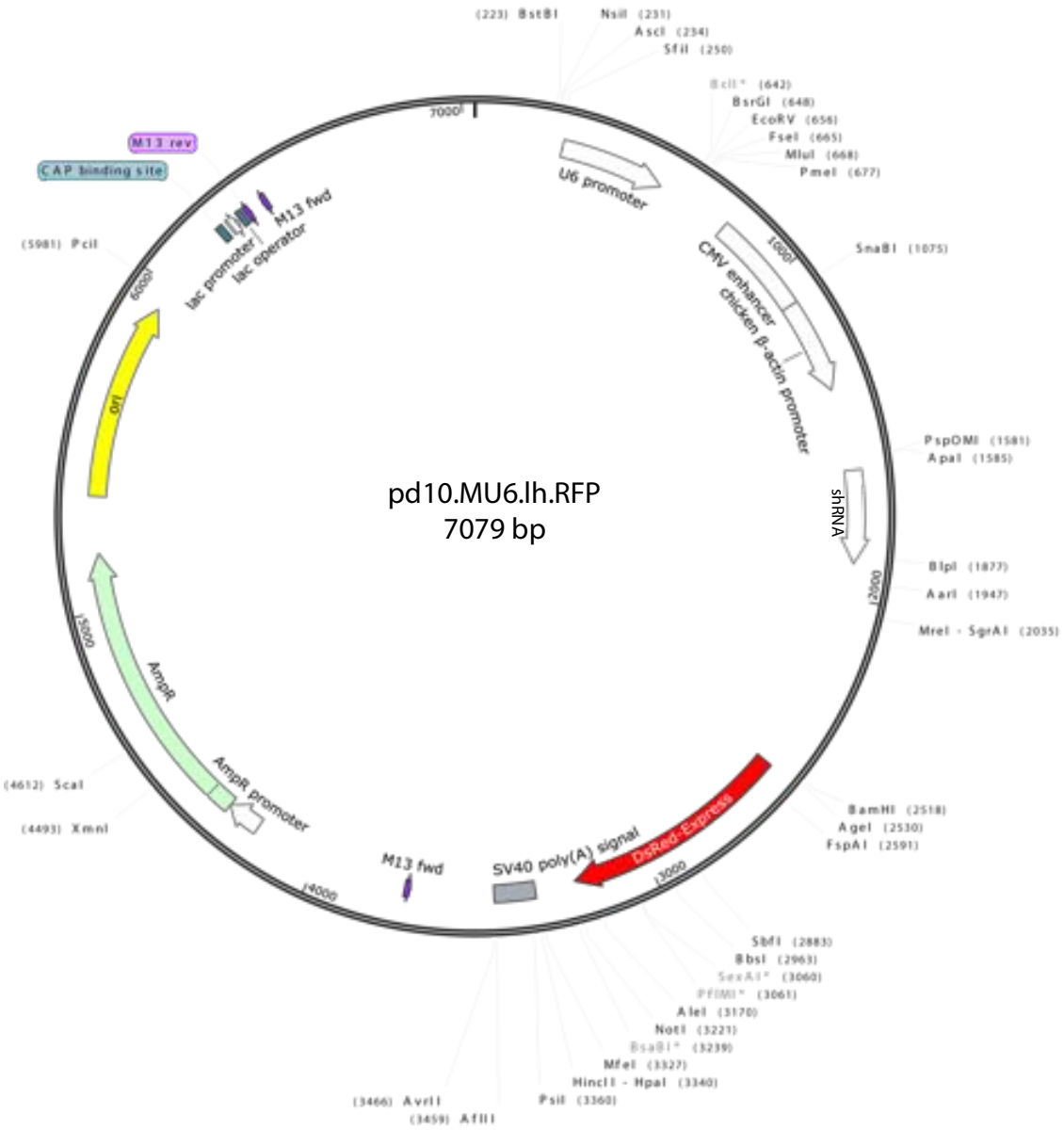

Figure 2.7 Plasmid map of pd10.MU6.lh.RFP vector.

The target hairpin was placed downstream of the U6 promoter to form an RNAi-expression cassette. The RNAi cassettes were excised and cloned into the AAV pD10.CBA/RFP backbone. The long shRNA (lh) targeting both Gfap and Vimentin was designed using shGfap targeting sequence linked by 3 nucleotides (CAC) to the shVimentin and cloned into the mU6pro plasmid.

2.3.3 Viral vector production

2.3.3.1 HEK 293T cell cultures

Human embryonic kidney cells, also known as HEK293T cells (American Type Culture Collection (ATCC)), were routinely grown in DMEM/GlutaMAX medium (Gibco, UK) with the addition of 10% (v/v) heat inactivated FCS (Gibco, UK) and 1% (v/v) AA (Thermo Fisher Scientific, UK) at 37^{o}C in a humidified 5% CO_2 incubator. Cells were grown on either 24-well plate or 15 cm^2 and used at confluence between 85-90% (see relevant sections).

2.3.3.2 Production of adeno-associated virus (AAV)

AAV was produced through a tripartite transfection of 293T cells using a three plasmid system and then purified by Fast protein liquid chromatography (FPLC, as described by others (Gao et al., 2002). A typical AAV production batch consisted of 20 x 15 cm^2 plate. Plasmids used for viral production were as follows:

(A) Viral Genomic plasmid based upon pd10.RFP backbone (see Section 2.3.2). This plasmid contains the viral genome to be packaged between AAV based inverted terminal repeat sequences. Providing this plasmid in trans to the replication and packaging genes minimises the risk of generating replication competent viral particles.

(B) Packaging Plasmid. This plasmid contains the AAV.ShH10.Y445F gene and Viral Capsid gene. Different packaging plasmids are used to produce different AAV serotypes; here AAV.ShH10.Y445F serotype of AAV2 was used as it was reported to transduce mainly Müller glial cells in the retina when administered to the intravitreal space (Klimczak et al., 2009).

(C) Helper Plasmid (pHGTI-Adeno1). This plasmid contains three large chunks of the Adenovirus four genome ligated together. This plasmid provides all the adenovirus genes that AAV requires to package and assemble.

The above plasmids were used in 1:1:3 (Genomic plasmid: Packaging plasmid: Helper plasmid). A total of 50 µg of total plasmid was introduced into 293T cells using polyethylenimine (PEI, Polysciences, Germany) transfection reagent at 1:2.25 weight per weight (w/w) ratio respectively.

All reagents were mixed in DMEM (without any supplements added) and incubated at room temperature (RT) for 15 min to allow DNA/PEI complex formation. After the incubation time, the mix was added to all prepared plates. Transfections were left o/n and replaced with fresh medium (with 10% FCS/1% AA) the following day. Three days post-transfection, cells were physically detached from the plates by scraping and collected together with a growth medium in the falcon tubes. Cells were pelleted at

2000 G for 10 min in a centrifuge. Supernatant medium was discarded and the cell pellet resuspended in 20 mL of 1X Tris density (TD) buffer.

In order to release the AAV virons, cells underwent 4 'Freeze - Thaw - Vortex' cycles comprising the following steps:

(A) Freeze – 20 min at -80°C

(B) Thaw – 20 min in at 37°C

(C) Vortex – 10 min at RT

After the 4th cycle, the resulting cell lysate was stored at -80°C until purification. On the day of viral purification, the cell lysate was defrosted at 37°C and treated with Benzonase (Sigma Aldrich, UK) at 37°C for 30 min at 50 U/mL concentration to destroy any non-packaged DNA remaining in the cell lysate.

Before viral purification 1X TD buffer was added to cell lysate to make a total volume of 40 mL which was then clarified by centrifugation and filtration as follows:

(A) Spun at 18,000 G for 20 min, pellet discarded.

(B) Syringe filter 5 µM dead-end.

(C) Spun at 18,000 G for 20 min, pellet discarded.

(D) Syringe filter 0.45 µM dead-end.

(E) Spun at 18,000 G for 20 min, pellet discarded.

(F) Syringe filter 0.22 µM dead-end.

The resulting clarified lysate was then purified using a two-step protocol performed on an AKTA Pure column using AVB Sepharose high performance affinity medium (GE Healthcare, UK). After purification, the viral fractions were concentrated by centrifugation at 5000 G using a Vivaspin 4 concentrator (10 kDa, Sartorius Stedim Biotech, Viral Fisher Scientific, UK) to 200 µl. 2 mL of PBS-MK was then added (to dilute out high salt elution buffer) and the eluate was concentrated to a final volume of 60 µl. Viral particle titres, in terms of viral genomes (vg)/mL, were determined by quantitative PCR relative to known reference standards. The resulting AAV preparations (AAV.ShH10.shControl.RFP, AAV.ShH10.shCrb1.RFP, AAV.ShH10.shGfap.RFP, AAV.ShH10.shVimentin.RFP and AAV.ShH10.lh.RFP) were titre matched before use.

2.3.4 siRNA intervention

2.3.4.1 Design of RNAi molecules targeting CRB1 protein

RNAi against *Crb1* mRNA was designed using the BLOCK-IT™ RNAi software (Thermo Fisher Scientific, UK). Two sequences were generated:

(A) 5′-ACTCCTGCTTCTGTGTGCCTGGATA-3′ (termed '672')

(B) 5′- GGAAGTGGATGAATGTGTTTCTGAT-3′ (termed '718')

and were obtained commercially (Thermo Fisher Scientific, UK). A proven non-targeting siRNA with 654-Alexa-Fluor was used as a negative control (All-Stars, Qiagen, UK). This negative control matched the general chemistry of the RNAi against *Crb1* mRNA molecule in length and modification and was used to determine any side effects of siRNA delivery and to provide a baseline to compare siRNA-treated samples.

All siRNAs were diluted to the desired concentration in RNAse-free DEPC-treated water (Thermo Fisher Scientific, UK).

2.3.4.2 RNAi transfection in vitro

HEK293T cells (see Section 2.3.3.1) were split and seeded onto a 24 well plate at a density of between 50,000 to 125,000 cells per cm^3 24 hrs before siRNA transfection. Müller glia cultures (see Section 2.2.2) were not split prior the RNAi experiment but they were used at 2 weeks in culture. Briefly, 20 μM siRNA was used as a standard stock solution. A co-transfection procedure (based on that available from www.Thermo Fisher Scientific.com) was used to simultaneously treat 293T cells with siRNA and a plasmid containing the murine *Crb1* cDNA. For Müller glia cultures, no plasmid was used as the Müller glia cells express endogenous *Crb1*. Transfection was performed by conjugating the RNAi with a lipid based transfection reagent (TR). 160 ng (40 pmol) of siRNA and 200 ng of the *Crb1* plasmid were added per well, along with 2 μl Lipofectamine 2000™ or Oligofectamine reagent (Thermo Fisher Scientific, UK), both diluted in OptiMEM reduced serum medium (Thermo Fisher Scientific, UK). Medium was changed after 6 hrs to DMEM/10% FCS/1% AA medium and cells were kept at 37°C in a humidified 5% CO_2 incubator for 48 hrs. After post-transfection period cells were either harvested for quantitative PCR or fixed for immunohistochemistry. The non-targeting siRNA Alexa Fluor 488 was used as a control for transfection efficiency. The wells with TR only were used as a negative control.

2.4 *In vivo* work

2.4.1 Anaesthesia

Animals were anaesthetized using a mixture of ketamine (100 mg/mL), medetomidine hydrochloride (1 mg/mL, Dormitor, Pfizer Pharmaceuticals, UK) and sterile water in

ratio 3:5:42. Postnatal mice (P10-P16) weighed approximately 0.2 g and adult animals weighed approximately 20 g received an intraperitoneal injection of 20 and 200 µL respectively. After the surgical procedure, anaesthesia was reversed with equal volume of intraperitoneal atipamezole hydrochloride (0.1 mg/mL, Antisedan, Pfizer Pharmaceuticals, UK). Animals were kept warm throughout the period of anaesthesia and recovery. Recovering animals were monitored constantly until fully awake and provided with soft bedding and softened food ad lib.

2.4.2 Eye injections

2.4.2.1 AAV.SHh10 administration in vivo

Intravitreal injections were performed under general anaesthesia using an operating microscope and were used for injections of the viral vectors. The eye was dilated using 1% tropicamide (Chauvin Pharmaceuticals, UK). Corneal reflective power was neutralised by placing a 5 mm coverslip (VWR, Germany) on the cornea covered with a coupling medium solution, Viscotears (Novartis Pharmaceuticals, UK). The fundus was brought into focus as a reference point. The eye was secured in position by grasping the conjunctiva using corneal notched forceps (John Weiss & Sons Ltd, UK). Where stated, a scleral puncture wound was performed at the level of the anterior chamber using a sterile 8 mm 34-gauge hypodermic needle mounted on a 5 µL Hamilton syringe (Hamilton, Switzerland). The tip of the needle penetrated the eye tangentially through the sclera just below the limbus above the edge of peripheral retina. The needle was guided through the vitreous towards the back of the eye into a position close to the optic nerve and without touching the lens at any point. 1-2 µL of the vector (10^{13} particles) was injected per eye. After injection, the needle was kept in place for 15 seconds while the intraocular pressure reduced slightly, before being slowly retracted from the eye in order to reduce reflux of the injected material. After procedure, animals were injected intraperitoneally with a reversal and kept on a heat mat until fully recovered. 1% chloramphenicol (Martindale Pharmaceuticals, UK) ointment was applied topically on the cornea as post-operative care for the eye.

2.4.2.2 RNAi transfection in vivo

RNAi sequences (see Section 2.3.4.1) were introduced subretinally at concentrations of 15 µM per eye. siRNA was mixed with Oligofectamine TR in OptiMEM and incubated at RT for 15 min to allow siRNA/TR complex formation. Formed complexes were administrated subretinally in a manner similar to intravitreal injections. Briefly, a Hamilton needle with bevel uppermost was inserted tangentially into the eye though the sclera below the equator of the globe into the subretinal space. The material was slowly injected into the space after which a retinal detachment could be observed. The needle was carefully withdrawn and any reflux of the material or change in the size of

the retinal detachment was noted, as described above. After surgery, mice were recovered as described above. Eyes were harvested after 48 or 72 hrs post-injections to assess effectiveness of RNAi, as reported previoulsy (Pearson et al., 2010; Yu et al., 2016).

2.4.2.3 Nrl.GFP$^{+/+}$ cell transplantation

The transplant procedure is illustrated in the methods schematic presented in Figure 2.3.

The use of the *Nrl*.GFP$^{+/+}$mouse as a source of donor cells provided a genetic marker for the identification of rod photoreceptors (Akimoto et al., 2006). NRL is a rod specific, basic motif-leucine zipper transcription factor (Landschulz et al., 1988; Swaroop et al., 1992; Rehemtulla et al., 1996) whose expression is switched on during terminal mitosis (Akimoto et al., 2006). In the *Nrl.*GFP$^{+/+}$ mouse, GFP is expressed under the *Nrl* promoter; hence GFP expression is restricted to post-mitotic rod photoreceptor cells (Akimoto et al., 2006). Cells for cell transplantations were prepared as described previously (Pearson et al., 2012). Cells were dissociated and prepared for FACS in the same manner as *Rlbp.*GFP$^{+/+}$ cells using papain-based kit (Section 2.2.1). After the sort, cell viability count was performed using trypan blue (Sigma Aldrich, UK) and a haemocytometer counting chamber. Dead or dying cells were identified by trypan blue labelling and excluded from live cell counts. *Nrl.*GFP$^{+/+}$ cells were made up to a final concentration of 200,000 live cells/µl in a solution containing DNase (100 U/ml) in EBSS and kept on ice until used for transplants unless otherwise stated. A total of 200,000 cells was injected into the superior subretinal space per eye in a single injection (Figure 2.8). Eyes were harvested and analysed three weeks post-injections.

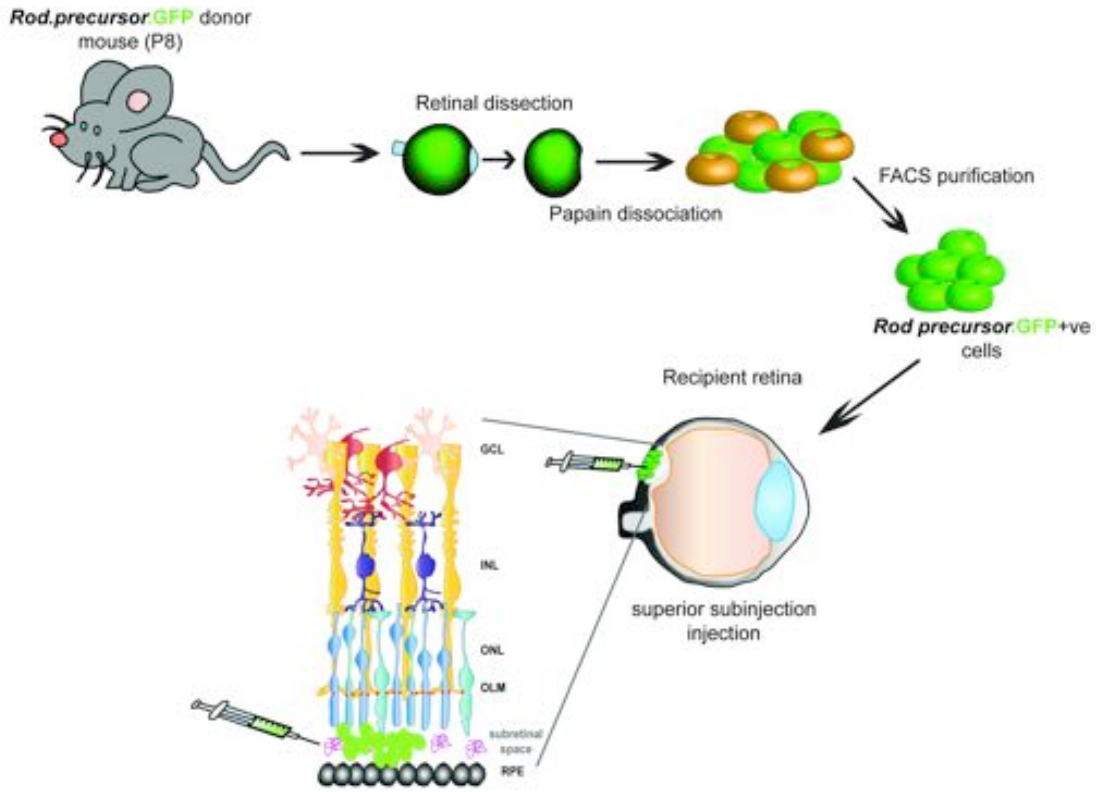

Figure 2.8 A schematic image of photoreceptor cell transplantation.

A schematic image of a dissection of the Nrl.GFP+/+ donor cells which is followed by a subretinal injection within the recipient retina.

2.4.2.4 Enzymatic treatment for CSPGs degradation

Bacterial Chondrotinase (Sigma Aldrich, UK) was prepared according to manufacturer's instructions and was reconstituted in 0.01% bovine serum albumin (BSA) aqueous solution. Immediately prior to use, subsequent dilutions were made with buffer (50nM Tris, 0.02% BSA), containing 60 mM sodium acetate to activate the ChABC. The buffer solution was adjusted to the optimal pH (8.0) for ChABC activity and was used at a final concentration of 0.025U/μL, containing 0.005% DNAse (Suzuki et al., 2007; Singhal et al., 2008).

Recombinant Human ADAMTS-4 enzyme (Millipore, UK) was prepared and used according to manufacturer's instructions. Enzyme was kept at -80^{o}C until the day of experiment and used at a final concentration of 100 ng/μL per eye.

Prior the subretinal injections, enzymes were incubated in water bath at 37^{o} C to allow their activation. Eyes were harvested for immunohistochemistry and Western Blot analysis after 24 - 48 hrs to assess the effectiveness of the enzymes in digesting CS sugar chains. EBSS was used as a control solution that followed the same preparation protocol as the enzymes.

2.5 RNA extraction, reverse transcription and quantitative polymerase chain reaction

2.5.1 Laser extraction of retinal tissue

To determine levels of CRB1 in a wild-type retina, the tissue was extracted from the superior and inferior regions using the laser capture technique. Frozen unfixed eyes were sectioned at 10 μm and 5-6 cryosections were collected on PEN polymer coated slides (Zeiss, Germany). Slides were fixed for 1 min with 70% ethanol, washed with distilled water and dipped in 100% ethanol to remove any excess of water. Slides were viewed on a Palm Zeiss laser microscope (Axiovert 200M, Zeiss, Germany) with 20X/0.4 objective using Palm Robo 3.1 computer software (Palm® Robo Software, MicroLaser Systems, Germany). Regions of the superior and inferior retina adjacent to optic nerve were cut with a laser (P.A.L.M MicroLaser Technologies AG, Germany) and collected in silicone-coated eppendorfs (Adhesive Cap 500, Zeiss, Germany). Captured tissue (5-6 sections) was homogenized with 300 μL of RLT buffer before being processed with RNeasy Micro Kit (Qiagen, UK) to extract RNA.

2.5.2 RNA extraction and quantitative polymerase chain reaction

Real-time quantitative polymerase chain reaction (qRT-PCR) was used to determine the relative gene expression levels. RNeasy Mini or Micro Kit (Qiagen, UK) was used

for RNA extraction of cultured cells, FACS sorted cells, laser-captured cells or whole retinae according to the manufacturer's instructions. RNA concentration and purity were measured with a NanoDrop® ND-1000 spectrophotometer (Thermo Fisher Scientific, USA). RNA was stored at -80°C.

For cDNA generation, the QuantiTect® Reverse or Whole Transcription kit (Qiagen, UK) was used according to the manufacturer's instructions. Standard qPCR reaction consisted of cDNA (50 ng/µL) diluted 1:16, TaqMan® Universal PCR Master Mix (Roche, UK), 2 µM forward primer, 2 µM reverse primer and 0.2 µM probe (Universal Probe Library; Roche, Germany). Primers for the target markers as well as endogenous reference control (β-actin) were designed and appropriate hydrolysis probes were chosen via the Universal Probe Library Design Centre (Roche, UK) (Table 2.2). QRT-PCR was run on an ABI Prism 7900HT Fast Real-time Sequence Detection System (Applied Bioscience, USA). All samples were run in triplicates. The general conditions used had an initial denaturation at 94°C of 2 min. Reactions followed by 40 cycles of:

(A) Denaturing step at 95°C for 30 sec.
(B) Annealing step at 42°C for 30 sec.
(C) Extension step at 72°C for 1 min.
(D) A final extension of 5 min at 72°C was performed to finish the reaction.

The relative expression between comparable samples in relation to the expression of the genes was normalised using the following methodology: signal thresholds were first manually determined and maintained for each individual experimental run on Sequence Detection Systems software 2.2.2 (Applied Biosystems, USA). They were chosen such that they laid in the middle of the linear part of log-based fluorescence amplification curves on fluorescence intensity vs. cycle number plots. To normalise target against β-actin control expression levels, cycle numbers at threshold (C_t) were used to calculate ΔC_t.

(A) $\Delta C_t = C_t\,(\text{target}) - C_t\,(\beta\text{-actin})$

To normalise sample (e.g. treated) against control levels of target expression (e.g. non-treated), $\Delta\Delta C_t$ was calculated:

(B) $\Delta\Delta C_t = \Delta C_t\,(\text{sample}) - \Delta C_t\,(\text{control})$

Finally, to obtain normalised relative target expression levels in '% of control levels', the following formula was applied:

(C) Normalised expression levels (%) = $(2^{-\Delta\Delta Ct}) \times 100$

Gene Name	Forward primer sequence (5'-3')	Reverse primer sequence (5'-3')	Probe (Universal Probe Library)
Mouse β-actin	AAGGCCAACCGT GAAAAGAT	GTGGTACGACC AGAGGCATAC	56
Human β-actin	CCAACCGCGAGA AGATGA	CCAGAGGCGTA CAGGGATAG	64
Crb1	CAACTCAGCCC ATGTCCTC	AAAACAGCCTT TGCGATACA	32
Crb2	CAGGATTCTCT GGCCAGTTC	CAGGCACTGCT ACCTCCAG	34
Gfap	GACAACTTTGCA CAG GACCTC	ATACGCAGCCAG GTT GTTCT	19
Gs	CATCGTGCAGGC TCACTACC	CCCTCACAGGGT CCTATCTG	67
Rlbp	CCCCTCGGATCT CAAGAAG	TTTGAACCTGGCT GGGAAT	1
Sox9	GTACCCGCATCT GCACAAC	CTCCTCCACGAA GGGTCTCT	66
S-100	ACAACTGGGCC AGGATCTTC	CCACCAGGACA ACAACTGC	17
Vimentin	TGCGCCAGCAGT ATGAAA	GCCTCAGAGAGG TCAGCAA	50

Table 2.1 Primer sequences.

2.6 Histology and immunochemistry

2.6.1 Immunochemistry

Immunochemistry was performed on both cryosections and cell cultures. For immunohistochemistry, mice were killed at various time points and their eyes were dissected out. A small corneal burn was used to provide a landmark for the superior retina. Eyes were embedded in optimal cutting temperature (OCT) embedding medium (TissueTek, Thermo Fisher Scientific, UK) using isopentane and liquid nitrogen. Tissue was left o/n at -20^{o}C. Serial transverse sections were cut at 18 µm on a Reichert-Jung 2050 microtome and collected onto Superfrost Plus slides (VWR International, UK) and air-dried for 30 min prior to staining. For immunocytochemistry on 293T and Müller glial cell cultures, the medium was aspirated out of the wells and cells were washed with phosphate buffer saline (PBS). Sections or cells were post-fixed in 1% (w/v) paraformaldehyde (PFA) for 5 or 30 min, respectively, and washed with phosphate buffer saline (PBS). Both slides and cells were blocked for 2 hrs at RT and then incubated with appropriate primary antibody o/n at 4^{o}C (see Table 2.3 for antibodies and staining protocols). The following day, retinal sections were washed with PBS (3 x 5 min) and incubated with secondary antibody (mouse or rabbit, 1:500 dilution in working solution) for 2 hrs at RT. After rinsing with PBS (3 x 5 min), slides were counterstained with Hoechst 33342 (stock solution 5 mg/mL diluted in 1:1000 with PBS for working solution) and cover-slipped with mounting medium. Negative controls were processed as above and in parallel, except that the primary antibody was omitted.

Primary antibody	Fixation	Blocking solution	Primary antibody dilution	Secondary antibody
Polyclonal rabbit anti-Aggrecan (Millipore, #AB1031)	1% PFA for 30 min at RT Pre-treated for 3 hrs with ChABC at 37°C	1% (w/v) NGS, 5% (w/v) milk, 0.1% (w/v) Triton-X in PBS	1:200 in BS	Goat- anti-rabbit Alexa 488 (Thermo Fisher Scientific 1:500 in BS
Monoclonal mouse anti-CRALBP (Abcam, #ab15051)	1% PFA post-fix for 30 min at RT	1% (w/v) NGS, 5% (w/v) milk, 0.05% (w/v) Triton-X in PBS	1:200 in BS	Goat- anti-mouse Alexa 488 (Thermo Fisher Scientific 1:500 in BS
Polyclonal rabbit anti-CRB1 (gift from J. Wijnholds)	no fixation or 1% PFA post-fix for 5 min (or 30 min for cell cultures) at RT	5% (w/v) NGS, 3% (w/v) BSA, 0.05% (w/v) Triton-X in PBS	1:300 in BS	Goat- anti-rabbit Alexa 546 (Thermo Fisher Scientific, #A-21085) 1:500 in BS
Monoclonal mouse anti-CS56 (Sigma Aldrich #C8035)	No fixation	1% (w/v) NGS, 5% (w/v) milk, 0.05% (w/v) Triton-X in PBS	1:200 in BS	Goat- anti-mouse Alexa 546 (Thermo Fisher Scientific 1:500 in BS

Primary antibody	Fixation	Blocking solution	Primary antibody dilution	Secondary antibody
Purified mouse anti-Glutamine Synthetase (BD Transduction Laboratories, #610517)	1% PFA post-fix for 30 min at RT	1% (w/v) NGS, 5% (w/v) milk, 0.05% (w/v) Triton-X in PBS	1:200 in BS	Goat- anti-mouse Alexa 488 (Thermo Fisher Scientific 1:500 in BS
Polyclonal rabbit anti-GFAP (Dako, #Z0334)	No fixation (1% PFA for 30 min at RT only for cell cultures)	1% (w/v) NGS, 5% (w/v) milk, 0.05% (w/v) Triton-X in PBS	1:500 in BS	Goat- anti-rabbit Alexa 488 (Thermo Fisher Scientific, #R37116) 1:500 in BS
Monoclonal mouse anti-GFAP (Sigma Aldrich, #G3893)	4% PFA for 1h Post-treatment in 30% sucrose	3% (w/v) NGS, 0.3% (w/v) Triton-X in PBS	1:200 in BS	Goat- anti-mouse Alexa 488 (Thermo Fisher Scientific 1:500 in BS
Monoclonal mouse anti-Laminin 1 A&B chains (Millipore, #MAB1904)	No fix	5% (w/v) NGS, 3% (w/v) BSA, 0.05% (w/v) Triton-X in PBS	1:200 in BS	Goat- anti-mouse Alexa 546 (Thermo Fisher Scientific 1:500 in BS

Primary antibody	Fixation	Blocking solution	Primary antibody dilution	Secondary antibody
Polyclonal rabbit anti-LAR (Santa Cruz, #sc25434)	No fix	5% (w/v) NGS, 3% (w/v) BSA, 0.05% (w/v) Triton-X in PBS	1:200 in BS	Goat- anti-mouse Alexa 633 (Thermo Fisher Scientific 1:500 in BS
Monoclonal mouse anti-S-100 (Abcam, #ab7852-500)	1% PFA post-fix for 30 min at RT	1% (w/v) NGS, 5% (w/v) milk, 0.05% (w/v) Triton-X in PBS	1:200 in BS	Goat- anti-mouse Alexa 488 (Thermo Fisher Scientific 1:500 in BS
Polyclonal rabbit anti-SOX9 (Millipore, #AB5535)	1% PFA post-fix for 30 min at RT	1% (w/v) NGS, 5% (w/v) milk, 0.05% (w/v) Triton-X in PBS	1:200 in BS	Goat- anti-rabbit Alexa 488 (Thermo Fisher Scientific 1:500 in BS
Monoclonal mouse anti-Vimentin (Sigma Aldrich #099K4753)	no fixation or 1% PFA post-fix for 5 min at RT	5% (w/v) NGS, 3% (w/v) BSA, 0.05% (w/v) Triton-X in PBS	1:200 in BS	Goat- anti-mouse Alexa 488 (Thermo Fisher Scientific 1:500 in BS
Monoclonal chicken anti-Vimentin (Millipore, #AB5733)	1% PFA for 30 min at RT for cell cultures	5% (w/v) NGS, 3% (w/v) BSA, 0.05% (w/v) Triton-X in PBS	1:200 in BS	Goat- anti-chicken Alexa 488 (Thermo Fisher Scientific 1:500 in BS

Primary antibody	Fixation	Blocking solution	Primary antibody dilution	Secondary antibody
Polyclonal rabbit anti-ZO-1 (Thermo Fisher Scientific, #40-2300)	no fixation or 1% PFA post-fix for 5 min at RT	5% (w/v) NGS, 3% (w/v) BSA, 0.05% (w/v) Triton-X in PBS	1:250 in BSA	Goat- anti-rabbit Alexa 546 (Thermo Fisher Scientific, #A-21085) 1:500 in BS

Table 2.2 Immunochemistry staining protocol.

(ChABC, chondrotinase ABC (Sigma Aldrich, UK); NGS, Normal Goat Serum (Abd serotec, UK); BSA, Bovine Serum Albumin (Sigma Aldrich, UK); PBS - 1X Phosphate Buffer Saline)).

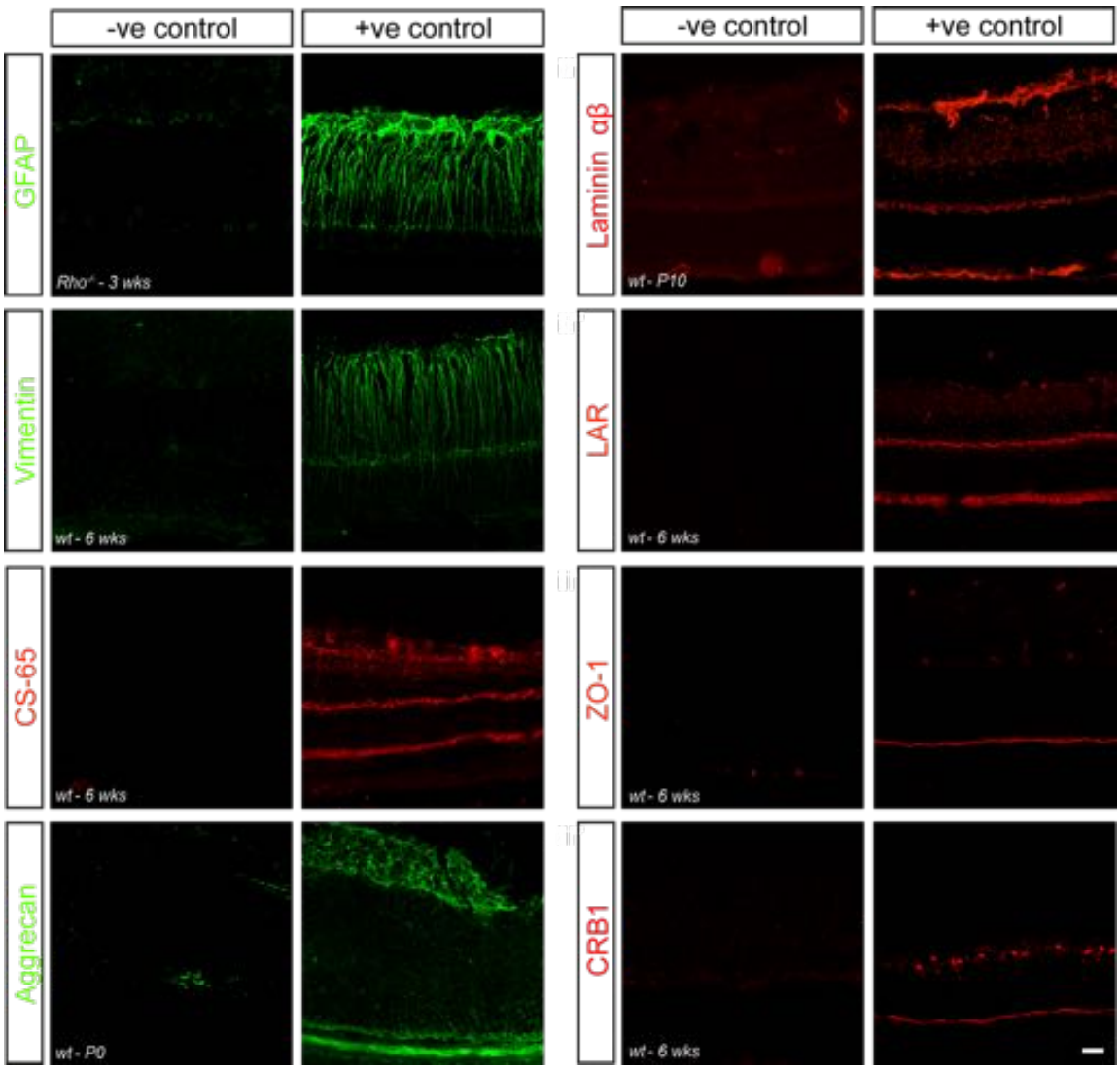

Figure 2.9 Immunohistochemistry controls.

A) Negative (no primary antibody) and positive controls for each of the antibodies used in this study. Scale bar, 25 μm.

2.6.2 Preparation of retinal flatmounts

Mice were killed using an approved Schedule 1 method and the eyes enucleated. The globe of the eye was punctured at the posterior pole using a 25-gauge needle and the eye was placed in a petri dish containing 4% PFA. The retina was dissected away from the rest of the globe with an orbital cut just posterior to the limbus. Any non-retinal tissue that came away attached to the retina was carefully removed. Once dissection was complete, four radial cuts were made in the 3, 6, 9 and 12 o'clock positions using a scalpel (No.15 Swann-Morton) to allow the retina to be flattened. Individual retinas were then fixed for a further 30 min. After fixation, the retina was placed on a microscope slide to allow its positioning for imaging with the layer of interest positioned upper most. The retina was then flattened on the slide using a pair of forceps before a 20-50 µL drop of fluorescent mounting medium (DAKO Ltd., Denmark) was placed upon the sample. A coverslip was then carefully placed upon the tissue and flattened on to the retina by a combination of capillary action and gentle pressure. The slide was then incubated left at RT for 30 min to allow the mounting medium to harden. All the flatmounts were imaged on the day of an experiment (Figure 2.10).

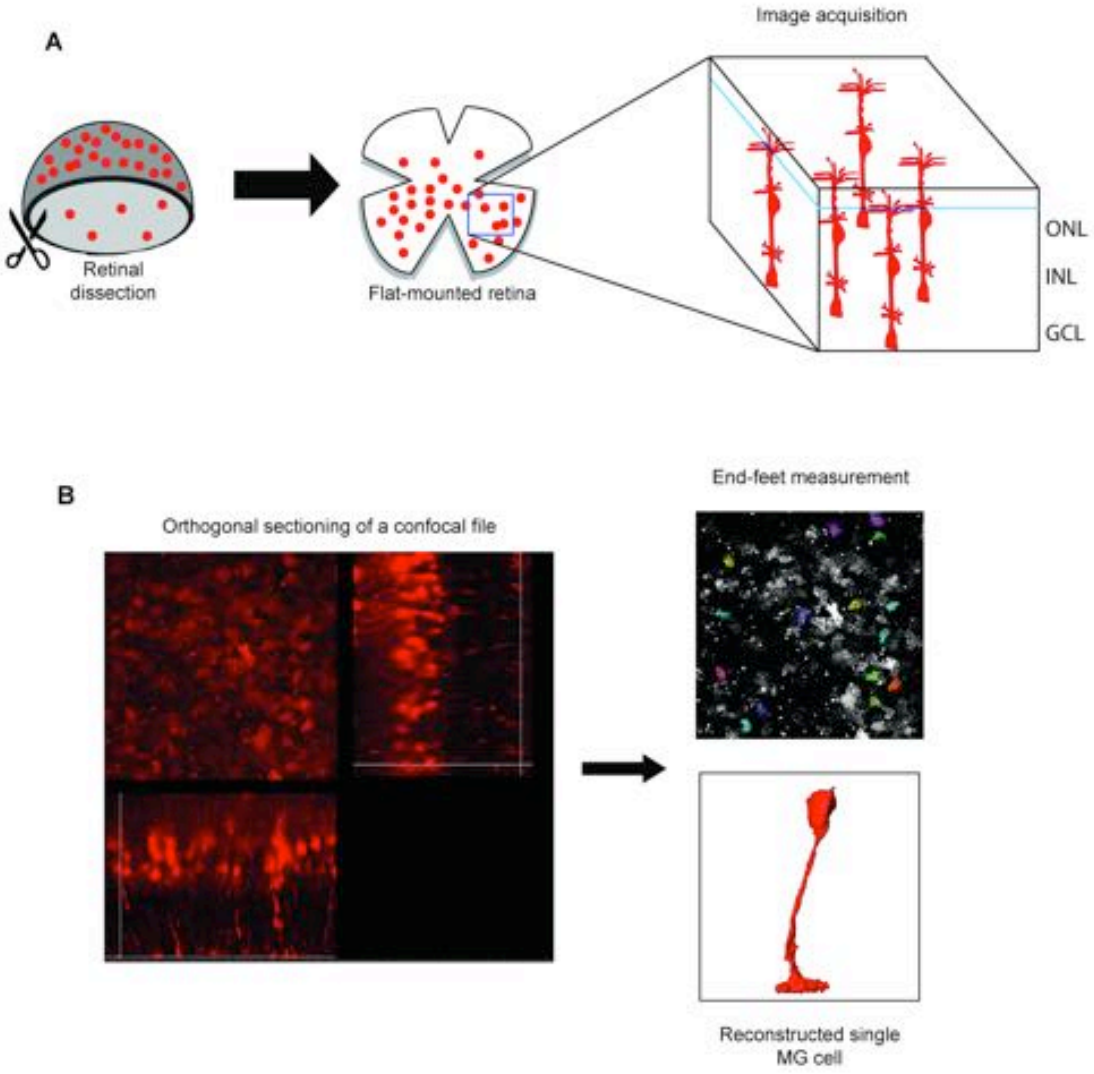

Figure 2.10 Retinal flatmount.

A) Schematic of the retina that was injected with AAV.shH10.RFP vector processed for a flatmount. B) Examples of the orthogonal confocal projections that were used for image analysis and 3*D* reconstruction of the Müller glial cells.

2.7 Microscopy

2.7.1 Confocal Microscopy

Leica TCS confocal microscope with 10x/0.30 and 40x/1.15 oil immersion objectives was used to capture fluorescence images of the retinal sections. (Leica TCS SPE, Leica Microsystems, UK). Images of the retinae were captured with Leica DFC360FX microscope camera and saved on the computer by using LAS AF software (Leica Microsystems, UK). Single confocal sections or merged projection images of a x-y-z stack are presented. Confocal stacks were approximately 15 µm thick with a step size of approximately 1 µm. Hoechst 33342 was excited by the 405 nm laser, Alexa-488 fluorophore using the 488 nm laser and the Alexa-546 fluorophore using the 543 nm. Images were taken at a resolution of 1024x1024. The images were taken using the same laser intensity, gain and offset settings wherever possible. For figures, digital images were adjusted for contrast using Adobe Photoshop CS4. All qualitative comparisons between conditions/models were made on the raw image files.

2.7.2 Electron Microscopy

Mice were sacrificed and the eyes were fixed in 3% glutaraldehyde/ 1% PFA (w/v) buffered to pH 7.4 with 0.08 sodium cacodylate HCl and left for one week at 4^{o}C. The cornea and lens were removed and a nasal stitch was made to orientate the eyecups, as previously described (West et al., 2008). Following a washing step (2.5% glutaraldehyde and 0.1M cacodylate buffered to pH 7.4 for 15 min), the eyes were osmicated for 2.5 hrs in a 1% aqueous solution of osmium tetroxide in the dark, followed by dehydration steps though ascending ethanol series (50-100%, 10 min per step with rotation). After three submersions in 1,2-epoxypropane (10 min each), the samples were left in a 50:50 mixture of 1,2-epoxypropane and araldite resin for a minimum of 3 hrs at RT with rotation. The submersion solution was changed to fresh araldite resin and specimens were left o/n with rotation at RT. The following day, the eyecups were embedded in fresh araldite resin and cured for 48 hrs at 60^{o}C. Semithin (0.7 µm) and ultrathin (0.07 µm) sections were taken using Leica ultracut S microtome (Diatome histoknife Jumbo or Diatome Ultrathin, respectively). Semithin sections were collected on Super Frost slides and stained with 1% toluidine blue and analysed using a Leitz Diaplan microscope with 100x/1.32 oil objective fitted with a Leica digital camera DC500 (Leica Microsystems, UK). Images were captured using Q-Capture Pro 5.1 software (QImaging Ltd., Canada). Ultrathin sections were collected on the copper grids and contrast-stained with lead citrate and evaluated using a JEOL1010 Transmission Electron Microscopy (80 kV). Images were taken using a digital camera and DigitView 1.82.366 software (Gatan Inc., USA).

2.8 Histology assessment

2.8.1 Degeneration assessments

The outer nuclear layer (ONL) thickness (from outer to inner edge of the ONL) and ONL density were measured using single section confocal images (Leica TCS SPE, Leica Microsystems, UK) taken at x80 magnification. Images were acquired from three standardised regions of the superior retina immediately adjacent to the optic nerve (here in termed superior-posterior) from at least three independent animals, for each model per time point. The rate of degeneration was calculated using the ONL thickness measurements: the total loss of ONL thickness between early and late stage degeneration was divided by the number of days over which the degeneration had taken place. In parallel, the number of photoreceptor rows was counted at each examined stage of disease. ONL density was calculated by counting the number of cell nuclei and normalised to the area of the ONL, and expressed as the number of nuclei per 100 μm^2. Measurements were taken using ImageJ software and analysed in a fully blinded manner.

2.8.2 Assessment of photoreceptor transplantation

Recent findings showed that transplantation of door labelled *Nrl.*$GFP^{+/+}$ cells leads to both 'true integration' and so-called material transfer/cytoplasmic fusion (Pearson et al., 2016; Santos-Ferreira et al., 2016; Singh et al., 2016). At the time when this study was designed and implemented, cell integration was genuinely thought to be the only biological mechanism that led to detection of $GFP^{+/+}$ cells within the host ONL. Due to the length of each experiment with the viral vectors, it was not possible to repeat the cell tranplantation experiments. Although, the presented findings do not enable to distinguish between true integration and material transfer/cytoplasmic fusion, they can indicate whether knockdown of IF proteins has any impact on the cell transplantation outcome.

Counts of GFP^{+} cells were taken using a fluorescence microscope (Axio Observer Z.1, Zeiss, UK) and were performed by Prof. Rachael Pearson according to previously established protocol (MacLaren et al., 2006; Pearson et al., 2012). The donor labelled cells were only counted if the whole cell body was correctly located within the recipient outer ONL, above the outer limiting membrane (OLM). Eyes were fixed in 4% PFA, cryopreserved and serially sectioned across three slides. The *Nrl.*$GFP^{+/+}$ cells were counted in every third section throughout the whole eye and multiplied by three to give a total number per retina. Eyes were omitted from analysis if there was a clear evidence of an injection having been inadvertently administrated into the vitreal cavity,

instead of subretinally, or if there was an absence of the cell mass in the subretinal space (defined as less than 200 cells in the SRS), which is an indication either of the reflux at the time of a cell transplant, or of acute inflammatory response (this occurs in approximately 20% of injections; (see (West et al., 2010)). For the experiments with the viral vectors additional condition, the transduction efficiency was also taken into account where eyes with poor transduction were omitted from the study. All counts were done in a fully blinded manner.

2.9 Western Blot Assessment

Neuronal retinae were dissected from 3-5 mice per time point, snap frozen in liquid nitrogen and stored in -80^{o}C. Retinal tissue was then lysed in 100 µl of RIPA buffer (Sigma Aldrich, UK) with 1 µl protease inhibitor (Sigma Aldrich, UK). Cell membranes were disrupted using a sonicator (Soniprep 150, MSE London, UK). Protein concentrations were determined with a BCA assay (Bio-Rad, UK). Equal amounts of protein (20 µg) were resuspended in Laemmli's loading buffer or non-reducing loading buffer (see Table 2.2 and 2.3). The samples were then run on a sodium dodecylsulphate-polyacrymalide gel for 90 min 120 mV. The separated proteins were electrotransfered to PVDF membranes (Millipore, UK) for 30 min 25 mV using Transfer System machine (Bio-Rad, UK) and then separated into two blots at 25 kDa. Membranes were incubated in an appropriate blocking solution for 1 hr at RT and incubated with primary antibody o/n at 4^{o}C (Table 2.3). The following day the membranes were washed with PBST (0.05% Tween in PBS) and incubated for 2 hrs with secondary antibody. Chemiluminescence detection was performed using a Fujifilm LAS-1000 Luminescence Image Analyser (Fujifilm Corp., Japan) after incubation with enhanced luminescence reagent (ECL Plus, GE Healthcare, UK). Band intensities were quantified using Image J software and normalized to Histone 2B (H2B) levels.

Antibody	Laemmli's Buffer	Blocking solution	Primary antibody	Secondary antibody
Monoclonal mouse anti-Histone-2B (Cell Signalling, #2934)	Reducing	5% BSA 0.05% PBST	1:10000 in 5% Non-fat milk 1% BSA 0.05% PBST	Goat-anti-mouse conjugated to HRP, (ThermoFisher Scientific, #31430) 1:10000 in BS
Polyclonal rabbit anti-Neurofilament L (Cell Signalling, #2837)	Reducing	5% BSA 0.05% PBST	5% BSA 0.05% PBST	Goat anti-rabbit conjugated to HRP, (ThermoFisher Scientific, #G-21234) 1:5000 in BS
Polyclonal rabbit anti-Brain 3B (Brn-3, Santa-Cruz, #sc-6026)	Reducing	5% BSA 0.05% PBST	1:2500 in BS	Goat anti-rabbit conjugated to HRP, (ThermoFisher Scientific, #G-21234) 1:5000 in BS
Polyclonal rabbit anti-GFAP (DAKO, #Z0334)	Reducing	5% Non-fat milk 1% BSA 0.05% PBST	1:2500 in BS	Goat anti-rabbit conjugated to HRP, (ThermoFisher Scientific, #G-21234) 1:5000 in BS

Antibody	Laemmli's Buffer	Blocking solution	Primary antibody	Secondary antibody
Monoclonal mouse anti- Vimentin (Sigma Aldrich, #V5255)	Reducing	5% Non-fat milk 1% BSA 0.05% PBST	1:3000 in BS	Goat-anti-mouse conjugated to HRP, (ThermoFisher Scientific, #31430) 1:10000 in BS
Monoclonal mouse anti-CS56 (Sigma Aldrich, #C8035)	Non-reducing	10% Non-fat milk 0.05% PBST	1:1500 in 5% Non-fat milk 0.05% PBST	Goat-anti-mouse conjugated to HRP, (ThermoFisher Scientific, #31430) 1:10000 in BS
Polyclonal anti-Aggrecan produced in rabbit (Millipore, #AB1031)	Non-reducing (pre-treatment with ChABC for 3 hrs at 37 ^{o}C)	5% Non-fat milk 1% BSA 0.05% PBST	1:3000 in BS	Goat anti-rabbit conjugated to HRP, (ThermoFisher Scientific, #G-21234) 1:5000 in BS

Table 2.3 Antibodies and protocols used for Western Blot analysis.

PBST, PBS-Tween-20; HRP, Horseradish peroxide; BS, blocking solution; BSA, Bovine Serum Albumin; ChABC, Chondroitinase ABC.

2.10 Image analysis and 3*D* reconstruction

2.10.1 Assessment and quantification of the adherens junctions

Nature and number of adherens junctions across different degenerative models at early and late ages were assessed using electronmicrograph images taken at x1000 using ImageJ software. Two grids with two independent regions taken at the optic nerve area from both middle inferior and superior retina were assessed. All the measurements were averaged and expressed as a total number of junctions counted over a distance of 100 μm.

2.10.2 Quantification of the Müller glia end-feet

Müller glia end feet were measured using a sub-stack projection that was created in Image J (from the confocal z-stack of a flatmount; (imagej.nih.gov/ij/), see Figure 2.6 B). The created image was then converted to RGB image and opened in GNU Image Manipulation Program (GIMP; Open Source; https://www.gimp.org/). Orthogonal views of the individual sub-stacks were used to track individual cells to their end-foot processes. Only those endfeet that could be clearly traced down to cell bodies that occupied an appropriate position in the inner nuclear layer were used for assessment. Sub-stack xy projections encompassing the first 15-20 μm at the apical margin of the retina were generated from the flatmount confocal xyz stacks described above. The resulting image was then opened using GIMP software and converted to grayscale. Threshold Alpha tool was used to separate signal from background and the same threshold was applied to all analysed images. Regions of interest (ROI) were selected using the free selection tool. The perimeter of each individual end-foot process was manually delineated and the histogram dialogue was used to quantify the total number of pixels within the selected area. The measured values for the total area were then converted to μm^2. All quantifications were performed in a fully blinded manner by an independent assessor.

2.10.2 3*D* reconstruction of Müller glial cells

Leica confocal xyz images (in tif format) were directly opened in Amira 5.5.0 (FEI.com). Data series were filtered using a noise reduction median filter and then individual cells were semi-automatically segmented using a Wacom drawing tablet. The segmentation data was smoothed with voxels smaller than or equal to the size value specified being removed. 3*D* surfaces were generated and shown using vertex normals. Three to five cells were reconstructed per file. All data were treated in the same way. An independent assessor performed all reconstructions in a blinded manner.

2.11 Statistics

All means are ± standard deviation, unless otherwise stated. *N* corresponds to a number of eyes examined where appropriate (one eye per animal was used for any given method of assessment) or independent cell cultures used per study. All experiments concerning RNAi/viral injections were conducted as paired experiments, whereby the contralateral eye served as a within- animal control. Pearson's test was used to determine normal distribution of data sets. Where appropriate, statistical significance was assessed using a Student's *t*-test with Holm-Sidak corrections or ANOVA test with Tukey's correction applied for multiple comparisons, using Graphpad Prism 5.0 software (Graphpad Inc., USA). *P* values are presented as $*P < 0.05$, $**P < 0.01$, $***P < 0.001$ and $****P < 0.0001$.

CHAPTER 3

Characterisation of the retinal environment in different murine models of retinopathy

3.1 Overview

The vast majority of degenerative retinal diseases lead either directly or indirectly to dysfunction and/or loss of photoreceptor cells. As degeneration progresses the microenvironment of the retina undergoes a number of significant changes. The loss of photoreceptors causes the cytoarchitecture of the nuclear layers together with the outer limiting membrane (OLM), a network of adherens junctions (AJs) formed between photoreceptors and Müller glia, to remodel. In addition, Müller glial cells undergo reactive gliosis, leading to the formation of a glial scar that can envelope the entire retina at later stages of degeneration (Jones et al., 2003a). This scar can act as a reservoir for the accumulation of extracellular matrix (ECM) molecules including chondroitin sulphate proteoglycans (CSPGs), which are known to be inhibitory to axonal growth and regeneration (Inatani et al., 2001; Jones et al., 2003b; Escher et al., 2008). Each of these processes is likely to have a significant impact upon the retina, its health and physiology. Previously, retinal gliosis has been shown to negatively impact on the efficiency of viral transduction in gene therapy (Grüter et al., 2005), photoreceptor transplantation outcome (reviewed in (Pearson et al., 2014; Hippert et al., 2016) and the ability of retinal grafts (reviewed in (Zhang et al., 2004)) and electronic implants (Pardue et al., 2001) to contact the underlying retina. Elsewhere in the CNS, reactive gliosis has long been considered as the major impediment to axonal regrowth after an injury (Fawcett and Asher, 1999; Busch and Silver, 2007). Nonetheless, the formation of a glial barrier around a lesion site is also an advantage, because it isolates the still intact CNS tissue from secondary lesions. In addition, there are reports to suggest that in certain conditions reactive astrocytes could even provide a permissive substrate for neurite extension (reviewed in (Ridet et al., 1997)). For these reasons, understanding the process of glial scar formation, how this process differs in different models of degeneration, and finding strategies to circumvent these barriers, represent major challenges to the advancement of many ocular therapies.

Typically, gliosis in the eye is characterized by a dramatic increase in intermediate filament (IF) expression and a pronounced activation of Müller cells (Fisher and Lewis, 2003). In addition to the upregulation of the IF proteins, Glial Fibrillary Acidic Protein (GFAP) and Vimentin, reactive Müller cells may undergo hypertrophy, presenting a proliferation of fibrous processes and deposition of proteoglycans, particularly CSPGs, at the outer edge of the retina (Lewis and Fisher, 2003; Jones et al., 2003b; Fisher et al., 2005; Jones and Marc, 2005; Inman and Horner, 2007). This process of gliosis is characteristic of many retinal disease models (Ekström et al., 1988; Sheedlo et al., 1995; Fan et al., 1996; Inatani et al., 2001; Escher et al., 2008), although the temporal relationship between the onset of gliosis and degeneration may vary between disease

models. Given the apparent complexities of the gliotic process, more precise dissections of the links between the onset of glial reactivity and progressive neurodegeneration are needed.

Over the past decade, progress in creating genetically engineered animal models that more accurately model human retinopathies has allowed scientists to advance our understanding of the mechanisms underlying disease pathology. As different biological causes may lead to changes in different physiological pathways, the assessment of the retinal microenvironment across a number of different murine models of retinal degeneration is needed. In this chapter, seven clinically relevant mouse models (three carrying a spontaneous gene mutation and four having been genetically modified) have been compared against wild-type controls across different time points in a course of disease progression.

3.2 Results

3.2.1 Assessment of retinal cytoarchitecture

Each of the studied murine models undergoes a progressive loss of photoreceptors over time ranging from a normal cell loss due to ageing to near complete reduction of all the cells in ONL. For the purpose of this thesis, the examined mouse models were divided into naturally occurring (spontaneous mutations) or genetically modified mutants (targeted genetic mutations) of inherited retinal degeneration (Table 3.1). The time points examined were chosen to encompass a range of degeneration stages within each model. These can be described broadly as early, mid, and late degeneration. These were further characterised in terms of ONL cell nuclei density, thickness and number of photoreceptor cell rows.

Model	Phenotype	Early time point	Mid time point	Late time point
Spontaneous genetic mutations				
Crb1$^{rd8/rd8}$	Focal retinal degeneration; 'rosette' formation; cones and rods present	3 weeks	6 weeks	12 weeks
Prph2$^{rd2/rd2}$	Mild retinal degeneration; rods die first	4 weeks	8 weeks	12 weeks
Pde6b$^{rd1/rd1}$	Early onset; severe retinal degeneration; rods die first	10 days	3 weeks	6-8 weeks
Targeted genetic mutations				
Rho$^{-/-}$	Moderate retinal degeneration; rods die first; lack of OS	4 weeks	6 weeks	10 weeks
Prph2$^{+/\Delta 307}$	Very slow progressive retinal degeneration	2 months	4 months	6 months
Nrl$^{-/-}$	Cone-like retina; 'rosette' formation	3 weeks	6 weeks	12 weeks
R9191; Nrl$^{-/-}$	Cone-like retina	3 weeks	6 weeks	12 weeks

Table 3.1 Summary of the different murine models with retinal phenotype and the stages of retinal degeneration studied.

3.2.1.1 Rate of photoreceptor degeneration

An indication of the rate of degeneration can be obtained by dividing the overall loss of ONL thickness by the number of days between early and late stage. In wild-type mice, ONL thickness is approximately 58 µm (± 7.8) at the early stage examined and stays stable over time (Table 3.2). Of the seven examined retinal phenotypes, the *Pde6b*$^{rd1/rd1}$ mouse demonstrates the most dramatic phenotype with photoreceptor degeneration starting as early as postnatal day (P) 10 (Carter-Dawson et al., 1978). Even though neurogenesis is not fully completed by this time, the number of cells is already reduced by ~20% in comparison to wild-type (Figure 3.1). By 3 weeks, the thickness of the ONL is lessened to only 15% of wild-type. At the latest examined stage, only sporadic cone nuclei are observed indicating that this model experiences an average loss of 3.4 µm per day from the ONL thickness (Table 3.2). In the *Rho*$^{-/-}$ mouse, by 6 weeks of age, the retina is already reduced to 50% of a wild-type and decreases to 20% by the age of 10 weeks (Figure 3.1) meaning that on average 0.5 µm of the ONL is lost per day (Table 3.2). The *Prph2*$^{rd2/rd2}$ model manifests a mild retinal phenotype of retinitis pigmentosa (RP), with the initial 36% loss in the ONL thickness to ~53% later on (Figure 3.1) which corresponds to an average loss of 0.44 µm per day (Table 3.2). Interestingly, two models that exhibit undulations of the ONL, commonly known as rosettes, the *Crb1*$^{rd8/rd8}$ and the *Nrl*$^{-/-}$ mouse, undergo a relatively small decrease in the ONL thickness of about 20% and 10% respectively (Figure 3.1) with an average loss between 0.016 and 0.12 µm per day respectively (Table 3.2). The cone-like retina of the *R91W; Nrl*$^{-/-}$ mutant shows little sign of photoreceptor degeneration with no major changes in the ONL thickness over time (Figure 3.1). *Prph2*$^{+/\Delta 307}$ mouse manifests a slow rate of degeneration with an initial reduction in the ONL thickness of ~20-25%, followed by almost 80% loss at 6 month of age (Figure 3.1).

Model	Early time point	Mid time point	Late time point
Wild-type	58.1±7.8	59.6±2.5	58.2±5.0
Crb1$^{rd8/rd8}$	48.1±14.2	46.9±3.0	47.9±6.5
Prph2$^{rd2/rd2}$	52.4±3.5	38.0±4.5	27.6±1.1
Pde6b$^{rd1/rd1}$	43.5±2.7	12.3±3.5	4.9±1.2
Rho$^{-/-}$	44.5±5.1	30.1±7.4	11.6±3.5
Prph2$^{+/\Delta 307}$	46.2±5.0	32.3±1.6	12.5±1.9
Nrl$^{-/-}$	54.2±5.8	±47.8±8.4	53.3±8.2
R9191; Nrl$^{-/-}$	64.5±6.9±	56.2±2.5	56.7±2.4

Table 3.2 The ONL thickness for each of the examined murine model at early, middle and late stage of retinal degeneration.

All the measurements are expressed in μm (±SD); n=3 animals examined per time point.

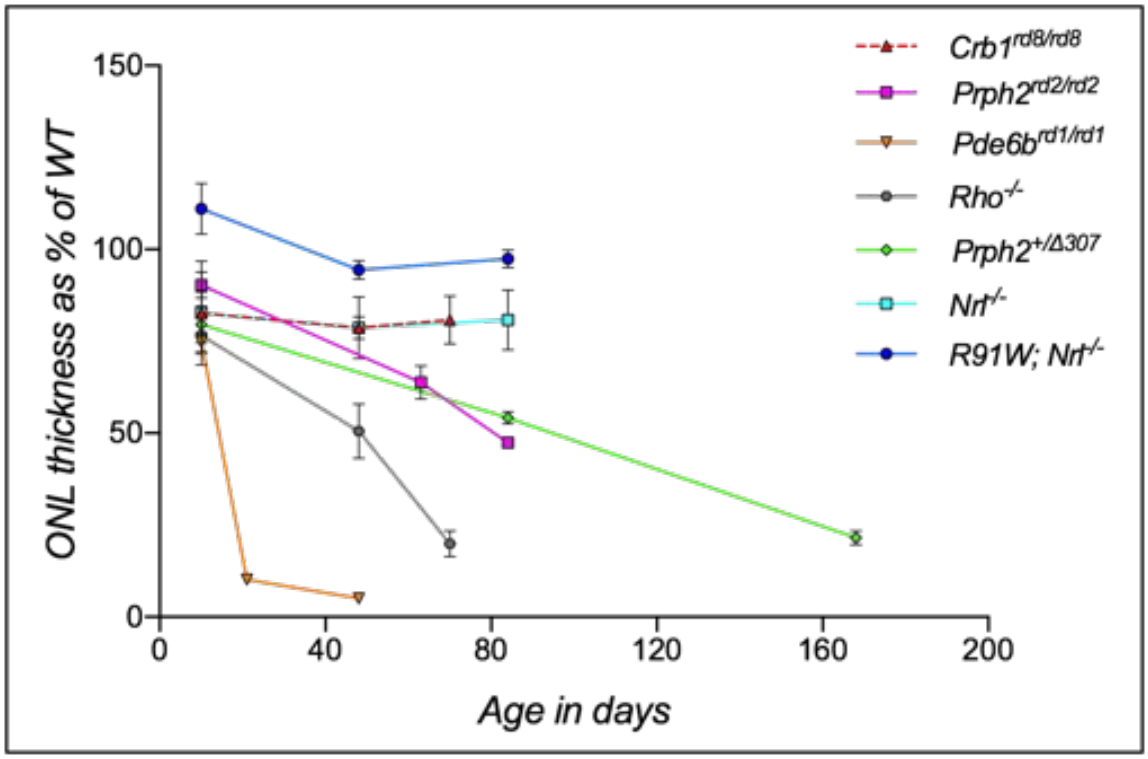

Figure 3.1 Rate of photoreceptor degeneration for each of the examined murine model expressed as a percentage of the wild-type ONL thickness.

Error bars, SD; n=3 animals examined per time point.

3.2.1.2 Impact of retinal degeneration on ONL cell density

Next, we sought to determine the impact of photoreceptor cell loss on cell density within the ONL. The comparison of the average cell density within the ONL showed that each of the examined models, including wild-type, undergoes some nuclei loss over time (Figure 3.2A). In *Prph2*$^{rd2/rd2}$ animals, changes in cell density were small and resembled that observed in the control mice. A marked reduction in nuclei density was observed in several mutants, including *Pde6b*$^{rd1/rd1}$ and *Prph2*$^{+/\Delta 307}$ animals. This was particularly evident at the latest examined stage. *Nrl*$^{-/-}$ and *R91W;Nrl*$^{-/-}$ models, which are notable for their cone-like retinae, exhibited a very similar and statistically significant reduction in ONL cell density over time for both mid and late stages. Interestingly, a small initial increase in cell density with degeneration was observed in *Crb1*$^{rd8/rd8}$ and *Rho*$^{-/-}$ mutants, which then followed a predicted decrease. These differences seen in the cell density may reflect the alterations in cell morphology and size of the photoreceptor nuclei as the course of a disease progresses. As the photoreceptors fail to function normally and start to die, their nuclei undergo significant changes that may lead to their shrinkage or bulging.

In the next instance, changes to the number of photoreceptor rows were assessed. In the adult wild-type retina there are on average 12.9 (±0.9) cell rows in the ONL, which then decreases to 11.6 (±0.5) with time (Figure 3.2B). This loss is associated with a normal ageing process as the oldest animals that we examined were 1 year of age. A similar decrease was observed in *Crb1*$^{rd8/rd8}$ mutants, where the number of photoreceptor rows dropped from 13 (±0.9) at the early stage to 11.4 (±0.5) at the late stage. In the *Nrl*$^{-/-}$ and *R91W;Nrl*$^{-/-}$ mice there were, on average, 9.4 (±2.1) and 10.8 (±0.7) cell rows, respectively; each was further reduced by approximately two rows over the time frame examined. The animal models that displayed mild and moderate rate of degeneration, including the *Rho*$^{-/-}$, *Prph2*$^{rd2/rd2}$ and *Prph2*$^{+/\Delta 307}$ have a decreased number of cell rows, about 10, compared to wild-type, even at the earliest stages examined here, which then decrease markedly as photoreceptors die leaving between 2-5 rows by the latest stage examined. The *Pde6b*$^{rd1/rd1}$ mutant, which undergoes a very rapid cell loss, already shows a noticeable reduction in row numbers (8.6 (±0.7) cell rows) even at P10. These reduced rapidly, to about 1.6 (±0.5) at 3 weeks of age and 0.8 (±0.4) at the latest examined age.

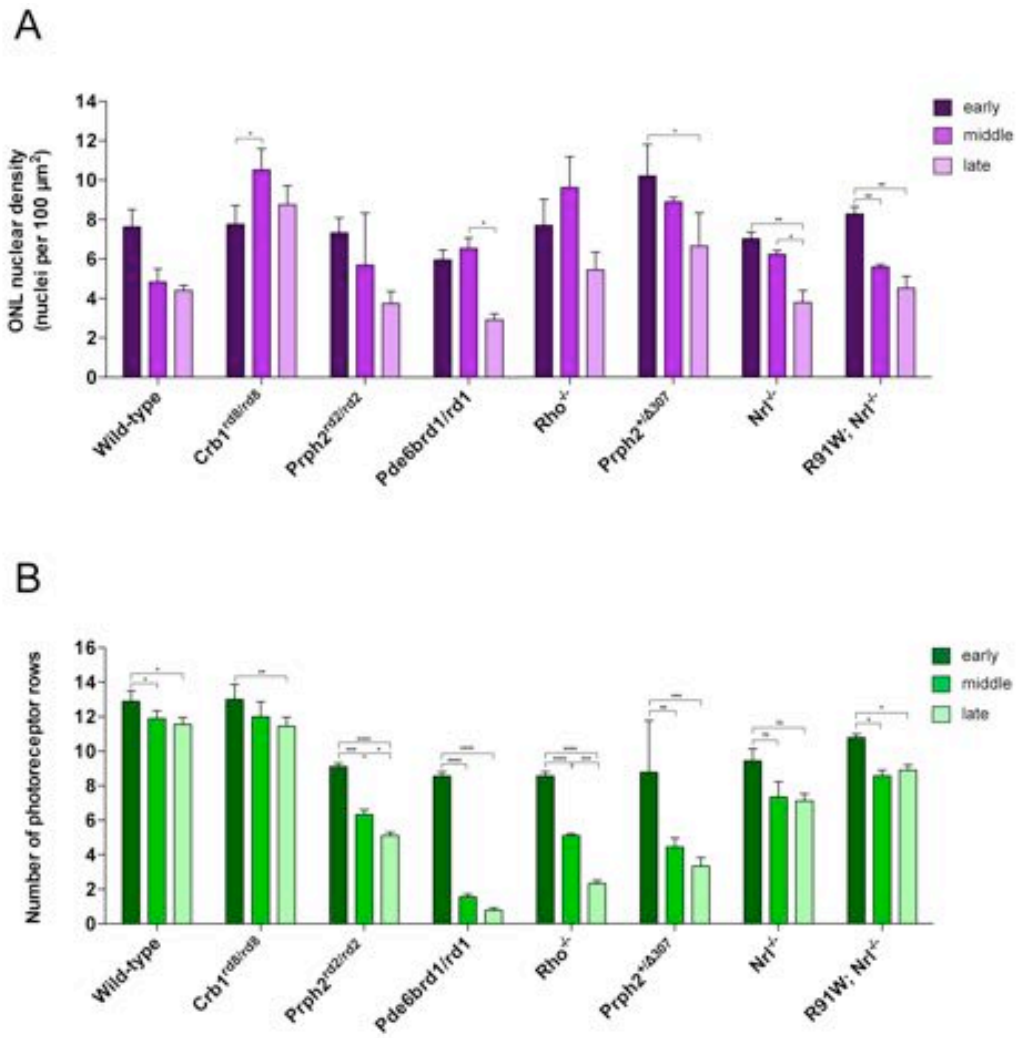

Figure 3.2 Changes in ONL cell density and photoreceptor row numbers at the early (dark purple), mid (purple) and late (pink) stages of a disease for all examined models.

A) ONL nuclear cell density expressed as a number of nuclei per 100 µm, and **B)** number of photoreceptor rows counted per each of the examined model per every time point. Statistical significance was assessed using one-way ANOVA with Tukey's corrections for multiple comparisons; **P* < 0.05, ***P* < 0.01, ****P* < 0.001, *****P* < 0.0001. Error bars: SEM; n=3 animals examined per time point.

3.2.2 Development of a glial scar in different models over disease progression

3.2.2.1 Alterations in IF protein levels

As mentioned before, progressive retinal degeneration is frequently associated with development of gliosis. Here, immunohistochemistry (IHC) and Western Blot (WB) analysis were used to perform qualitative and semi-quantitative assessments of regional changes in the levels of IF proteins GFAP and Vimentin. There are reports showing that a given disease type may lead to some geographical differences; for example, the inferior region may manifest a faster rate of photoreceptor degeneration (LaVail and Battelle, 1975; LaVail et al., 1992; García-Fernández et al., 1995; LaVail et al., 1997; Lin et al., 2009). Therefore, in each model, both the superior and inferior retina were examined at the anterior margin, equatorial region and the posterior retina immediately adjacent to the optic nerve (positions indicated in schematics on each figure). Main figures show representative examples of staining at the equatorial region for each model at early, mid and late-stage degeneration. Full representation of all regions examined in each of the models is shown in Appendix A-Y. Changes in global protein levels were assessed with WB of whole neural retina.

A primary objective of studying protein expression is to define the patterns that could allow the distinction between normal and pathological conditions. In many studies, especially those involving WB analysis, the protein of interest is usually compared against the levels of 'housekeeping' proteins. However, there is a growing body of evidence to illustrate the variability in the expression of commonly used internal standards between different tissues and diseased states (Blanquicett et al., 2002; Ferguson et al., 2005). For example, in models such as *Pde6b*$^{rd1/rd1}$ the death of photoreceptors occurs very rapidly, which may lead to significant changes in gene expression, including housekeeping genes; therefore, an appropriate control marker for WB analysis is needed. To address this issue, three independent markers were examined to determine which is least affected by retinal degeneration. They were Histone2-B (H2B) and two markers of the (largely unaffected) ganglion cells, Neurofilament 68 (NF-68) and Brain-3b (Brn3b). These markers were tested in the *Pde6b*$^{rd1/rd1}$ model at different disease stages, as well as in age-matched wild-type controls. Previous reports showed that despite the axonal arborisation during the period of rod and cone death, cells within the inner nuclear layer (INL) and ganglion cell layer (GCL) survive in significant numbers (Grüter et al., 2005; Punzo and Cepko, 2007; Mazzoni et al., 2008). Although, no major changes to these cell types were observed, the levels of Brn3b and NL-68 proteins did vary between different ages even in wild-type (Figure 3.3). These inconsistencies in the protein expression could be

explained by the fact that both Brn3b and NL-68 are markedly up-regulated during axonal growth and stabilisation of the neuronal connections respectively. Moreover, photoreceptor death causes alterations in the dendritic arbors of the neuronal cells. A study by Punzo and Cepko (2007) argued that retinal remodelling, especially in the *Pde6b*$^{rd1/rd1}$ mutant, may lead to changes in gene expression in all retinal cell types as the retina tries to adapt to the new environment (Punzo and Cepko, 2007). These findings could explain the significant variations in Brn3b and NF-68 levels between different disease stages in the *Pde6b*$^{rd1/rd1}$ samples (Figure 3.3B). Interestingly, H2B levels remained broadly constant across all examined time points in both animal models in comparison to NF-68 and Brn3b (Figure 3.3).

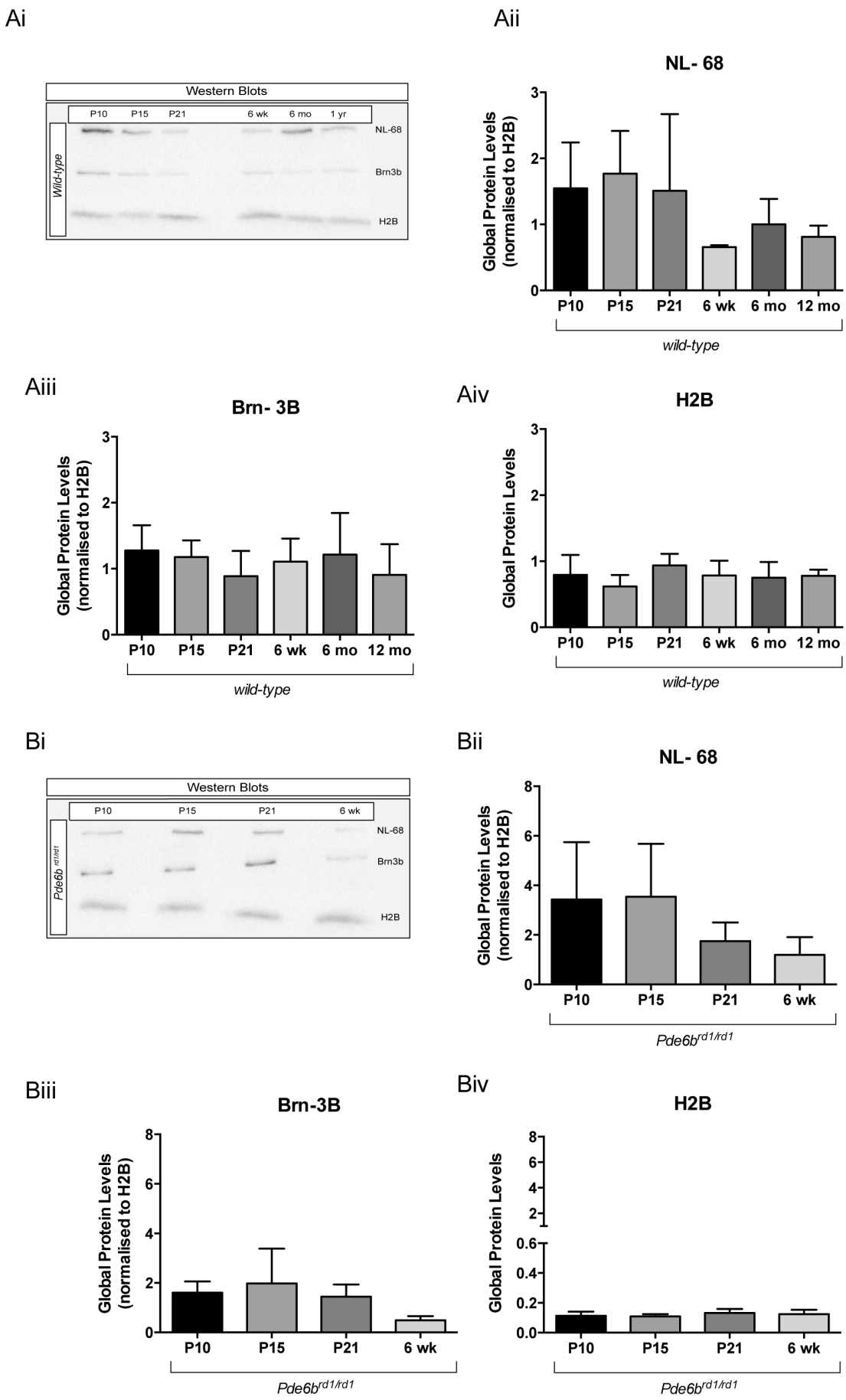

Figure 3.3 Comparisons of the three protein markers for semi-quantitative WB analysis in a wild-type and Pde6b$^{rd1/rd1}$ mutant across four different time points.

Ai-iii) Protein levels in a wild-type (*Ai* NL-68, *Aii* Brn3b and *Aiii* H2B). **Bi-iii)** Protein levels in *Pde6b*$^{rd1/rd1}$ retinae (*Bi* NL-68, *Bii* Brn3b and *Biii* H2B). All the samples were normalised to H2B levels at 3 weeks as a reference point for protein expression. Statistical significance was assessed using one-way ANOVA with Tukey's corrections for multiple comparisons. No statistical differences were assessed. Error bars, SEM; n=3 animals examined per time point.

C57Bl/6J wild-type mice were used as background-matched (either wholly or partially) non-degenerating controls. As expected, there was little evidence of GFAP expression in either the inferior or superior wild-type retina at 6 weeks of age and this did not change significantly with time (Figure 3.4A i-vi; Appendix A). GFAP^{+ve} processes within the retina were largely restricted to astrocytes at the inner retinal margin, adjacent to the ganglion cell layer (GCL). Some GFAP^{+ve} basal processes of Müller glia were also observed; these were mostly restricted within the anterior margin of the retina and there were no appreciable differences between the inferior and superior retina. WB analysis revealed no significant change in global GFAP across the three ages examined (Figure 3.4A vii). In contrast, robust levels of Vimentin were observed in both the superior and inferior retina (Figure 3.6A i-vi; Appendix B). Vimentin^{+ve} Müller glial fibres could be seen extending up into the inner nuclear layer (INL) as far as the outer plexiform layer (OPL) at all ages examined. Interestingly, this appeared to increase with age. Similarly, WB analysis also indicated a trend of increasing global levels of Vimentin over time, although this was not statistically significant (Figure 3.6A vii).

Degeneration occurs in a focal manner in the *Crb1*$^{rd8/rd8}$ mouse (Mehalow et al., 2003; van de Pavert et al., 2004; Barber et al., 2013). Interestingly, the undulations of the ONL that have been previously reported in the inferior nasal quadrant of the fundus in these mice were also seen in the superior posterior part of the retina (Appendix D). Similar to the wild-type mouse, only very few GFAP^{+ve} processes were observed in the retina at early and mid-stage disease with the majority restricted to the anterior margins of the retina (Figure 3.4B i, ii, iv, v). However, at the latest stage examined, many more Müller glial fibres contained GFAP and GFAP^{+ve} filaments extended into the apical processes within the ONL (Figure 3.4B iii, vi). Such patterns of GFAP localisation were typical around sites of rosette formation, which were most numerous in the posterior retina (Appendix D; arrows). These changes were mirrored by a statistically significant increase in global GFAP (Figure 3.4B vii). In contrast, significant levels of Vimentin were observed throughout the retina at the earliest stages examined and this was maintained as degeneration progressed (Figure 3.6B i-vi; Appendix E). A qualitative assessment of Vimentin staining indicates that the level was higher in *Crb1*$^{rd8/rd8}$ retinae than in wild-type retinae at all stages examined. Analysis of global Vimentin by WB also indicated a small increase in protein levels at the latest time point examined, although this was not statistically significant (Figure 3.6B vii).

When assessing the microenvironment of *Prph2*$^{rd2/rd2}$ mice using IHC, we observed markedly higher levels of GFAP at all-time points examined, compared to wild-type (Figure 3.4C i-vi; Appendix G). Even at the earliest stage examined (4 weeks), when the ONL is of similar thickness to wild-type, GFAP^{+ve} processes were observed extending throughout the retina towards the OPL. By 12 weeks, glial GFAP^{+ve}

processes expanded throughout the ONL, with many extending beyond the limits of the ONL and intertwining along the outer edge of the neuroretina. These changes were confirmed using WB as a significant upregulation of GFAP over time was noted (Figure 3.4C vii). IHC analysis of Vimentin also showed an increase with time (Figure 3.6C i-vi; Appendix H). A global increase in Vimentin levels was also observed at the later stages of degeneration, in comparison to levels at the first assessed time point (Figure 3.6C vii).

In the *Pde6b*$^{rd1/rd1}$ mouse, IHC indicated a bimodal pattern for GFAP, with levels being particularly strong at the middle stage, but decreasing thereafter. At the earliest time point examined, P10, the retina is still undergoing neurogenesis. GFAP staining was similar to that seen in adult wild-type retinae and was restricted to a few basal processes only (Figure 3.4D i, iv; Appendix J). However, from as early as P15 (Appendix L) onwards the vast majority of Müller cells contained GFAP and protein expression extended throughout the thickness of the retina into the apical processes (Figure 3.4D ii, v). Notably, by very late stage degeneration, when the ONL is reduced to a single layer of cone photoreceptors (6 weeks), GFAP was much reduced, particularly around the remaining ONL (Figure 3.4D iii, vi; Appendix J). WB analysis also revealed a statistically significant upregulation of global GFAP levels between early and mid-degeneration although the decrease seen by IHC in very late degeneration was not reflected at the global level (Figure 3.4D vii). Surprisingly, and in contrast to the other models of degeneration, Vimentin levels appeared to remain fairly low in the *Pde6b*$^{rd1/rd1}$ mouse throughout degeneration with Vimentin^{+ve} processes largely being restricted to the inner retina. As degeneration Vimentin^{+ve} processes started to project into the remaining ONL (Figure 3.6D i-vi; Appendix K). A statistically significant increase in global Vimentin levels was observed between the early and latest time points examined.

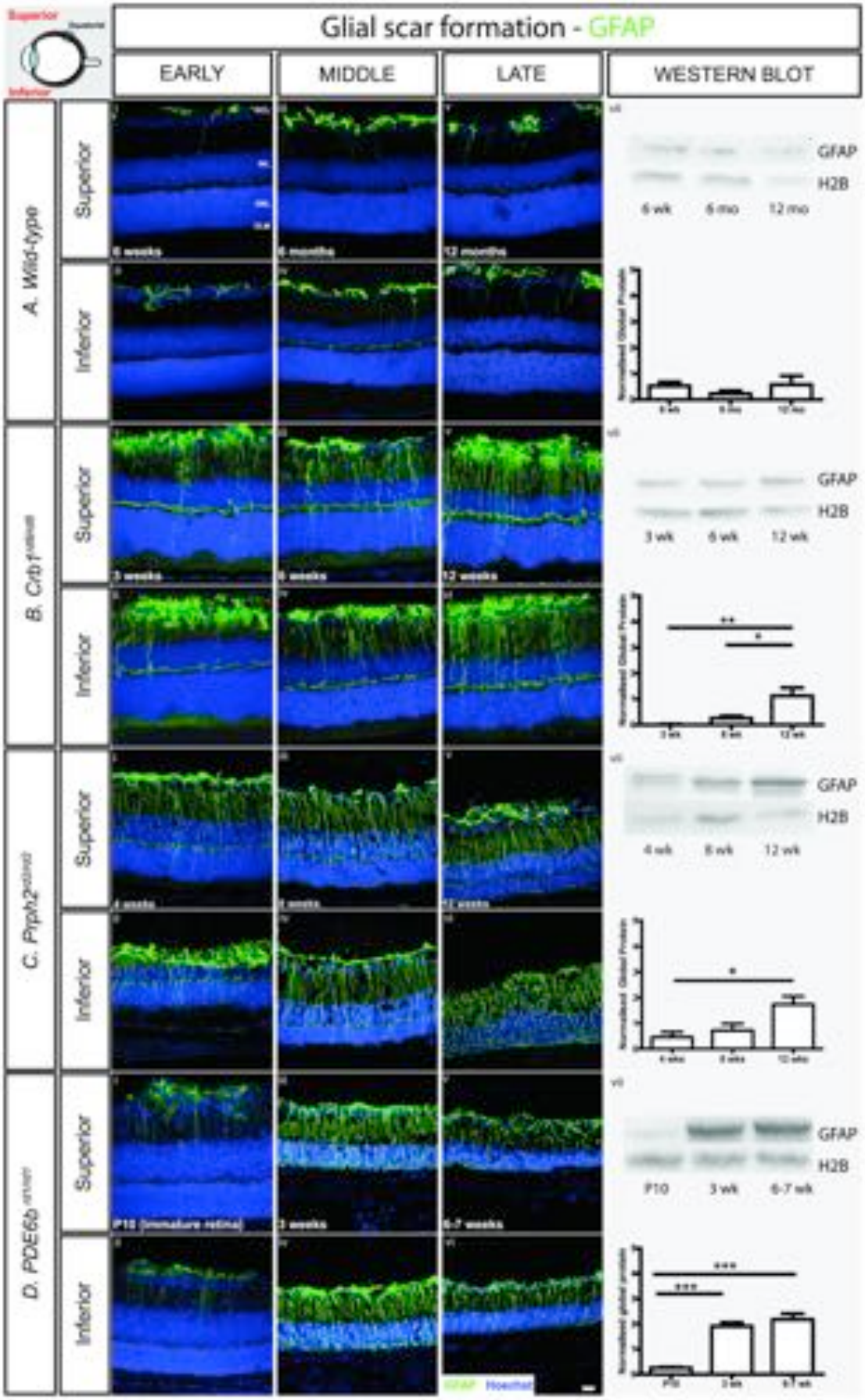

Figure 3.4 GFAP expression in the animal models carrying a spontaneous mutation.

Ai-vii) *C57Bl/6J* wild-type; **Bi-vii)** *Crb1*$^{rd8/rd8}$; **Ci-vii)** *Prph2*$^{rd2/rd2}$; **Di-vii)** *Pde6b*$^{rd1/rd1}$. Cryosections were immunostained for GFAP (*green*) and counterstained with nuclei marker Hoechst 33342 (*blue*). Semi-quantitative assessments of GFAP levels in whole neural retina were determined by Western blot. GFAP was normalized against H2B. Statistical significance was assessed with a one-way ANOVA test with Tukey's correction for multiple comparisons; $*P < 0.05$, $**P < 0.01$, and $***P < 0.001$. Error bars, SEM; n=3 animals examined per time point.

GCL, ganglion cell layer; IPL, inner plexiform layer; INL, inner nuclear layer; OPL, outer plexiform layer; ONL, outer nuclear layer; IS/OS, photoreceptor inner/outer segment region. Scale bar, 25 μm.

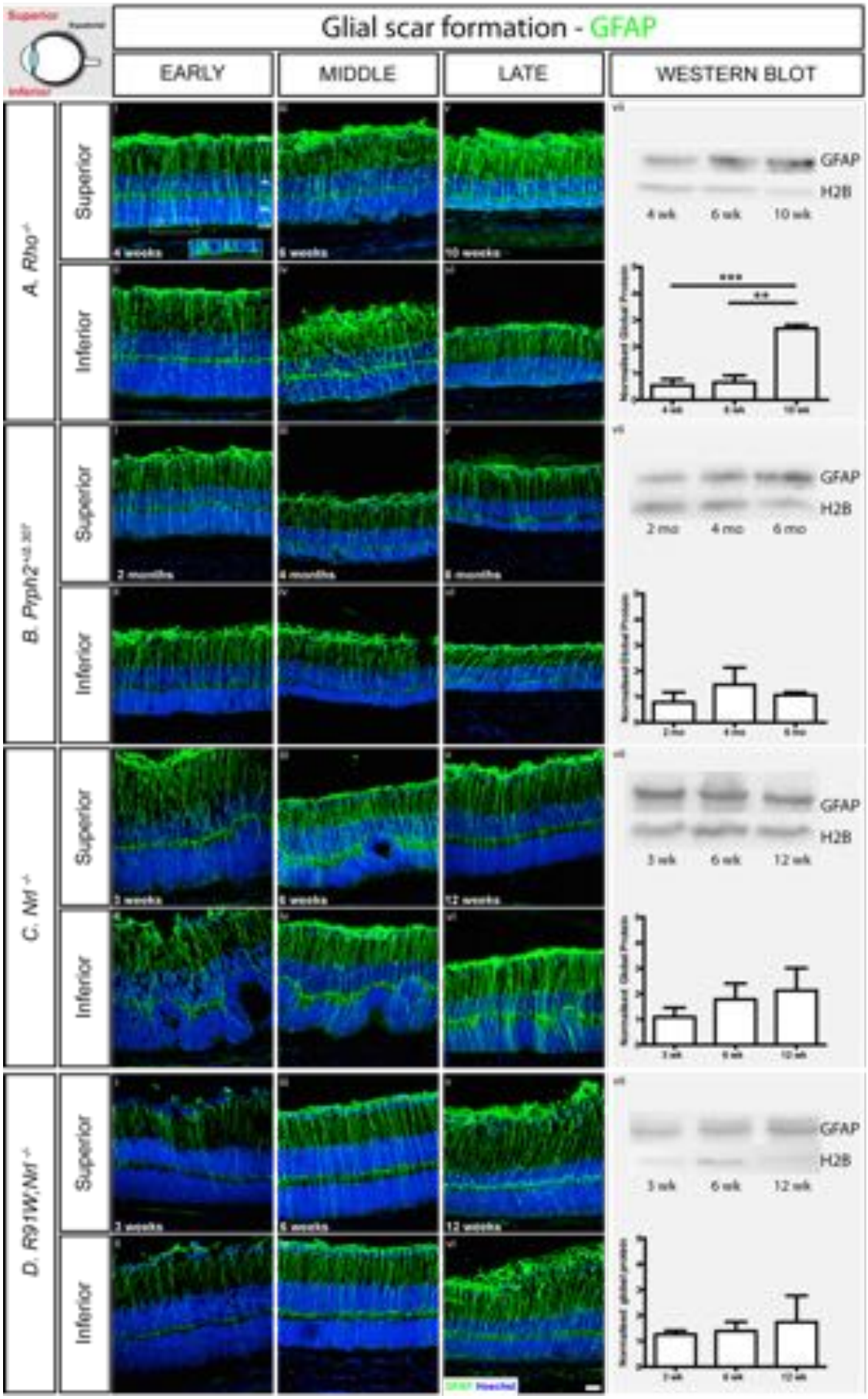

Figure 3.5 GFAP expression in animals carrying a targeted genetic mutation.

Ai-vii) *Rho*$^{-/-}$; **Bi-vii)** *Prph2*$^{+/\Delta 307}$; **Ci-vii)** *Nrl*$^{-/-}$ **Di-vii)** *R91W;Nrl*$^{-/-}$. Cryosections were immunostained for GFAP (*green*) and counterstained with nuclei marker Hoechst 33342 (*blue*). Semi-quantitative assessments of GFAP levels in whole neural retina were determined by Western blot. GFAP was normalized against H2B. Statistical significance was assessed with a one-way ANOVA test with Tukey's correction for multiple comparisons; $^{**}P < 0.01$, and $^{***}P < 0.001$. Error bars, SEM; n= animals examined per time point.

GCL, ganglion cell layer; IPL, inner plexiform layer; INL, inner nuclear layer; OPL, outer plexiform layer; ONL, outer nuclear layer; IS/OS, photoreceptor inner/outer segment region. Scale bar, 25 μm.

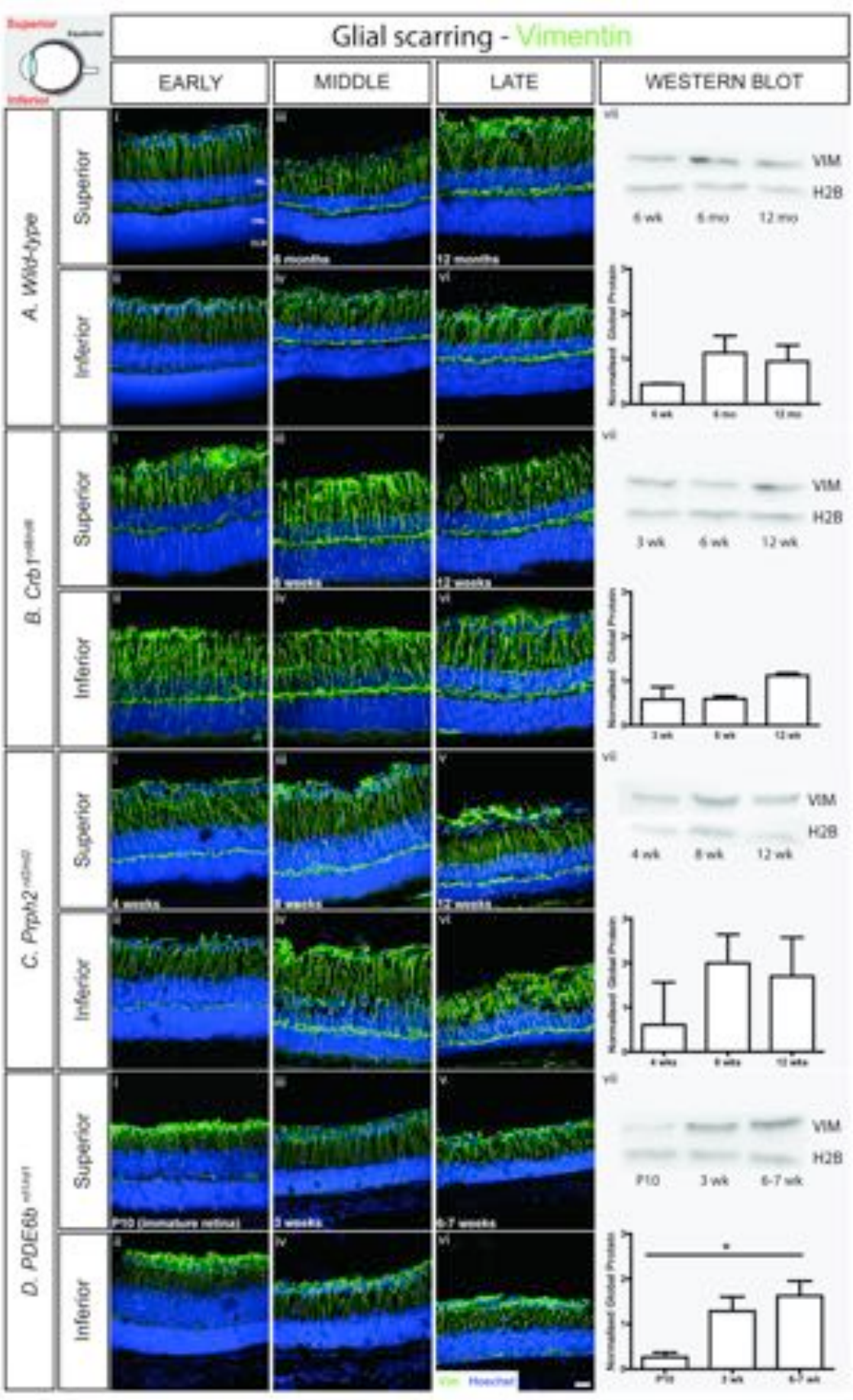

Figure. 3.6 Vimentin expression in the animal models carrying a spontaneous mutation.

Ai-vii) *C57Bl/6J* wild-type; **Bi-vii)** *Crb1*$^{rd8/rd8}$; **Ci-vii)** *Prph2*$^{rd2/rd2}$; **Di-vii)** *Pde6b*$^{rd1/rd1}$. Cryosections were immunostained for Vimentin (*green*) and counterstained with nuclei marker Hoechst 33342 (*blue*). Semi-quantitative assessments of Vimentin levels in whole neural retina were determined by Western blot. Vimentin was normalized against H2B. Statistical significance was assessed with a one-way ANOVA test with Tukey's correction for multiple comparisons; $*P < 0.05$. Error bars, SEM; n= animals examined per time point.

GCL, ganglion cell layer; IPL, inner plexiform layer; INL, inner nuclear layer; OPL, outer plexiform layer; ONL, outer nuclear layer; IS/OS, photoreceptor inner/outer segment region. Scale bar, 25 μm.

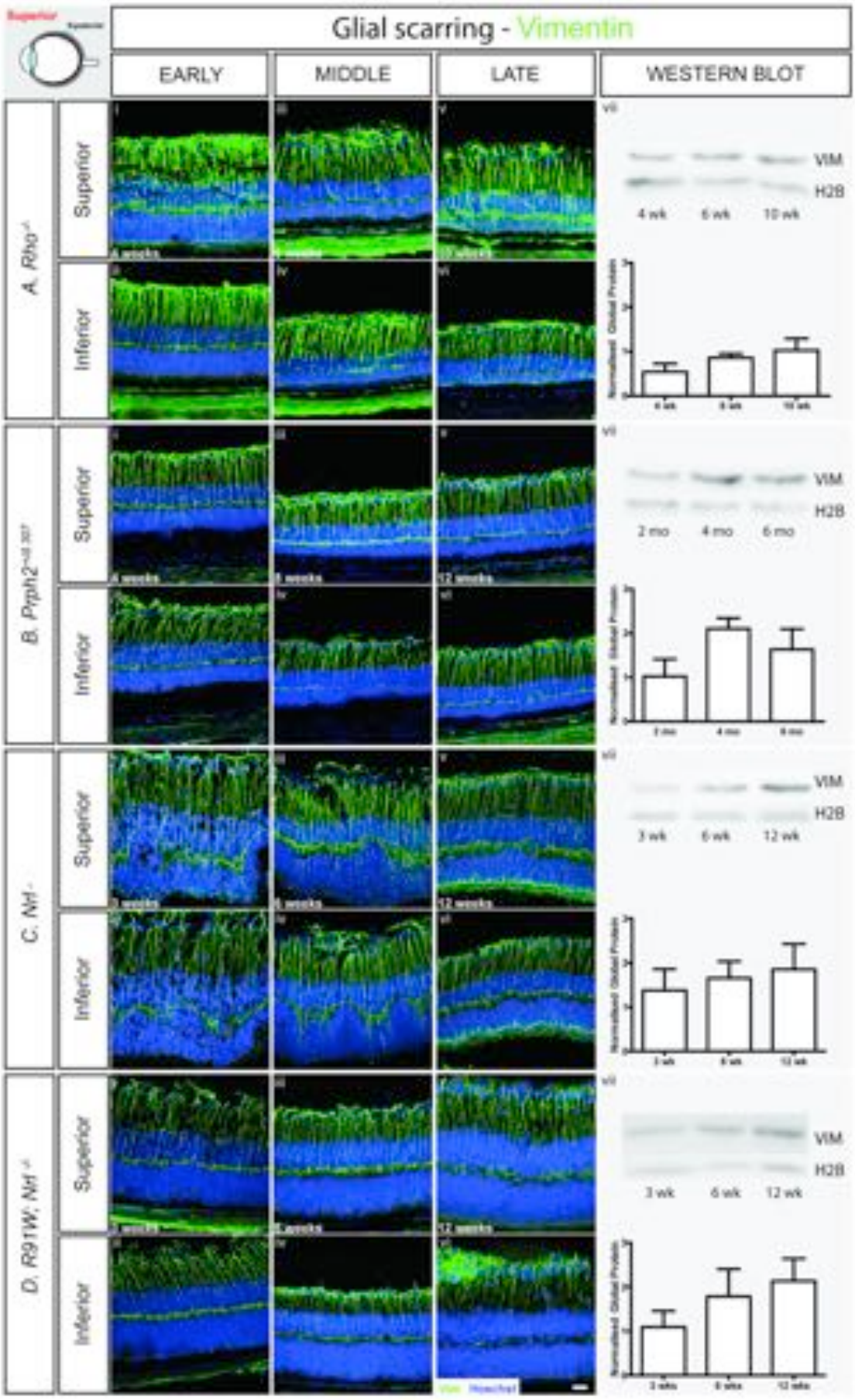

Figure 3.7 Vimentin expression in animals carrying a targeted genetic mutation.

Ai-vii) *Rho*$^{-/-}$; **Bi-vii)** *Prph2*$^{+/\Delta 307}$; **Ci-vii)** *Nrl*$^{-/-}$ **Di-vii)** *R91W;Nrl*$^{-/-}$. Cryosections were immunostained for Vimentin (*green*) and counterstained with nuclei marker Hoechst 33342 (*blue*). Semi-quantitative assessments of Vimentin levels in whole neural retina were determined by Western blot. Vimentin was normalized against H2B. Statistical significance was assessed with a one-way ANOVA test with Tukey's correction for multiple comparisons. Error bars, SEM; n=3 animals examined per time point.

GCL, ganglion cell layer; IPL, inner plexiform layer; INL, inner nuclear layer; OPL, outer plexiform layer; ONL, outer nuclear layer; IS/OS, photoreceptor inner/outer segment region. Scale bar, 25 μm.

Of all the models examined, the *Rho*$^{-/-}$ mouse presented the most marked upregulation of expression of IFs. IHC for GFAP showed a significant increase in protein levels as degeneration progressed. Even at the earliest stage examined, the vast majority of Müller glia contained GFAP throughout both basal and apical processes. Moreover, GFAP^{+ve} apical processes were observed extending to the outer edges of the retina and there was evidence of hypertrophy, with processes extending along the outer edge of the retina (Figure 3.5A i). This pattern of GFAP localisation was seen at all stages examined (Figure 3.5A ii, iii, v, vi; Appendix N). Interestingly, both basal and apical Müller glial processes appeared thicker compared to other models, although further histological analysis would be required to confirm whether this reflects a true morphological change or simply reflects the high levels of GFAP within any given process. WB revealed a statistically significant increase in global GFAP levels between early and late stage disease (Figure 3.5A vii). Vimentin levels also increased with age and degeneration, although staining of the apical processes was not as strong as that of GFAP, at least at the earlier time points. As for GFAP, Vimentin^{+ve} processes appeared thicker compared to wild-type (Figure 3.7A i-vi; Appendix O). A trend of global Vimentin levels increasing with disease progression was noted, although this was not statistically significant (Figure 3.7A vii).

When assessing the microenvironment of *Prph2*$^{+/\Delta 307}$ mice using IHC, markedly higher levels of GFAP were noticed at all time points examined, compared to wild-type (Figure 3.5B i-vi). Even at the earliest stage examined (2 months), when the ONL is of similar thickness to wild-type, GFAP^{+ve} processes were observed extending throughout the retina to the outer edges of the ONL. Strikingly, however, although there was no significant decrease in global GFAP levels with degeneration as assessed by WB (Figure 3.5B vii), IHC revealed that while the basal processes of the Müller glia continue to stain for GFAP, there was a consistent and marked reduction of GFAP in the apical processes over time (Figure 3.5B i-vi; Appendix Q). IHC analysis of Vimentin showed a pattern similar to wild-type with time, although overall levels were qualitatively higher at all stages examined, particularly in the basal processes (Figure 3.7B i-vi; Appendix R). WB revealed a slight increase in global Vimentin levels at the latest stages examined compared to early stage of degeneration (Figure 3.5B vii).

The *Nrl*$^{-/-}$ mutant presented a marked upregulation in IFs from the earliest examined time-point with a gradual progression in a thickening of GFAP^{+ve} processes over time (Figure 3.5C i-vi). Even at the earliest stage examined, the vast majority of Müller glia stained for GFAP with many of them extending throughout the apical surface. Surprisingly, the GFAP^{+ve} glial processes were absent around sites of rosette formation, which were present in both superior and inferior regions of a retina (Appendix T; arrows). Upregulation in GFAP was also evident, as assessed by WB

analysis, with much higher protein levels in comparison to wild-type (Figure 3.5C vii). No striking differences in Vimentin staining were observed between the examined ages (Figure 3.7C i-vi); however a noticeable band of Vimentin^{+ve} processes was noticed at the outer edge of the photoreceptor layer especially at the the latest examined time point compared to wild-type or any other examined phenotype (Figure 3.7C v-vi; Appendix U). A small trend of global Vimentin levels increasing with disease progression was noted, although this was not statistically significant (Figure 3.7C vii).

The *R91W;Nrl*$^{-/-}$ mouse is a relatively new genetically engineered murine model designed for the study of the mechanisms of cone specific degenerations (Samardzija et al., 2014). As there is only one study that used this mutant, a comprehensive assessment of these animals was carried out as part of this project. The *R91W;Nrl*$^{-/-}$ phenotype has a functioning all-cone retina, which manifests with a very slow rate of degeneration. In comparison to the *Nrl*$^{-/-}$ model, it expresses a hypomorphic *Rpe65* allele (R91W), which appears to prevent the development of rosettes (Samardzija et al., 2014). Although the maximum retinal thickness is similar to the wild-type and the rate of photoreceptor loss is minimal, this model presents with a significant Müller glia cell reactivity, as shown with GFAP staining (Figure 3.5D; Appendix W). IHC indicated that GFAP^{+ve} processes were seen as early as 3 weeks of age, with a gradual increase in their number over time. Interestingly, with time more GFAP^{+ve} processes extended towards the ONL (Figure 3.5D iii-vi). Global levels of GFAP also increased over time, as assessed by WB, although these changes were not statistically significant (Figure 3.6D vii). This is in contrast to previously reported findings, which showed no GFAP^{+ve} glial processes other than those observed in astrocytes at the GCL level (Samardzija et al., 2014). To examine these apparently contradictory results, a further analysis was performed using the same IHC protocol, including GFAP antibody, as that reported in the Samardzija *et al.* study. In parallel, the antibody was tested with antigen retrieval pre-treatment, as suggested by the manufacturer (Sigma Aldrich, UK). Using the same IHC protocol, no GFAP staining was observed at 6 weeks of age in *R91W;Nrl*$^{-/-}$ apart from a thin layer at the GCL (Figure 3.8A). In comparison, a section from the same eye, but pre-treated with antigen retrieval, revealed a positive GFAP staining of the Müller glia processes (Figure 3.8B) similar to those presented in Figure 3.5D. Although Grimm's group did report an upregulation in *Gfap* mRNA levels with progressive degeneration, which corresponds with our WB analysis, they did not show this data in the paper (Samardzija et al., 2014). As for Vimentin, a qualitative assessment using IHC showed no major differences between the *R91W;Nrl*$^{-/-}$ mutant and wild-type controls (Figure 3.7D i-vi; Appendix X). Although, a gradual upregulation in global protein levels was noticed, no significant differences between the examined ages were observed (Figure 3.7D vii).

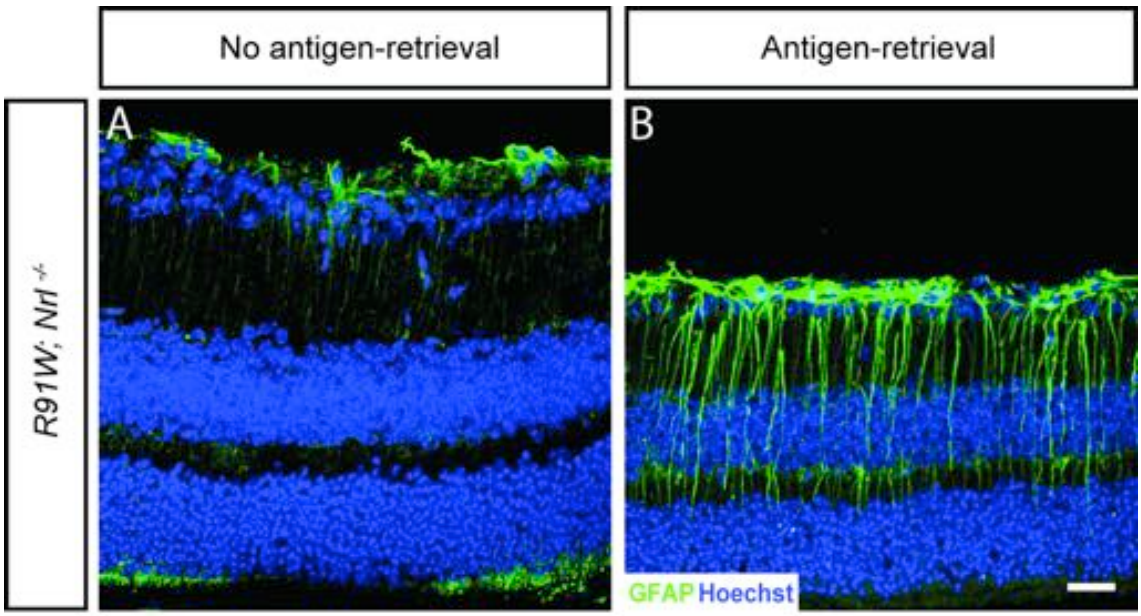

Figure 3.8 Differences in the GFAP staining in R91W;Nrl$^{-/-}$ mutant.

Images of the *R91W;Nrl*$^{-/-}$ retina (6 week old) stained with GFAP antibody (Sigma Aldrich, UK) **A)** without and **B)** with antigen retrieval treatment. Cryosections were immunostained for GFAP (*green*) and counterstained with nuclei marker Hoechst 33342 (*blue*). Scale bar, 25 µm.

3.2.2.2 Changes in CSPG levels with degeneration

In the CNS, glial cell reactivity is accompanied by changes in the deposition of CSPGs (reviewed in (Sharma et al., 2012a)). In this study, the CS-56 antibody was used for both IHC and WB to assess whether there were any global alterations in these proteins with degeneration. This is a well-characterised antibody, which targets a large panel of CSPGs (Inatani and Tanihara, 2002; Escher et al., 2008; Bringmann et al., 2009a), providing an overview of CSPG deposition. In wild-type retinae, CSPGs were sparsely distributed throughout the photoreceptor inner/outer segment (IS/OS) region and inner plexiform layer (IPL), with much higher levels, exhibited as dense staining, in the OPL and in the GCL at all-time points examined (Figure 3.9A i-vi; Appendix C). No consistent differences were observed in the pattern of CSPG level between the superior and inferior retina. A gradual increase in CS-56 staining was observed with age and was particularly noticeable within the IS/OS region. This was mirrored by a statistically significant increase in global CSPG levels with age, as assessed by WB (Figure 3.9A vii).

A qualitative assessment of IHC in the *Crb1*$^{rd8/rd8}$ mouse indicated that CSPG deposition, as assessed by CS-56 staining, appeared to be reduced compared to that seen in the wild-type retina. Protein was most noticeable at the outer edge of the ONL in the IS/OS region (Figure 3.9B i-vi), and around sites of presumptive rosette formation (see posterior retina in Appendix F; arrows). Notably, and in contrast to the wild-type retina, staining for CSPG in the GCL was largely restricted to the posterior retina with very little labelling in equatorial and anterior regions of the retina (Appendix F). There were no noticeable differences in the CSPG levels between superior and inferior regions of the retina. WB analysis revealed a trend for increasing global CSPG with age, which correlates with the increase in GFAP and Vimentin (Figure 3.4B and Figure 3.6B), although this was not statistically significant.

In *Prph2*$^{rd2/rd2}$ mutants, CS-56 staining was evident in the IS/OS region and the GCL (Figure 3.9C i-vi, Appendix I), although appeared more intense in the IS/OS region. Staining presented as a thin band abutting the ONL indicating a more dense deposition of CSPGs, compared to wild-type, at 3 weeks, the earliest examined time point (Figure 3.9C i-ii). As degeneration progressed, the intensity and size of the CS-56 band at the IS/OS region gradually decreased. These reductions were also reflected in the global levels of CSPGs, as examined by WB, with a marked reduction by 12 weeks (Figure 3.9C vii).

In the *Pde6b*$^{rd1/rd1}$ mice at P10, a thin band of CSPGs was observed at the outer margin of the ONL with some sating at the GCL level (Figure 3.9D i, iv; Appendix M). By mid-stage degeneration, CSPGs were seen throughout the remaining ONL, extending into

the OPL and IPL, before decreasing at very late stages of degeneration (Figure 3.9D ii, iii, v, vi; Appendix M). Notably, CSPG deposition was also significantly reduced in the inner retina, with little CS-56 staining in the astrocyte layer. These changes were mirrored by a significant reduction in global CSPG levels over time (Figure 3.9D vii).

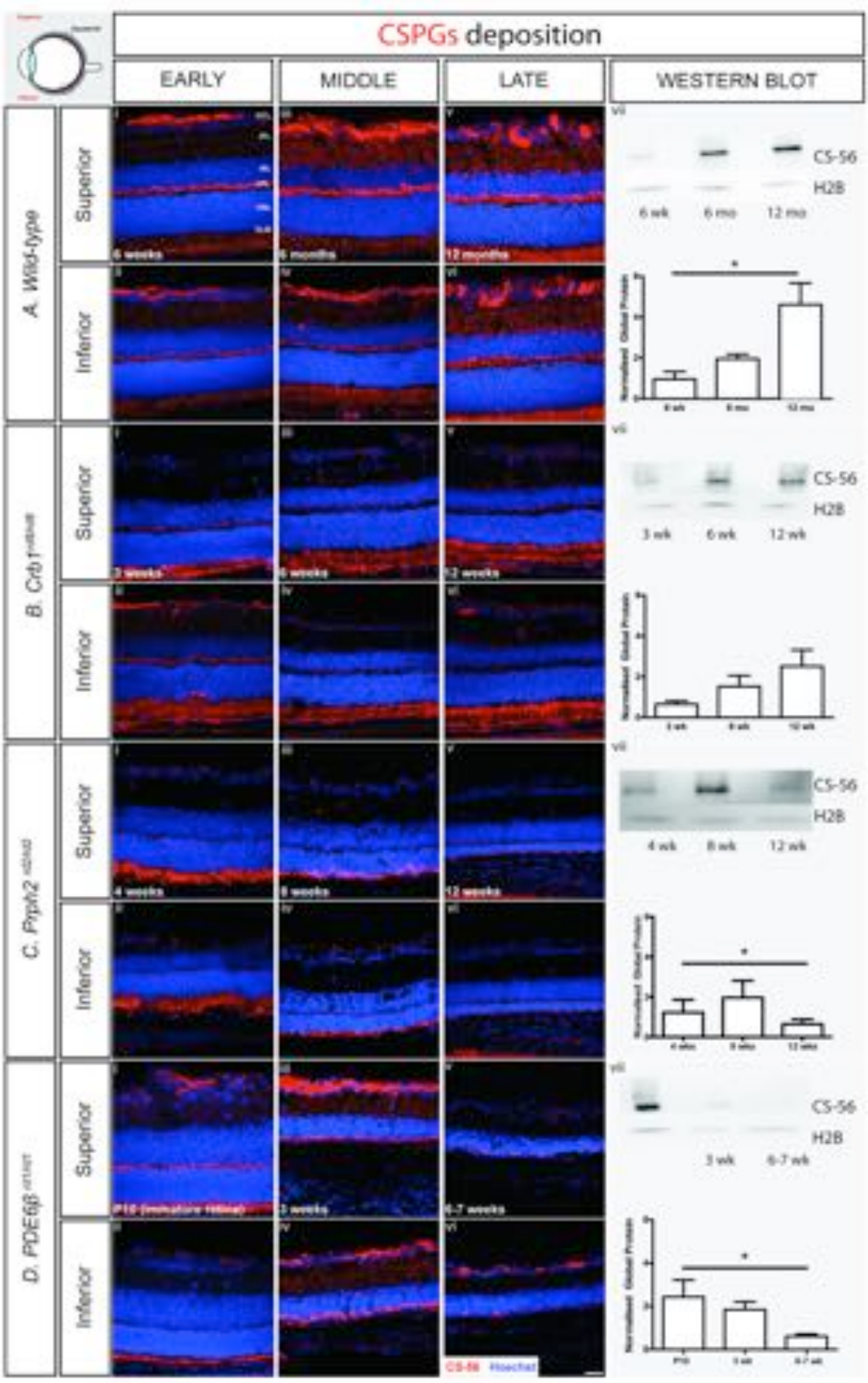

Figure 3.9 CSPG deposition in the naturally occurring mutants.

Ai-vii) *C57Bl/6J* wild-type; **Bi-vii)** *Crb1*$^{rd8/rd8}$; **Ci-vii)** *Prph2*$^{rd2/rd2}$; **Di-vii)** *Pde6b*$^{rd1/rd1}$. Cryosections were immunostained for CS-56 (*red*) and counterstained with nuclei marker Hoechst 33342 (*blue*). Semi-quantitative assessments of CSPGs levels in whole neural retina were determined by Western blot. CSPGs were normalized against H2B. Statistical significance was assessed with a one-way ANOVA test with Tukey's correction for multiple comparisons; $*P < 0.05$. Error bars, SEM; n=3 animals examined per time point.

GCL, ganglion cell layer; IPL, inner plexiform layer; INL, inner nuclear layer; OPL, outer plexiform layer; ONL, outer nuclear layer; IS/OS, photoreceptor inner/outer segment region. Scale bar, 25 μm.

When assessing the microenvironment of *Rho*$^{-/-}$ mice by IHC, we found that the distribution of CSPGs was largely restricted to the IS/OS, IPL, OPL and GCL at all-time points examined (Figure 3.10A i-vi). However, staining was particularly noticeable in the IS/OS region and even extended into the ONL in the later time points (Figure 3.10A v-vi; Appendix P). Surprisingly, and in contrast to the other models examined, CSPG levels appeared to be reduced in the inferior part of the retina in the late time point, particularly around the equatorial region (Figure 3.10A vi; Appendix P), which could suggest that the inferior retina degenerates faster than the superior. Interestingly, for each stage studied, CSPG staining seemed stronger in the GCL, compared to the same region in the wild-type. WB analysis revealed a significant increase in global CSPG levels between early and mid/late degeneration (Figure 3.10A vii).

In *Prph2*$^{+/\Delta 307}$ mice, the overall distribution of CSPGs was broadly similar to that seen for wild-type mice and this did not change significantly with degeneration. CS-56 staining was evident in the IS/OS region, the OPL, the IPL and the GCL (Figure 3.10B i-vi) although appeared to be more intense in the IS/OS region, compared to wild-type, and formed a thin band abutting the ONL, indicating a denser deposition of CSPGs. Interestingly, qualitative assessments of IHC indicated some regional differences between the superior and the inferior retina (Appendix S); CSPG levels appeared to be higher within the inferior, compared to the superior retina. When examining global amounts of CSPGs by WB, the *Prph2*$^{+/\Delta 307}$ animals showed a significant increase in CSPG levels with disease progression between early and late time-points (Figure 3.10B vii).

Although *Nrl*$^{-/-}$ mutant retinae showed high levels of glial reactivity, as indicated by a significant upregulation in GFAP, the levels of CSPGs stayed relatively low at all examined time points (Figure 3.10C i-vi; Appendix V). CS-56 staining was only observed within the IS/OS region and within presumptive rosettes, as also seen in the *Crb1*$^{rd8/rd8}$ animals. No noticeable differences between any of the analysed retinal regions were observed. Further, WB analysis showed no changes in global levels of CSPGs over time (Figure 3.10C vii).

As shown in Figure 3.5D, Müller glia become reactive in the *R91W;Nrl*$^{-/-}$ model as early as 3 weeks of age, which might suggest that the levels of CSPGs may be also altered. IHC analysis with CS-56 antibody showed that these proteins were restricted to the IS/OS region (Figure 3.10D i-vi; Appendix Y). Further WB assessment revealed no significant changes at the global protein levels with disease progression (Figure 3.10C vii) indicating that levels of CSPGs do not change over a course of retinal degeneration in this model.

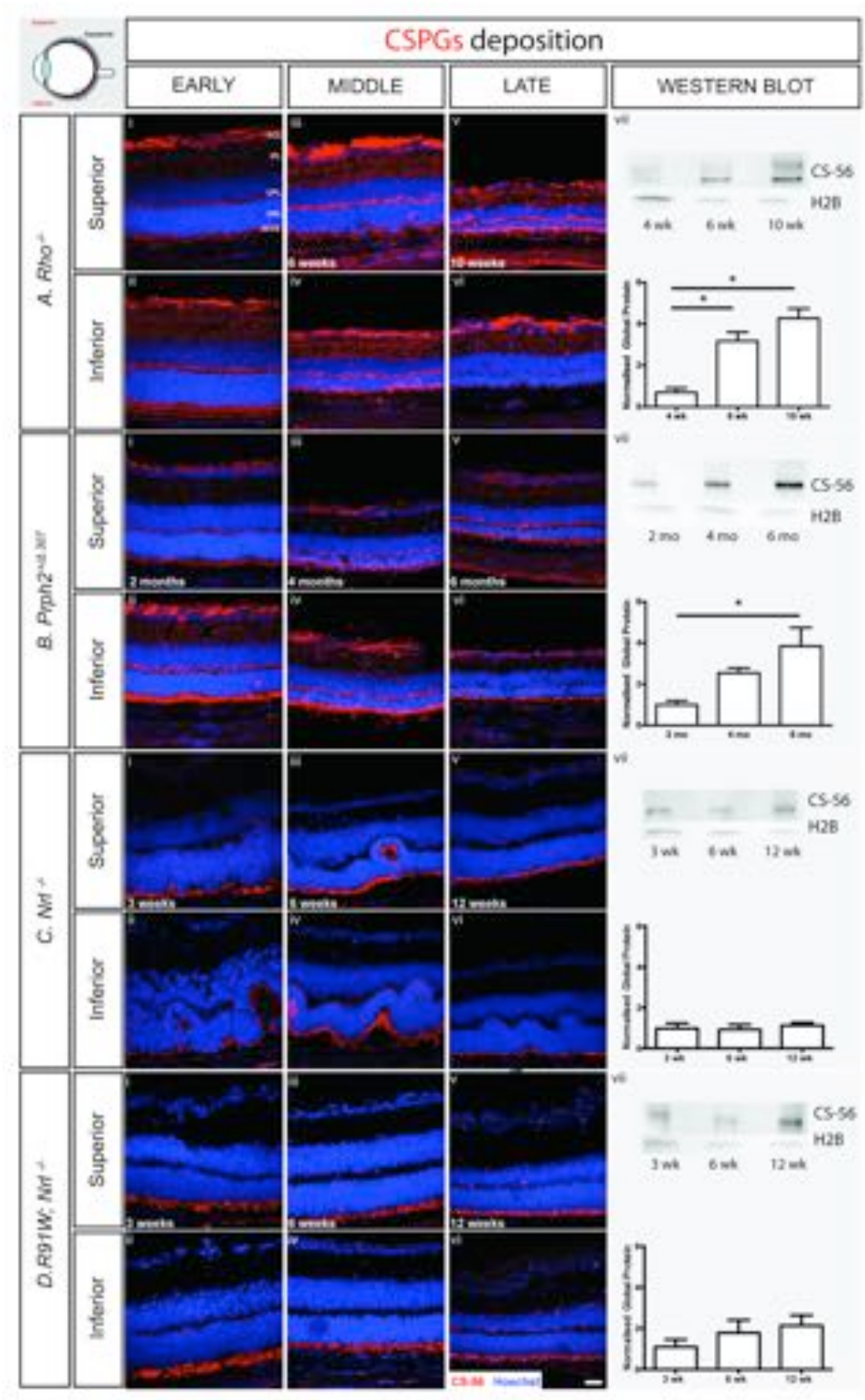

Figure 3.10 CSPG deposition in the genetically engineered mutant mice.

Ai-vii) *Rho*$^{-/-}$; **Bi-vii)** *Prph2*$^{+/\Delta 307}$; **Ci-vii)** *Nrl*$^{-/-}$ **Di-vii)** *R91W;Nrl*$^{-/-}$. Cryosections were immunostained for CS-56 (*red*) and counterstained with nuclei marker Hoechst 33342 (*blue*). Semi-quantitative assessments of CSPGs levels in whole neural retina were determined by Western blot. CSPGs were normalised against H2B. Statistical significance was assessed with a one-way ANOVA test with Tukey's correction for multiple comparisons; $*P < 0.05$. Error bars, SEM; n=3 independent eyes examined.

GCL, ganglion cell layer; IPL, inner plexiform layer; INL, inner nuclear layer; OPL, outer plexiform layer; ONL, outer nuclear layer; IS/OS, photoreceptor inner/outer segment region. Scale bar, 25 μm.

3.3 Discussion

The degenerating retina represents a complex environment, which undergoes constant changes over the course of disease. While variations in the timing and magnitude of response have been reported by various studies looking at different initiating insults, there have been no within-study comparative assessments of gliosis across time in multiple models of retinal degeneration. The results presented in this chapter show that each of the seven examined mouse models of inherited retinal degeneration manifests a unique pattern of alteration to the retinal microenvironment. Moreover, they show that the nature of the Müller glial response and its magnitude are not correlated with disease severity. These observations emphasise that the aetiology of a given retinal degenerative disease, including age, retinal cytoarchitecture and disease stage, is likely to represent an important factor that must be considered when developing any clinical intervention.

Gliosis in the retina can be induced by retinal degeneration (Kinouchi et al., 2003; Zhang et al., 2003b), mechanical insult (Lewis et al., 2010), inflammation (Dinet et al., 2012) and/or ageing (Kim et al., 2004). Reactive gliosis encompasses a wide range of molecular, biochemical, and morphologic events and is easily demonstrated by IHC due to the overproduction of the IF proteins, GFAP and Vimentin, and hypertrophy of the terminal processes of Müller glial cells. Despite numerous studies, to date there is no clear answer for the function and purpose of the glial scarring. Previous reports have shown that gliosis has both protective and detrimental effects, potentially determined by whether it is initiated by an acute insult or by a prolonged chronic condition ((Sofroniew, 2005), reviewed in (Ridet et al., 1997)).

Initially, upregulation of IFs is thought to stabilise the processes of Müller glia, which attempt to undergo hypertrophy in order to limit the extent of a lesion (Lundkvist et al., 2004). As the retina starts to remodel, these glial cells help to maintain the integrity of the tissue and provide a protection from a further mechanical damage (Verardo et al., 2008). On the other hand, chronic reactivity of the glial cells may interfere with neuronal survival and regeneration. Following extensive loss of the photoreceptors within the ONL, the hypertrophied side branches of Müller cells may grow into the OPL in an attempt to protect the inner retina from further degeneration. However, this action may also limit synaptic remodelling by the remaining neurons (Coulombe and Wong, 2004; Vázquez-Chona et al., 2011). On the other hand, glial scarring has been linked to severity of the retinal detachment and the loss of photoreceptor OS (Linberg et al., 2002).

As anticipated, in this study we found that the levels of GFAP and Vimentin typically increased with disease progression (and age) in the majority of examined models,

including wild-type animals. This upregulation was particularly striking in the *Rho*$^{-/-}$ and *Prph2*$^{rd2/rd2}$ models of RP, where GFAP^{+ve} Müller glial fibres extended beyond the ONL and along the outer margins of the retina, similar to the glial scars formed in the brain (Myer et al., 2006). The two mutants, *Nrl*$^{-/-}$ and *Crb1*$^{rd8/rd8}$, which suffer from rosette formation in the ONL, exhibited high levels of IFs around these presumptive rosettes, which could be linked to the changes associated with retinal structural remodelling. Interestingly, in the cone-only retina of *R91W;Nrl*$^{-/-}$ mice, a marked upregulation of GFAP and Vimentin was also observed despite the fact that this model is comparatively normal, lacks rosette formation and does not undergo significant photoreceptor degeneration over time (Samardzija et al., 2014). More surprising, however, was the observation that the levels of both GFAP and Vimentin, although increasing initially, undergo a regional decrease in the outer retina in both *Prph2*$^{+/\Delta 307}$ and *Pde6b*$^{rd1/rd1}$ animals at the later stages of degeneration. This is striking, when one considers that these models represent very different rates of degeneration (slow and fast, respectively). Conversely, the same phenomenon was not seen in the *Rho*$^{-/-}$ or *Prph2*$^{rd2/rd2}$, models that fall in between these two in terms of degeneration rate.

Cepko and colleagues performed a microarray data analysis on single Müller cells isolated from *Rho*$^{-/-}$ and *Pde6b*$^{rd1/rd1}$ neural retinae where they examined expression of *Gfap* (Roesch et al., 2012). In the Rho$^{-/-}$ mutant, at 8 weeks of age, which corresponds with a peak of rod degeneration, four out of five examined Müller cells were positive for GFAP expression. However, at the peak of cone death at 22 weeks, only one cell showed significant levels of GFAP. In contrast, our study reported that in 22 weeks old mice, immunostaining for GFAP was still robust, with no evidence of a decrease (Hippert et al., 2015). Similarly, when Roesch *et al*. looked at the *Pde6b*$^{rd1/rd1}$ model, they found a robust expression of *Gfap* in four of five of the *Pde6b*$^{rd1/rd1}$ Müller cells at early postnatal age (P12). In this study, little GFAP at the slightly earlier time point of P10 was found, but robust levels by P15 were observed (Appendix L). However, at 5 weeks, Cepko and colleagues reported a significant expression of *Gfap* in five out of five cells (Roesch et al., 2008). This is in contrast to the findings here and those of Strettoi *et al.* where a reduction in GFAP protein was reported (Strettoi et al., 2002). The apparent discrepancies almost certainly lie in the different techniques used. In the Roesch *et al.* study, they used a powerful, single cell profiling approach, which reflects RNA levels at a given point in time while most studies, including this one, examined GFAP protein, which may undergo changes on a different timescale. In addition, there are many studies, which report a significant heterogeneity among Müller cells in levels of different proteins that could provide a valid explanation for the discrepancies found between this, and Roesch *et al.* study. Since cell death in the RP retina typically spreads from the centre to the periphery of the mouse retina, cells originating from the

centre can differ significantly from those at the periphery. The data in the study by Cepko and colleagues come from only a very small number of cells (5 in each condition) and thus may not reflect the overall changes occurring in the diseased retina as a tissue.

Another reported feature of reactive gliosis associated with disease and injury is an increase in a deposition of CSPGs. CSPGs belong to a large family of glycoproteins that are found both on the cell surface and in the extracellular space and are the major proteoglycans found in the retina. They consist of a core protein covalently attached to long carbohydrate chains known as glycosaminoglycans (GAGs). These GAG chains can vary markedly in length, number and sulphation pattern, which in turn influences the unique functions of different proteoglycans within and between classes (Properzi et al., 2003; Wang et al., 2008). By interacting with other components of the ECM, proteoglycans play an important role in many biological processes, including cell development, migration and regulation of synaptic plasticity (Fawcett and Asher, 1999). In the spinal cord and brain, CSPGs are upregulated by reactive astrocytes in response to injury and disease and participate in the inhibition of axon regeneration, mainly through their GAG side chains ((McKeon et al., 1991; Crespo et al., 2007), reviewed in (Busch and Silver, 2007)). However, our understanding of CSPG biosynthesis and the role of these molecules in retinal degeneration is very limited. Here, CSPGs were found in several regions of the healthy neural retina including the GCL, IPL, OPL, and the IS/OS region. Taylor *et al.* reported alterations in the biosynthesis and turnover of proteoglycans with age (Taylor, 2006), which is supported by the observations from this study of an increase in CS-56 staining in aged (1 year), compared to young (6 weeks), wild-type mice. Importantly, others have linked age-related changes in the glycomatrix to the development of AMD pathogenesis (Clark, 2006; Day et al., 2011). Here, we report that in the degenerating retina CSPG levels usually, but not always, followed the trends in IF expression, becoming highly expressed in the *Rho*$^{-/-}$ model, but decreasing in the *Prphr2*$^{rd2/rd2}$ and *Pde6b*$^{rd1/rd1}$ mutants. Interestingly, in models such as *Nrl*$^{-/-}$, the expression of CSPGs was relatively low despite major alterations to retinal architecture and high levels of GFAP and Vimentin.

Having identified marked, but contrasting, changes in the expression of CSPGs as assessed with the broad-spectrum CSPG marker, CS-56, further work is required to examine changes in specific CSPGs within the diseased retina. While a number of different proteoglycans have been identified, only a few have been studied in any detail in the eye. One that has received attention is Neurocan (*Ncan*). *Ncan* gene expression is increased in retinae injured by transient ischemia, *Rho*$^{-/-}$ and *Pde6b*$^{rd1/rd1}$ mutants, and the Royal College of Surgeons (RCS) rat model of inherited retinal degeneration

(Inatani et al., 2001; Zhang et al., 2003b; Singhal et al., 2008). Interestingly, it has also been shown that Neurocan inhibits the outgrowth of RGCs *in vitro* (Inatani et al., 2001). This inhibition persists even after removal of chondroitin sulphate sugar chains from the core protein, suggesting that the Neurocan core protein itself is inhibitory. Similarly, *Acan*, one of the major CSPGs expressed in nervous tissue (Oakley and Tosney, 1991; Schwartz et al., 1996), is expressed in the optic nerve and the inner retinal layers from embryonic day 16 (rat) and 18 (mouse) (Popp et al., 2004; Ali et al., 2011). In development, Aggrecan is produced by glial precursor cells and plays a significant role in neurite outgrowth (Domowicz et al., 2008; Afshari et al., 2010a) and astrocyte differentiation (Smith and Strunz, 2005), amongst other roles. IHC analysis of the adult wild-type retina showed Aggrecan in the GCL, INL, ONL and weak staining in the plexiform layers, which is similar to what has been shown in human retina (Keenan et al., 2012). Several groups have also identified glial scarring, and, more specifically the accumulation of CSPGs, as a potential factor involved in transplantation success both in the retina and the CNS (Moon et al., 2001; Bradbury et al., 2002; Kim et al., 2006; Suzuki et al., 2007; Bull et al., 2008; Bradbury and Carter, 2011). Findings from many studies corroborate the findings presented by other groups where the number of GFP^{ve+} cells was increased following enzymatic degradation of subretinal CSPGs using chondrotinase ABC (ChABC) (Suzuki et al., 2007; Bull et al., 2008; Singhal et al., 2008). The role of CSPGs in axon regeneration inhibition is well documented (Dou and Levine, 1994; Friedlander et al., 1994; Emerling and Lander, 1996; Mitashov, 2001; Bradbury et al., 2002; Jones et al., 2002; Kim et al., 2006; Bradbury and Carter, 2011), however, there are several subtypes of CSPG, including Neurocan and Versican, and ChABC has a different enzymatic affinity for each subtype. The exact expression profile in each model maybe different and further profiling may facilitate a more targeted enzymatic approach to degrade these specific subtypes and produce a greater improvement in transplanted cell integration. Indeed, a variety of different CSPGs, including Neurocan, Versican, Aggrecan, Phosphacan and NG2, are upregulated in the brain at varying rate after injury (Dou and Levine, 1994; Lemons et al., 1999; Asher et al., 2000) and this is likely to be the case in the retina. Furthermore, degradation of extracellular matrix proteins via induction of matrix metalloproteinase-2 (MMP-2) has been shown to increase neurite outgrowth in retinal explants (Suzuki et al., 2006) and *in vivo* in the *PDE6b*$^{rd1/rd1}$ mouse (Zhang et al., 2007). Further, when co-injected with RPCs, polymer scaffolds that deliver MMP2 were shown to degrade the ECM proteins, CD44 and Neurocan, in the degenerating retina and enhance donor cell integration (Tucker et al., 2008).

Gliosis has also been reported to have a detrimental effect on the application of viral vectors. Lentiviral vector is known to have better transduction efficiency in newborn

photoreceptors and immature retinae than in adult mice after either intravitreal or subretinal injection (Miyoshi et al., 1997; Takahashi et al., 1999; Kostic et al., 2003). Arsenijevic and colleagues hypothesised that this might be because in adult mice the CSPG-rich interphotoreceptor matrix acts as a physical barrier (Grüter et al., 2005). By applying CSPG-digesting enzymes to the subretinal space in conjunction with lentiviral vector delivery, they obtained an improvement of viral diffusion and transduction of photoreceptors. It is interesting to note, however, that the transduction efficiency of lentivirus is still markedly lower than that achieved by adeno-associated virus (AAV) vectors without any treatment. One of the major differences between these two vectors is their viral particle size, ~20 nm for AAV vectors compare to ~80-100 nm for the lentiviral vector. The smaller particle size may facilitate the diffusion of the AAV vector through barriers, such as the OLM, and so enhance its access to the photoreceptor layer.

This study shows that gliosis, as assessed by IF expression, and the associated changes in CSPG deposition do not change in an equivalent manner between different degenerations and, importantly, are unrelated to disease severity. Here we examine only inherited causes of retinal degeneration and further studies are required to directly compare these with age-related pathology and injury-induced changes. It is also important to remember that the changes in GFAP, Vimentin and CSPGs deposition represent just a few changes in what is an incredibly complex event. Nonetheless, the presented findings underlie the need to study these processes and how they differ in various disease models. Such knowledge will be crucial to designing therapeutic strategies that will be required to circumvent these obstacles in the diseased retina by either preventing the formation of the glial scar or breaking aspects of the scar down.

Chapter 4

Modulation of intermediate filament proteins in a murine model of retinitis pigmentosa

4.1 Overview

Müller glia are very sensitive to any type of environmental change and can therefore serve as an early indicator of the retinal stress. In response to virtually any pathological condition, these cells undergo gliosis, a cellular hypertrophy that includes (but is not limited to) an elevation in expression of the intermediate filament (IF) proteins glial fibrillary acidic protein (GFAP) and Vimentin. Following their activation, reactive Müller glia undergo changes in their biomechanical properties, enlarging their cell bodies and becoming stiffer, especially in the inner stem processes and the apical terminal region, due to an increase in the density of IFs (Lu et al., 2011). The upregulation of IFs in Müller glia is also associated with hypertrophy of the glial processes, which contributes to the formation of a glial scar at the outer edge of the neuroretina (Fisher and Lewis, 2003), similar to that observed elsewhere in the CNS (Eng and Ghirnikar, 1994). This subretinal scar formed at the outer surface of the photoreceptors may impede tissue regeneration, including the outgrowth of photoreceptor outer segments (OS) following retinal detachment (Fisher and Lewis, 2003), or interactions between grafted tissues or cells and the underlying recipient retina (Zhang et al., 2003a). Modulating these changes in reactive Müller glia may therefore be important for the development of new therapeutical strategies.

Despite numerous studies, to date the purpose of IF upregulation in the process of gliosis remains a matter of considerable debate. Researchers propose that it can have both protective and detrimental effects, depending upon whether there is an acute insult or prolonged chronic condition (reviewed in (Ridet et al., 1997; Sofroniew, 2005)). In particular, the role of GFAP in the retina has been the subject of many apparently contradictory findings. In the degenerative retina, it has been suggested that the increased production of GFAP and Vimentin helps Müller glia stabilise the retinal architecture, which necessarily undergoes cellular remodelling after pathological insult (Fisher and Lewis, 2003). Moreover, it has been proposed that the hypertrophied apical terminals help to seal the neuroretina, by building a glial barrier at the outer edge of the ONL, to prevent neurovascularisation and any potential increase in monocyte infiltration (Nakazawa et al., 2007).

Alterations in glial reactivity have been suggested to present challenges for therapeutic interventions, such as gene therapy (Calame et al., 2011) or cell transplantation (Barber et al., 2013). One prominent study used the *Gfap*$^{-/-}$*/Vim*$^{-/-}$ double knockout mouse and reported significantly improved integration of early postnatal retinal cells compared to wild-type control recipients (Kinouchi et al., 2003). However, the *Gfap*$^{-/-}$*/Vim*$^{-/-}$ model does not degenerate and it may not, therefore, accurately reflect the role of these two IF proteins in the diseased environment. Indeed, GFAP positive glial cells

have been proposed to provide a permissive substrate for retinal axonal regrowth and neural stem cells transplanted into the mechanically injured retina preferentially integrated in regions that coincided with increased *Gfap* expression (Nishida et al., 2000). Here, we sought to examine the role of IF proteins in a model of chronic retinal degeneration and the effect of suppressing their expression on photoreceptor cell transplantation outcome.

4.2 Results

In this study shRNA-containing AAVShH10-Y445F viral vectors (Klimczak et al., 2009) were developed to selectively knockdown the expression of *Gfap* and *Vimentin* and applied to the degenerating murine retina. The initial design and characterisation of the vectors to knockdown GFAP and Vimentin proteins was performed by Dr Claire Hippert (Hippert, Graca et al., in review) and only the most pertinent data is presented here. The three most effective plasmids (pshGfap2, pshVim4 and plh) of those designed were used to generate AAVShH10-Y445F viral particles that were titre matched before use. Each shRNA plasmid construct also contained an RFP reporter gene under the control of a CMV promoter. This reporter allowed viral transduction efficiency to be quickly and easily assessed. Herein, these will be referred to as AAV.shGfap, AAV.shVim and AAV.Lh, respectively. AAV.shCon vector was used as a control for transduction efficiency.

4.2.1 Müller glia primary culture to study the RNAi vectors

To assess whether knockdown of GFAP or Vimentin has any effect upon the development of gliosis, the effectiveness of the designed vectors was first tested *in vitro* by transducing primary Müller glia cultures. A full description of the methods employed to establish purified Müller glial cultures is provided in Chapter 2, Section 2.2. Briefly, retinae of *Rlbp1.*GFP$^{+/+}$ mice, in which GFP expression is restricted to Müller glia by the *Rlbp1* promoter (Vázquez-Chona et al., 2009), were dissociated enzymatically using a papain-based kit, then FACS sorted and left in culture for 2 weeks before being used in the study. As this cell system was a relatively new method within our lab, a full characterisation of the cultured Müller glia using immunocytochemistry (ICC) and quantitative RT-PCR analysis was performed to confirm their glial identity (Figure 4.1). Five glial markers were chosen including CRALBP (RLBP1), Vimentin, GFAP, SOX9 and Glutamine Synthetase (GS).

ICC analysis confirmed that all the markers detailed above were expressed in the cultured cells (Figure 4.1A), and this was confirmed with QRT-PCR (Figure 4.1 B). Surprisingly, the GFP fluorescence that was used for FACS purification (Figure 4.2B ii) was not retained by these cells *in vitro* (Figure 4.2B iii-vii), despite CRALBP being detectable both by ICC (Figure 4.1A i) and QRT-PCR (Figure 4.1B).

In this study, GFAP staining of the glial cells was found to be quite variable between individual cells, even within the same well (Figure 4.1A v and Figure 4.3B i) similar to that reported by Abrahan *et al.* (Abrahan et al., 2009). In contrast, Vimentin was highly, and quite uniformly, expressed by cells in the same culture, as confirmed by ICC (Figure 4.1A iv). QRT-PCR confirmed a robust expression in all wells examined

(Figure 4.1B). Having shown the expression of *Gfap* and *Vimentin* mRNA in cultured Müller glia, we then used this system to examine the effectiveness of the designed vectors in reducing the levels of both IFs within this cell type.

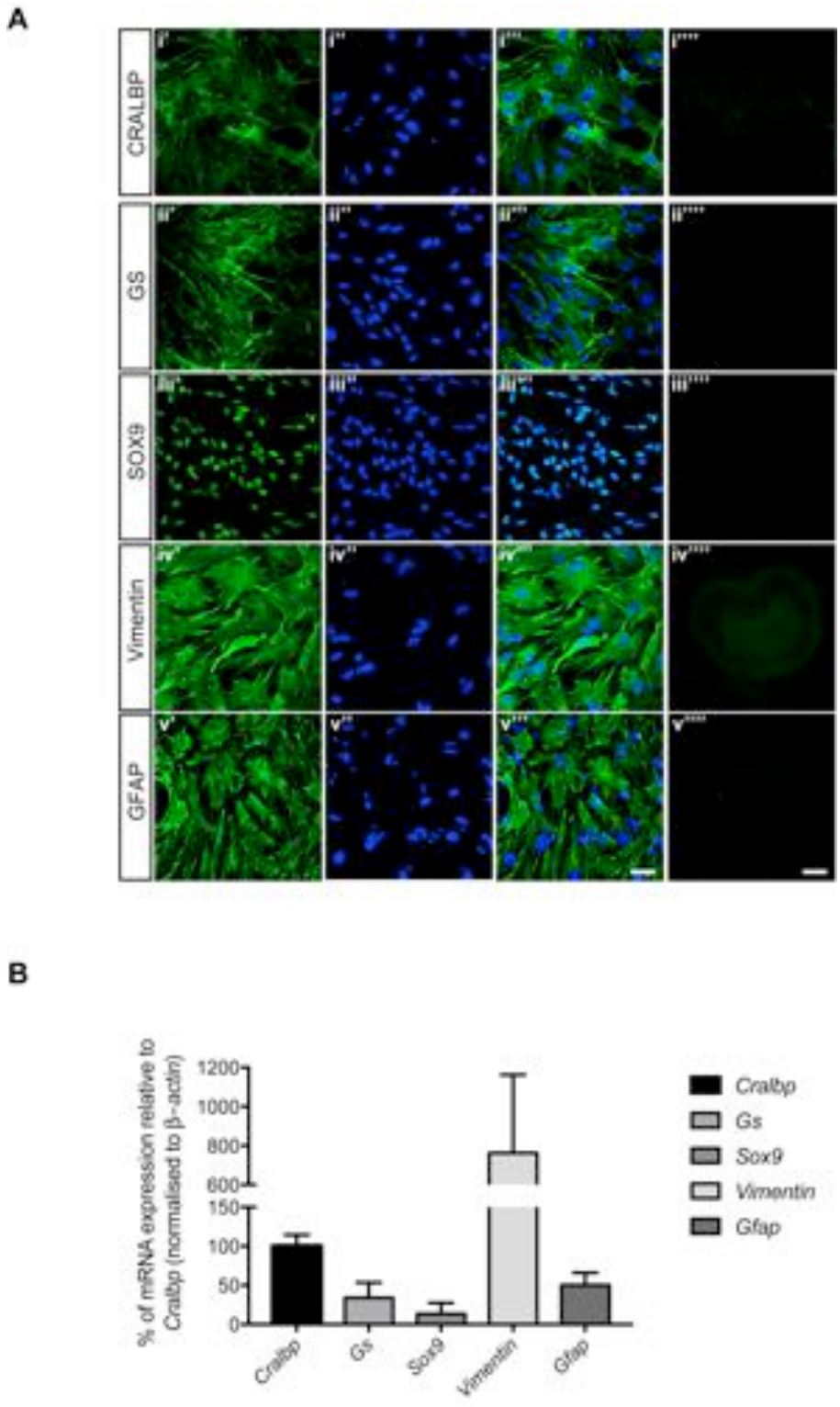

Figure 4.1 Typical glial markers are expressed by primary Müller glial cells in culture.

Ai-v) Müller glia showed a positive staining for **Ai)** CRALBP; **Aii)** GS; **Aiii)** SOX9; **Aiv)** Vimentin and **Av)** GFAP (*white*). Images of the negative controls with no primary antibodies added (i''''-v''''). Cells were counter-stained with nuclei marker Hoechst 33342 (*blue*). Scale bar, 25 μm. **B)** QRT-PCR analysis confirmed the RNA expression of all the examined glial markers. Error bars: SD, n=3 independent cultures examined.

4.2.2 Endogenous Gfap and Vimentin are effectively knockdown with AAV.shGfap and AAV.shVim vectors in Müller glia cells in vitro

As shown in Section 4.2.1, Müller glia express *Vimentin* and *Gfap,* among other glial markers, *in vitro*. Having established that AAV.shGfap, AAV.shVim and AAV.lh are able to silence exogenous expression of *Gfap* and *Vimentin* in HEK-273T cells *in vitro* (see Appendix Z; Hippert, Graca et al., in review), in the next instance the efficiency of the designed plasmids was tested in cultured Müller glia. After 2 weeks in culture, Müller glial cells were transduced with each of the four vectors (AAV.shGfap, AAV.shVim, AAV.lh and AAV.shCon) and assessed against non-transduced control cultures (Figure 4.2B ii) after 1 week post-transduction. RFP expression was used as a read-out for viral transduction efficiency and assessed by fluorescence microscopy (Figure 4.2A i-v) and FACS analysis (Figure 4.2B i-vii). Each of the four used vectors robustly transduced Müller glia *in vitro* and the RFP signal was detectable as early as 2 days after infection with the virus (Figure 4.2A i). FACS analysis showed that after 1 week post-transduction more than 95% of cells subject to AAV.shCon (Figure 4.2A ii, B iv), AAV.shGfap (Figure 4.2A iv, B v) and AAV.shVim (Figure 4.2A iii, B vi), treatment, and 75% of cells transduced with AAV.lh (Figure 4.2A v, B vii) expressed RFP *in vitro.*

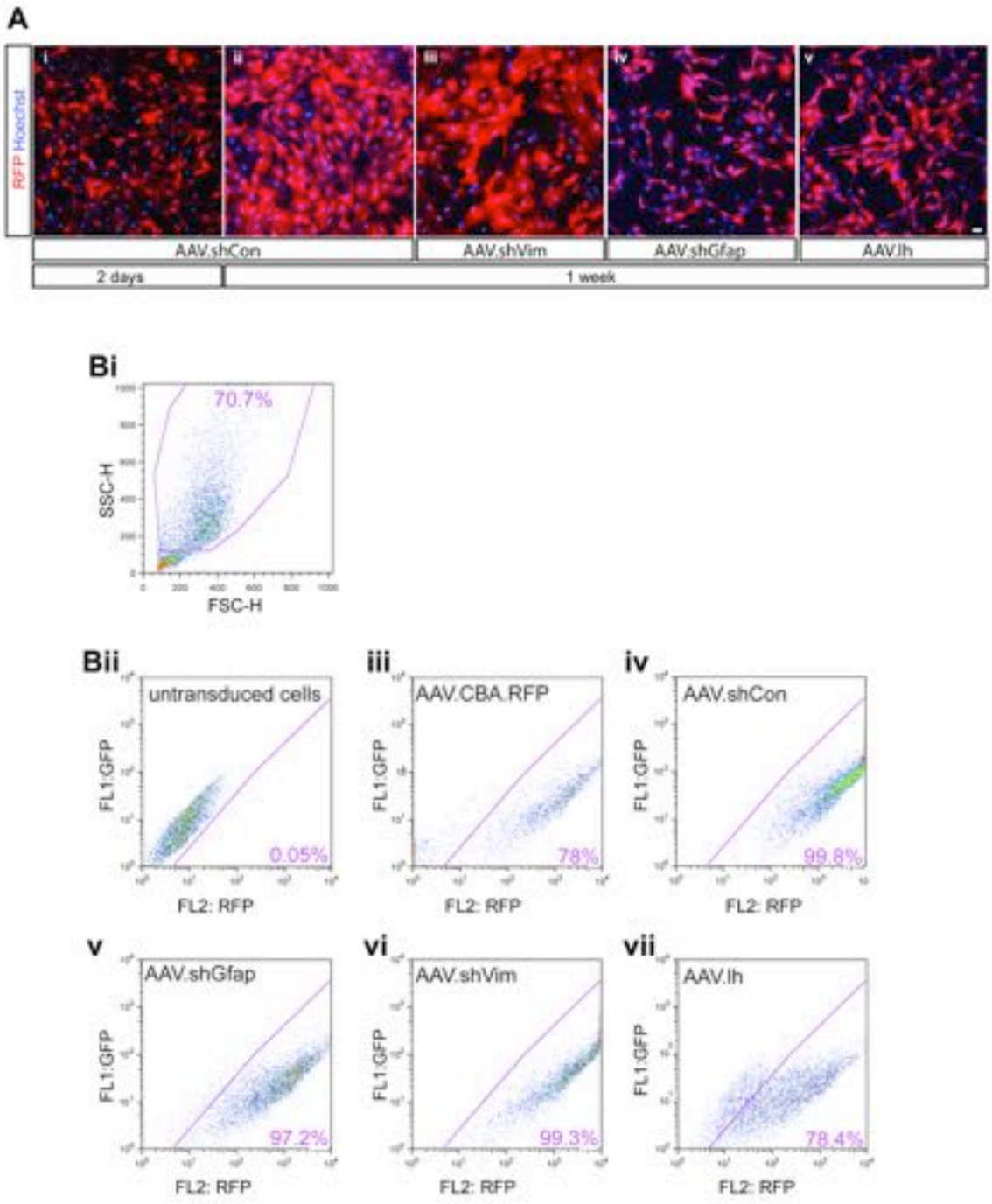

Figure 4.2 AAVShH10-Y445F vectors successfully transduce Müller cells in vitro.

Ai-v) After 2 weeks in culture, Müller cells were treated with AAV.SHh10 RNAi vectors. **Ai)** Robust expression of RFP (*red*) was seen within 2 days after treatment with AAV.shCon and **Aii)** almost all cells expressed RFP by 1 week post-transduction. Cells transduced with **Aiii)** AAV.shVim; **Aiv)** AAV.shGfap or **Av)** AAV.lh. Cells were counterstained with nuclei marker Hoechst 33342 (*blue*). Scale bar: 25 µm. **Bi-vii)** AAV-RNAi vectors rapidly and robustly transduced Müller glial cells *in vitro*. Representative FACs plots taken at 1 week post-transduction of Müller glial primary cultures showing **Bi)** viable cells only; **Bii)** the GFP (y axis) and RFP (x axis) expression in non-transduced cells; the GFP (y axis) and RFP (x axis) expression in Müller cells transduced with **Biii)** AAV.CBA.RFP; **Biv)** AAV.shCon; **Bv)** AAV.shGfap; **Bvi)** AAV.shVim or **Bvii)** AAV.lh. More than 97% of Müller glial cells expressed the RFP reporter following

transduction with AAV.shCon, AAV.shGfap, or AAV.shVim and more than 78% did so following transduction with AAV.CBA.RFP or AAV.lh.

Next, ICC and QRT-PCR were used to assess the efficiency with which these vectors knockdown endogenous GFAP and Vimentin in cultured Müller glia. As mentioned previously (Section 5.2.1), the endogenous levels of GFAP protein are not uniform between Müller glia as observed in non-transduced Müller glia cultures (Figure 4.3A i). A similar pattern was observed in the wells transduced with AAV.shCon, where GFAP was expressed to varying extents, both in transduced (RFP^{+ve}) cells and non-transduced (RFP^{-ve}) cells in the same well (Figure 4.3A ii). In contrast, GFAP expression was much lower in wells subject to AAV.shGfap treatment and was restricted to non-transduced, RFP^{-ve} cells (Figure 4.3A iii). GFAP staining was also much lower in the RFP^{+ve} cells in cultures transduced with AAV.lh (Figure 4.3A iv). Further, QRT-PCR analysis showed that *Gfap* RNA levels were significantly reduced, both by AAV.shGfap and by AAV.lh, to 2.4% ±1.9 and 13.6% ±5.4 of the AAV.shCon levels, respectively (Figure 4.3B).

In Section 4.2.1, it was shown that Vimentin is highly expressed in the vast majority of Müller glia *in vitro.* This expression was visibly reduced in the RFP^{+ve} cells transduced with AAV.shVim (Figure 4.3C iii), in comparison to RFP^{+ve} cells treated with the control vector (Figure 4.3C ii) and non-transduced controls (Figure 4.3C i). Reduction in Vimentin staining was also noted in AAV.lh transduced cells, although some of the RFP^{+ve} cells retained a degree of Vimentin expression (Figure 4.3C iv). QRT-PCR results revealed a significant knockdown of endogenous *Vimentin* RNA levels after AAV.shVim treatment, to 1.4 % ±0.4 of the AAV.shCon (Figure 4.3D; n = 3 independent culture plates for each experimental condition). Application of AAV.lh also led to a statistically significant, but much smaller, decrease in *Vimentin* mRNA (to 57.1% ±6.8 of the control vector levels).

Interestingly, a closer examination of the morphology of the transduced cells revealed changes associated with a treatment with different viral vectors. Those transduced with AAV.shVim (Figure 4.3C iii) showed an enlarged, flattened morphology, compared to cells transduced with AAV.shCon (Figure 4.3A ii or 5.3C ii), while those transduced with AAV.shGfap (Figure 4.3A iii) or AAV.lh (Figure 4.3A iv or 5.3C iv) became thinner and with a more elongated profile. No obvious differences in cell number were apparent, although this was not quantified.

Having confirmed the efficacy of AAV.shGfap and AAV.shVim to silence *Gfap* and *Vimentin* expression *in vitro*, in the next instance, the effectiveness of these vectors was tested in the mouse retina.

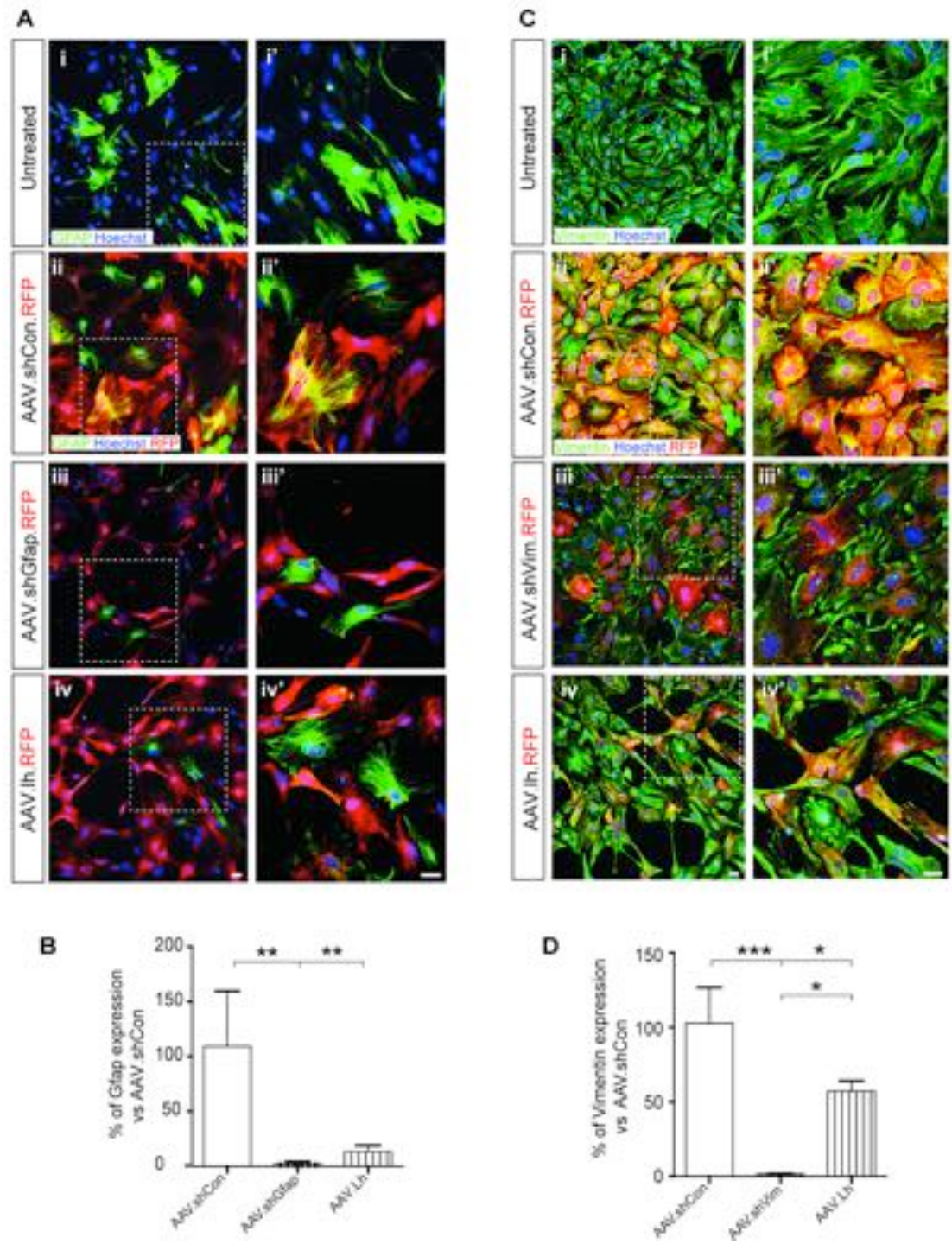

Figure 4.3 RNAi targeting vectors mediate robust knockdown of GFAP and Vimentin in cultured Müller glia in vitro.

Ai-iv) Immunocytochemistry shows that GFAP expression (*green*) is highly variable between cells both in **Ai** untreated and **Aii** AAV.shCon treated (*red*) cultures. However, GFAP was significantly reduced in cells transduced with **Aiii** AAV.shGfap (*red*) or **Aiv** AAV.lh (*red*), compared to controls. (**Ai'-iv'** show ROIs outlined in **Ai-iv)**. **B)** Histogram shows RNA levels, assessed by QRT-PCR one week post-transduction, for *Gfap* following transduction of Müller glial cultures with AAV.shGfap or AAV.lh. Both vectors mediated a significant reduction in *Gfap* mRNA, compared to AAV.shCon. **Ci-iv)** Immunocytochemistry shows robust expression of Vimentin (*green*) in the majority of **Ci** untreated and **Cii** AAV.shCon treated (*red*)

cells. Expression was markedly reduced in cells transduced with **Ciii** AAV.shVim (*red*) or **Civ** AAV.lh (*red*), compared to controls. **D)** Histogram shows RNA levels, assessed by QRT-PCR one week post-transduction, for *Vimentin* following transduction of Müller glial cultures with AAV.shVim or AAV.lh. Both vectors mediated a significant reduction in *Vimentin* mRNA, compared to AAV.shCon, albeit that AAV.lh mediated a smaller reduction here than seen in 293T cells (Hippert, Graca et al., MS in prep). Cells were counterstained with nuclei marker Hoechst 33342 (*blue*). *$P < 0.05$, **$P < 0.01$ and ***$P < 0.001$ with a one-way ANOVA. Error bars: SEM; n=3 independent cultures examined. Scale bar: 25 µm.

4.2.3 AAV.shGfap and AAV.shVim mediate effective knockdown of endogenous GFAP and Vimentin in *Rho*$^{-/-}$ mice

An increase in IF protein levels is considered the hallmark of reactive gliosis and occurs in response to various pathologies, including retinal degeneration (Okada et al., 1990a; Hippert et al., 2015), but the functional changes associated with this increase are not fully understood. The *Rho*$^{-/-}$ mouse model was chosen as it manifests a marked upregulation of both GFAP and Vimentin and a moderate rate of degeneration of photoreceptors (see Chapter 3, Section 3.2). Since majority of the retinogenesis is complete by P10 (Young, 1985; Close et al., 2005) and Müller cells become reactive by three weeks of age in the *Rho*$^{-/-}$ mouse (Humphries et al., 1997), P10 was picked as an appropriate time to administer the vectors. First, to confirm reports that AAV.ShH10-Y445F preferentially transduces Müller glia following intravitreal injection (Klimczak et al., 2009), recipient wild-type mice received AAV.shCon at P10 and were assessed 3 weeks later by IHC. A widespread transduction of about 70% of Müller glial cells was observed (Figure 4.4). Next, recipient P10 *Rho*$^{-/-}$ mice received intravitreal administration of either AAV.shCon, AAV.shGfap, AAV.shVim and were initially assessed 3 weeks later by QRT-PCR and IHC.

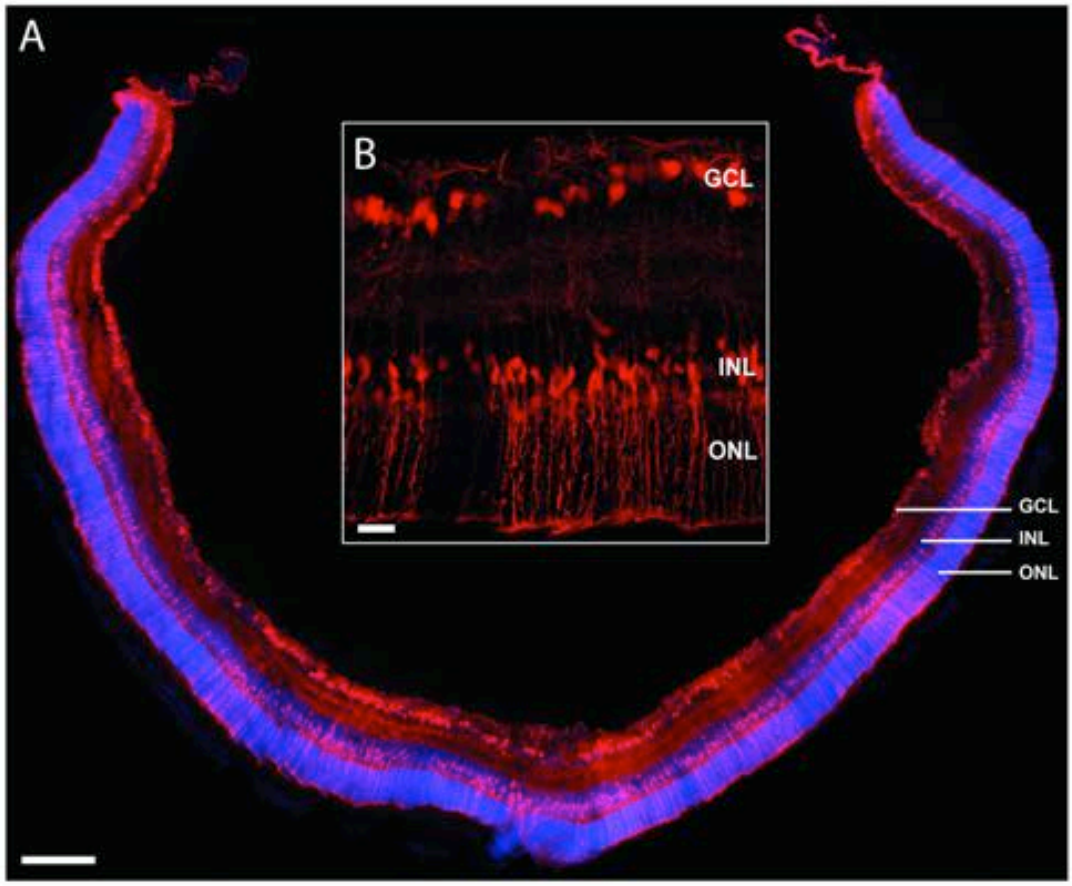

Figure 4.4 Robust transduction of Müller glia in vivo by AAV.SHh10 vector.

Representative confocal projection image of a mouse wild-type retina injected with AAV.shCon postnatal day 10. **A)** At 3 weeks post-transduction, widespread expression of RFP (red) was observed and **B)** this was predominantly restricted to Müller glial cells, as assessed by morphology. Scale bars: A, main panel = 100 µm; B, insert = 20 µm.

In the first instance, the generated vectors were tested for their ability to prevent *Gfap* upregulation during chronic degeneration. In the untreated P10 *Rho*$^{-/-}$ mouse, GFAP expression is very low (Figure 4.5A i and 5.5B i), but is markedly upregulated during the course of degeneration (Figure 4.5A i and 5.5B ii; (Hippert et al., 2015)). As assessed with IHC, at P10 GFAP staining is largely restricted to astrocytes that reside at the vitreal side of the inner retina, with some additional labelling around the OPL (Figure 4.5B i). Three weeks later, GFAP expression is widespread and demarcates the full extent of both apical and basal Müller glial processes, which also appeared thickened and with increased branching from the central process (Figure 4.5B ii). Close inspection of the apical margin of the neural retina revealed the lateral extension of GFAP^{+ve} terminal processes along the outer edge of the ONL (Figure 4.5B iii).

QRT-PCR analysis showed that administration of AAV.shCon alone led to a small decrease in *Gfap* mRNA when compared to untreated controls (Figure 4.5A i). Although statistically significant, this did not translate to a visible reduction in GFAP staining, as assessed by IHC (Figure 4.5C i-ii). Nonetheless, given this small effect of viral administration, the effects of AAV.shGfap, AAV.shVim and AAV.lh were compared against the control vector rather than untreated controls.

Levels of *Gfap* RNA were significantly decreased by both AAV.shGfap and AAV.lh, to 31.5% ±23.2 and 44.9% ±13.8 of AAV.shCon, respectively (Figure 4.5A ii). Further analysis with IHC showed that GFAP staining was absent in those Müller glia transduced with AAV.shGfap (Figure 4.5C iii-iv). Similarly, a noticeable reduction in GFAP protein levels was also observable in the retinae transduced with AAV.lh (Figure 4.5C v-vi) compared to those transduced with AAV.shCon (Figure 4.5Ci-ii).

As it was reported that Vimentin indirectly affects GFAP expression (Galou, 1996), we also assessed whether AAV.shVim had any indirect effects on the expression of endogenous *Gfap*, but no significant changes in *Gfap* mRNA levels were observed (Figure 4.5A ii).

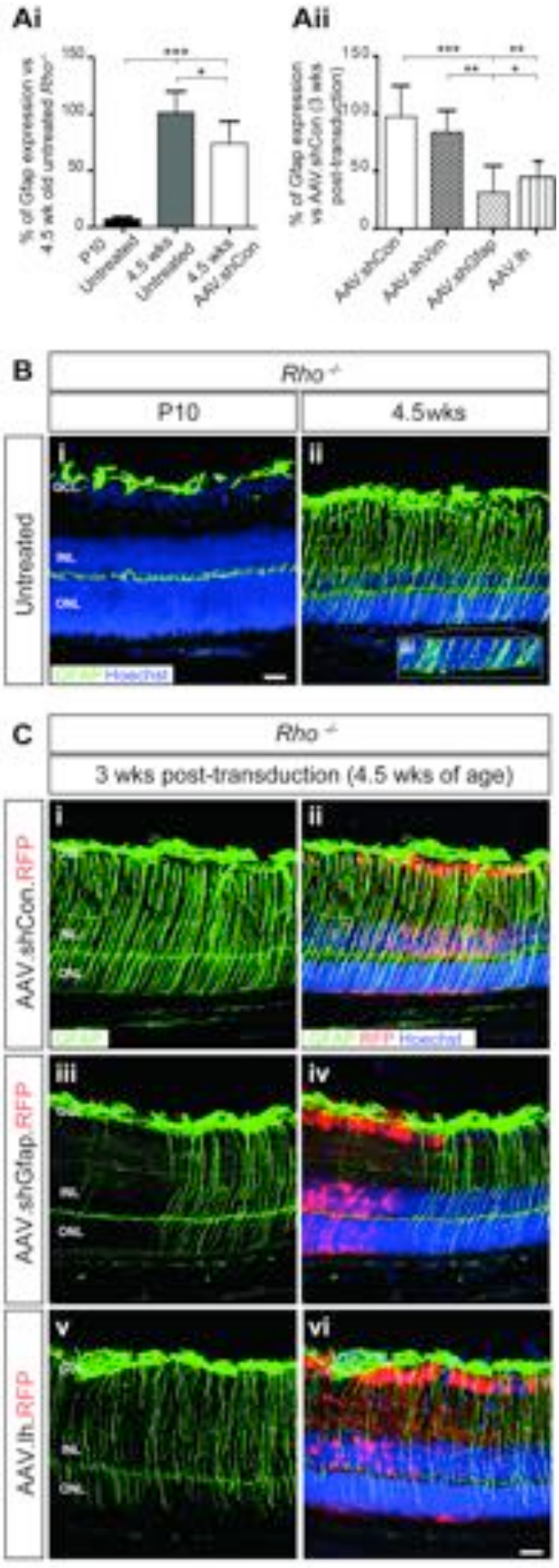

Figure 4.5 RNAi targeting vectors mediate knockdown of GFAP in Müller glia in vivo in the degenerating Rho$^{-/-}$ retina.

Ai) Histograms show that *Gfap* mRNA levels, as assessed by QRT-PCR, are low at the time of administration (P10), but increase significantly during the course of degeneration. Administration of AAV.shCon vector led to a small but significant reduction in *Gfap* mRNA. **Aii)** Transduction with both AAV.shGfap or AAV.lh mediated significant reductions in *Gfap* mRNA, compared to AAV.shCon, while AAV.shVim had no significant effect. **P* < 0.05, ***P* < 0.01 and ****P* < 0.001 with a one-way ANOVA. Error bars: SEM; n=3 animals examined per time point. **Bi)** Immunohistochemistry shows that in the P10 *Rho*$^{-/-}$ retina, GFAP expression (*green*) appears largely restricted to astrocytes that reside at the vitreal surface of the ganglion cell layer (GCL), with some additional expression around the outer plexiform layer (OPL). **Bii)** By 4.5 weeks of age, in *Rho*$^{-/-}$ retina, GFAP is expressed by the majority of Müller glia cells and throughout the entire length of their processes. **Biii)** Close inspection of the outer retina reveals the extension of apical Müller glia GFAP^{+ve} processes along the outer edge of the outer nuclear layer (ONL), which led to development of a 'glial scar'. **Ci-ii)** GFAP expression was unchanged in the eyes injected with AAV.shCon vector at 3 weeks post-transduction (4.5 weeks of age). **Ciii-iv** In those eyes receiving AAV.shGfap, GFAP expression was largely absent in transduced cells (*red*) and only seen in non-transduced cells. **Dv-vi)** GFAP expression was also reduced in cells transduced with AAV.lh, albeit to a lesser extent. Retinal cryosections were counterstained with nuclei marker Hoechst 33342 (*blue*). GCL, ganglion cell layer; INL, inner nuclear layer; ONL, outer nuclear layer. Scale bar: 25 μm.

It is worth noting that both AAV.shGfap and AAV.lh failed to transduce the astrocytes located at the inner edge of the retina, as GFAP labelling remained in this region unchanged (Figure 4.5C iii-vi). This is surprising, as a previous study reported a robust transduction of brain astrocytes *in vitro* with an AAV.ShH10-Y445F vector (Klimczak et al., 2009). To test this, mouse astrocyte primary glial cultures derived from P7-8 brains were established and were subject to AAV.shCon vector treatment. In parallel, P10 wild-type animals were injected with the same vector, as GFAP expression in the uninjured wild-type is largely restricted to astrocytes. After 1 week, cultured astrocytes stained for GFAP, but as with Müller glial cells GFAP expression varied between the individual cells (Figure 4.6A i). When transduced with AAV.shCon, cultured astrocytes showed robust RFP expression (Figure 4.6A ii) similar to that observed in cultured Müller glial cells (Figure 4.2A ii). In contrast, the transduction efficiency of retinal astrocytes *in vivo* was extremely low and GFAP protein levels in these cells remained unchanged (Figure 4.6B). Based on our findings, it appears that AAV.ShH10-Y445F does not effectively transduce retinal astrocytes *in vivo*.

This result likely explains the smaller magnitude of the *Gfap* mRNA reduction following the AAV.shGfap transduction *in vivo*, which encompasses the whole neural retina, as compared to the *in vitro* examination of the pure population of Müller glial cells. No gross morphological changes in retinal architecture were observed following the reduction in GFAP levels following AAV.shGfap or AAV.lh administration. Together, these data show that injection of AAV.shGfap and AAV.lh prevent effectively the upregulation of GFAP protein in *Rho*$^{-/-}$ mouse Müller glial cells that normally occurs with retinal degeneration.

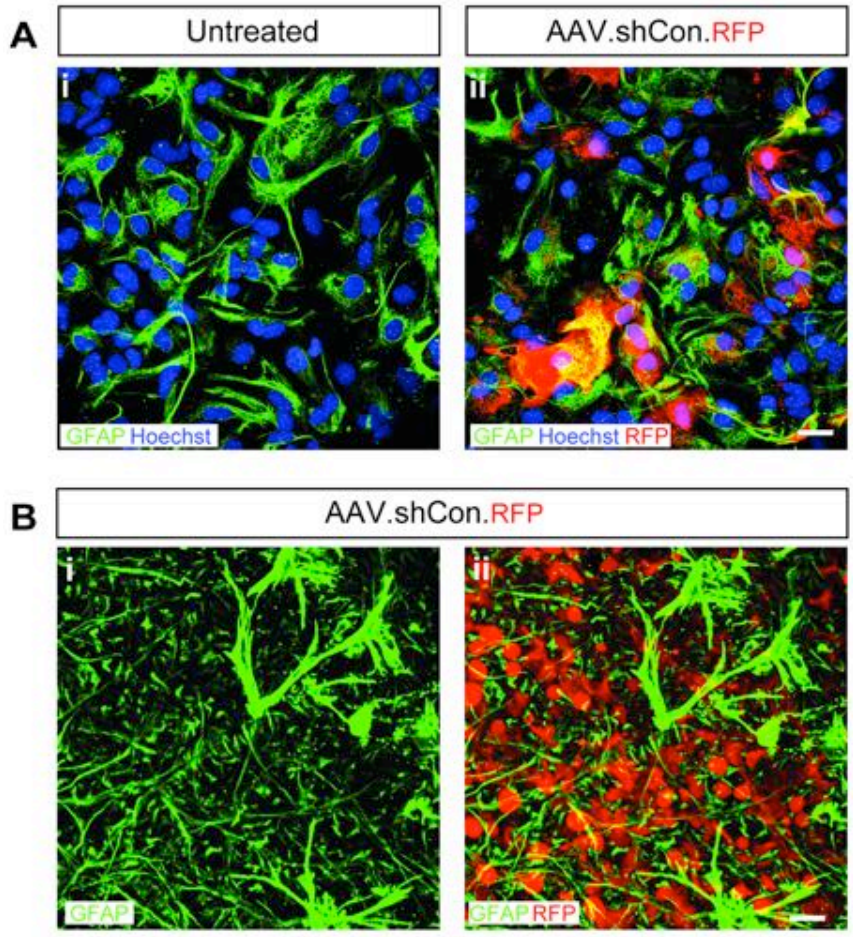

Figure 4.6 AAV.SHh10 vector can transduce astrocytes in vitro but not in vivo.

Ai-ii) Transduction of astrocytes with AAV.shCon resulted in these cells expressing RFP (*red*) as early as 2 days post-administration. As with Müller glia, the expression of GFAP (*green*) is not homogeneous in the astrocyte cultures. **Bi-ii)** Using the same vector *in vivo*, RFP was robustly expressed by inner retinal neurons, but not by $GFAP^{+ve}$ astrocytes, when examined in retinal flat-mounts. Cultured cells and retinal flat-mounts were immunostained with GFAP (*green*) and counterstained with nuclei marker Hoechst 33342 (*blue*). Scale bars: 25 µm.

Next, the effects of administration of AAV.shVim on Vimentin levels were assessed *in vivo*. In the untreated P10 *Rho*$^{-/-}$ mouse, Vimentin is expressed throughout the retina and its levels increase over the course of degeneration (Figure 4.7A i and 5.7B ii-iv; (Hippert et al., 2015)). Administration of AAV.shCon did not lead to any indirect effect on *Vimentin* mRNA levels (Figure 4.7A i) or Vimentin protein levels (Figure 4.7C i-ii), compared to untreated eyes at 3 weeks post-transduction (Figure 4.7B iii). Although no significant differences were found between AAV.shCon transduced and untreated controls, all presented data is normalised against the control vector for consistency with the analysis for AAV.shGFAP. As expected based on the *in vitro* results, AAV.shVim significantly reduced *Vimentin* RNA levels, to 57.5 ±14.5% of AAV.shCon levels (Figure 4.7A ii). Surprisingly, this knockdown was not reflected in a decrease in Vimentin staining (Figure 4.7C ii-iv) at this age. However, Vimentin expression is widespread, even in the normal wild-type P10 retina (Figure 4.7B i). Moreover, Privat and colleagues reported a significant delay in the time between RNAi-mediated knock down of the *Vimentin* mRNA and reduction in Vimentin protein in the injured spinal cord (Desclaux et al., 2015). Based on this report, it was reasoned that it might take longer for the knockdown in retinal *Vimentin* RNA to be reflected in a change at the levels of Vimentin protein. To test this hypothesis, *Rho*$^{-/-}$ eyes were transduced with AAV.shCon or AAV.shVim and compared against untreated controls at 6 weeks post-transduction (7.5 weeks of age). IHC analysis showed that there were no major differences in Vimentin protein levels between the untreated controls (Figure 4.7B iv) and AAV.shCon transduced retinae (Figure 4.7D i-ii). In contrast, Vimentin expression, while not completely abolished, was markedly reduced in transduced Müller glial cells following AAV.shVim administration (Figure 4.7D iii-iv). No gross changes in retinal architecture were observed following the knockdown of Vimentin. AAV.shGfap had no indirect effects on *Vimentin* mRNA expression (Figure 4.7A ii).

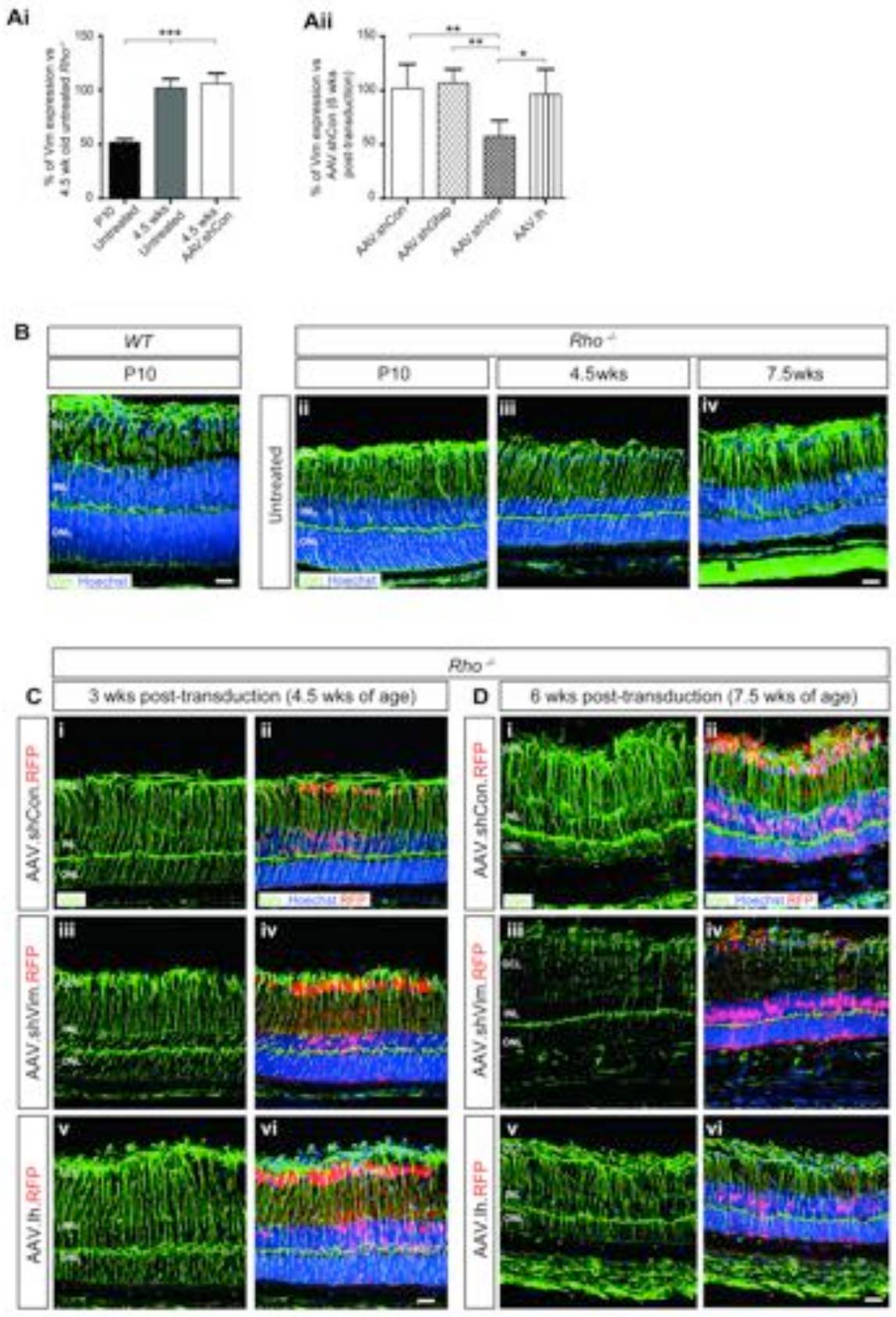

Figure 4.7 RNAi targeting vectors mediate knockdown of Vimentin in Müller glia in vivo in the degenerating Rho$^{-/-}$ retina.

Ai) Histograms show that *Vimentin* mRNA levels, as assessed by QRT-PCR, are already abundant at the time of injection (P10) and increase significantly during the course of degeneration. Administration of AAV.shCon vector had no effect on this increase. **Aii)** Administration of AAV.shVim led to a significant decrease in *Vimentin* mRNA at 3 weeks post-transduction (4.5 weeks of age), compared to AAV.shCon while AAV.shGfap had no effect. In contrast to the results *in vitro*, AAV.lh did not significantly reduce *Vimentin* mRNA *in vivo*. **P* < 0.05, ***P* < 0.01 and ****P* < 0.001 with a one-way ANOVA. Error bars: SEM; n=3 animals examined per time point. **Bi-iv)** Immunohistochemistry shows that Vimentin (*green*) expression is widespread in Müller glia in both P10 **Bi** wild-type and **Bii** *Rho*$^{-/-}$ animals, and **Biii-iv** increases throughout the course of degeneration. **Ci-iv)** Examination of the retinae transduced with RNAi targeting vectors (*red*) showed that at 3 weeks post-transduction there were no notable changes in Vimentin expression in any of the four conditions, compared to untreated age-matched eyes. **Di-iv)** Examination at a later time point (6 weeks post-transduction) showed that Vimentin expression remained robust in **Di-ii** AAV.shControl treated eyes. However, in those eyes that received **Diii-iv** AAV.shVim, Vimentin expression was reduced in transduced cells (*red*). **Dv-vi** No marked differences in Vimentin expression were observed in eyes receiving AAV.lh. Retinal cryosections were counterstained with nuclei marker Hoechst 33342 (*blue*). GCL, ganglion cell layer; INL, inner nuclear layer; ONL, outer nuclear layer. Scale bar: 25 μm.

Disappointingly, despite introducing a moderately robust knockdown of Vimentin *in vitro*, AAV.lh failed to reduce either *Vimentin* mRNA (Figure 4.7A ii) or protein *in vivo* to any significant degree at either time point examined (Figure 4.7C v-vi and 5.7D v-vi). The reasons for this are not fully understood, but we hypothesise that this may relate to *in vivo* differences in the processing of the lh RNA sequences. As an alternative, we combined AAV.shGfap and AAV.shVim together in a 1:1 ratio and injected the mix into the same eye. This application of AAV.shGfap/AAV.shVim together led to a notable reduction in GFAP protein levels at 3 and 6 weeks post-transduction (Figure 4.8A i-ii and 5.8B i-ii) and in Vimentin levels at 6 but not 3 weeks post-transduction, as assessed by IHC (Figure 4.8B iii-iv). However, this was also often (6/9 eyes) associated with exacerbated retinal degeneration including the ONL thinning and retinal detachment as well as other ocular complications. Conversely, retinae receiving titre-matched AAV.shCon showed no such changes, suggesting that the absence of two principal IF proteins may have a detrimental effect on a degenerating retina. In summary, these data show that administration of AAV.shGfap is effective in preventing the upregulation of GFAP, while transduction with AAV.shVim may reverse the upregulation of Vimentin; however targeting both IFs simultaneously may be associated with ocular pathologies in the *Rho*$^{-/-}$ mouse.

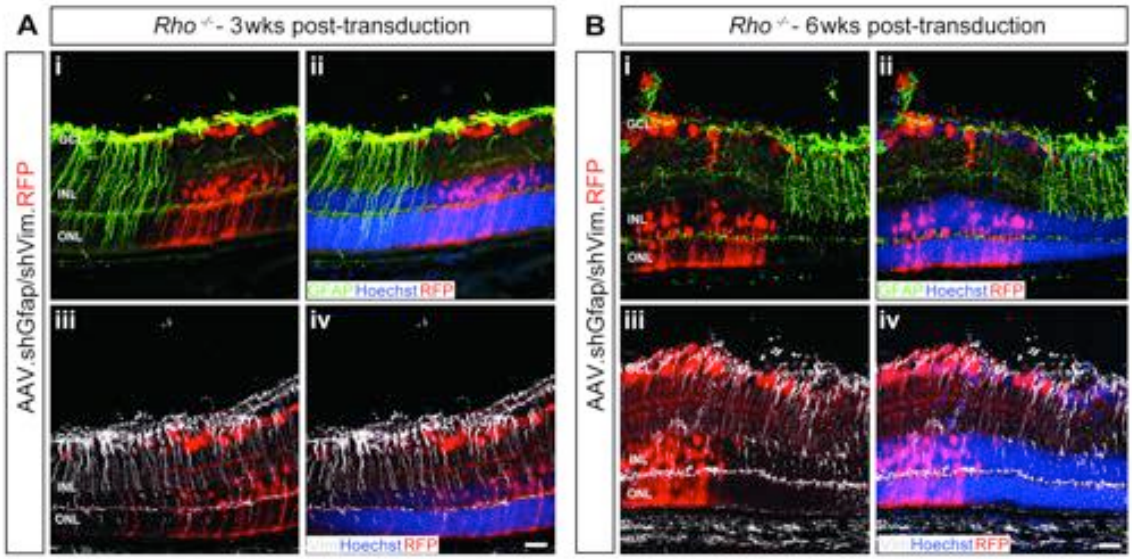

Figure 4.8 Co-transduction with AAV.shGfap and AAV.shVim resulted in marked changes to retinal architecture in the Rho$^{-/-}$ mouse.

Confocal projection images of GFAP and Vimentin expression following co-transduction with AAV.shGfap and AAV.shVim (1:1 ratio) into the same eye. At both **Ai-ii)** 3 (4.5 weeks of age) and **Bi-ii)** 6 weeks post-transduction (7.5 weeks of age), a mark decrease in GFAP levels (*green*) was observed in transduced Müller glia cells (*red*). **Aiii-iv)** As before, there was little change in Vimentin expression (*grey*) at 3 weeks post-transduction. **Biii-iv)** At 7.5 weeks of age, Vimentin expression was reduced in transduced Müller glia. Retinal cryosections were counterstained with nuclei marker Hoechst 33342 (*blue*). GCL, ganglion cell layer; INL, inner nuclear layer; ONL, outer nuclear layer. Scale bar: 25 μm.

4.2.4 Photoreceptor number is not affected by a knockdown of IF proteins

Previous studies indicated that absence of the IF proteins, GFAP and Vimentin, may attenuate photoreceptor apoptosis due to increase in monocyte infiltration (Nakazawa et al., 2007). In order to test whether the absence of GFAP or Vimentin has any effect on photoreceptor survival, we examined ONL thickness and the number of photoreceptor rows across all experimental conditions and compared the results against the uninjected eyes.

Following the administration of AAV.shCon, the ONL was slightly thicker in comparison to untreated controls (60.4 (±7.5) μm vs 51.0 (±4.0) μm), AAV.shGFAP and the animals that received AAV.shGfap/AAV.shVim combined injection (50.6 (±6.1) μm at 3 weeks post-transduction (Figure 4.9A i). This difference between AAV.shCon and untreated eyes had resolved by 6 weeks (AAV.shCon treated, 36.0 (±8.6) μm; uninjected controls, 29.1 (±7.1) μm) (Figure 4.9A ii). Conversely, the ONL of AAV.shGfap/AAV.shVim co-transduced mutants appeared thinner than in any other condition, although this was not statistically significant (27.4 (±5.8) μm; Figure 4.9A ii). The assessment of the eyes transduced with AAV.shGFAP at 3 (55.9 (±4.2) μm) and 6 (33.4 (±4.2) μm) weeks post-transduction or AAV.shVim at 3 (58.6 (±4.6) μm) and 6 (42.1 (±8.8) μm) weeks post-transduction showed no major differences in the ONL thickness at any of the examined ages and was similar to that of the uninjected mutants (Figure 4.9A i-ii). When assessing the number of photoreceptor rows no significant changes between the untreated controls and the eyes transduced with different AAV vectors were observed apart from the ones that were co-transduced with AAV.shGfap and AAV.shVim (Figure 4.9B i-ii). This suggests that only the simultaneous downregulation of GFAP and Vimentin exacerbates the rate of photoreceptor degeneration.

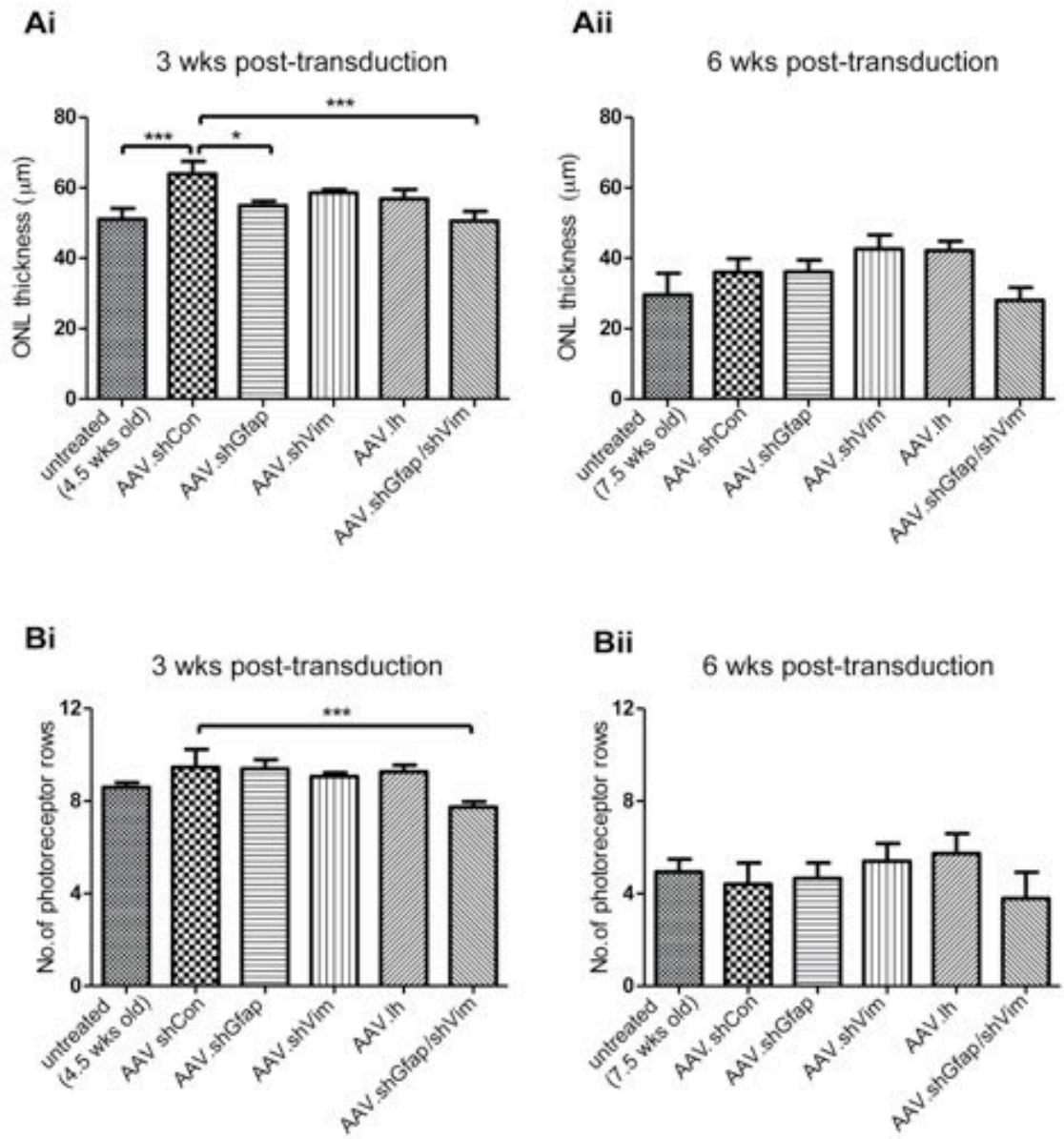

Figure 4.9 Knockdown of GFAP and Vimentin does affect photoreceptor cell number in degeneration.

Ai) Administration of AAV RNAi vectors by intravitreal injection results in some subtle changes to ONL thickness, compared to untreated age-matched controls. At 3 weeks post-transduction, AAV.shCon resulted in a small but statistically significant increase to ONL thickness. **Aii)** No significant differences were observed at 6 weeks post-transduction in any of the cohorts examined. **Bi-ii)** No significant differences were observed when examining the number of photoreceptor rows at either 3 or 6 weeks post-transduction, with the exception of a small, but significant, decrease in those eyes co-transduced with AAV.shGfap and AAV.shVim, compared to AAV.shCon transduced eyes. **Bii)** This decrease was maintained at 6 weeks post-transduction, although no longer statistically significant. *$P < 0.05$ and ***$P < 0.001$, with a one-way ANOVA with Tukey's correction for multiple comparisons. Error bars: SD; n≥5 independent eyes examined.

4.2.5 Hypertrophy of the Müller cells apical terminals is reduced in mutants treated with AAV.shVim

One of the hallmarks of reactive gliosis in the retina is hypertrophy of the Müller glia apical processes (reviewed in (Bringmann et al., 2006)). Having shown that the generated AAV.shVim and AAV.shGFAP vectors can successfully reduce Vimentin levels and prevent the upregulation of GFAP in Müller glia cells, respectively, we next sought to determine their impact on hypertrophy at the outer margin of the retina. By using serial reconstructions of individual RFP^{+ve} Müller glial cells, the morphology of these cells and the extent of lateral spread of their terminal processes at the apical margin of the retina was exmained (Figure 4.10). As previously shown, intravitreal injection of AAV.shCon vector at P10 results in widespread transduction of the whole Müller glia cell, which allows for identification of individual cells throughout the depth of the retina (see Figure 4.4). Following the injection of AAV, *Rho*$^{-/-}$ retinae were fixed and flat-mounted at 3 (AAV.shGfap) or 6 (AAV.shVim) weeks post-transduction, respectively, and high-resolution xyz confocal stacks were taken throughout the thickness of the retina and individual Müller glial cells were 3*D* reconstructed using Amira software. All assessments were compared to the appropriate age-matched AAV.shCon injected controls. As the size of the Müller glia apical terminals has not been assessed before, we also injected wild-type mice with AAV.shCon in parallel to *Rho*$^{-/-}$ animals to determine the normal size of the glial processes at the ONL margin.

In the wild-type retina, the average lateral spread achieved by Müller glial apical terminal processes was 73.4 (±19.7) μm^2 in AAV.shCon treated animals at 3 weeks of age and did not significantly change over time; the lateral spread achieved at 6 weeks was 85.8 (±22.6) μm^2 (Figure 4.10A i). In *Rho*$^{-/-}$ retinae receiving the same control vector, we noticed a marked enlargement of the apical terminal region at 3 weeks post-transduction, compared to age-matched wild-type controls (Figure 4.10A i). The average lateral spread of the glial terminals at 3 weeks of age was 93.4 (±25.8) μm^2 and this increased significantly, to 135.4 (±42.6) μm^2, by 6 weeks post-transduction (Figure 4.10A i-ii). Further analysis of the overall morphology of 3-*D* reconstructed glia cells showed that wild-type Müller glia possess a single thin, apically-directed central process, which projects from the cell body and branches out into a number of fine processes at the level of the apical margin (Figure 4.10B i-ii). In contrast, in the *Rho*$^{-/-}$ mutant, the central process was much thicker and often bore many smaller lateral processes (Figure 4.10 i-ii). These results demonstrate that marked changes occur in Müller glial cell hypertrophy at the apical margin of the retina during chronic retinal degeneration.

We next examined the impact of GFAP or Vimentin removal on Müller glial hypertrophy. *Gfap* mRNA was robustly suppressed and GFAP protein was largely absent in transduced Müller glial cells at 3 weeks post-transduction with AAV.shGfap (see Figure 4.5). However, this had little or no effect on the lateral spread achieved by Müller glial apical terminal processes in AAV.shGfap injected eyes (88.5 (±23.3) μm^2), compared to age-matched AAV.shCon injected *Rho*$^{-/-}$ mutants (Figure 4.10A ii). In contrast, when compared against AAV.shCon transduced wild-type eyes, the lateral spread of the Müller glial apical terminal processes transduced with AAV.shGfap vector was significantly higher. There were no major differences in the morphology of reconstructed glial cells transduced with AAV.shGfap (Figure 4.10C v), compared to AAV.shCon ones.

As noted above, AAV.shVim vector successfully reduced *Vimentin* mRNA *in vivo* at 3 weeks post-transduction, although this did not translate into a robust reduction at the protein level until 6 weeks post-transduction (see Figure 4.7). In keeping with the delayed timecourse of Vimentin knockdown, AAV.shVim treated glial cells presented a gross morphology (Figure 4.10C iii) and lateral spread of the apical terminal processes (92.4 (±20.9) μm^2; Figure 4.10A ii) very similar to that of Müller glia transduced with AAV.shCon in the *Rho*$^{-/-}$ mutants. As noted above, by 6 weeks post-transduction, Müller glia transduced with AAV.shCon showed marked changes in morphology and increased lateral spread of the apical terminal region. In contrast, we did not observe any increase in the lateral spread of the apical terminals of Müller glia transduced with AAV.shVim (62.1 (±16.3) μm^2; Figure 4.10A ii). In addition, 3*D* reconstructions revealed that at 6 weeks post-transduction Müller glia transduced with AAV.shVim more closely resembled those seen at 3 weeks post-injection (both AAV.shCon and AAV.shVim) (Figure 4.10C iv). These findings indicate that Vimentin is required for the development of degeneration-associated Müller glia hypertrophy at the outer edge of the neuroretina.

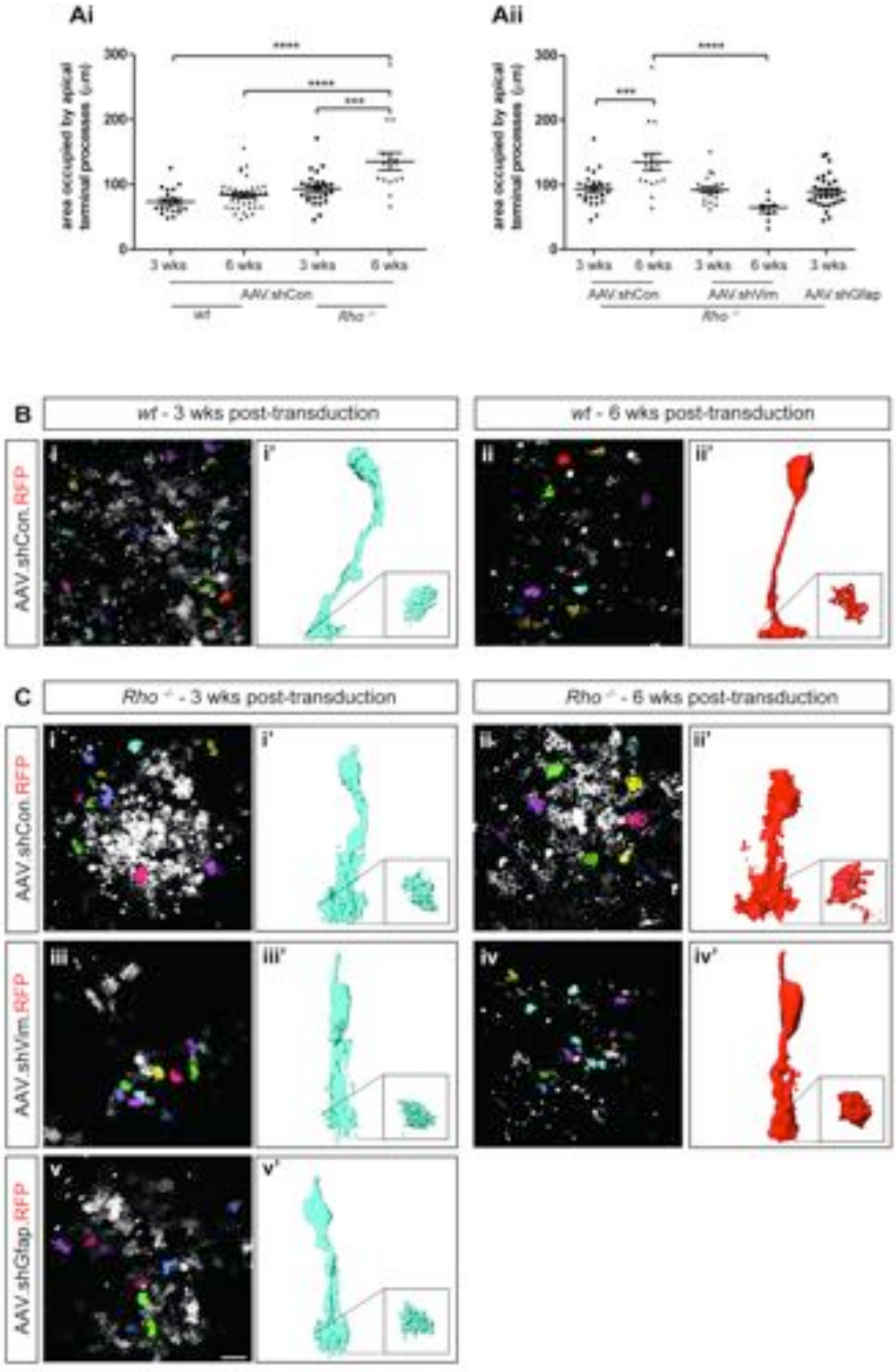

Figure 4.10 Vimentin plays a role in hypertrophy of Müller glial apical processes.

Ai) Scatter plots show the area occupied by the apical terminal processes of Müller glia in *Rho*$^{-/-}$ and wild-type animals transduced with AAV.shCon. At 3 weeks post-transduction (4.5 weeks of age) there were no significant differences between the two strains, but at 6 weeks post-transduction (7.5 weeks of age) *Rho*$^{-/-}$

Müller glial apical terminal processes were hypertrophic and occupied a significantly larger area, compared to Müller glia in both 4.5 week old *Rho*$^{-/-}$ and 7.5 week old wild-type controls. **Aii)** Comparison of the four RNAi vectors across two examined time points showed that AAV.shVim, but not AAV.shGfap, prevents the increase in area occupied by Müller glial apical terminal processes. **P* < 0.05 with a one-way ANOVA with Dunett's post-test for multiple comparisons. Error bars: SEM; n≥3 i animals examined per time point. **Bi-ii)** Representative confocal images of analysed apical surface areas and **Bi',ii')** typical examples of 3*D* reconstructed wild-type Müller glia at 3 and 6 weeks post-transduction with AAV.shCon. **Ci-v)** Representative confocal images of analysed apical surface areas and **Ci'-v')** typical examples of 3*D* reconstructed *Rho*$^{-/-}$ Müller glia at 3 and 6 weeks post-transduction with **Ci-ii)** AAV.shCon; **Ciii-iv)**; AAV.shVim and **Cv)** AAV.shGfap. At 3 weeks post-transduction (4.5 weeks of age), *Rho*$^{-/-}$ Müller glia apical processes already contain many more branching points than wild-type, a feature that increased with degeneration, and (*inserts*) the area occupied by the terminal processes at the apical surface expanded. In contrast, in eyes transduced with AAV.shVim, Müller glia retained a more normal morphology throughout the time period examined. Scale bar: 20 μm.

4.2.6 CSPG deposition is not affected by reduction in IF protein levels

Upregulation of GFAP during gliosis in the CNS is typically associated with an increase in the expression of CSPGs and other related ECM molecules (reviewed in (Busch and Silver, 2007)). As described in Chapter 3, *Rho*$^{-/-}$ animals manifest high levels of CSPGs, therefore, we assessed whether reducing GFAP and Vimentin levels had any effect on CSPG deposition (Figure 4.11). In the untreated *Rho*$^{-/-}$ controls, staining for CS-56, a broad-spectrum marker of CSPGs, showed a modest increase in expression between 4.5 (Figure 4.11A i) and 7.5 weeks of age (Figure 4.11A ii), similar to previous observation for this model (Chapter 3, Section 3.2.2.2). Injecting AAV.shCon (Figure 4.11B/C i-ii), AAV.shGFAP (Figure 4.11B/C iii-iv) or AAV.shVim (Figure 4.11B/C v-vi) at P10 had no effect on thie increase of CSPGs deposition at either 3 weeks post-transduction (4.5 weeks of age) (Figure 4.11B) or 6 weeks post-transduction (7.5 weeks of age) (Figure 4.11C), compared to the relevant controls. This suggests that downregulation of GFAP or Vimentin, alone, has no indirect effect on CSPG production by Müller glial cells.

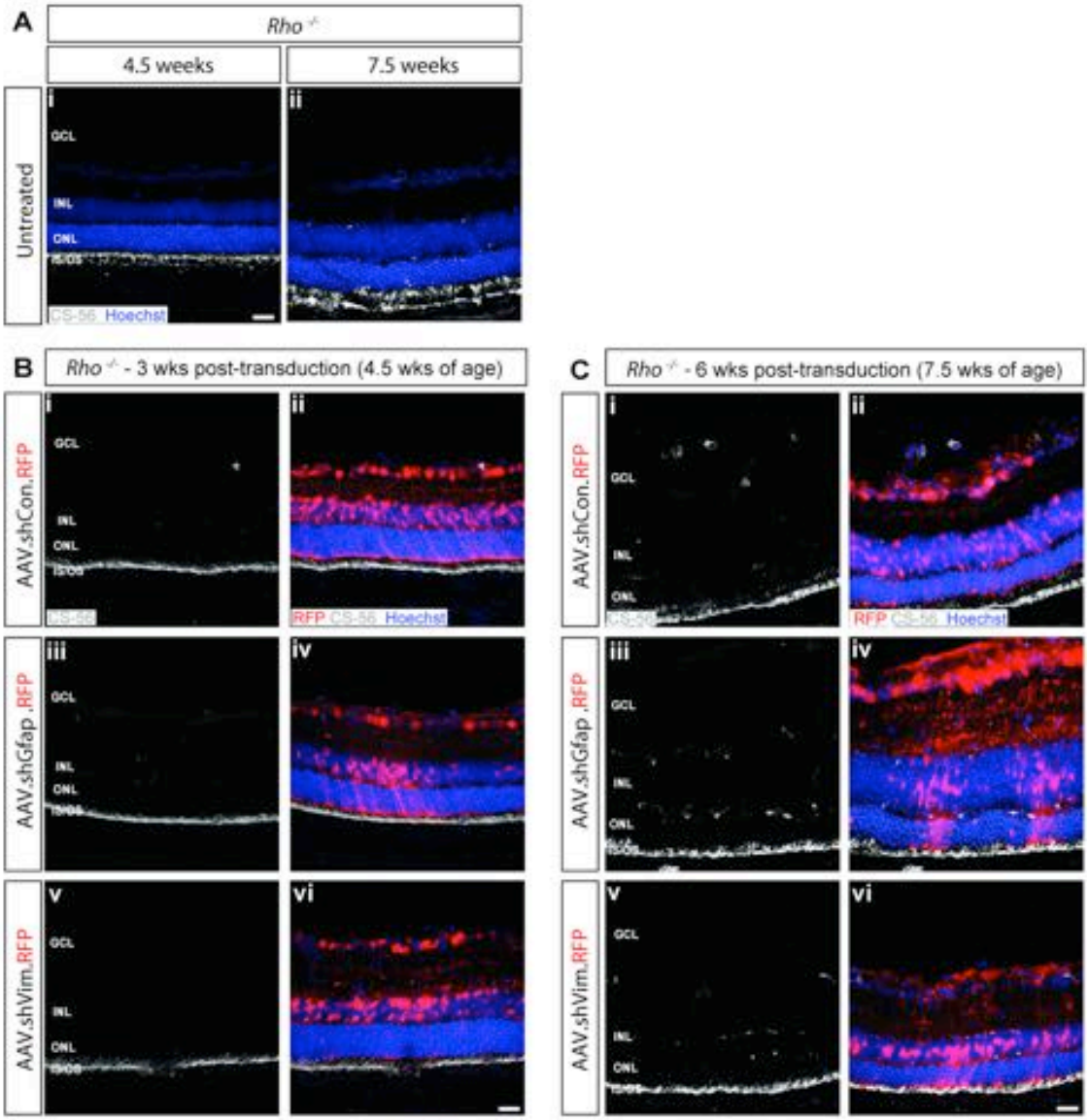

Figure 4.11 Knockdown of the IF proteins GFAP and Vimentin has no discernible effect on CSPG deposition in the degenerating Rho$^{-/-}$ retina.

Reactive gliosis is typically associated with upregulation of CSPG molecules within the extracellular environment. **Ai-ii)** Staining for CS-56 (*grey*), a broad-spectrum marker of CSPGs, showed that CSPGs are robustly expressed within the photoreceptor segment region of *Rho*$^{-/-}$ retinae at both **Ai** 4.5 and **Aii** 7.5 weeks of age in untreated mutants, increasing moderately with age. Administration of RNAi targeting vectors (*red*) had no effect on CSPGs deposition within the photoreceptor segment region and no visible differences between any of the four examined vectors were observed at either **Bi-vi)** 3 (4.5 weeks of age) **Ci-vi)** 6 weeks post-transduction (7.5 weeks of age). Retinal cryosections were counterstained with nuclei marker Hoechst 33342 (*blue*). GCL, ganglion cell layer; INL, inner nuclear layer; ONL, outer nuclear layer; IS/OS – inner/outer segment region. Scale bars: 20 µm.

4.2.7 Downregulation of IF protein levels has no effect on the number of integrating cells following photoreceptor transplantation

Previous studies have indicated that reactive gliosis and increased levels of IFs are associated with a poor photoreceptor transplantation outcome (Barber et al., 2013), and the impaired ability of retinal grafts (Zhang et al., 2004) and electronic implants (Pardue et al., 2001) to contact the host retina. However, it is not clear if these are causative, or simply correlative. Having shown that *Gfap* and *Vimentin* can be effectively suppressed in the degenerating retina, we next sought to assess whether or not these changes influence photoreceptor transplantation outcome. First, P10 *Rho*$^{-/-}$ recipient mice received AAV.shCon in one eye and either AAV.shGfap or AAV.shVim in the contralateral one. After 3 (for AAV.shGfap) or 6 (for AAV.shVim) weeks, both eyes received a single injection of P8 donor *Nrl.GFP*$^{+/+}$ cells into the subretinal space, between the host neural retina and the RPE, as previously described (Pearson et al., 2012). The number of GFP^{+ve} labelled cells within the host ONL was assessed 3 weeks post-cell transplantation.

All recipient retinae, receiving AAV.shCon, AAV.shGfap or AAV.shVim followed by cell transplantation, tolerated the double surgery well and presented normal retinal structure with little or no signs of inflammation. Since transduction efficiency could only be determined post-hoc, only those retinae presenting robust expression of RFP in the same region as the donor cell mass were included in the assessments of transplantation outcome; in this instance, RFP expression serves as an indirect indicator of GFAP/Vimentin knockdown, as shown earlier. Each of the cohorts receiving the control vector presented low numbers of GFP^{+ve} cells within the host ONL, similar to those seen in untreated 4 week old *Rho*$^{-/-}$ recipients (Barber et al., 2013). Despite widespread viral transduction, we observed no significant differences in the number of GFP^{+ve} cells within the host ONL in the eyes transduced with either AAV.shGfap (Figure 4.11A) or AAV.shVim (Figure 4.11B), compared to the contralateral ones treated with AAV.shCon (Figure 4.11). Others have reported significantly increased numbers of reporter labelled donor cells in the host retina following transplantation into retinae where both GFAP and Vimentin proteins are abolished (Kinouchi et al., 2003). To test this hypothesis, donor cells were transplanted into eyes injected with a combination of AAV.shGfap and AAV.shVim at 6 weeks post-viral transduction and assessed transplantation outcome 3 weeks after that. As mentioned in Section 4.2.4, combining the two vectors is associated with a high incidence of ocular abnormalities; however, in the three eyes that retained reasonable retinal architecture, we observed numbers of GFP^{+ve} cells similar to that seen in AAV.shCon treated retinae (Figure 4.11C). Taken together, these results indicate that

manipulating GFAP and Vimentin and the subsequent prevention of Müller glial hypertrophy at the apical margin of the degenerating retina does not affect photoreceptor transplantation outcome. The observed discrepancy between this and other studies could be explained by the fact that the majority of previous findings come from studies of the *Gfap* or *Vimentin* knowckout animals or where animal model suffered from an acute injury, rather than a chronically diseased state. Howver, findings presented int this chatpter are in line with previous reports where reporter labelled cells were observed in the retinae of other degenerative mutants including *rds* that showed elevated levels of IFs (Barber et al., 2013; Santos-Ferreira et al., 2014). In light of recent publications on cell transplantation (Pearson et al., 2016; Santos-Ferreira et al., 2016; Singh et al., 2016), it is not possible to give any indication on whether the reporter labelled cells observed in the recipient retina were the truly integrated cells or whether they were a result of a material transfer/cytoplasmic fusion. Future studies should investigate this issue further as it would be interesting to see whether the removal of IFs and/or decreased glial hypertrophy have any direct impact on cell integration or material transfer/cytoplasmic fusion.

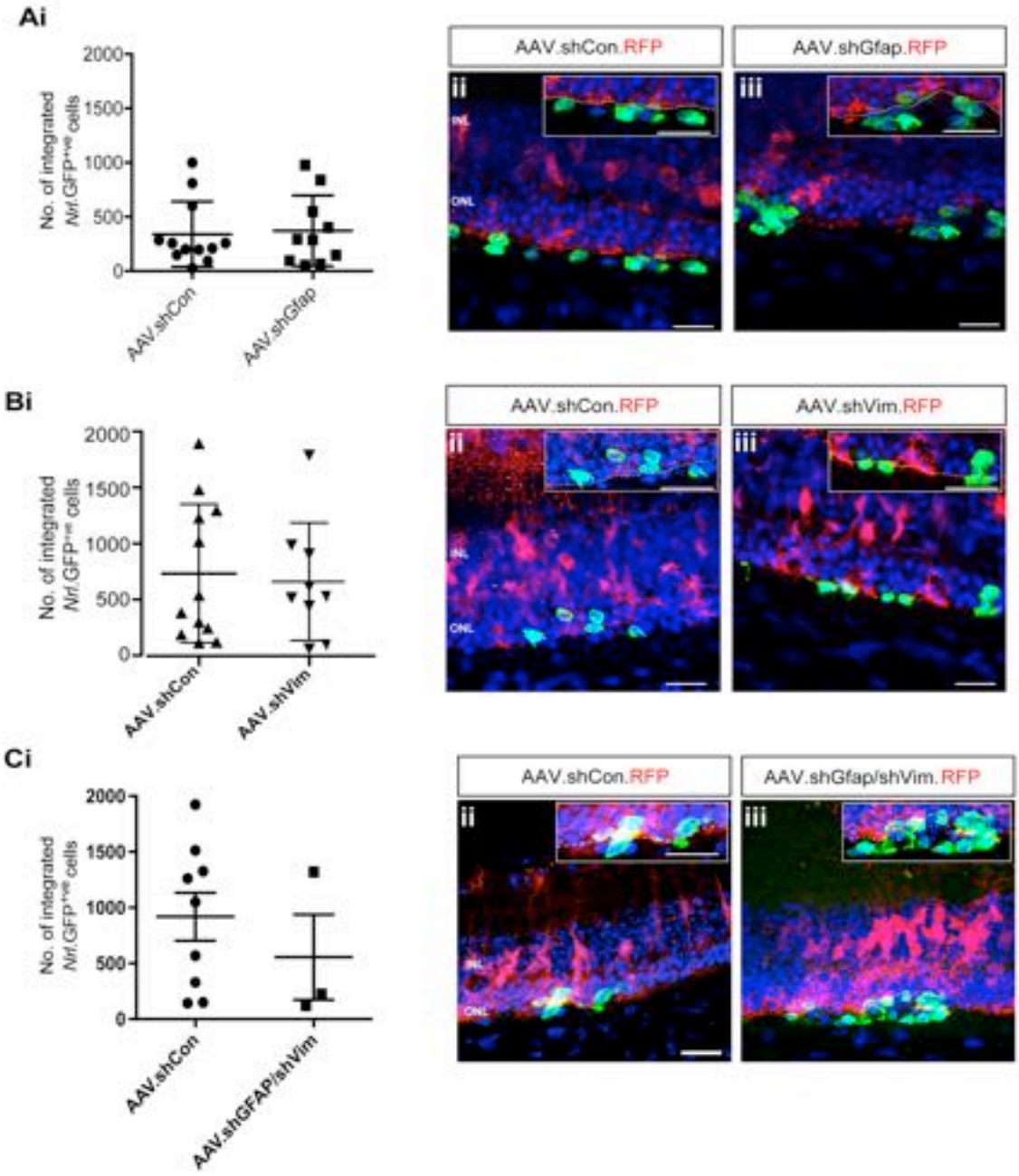

Figure 4.12 Knockdown of Gfap or Vimentin and inhibition of Müller Glial hypertrophy does not affect photoreceptor transplantation outcome in the degenerating retina.

Ai) Scatter plots show number of GFP^{+ve} photoreceptors in the host ONL following transplantation into 4.5 week old *Rho*$^{-/-}$ *at* 3 weeks post-transduction with AAV.shCon or AAV.shGfap. No difference between these two groups was observed. **Aii-iii)** Representative confocal projection images of GFP^{+ve} cells (*green*) in **Aii)** AAV.shCon- and **Aiii)** AAV.shGfap-transduced (*red*) retinae. **Bi)** Scatter plots show number of GFP^{+ve} photoreceptors in the host ONL following transplantation into 7.5 week old *Rho*$^{-/-}$ mice, at 6 weeks post-transduction with AAV.shCon or AAV.shVim. No difference between either two groups was observed. Representative confocal projection images of transplanted *Nrl*.GFP$^{+/+}$ cells (*green*) in **Bii)** AAV.shCon- and **Biii)** AAV.shVim-transduced (*red*) retinae. **Ci)** A higher-than-average failure rate was observed in AAV.shGfap/shVim co-transduced eyes (5) eyes injected showed number of surviving donor cells (12

eyes in total received the combined injection). In those eyes treated with AAV.shGfap/shVim that retained donor cell masses (n = 3/8), the number of GFP^{+ve} cells in the host ONL was unchanged, compared to eyes treated with AAV.shCon. Representative images of GFP^{+ve} cells in **Cii)** AAV.shCon and **Ciii)** AAV.shGfap/shVim dual-treated retinae. Unpaired Student's *t* - test. Error bars: SEM; n≥3 independent eyes examined. Retinal cryosections were counterstained with nuclei marker Hoechst 33342 (*blue*). INL, inner nuclear layer; ONL, outer nuclear layer. Scale bars: 20 μm.

4.3 Discussion

Reactive gliosis is a complex process that is considered to represent a cellular response to protect the retina from further damage and to promote its repair following pathological insult. It includes morphological, biochemical, and physiological changes, which may vary depending on a type and degree of the initial injury. Given the contradicting evidence on the role of IF proteins in this process, we sought to assess GFAP and Vimentin in a mouse model of chronic retinopathy. This study showed that levels of GFAP and Vimentin in the *Rho*$^{-/-}$ mutant could be effectively reduced using AAV vectors. Interestingly, reducing levels of Vimentin prevented Müller glial cells from undergoing degeneration-associated hypertrophy at their apical terminal processes. With regard to therapeutic application, neither AAV.shGfap nor AAV.shVim had any significant effect on photoreceptor transplantation outcome.

In the vertebrate retina, Müller cells account for approximately 90% of the glial population and exhibit a complex structural architecture spanning its entire thickness. Together, with astrocytes, these cells perform a variety of physiological roles, including supplying metabolic support by means of glutamine and taurine in the normal retina, maintaining K^+, H^+, and water balance, protecting against oxidative stress, recycling cone photopigments, releasing neuro- and vasoactive substances, and serving as scaffolds for neurovascular guidance (reviewed in (Bringmann et al., 2006)). Under normal conditions, retinal Müller cells are quite flexible and they predominately express Vimentin. After injury, however, they undergo a rapid change in the composition of their cytoskeleton, including the increase in the density of the IFs (Lu et al., 2011) and sprouting of their processes that grow widely throughout the retina (Lewis et al., 1989; Lewis and Fisher, 2003). Over the years, researchers have tried to identify the role that IF proteins may have in the development of gliosis, but there remains significant debate and little consensus, especially with reference to GFAP.

In contrast to actin filaments, IF proteins are cell-specific, meaning they are found in a limited number of cell types and their expression may differ between developmental stages and adulthood as well as different pathological conditions. Interestingly, the filaments themselves may be composed of different IF proteins that co-depend on each other to assemble into a typical 10-nm IF bundle (Lewis and Fisher, 2003). Most cells retain relatively small amounts of soluble tetrameric oligomers of Vimentin and GFAP compared with their polymerized filamentous forms. Under normal conditions, Müller glial cells maintain high levels of filamentous Vimentin but GFAP is expressed only minimally. GFAP is, however, abundantly expressed in the retinal ganglion layer (GCL) astrocytes (Fernández-Sánchez et al., 2015). Although, Vimentin is the main IF protein expressed by both immature retinal progenitors and adult Müller glial cells, it is GFAP

that has received the most attention for study as it has been perceived as an indicator of retinal 'stress'.

In the uninjured retina, GFAP is normally found in astrocytes and inner half of the retinal Müller cells and their end feet terminals; however basal levels of GFAP in Müller glia may vary between different species, as well as between individual cells within the same retina (Dreher et al., 1992; Sarthy and Ripps, 2001; Lewis and Fisher, 2003). This likely explains why we found the levels of GFAP in cultured Müller glia fluctuating between individual cells even within the same well (Figure 4.3). In contrast, GFAP was reported to be uniformly distributed within the cytoplasm of astrocytes. Following trauma to the retina, such as retinal detachment, GFAP undergoes rapid upregulation in the Müller glia (Guérin et al., 1990; Fisher and Lewis, 2003). Elevated levels of GFAP have also been found after the introduction of retinal ischemia (Kim et al., 1998) or hypoxia (Kaur et al., 2007). In studies on experimental glaucoma, increases in the expression of *Gfap* and another IF, *Nestin* were reported as early as 2h after induction of elevated intraocular pressure (Xue et al., 2006). Although, the *Gfap* mRNA levels rapidly increase in Müller cells following the initial retinal insult, they do revert to normal levels a few days later (Sarthy and Egal, 1995); however, the newly formed filaments may remain in the glial cells for many months after injury (Seoane et al., 1999). Cao *et al.* reported that the magnitude of the GFAP response to mechanical insult is age-dependent, meaning that the older the retina, the more marked the response (Cao et al., 2001). In contrast, in the models of inherited retinopathies, the increase in GFAP levels is a gradual process and it may take weeks or months depending on the type of retinal condition (Ekström et al., 1988; Hippert et al., 2015). In this study, AAV.shGfap successfully prevented upregulation of GFAP in the transduced Müller glia of the *Rho*$^{-/-}$ mutant (Figure 4.5); however, it did not lower the levels of GFAP in astrocytes (Figure 4.5). One possible explanation for this discrepancy is the inability of the designed vector to transduce astrocytes *in vivo* (Figure 4.6). Another possibility is that although the vector may have been able to lower *Gfap* mRNA levels, but no observable effects at the protein level were observed in astrocytes as it takes time to remove the formed IF bundles (Lewis et al., 1989; Humphrey et al., 1997; Seoane et al., 1999). Future experiments to look at a later time point should be able to rule out this possibility. Another explanation is the difference in the GFAP response that could be cell specific. It is well known that in Müller glia, *Gfap* transcription is triggered by a variety of regulatory elements that differ from those that control *Gfap* expression in astrocytes (Brenner, 1994; Brenner et al., 1994; Verderber et al., 1995).

Vimentin is present during development and its expression is maintained throughout adulthood (Cochard and Paulin, 1984). As one of the major IFs in the glial cells, Vimentin has multiple functions, including the regulation of cell cytoskeleton via its

intimate relationship with microtubules (Goldman et al., 1996). Ivaska *et al.* reported that Vimentin takes part in the regulation of proteins that are associated with cell migration, cell adhesion and signalling (Ivaska et al., 2007). They suggested that in the absence of Vimentin, or its malfunction, some processes become compromised, which could lead to abnormal protein expression or perturbations in normal signalling pathways. For example, it was reported that wounded mice that lack the *Vimentin* gene heal slower than their wild-type counterparts (Eckes et al., 2000).

Although the precise role of GFAP and Vimentin is yet to be determined, studies with the use of transgenic animals helped to shed some light on the topic. Under normal conditions, Müller glia are much softer than neurons, which helps them to maintain structural integrity within the retina and protect neuronal cells in case of a mechanical insult. Following retinal damage and development of reactive gliosis, Müller glia lose this flexibility and become more rigid (Lundkvist et al., 2004), most likely due to an increase in the density of IFs (Lui et al., 2011; Lu et al., 2013). This increase in stiffness is a major factor that contributes to viscoelastic properties of the glial cells and is coupled with a remodelling of the glial network and is associated with changes in the retinal architecture, such as folding and shrinkage (Lu et al., 2011). Interestingly, in mutant mice lacking both GFAP and Vimentin, Müller glia show similar biomechanical properties as Müller glia in the uninjured wild-type retina, even when exposed to mechanical damage (Lu et al., 2011). Although, the exact purpose of this increased stiffness is not known, it has been suggested that it may serve as a regulatory mechanism that helps to stabilise the delicate neuronal network and compensate for any loss of mechanical tension caused by the loss of photoreceptors (or other retinal cells). This stiffness could also have a negative impact on regeneration and therapeutic interventions, as rigid scars may impair neurite outgrowth and may contribute to poorer regenerative abilities of the mammalian retina. Therefore, inhibition of the upregulation of IF proteins in Müller glia may ease neuronal plasticity and axonal sprouting after the retinal injury (Cho et al., 2005).

In pathological conditions associated with photoreceptor degeneration, the upregulation of IFs in Müller glia is associated with their hypertrophy, which contributes to the formation of a glial scar at the outer edge of the neuroretina (Fan et al., 1996; Lewis and Fisher, 2000). For example, any trauma to a retina result in dramatic changes in Müller glia morphology which are mirrored by the alterations in IFs levels in the majority of the vertebrates. There are striking exceptions, however; Müller glial cells in the ground squirrel retina do not become activated and do not show any upregulation of IF proteins in response to retinal injury (Linberg et al., 2002). Studies on *Gfap*$^{-/-}$/*Vim*$^{-/-}$ knockout mice have reported that, following retinal detachment, the absence of IFs results in fewer morphological alterations in the glial cells and a marked

reduction in reactive gliosis (Kinouchi et al., 2003; Lundkvist et al., 2004). On the other hand, in single *Gfap*$^{-/-}$ mutant mice, Tatzelt *et al.* reported that following scrape-induced neurodegeneration, the glial response was similar to that of wild-type animals (Tatzelt et al., 1996). This could be explained by the fact that formation of the 'functional' IFs depends on copolymerisation of different IF proteins and that in the absence of GFAP, IF can still be formed due to the presence of other IFs proteins, such as Vimentin. In a study by Pekny *et al*., the authors reported that in the 'uninjured' brain of the *Gfap*$^{-/-}$ mutant, Vimentin is enable to self-polymerise in the absence of GFAP to form IFs in astrocytes (Pekny et al., 1995). In contrast, following the mechanical insult and activation of astrocytes, IFs were formed due to an increase in Nestin expression and its copolymerisation with Vimentin, which also led to development of the glial scar. In the current study of a model of RP, despite successful prevention of GFAP upregulation, Müller glial cells still underwent morphological changes associated with glial hypertrophy (Figure 4.5 and Figure 4.10). In line with these findings, Cuenca *et al.* also demonstrated that knockdown of *Gfap* gene in *Xenopus* does not prevent Müller glia from a formation of a glial scar (Martinez-De Luna et al., 2016). Interestingly, our study indicates that Vimentin may play a previously underappreciated role in establishing Müller glial cell hypertrophy; reducing Vimentin in a model of chronic retinal degeneration results in changes in glial hypertrophy and a reduction in the extent of the glial scar, compared to (degenerating) control retinae (Figure 4.10). This finding is in accordance with Lewis and Fisher study in the feline retina, where only the Vimentin^{+ve} Müller glial processes grew into the subretinal space and formed the glial scar following the retinal detachment (Fisher and Lewis, 2003; Lewis and Fisher, 2003). Further evidence for the role of Vimentin in the extension of Müller glia processes may come from the studies on the retina of ground squirrels. As mentioned previously, following retinal detachment Müller glia do not become reactive, proliferate or migrate in this species and show no upregulation of GFAP protein (Linberg et al., 2002; Merriman et al., 2016). Interestingly, Linberg *et al.* reported an increase in Vimentin levels in the Müller glia end feet and around surviving photoreceptors (Linberg et al., 2002). They also reported that despite the lack of Müller glia reactivity, the glial processes were still able to fill the empty spaces left by dead photoreceptors, preserving the general retinal structure. Moreover, it has been found that in *Vimentin* knockout mice, reactive brain astrocytes are able to form some IF that consist mainly of GFAP, but the filaments instead of assembling into loose bundles, form abnormal packed ones (Eliasson et al., 1999). This is perhaps not surprising as Vimentin has an intimate relationship with microtubules and it has been suggested that it serves as a facilitator in the assembly of other IF proteins, including GFAP (Galou, 1996). In this study following downregulation of Vimentin with AAV.shVim we did not observe any

major structural abnormalities. Müller glia apical terminals did not increase over time as in the AAV.shCon transduced eyes, but the knockdown effect was only visible at the later time point (Figure 4.7 and Figure 4.10). Moreover, studies of Vimentin knockout mice showed that in the injured brain, astrocytes may be able to form some GFAP-only IFs, as alterations of Vimentin significantly decrease Nestin and Synemin protein expression (Eliasson et al., 1999). Of the latter, Jing *et al.* reported that accumulation of Synemin at the protein level requires functional Vimentin (Jing et al., 2007). Further support for the intimate relationship between IF proteins comes from our study, as targeting both GFAP and Vimentin resulted in more prominent structural abnormalities in chronic retinal degeneration (Figure 4.8). These findings could indicate that the formation of IFs in Müller glia requires at least one of the two IFs studied, but when both of them are removed, functional IFs may not be able to form efficiently, if at all. Although, the lateral spread of Müller glia processes was not inhibited in the AAV.shGfap injected eyes at 3 weeks post-transduction, future experiments should look into the 6 weeks time-point to confirm this result. It would also be interesting to examine the impact of Vimentin removal from Müller glia in the non-degenerating retina, as in the non-activated state, Vimentin is the primary IF protein expressed in this cell type. Further experiments should also look into the expression of different IF proteins, such as Nestin and Synemin, in those retinae treated with AAV.shGfap and AAV.shVim, as well as examining the assembly of IFs following the removal of the Vimentin using electron microscopy.

Retinal glial cells are responsible for the maintenance of the inner and outer blood-retinal barrier integrity, which consists of densely-packed tight junctions between endothelial cells (Kaur et al., 2007). Disruptions to it and abnormal migration of microglial and vascular cells into the vitreous are common to a variety of retinal pathologies, including diabetic retinopathy and retinal detachment (reviewed in (Bringmann et al., 2009a)). These migrated cells exert traction on the retina, which can lead to retinal detachment. The formation of the glial scar has been proposed to protect the neuroretina from further damage, especially pathogenic factors present in the vitreous and/or injured RPE. In order to increase the neuronal cell survival, activated Müller glia start to produce a number of neurotrophic, and other, growth factors including FGF, as well as several antioxidants, molecules that are not normally secreted in the healthy retina (reviewed in (Bringmann and Wiedemann, 2012)). Studies with *Gfap*$^{-/-}$*/Vim*$^{-/-}$ animals showed that genetic removal of GFAP and Vimentin leads to accelerated monocyte infiltration and faster degeneration of photoreceptors following retinal trauma (Nakazawa et al., 2007). In the genetic absence of both GFAP and Vimentin together, the end terminals of Müller glia become thinner, which leads to abnormal morphology of the glial cells and shearing of the glial end feet. As a result,

the glial terminals may separate from the rest of the cell body and eventually detach from the neuroretina (Lundkvist et al., 2004; Verardo et al., 2008). Moreover, it was reported that mortality rate is much higher in *Gfap*$^{-/-}$*/Vim*$^{-/-}$ animals following a brain trauma, in comparison to controls (Lundkvist et al., 2004). In this study, the combined injection of AAV.shGfap and AAV.shVim resulted in major structural defects including collapse of the neuroretina, retinal detachment or the failure of the eye to develop in the majority of injected eyes, which further supports the importance of IFs in maintaining the retinal architecture under degenerative conditions. However, others have reported that neural regeneration increased and CNS functions improved following pathological insult to *Gfap*$^{-/-}$*/Vim*$^{-/-}$ retina (Kinouchi et al., 2003; Verardo et al., 2008) or spinal cord (Menet et al., 2011). Moreover, it has been illustrated that in the injured spinal cord, silencing of GFAP and Vimentin mediated by RNAi-containing lentiviral vectors (under the PGK promoter and pseudotyped with the Mokola envelope for glial specificity) leads to a significant reduction in the extent of astrogliosis, increase in axonal sprouting and improvement in functional motor recovery (Desclaux et al., 2015). However, the majority of these reports come from studies using an acute injury or induced pathological condition, rather than a chronically diseased state. In this study, we assessed the impact of GFAP and Vimentin removal paired with photoreceptor cell transplant in a mouse model of degenerative retinopathy, which is caused by a knockout of *Rhodopsin* gene that leads to photoreceptor loss. We found that reduction of GFAP and/or Vimentin had no effect on the outcome of the cell transplantation, which is in line with previous findings where donor cells successfully integrated in the retinae of other degenerative mutants that showed elevated levels of IFs (Barber et al., 2013; Santos-Ferreira et al., 2014).

Taking into account contradicting reports from numerous studies, it is reasonable to conclude that the absence or malfunction of IF proteins has different effects on vulnerability of the retina based on both the type of the pathological insult and the species. This is supported by findings from a variety of studies examining signalling pathways that are proposed to inhibit the up-regulation of IFs. For example, upregulation of GFAP and glial scarring following retinal detachment were reduced by introducing exogenous brain derived neuronal factor (BDNF) (Lewis et al., 1999). The same approach, however, did not affect the GFAP up-regulation induced by optic nerve crush (Chen and Weber, 2002), which further supports the complexity of the IF responses.

The complexity of retinal glial reactivity to pathological insult is further complicated by the heterogeneity of Müller cells, which may lead to different responses among individual cells and between Müller cells in different species. As mentioned before, there are species-specific differences in the distribution of IF proteins even in non-

reactive Müller glial cells. For example, in mouse, squirrel and rabbit Vimentin is found in high levels across the entire Müller cell, whereas in feline and human cells Vimentin is only expressed in their outer glial terminals (Okada et al., 1990b). In most mammalian species, retinal detachment results in Müller cell proliferation, hypertrophy, and an increase in the expression of GFAP. However, these alterations were not observed after detachment of the cone-dominant ground squirrel retina (Linberg et al., 2002; Merriman et al., 2016). In the chick retina, NMDA-induced retinal damage caused heterogeneity of glial response even within the same region of the retina (Lewis and Fisher, 2003). In the injured regions, around 65% of the Müller cells re-entered the cell cycle, while the remaining 35% did not. Luna et al. showed that following retinal injury Müller cells started to upregulate GFAP, Vimentin and Nestin on individual basis rather than across all the cells in a uniform manner (Luna et al., 2010). Moreover, it was suggested that GFAP plays a role in regulating glial proliferation as only cells that failed to increase GFAP expression re-entered cell cycle (Fisher and Lewis, 2003). This heterogeneity of glial responses has also been reported following spinal cord injury. In recent study by Wanner *et al*. reactive astrogliosis was noted to be very heterogeneous and it can be graded with respect to distance from the injury and the type of activated astrocytes found around the lesion site (Wanner et al., 2013). Additionally, as in the retina, neighbouring astroglial cells have also been reported to present a unique pattern of molecular expression that further contributes to complexity of glial responses. Such observations raise some fundamental questions about the heterogeneity of signalling pathways that activate the glia cells, a diversity of glia participating in the cellular response, and the signalling mechanisms that are activated in response to different types of injury. The above examples only highlight the complexity of gliosis, indicating that it is not a simple all or nothing response, but rather a variable process with respect to alterations in cell morphology, proliferation and molecular expression, all of which are tuned in a situation-specific manner to different pathological stimuli.

In the retina of warm-blooded vertebrates, development of the glial scar within and at the margin of the injured tissue is one reason for the failure of the system to regenerate. In contrast, cold-blooded vertebrates such as fish and amphibians retain the capability of full retinal regeneration into adulthood. It is tempting to ask what the relationship between the development of gliosis and regeneration is, and whether gliosis is just a failed regenerative programme in the mammalian retina. Numerous studies showed that activation of Müller cells causes upregulation of Vimentin and Nestin, which are the markers of progenitor cells. The re-expression of Nestin by reactive glia in the injured mature retina may reflect the differentiation of the cells toward becoming neurogenic progenitors (Goel and Dhingra, 2012). It was reported

that after retinal detachment, Nestin is localised to the foremost processes of the glial cells that grew into the subretinal space, as well as in proliferating Müller glia (Luna et al., 2010). Lewis *et al.* demonstrated that following the detachment the nuclei of Müller cells migrate towards the outer retina using Vimentin filaments, where they proliferate and re-enter the cell cycle (Lewis et al., 2010). Future studies should look into this idea to see how GFAP and Vimentin knockdown affects other IFs and whether this may have any impact on cell proliferation.

To conclude, in this study we showed that two IFs, Vimentin and GFAP, could successfully be decreased in a mouse model of chronic retinal degeneration using AAV vectors. We showed that, in this context, knockdown of Vimentin alone is sufficient to largely prevent Müller cell hypertrophy indicating that the role of Vimentin in glial scarring may have been largely overlooked. Although we did not see any significant impact on the outcome of cell transplantation, decreasing levels of IF proteins may be still of therapeutical interest. For example, reactive Müller cells contribute to two causes of blindness: subretinal fibrosis and proliferative vitreoretinopathy. In this study, the hypertrophy of the Müller processes was shown to be minimised following RNAi. This strategy may help to regenerate the photoreceptor OS following retinal reattachment. Moreover, the designed vectors may be of potential use when considering the implantation of retinal prosthetics or retinal sheets as glial remodelling may be a major limiting factor with these therapeutic approaches. It has been suggested that development of the glial scar impedes the contact between the implants/grafts and the host neuroretina by creating a physical barrier between the two. For example, transplantation of the whole retinal sheets was proved to be feasible with the establishment of proper neuronal connections between the graft and host retina; however in many cases the transplanted retina and the host were not well integrated (Radtke et al., 1999; Peng et al., 2008; Seiler et al., 2009). The same applies to electric retinal implants such as Angus III as the glial scarring may have a significant impact on these devices especially when implanted subretinally limiting their contact with the host neuroretina (Stingl et al., 2013). This study may therefore help to optimise or even ease some of the therapies for patients suffering from advanced retinopathies.

Chapter 5

CSPGs modulation in the mouse model of retinitis pigmentosa

5.1 Overview

In the central nervous system (CNS), the majority of damaged axons fail to regenerate following injury. This failure is due in part to the response by glial cells, including the upregulation of inhibitory molecules in the extracellular matrix (ECM), which may present a potent barrier to neuronal regeneration (Yiu and He, 2006).

An important class of inhibitory ECM molecules are the chondroitin sulphate proteoglycans (CSPGs), a diverse group of glycoproteins, which also represent one of the most abundant groups of ECM proteins. The inhibitory action of CSPGs has been attributed to the abundance of negatively charged glycosaminoglycan (GAG) chains that decorate the core protein (Galtrey and Fawcett, 2007). These GAG chains vary in length, number and sulphation pattern and were shown to determine the unique functions of different proteoglycans (PGs). Several types of CSPGs, including Aggrecan, Versican, Neurocan, Brevican and Phosphacan, are found in adult CNS tissue and are variously expressed throughout the brain, spinal cord and eye, where they are condensed into perineuronal nets surrounding CNS neurons (Brückner et al., 2000). By interacting with other components of the ECM environment, these PGs regulate a wide range of different cellular processes including cell adhesion and growth, receptor binding, cell migration and synaptic plasticity. Following CNS injury, CSPGs are upregulated (McKeon et al., 1995; Fitch et al., 1999; Jones et al., 2002; Morgenstern et al., 2002; Jones et al., 2003a) and appear to inhibit neurite outgrowth from adult neurons (Snow et al., 1990; Davies et al., 1999). Digestion of the GAG side chains using a bacterial chondroitinase ABC (ChABC) enzyme abrogates CSPG-dependent neurite outgrowth inhibition *in vitro* and improves neurite sprouting and functional recovery after spinal cord injury (SCI) (McKeon et al., 1995; Zuo et al., 1998; Bradbury et al., 2002; Grimpe et al., 2005). Interestingly, the upregulation of CSPGs has also been linked to some psychiatric conditions including bipolar disorder, schizophrenia and ADHD (reviewed in (De Luca and Papa, 2016)). In recent years, Protein tyrosine phosphatase sigma (PTPsigma), Leukocyte common antigen related phosphatase (LAR) and Nogo R have been identified as neuronal receptors that functionally interact with and mediate CSPG-dependent inhibition of axonal growth (Shen et al., 2009; Fisher et al., 2011; Dickendesher et al., 2012).

In adult retina, CSPGs are found in several regions including the optic nerve, inner (IPL) and outer plexiform layer (OPL) and the photoreceptor inner/outer segment (IS/OS) region (Zhang et al., 2003b; 2007; Hippert et al., 2015). Numerous studies have reported that CSPG levels are increased in a wide spectrum of retinopathies, including optic nerve damage and transient retinal ischemia (Inatani et al., 2000; 2001; Zhang et al., 2007; Singhal et al., 2008). Recently, a comprehensive assessment by

our group showed spatio-temporal differences in the expression of CSPGs between different models of inherited retinopathy (see Chapter 3; (Hippert et al., 2015)). Such changes have also been linked to poorer therapeutic outcome. Findings from studies of cell replacement strategies have indicated that increased CSPGs deposition in the diseased retina is correlated with poor cell transplantation outcome, while enzymatic reduction of CS GAGs results in increased numbers of donor-labelled cells in the host retinae (Suzuki et al., 2007; Singhal et al., 2008; Barber et al., 2013). For example, *Rho*$^{-/-}$ animals, where the number of GFP^{+} cells in the recipient retina after transplantation was very low (Barber et al., 2013) presented high levels of CSPGs from the onset of degeneration, and this continued to rise throughout the course of disease (see Chapter 3, and (Barber et al., 2013; Hippert et al., 2015)). In contrast, in *PDE6b*$^{rd1/rd1}$ recipients, where the number of observable donor-labelled cells in the host retina was higher (Barber et al., 2013), there was a marked decrease in global CSPGs expression over time (see Chapter 3 and (Hippert et al., 2015)).

While it has been generally accepted that CSPGs exert a largely inhibitory impact to the regenerative process, this may be an oversimplification. For example, growth-promoting features have been attributed to several CSPGs in their soluble (Brittis and Silver, 1994; Greenfield et al., 1999) and over-sulphated form (Bicknese et al., 1994; Nakanishi et al., 2006; Sato et al., 2008). Moreover, CSPG distribution may not be uniform at the lesion site, with different CSPGs having unique patterns of expression (Tang et al., 2003). This suggests that different PGs may have different roles in modulating the spread of the injury. In keeping with this idea, a reduction in Neurocan and Versican have both been reported to be beneficial to cell transplantation outcome (Zhang et al., 2007; Singhal et al., 2008); however as both PGs were shown to be expressed in the wild-type retina in the IS/OS region (Zhang et al., 2003b), it is possible that upregulation of other PGs may be detrimental to therapeutic interventions.

Aggrecan is one of the major CSPGs expressed in the central and peripheral nervous system of embryos and adults (Oakley and Tosney, 1991; Schwartz et al., 1996). In the normal CNS, this PG is produced by glial precursor cells and strongly influences neurite outgrowth (Domowicz et al., 2008; Afshari et al., 2010a). It is also required for normal astrocyte differentiation (Smith and Strunz, 2005). In the eye, Aggrecan has been proposed to be involved in the maintenance of the normal laminar structure of the adult retina (Lemons et al., 1999; Ali et al., 2011; Chen et al., 2012a). Findings from the injured CNS showed that Aggrecan has a negative impact on Schwan cell migration following transplantation after SCI by inhibiting integrin mediated cell adhesion (Afshari et al., 2010b). Later, Chen et al. reported that Aggrecan is markedly upregulated in a rat model of retinal dystrophy, particularly around the IPL (Chen et al., 2012b). To date,

no reports on Aggrecan expression in mouse models of retinitis pigmentosa (RP) have been published. Given the negative role of Aggrecan on neuronal regeneration in other systems, this study sought to establish whether changes in the levels of Aggrecan could, either wholly or partially, account for the reported differences in cell transplantation outcome by Barber *et al.* (Barber et al., 2013). In this chapter, two models of RP, *Rho*$^{-/-}$ and *Pde6b*$^{rd1/rd1}$, were chosen to study the expression patterns of Aggrecan as disease progressed, compared against wild-type controls. The expression pattern of the CSPG receptor LAR in the wild-type and diseased mouse retina was also assessed. Finally, an alternative enzymatic treatment to ChABC was also made and tested *in vivo*.

5.2 Results

5.2.1 Müller glia primary culture to study effects of elevated CSPGs

Following CNS injury, there is a marked upregulation of CSPGs, which are believed to contribute to reactivity of the glial cells and development of the glial scar (reviewed in (Properzi et al., 2003)). To test whether CSPGs can directly influence Müller glial cell reactivity, *Rlbp*.GFP$^{+/+}$ cells were cultured on CSPGs substrate and compared against untreated controls.

Two different concentrations (10 and 20 µg/ml of a commercially prepared mix of CSPGs (Millipore, UK) were chosen to coat cell plates, according to previously published reports (Siebert and Osterhout, 2011; Tan et al., 2011), before adding FACS sorted *Rlbp*.GFP$^{+/+}$ cells. A full description of the protocol is provided in Chapter 2, Section 2.2. Cells that grew on laminin-only substrate were used as a negative control. After 2 weeks in culture, ICC analysis was performed to look for changes in Müller glia reactivity, resulting from the presence of high levels of CSPGs.

Cultured Müller glial express a variety of typical glial markers, including the intermediate filament (IF) proteins, Vimentin and Glial fibrillary acidic protein (GFAP) (see Chapter 3). These two IFs have been shown to be markedly upregulated by activated Müller glial cells in both injured and diseased retina models (Ekström et al., 1988; Sheedlo et al., 1995; Fan et al., 1996; Inatani et al., 2001; Escher et al., 2008; Hippert et al., 2015). As already demonstrated in Chapter 4, Vimentin is highly expressed by Müller glial cells *in vitro* with no major differences between individual cells (Figure 5.1A'). In contrast, GFAP staining was found to be very sparse in Müller glia grown in the absence of CSPGs (Figure 5.1A'), which is in line with previous reports (Chapter 4; Abrahan et al., 2009). Interestingly, there was a notable increase in the number of cells expressing GFAP in the wells coated with CSPG mix (Figure 5.1B'-C'), compared to untreated controls. A closer examination of the morphology of the cells grown on CSPGs substrate revealed changes that were concentration dependent. Those that were cultured on CSPGs had smaller nuclei and were thinner, with a more elongated profile, compared to cells grown on laminin only coated plates. Interestingly, in the presence of high concentrations of CSPGs, the glial processes appeared increasingly tangled and formed aggregates, which were not observed in the control cultures. These morphologies were particularly evident in the wells with higher concentration of CSPGs (Figure 5.1A).

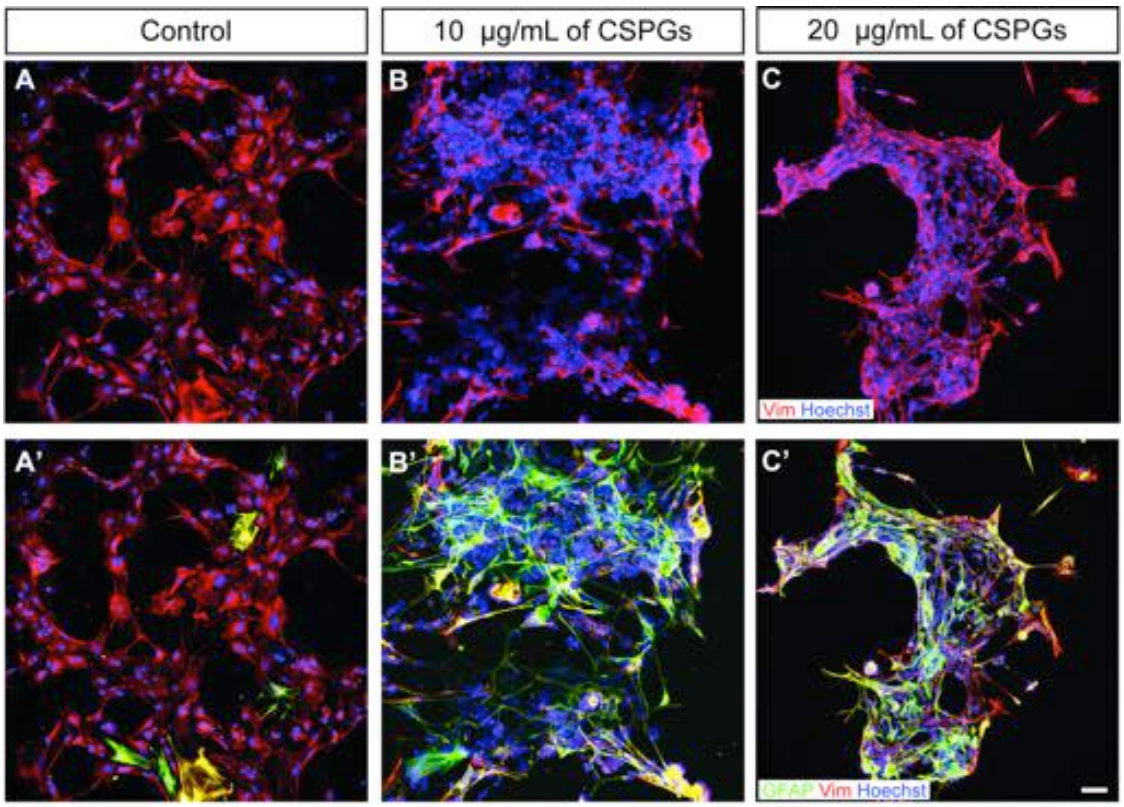

Figure 5.1 Müller glia morphology is altered in the presence of high CSPGs levels in vitro

A) After 2 weeks in culture on laminin-coated plates, Müller cells showed a robust expression of **A)** Vimentin (*red*), but only a very sparse staining for **A')** GFAP (*green*), with no visible changes to cell morphology. **B - C)** Cells that grew in the presence of high levels of CSPGs visibly changed appearance, with smaller nuclei and a more condensed morphology, in a concentration-dependant manner. Moreover, high levels of CSPGs resulted in Müller glial cells forming aggregates 20 µg/mL of CSPGs substrate. All of these morphological changes were accompanied by a visible upregulation in GFAP. Cells were counterstained with nuclei marker Hoechst 33342 (*blue*). Scale bar: 50 µm.

To test whether the observed changes in Müller glia were caused by high levels of CSPGs, rather than a lack of adhesion, Müller glial were first cultured for 2 weeks on laminin-only coated plates, and pre-assessed under a white-light microscope before the addition of CSPGs mix. Two concentrations were used and added to cultures at intervals of 2 days for one week to account for any intrinsic degradation mechanisms (Figure 5.2). Cells were assessed for morphological changes 1 week post-treatment with ICC analysis.

In the absence of CSPGs (Figure 5.2A), cultured Müller glia showed flattened morphology similar to that observed in the control wells presented in Figure 5.1A. Following the addition of the CSPG mix at 2 weeks in culture, there were visible changes in glial morphology, although these were not as marked as when the cells had been grown on the CSPG substrate from the start of culturing (Figure 5.1B-C). Although cells appeared to be more sparsely distributed at first, closer examination showed that, in the presence of CSPGs, Müller glia were more likely to form numerous cell clusters. These aggregates were very prominent in the wells with the highest concentration of CSPGs (Figure 5.2C). The nuclei of the cells also appeared to be smaller in comparison to the nuclei in the control wells with the glial processes being thinner and more elongated. Together, these findings suggest that CSPGs may have an impact on Müller glia behaviour, which could be linked to development of the glial scar.

CSPGs have been reported to have an inhibitory role on neurite extension after SCI (reviewed in (Fawcett and Asher, 1999; Sharma et al., 2012a)). In other work carried out in the lab, *Nrl*.GFP$^{+/+}$ photoreceptor precursor cells were shown to extend their processes as early as few hours after being added to cultured Müller glial cells (Warre-Cornish, PhD thesis, 2013). To test whether the presence of CSPGs has any inhibitory effect on the outgrowth of *Nrl*.GFP$^{+/+}$ processes, on average 10,000 *Nrl*.GFP$^{+/+}$ cells were added per well 24 hours after the first dose of CSPGs mix and cultured for 7 days before plates were fixed and analysed.

Qualitative assessment showed no observable differences in the number of GFP^{+ve} cells between the three (control, low CSPG and high CSPG addition) experimental conditions, suggesting that the presence of CSPGs does not have any significant impact on photoreceptor precursor survival *in vitro* (Figure 5.2B i-iii). Closer inspection of the cells revealed that in the control wells, numerous GFP^{+ve} cells were observed extending long processes out from the cell body (on average 2.7±0.77 processes with the average length of 15.84±1.42 µm) and apparently forming contacts with other cells (Figure 5.2B i). The presence of high levels of CSPGs did not have a significant impact on the measurable length of extended *Nrl*.GFP$^{+/+}$ processes (11.48±2.97 in 50 µg/mL

of CSPGs; and 12.05±3.1 µm in 100 µg/mL of CSPGs respectively; Figure 5.3C i, *P*=0.083), but the average number of outgrown processes was markedly decreased (1.49±0.61 in 50 µg/mL of CSPGs; and 1.33±0.26 µm in 100 µg/mL of CSPGs respectively; Figure 5.3C ii, *P*<0.05). This suggests that in the presence of high concentrations of CSPGs, *Nrl*.GFP$^{+/+}$ cells are less likely to extend a process, which may be of particular importance for cell transplantation where cells are expected to grow their processes to make a contact with the host retina.

Of note, a similar experiment was also performed with Müller glial cells cultured on CSPG substrate from the outset (as opposed to adding CSPGs after 2 weeks in culture). Unfortunately, no *Nrl*.GFP$^{+/+}$ cells were observed at 2 days post-addition in any of the wells that had the CSPGs mix used as a substrate (n = 4 independent cultures examined; data not shown). This may indicate an unfavourable environment, preventing the survival of these cells. Although the composition of the medium that cells grew in was not tested, post-culturing, it is possible that in such conditions reactive Müller glia release cytokines, which are detrimental to photoreceptor precursor cell survival (Fernández-Sánchez et al., 2015).

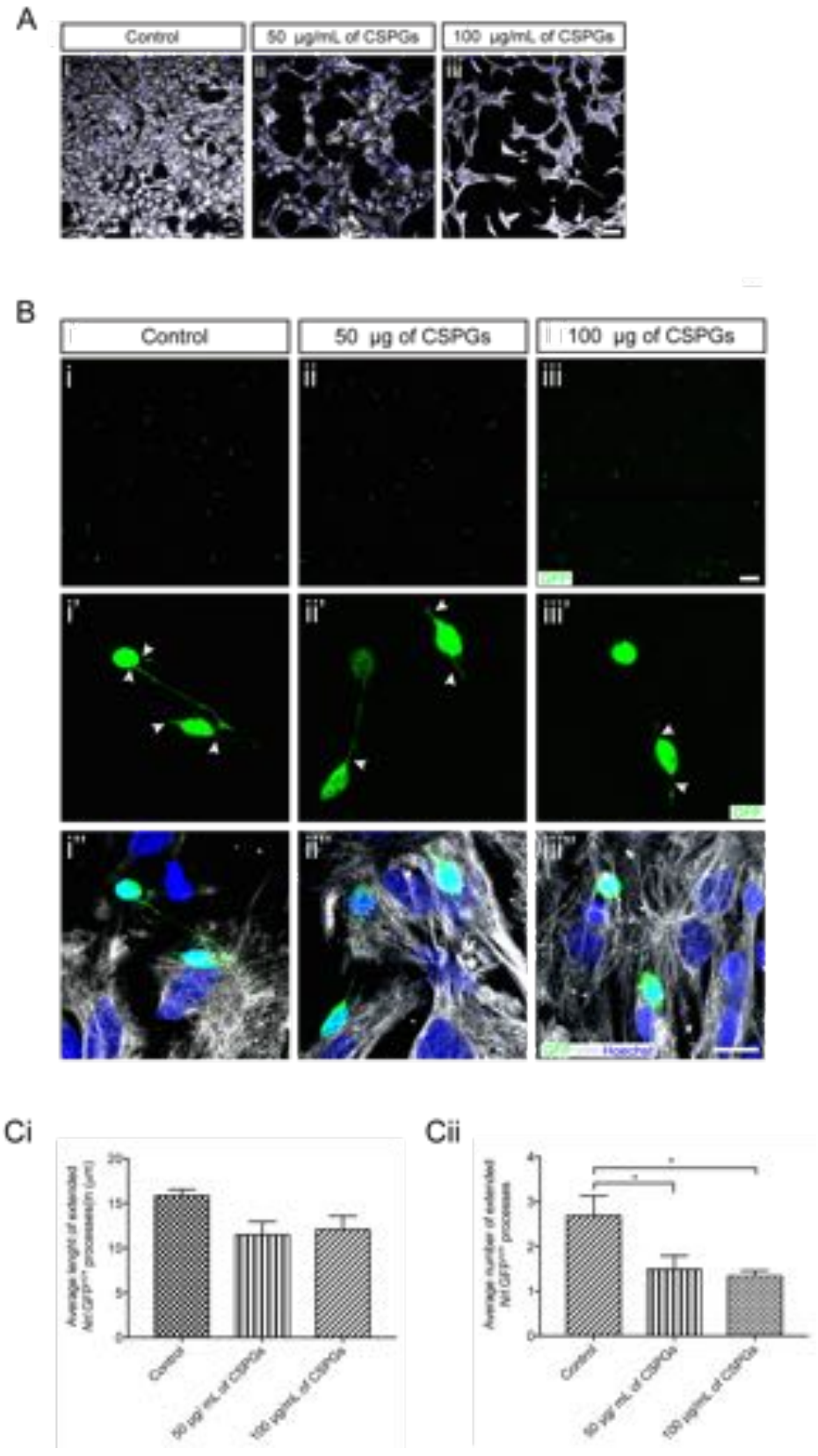

Figure 5.2 CSPGs alter Müller glia morphology and inhibit extension of Nrl.GFP$^{+/+}$ processes in vitro.

Ai-iii) ICC analysis of Müller glia stained with Vimentin antibody (*grey*). **Ai)** After 3 weeks in culture, Müller glia in control wells typically showed a flattened morphology with cell processes covering majority of the area. **Aii)**. Cells that grew in the presence of 50 µg CSPGs demonstrated visible changes in their appearance with smaller nuclei with Müller glia aggregating into small clumps, **Aiii)** with more clusters being formed at higher levels of CSPGs.

Bi-iii) Low magnification images showing a good number of *Nrl*.GFP$^{+/+}$ (*green*) after 1 week in culture in both control and CSPGs treated wells. **Bi'-I'')** In control wells, *Nrl*.GFP$^{+/+}$ extended long processes to establish a contact with other *Nrl*.GFP$^{+/+}$ cells and Müller glia (*white* arrows). **Bii'-ii'')** The length of *Nrl*.GFP$^{+/+}$ outgrowths (white arrows) appeared to be shorter in the presence of 50 µg CSPGs. **Biii'-iii'')** with more clusters being formed at higher levels of CSPGs. Cells were counterstained with nuclei marker Hoechst 33342 (*blue*). Scale bars: Ai-iii) and Bi-iii); 50 µm; Ai-iii), 25 µm. **Ci-ii)** Quantitative analysis of the extended *Nrl*.GFP$^{+/+}$ processes showed that **Ci)** although there was no significant decrease in the length of the processes in the presence of CSPGs, **Cii)** the number of extended processes was. $*P < 0.05$ with a one-way ANOVA. Error bars: SD; n=3 independent cultures examined. Scale bar: 25 µm.

5.2.2 Aggrecan expression undergoes disease-specific changes in different models of retinal degeneration

As shown in Chapter 3, the *Rho*$^{-/-}$ mutant exhibits marked upregulation in CSPGs levels with degeneration, whereas in the *Pde6b*$^{rd1/rd1}$ mice CSPGs were found to decrease (Hippert et al., 2015). These differences between these two models may explain why cell transplantation outcome differed between the two models, with very low numbers of donor-labelled cells reported in the *Rho*$^{-/-}$ recipients (Barber et al., 2013). Above, it has been demonstrated that photoreceptor process outgrowth is altered in the presence of CSPGs *in vitro.* One of the main components of the CSPG mix used in section 5.2.1 is Aggrecan, which has been shown to similarly influence process outgrowth of brain-derived neuronal cells (Snow and Letourneau, 1992; Challacombe et al., 1997). To examine whether there are any differences in Aggrecan expression between the two models of inherited retinal degeneration, semi-quantitative Western blot (WB) analysis was performed and results were compared to age-matched wild-type controls.

As previously reported, in a mouse retina, levels of Aggrecan are elevated during development but decrease during adulthood (Ali et al., 2011). In wild-type retina, Aggrecan was detectable as early as P10 (Figure 5.3A) with levels decreasing with age. In the P10 *Rho*$^{-/-}$ mutant, levels of Aggrecan were high, but decreased by 3 weeks of age, after this time they have started to increase again (Figure 5.3B). Statistical analysis showed that there was a marked difference between 3 weeks and 10 weeks of age, indicating that there is a significant upregulation of Aggrecan in this model of RP (P<0.05; Figure 5.3B). Interestingly, in the *Pde6b*$^{rd1/rd1}$ mice, the pattern of Aggrecan expression was reversed, with global levels of Aggrecan significantly decreasing with disease progression (between P10 and 6-8 weeks of age; P<0.05; Figure 5.3C). These findings are in line with the findings presented in Chapter 3, where global levels of CSPGs, as assessed with CS-56, were shown to decrease between early and late stages of disease progression in the same model.

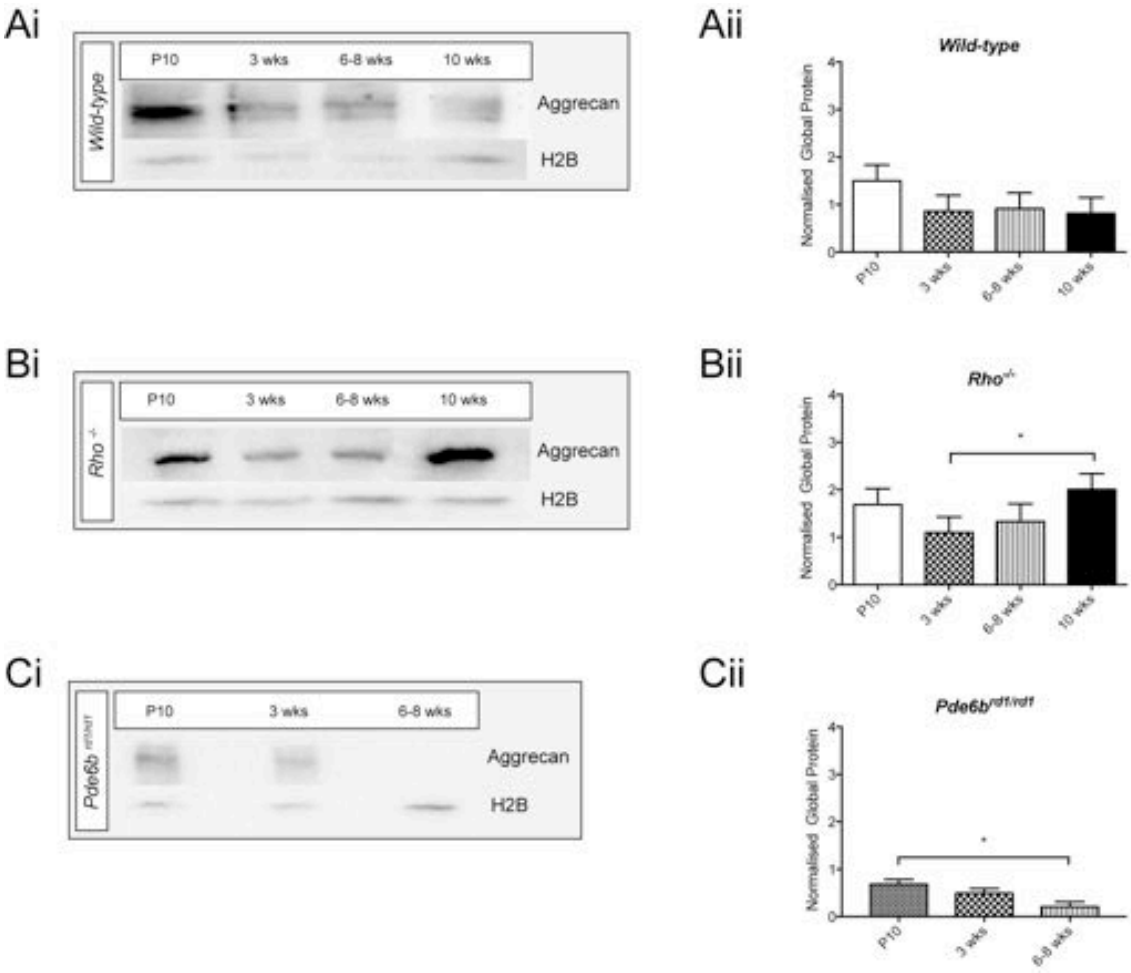

Figure 5.3 Aggrecan levels are elevated in Rho$^{-/-}$ mice.

Semi-quantitative assessments of Aggrecan levels in whole neural retina of **A)** a wild-type; **B)** *Rho*$^{-/-}$ and **C)** *Pde6b*$^{rd1/rd1}$ mutants. Semi-quantitative assessments of CSPG levels in whole neural retina were determined by Western blot. Aggrecan levels were normalized against H2B. Statistical significance was assessed with a one-way ANOVA test with Tukey's correction for multiple comparisons; *P < 0.05. Error bars: SEM, n=3 animals examined per time point.

5.2.3 Injection of ADAMTS-4 enzyme into subretinal space digests some but not all CSPG sugar chains

Application of ChABC is the predominant strategy used to digest CSPGs. Although ChABC has been shown to effectively remove GAG chains and resulted in an increase in axonal sprouting following CNS insult in rodents ((Bradbury et al., 2002; Caggiano et al., 2005), also reviewed in (Bradbury and Carter, 2011)), there are several disadvantages of using it clinically, including a potential risk of immune response due to ChABC's bacterial origin. Moreover, given the complexities of the roles of CSPGs in promoting and inhibiting regeneration, it may be of greater benefit to target specific CSPGs, rather than relying on broad spectrum digestion. Upregulation of the proteases that are involved in the turnover of the proteoglycans could be an alternative method to reduce levels of CSPGs in the ECM environment. For example, treatment with naturally occurring catabolic protein, Aggrecanase, also known as ADAMTS-4 ('A Disintegrin and Metalloproteinase with ThromboSpondin Motifs'), could be one alternative (Lemke et al., 2010). In humans, this protease is naturally expressed in the CNS, including the brain and retina (Tortorella, 1999; Tang, 2001) and was found to be capable of cleaving all the large CSPGs, including Aggrecan. As Aggrecan levels increase in the *Rho*$^{-/-}$ mutants with degeneration, the aim of this experiment was to determine whether ADAMTS-4 enzyme is capable of reducing its levels *in vivo*.

To assess the effectiveness of Aggrecanase in removing CSPGs in the *in vivo* retina, *Rho*$^{-/-}$ mutants and wild-type animals received a subretinal injection of a recommended dose (100 ng/µL per eye) of ADMATS-4 enzyme to either superior or inferior retina at 6 weeks of age and were analysed 48 hrs later. In parallel, some animals were injected with ChABC and were used as a positive control for CSPG degradation. Earle's Balanced Salt Solution (EBSS) injected eyes were used as a negative control, to control for the injection itself. All the retinae were analysed with IHC using CS-56 antibody, which binds to sulphated sugar chains, to assess any alterations in the levels of CSPG GAG chains following the enzymatic treatment.

In wild-type retina, CSPGs are abundant in the IS/OS region (see Chapter 3). Figure 5.4 shows that subretinal injection of EBSS had little or no effect on CSPG deposition within the IS/OS region (Figure 5.4A); CS-56 staining was robust even around the site of retinal detachment (Figure 5.4A i'; *arrow*). Similarly, no differences were observed between the injected and uninjected regions (Figure 5.4A i''). A similar pattern of CS-56 staining was observed in *Rho*$^{-/-}$ animals injected with EBBS (Figure 5.4B i). Although, the extent of the retinal detachment following injection in the *Rho*$^{-/-}$ retina was greater, the intensity of CS-56 staining intensity was comparable between the injected (Figure 5.4B i') and uninjected sites (Figure 5.4B i'').

In contrast, injection of ChABC into wild-type led to a marked reduction in CS-56 staining (Figure 5.4A ii'), compared to the uninjected region (Figure 5.4A ii''). A similar pattern was observed in *Rho*$^{-/-}$ animals, where CS-56 staining was strong in uninjected regions (Figure 5.4B ii'), but almost absent in the region injected with ChABC. Injection of ADAMTS-4 enzyme into wild-type retinae led to a slight reduction in CS-56 staining, in comparison with the uninjected region (Figure 5.4A iii''), and those retinae receiving EBSS, although robust staining was still detectable in the IS/OS region (Figure 5.4A iii'). In the retina of the *Rho*$^{-/-}$ mutant, ADAMTS-4 led to a visible reduction in detectable CSPGs in the subretinal region (Figure 5.4B iii'), compared to uninjected and EBSS treated controls (Figure 5.4B iii''). These results suggest that the enzymatic treatment with ADAMTS-4 leads to removal of CSPGs around the segment region that may not be present in a healthy retina.

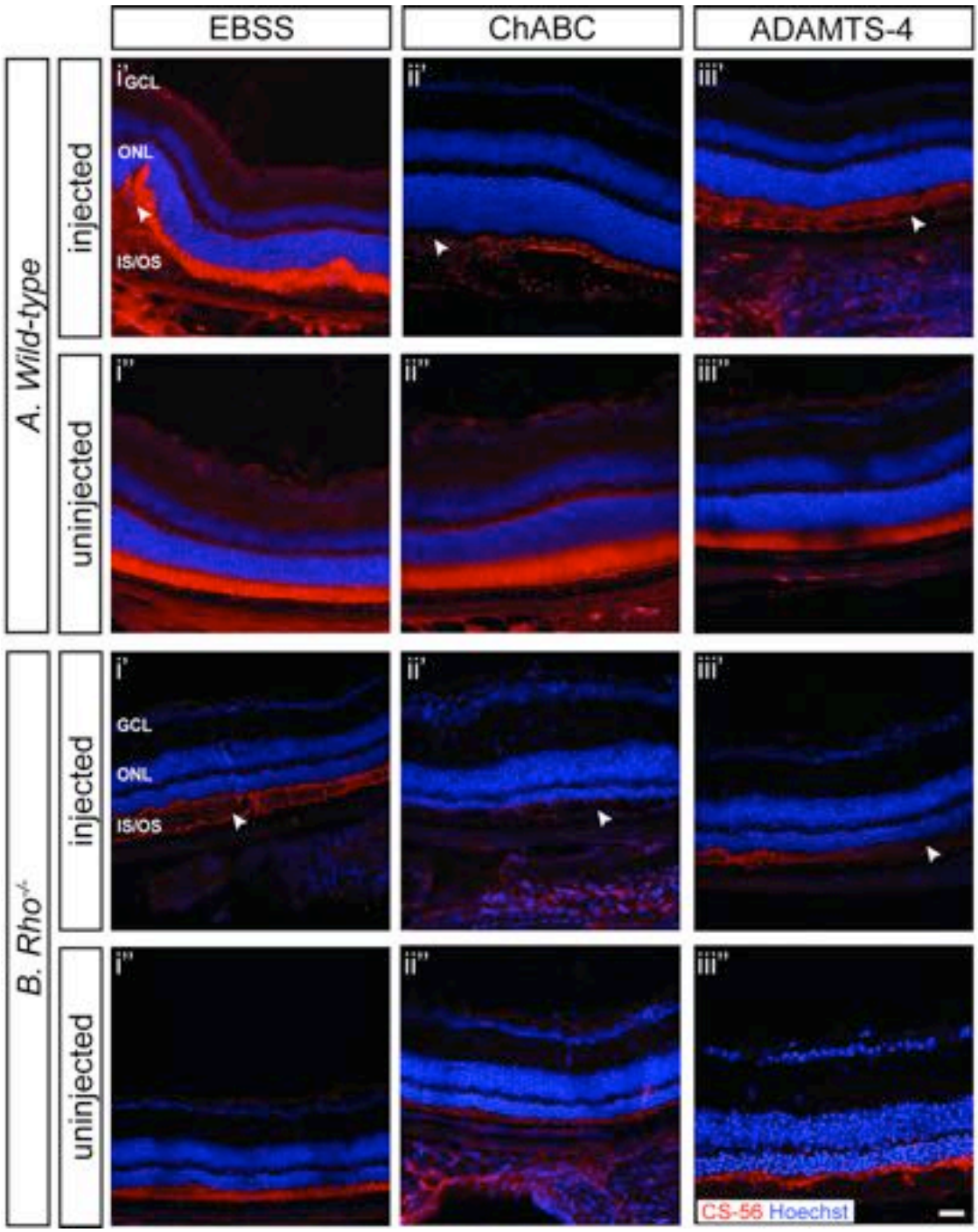

Figure 5.4 ADAMTS-4 reduces CSPGs in the photoreceptor segment region of the degenerating retina.

A-B) IHC analysis of CSPGs levels (*red*) following subretinal injection into a wild-type and *Rho*$^{-/-}$ retinae at 6 weeks of age. **Ai')** In a wild-type retina that was injected with EBBS control solution, CS-56 staining was very similar to that observed **Ai")** in the uninjected region, even at the site of retinal detachment (arrows). **Aii')** In contrast, treatment with ChABC resulted in almost complete abolishment of CS-56 staining **Aii")** in comparison to uninjected site of a retina. **Aiii')** Injection of ADAMTS-4 enzyme into a healthy retina led to a visible reduction in CS-56 staining in comparison to **Aiii")** the uninjected retina, with some staining still being detectable in the IS/OS region.

Bi') EBSS injection did not reduce CS-56 staining (*red*) in the *Rho*$^{-/-}$ mutants; although the retinal detachment was bigger to that seen in a wild-type. **Bii')** As in a healthy retina, ChABC injection led to complete absence of CS-56 staining detectable in the IS/OS region in comparison to **Bii")** the uninjected region. **Biii')** ADAMTS-4 enzyme treatment resulted in a noticeable decrease in CS-56 staining (*red*) **Biii")** in comparison to uninjected region. n=4 animals examined per each experimental condition.
Cryosections were counterstained with nuclei marker Hoechst 33342 (*blue*). GCL, ganglion cell layer; INL, inner nuclear layer; ONL, outer nuclear layer; IS/OS, photoreceptor inner/outer segment region. Scale bar, 25 μm.

To test whether enzymatic treatment with ADAMTS-4 altered global protein expression of CSPGs, and Aggrecan in particular, WB analyses were performed. In the ADAMTS-4 treated retina, immunoblotting with CS-56 antibody, which detects the GAG portion of native CSPGs, showed a small but not significant decrease in wild-type retina eyes (P=0.8741; Figure 5.5A). In contrast, a marked decrease in detectable CSPGs in the *Rho*$^{-/-}$ mutant, in comparison to EBSS-injected eyes (P<0.05; Figure 5.5B). Surprisingly, despite the observed reduction in CS-56 staining (Figure 5.4A), no difference in the global protein levels of Aggrecan was observed in a wild-type controls (P=0.9191; Figure 5.5A) or the *Rho*$^{-/-}$ mutants (P=0.9681; Figure 5.5B), indicating that while ADAMTS-4 enzyme cleaves some CSPGs present in the segment region when injected into the subretinal space (Figure 5.4B), this may not include Aggrecan. Taken together, these results indicate that ADAMTS-4 can robustly digest CSPGs that are specific to the IS/OS region and that are abundant in the diseased retina (Figure 5.5A). However, it also suggests that Aggrecan, whilst expressed in the retina, is unlikely to be present at significant levels in the segment region.

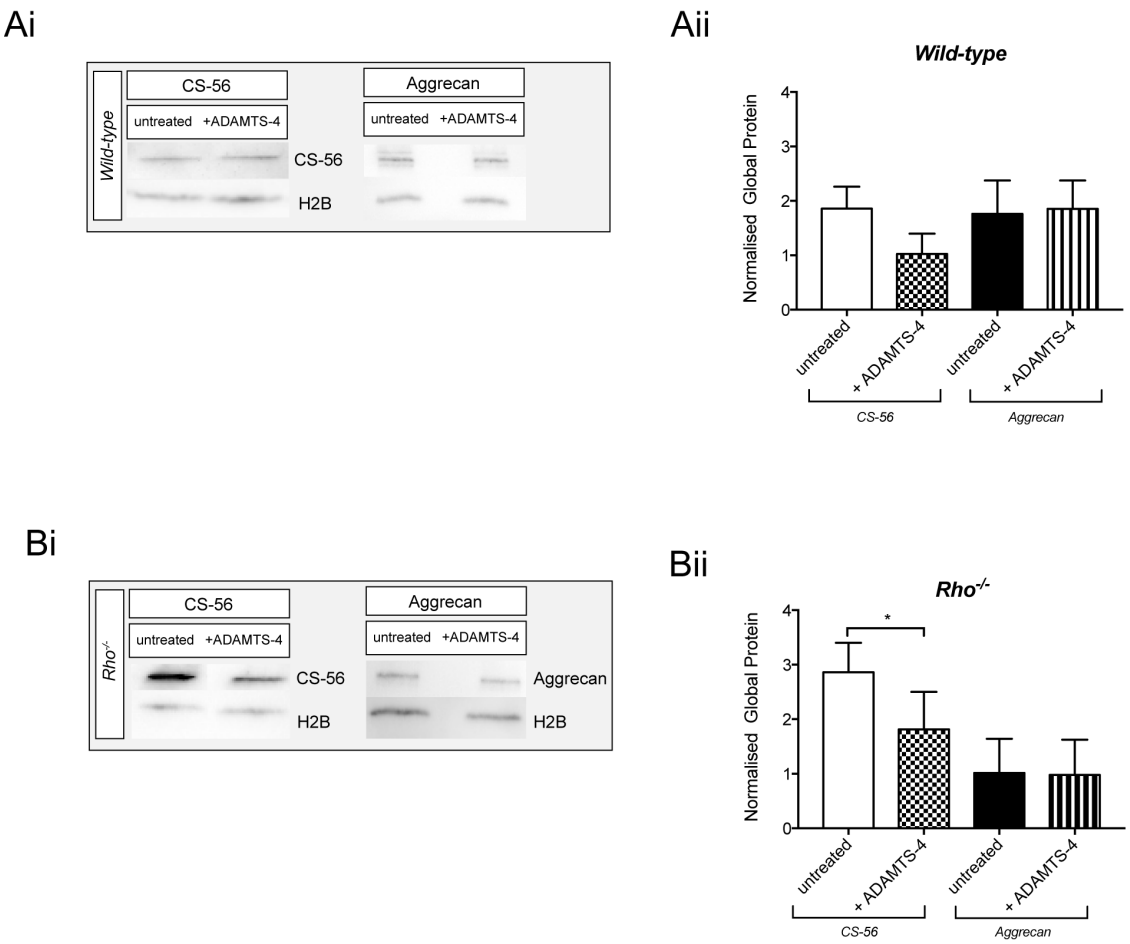

Figure 5.5 Global Aggrecan expression was not affected by subretinal administration of ADAMTS-4.

Semi-quantitative assessments of CSPGs and Aggrecan levels in **A)** a wild-type retina and **B)** the *Rho*$^{-/-}$ mutant. Semi-quantitative assessments of CSPGs and Aggrecan levels in whole neural retina were determined by Western blot. Protein levels were normalized against H2B. Statistical significance was assessed with a Student's *t*-test. *P* <0.5; Error bars: SEM, n=4 animals examined per each experimental condition.

5.2.4 Aggrecan is not a major component of CSPG deposits in the photoreceptor segment region

Given the lack of reduction in global levels of Aggrecan protein following the enzymatic treatment, the spatio-temporal distribution of Aggrecan was examined in two models of RP and compared to healthy wild-type controls. Ali *et al.* reported Aggrecan to be present throughout all neuronal layers, including the ONL, in the adult wild-type mouse retina (Ali et al., 2011). Having developed a working IHC protocol for Aggrecan (using the same antibody as the one used for WB analysis), the pattern of Aggrecan distribution was examined in the wild-type, *Rho*$^{-/-}$ and *Pde6b*$^{rd1/rd1}$ retina.

In the P10 wild-type retina, Aggrecan was robustly expressed in the IPL and GCL, with some weak staining observed in the OPL (Figure 5.6A i). This pattern of distribution was maintained throughout adulthood, although the expression in the IPL appeared to decrease with age (Figure 5.6A ii-iv). No Aggrecan expression was observed in the ONL or segment region, but positive staining was detectable in the choroid (Figure 5.6A ii-iv).

In the P10 *Rho*$^{-/-}$ retina, the distribution of Aggrecan was similar to that observed in a wild-type, but staining appeared stronger in the OPL and weak expression was also detectable in the IS/OS region (Figure 5.6B i). As degeneration progressed, the staining in the OPL decreased (Figure 5.7B ii-iii). At the later examined time points, 6-12 weeks, Aggrecan staining was restricted to the ONL and INL with an increased deposition within the GCL. These increases are in line with the WB findings presented in Figure 5.3B, where Aggrecan expression was significantly higher at 10 weeks of age, in comparison to P10 retina.

In the P10 *Pde6b*$^{rd1/rd1}$ retina, the expression of Aggrecan was quite similar to wild-type control (Figure 5.6C i). As degeneration progressed, Aggrecan staining in the IPL gradually decreased (Figure 5.6C ii-iv), being quite sparse at the latest examined time point (7-8 week old) even within the plexiform layers and the GCL (Figure 5.6C iv).

Taken together, these data suggest that while Aggrecan is present in the normal wild-type retina and its expression is increased in degeneration, it is predominantly found in the plexiform layers and not at the IS/OS.

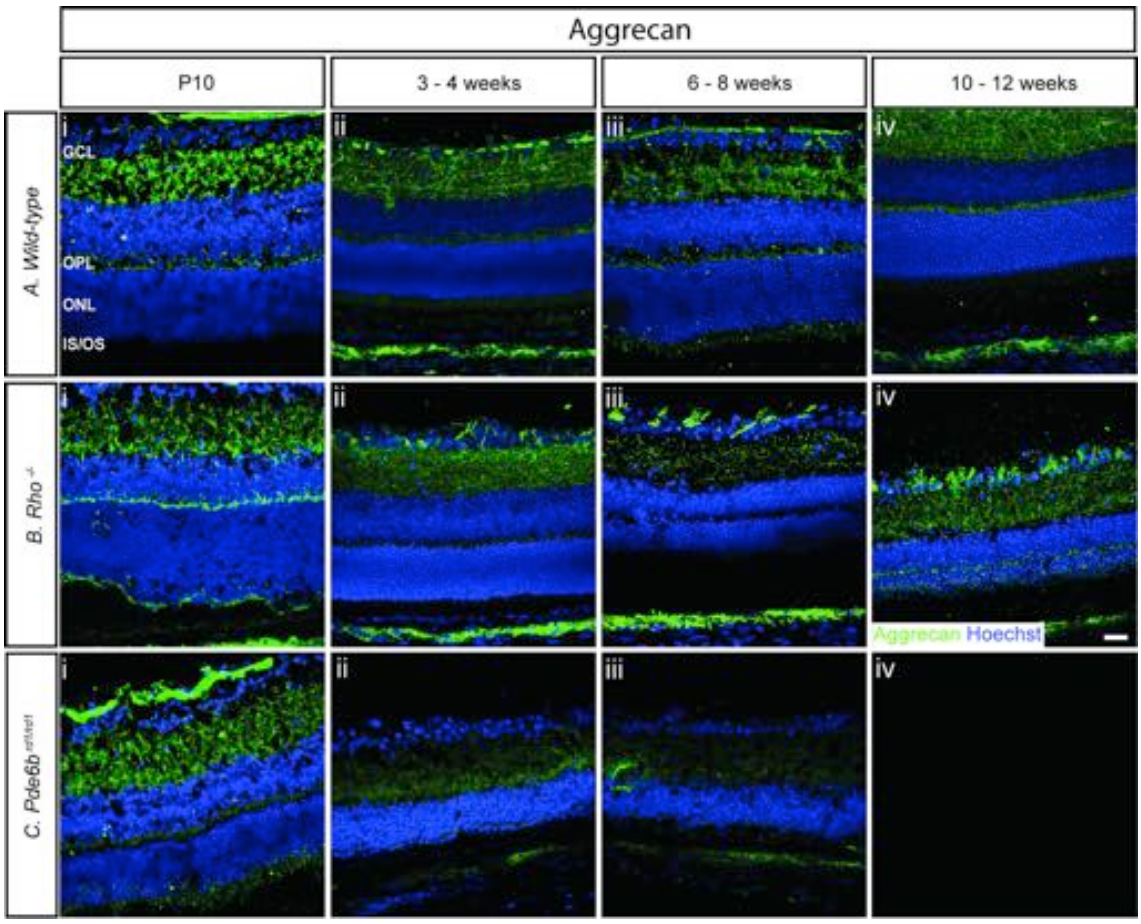

Figure 5.6 Aggrecan staining is absent from the photoreceptor segment region.

Ai-iv) *C57Bl/6J* wild-type; **Bi-iv)** *Rho*$^{-/-}$ and **Ci-iv)** *Pde6b*$^{rd1/rd1}$. Cryosections were immunostained for Aggrecan (*green*) and counterstained with nuclei marker Hoechst 33342 (*blue*).

GCL, ganglion cell layer; IPL, inner plexiform layer; INL, inner nuclear layer; OPL, outer plexiform layer; ONL, outer nuclear layer; IS/OS, photoreceptor inner/outer segment region. Scale bar, 25 µm.

5.2.5 The CSPG receptor LAR is expressed in the murine retina and undergoes disease specific changes in expression

The potent inhibition of neuronal regeneration by CSPGs has been known for more than two decades, with the sulphated GAG chains understood to play the major role in this inhibition (Snow et al., 1990; McKeon et al., 1995).However, the CSPG binding receptors have only been discovered recently (Shen et al., 2009; Fisher et al., 2011; Dickendesher et al., 2012). In particular, two members of the LAR subfamily were shown to bind CSPGs with high affinity and mediate their suppression of axon elongation (Fisher et al., 2011). To date there have been no published reports on their expression in a mouse retina. As a first step to examine the potential roles, IHC analysis was performed on wild-type and the same two models of RP as described above, to assess spatial distribution of LAR in a retina.

In P10 wild-type retinae, LAR staining was detectable in the IS/OS region with sparser distribution in the OPL and in the GCL (Figure 5.7A i). In 3 week old adult retina, LAR staining was additionally prominent within the INL and IPL (Figure 5.7A ii-iv), which probably reflects maturation of the synaptic processes (Dunah et al., 2005). Interestingly, LAR distribution largely mirrored the pattern of CS-56 staining reported in Chapter 3. Unfortunately, both antibodies were raised in mouse, so it was not possible to perform co-localisation studies of LAR and CPSG expression.

When assessing the P10 retina of *Rho*$^{-/-}$ mice by IHC, LAR was located broadly throughout the IS/OS, OPL, IPL and GCL regions (Figure 5.7B i). Surprisingly, as the retina matured, LAR expression became reduced in the IPL and the GCL regions, but was very prominently expressed in the photoreceptor segment region (Figure 5.7B ii-iv). At the latest examined stage (10 weeks of age), LAR staining was also detectable in the ONL (Figure 5.7B iv).

In P10 *Pde6b*$^{rd1/rd1}$ retina, LAR expression within the neural retina was initially quite similar to wild-type, although levels in the OPL appeared lower (Figure 5.7C i). Staining within the segment region was initially high and presented as a thick band. This reduced markedly with (Figure 5.7C ii) and by the latest examined stage (6-8 weeks of age), LAR became almost undetectable in the *Pde6b*$^{rd1/rd1}$ retina (Figure 5.7C iv).

To date, this is the first study that demonstrated the expression of LAR within the mouse retina, particularly within the segment region, and the first to examine changes in LAR expression in two models of RP. These findings suggest that LAR should be considered as a potential candidate for combined therapeutic interventions with cell transplants or retinal implants.

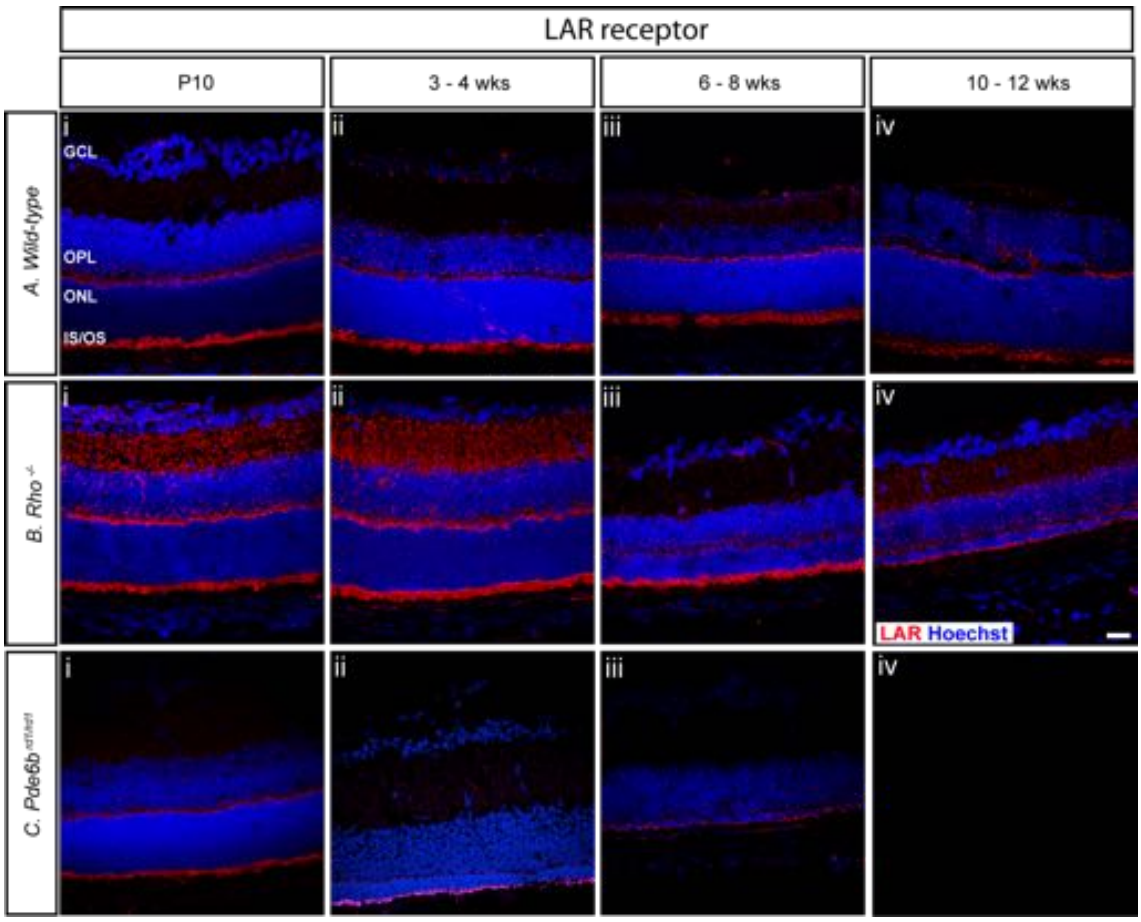

Figure 5.7 CSPGs receptor LAR is detectable in a mouse retina of a wild-type and two models of RP.

Ai-iv) *C57Bl/6J* wild-type; **Bi-iv)** *Rho*$^{-/-}$ and **Ci-iv)** *Pde6b*$^{rd1/rd1}$. Cryosections were immunostained for LAR (*red*) and counterstained with nuclei marker Hoechst 33342 (*blue*).

GCL, ganglion cell layer; IPL, inner plexiform layer; INL, inner nuclear layer; OPL, outer plexiform layer; ONL, outer nuclear layer; IS/OS, photoreceptor inner/outer segment region. Scale bar, 25 µm.

5.2.6 Laminin expression in the diseased retina

Recent studies have shown that CSPGs form non-permissive perineuronal nets, which cause attenuation of adhesion molecules such as laminins that also bind to CSPGs and LAR (Tan et al., 2011). Laminins are large glycoproteins consisting of α, β, γ chains that are found in at least three different genetic variants resulting in a formation of a diverse group of heterodimers. These molecules have been reported to be differentially expressed, both temporally and spatially, which likely reflects the variety of functions these molecules may have. To test whether the expression of Laminins is altered in the diseased retina, IHC analysis of the *Rho*$^{-/-}$ and *Pde6b*$^{rd1/rd1}$ retinae was performed.

In wild-type retinae, at P10, staining for Laminin αβ chains was detectable in the IS/OS region, the OPL, the INL and in the GCL (Figure 5.8A i), which is in line with previously published reports (Libby et al., 2000). This pattern of expression continued throughout adulthood with no major changes in levels or localisation over time (Figure 5.8A ii-iv).

At P10 and 3 weeks of age, *Rho*$^{-/-}$ mutant retinae presented a very similar distribution of Laminin αβ chains to that observed in age-matched wild-type retinae, with Laminin staining detectable in the IS/OS region, the OPL, the INL and in the GCL (Figure 5.8B i-ii). As degeneration progressed, Laminin staining became more prominent in the photoreceptor layer (Figure 5.7B iii-iv), especially at 10 weeks of age, the latest examined time point (Figure 5.7B iv).

In the P10 retina of *Pde6b*$^{rd1/rd1}$ mice, the expression of Laminin αβ chains in the IS/OS region differed from that observed in wild-type and *Rho*$^{-/-}$ mutant (Figure 5.8C i). In a wild-type retina, Laminins formed a band at the edge of the ONL, whereas in the *Pde6b*$^{rd1/rd1}$ retina this band appeared more diffuse, extending into the photoreceptor layer. As degeneration progressed, Laminins were found throughout almost all retinal layers apart from the IPL (Figure 5.8C ii-iii). IHC analysis also revealed labelling of blood vessels in the two models of RP, which is in line with previously published report showing that Laminins are associated with neovascularisation and growth of new blood vessels in the diabetic retina (reviewed in (Edwards and Lefebvre, 2013)).

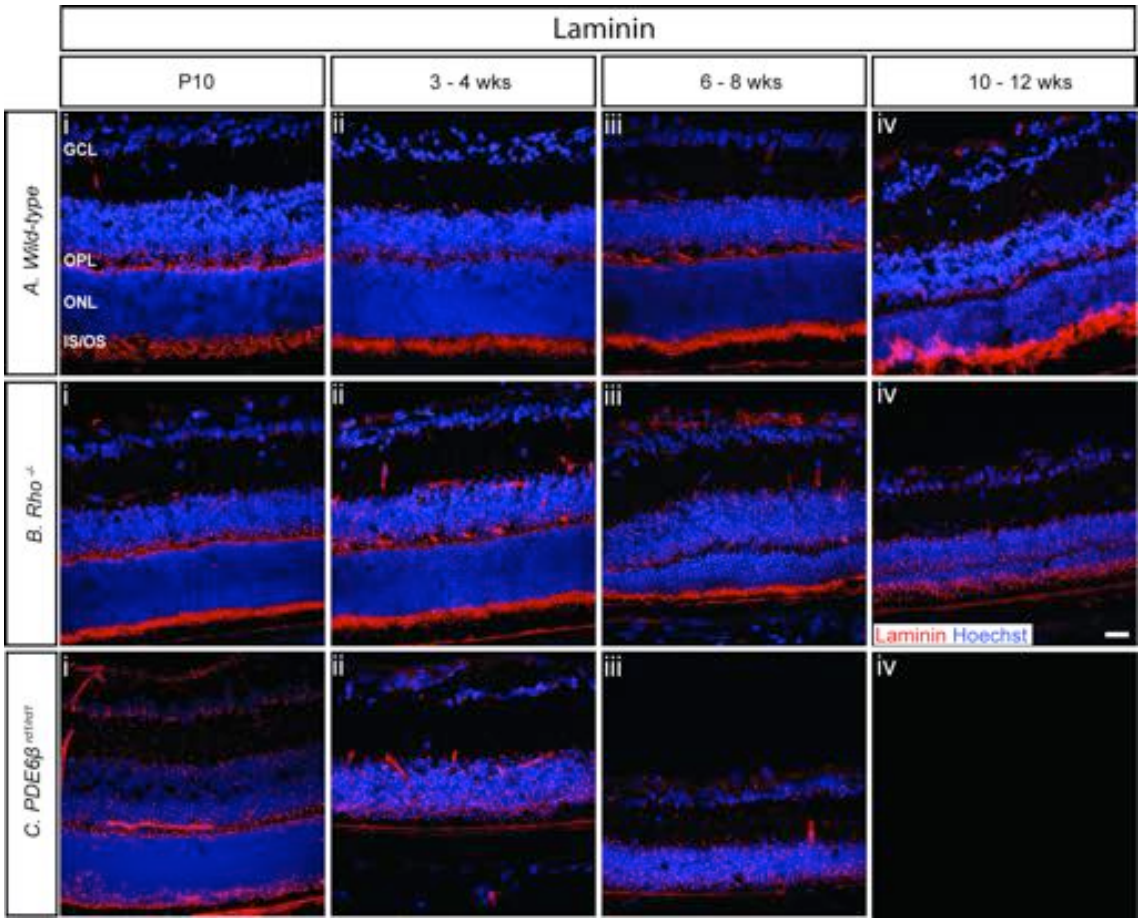

Figure 5.8 Expression of Laminin αβ chains is altered in the mouse model of RP.

Ai-iv) *C57Bl/6J* wild-type; **Bi-iv)** *Rho*$^{-/-}$ and **Ci-iv)** *Pde6b*$^{rd1/rd1}$. Cryosections were immunostained for Laminin αβ chains (*red*) and counterstained with nuclei marker Hoechst 33342 (*blue*).

GCL, ganglion cell layer; IPL, inner plexiform layer; INL, inner nuclear layer; OPL, outer plexiform layer; ONL, outer nuclear layer; IS/OS, photoreceptor inner/outer segment region. Scale bar, 25 μm.

5.3 Discussion

For the past three decades, CSPGs have earned a negative reputation as being one of the main driving forces that impede axonal regeneration following CNS injury (Properzi et al., 2003; Matsui and Oohira, 2004; Galtrey and Fawcett, 2007). In the retina, CSPGs were found to be markedly upregulated in different models of inherited retinal degenerations, glaucoma, optic nerve injury or diabetic retinopathy (Inatani et al., 2000; Zhang et al., 2003b; Hippert et al., 2015), which has led to the notion of CSPGs being potentially detrimental to therapeutic approaches, including electronic grafts, gene therapy and cell transplants ((Grüter et al., 2005; Singhal et al., 2008; Tucker et al., 2008; Barber et al., 2013)). For example, subretinal implant devices and cell transplants are typically administered into the subretinal space, but must make contacts with the host neuroretina. This may be impeded by CSPGs located within the segment region (reviewed in (Johnson et al., 2010; Pearson, 2014; Pearson et al., 2014; Zarbin, 2016)). It is important to note too, however, that compelling evidence has been gathered suggesting that not all CSPGs are inhibitory, with some of them actually promoting CNS recovery (Akita et al., 2004). As CSPGs represent a large family of proteins and there are a limited number of studies that have looked at their role in the injured and/or diseased retina, the assessment for specific CSPGs is needed to better understand the underlying pathological mechanisms. As a first step towards this goal, the current study examined the expression pattern of one of the major CSPGs, Aggrecan, and the CSPG receptor LAR in the murine wild-type and diseased retina as both proteins have both been reported to have negative roles in axon regeneration (Kuboyama et al., 2010; Afshari et al., 2010b; Fisher et al., 2011; Tan et al., 2011; 2012; Sharma et al., 2012b). Here, two models of RP were chosen to investigate possible alterations in their expression in the diseased retina. Although CS-56 staining is robust in the segment region and the administration of Aggrecanase to the subretinal space led to a reduction in CS-56 staining, expression of Aggrecan itself appears to be largely restricted to the inner retina and the choroid. In contrast, the expression of newly discovered CSPG receptor, LAR, was found to be mainly restricted to the IS/OS region, suggesting that LAR may be of potential use for future therapeutic strategies.

During CNS development, CSPGs are expressed in a highly organised manner creating gradients and boundaries that help to navigate growing neurons towards their correct locations (Letourneau et al., 1994; Laabs et al., 2005). In the injured CNS, including the retina, CSPGs were thought to be upregulated by the reactive glia (Inatani et al., 2000; Inatani and Tanihara, 2002), which makes them one of the major contributors to formation of a barrier for regenerating neurons (McGraw et al., 2001; Massey et al., 2008; Fawcett, 2009). Recent research findings suggest that CSPGs play a role in the pathology of diseases such as Alzheimer's disease, stroke and

epilepsy (reviewed in (Siebert et al., 2014)). Higher expression of Aggrecan, Neurocan and Versican was also reported in human brain of patients with multiple sclerosis (Sobel and Ahmed, 2001). Several approaches to remove CSPGs after injury have been made including the well characterised use of enzymatic treatment with locally applied bacterial ChABC. Although very effective, ChABC has many disadvantages making it less suitable for therapeutic use in patients (Lee et al., 2010; Sharma et al., 2012a). Broad spectrum removal of all CSPGs may not be beneficial to the tissue, as CSPGs are important for the maintenance of synaptic plasticity and other cellular processes (reviewed in (Vecino et al., 2016)), thus an alternative is needed. Here, a naturally occurring enzyme, ADAMTS-4 (Lemke et al., 2010), was tested in the retina of wild-type and *Rho*$^{-/-}$ mutants and found to be effective in digesting CSPGs deposited within the subretinal space. This suggests that ADAMTS-4 could be of potential interest in the studies on therapeutic interventions as the removal of CSPGs has been shown to enhance viral diffusion and transduction of photoreceptors, and transplantation (Zhang et al., 2007; Barber et al., 2013).

CSPGs represent a diverse group of molecules with some undergoing significant changes in their expression in the injured and diseased retinae of rodents (Chaitin and Brun-Zinkernagel, 1998; Inatani et al., 2000; Zhang et al., 2003b). Microarray analysis of individual Müller glial cells from a mouse model of RP identified a significant increase in Neuroglycan (Roesch et al., 2012). Zhang and colleagues reported that global levels of Neurocan appeared to be increased in the retina of S334ter-line-3 rat, which represents a transgenic model of retinal degeneration (Zhang et al., 2003b). They also reported that removal of Neurocan using ChABC enzyme from a diseased retina of *Rho*$^{-/-}$ mutant results in a higher number of observable donor-labelled cells in the recipient eye (Zhang et al., 2007). Another study demonstrated the presence of Neurocan and Versican in the dystrophic retina of the Royal College of Surgeons (RCS) rats by comparing it to normal retina of the Lister Hooded rat strain (Singhal et al., 2008). The same study reported that treatment with ChABC at the time of transplantation of Müller stem cells leads to a dramatic increase in the number of reporter-labelled cells in the host retina and these appeared to invade all layers of the retina (Singhal et al., 2008). These findings suggested that both Neurocan and Versican may be inhibitory to transplanted donor cells. However, despite a reported upregulation in the global protein levels of Neurocan, IHC analysis showed that Neurocan was abundant in the segment region in wild-type retinae and the overall distribution of Neurocan in the S334ter mutant appeared similar to that seen in control retinae (Zhang et al., 2003b). Interestingly, the same study showed that as degeneration progressed and photoreceptor cells died, the staining for Neurocan disappeared from the subretinal space, but increased at the level of the GCL in the

S334ter mutant (Zhang et al., 2003b). As mentioned before, Singhal *et al.* also identified Neurocan as having an inhibitory role in the retina, reporting Neurocan deposition in the dystrophic rats but not in the control retina (Singhal et al., 2008). However, in their study there was no age-matched comparison, with the neonate wild-type retina being compared to 5 week-old RCS eyes. This age mismatch may over-represent the actual changes in Neurocan and Versican at the segment region between control and diseased eyes. Moreover, in the study by Singhal *et al.*, no cell transplants were performed in the control retinae following ChABC treatment. In the future, it would be interesting to see whether the treatment with ChABC of the healthy retina also leads to a similar increase in a number of observable transplanted cells within the recipient retina.

To the best of my knowledge, the expression of Aggrecan has never been studied in models of retinal degenerations, despite clear evidence that Aggrecan has an inhibitory role in the CNS on neuronal extension. In the brain, Aggrecan is the main constituent of the perineuronal nets (PNN) (Giamanco et al., 2010). *In vitro*, axonal attachment and growth were reported to be blocked in the presence of purified Aggrecan (Domowicz et al., 2008; Afshari and Fawcett, 2011). Chen and colleagues reported that Aggrecan is upregulated in a rat model of diabetic retinopathy (Chen et al., 2012a). In the data reported here, the WB assessments showed an upregulation of Aggrecan over time in the *Rho*$^{-/-}$ animals and marked decrease in the *Pde6b*$^{rd1/rd1}$mutants. However, no deposition in the segment region was found in any of the examined models, including wild-type, as assessed by IHC. The observed upregulation in the retina of *Rho*$^{-/-}$ mice could be linked to an increase of Aggrecan expression in the IPL, potentially due to synaptic remodelling between the remaining retinal neuronal cells. As *Pde6b*$^{rd1/rd1}$ is a very fast degenerative model, it is possible that there is insufficient time for this PG to become aggregated in this mutant retina or there is redundancy in the system and a compensatory increase in a different CSPG. These results suggest that, at least in the models of inherited retinal degeneration used here, Aggrecan is not a primary component of the CSPGs deposited in and around the segment region of the neuroretina, where Müller glia build a glial seal. In keeping with this, subretinal administration of ADAMTS-4 enzyme did decrease the overall expression of CSPGs, but Aggrecan levels remained unchanged. Interestingly, a very recent study by Anderson *et al.* demonstrated that despite previous evidence for an inhibitory role of Aggrecan in CNS regeneration, no deposition of this PG was observed at the lesion site weeks after SCI in a mouse (Anderson et al., 2016). Moreover, the same study reported that scar-forming astrocytes produce two growth-supportive CSPGs, CSPG4 and CSPG5, and that both astrocytes and non-astrocyte cells in SCI lesions express multiple axon-growth-supportive molecules such as Laminins. Surprisingly, Anderson

et al. found that CSPGs are upregulated in the absence of the astrocytes, suggesting that other cells including neurons may contribute to CSPG deposition following injury. It is tempting to speculate whether, in the retina, photoreceptors are involved in CSPG production, and if this might explain why in the very rapidly degenerating *Pde6b*$^{rd1/rd1}$ model, CSPG reduction correlates with photoreceptor depletion (Landers and Hollyfield, 1992; Hippert et al., 2015). Although not examined in this study, future studies should investigate in more detail the role of microglia in the upregulation of CSPGs in a diseased retina. Activated microglia cells are an important part of the CNS response to injury and infection because of the various products they secrete, including cytotoxic molecules (free radicals, i.e., superoxides), neurotrophic molecules (nerve growth factor, e.g.), and a variety of pro- and anti-inflammatory cytokines and chemokines (reviewed in (Rock et al., 2004)). The release of cytokineses is particularly important as these molecules can stimulate the expression of CSPGs in a variety of cells in and around the lesion side. Most important are the astrocytes, which also undergo a reactive gliosis and in response to various cytokines they become hypertrophic and begin secreting CSPGs, leading to the formation of a glial scar at the vitreous side (reviewed in (Siebert et al., 2014)).

Although the potent negative role of CSPGs on neuronal regeneration has been studied for decades, only in recent years have the CSPG binding receptors been discovered (Shen et al., 2009; Fisher et al., 2011; Dickendesher et al., 2012) increasing our understanding of CSPG-mediated inhibition. Using a CSPG gradient crossing assay, Shen *et al.* provided evidence that PTPsigma-dependent interactions with CSPGs maintain growth cones in a dystrophic state (Shen et al., 2009). A regrowth of sensory axons into scar tissues was enhanced in PTPσ deficient adult mice (Shen et al., 2009; Dickendesher et al., 2012). Fisher *et al.* reported that LAR receptor can be blocked pharmacologically with small peptides and stimulated regrowth of serotonergic axons (Fisher et al., 2011), while a more recent study showed that locomotor functional recovery is significantly better in mice deficient in LAR in comparison to normal controls following caudal SCI (Xu et al., 2015). However, many critical issues regarding CSPG receptor function remain unknown, including their expression in the retina. A better understanding of CSPG receptor function may facilitate our ability to modulate scar-mediated growth inhibition and developing more effective therapies. Here, for the first time, the assessment of LAR receptor in the healthy mouse retina was performed and compared to two models of inherited retinal degenerations. LAR was found to be highly abundant in the IS/OS region, the IPL and the GCL in all three examined models, but its expression gradually decreased in the *Pde6b*$^{rd1/rd1}$ mutant over time. Knowing that LAR is being expressed in a retina, pharmacological targeting of this CSPG receptor could be used as a potential

intervention as it does not present the risk of undigested GAG chains, as in case of the enzymatic treatment. Lemons *et al.* reported that these partially digested carbohydrate sugar chains left on the molecules may still exhibit their inhibitory effects on the neuronal outgrowth (Lemons et al., 2003). Secondly, in the injured CNS, the CSPGs are constantly released by the cells; therefore single injection of the enzyme would not be sufficient to override the CSPGs inhibition. A course of several ChABC injections could potentially induce an immune response that could lead to further damage of the injured area. Moreover, as CSPGs represent a large family of proteins, which may be differentially expressed at the lesion site, targeting CSPGs receptors may be an easier way to override CSPG-mediated inhibition.

In conclusion, understanding the changes in the expression of CSPGs and their receptors in the injured or diseased retina may be crucial in designing effective therapeutic strategies. In this study, for the first time, the spatio-temporal expression of the CSPG, Aggrecan, and the CSPG receptor LAR were assessed in the degenerating mouse retina, which opens a door for future experimental work on how to manipulate the inhibitory role of CSPGs.

CHAPTER 6

Remodelling of the outer limiting membrane in retinal degeneration

6.1 Overview

The retina is a laminar tissue that can be divided into two distinct compartments. Each compartment is composed of a monostratified cell layer in which neuronal elements are embedded and each is supplied by a different blood supply (Mestrinerr and Haddad, 1994). The inner compartment extends from inner blood-retina barrier until the outer edge of the outer nuclear layer (ONL), and it is sometimes referred to as a glial compartment since it lays between the Müller glia basal and apical processes. The outer compartment, also referred to as retinal pigmented epithelium (RPE), extends from the edge of the neuroretina and Brunch's membrane. These two compartments are separated from each other by a structure comprised of specialised adherens junctions (AJs), the outer limiting membrane (OLM). The OLM is considered to play a role in the maintenance of photoreceptor orientation through mechanical strength, especially in the retinae of birds and teleosts, where photoreceptors are motile (Ali, 1971; Burnside, 1978; Burnside and Nagle, 1983; Drenckhahn and Wagner, 1985). However, the emerging evidence points to the OLM being part of the retinal barrier due to its permeability properties. The AJs, mainly formed between photoreceptor inner segments (IS) and the Müller glia apical processes, appear to provide a semipermeable diffusion for extracellular components with Stokes radii greater than 30-36A (Bunt-Milam et al., 1985). In recent years, the OLM has also been identified as a possible obstacle to transplanted cells, as the number of GFP^+ cells within the recipient retina is higher in animal models where OLM integrity is compromised (West et al., 2008; Pearson et al., 2010; Barber et al., 2013).

The OLM is an unusual structure for a number of different reasons. First, the AJs are usually formed between only one cell type, whereas in the OLM the junctions are heterotypic, with three different cell types being involved (Bunt-Milam et al., 1985). Secondly, these junctions are referred to as specialised AJs as they consists of a mixture of proteins that are usually associated with tight junctions (TJ) and proteins found in a typical AJ (Randlett et al., 2011). OLM junctions contain typical TJ proteins, such as claudins, occludin and junction adhesion molecules (JAMs), and typical AJ markers, including E-cadherins, β-catenin and α-catenin (Tsukita and Furuse, 1999; Tsukita et al., 1999; Omri et al., 2010). Cadherin adhesion molecules are the core of the OLM junctional component (Takeichi, 1991). All cadherins contain two or more extracellular cadherin domains and a highly conserved cytoplasmic tail that interacts with a defined set of cytoplasmic proteins, the catenins. P120-catenin and β-catenin bind the cytoplasmic tail of cadherins, and β-catenin binds to α-catenin to form the cadherin–catenin complex (Perez-Moreno and Fuchs, 2006; Pokutta and Weis, 2007; Nishimura and Takeichi, 2009). These catenins in turn associate with a variety of other

molecules, including cytoskeletal proteins and their regulators. As in the ear hair cells, the junctional plaques are linked to cell's cytoskeleton via the actin filaments through zonule occludens 1 (ZO-1) (Fanning et al., 2002). Within the OLM, there is also a specialised apical region (SAR) that contributes to localisation and organisation of the AJs. The SAR, which apically localises to the AJs, is comprised of two protein complexes, portioning defective (PAR) and the Crumbs homologue (CRB) (Figure 6.1). In the mammalian retina, the PAR complex consists of PAR6, PAR3, atypical protein C (aPKC) and cell division control 42 (CD42) (reviewed in (Martin-Belmonte and Perez-Moreno, 2012)). The core CRB complex is composed of CRB family members, which interact with the associated cytoplasmic proteins Protein Associated with Lin Seven 1 (PALS1) also known as Membrane Protein Palmitoylated 5 (MPP5), and PALS1-associated tight junction protein (PATJ), or the Multi-PDZ Domain Protein 1 (MUPP1) (Bulgakova et al., 2008; Assémat et al., 2013). Both of these structures are very dynamic as many of their components undergo changes depending on the developmental stage. This apical junctional region is especially important in establishing proper cell polarity during retinal development, as loss-of-function or a defect in any of these complexes leads to detachment of the progenitor cells and perturbations in retinal laminations. These spatio-temporal alterations in retinogenesis can result in mild to severe impairment of retinal function and retinal degeneration (Pujic and Malicki, 2004; van Rossum et al., 2006; Alves et al., 2012; Pellissier et al., 2013). For example, during retinogenesis, AJs are important for the anchorage of newborn progenitor cells to the apical surface of the epithelium (reviewed in (Alves et al., 2014b)). These retinal progenitor cells elongate along the apico–basal axis forming long processes, which are important for interkinetic cell migration (Baye and Link, 2007). Later studies showed that the migration of retinal progenitors is strictly dependant on the expression of OLM proteins (Pujic and Malicki, 2004; van Rossum et al., 2006; Alves et al., 2012; Pellissier et al., 2013). Moreover, it has been shown that AJ proteins take part in the regulation of cell proliferation and disruptions in levels of any of these molecules cause loss of cell polarity and epithelial adhesion, and concomitant detachment from the apical lamina (reviewed in (Alves et al., 2014b)). In the mouse retina, β-catenin links AJs to the cytoskeleton as well as acting as an effector of canonical wingless (Wnt) signalling pathway, which regulates cell differentiation during neurogenesis (Logan and Nusse, 2004). Removal of β-catenin during development results in loss of the typical radial spanning of retinal progenitor cells, together with loss of cell adhesion, OLM disruption, and a decrease in cell survival (Fu et al., 2006). Studies of the chick eye demonstrated that constitutively active β-catenin or Wnt2b signalling pathway have an impact on the identity of retinal progenitor cells, pushing progenitors towards the peripheral cell fate of the ciliary body

or iris (Cho and Cepko, 2006). The removal of another AJ protein, aPKC, from postmitotic photoreceptors results in abnormal lamination and photoreceptor cell morphology as well as the defects in establishment of proper neuronal connections (Koike et al., 2005). Moreover, in the absence of aPKC the photoreceptor differentiation is impaired and takes place at different regions in the retina. In 2012, Alves *et al.* study demonstrated that CRB2 protein restricts proliferation of retinal progenitors in mouse and that deletion of it leads to severe retinal disorganisation and progressive degeneration with concomitant loss of vision (Alves et al., 2012). Furthermore, their study demonstrated that CRB2 removal results in reduction of loss of other SAR and AJs proteins suggesting destabilisation of the entire junctional complexes. Later studies that used different *Cre* mouse lines and AAV expressing vectors targeting *Crb2* expression revealed that CRB2 has a cell specific role (Alves et al., 2014a). The deletion of CRB2 from photoreceptor cells during retinal development leads to loss of cell adhesion, OLM disintegrity, progressive morphological deterioration and loss of retinal lamination. In contrast, when CRB2 is removed from Müller cells, the phenotype is milder with moderate disruptions to OLM continuity and nuclei mislocalisation, mainly observed at the peripheral retina (Alves et al., 2014a). Surprisingly, silencing of CRB2 with AAV vectors in adult retinae results in no changes to retinal morphology or function suggesting that CRB2 plays no part in the maintenance of AJs in the adulthood (Alves et al., 2014a). Interestingly, the developed mouse mutant strikingly resembled a human phenotype observed in RP patients linked to *CRB1* mutation.

Finally, the junctional proteins have been found to be asymmetrically distributed between photoreceptors and Müller cells, with the junctional plaques being much larger in Müller cells than in photoreceptors (Williams et al., 1990). The expression of junctional proteins also varies between different cell types or different species. For example, in a mouse retina CRB1 is restricted to apical processes of Müller glial cells, whereas CRB2 is expressed in both Müller cells and photoreceptor inner segments. Interestingly this pattern of expression was found to be reversed in humans (reviewed in (Alves et al., 2014b). These discrepancies between the typical epithelial AJs and OLM are thought to reflect an adaptation of the OLM for the specialised roles it has to perform in the retina.

Given the importance of the OLM in the retina, we sought to determine whether and how this structure changes in a diseased state. Previous reports have shown that in chronic pathological conditions, including diabetic retinopathy (DR), the OLM is compromised with a loss of the typical honeycomb pattern (Omri et al., 2013). Any breach to this barrier between photoreceptor segments and the neuroretina may play an important role in development of further pathological changes or acceleration of the

degeneration. Better understanding of these alterations should provide insight into a pathological environment and help to design more efficient therapeutic approaches for patients whose retinae deteriorate.

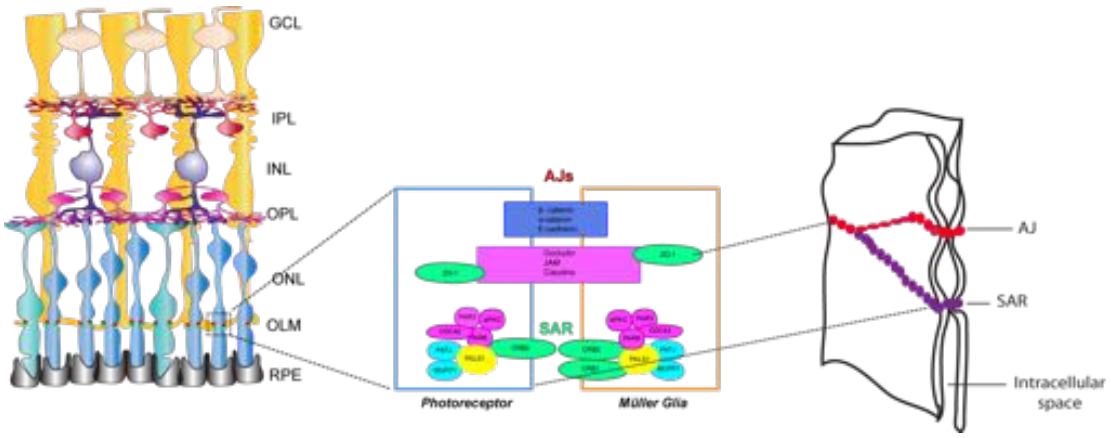

Figure 6.1 Schematic representation of the OLM in the mouse retina.

OLM junctions comprise of the tight junction (TJ) proteins, Claudin, Occludin and JAM, as well as proteins associated with typical adherens junctions (AJs), such as β-catenin, α-catenin and E-cadherin (reviewed in (Alves et al., 2014b)). Cytoplasmic protein ZO-1 links the AJ proteins to the cell's cytoskeleton. The CRB complexes are located at the subapical region above the adherens junctions at the OLM. The core of the CRB complex is formed by CRB1 and CRB2 that connect to PALS1, which links with PATJ and MUPP1. The CRB proteins and PALS1 are also able to bind to the PAR complex member PAR6, which associates with aPKC, PAR3 and CDC42. In a mouse retina, CRB1 is restricted to Müller glia. The fact that OLM shares similar proteins with the TJs within the RPE suggests that it can function as a retinal barrier. GCL, ganglion cell layer; IPL, inner plexiform layer; INL, inner nuclear layer; OPL, outer plexiform layer; ONL, outer nuclear layer; OLM, outer limiting membrane; AJs, adherens junctions; SAR, subapical region.

6.2 Results

Here, the OLM integrity was examined at the early and late time points in all models of retinal degeneration introduced in Chapter 3. A global overview of OLM contiguity in superior and inferior regions was performed using immunohistochemistry (IHC) for ZO-1 expression, which is associated with AJs. In parallel, IHC analysis for CRB1 was performed, to assess possible alterations to the core complex of SAR. To determine possible changes in a number and/or types of AJs in a diseased retina, electron micrographs (EM) of each mutant model were examined and compared to healthy age-matched wild-type retinae.

6.2.1 OLM integrity is largely maintained in the majority of the retinal degenerations

Although, a systematic assessment of both superior and inferior retina was conducted, no visible differences between the two regions were found. For the purpose of this thesis, representative images of both superior and inferior regions of the retina are included in the figures presented, but the qualitative description applies globally with no distinction between the two regions.

In the wild-type inferior and superior retina at 6 weeks of age (early) ZO-1 staining formed a continuous line at the edge of the ONL with no nuclei intruding into the subretinal space, indicating that the OLM was intact (Figure 6.2A i-ii). This pattern was preserved over time, with no differences observed in 6 month-old animals, compared to 6 week-old mice (Figure 6.2A iii-iv). CRB1 staining followed the same pattern as ZO-1 with no noticeable dissimilarities between superior and inferior regions (Figure 6.2A v-viii).

In the next instance the retina of *Crb1*$^{rd8/rd8}$ mouse was assessed. This naturally occurring mutant has a 1bp deletion in *Crb1* gene, which truncates the transmembrane and cytoplasmic domain of CRB1 (Mehalow et al., 2003). As a result, focal disorganisation in retinal lamination can be observed with characteristic undulations of the ONL. Mehalow *et al.* reported that the OLM disintegrity starts as early as 2 weeks after birth, accompanied by the structural alterations in both photoreceptors and Müller glial cells (Mehalow et al., 2003). At 6 weeks of age, the staining for ZO-1 appeared fragmented across the entire retina indicating that the integrity of the OLM was already compromised (Figure 6.2B i-ii) and became even more prominent at later stage examined (Figure 6.2B iii-iv). CRB1 staining was, as expected for this model, mostly absent or diffused (Figure 6.2B v-viii). A displacement of photoreceptor cells into the

subretinal space was also observed (Figure 6.2B i-viii, arrows), providing a further evidence for the breakdown of the OLM barrier.

The *Rds*$^{rd2/rd2}$ mutant lacks photoreceptor OSs and undergoes a mild progressive retinal degeneration. At 4 weeks of age, some occasional absences of ZO-1 expression at the level of the OLM were observed (Figure 6.2C i-ii, white arrows) with more breaks in ZO-1 staining as degeneration progressed (Figure 6.2C iii-iv, white arrows). Further IHC assessment showed that CRB1, although not absent, seemed to be more diffused into the segment region (Figure 6.2C v-viii) in comparison to wild-type retina. Sporadic nuclei intrusions into the subretinal space were also noticeable. These OLM alterations were prominent in both superior and inferior regions.

In the *Pde6b*$^{rd1/rd1}$ mouse, which is a very fast degenerative model, the majority of rod photoreceptor cells are lost by the 4th week of age. At the earliest time point examined, staining for ZO-1 formed a uniform line at the edge of the outer retina but some small breaches to its continuity were apparent (Figure 6.2D i-ii). These disruptions became more noticeable in mid (3 weeks of age) and late ages (Figure 6.D iii-iv) with a marked increase in the breaks in ZO-1 staining over time, indicating significant disruptions of the OLM in this model. The ectopic presence of ZO-1 at the level of the outer plexiform layer (OPL) was also noticeable between the inner nuclear layer (INL) and the remaining ONL from 3 weeks onwards, which is probably associated with the growth of new blood vessels. Similar to ZO-1, CRB1 expression was preserved at the early time point (Figure 6.2D v-vi), but as degeneration progressed the staining was either fragmented or as in the *Rds*$^{rd2/rd2}$ mutant diffused into the segment region (Figure 6.2D vii-viii).

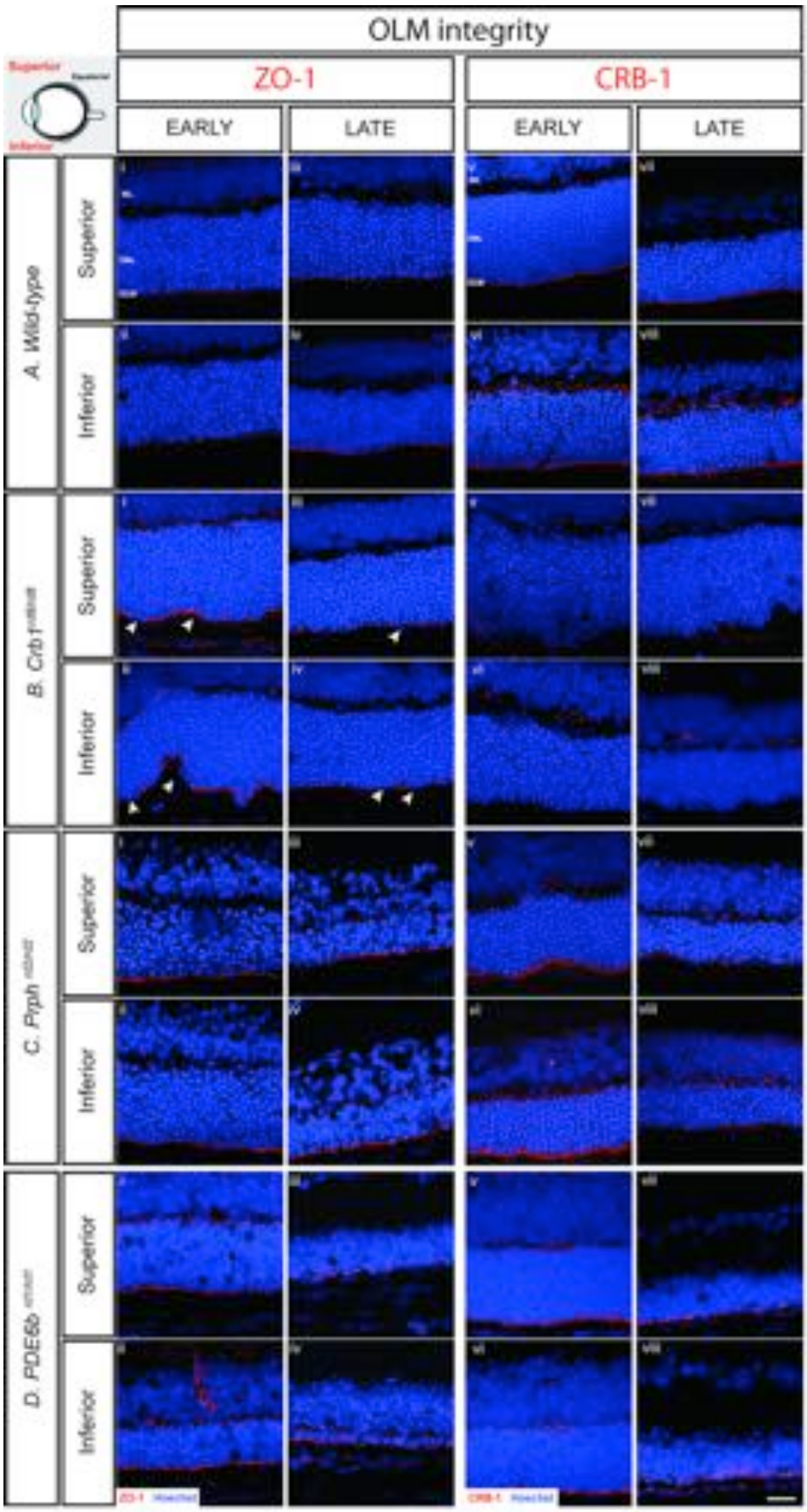

Figure 6.2 IHC assessment of OLM integrity in animal models carrying a spontaneous mutation.

Ai-viii) *C57Bl/6J* wild-type; **Bi-viii)** *Crb1*$^{rd8/rd8}$; **Ci-viii)** *Prph2*$^{rd2/rd2}$ and **Di-viii)** *Pde6b*$^{rd1/rd1}$. Cryosections were immunostained for ZO-1 and CRB1 (*red*) and counterstained with nuclei marker Hoechst 33342 (*blue*); *arrows,* indicate displaced photoreceptors. Scale bar, 25 µm. INL, inner nuclear layer; OPL, outer plexiform layer; ONL, outer nuclear layer; OLM, outer limiting membrane.

Rho$^{-/-}$ mice do not develop rod photoreceptor OSs and lose their photoreceptor cells within the first 3 months (Humphries et al., 1997). In contrast to previous reports (Campbell et al., 2007), we found that the OLM appears to be maintained throughout the course of photoreceptor degeneration: IHC for ZO-1 staining was strong and formed a single continuous line at the edge of the outer neuroretina (Figure 6.3A i-ii) with some evidence of disruption at the later stage of degeneration (Figure 6.3A iii-iv). Surprisingly, however, despite the OLM preservation, staining for CRB1 appeared to be very weak in this model (Figure 6.3A v-viii).

In *Prph2*$^{+/\Delta 307}$ mice that are heterozygous for the codon 307 mutation of the *Peripherin* gene (McNally et al., 2002) there is a marked, but fairly slow, reduction in rod cell number, in comparison to wild-type retina. In this mutant, the remaining photoreceptor cells have shorter OSs that are severely disrupted in number and configuration. The OLM in both the inferior and superior retina appeared disrupted even at the beginning of degeneration (Figure 6.3B i-ii), but became progressively more disrupted with disease, as indicated by marked disruptions in ZO-1 (Figure 6.3B iii-iv) and CRB1 expression (Figure 6.3B v-viii).

Nrl$^{-/-}$ retina lacks rod cells; therefore, the AJ formation involves only two cell types, Müller glia and so–called 'cods' (Mears et al., 2001). Similar to the *Crb1*$^{rd8/rd8}$ mutant, *Nrl*$^{-/-}$ retina develops numerous ONL undulations in both superior and inferior regions, with the appearance of the first rosettes as early as P8 (Stuck et al., 2012). Stuck *et al.* showed that the formation of AJs is not uniform in the *Nrl*$^{-/-}$ retina, which leads to protrusion of a population of photoreceptors into the subretinal space during retinal development. Recently, the rosette morphogenesis was suggested to be linked to the presence of functional RPE65 protein as rosette development was prevented only in mutants with reduced RPE65 levels (Samardzija et al., 2014). In keeping with these results, and similar to *Rho*$^{-/-}$, we founded that ZO-1 expression was very robust in this model at both early (Figure 6.3C i-ii) and late time points (Figure 6.3C i-ii) examined, but with clear signs of OLM discontinuity and nuclei mislocalisation (Figure 6.3C i-iv; white arrows). The CRB1 staining followed the ZO-1 pattern with no visible signs of protein diffusion into the segment region (Figure 6.3C v-viii).

As discussed in Chapter 3, the cytoarchitecture of the retina in the *R91W; Nrl*$^{-/-}$ mouse is well preserved, despite the lack of rods. Moreover, unlike the *Nrl*$^{-/-}$ mutant, the *R91W;Nrl*$^{-/-}$ model lacks rosettes, which was suggested to be due to a reduction in levels of visual chromophore (Samardzija et al., 2014). IHC analysis showed that ZO-1 expression is strong, with no clear signs of disruption in the OLM at either of the examined time points (Figure 6.3D i-iv), and comparable to ZO-1 labelling in the wild-type. CRB1 expression was also preserved in this model, with clear and strong staining

at the apical margin of the retina (Figure 6.3D v-viii), indicating that OLM may be intact in this double mutant. The IHC data presented above indicates that the OLM may be disturbed to varying degrees in different models of retinal degeneration.

Although not relevant to this study, it is worth mentioning, that a punctate ZO-1 staining was also present in the OPL of all examined models examined but it was most prominent in the *Nrl*$^{-/-}$ and *R91W;Nrl*$^{-/-}$ mutants. ZO-1 is a well known intracellular component of tight and adherens junctions, which also localises to gap junctions formed between horizontal and photoreceptor cells (Puller et al., 2009). It has been demonstrated that ZO-1 co-localises with connexins at rod spherules and at the cone pedicle base (Puller et al., 2009). As both mutants are cone-dominant retinae, it would be interesting to investigate in a future whether this increased expression in the OPL is linked to a formation of different types of gap junctions.

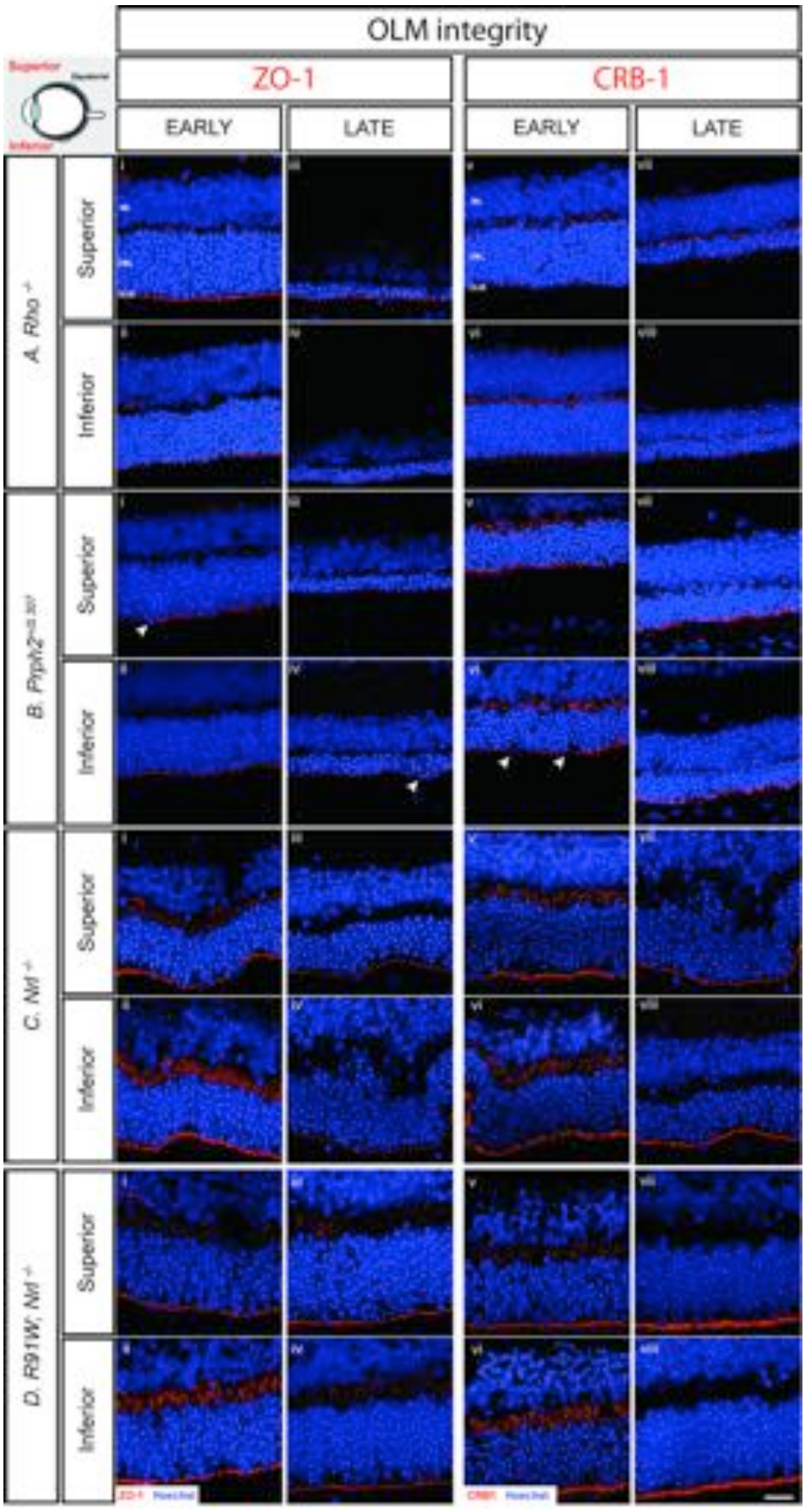

Figure 6.3 IHC assessment of OLM integrity in animal models carrying a targeted mutation.

Ai-viii) *Rho*$^{-/-}$; **Bi-viii)** *Prph2*$^{+/\Delta 307}$; **Ci-viii)** *Nrl*$^{-/-}$ and **Di-viii)** *R91W;Nrl*$^{-/-}$. Cryosections were immunostained for ZO-1 and CRB1 (*red*) and counterstained with nuclei marker Hoechst 33342 (*blue*); *arrows,* indicate displaced photoreceptors. Scale bar, 25 μm. INL, inner nuclear layer; OPL, outer plexiform layer; ONL, outer nuclear layer; OLM, outer limiting membrane.

6.2.2 Adherens junctions undergo significant remodelling during retinal degeneration in order to maintain OLM integrity

As retinal degeneration progresses, the OLM starts to remodel, a phenomenon that has been previously reported, individually, for some of the examined mutants (Mehalow et al., 2003; Campbell et al., 2006; 2007). Here, qualitative and quantitative analysis of the AJs was performed in different models of retinal degenerations using EM. Similar to IHC results, EM demonstrated that, in wild-type retinae, the OLM appears as a series of highly ordered, regularly spaced AJs at the outer edge of the ONL and this appearance remains unbroken throughout the time frame examined (Figure 6.4A i-ii, v-vi). Assessment at the ultra-structural level confirmed previous reports (reviewed in (Alves et al., 2014b)) that the vast majority of these AJs are formed between rod/cone photoreceptor IS and Müller glia apical processes, creating a neatly aligned OLM structure (Figure 6.4A iii-iv, vii-viii; red boxes).

As expected, in the *Crb1*$^{rd8/rd8}$ model the OLM did not present a straight line, as seen in a wild-type, but instead exhibited visible undulations of the ONL and displacement of the photoreceptor nuclei beyond the limits of the AJs, into the segment region (Figure 6.4B iii-iv; arrows), providing further evidence for a loss of OLM integrity (Figure 6.4B i-ii, v-vi; arrows). Interestingly, upon closer inspection at the ultrastructural level, the AJs were still numerous. Moreover, the IS seemed also abnormal in their length and comparatively thinner than those of the wild-type.

Analysis of semithin retinal sections of the *Rds*$^{rd2/rd2}$ mouse confirmed the OLM disruption seen with IHC. This was particularly evident at the late stage, as the OLM appeared uneven at the outer edge of the retina (Figure 6.4B i-ii, v-vi). Ultra-structural EM revealed that AJs were well-maintained at the early stage of degeneration (Figure 6.4C iii-iv), but as diseased progressed the junctions seemed to become more elongated (Figure 6.4C vii-viii), which could indicate AJ protein mislocalisation or diffusion, which has been previously suggested by Williams *et al.* (Williams et al., 1990). Moreover, there were also visible signs in the alterations to ONL lamination, with photoreceptor nuclei become sparser over time and clear signs of Müller glia hypertrophy.

As might be expected, *Pde6b*$^{rd1/rd1}$ retina showed significant changes in the laminar organisation within both the ONL itself and the OLM between early (Figure 6.4D i-ii) and late stages of degeneration (Figure 6.4D v-vi). Analysis at the ultra-structural level revealed that the alignment of the AJs at the outer margin of the ONL was relatively normal at the early stage examined (Figure 6.4D iii-iv) but was lost by the latest stage (Figure 6.4D vii-viii). At P10 (early stage), most junctions were still formed between Müller glia end feet and nascent photoreceptor segments. However, as degeneration

progressed, and unsurprisingly in the absence of photoreceptors, the vast majority of AJs formed were between the apical processes of two Müller glial cells or Müller glia and other retinal cells whose identity could not be confirmed with certainty on the basis of location and morphology, due to the extensive degeneration. Together, these results indicate that the OLM undergoes significant remodelling, including changes in the type of junctions formed, in this model in the face of almost complete loss of the photoreceptor layer.

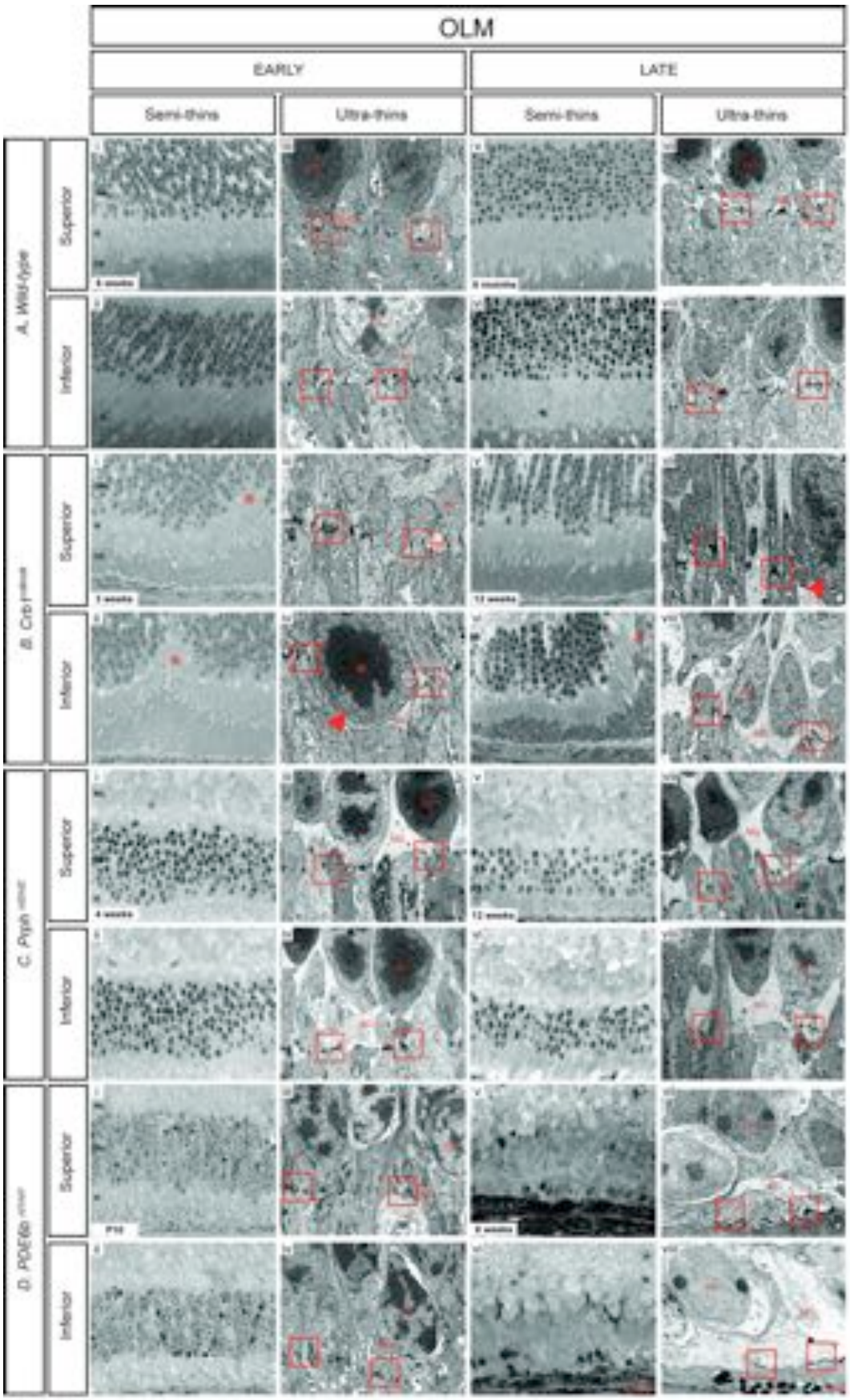

Figure 6.4 Ultratructural assessment of the adherens junctions in animal models carrying a spontaneous mutation.

Ai-viii) *C57Bl/6J* wild-type; **Bi-viii)** *Crb1*$^{rd8/rd8}$; **Ci-viii)** *Prph2*$^{rd2/rd2}$ and **Di-viii)** *Pde6b*$^{rd1/rd1}$. OLM integrity was assessed at early and late stage of retinal degeneration using semithin sections (Scale bar: 25 µm) and ultrathin electron microscopy (Scale bar: 1 µm). Red boxes: AJs; PR, photoreceptor; MG, Müller glia; arrows indicate displaced photoreceptors. ONL, outer nuclear layer; OLM, outer limiting membrane; IS, inner segment; OS, outer segment.

Examination of semithin sections of *Rho*$^{-/-}$ mouse showed that at early stage of retinal degeneration (Figure 6.5A i-ii), the laminar structure is comparable to a wild-type retina (Figure 6.5A i-ii). As degeneration progresses, the photoreceptor morphology changes with the nuclei becoming smaller and the ISs becoming shorter (Figure 6.5A v-vi). Further EM analysis revealed the presence of numerous AJs at the early time point (Figure 6.5A iii-iv), but as photoreceptor death progressed, the distance between junctions increased (Figure 6.5A vii-viii). By the latest stage examined, when the vast majority of photoreceptors have died, much of the space at the outer retinal margin appeared to be occupied by the terminal processes of the Müller glia. This is reflected in a shift in the type of AJs; at the ultra-structural level, many more Müller-to-Müller cell AJs were observed in the late stage, in comparison with the early stage.

In the *Prph2*$^{+/\Delta 307}$ retina, there was a moderate disorganization at the margin of the ONL including the mislocalisation of photoreceptor cell bodies into the segment region at both early (Figure 6.5B i-ii) and late time points (Figure 6.5B v-vi). Ultra-structural analysis confirmed that while junctions remained quite neatly aligned at both stages examined, they were less numerous in the late stage (Figure 6.5B vii-viii) in comparison to 2 months old retina (Figure 6.5B iii-iv). Additional morphological changes in the Müller cells were observed at the late stages of degeneration, including hypertrophy of the end feet and an increase in a number of Müller to Müller junctions.

As in the *Crb1*$^{rd8/rd8}$ model, the OLM of the *Nrl*$^{-/-}$ mutant undergoes significant fragmentation and displacement of photoreceptor nuclei into the segment region is apparent (Figure 6.5C i-ii, v-vi; arrows). Surprisingly though, inspection at the ultra-structural level showed that the AJs were still numerous, including in the regions where rosettes were formed (Figure 6.5C iii-iv; arrows). The photoreceptor segments also appeared to be shorter than those of a wild-type. No major alterations were observed between early and late stages.

Similar to wild-type retinae, the OLM is well preserved in the *R91W;Nrl*$^{-/-}$ retina throughout the time frame examined (Figure 6.5D i-ii, v-vi). Assessment at the ultrastructural level showed the AJs were neatly aligned with the majority of junctions being formed between photoreceptor segments and Müller apical terminals (Figure 6.5D iii-iv, vii-viii; red boxes). As in the wild-type, no observable changes in the alignment of the AJs were observed between early and late time points examined.

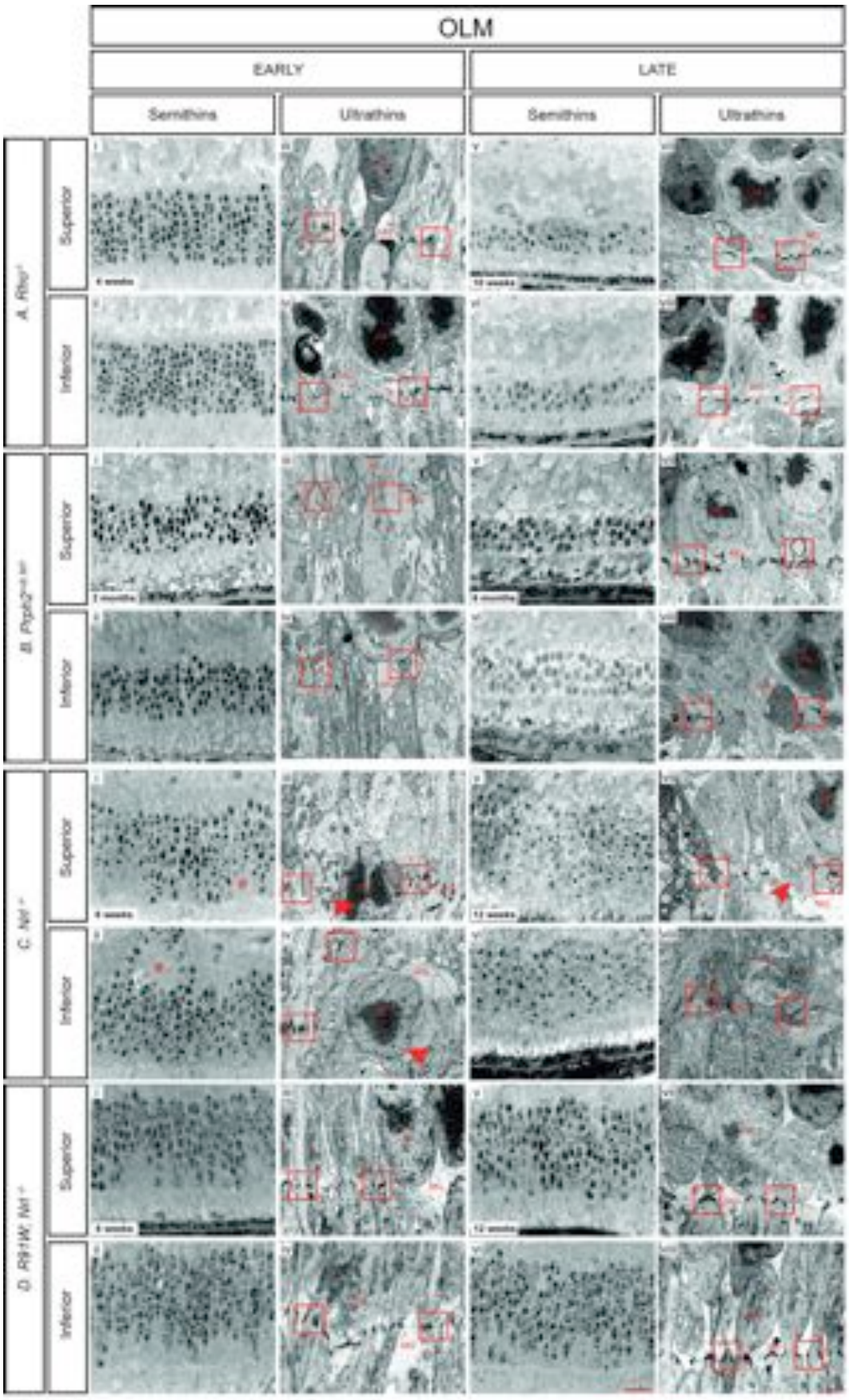

Figure 6.5 Ultrastructural assessment of the adherens junctions in animal models carrying a targeted mutation.

Ai-viii) *Rho*$^{-/-}$; **Bi-viii)** *Prph2*$^{+/\Delta 307}$; **Ci-viii)** *Nrl*$^{-/-}$ and **Di-viii)** *R91W;Nrl*$^{-/-}$. OLM integrity was assessed at early and late stage of retinal degeneration using semithin sections (Scale bar: 25 µm) and ultrathin electron microscopy (Scale bar: 1 µm). Red boxes: AJs; PR, photoreceptor; MG, Müller glia; arrows indicate displaced photoreceptors. ONL, outer nuclear layer; OLM, outer limiting membrane; IS, inner segment; OS, outer segment.

Having noted clear differences in the appearance of the AJs between early and late stages of retinal degeneration in some of the examined mutants, a quantitative assessment of the AJs was performed (Figure 6.6). Using EM micrographs, a number of data analyses was performed including the total number of AJs, and a proportion of i) AJs formed between photoreceptor IS and Müller glia apical terminals, ii) AJs between two Müller glial cells, iii) AJs between two photoreceptor cells and iv) atypical AJs that formed between cellular structures whose identity could not be fully defined due to advanced retinal degeneration. Unfortunately, the *Crb1*$^{rd8/rd8}$ and *Prph2*$^{+/\Delta 307}$ mutants had to be excluded from these data analysis as the two lines were lost prior to sufficient number of samples being collected for each time point. The number of junctions counted in the middle superior and inferior regions was combined, and expressed as an average number of AJs per retina per 100 µm. Early and late stages of degeneration were compared using an unpaired Student's *t*-test with Holm-Sidak corrections.

In wild-type retinae, we did not observe any major changes in absolute number of AJs between early and late stages examined (early, 158±12; late, 132±14 junctions per 100 µm; Figure 6.6A). The majority of the AJs counted were formed between photoreceptor IS and Müller glia apical processes. There was a small, but non-significant drop in this number with age (Figure 6.6B) (early, 141±13; late, 110±17). As predicted, only a very small number of the AJs were formed between two Müller glia cells (early, 18±4; late, 15±2; Figure 6.6C). A few junctions forming directly between two photoreceptor cells were also observed at early stages but this did not change with time (early, 7±4; late, 7±4; Figure 6.6C). No atypical AJs were found in a wild-type.

In the slowly degenerating *Rds*$^{rd2/rd2}$ mutant, the total number of junctions per 100 µm fell markedly, from 107±4 at the early stage to 76±7 at the late age (P<0.002*;* Figure 6.6A). A small, but non-significant, drop in a number of AJs between photoreceptors and Müller glia was seen between early (70±20) and late (53±9) time points (Figure 6.6B) and there was a concomitant increase in the number of AJs formed between two Müller glial cells (early, 10±4; late, 16±1; P<0.05*;* Figure 6.6C). No other significant changes were found in the *Rds*$^{rd2/rd2}$ model.

The most dramatic changes to AJ number and type were seen in the rapidly degenerating *Pde6b*$^{rd1/rd1}$ mutant. In this model, the total number of AJs per 100 µm dropped from 111±12 in the early stage of disease to 52±4 by the late age (P<0.001; Figure 6.6A). There was a dramatic decrease in a number of photoreceptor IS to Müller glial type AJs, with 97±9 AJs counted at the early stage but almost none in the late stage (P<0.001*;* Figure 6.6B). As degeneration progressed, the Müller glial processes extended along the outer edge of the neuroretina and there was a marked increase in

the number of AJs formed between two glial cells (early, 10±1; late, 38±9; *P*<0.01; Figure 6.6C). At the late stages of retinal degeneration, and most likely due to the extensive degeneration and morphological reorganisation of the retina, we also observed a significant number of AJs that were formed between cellular structures whose identities were difficult to define (12±1; *P*<0.001; Figure 6.6E).

The rod OSs of *Rho*$^{-/-}$ mutants do not develop and these animals lose their photoreceptor cells within the first 3 months of age (Humphries et al., 1997). Nonetheless, as shown by the IHC and ultrastructural analyses, the OLM integrity appears largely preserved. Interestingly, the total number of AJs did decrease significantly over the course of degeneration, falling from 116±5 counted per 100 µm at the early stage to 61±6 at the late time point (*P*<0.001*;* Figure 6.6A). The number of AJs formed between photoreceptors and Müller glia dropped markedly, between the early (98±1) and late (33±9) time points (*P*<0.001*;* Figure 6.6B). Surprisingly, despite the progressive loss of photoreceptors, there was no significant increase in the number of AJs formed between two glial processes (early, 17±4; late, 20±5*;* Figure 6.6C), although a small number of atypical AJs was also observed in the late time point examined (4±2*;* Figure 6.6E), which could be a result of the extended retinal remodelling.

Nrl$^{-/-}$ retina lacks rod cells; therefore the AJ formation involves only two cell types, Müller glia and so–called 'cods' (Mears et al., 2001). Moreover, *Nrl*$^{-/-}$ mice develop numerous rosettes, with many photoreceptor cells being mislocalised in the segment region (Stuck et al., 2012). Analysis of the EM micrographs revealed that although the total number of AJs was typically lower than that seen in wild-type retina, this did not change with age; an average of 70±2 AJs per 100 µm were observed at the early, compared to 80±30 at the late, time point (Figure 6.6A). No obvious changes in the type of AJs were observed with age, although the number of AJs formed between photoreceptors and Müller glia cells was notably lower than that seen in wild-type (early, 46±2; late, 52±21; Figure 6.6B). Despite extensive gliosis throughout these retinae, no major changes in the number of Müller glia to Müller glia AJs was observed over time (early, 23±2; late, 28±12; Figure 6.6C).

The all-cone retina of the *R91W; Nrl*$^{-/-}$ mouse had a similar number of AJs to the *Nrl*$^{-/-}$ mutant, with no significant changes over time (early, 86±7; late, 83±8 AJs per 100 µm Figure 6.6A). Although the total number of AJs was again lower in comparison to wild-type, including the number of AJs formed directly between photoreceptor IS and Müller glia terminals (early, 57±7; late, 56±7; Figure 6.6B), this does not appear to result in any obvious breaks to OLM integrity, and the lamination of the ONL remains intact. No

change in a number of junctions formed between two Müller glial cells was observed, which was expected given the fact that this model does not really degenerate.

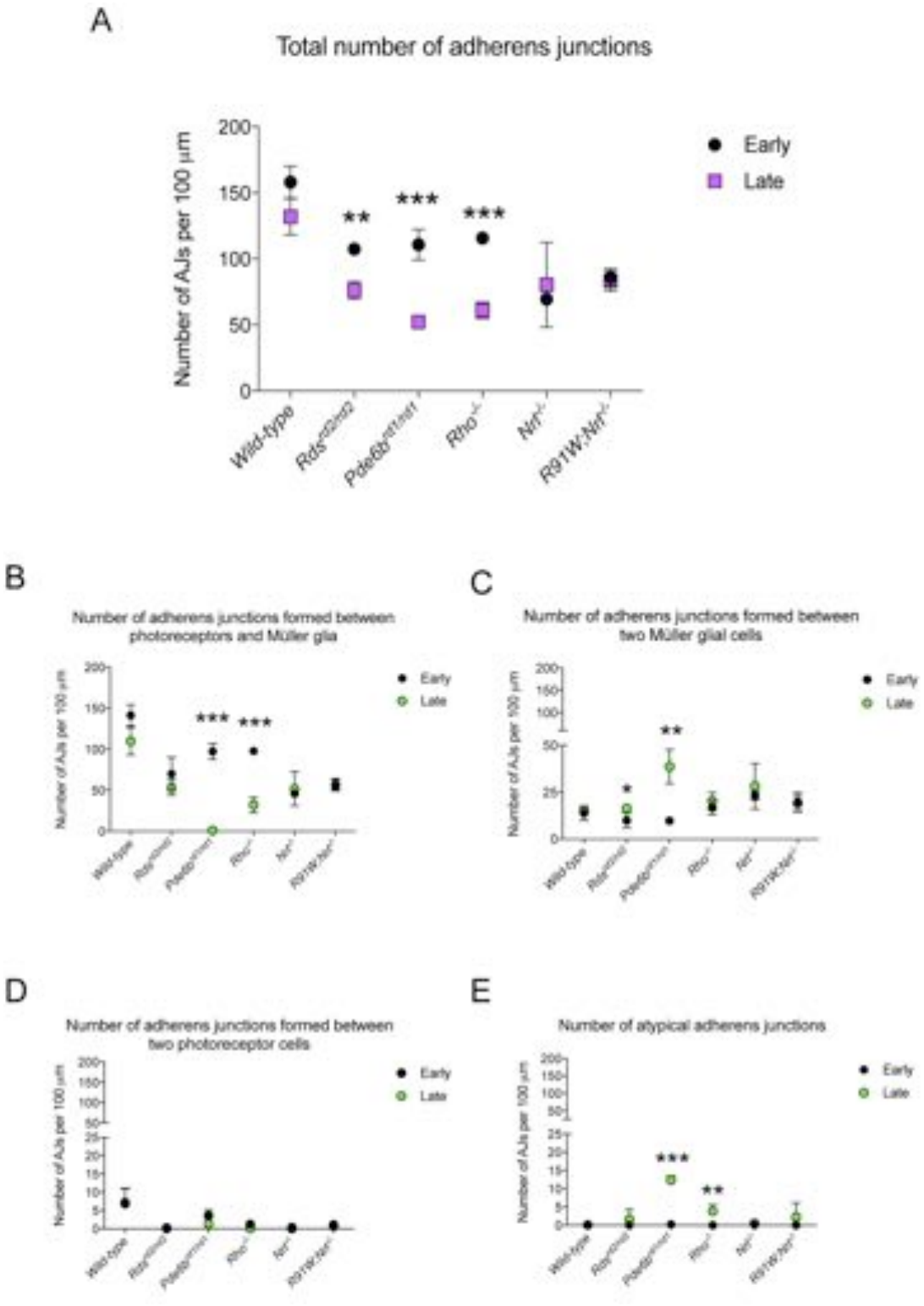

Figure 6.6 Assessment of the number of adherens junctions between early and late stages of retinal degeneration.

A) Total number of AJs; **B)** Number of AJs formed between photoreceptors and Müller glial cells; **C)** Number of AJs formed between two Müller glial cells; **D)** Number of AJs formed between two photoreceptor cells and **E)** Number of the atypical AJs formed. All the counts are expressed per 100 µm. Statistical significance was assessed using unpaired Student's *t*-test with Holm-Sidak corrections. ***P* <

0.01 and ***P < 0.001. Error bars: SD, n=3 animals examined per time point (with ≥2 retinal sections assessed per animal in at least two independent ROI).

6.3 Discussion

The OLM is considered by many to be the third retinal barrier. In this study, it has been shown that in a number of murine models of inherited retinal degenerations, this barrier undergoes significant remodelling during degeneration. As the photoreceptor cells die, both the number and the composition of those AJs between the remaining cells changes, with a significant shift in favour of junctions formed between two Müller glia cells, rather than between Müller glia and photoreceptor cells. Both in the current study, and previous reports (Barber et al., 2013; Hippert et al., 2015), these changes can be correlated with the rate of photoreceptor death, with the most striking OLM remodelling seen in the *Pde6b*$^{rd1/rd1}$ mutant, which undergoes a very rapid loss of photoreceptors.

In the retina, Müller glia are arranged in a regular pattern. Each individual glial cell constitutes the core of a column of retinal neurons, which represents the smallest functional unit in the retina. It has been illustrated that for each Müller cell there is one cone and a variable number of rods and inner neurons (reviewed in (Bringmann et al., 2006)). It is possible then that the AJ connections between Müller cells could represent the borders of such units. It is tempting to speculate that the protein expression may be different at the 'unit border' enabling the junctions to specialise and perform some specific function or lead to some differences in permeability to ECM molecules. This could be of particular importance in diseased conditions where these individual units become rearranged due to loss of cell contacts, leading to an increase in OLM permeability and/or decrease in the strength of AJs and susceptibility to retinal detachment. Various clinical studies have demonstrated that eyes with a continuous IS/OS junctions have a better visual acuity than those in which IS/OS line is disrupted prior the surgery making them more prone to increased vascular leakage upon mechanical stress (Mitamura et al., 2013). In the majority of the mouse models of inherited retinal degeneration examined in the current study, there were clear signs of OLM remodelling, although the nature and extent this remodelling varied markedly between different mutants. In addition to these changes, a mislocalisation of photoreceptor cells into the segment region was observed, particularly in the areas where the OLM was clearly compromised. Interestingly, despite severe loss of photoreceptor cells, the retina's attempt to maintain OLM integrity is remarkable. This is evident in the increased number of AJs formed between Müller glia processes in a number of different models, demonstrating the importance of this structure in the maintenance of retinal architecture.

During retinal development, the SAR complex localises apically in the neuroepithelium, where it helps to form an adhesive OLM belt and plays an important role in the

maintenance of the AJs (Mehalow et al., 2003; Alves et al., 2014b). These proteins have also been implicated in photoreceptor survival and maintenance. For example, mutations in *CRB1*, which is part of the SAR complex, have been associated with a variety of autosomal recessive retinal dystrophies, including Leber's congenital amaurosis, retinitis pigmentosa type 12, retinitis pigmentosa with Coats-like exudative vasculopathy and other early-onset forms of retinitis pigmentosa (Bujakowska et al., 2011; Pellissier et al., 2014; Zhao et al., 2015). In mouse, the loss of CRB1 protein leads to displaced photoreceptors and focal degeneration of all neural layers. This is attributed to loss of adhesion between photoreceptors and Müller cells (Mehalow et al., 2003; van de Pavert et al., 2004), although more recent reports have indicated this phenomenon is background-specific (Luhmann et al., 2015). As described by others, in this study the OLM integrity was found to be increasingly compromised with degeneration in the *Crb1*$^{rd8/rd8}$ mouse mutant. This manifests as ONL undulations, commonly known as ‘rosettes’. Moreover, expression of ZO-1 appears reduced in comparison to wild-type. In contrast, in the *Nrl*$^{-/-}$ mouse, another model that also develops ONL 'rosettes', both ZO-1 and CRB1 were robustly expressed despite numerous OLM breaks and visible displacement of photoreceptors into the segment region. Interestingly, in this model, the retinal cells still managed to form AJs within the 'rosettes'; however, these appeared to be abnormal and did not form a continuous line. Previous reports have shown that mutations in the *Nrl* gene results in a number of pathological functions, including aberrant photoreceptor packing, abnormal association between photoreceptors and RPE, retinal detachment, changed dendritic fields and axon terminals in horizontal cells, vascular leakage, and ganglion cell death (Mears et al., 2001; DeAngelis et al., 2002). The exact cause of the OLM disruption in the *Nrl*$^{-/-}$ retina still remains unclear, although recent study by Feathers *et al.* pointed towards the involvement of retinoid intermediates, since *Nrl*$^{-/-}$ mutants with no functional RPE65 protein failed to develop rosettes (Feathers et al., 2008). Moreover, it still remains unclear why disruptions in the OLM in both *Nrl*$^{-/-}$ and *Crb1*$^{rd8/rd8}$ mutants appear as localized disruptions, resulting in focal rosettes, instead of a uniform failure of OLM formation across the retina. One possible explanation is that there are differences in the protein expression between different AJ types, making some of the junctions weaker or more susceptible to disruption. For example, Daniele and colleagues reported that in the *Nrl*$^{-/-}$ retina, which is 'cone' dominant, JAM-C protein, a part of the AJs complex, is significantly overexpressed compared to wild-type retina. The authors propose that JAM proteins play a specific role in cone polarisation and function (Daniele et al., 2007), but these could also lead to functional differences in AJs between cone photoreceptors, rod photoreceptors and Müller glia. A previous study in diabetic patients reported that S-cones, which are absent from the fovea, are the most

prone to retinal degeneration (Hollyfield et al., 1999; Cho et al., 2000). Omri *et al.* reported that in a rat animal model of diabetic retinopathy there was a marked drop of S-cone photoreceptors (Omri et al., 2013). They also showed that this mutant manifests clear signs of OLM discontinuity with both Occludin, which is mainly found in the AJs between Müller glia and cones (Omri et al., 2010), and aPKC protein (Omri et al., 2013), to be visibly decreased. Of note, the current study shows that there are observable differences in the expression of ZO-1 and CRB1 between different models of retinal degenerations, as well as differences in the number and type of the remaining AJs. These discrepancies may be related to the fact that there are regional differences in both quantity and density of surviving photoreceptors (LaVail and Battelle, 1975; Carter-Dawson et al., 1978; LaVail et al., 1992; García-Fernández et al., 1995; LaVail et al., 1997; Lin et al., 2009), which may depend on preservation of the OLM. In normal mice, the majority of the AJs form between photoreceptor ISs and Müller glia apical terminals. However, in the *Pde6b*$^{rd1/rd1}$ mouse model of RP, for example, where the majority of rod photoreceptors are gone by P21, there is extensive junctional remodelling and the majority of AJs form between two Müller glial apical terminals. At this stage, only the cone photoreceptors remain and wrapped tightly by the gliotic processes of Müller cells. These findings suggest a robust attempt by the retina to preserve the OLM and retinal architecture. Moreover, qualitative analysis at the ultrastructural level showed that the newly AJs seem to extend further than the junctions observable in a wild-type, which may suggest that the junctions enlarge or the junctional proteins mislocalise or diffuse along the junction. The same phenomenon was observed in *Rho*$^{-/-}$ mice especially at the later examined time-point. This corresponds with the results presented in Williams *et al.* study that showed that the cytoplasmic plaques of the OLM junctions are larger in Müller cells than the ones in photoreceptors (Williams et al., 1990). They speculated that these large aggregates of junctional proteins may control the extracellular pore size of the AJ and thus the permeability of the OLM. Although the described changes may be due to sectioning artefact, it is possible that in reactive glia the expression of the junctional proteins is altered which could lead to abnormities in the newly formed AJs.

Interestingly, in the *Rho*$^{-/-}$ model where the loss of the ONL occurs moderately quickly, the OLM seemed to stay linear and uninterrupted until at least 6 weeks, by which time only 2-3 rows of PRs remain (see Chapter 3). It was only at the latest time point examined that some disruption in the OLM was evident, and significant preservation even as late as 22 weeks of age (Appendix AA; (Hippert et al., 2015)). These observations contrast those of Campbell *et al.* who reported reduced levels of ZO-1 and catenin proteins in *Rho*$^{-/-}$ mice as early as 3 weeks of age and no staining of the same AJ proteins after 5 weeks (Campbell et al., 2007). In this study, ZO-1 staining

was very visible and even appeared stronger than in a wild-type retina. The reasons for these discrepancies are unclear. EM analysis showed that the total number of AJs significantly drops in *Rho*$^{-/-}$ mutant between early and late ages; however, IHC analysis did not indicate any major changes to OLM continuity. As mentioned before, the AJs especially those formed between two glial cells appeared to be elongated as shown at the ultrastructural level. This could explain why ZO-1 staining appeared to be unbroken. Interestingly, we did not observe any ring formation of cones as has been previously reported in rat model of RP, where a mutation in *Rhodopsin* gene led to the loss of rod photoreceptors triggering a reorganisation of cones into an array of rings (Lee et al., 2011; Yu et al., 2016). Lee *et al.* reported that these rings formed around the zones of rod cell death, which were then enwrapped by Müller glia processes and formed junctional connections with the cones' IS (Lee et al., 2011). IHC analysis showed that OLM was also compromised with an alteration in ZO-1 expression and clear remodelling of Müller glia processes, but strong ZO-1 expression was observed at the ring boundaries. Interestingly, these Müller glia-cone interactions were disrupted following the injection of DL- aminoadipic acid (AAA), which is commonly used to disrupt Müller glial cell metabolism (Lee et al., 2011), indicating that Müller glia compel cones to migrate to specific areas of rod death to form rings. Another study, by Xia *et al.* showed that this ring formation can be prevented by injection of Oncostatin M (OSM), which is a member of the IL-6 cytokine family (Xia et al., 2011). In the past, cytokinesis have been reported to alter tight junctions (Abe et al., 2003; Villarroel et al., 2009; Aveleira et al., 2010); hence it has been suggested that OSM may modulate the formation or the strength of the cone-glia AJs. This hypothesis was further tested by Yu *et al.* who showed that treatment of the same mutant with high concentrations of siRNA against *Zo-1* mRNA leads to the homogenous spread of cones within the ONL without any reduction in their number (Yu et al., 2016). These findings suggest that AJs represent at least one critical component for cone rearrangement in RP retina. ZO-1 is known to act as a molecular scaffold that organizes, assembles, and links the TJ complexes to the cytoskeleton through a number of protein-protein interactions providing structural integrity to the cells (Wittchen et al., 1999; Van Itallie et al., 2009); hence any breakages can result in the loss of the cellular structure. Moreover, any inhibition of the ZO-1 expression may result in weakening of the bundles of filament by affecting the AJ complexes and, as a consequence, have an impact on the glial scar that forms in many diseased conditions at the outer edge of the neuroretina (reviewed in (Hippert et al., 2016)). Equally, it is possible that any intervention that inhibits the formation of the glial seal, including downregulation of the intermediate filament proteins (e.g. Chapter 5), may lead to a disruption of OLM remodelling.

Understanding the composition of retinal barriers, including the specific differences that may exist between the AJs in normal and diseased conditions, is a prerequisite for understanding why certain pathological events are region specific such as oedema that localises to the macula. The macula is the only place in the retina where cones out-number rods. In this region, the AJs between Müller cells and cone photoreceptors were reported to be shorter, in comparison to AJs elsewhere within the retina, and to have a structure typical of desmosomes, with dense intermediate filament extensions (Omri et al., 2010). At this region, Müller glial cell apices are almost in contact with the cone OS leading to a decrease in the glial free SAR that surrounds the fovea. Moreover, although it has generally been accepted that the OLM is continuous throughout the entire retina, one observation reported that in the centre of the fovea of the rabbit retina, there might be areas in which the OLM becomes discontinuous, as there is a lack of AJs between some cone IS and Müller glial apical terminals (Bunt-Milam et al., 1985). These findings could explain why this region is more susceptible to pathologies, such as the macular oedema that is associated with AMD disease. Macular oedema in humans is a result of diffuse capillary leakage and micro-aneurysms in the macular region. Geiger *et al.* showed that exposure to toxic levels of blue-light of the all-cone retina of the *R91W;Nrl*$^{-/-}$ mutant leads to vascular leakage, retinal swelling and the appearance of cystoid spaces in both INL and ONL indicating oedema (Geiger et al., 2015). In AMD, like RP is a collection of defects where the macular area and fovea become compromised leading to retinal remodelling including the remodelling of the AJs. Geiger and colleagues reported that the expression levels of ZO-1 were markedly reduced in *R91W;Nrl*$^{-/-}$ in comparison to wild-type controls (Geiger et al., 2015). Interestingly, in the current study, I found ZO-1 expression to be robust, as assessed by IHC, however ZO-1 expression was not quantified, either by PCR or WB. Nonetheless, in keeping with Geiger *et al.* study, here the total number of AJs was shown to be much lower, in comparison to wild-type controls, including the number of AJs formed directly between photoreceptor IS and Müller cell processes, although retinal lamination remained normal. Together, these findings suggest that the susceptibility of the *R91W;Nrl*$^{-/-}$ mutant to develop vascular leakage may be linked to the more sparse distribution of AJs. Recent studies in humans showed that OLM integrity is viewed as an important prognostic factor in treatment of the epiretinal membrane (Cobos et al., 2013). It has been reported that the presence of an intact IS/OS junction on the preoperative spectral-domain optical coherence tomography scan was an important predictor of better visual recovery after epiretinal membrane surgery. Mitamura *et al.* demonstrated that the IS/OS junction is important in predicting postoperative visual acuity and that the improvement of retinal microstructure after surgery is better in patients with fewer OLM discontinuities (Mitamura et al., 2013).

It is increasingly evident that understanding the diseased retinal environment is of paramount importance when designing effective therapeutic strategies for the treatment of retinal degeneration. In the past few years, great progress has been made in the development of novel ocular therapies such as electronic implants (Stingl and Zrenner, 2013) and in the field of both cell (MacLaren et al., 2006; Gonzalez-Cordero et al., 2013; Santos-Ferreira et al., 2014) and gene (Bainbridge et al., 2008; Maguire et al., 2008; Jacobson, 2012) therapy. A compromised OLM may promote gene delivery or cell transplantation efficiency by increasing accessibility of the virus or the donor cell into the target tissue. A number of different studies demonstrated that combining a reversible disruption of the OLM with photoreceptor transplantation increases the number of donor-reporter labelled cells observable within the recipient retina (West et al., 2008; Pearson et al., 2010; Barber et al., 2013). Previously, transplantation of donor cells was thought to lead to their migration from the site of transplantation in the sub-retinal space, across the OLM and into the recipient retina. Real-time imaging of explants of transplanted retina have confirmed these findings (Pearson et al., 2016). However, in the same study, Ali and colleagues found that this process accounts for only a minority of apparently integrated cells within the host ONL. Instead, donor and host photoreceptor cells engage in the exchange of RNA and/or protein, in a process termed material transfer. The precise cellular mechanism underlying this process remains unclear. What is known is that it does not involve uptake of free protein, RNA or DNA nor does it involve classic cell-cell fusion mechanisms or nuclear transfer. At the time of writing, the release by donor photoreceptor cells and subsequent uptake by host photoreceptors (and to a lesser extent vice versa) of microvesicles is a working hypothesis. Whatever the underlying process, material transfer is surprisingly robust, resulting in host cells be able to express a wide variety of photoreceptor specific proteins with high fidelity; for example, around 85% of GFP^{ve+} cells in the ONL of *Gnat1*$^{-/-}$ hosts also express rod α-transducin, the protein missing for host photoreceptors. A number of reports have demonstrated improvements in visual function following photoreceptor transplantation (Lamba et al., 2009; Pearson et al., 2012; Santos-Ferreira et al., 2014; Barnea-Cramer et al., 2016).

Intriguingly, the number of GFP^{ve+} cells in the host ONL is markedly higher in models that show a disrupted OLM than in models where the OLM remained intact. Moreover, disruption of OLM in a wild-type mice using pharmacological (West et al., 2008) and siRNA techniques (Pearson et al., 2010) led to a significant increase in the number of GFP^{+} cells within the host retina. It is not clear at present whether these improvements are due to improving the number of real integration events or the frequency of material transfer events, although the frequency of material transfer events versus true integration events seen in the normal retina would make the latter more likely. These

findings may help us in elucidating the mechanisms underlying material transfer. Previous studies have shown that after the lamination of the retina is complete, the OLM creates as barrier to limit the diffusion of macromolecules including Retinoid-binding protein into the neuroretina from the IS/OS region depending on their molecular weight (Carter-Dawson and Burroughs, 1992). Although the recent studies on photoreceptor transplantation showed that material transfer does not result from the uptake of free proteins from the extracellular milieu(Pearson et al., 2016; Santos-Ferreira et al., 2016), if the OLM is a semipermeable barrier (Bunt-Milam et al., 1985), it may restrict the passage of microvesicles from donor to host and/or access to the uptake mechanisms. This could explain why in the retina with a compromised OLM, the number of GFP^+ cells is higher in comparison to healthy retinae. If the underlying biological mechanisms of material transfer can be revealed, they may represent a new therapeutic strategy for a broad-spectrum of inherited retinal diseases by introducing functional proteins into otherwise diseased photoreceptors.

In conclusion, disruption to the OLM is an expected outcome of photoreceptor loss and is predicted to have significant consequences for the overall homeostasis of the retina (Omri et al., 2010). Remarkably, however, our data show that while there is undoubtedly significant junctional remodelling, depending upon the model, the OLM very often remains intact even at advanced stages of degeneration, suggesting a significant attempt by the retina to protect itself from further damage. A better understanding of the OLM is needed for our understanding of disease progression. This is particularly important when designing therapeutic interventions, as any disruption to it, particularly in a diseased condition, may result in acceleration of retinal degeneration.

CHAPTER 7

Disruption of OLM integrity

7.1 Overview

In the vertebrate retina, the apical processes of Müller cells are attached to each other and to the inner segments (IS) of the photoreceptors by continuous heterotypic adherens junctions (AJs) that collectively form the outer limiting membrane (OLM). This continuous belt of AJs helps to maintain the integrity of the retinal lamination as it creates a barrier which seals off the neuroretina from the retinal pigmented epithelium (RPE) and choroid. In recent years, a number of different proteins that contribute to localisation and organisation of the AJ 'building blocks' have been studied, including proteins of the SAR region. The SAR region, which is located apically to the AJs, is comprised of the two complexes, PAR and Crumbs, which directly interact with each other. The core of the Crumbs/CRB complex (formed by the CRB proteins, PALS1, PATJ and MUPP1 (Richard et al., 2006) has received particular attention from the scientific and clinical community because thus far only the Crumbs complex member, CRB1, has been associated directly with human disease.

CRB1 is a large (153 kDa) transmembrane protein, which is one of the three homologs to Drosophila protein Crumbs found in human genome (Tepass et al., 1990; Pellikka et al., 2002). In the mouse retina, CRB1 is expressed from embryonic (E) day 12.5 onwards at the SAR adjacent to AJs in retinal progenitor cells (Hollander et al., 2002). As the retina matures, the CRB1 expression becomes restricted to Müller cells (Pellikka et al., 2002; van de Pavert et al., 2004), where it acts as an anchor between Müller glia microvilli and photoreceptor IS, ensuring the integrity of the OLM (Gosens et al., 2008). In 1999, the *CRB1* gene was found to be mutated in a specific group of patients with RP (Hollander et al., 1999) and shortly after, mutations in the human *CRB1* gene were found to be associated with autosomal recessive RP and autosomal Leber's congenital amaurosis (LCA) retinopathy (Jacobson et al., 2003; Hollander et al., 2004; Bujakowska et al., 2011). To date, several animal models have been studied that provided some insight into the pathology of CRB defects. The *Crb1*$^{rd8/rd8}$ mouse is a naturally occurring mutant, where a single base deletion in the *Crb1* gene causes discontinuity and fragmentation of the AJ complexes (van de Pavert et al., 2004; Hippert et al., 2015; Figure 7.1 B, white arrows), as well as defects in the photoreceptor IS and outer segment (OS) (Mehalow et al., 2003). Moreover, it has been reported that mutations of *Crb1* lead to retinal folding and the formation of so-called rosettes (see Chapter 3 and 6), and subsequent photoreceptor cell death (van de Pavert et al., 2004). Two studies have demonstrated that the number of GFP cells following transplantation of *Nrl.*GFP$^{+/+}$ photoreceptor precursors was significantly higher in the *Crb1*$^{rd8/rd8}$ animals compared with co-transplanted wild-type animals (Pearson et al., 2010; Barber et al., 2013). This contrasts with the very low numbers of GFP cells

typically observed in the recipient retina following cell transplantation into other models of retinal degeneration, including the *Rho*$^{-/-}$ mutant (Barber et al., 2013), where the OLM integrity is preserved (see Chapter 6). To test the hypothesis that the OLM may represent a barrier to cell transplantation, two molecular approaches were developed and tested to downregulate *Crb1* expression in a C57BL/6J wild-type retina to assess whether CRB1 is a suitable target for OLM disruption.

In 2010, a study by Pearson *et al.* showed that using siRNAs against a junctional adaptor (ZO-1) leads to a discontinuity in OLM integrity. Moreover, when combined with photoreceptor precursor cell transplantation, they reported significantly more integrated cells within the recipient retina in both wild-type mice and, importantly, in a model of retinal degeneration (Pearson et al., 2010). However, ZO-1 is not exclusively expressed in the OLM. It has been shown that ZO-1 is also part of the junctional complex within the RPE; thus it is possible that a subretinal injection of siRNA against *Zo-1* will also interfere with junctions in the RPE. Interestingly, recent work by Daniele *et al.* demonstrated that there are some differences in the expression of tight junction proteins in the OLM compared with the AJs of the RPE, which may help to find an alternative target for OLM disruption (Daniele et al., 2011). One such possible target for an RNAi strategy is *Crb1*, because its expression in the eye is restricted to the OLM (Hollander et al., 2002). It is therefore possible that knocking down mouse CRB1 might lead to a more specific disruption of the OLM without the risk of associated damage to the RPE.

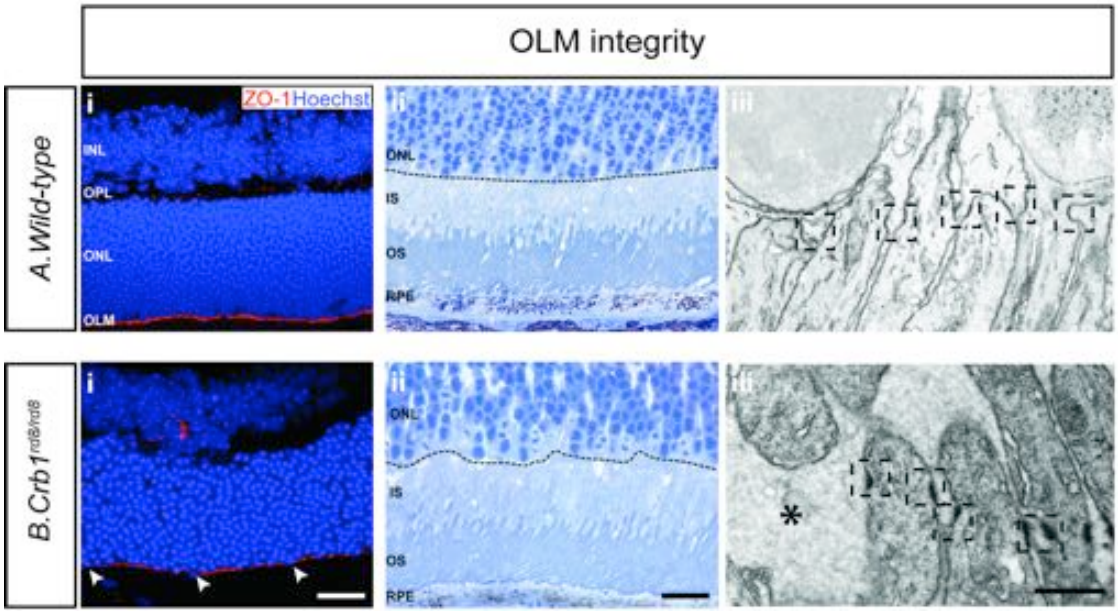

Figure 7.1 The OLM integrity in a wild-type and Crb1$^{rd8/rd8}$ mouse retina.

Ai) In a wild-type ZO-1 (*red*) staining forms a uniform, unfragmented line. **Aii)** Semithin sections demonstrate OLM continuity, as indicated by black dashed line. **Aiii)** Ultrastructural images show the continuous formation of AJs at the OLM level (dashed boxes). **Bi)** In *Crb1$^{rd8/rd8}$* model a clear disruption of the OLM can be seen (arrows) as ZO-1 staining (red) appears to be fragmented. **Bii)** Semithin sections show ONL nuclei being displaced as the OLM continuity is being compromised (black dashed line). **Biii)** Assessment of OLM integrity at the ultrastructural level shows missing AJs in the *Crb1$^{rd8/rd8}$* mutant (asterisk). Retinal cryosections were co-stained with the nuclear marker Hoechst 33342 (*blue*). INL, inner nuclear layer; OPL, outer plexiform layer; ONL, outer nuclear layer; IS, inner segment; OS, outer segment; RPE, retinal pigmented epithelium (see also Hippert et al., 2015). Scale bars: Ai and Bii, 25 µm; Aii and Bii, 10 µm; Aiii and Biii, 0.5 µm.

7.2 Results

7.2.1 CRB1 in a *C57BL/6J* wild-type retina

It has been previously suggested that CRB1 levels might vary between different retinal regions, based on the fact that the inferior quadrant of the retina is structurally more impaired in the *Crb1* mouse mutant (Mehalow et al., 2003). To assess whether there is any variation in the distribution of CRB1 in a wild-type retina, IHC and QRT-PCR analysis were performed on the samples from superior and inferior regions.

A confocal montage of immunostained wild-type retina (Figure 7.2A i) indicates that CRB1 expression is uniform across the whole retina, with no noticeable differences between the superior (Figure 7.2A ii) and inferior (Figure 7.2A iii) regions. As expected, there were no signs of OLM fragmentation or nuclei displacement into the subretinal space.

Further QRT-PCR analysis on laser-captured samples from orientated retinae showed that the levels of *Crb1* mRNA were similar between the superior (119.9±36.5%) and inferior (118.6±44.5%) parts of the retina (P=0.447; Figure 7.2B). In contrary to previous reports (Mehalow et al., 2003), no significant variations between the wild-type superior and inferior retinae were detected; however the inter-sample variations in detected mRNA levels were high in both regions assessed. Having shown that CRB1 is homogenously present in the wild-type retina and can be detected using ICH and QRT-PCR, I then moved to designing tools to knockdown its expression.

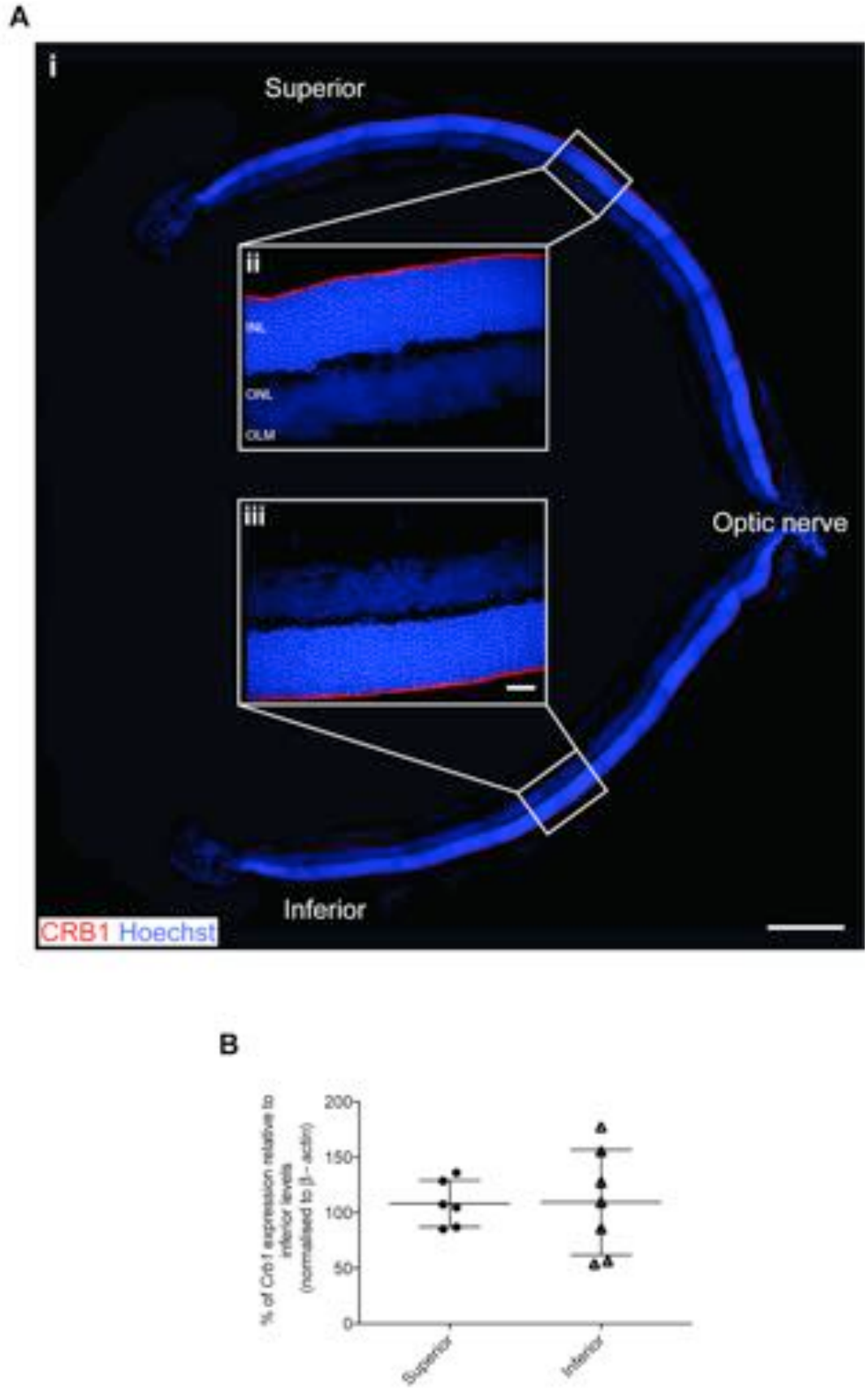

Figure 7.2 CRB1 expression in the superior and inferior regions of a wild-type retina.

Ai-iii) Representative images of the CRB1 staining (*red*) in a wild-type retina. **Ai)** A montage image showing a uniform and continuous belt of CRB1 at the OLM level across the entire retina. **Aii-iii)** Higher magnification images of the superior and inferior OLM regions. Retinal cryosections were counterstained

with the nuclei marker, Hoechst 33342 (*blue*). **B)** QRT-PCR analysis on the laser captured samples revealed no marked differences in the *Crb1* mRNA levels between superior and inferior quadrants (P<0.447, two-tailed paired Student's *t*-test. Error bars: SEM; n≥6 independent retinal samples examined). INL, inner nuclear layer; OLM, outer limiting membrane; ONL, outer nuclear layer. Scale bars: Bi, 500 µm; Bii-iii, 25 µm.

7.2.2 pCMV6.Crb1.GFP vector expression is effectively silenced in cultured HEK-293T cells by RNAi

Two sequences, starting at base pair 672 and 718 (courtesy of Dr Jan Wijnholds, Netherlands) were used to generate the RNAi arrays (Thermofisher, UK). Herein, these will be referred to as siCrb1.672 and siCrb1.718, respectively. A non-targeting stealth RNAi was used as a control (siCon). The effectiveness of silencing the mouse *Crb1* mRNA expression was first tested *in vitro* using HEK-293T cells that were co-transfected with commercially available pCMV6.Crb1.GFP vector (OriGene Technologies Inc., USA) to induce exogenous mouse *Crb1* cDNA. The efficiency of transfection and the effectiveness of siRNA in silencing the *Crb1* mRNA transcript were assessed 72 hrs post-transfection by ICC and QRT-PCR analysis. Cells transfected with pCMV6.Crb1.GFP only were used as a positive control.

To assess the efficiency of RNAi transfection, a non-targeting RNAi control sequence with an attached AlexaFluor was used as a positive reporter (Thermo Fisher Scientific, UK). First, the RNAi transfection protocol was optimised in HEK-293T cells by testing different concentrations of siCon (20, 40, and 100 pM). Transfected cells were analysed with IHC for AlexaFluor expression (Appendix AB). The untreated cells were used as a negative control. All three concentrations successfully transfected HEK-293T cells and little or no cell death was observed at any of the transfected wells. Among the three tested concentrations, the 40 pM dose of siCon was determined to be the most effective in transfecting HEK-293T cells, thus this dose was used in further experiments.

As HEK-293T cells do not endogenously express CRB1, the cells were first transfected with pCMV6.Crb1.GFP vector, to drive expression of CRB1 and GFP reporter. Fluorescent microscopy of the transfected cells showed that in wells transfected with pCMV6.Crb1.GFP vector ~80% of the cells were GFP^{+ve} (Figure 7.3A i') and that they stained for CRB1 protein (Figure 7.3A i''). Having confirmed a successful expression of CRB1 *in vitro,* HEK-293T cells were transfected with pCMV6.Crb1.GFP plasmid in conjunction with the generated RNAi sequences.

As expected, no noticeable differences in CRB1 expression were observed in the wells co-transfected with a non-targeting RNAi (Figure 7.3A ii). All the examined siCon wells demonstrated a robust expression of GFP (Figure 7.3A ii') and staining for CRB1 protein (Figure 7.3A ii''). Further QRT-PCR analysis confirmed the ICC results showing that the *Crb1* mRNA levels were comparable between the RNAi-untreated cells and those co-transfected with siCon (Figure 7.3B). In contrast, the expression of both CRB1 and GFP from pCMV6.Crb1.GFP was visibly decreased in the cells co-transfected with siCrb1.672 (Figure 7.3A iii) and siCrb1.718 (Figure 7.3A iv). This

silencing of CRB1 was confirmed by further QRT-PCR results which showed a significant drop in the expression of *Crb1* mRNA transcript in the cells that were transfected with pCMV6.Crb1.GFP vector in conjunction with either siCrb1.672 (33.3±10.0% of the levels in untreated cells, $P<0.01$) or siCrb1.718 (6.8±2.3% of the levels in untreated cells, $P<0.001$) with the latter producing a more dramatic effect in comparison with siCon treated cells (104.4±9.5% of the levels in untreated cells, $P=0.9999$) or untreated controls (Figure 7.3B). Together this data shows that the two generated RNAi sequences are capable of silencing CRB1 expression *in vitro*.

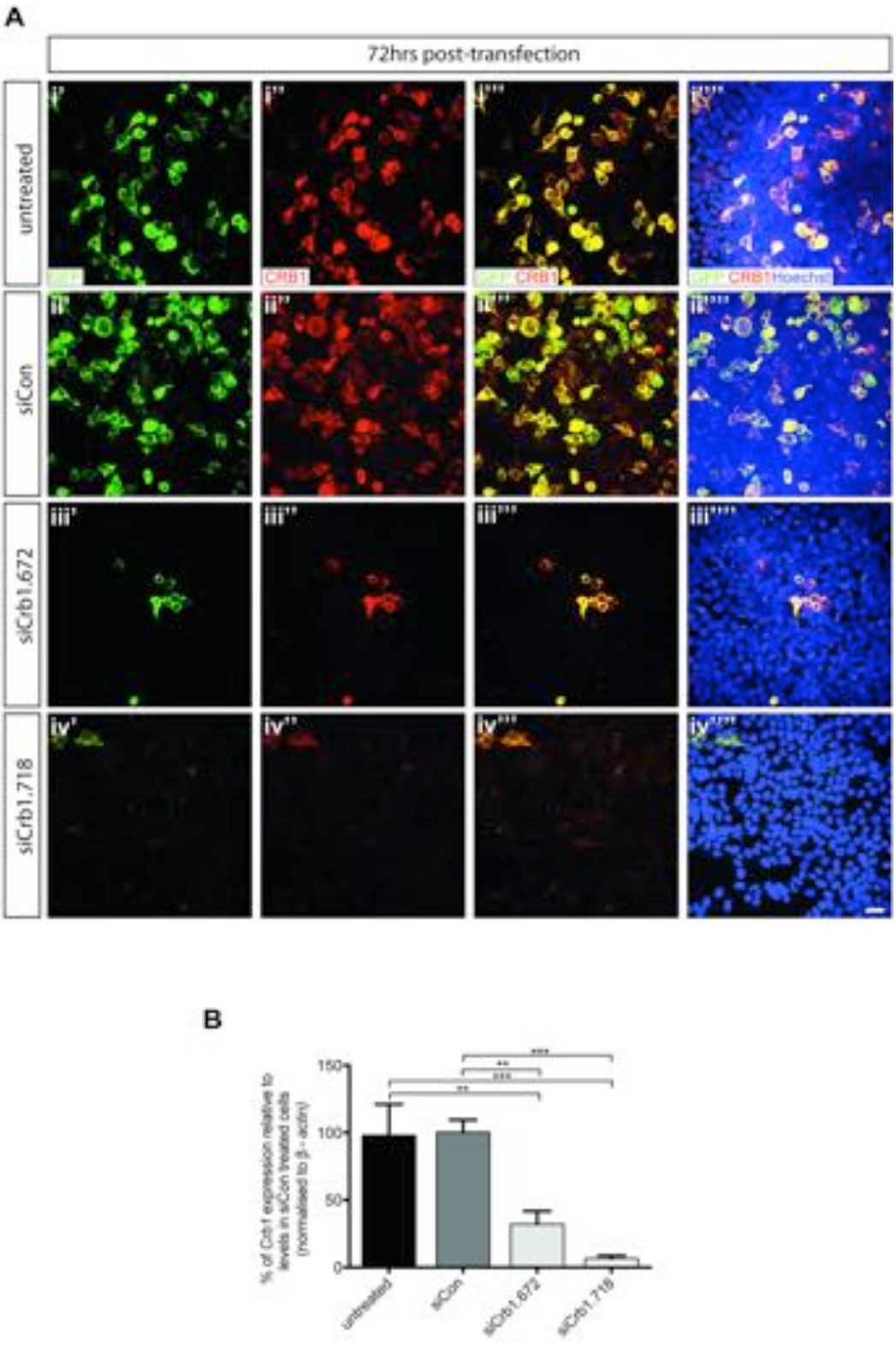

Figure 7.3 RNAi targeting sequences mediate robust silencing of exogenous mouse CRB1 expression in cultured HEK-293T cells.

Ai-iv) Transfection with pCMV6.Crb1.GFP vector induced CRB1 expression in HEK-293T cells (*red*), **Ai)** which was preserved in A**ii)** siCon treated wells. This robust CRB1 expression co-localised with the GFP reporter. In contrast, wells treated with either **Aiii)** siCrb1.672 or **Aiv)** siCrb1.718 showed a marked reduction in both GFP and CRB1 expression with siCrb1.718 leading to a more effective knockdown. Cells

were counterstained with the nuclei marker, Hoechst 33342 (*blue*). Scale bar, 25 μm. **B)** Histogram shows mRNA levels, assessed by QRT-PCR 72hrs post-transfection, for *Crb1*, following treatment with siCon, siCrb1.672 and siCrb1.718. Both targeting RNAi sequences mediated a significant reduction in *Crb1* mRNA expression, compared to siCon transfected cells or RNAi-untreated controls. **P*<0.05, ***P*<0.01, ****P*<0.001 and *****P*<0.0001 with a one-way ANOVA and Tukey's correction for multiple comparisons. Error bars: SEM; n≥3 independent cultures examined.

7.2.3 Endogenous CRB1 is effectively decreased in cultured Müller glia by RNAi

Having established that *Crb1* mRNA expression can be silenced in HEK-293T cells *in vitro*, the designed RNAi sequences were next tested to determine if they can also effectively reduce endogenous CRB1 in cultured Müller glial cells.

As shown in Chapter 4, Müller glia can be isolated from P7-8 *Rlbp*.GFP$^{+/+}$ mouse using FACS and subsequently grown *in vitro*. After two weeks in culture, *Crb1* mRNA was detectable in untreated Müller cells (Figure 7.4A) and a robust positive staining for CRB1 was observed (Figure 7.4B i''). A similar pattern of CRB1 expression was manifested by the cells treated with siCon with the attached Alexa Fluor488 that served as a reporter for successful transfection (Figure 7.4Bii'). Further ICC analysis showed that staining for CRB1 was not affected by RNAi in the wells transfected with siCon (Figure 7.4B ii'') with no detectable changes in *Crb1* mRNA levels (100.1±6.2 % of the untreated cells; P=0.993; Figure 7.4A). In contrast, cells that received *Crb1* RNAi targeting sequences, siCrb1.672 and siCrb1.718, showed a significant reduction in the mRNA expression (to 13.31±2.1% and 5.9±3.3% of the levels seen in untreated cells; P<0.001 and P<0.0001, respectively; Figure 7.4A). The application of either siCrb1.672 (Figure 7.4B iii''-iii''') or siCrb1.718 (Figure 7.4B iv''-iv''') also led to noticeable reduction in CRB1 staining in comparison with the untreated cells or cells that were transfected with a non-targeting RNAi. In line with the experiments in HEK-293T cells, siCrb1.718 was found to be more effective in silencing *Crb1* expression in Müller glia than si672. No changes in the overall morphology of the treated cells were noticed in any of the experimental conditions. These results further confirmed the effectiveness of the designed RNAi sequences in decreasing CRB1 expression.

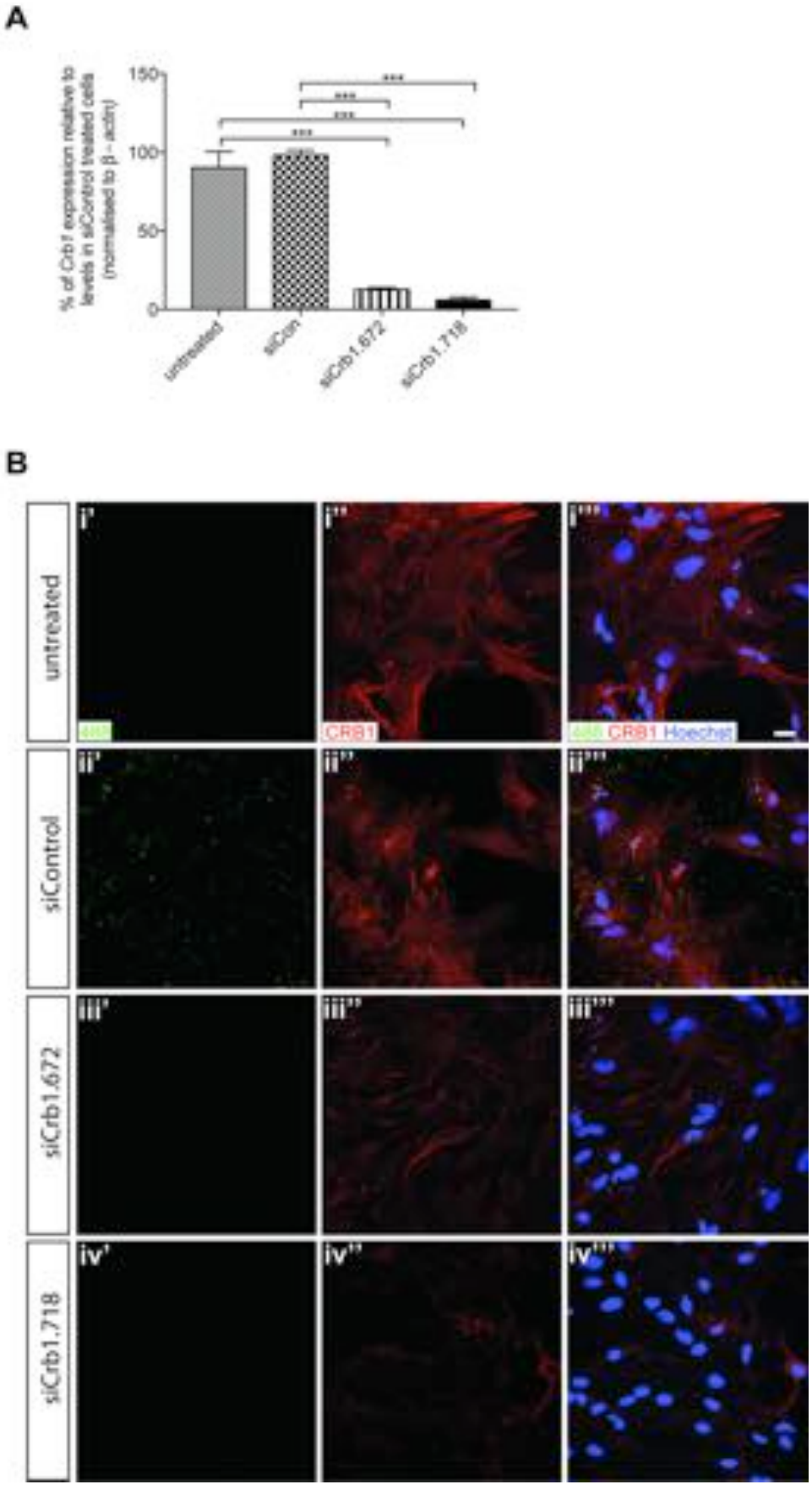

Figure 7.4 RNAi targeting sequences successfully knockdown endogenous CRB1 in cultured Müller cells.

A) Histogram shows that *Crb1* mRNA levels, as assessed by QRT-PCR, are robust in untreated Müller glia *in vitro,* and are not affected by siCon RNAi treatment. In contrast, administration of siCrb1.672 or siCrb1.718 both mediated a marked reduction in mRNA expression with the latter producing a more dramatic effect, compared to siCon treated cells. **P*<0.05, ***P*<0.01, ****P*<0.001 and *****P*<0.0001 with a one-way ANOVA and Tukey's correction for multiple comparisons. Error bars: SEM; n= 3 independent cultures examined. **Bi-iv)** CRB1 protein can be detected *in vitro*. **Bi)** ICC analysis show that untreated cells stained uniformly for CRB1. **Bii)** RNAi transfection itself (as assessed by the AlexaFluor signal (*green*)) had no visible effect on Müller glia morphology or CRB1 levels as shown in siCon treated wells. In contrast, administration of the two RNAi targeting sequences (**Biv)** siCrb1.672 and **Biv)** siCrb1.718) led to noticeable reduction in CRB1 staining, which was almost marked in the wells treated with siCrb1.718. Cells were counterstained with nuclei marker Hoechst 33342 (*blue*). Scale bar, 25 μm.

7.2.4 RNAi sequences are unsuccessful in downregulating CRB1 in the wild-type retina

Previous reports showed that in the mouse retina, CRB1 is normally localised at the apical process of the Müller glia where it is part of the AJ complex at the OLM (Mehalow et al., 2003). Loss of CRB1 or its mislocalisation during development leads to impairment of OLM integrity, delamination of the photoreceptor layer and eventual retinal degeneration in both the mouse and humans (van de Pavert et al., 2004); hence any knockdown of CRB1 should only be temporary. Previous studies have shown that it is possible to introduce a transient silencing of ZO-1 (also an AJ protein) using RNAi, which resulted in a temporary fragmentation of the OLM that resolved itself within one week post-injection (Pearson et al., 2010). Having established that the two RNAi sequences designed here successfully decrease levels of CRB1 *in vitro*, their effectiveness was then tested in an adult retina of a wild-type mouse. Both eyes received a single injection of 2 µL into the subretinal space (see Chapter 2, Section 2.3.4 for the details on the specific RNAi concentrations), between the neural retina and the underlying RPE in the superior hemisphere, as previously described (Pearson et al., 2010). This route of injection was favoured over the intravitreal one due to close proximity of the injection side to the OLM, which should lower the risk of siRNA degradation. Eyes were examined between 48 hrs to 1 week post-injection.

All the recipient retinae receiving the subretinal injection tolerated the surgery well and presented normal retinal structure with no signs of retinal damage at any time point examined. PBS injected eyes were used as a control for any unspecific effect of the injection itself. The uninjected region (the inferior quadrant) was used as an internal control. As predicted, no direct effect on CRB1 localisation was noticed in PBS injected eyes (Figure 7.5A i'-i''). Also administration of non-targeting RNAi resulted in no alterations to *Crb1* mRNA levels (107.0 ±19.3% of the PBS injected, *P*=0.7821; Figure 7.5B i) or any visible changes in CRB1 staining (Figure 7.5A ii'-ii''). Unfortunately, despite robust knockdown of CRB1 *in vitro,* no significant modifications were observed in the levels of *Crb1* mRNA (152.2±33.6% for siCrb1.672 (*P*=0.074) and 108.7±12.4% for siCrb1.718 injected eyes (*P*=0.998), respectively; Figure 7.5A i) nor any detectable disruptions within OLM integrity following siCrb1.672 (Figure 7.5A v-vi) or siCrb1.718 administration (Figure 7.5A vii-viii). The CRB1 staining looked comparable across all experimental conditions, forming a distinct continuous belt with no observable fragmentation nor any nuclei drop. Given the close interaction of CRB1 with CRB2, the impact of the RNAi injection on C*rb2* mRNA levels was also assessed. As shown in Figure 7.5B ii, the levels of C*rb2* mRNA remained unchanged and were very similar to

the levels detected in the PBS treated retinae (102±24.7% for siCon; 111.7±29.16% for siCrb1.672 and 147.2±65% for siCrb1.718.

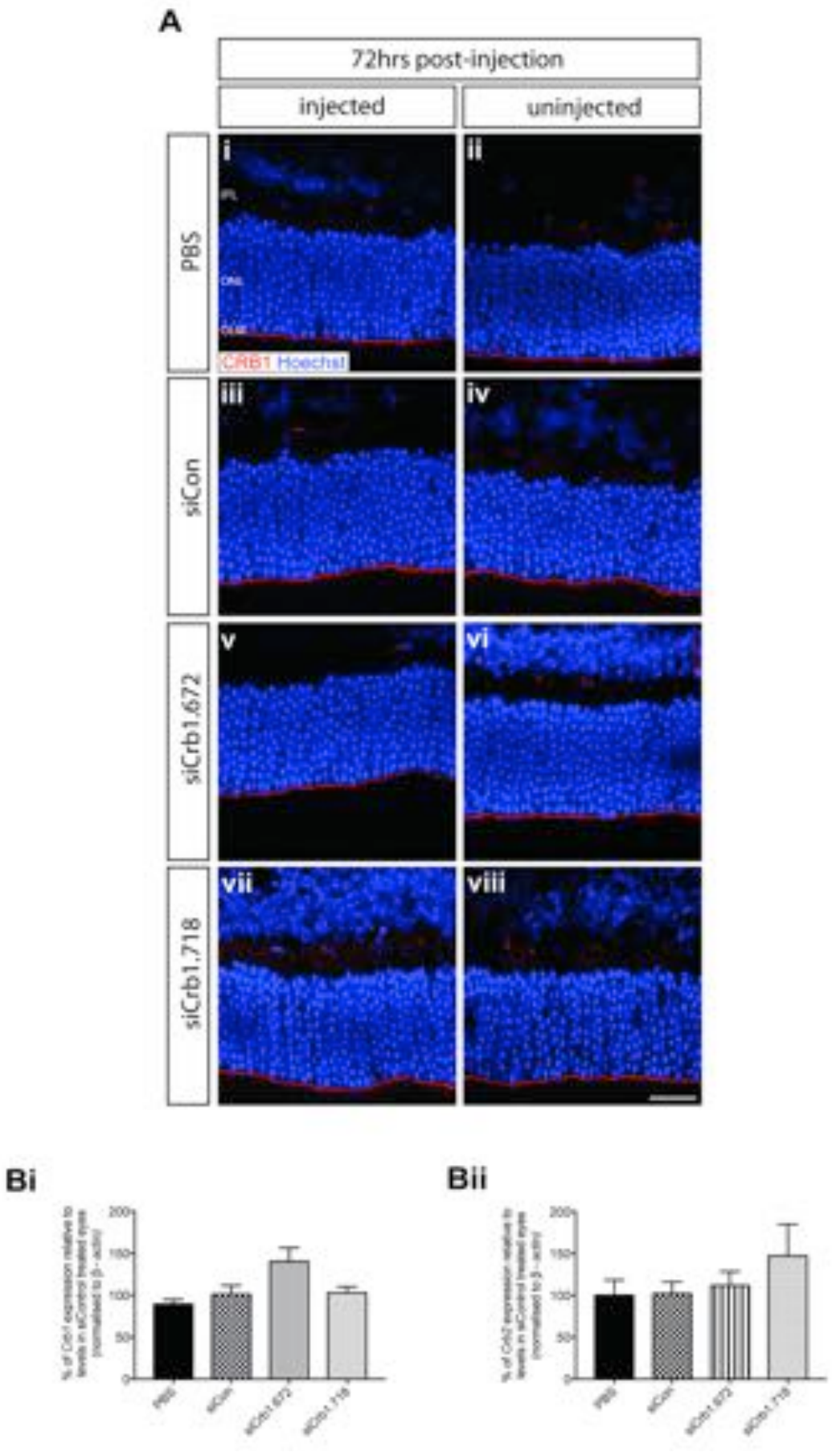

Figure 7.5 RNAi does not mediate a successful knockdown of CRB1 in vivo in a wild-type adult retina.

Ai-viii) IHC analysis showed that injection of RNAi against *Crb1* causes no disruption to OLM integrity or CRB1 staining, both look comparable across all the experimental conditions. No visible changes were detected between **Ai-ii)** PBS; **Aiii-iv)** siCont; **Av-vi)** siCrb1.672 or **Avii-viii)** siCrb1.718 treated retinae in CRB1 staining (*red*) which formed a nice uniform line at the OLM level. Retinal cryosections were counterstained with nuclei marker Hoechst 33342 (*blue*). INL, inner nuclear layer; ONL, outer nuclear layer; OLM, outer limiting membrane. Scale bar, 25 µm. **Bi)** QRT-PCR histogram shows that *Crb1* mRNA expression does not change following the administration of RNAi. **Bii)** Also levels of *Crb2* mRNA remained unchanged in the RNAi injected retinae. Statistical significance was assessed with one-way ANOVA and Tukey's correction for multiple comparisons. Error bars: SEM; n=3 animals examined per experimental condition.

As it has been previously shown that RNAi targeting *Zo-1* successfully caused disruption of the OLM (Pearson et al., 2010) the absence of CRB1 knockdown was surprising. To confirm the effectiveness of RNAi in silencing an OLM protein in a wild-type retina, the ZO-1 experiment was repeated according to previously published protocol (Pearson et al., 2010). The wild-type animals received the same doses of siRNA against *Zo-1* into the adult superior retina and the eyes were examined 72 hrs post-injection. The inferior region was used as an internal control. No visible differences in ZO-1 staining were detected between uninjected (Figure 7.6A i-ii) and PBS-treated retinae (Figure 7.6B i-ii). Unexpectedly, no visible changes in the OLM integrity, or ZO-1 expression following the injection of RNAi targeting *Zo-1* were found at any of the two experimental concentrations, 15 μM (Figure 7.6B iii-iv) and 30 μM (Figure 7.6B v-vi). A clear explanation for these discrepancies is not known. Despite using the same concentrations of siRNA, carrier agents as well as the same time-points for the post-injection assessment, it was not possible to replicate the findings published by Pearson *et al.* study. Having failed to successfully decrease CRB1 or ZO-1 using siRNA method *in vivo*, an alternative experimental approach to knockdown CRB1 was adopted.

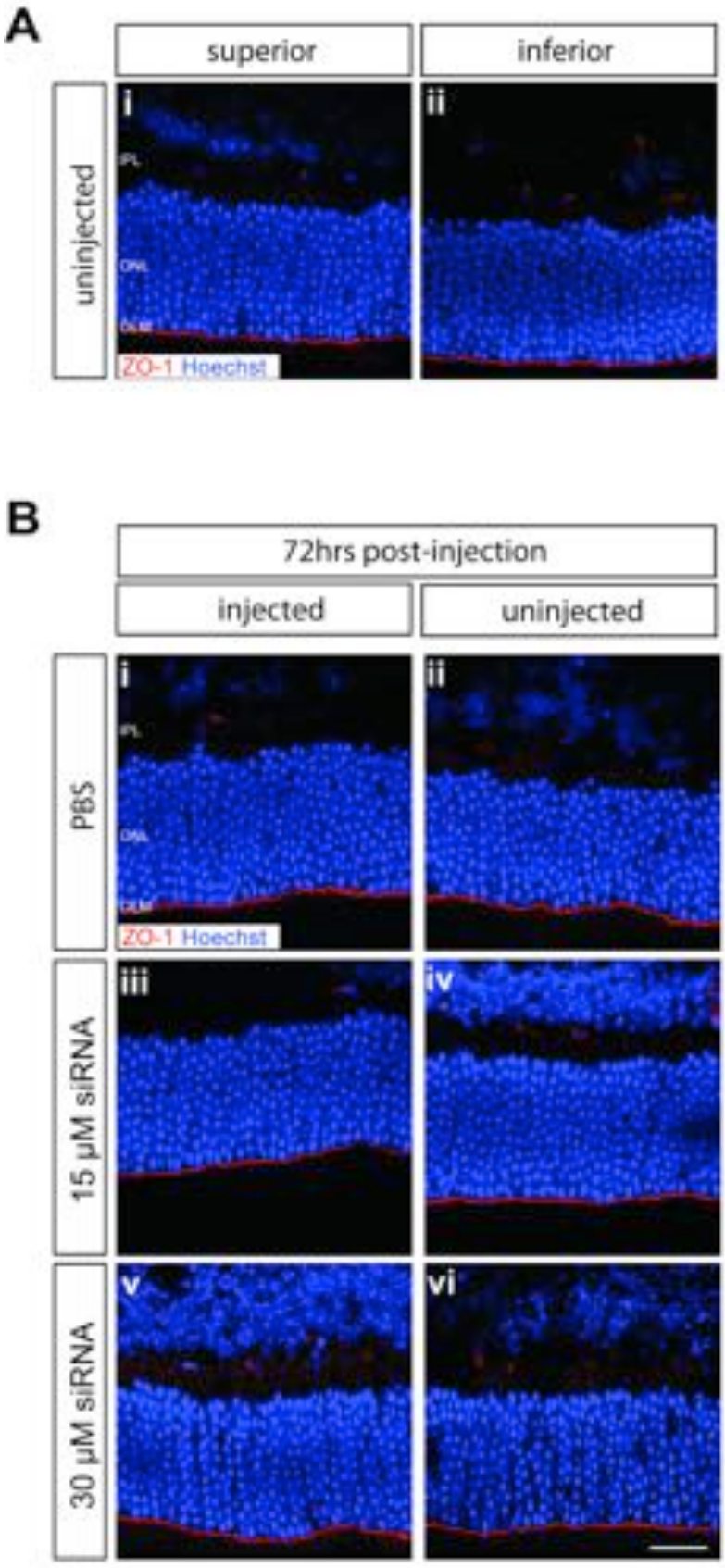

Figure 7.6 Administration of RNAi targeting Zo-1does not cause any disruption to OLM integrity.

Ai-ii) In the uninjected retina, ZO-1 forms a continuous band at the OLM level (*red*). **Bi-ii)** Administration of PBS did not lead to any fragmentation in the ZO-1 staining. **Biii-vi)** Injection of RNAi to silence ZO-1 had no effect on the OLM integrity. Neither **Biii-iv)** 15 µM nor **Bv-vi)** 30 µM caused any visible differences in ZO-1 levels or led to any dislocation of the cell nuclei as previously reported. Retinal cryosections were counterstained with nuclei marker Hoechst 33342 (*blue*). INL, inner nuclear layer; ONL, outer nuclear layer; OLM, outer limiting membrane. Scale bar, 25 µm; n=3 animals examined per experimental condition.

7.3.5 AAV.shCrb1 successfully reduces p.CMV6.Crb1.GFP plasmid expression *in vitro*

As the aim of this study was to assess whether post-developmental knockdown of CRB1 causes any disruption to OLM integrity, an AAV vector was developed to silence CRB1 expression *in vivo*. Having established that the two RNAi sequences are successful in knocking down CRB1 *in vitro*, the more effective one (siCrb1.718) was used as the basis of a short hairpin construct to be packaged into and expressed by an AAVShH10-Y445F vector. As mentioned in Chapter 4, this AAV serotype exhibits a specific tropism for Müller glia (Klimczak et al., 2009; Alves et al., 2014a) and since CRB1 is normally expressed at the apical terminals of Müller glia (van Rossum et al., 2006) it represents a good tool for use in the current study. A non-targeting sequence was used as a control. The two generated vectors will be referred to as AAV.shCon and AAV.shCrb1.

First, the two designed vectors were tested *in vitro* in HEK-293T cells that were additionally transfected with pCMV6.Crb1.GFP plasmid, expressing GFP. As both AAV.shCon and AAV.Crb1 vectors included RFP as a reporter protein, AAVShH10-Y445F transduction efficiency was followed by fluorescence microscopy. As in the siRNA experiments described earlier, HEK-293T cells were first transfected with pCMV6.Crb1.GFP plasmid and checked for GFP expression after 72 hours and then cells were infected with the generated viral vectors (Figure 7.7B i', ii', iii'). The transduction efficiency was assessed after one week by ICC and QRT-PCR analysis (Figure 7.7). As expected, viral transduction with AAV.shCon and AAV.shCrb1 was very efficient with more than 90% of the cells expressing RFP (Figure 7.7A ii'' and Figure 7.7A iii'', respectively). No RFP signal was observed in the non-transduced wells (Figure 7.7A i''). No noticeable differences in GFP signal were noticed between the non-transduced wells (Figure 7.7A i''') and wells treated with AAV.shCon (Figure 7.7A ii'''). Further QRT-PCR analysis confirmed the ICC results showing that the *Crb1* mRNA levels were comparable between the control cells and that infected with AAV.shCon (78.9±14.1% of the levels in non-transduced cells; P=0.287; Figure 7.7B). In contrast, the expression of pCMV6.Crb1.GFP vector was visibly decreased in the cells that received AAV.shCrb1 vector (Figure 7.7A iii'''). This silencing of CRB1 was confirmed by further QRT-PCR results, which showed a significant drop in the expression of *Crb1* mRNA transcript in the cells that were transduced with AAV.shCrb1 in comparison to untreated cells (18.1±8.6% of the levels in untreated cells; P<0.001) or cells treated with AAV.shCon (P=0.001; Figure 7.7B). Together, these results showed that the designed AAV vector is capable of silencing CRB1 *in vitro.*

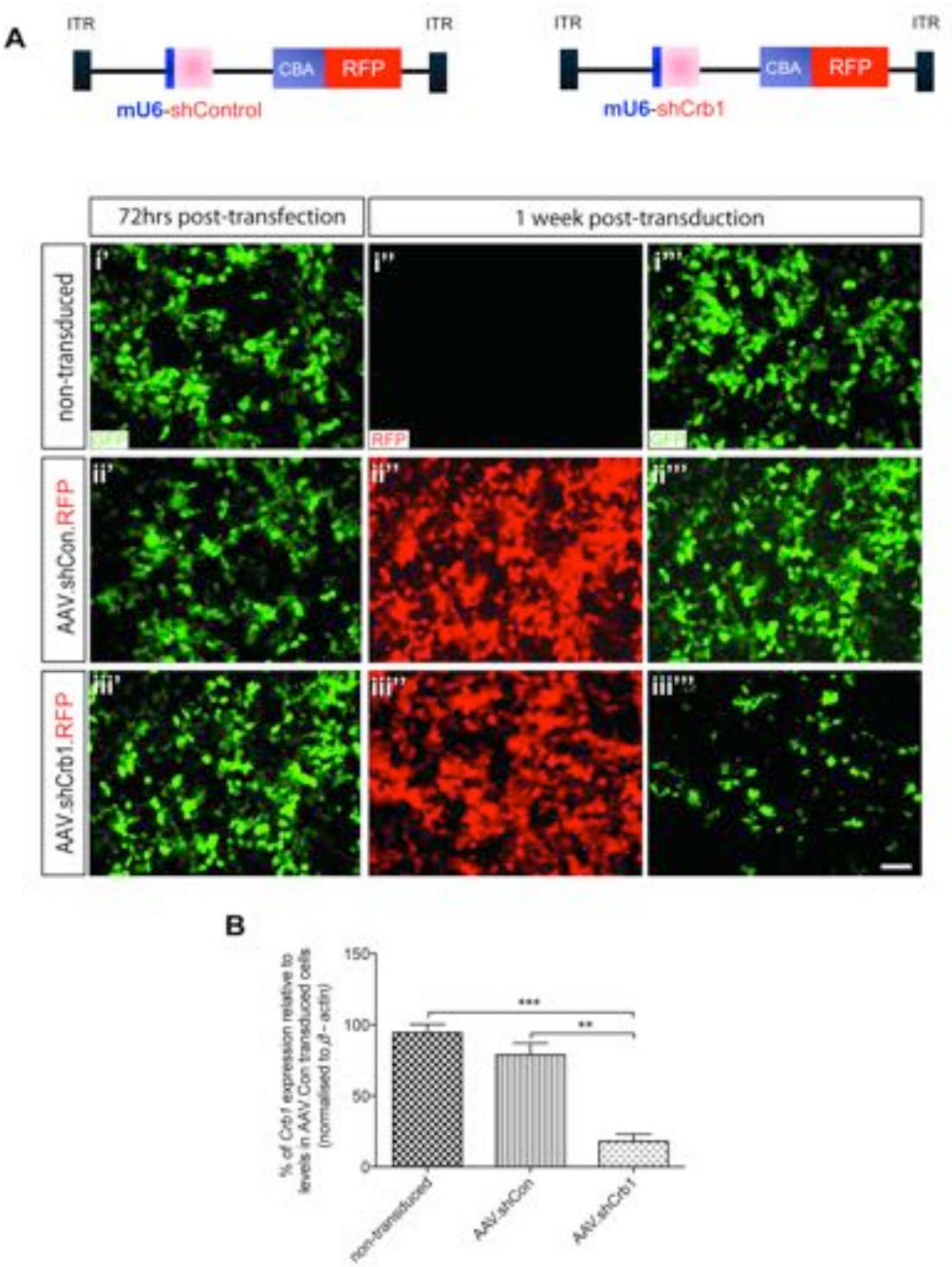

Figure 7.7 AAV.shCrb1 mediate robust silencing of Crb1 mRNA expression in cultured HEK-293T cells.

Transfection with pCMV6.Crb1.GFP vector induced *Crb1* expression in HEK-293T cells (*green*) **Ai)** which was preserved in **Aii)** AAV.shCon treated wells. In contrary, wells treated with **Aiii)** AAV.shCrb1 had a visible reduction in GFP expression. Cells were counterstained with nuclei marker Hoechst 33342 (*blue*). Scale bar, 25 μm. **B)** Histogram shows mRNA levels, assessed by QRT-PCR 72hrs post-transfection, for *Crb1*, following treatment with AAV.shCon and AAV.shCrb1. Only AAV.shCrb1 mediated a significant reduction in *Crb1* mRNA expression, compared to RNAi-untreated controls. ****P*<0.001 and *****P*<0.0001

with a one-way ANOVA and Tukey's correction for multiple comparisons. Error bars: SEM; n=3 independent cultures examined.

7.3.6 AAV.shCrb1 mediates effective knockdown of endogenous *Crb1* in a *C57BL/6J* wild-type retina

Having confirmed the efficacy of AAV.shCrb1 *in vitro*, the ability of this vector to suppress *Crb1* expression was then tested *in vivo*. As shown in Chapter 4, intravitreal delivery of AAVShH10-Y445F robustly transduces Müller glial cells at an early postnatal age and the surgery itself does not have any major impact on the neuroretina. Here, recipient *C57BL/6J* wild-type mice received titre matched AAV.shCon and AAV.shCrb1 in contralateral eyes, and were assessed three weeks later by QRT-PCR and IHC.

In a wild-type retina, CRB1 staining forms a uniform line at the outer edge of the ONL (Figure 7.8A). A global view of the AAV.shCon injected retina showed a widespread RFP expression in Müller glial with no visible alterations to the retinal architecture (Figure 7.8B i). Surprisingly, intravitreal delivery of AAV.shCon at P8 led to significant reduction in *Crb1* at the RNA level in comparison to uninjected eyes (59±2.9% of the levels in untreated retina; $P<0.001$; Figure 7.8C i), but this did not translate into any visible decrease in CRB1 protein as assessed by IHC (Figure 7.8B ii'-ii''), similar to that described for GFAP in Chapter 4 following the administration of AAV.shCon into *Rho*$^{-/-}$ retina. No observable differences in CRB1 staining were noted between transduced and non-transduced regions (Figure 7.8B ii') or between AAV.shCon treated eyes and uninjected controls (Figure 7.8A), with the OLM remaining intact and no visible signs of nuclei drop into the subretinal space. In contrast, robust transduction of AAV.shCrb1 resulted in major changes to retinal architecture including retinal folding (asterisks; Figure 7.8B iv-v) and nuclei displacement (arrows; Figure 7.8B v''). These morphological changes are typical characteristics reported in *Crb1*$^{rd8/rd8}$ mutant (Mehalow et al., 2003). Closer inspection of the outer edge of the neuroretina demonstrated a marked reduction in CRB1 staining, when compared to transduced region (Figure 7.8B v') or when compared to AAV.shCon injected retina (Figure 7.8B ii'). The observed alterations within the AJ 'belt' were also confirmed with staining for ZO-1, which showed clear breaks to OLM especially around the rosettes formed in the ONL in the retina treated with AAV.shCrb1 (arrows; Figure 7.8 B vi'-vi''). The reduction of CRB1 immunoreactivity was further confirmed by QRT-PCR analysis which showed a statistically significant knockdown of *Crb1* mRNA when compared to untreated or AAV.shCon injected eyes (9.49±2.1% of the levels in untreated retina; $P<0.0001$; Figure 7.8C i).

Given an intimate relationship between CRB1 and CRB2 in a mouse retina (Pellissier et al., 2014) the impact of *Crb1* silencing on the *Crb2* mRNA expression was also examined (Figure 7.8C ii). A small, but non-significant, drop in RNA levels were

observed in the eyes treated with AAV.shCon (89.8±9.4% of the levels in untreated retina; *P*=0.186; Figure 7.8C ii) in comparison to untreated controls. Interestingly, AAV.shCrb1 administration and *Crb1* silencing had an effect on *Crb2* expression causing a marked decrease (23.3±5.8% of the levels in untreated retina; *P*<0.001; Figure 7.8C ii). Taken together, these results show that it is possible to knockdown CRB1 *in vivo* via this methodology, but also that global removal of CRB1 leads to unwanted pathological changes in retinal architecture.

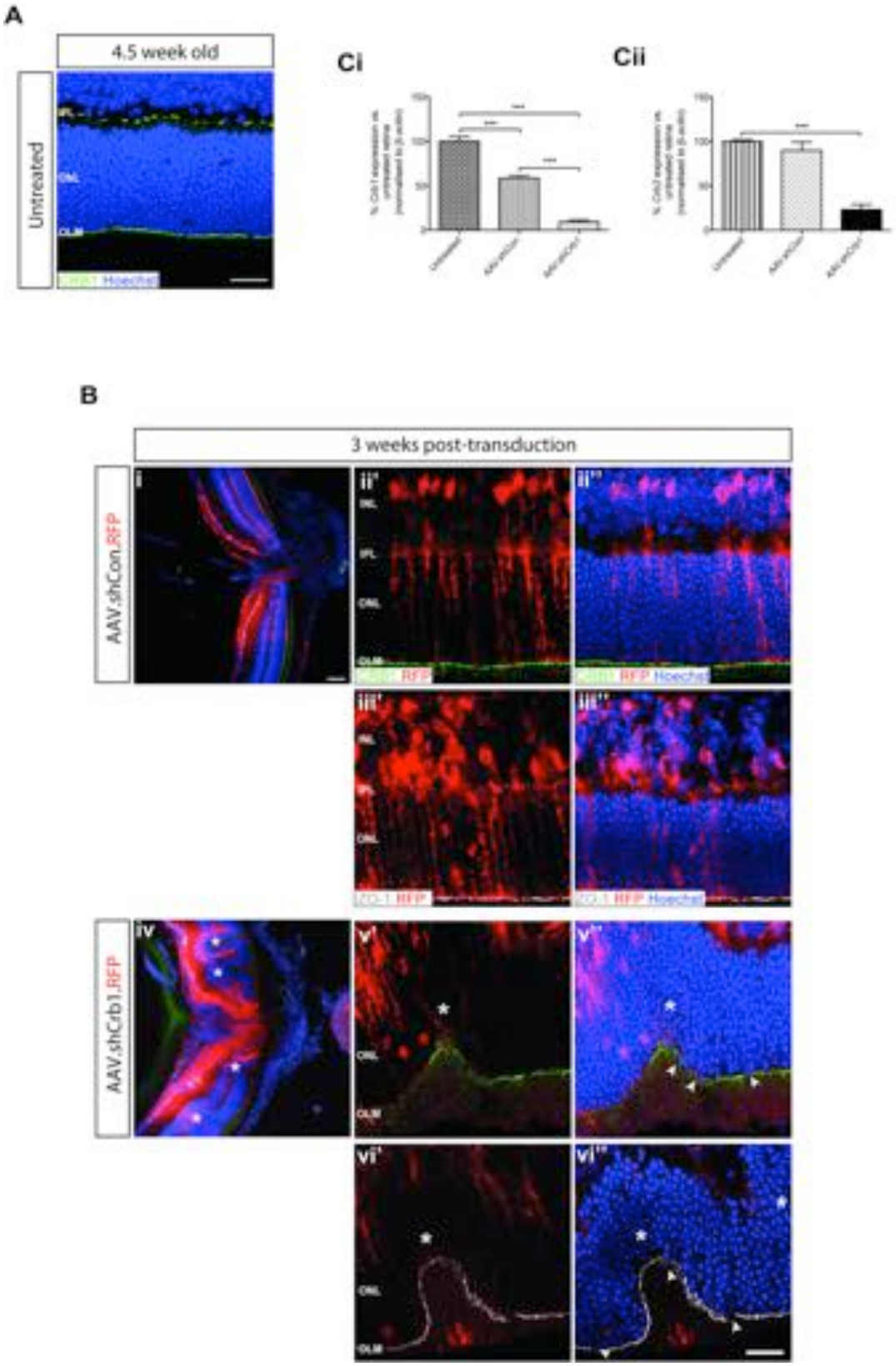

Figure 7.8 Knockdown of CRB1 in Müller glia of C57BL/6J wild-type mouse following a delivery of AAV.shCrb1 led to OLM disruption and prominent undulations of the ONL.

Ai) Immuoreactivity for CRB1 (*green*) in 4.5 week old C57BL/6J wild-type retina shows a continuous, uniform line at the OLM level. **Bi-ii)** The observed knockdown in *Crb1* mRNA AAV.shCon eyes was not

translated at the protein level as CRB1 immunoreactivity was comparable to that seen in untreated controls. No alterations to OLM continuity were observed which was also confirmed with **Biii'-iii'')** staining for ZO-1 (*grey*). **Biv-v)** In contrast, AAV.shCrb1 injection led to a visible reduction in CRB1 immunoreactivity, formation of so-called rosettes (asterisks), and nuclei drop into the subretinal space (arrows). **Bvi'-vi'')** The OLM disruption was further confirmed with IHC analysis for ZO-1, which was especially compromised in the areas of the retinal folds. Retinal sections were counterstained with nuclei marker Hoechst 33342 (*blue*). Scale bar = 25 μm, all other images at the same magnification except Bi and Biv, Scale bar = 100 μm. **Ci)** Histogram shows mRNA levels for *Crb1*, assessed by QRT-PCR 3 weeks after intravitreal injection at P8 of either AAV.shCon or AAV.shCrb1. Both AAV.shCon and AAV.shCrb1 mediated a marked reduction in *Crb1* mRNA expression, compared to untreated controls. **Cii)** Delivery of AAV.shCrb1 also resulted in a significant drop in *Crb2* mRNA levels which was not observed in the retinae treated with AAV.shCon. ***$P<0.001$ and ****$P<0.0001$ with a one-way ANOVA and Tukey's correction for multiple comparisons. Error bars: SEM; n≥3 animals examined per experimental condition.

In order to avoid the introduction of pathological changes to a wild-type retina, I decided to test whether a sparse knockdown of CRB1 was possible. Recent findings demonstrated that AAVShH10-Y445F is not very effective in transducing adult retina, with only patches of Müller glial cells being infected with the virus (Klimczak et al., 2009; Alves et al., 2014a). As morphogenesis is complete by P16 (Xu and Tian, 2007), the generated vectors were delivered at P18 and assessed the injected eyes 3 weeks later against uninjected controls.

At six weeks of age, a continuous line at the level of the OLM can be seen following a staining with CRB1 antibody in the uninjected wild-type retina (Figure 7.9A). No changes in CRB1 staining were observed. In agreement with previous reports, the transduction of the more mature retina with AAVShH10-Y445F was not as effective in comparison with transduction at P8-P10. A sparse expression of RFP in Müller glial cells was observed in both AAV.shCon (Figure 7.9B i) and AAV.shCrb1 (Figure 7.9v iv) treated eyes. QRT-PCR analysis demonstrated that *Crb1* mRNA levels were unaffected by AAV.shCon administration and where similar to those seen in the uninjected animals (91.51±17.8% of the levels in untreated retina; P=0.12; Figure 7.9C i). Similarly, IHC labeling of CRB1 showed no visible differences between AAV.shCon treated (Figure 7.9B ii') and untreated retinae (Figure 7.9A) which was further confirmed with staining for ZO-1 (Figure 7.9B iii'). In contrast, *Crb1* expression, while not completely abolished, was markedly reduced in the eyes treated with AAV.shCrb1 (61.2±22.9% of the levels in untreated retina; P<0.05; Figure 7.9C i). Additionally, a decrease in the level of CRB1 staining was notable in areas transduced by AAV.shCrb1 (Figure 7.9B v'). No major abnormalities ether within the integrity of the OLM or immunoreactivity for ZO-1 (Figure 7.9B vi') were observed. Although there was a clear reduction in CRB1 levels, no marked changes to cytoarchitecture were detected with the gross retinal lamination being preserved.

Interestingly, delivery of AAVShH10-Y445F vectors at P18 had no indirect effect on levels of *Crb2* as assessed at the RNA levels by QRT-PCR (123.2±8.4% and 87.4±12.0% of the levels in untreated retina for AAV.shCon and AAV.shCrb1, respectively; P=0.698; Figure 7.9C ii). The injection of AAV.shCrb1 at P18 did not lead to a drop in *Crb2* expression, as was observed in the eyes injected at P8; this most likely explains the concomitant reduction in the occurrence of ONL undulations.

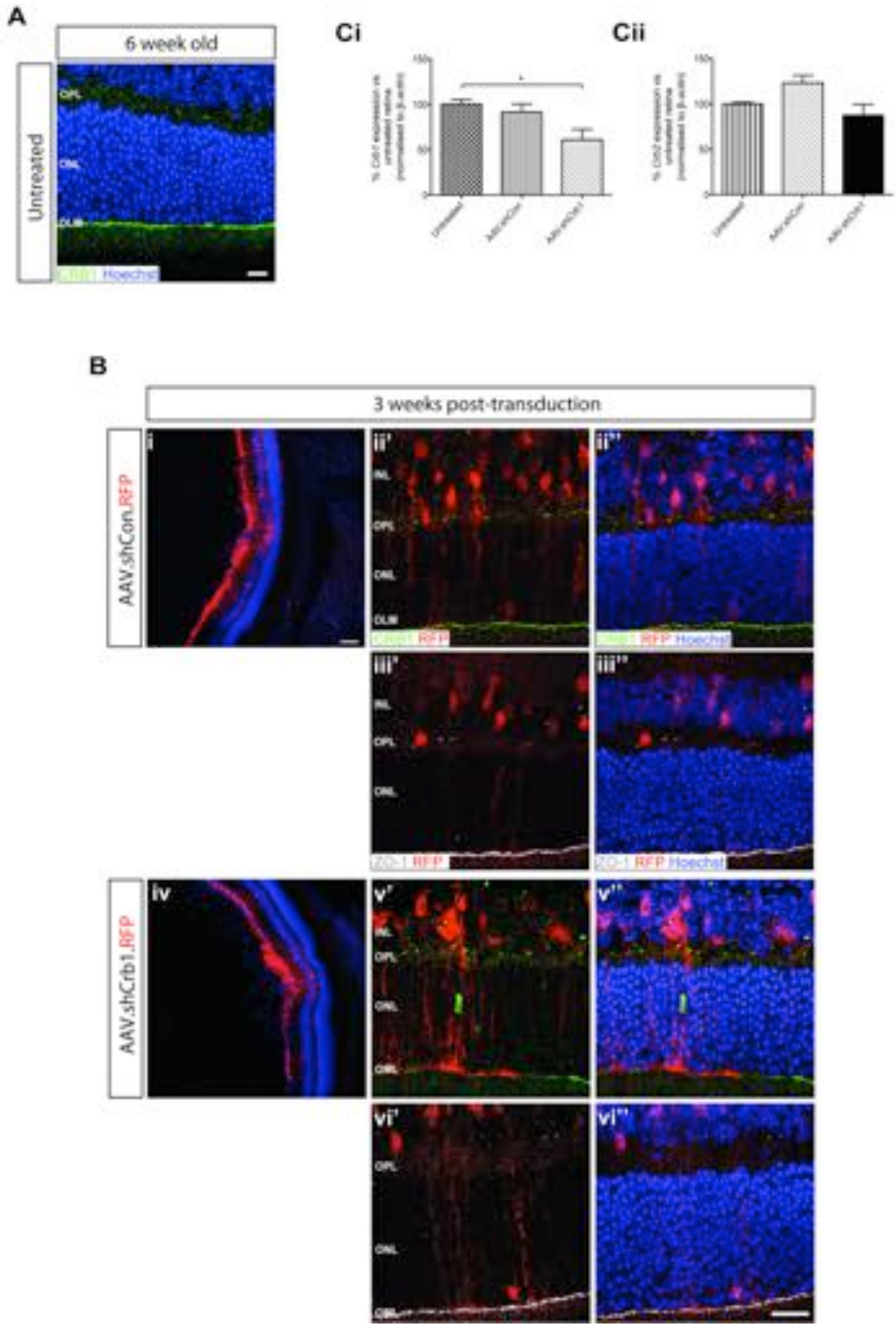

Figure 7.9 Delivery of AAV.shCrb1 at P18 results in a reduction of CRB1 in Müller glia of C57BL/6J wild-type mouse but no prominent undulations of the ONL.

Ai-ii) Immuoreactivity for CRB1 (*green*) in 6 week old C57BL/6J wild-type retina shows a continuous and uniform line at the OLM level. **Bi-ii0** The CRB1 immunoreactivity in AAV.shCon injected retinae was comparable to that seen in untreated controls. **Biii'-iii'')** No alterations to OLM continuity were observed which was also confirmed with staining for ZO-1 (*grey*). **Biv-v)** Administration of AAV.shCrb1 led to reduction in the signal of CRB1 staining in transduced areas (*red*); however no visible abnormalities within the integrity of the OLM were observed. **Bvi'-vi'')** IHC analysis of ZO-1 immunoreactivity confirmed the

continuity of OLM and preservation of retinal. Retinal sections were counterstained with nuclei marker Hoechst 33342 (*blue*). Scale bar = 25 μm, all other images at the same magnification except Bi and Biv, Scale bar = 100 μm. **Ci)** Histogram shows mRNA levels, assessed by QRT-PCR 3 weeks after intravitreal injection at P18, for *Crb1*, following treatment with AAV.shCon and AAV.shCrb1. Only AAV.shCrb1 mediated a marked statistically significant reduction in *Crb1* mRNA levels, compared to AAV.shCon injected eyes or shRNA untreated controls. **Cii)** Delivery of AAV.shCrb1 did not alter *Crb2* mRNA expression. **P*<0.05 with a one-way ANOVA and Tukey's correction for multiple comparisons. Error bars: SEM; n≥3 animals examined per experimental condition.

As illustrated in Chapter 3, the *Crb1*$^{rd8/rd8}$ mouse manifests clear signs of reactive gliosis; therefore it was hypothesised that the ablation of CRB1 in Müller glia may lead to their activation. One of the best markers for reactive glia is GFAP upregulation, as in a healthy wild-type retina GFAP immunoreactivity is restricted to astrocytes (see Figure 7.10A and Chapter 3).

The delivery of AAV.shCrb1 resulted in marked upregulation in IF with visible GFAP^{+ve} processes spanning the entire thickness of a retina even after 3 weeks post-injection, both in retinae injected at P8 (Figure 7.10i-ii) or at P18 (Figure 7.10iii-iv). The GFAP immunoreactivity was especially prominent around the rosettes, which is in agreement with the observations reported in *Crb1* mutant (reviewed in (Hippert et al., 2016)). Moreover, the processes of the Müller glia in the retina injected at P8 appeared (on average) to be much thicker than the processes of the glia cells examined in the eyes injected at P18. A possible explanation for this could be that reduction of CRB1 in a retina that is not fully developed at P8 has greater consequences on retinal morphology and homeostasis than its removal when fully formed. It has been shown that AJ proteins, including CRB1 and CRB2, take part in the regulation of cell proliferation and any mutation or disruption in their levels may lead to loss of cell polarity and epithelial adhesion, and concomitant detachment from the apical lamina (reviewed in (Alves et al., 2014b)). It is worth noting that upregulation in GFAP levels was also observed after administration of AAV.shCon, albeit smaller than that following administration of AAV.sCrb1, which may indicate the extreme sensitivity of Müller glia to any change within the retinal environment, particularly during development. These changes further illustrate the effectiveness of the generated vector in silencing *Crb1* but also demonstrate the risk to, and possible consequences for, retinal health when manipulating the expression of a junctional protein.

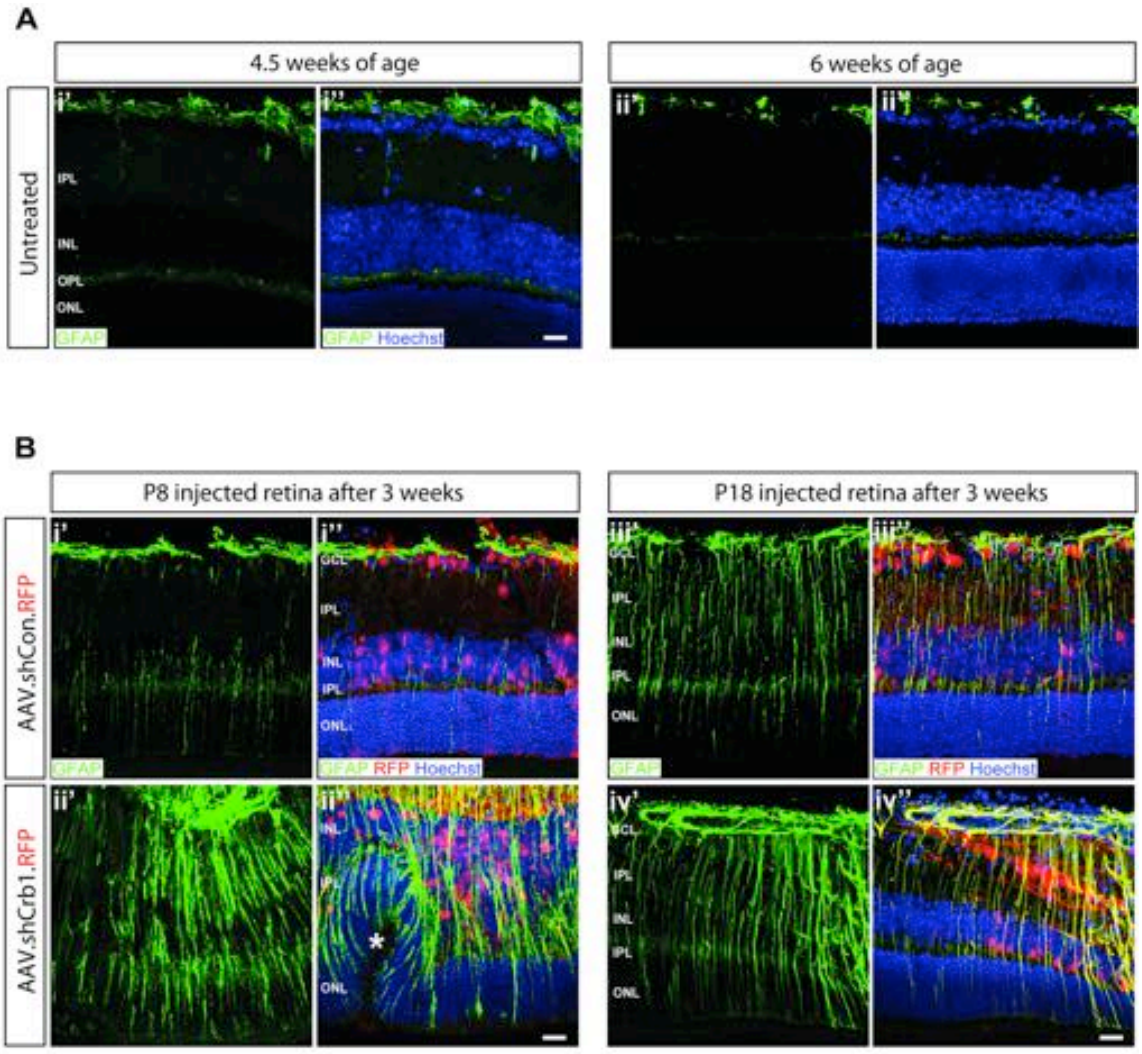

Figure 7.10 AAV.shCrb1 administration and reduction in CRB1 levels leads to activation of Müller glia in C57BL/6J wild-type.

Ai-ii) In a normal retina, there are no signs of activated Müller glia when assessed with IHC for GFAP immunoreactivity. **Bi-iv)** After administration of the generated AAVShH10-Y445F vectors at P8 and P18, the injected eyes were assessed after 3 weeks. **Bii'-ii")** Targeted ablation of CRB1 in postnatal retina results in visible upregulation of GFAP especially in areas close to retinal folds which develop after AAV.shCrb1 injection at P8. **Biv'-iv")** Although delivery of AAV.shCrb1 at P18 did not lead to any visible abnormalities within the retina, decrease in *Crb1* levels still resulted in activation of Müller cells. **Bi'-i"); Biii'-iii')** Surprisingly, the delivery of AAV.shCon also resulted in glial activation which demonstrates the sensitivity of a retina to any retinal insult including the intravitreal surgery. Retinal sections were counterstained with nuclei marker Hoechst 33342 (*blue*). Scale bar, 25 µm.

7.3 Discussion

Consistent with the idea of the OLM as a barrier to therapeutic interventions, a molecular tool to silence *Crb1*, one of the key regulators of AJs in the mouse retina was developed. In this study, the designed AAV-ShH10-Y445F.shCrb1 vector was shown to be capable of silencing the expression of *Crb1* mRNA in wild-type C57BL/6J Müller glia cells when injected into early postnatal eye. The removal of CRB1 led to defects in retinal lamination and development of gliosis, which is in line with previous findings from studies of *Crb1* mutants.

In adult murine retina, CRB1 has been shown to be involved in retinal lamination and the maintenance of AJs between Müller glial cells and photoreceptors ensuring the integrity of the OLM (van de Pavert et al., 2004). Loss of CRB1 or its mislocalisation leads to impairment of OLM integrity, delamination of the photoreceptor layer and eventual retinal degeneration in both mice and humans (van de Pavert et al., 2004). In affected retinal areas, staining for typical AJ or SAR markers is usually reduced or lost, which indicates disruptions to OLM continuity (van de Pavert et al., 2004; van Rossum et al., 2006). This focal loss of adhesion between photoreceptors and Müller glia can then result in ONL undulation and formation of so-called rosettes (Mehalow et al., 2003). Findings from a study on the *Crb1* mutant demonstrated that the rosettes become bigger with age and in some areas the retinal lamination was completely lost (van de Pavert et al., 2004). It has also been reported that loss of *Crb1* in Müller glia results in irregularities in the number and size of their apical villi (van de Pavert et al., 2007). However, all these changes were usually more prominent in the inferior quadrant with significantly more signs of retinal disorganization in this region. These changes were proposed to be due to differing levels of CRB1 expression between superior and inferior retina (Mehalow et al., 2003; van de Pavert et al., 2004; van Rossum et al., 2006). A recent study by Krol *et al.* showed that CRB1 is post-transcriptionally regulated by miR-183/96/182. Moreover, they demonstrated that the photoreceptors and not Müller cells represent the main source of CRB1 in the OLM of the early postnatal retina (Krol et al., 2015). In early post-mitotic photoreceptors, when mature miR-183/96/182 is not present, CRB1 was found to be expressed at a high level to ensure the formation of a strong adhesion between Müller glia and photoreceptors. During retinogenesis, this adhesion was proposed to help confine retinal progenitors within the tight borders created by the inner and outer limiting membranes. After the lamination of the retina is complete, these barriers limit the diffusion of important molecules including Retinoid-binding protein into the neuroretina (Carter-Dawson and Burroughs, 1992). As the retina matures, it has been demonstrated that CRB1 expression becomes suppressed by miR-183/96/182, which

may lead to a weakening of the OLM barrier. In terms of this hypothesis, one could explain the formation of the retinal folds in *Crb1* mutants as regions where retinal progenitor migration pushes against these flimsy margins, which may result in a breech in the AJs and subsequent cellular protrusions into the subretinal space.

Given the importance of CRB1 in the maintenance of AJs in the mouse retina and the fact it was shown be restricted only to OLM region, this study aimed to develop a molecular tool to temporarily silence its expression and potentially open a window for therapeutic intervention. Despite encouraging results from initial *in vitro* studies, designed siRNA sequences failed to reduce CRB1 levels or cause any transient disruption in OLM integrity in a C57BL/6J wild-type retina. Surprisingly, this RNAi technique was also unsuccessful in decreasing levels of ZO-1 *in vivo*, even though the group has previously found it to be effective (Pearson et al., 2010). The reason for these discrepancies is not fully understood but one could speculate that they result from the lack of an efficient system for siRNA delivery *in vivo* to Müller glia, degradation of the siRNA by endogenous RNAses, or instability of the designed siRNAs. Another possibility is that 72 hrs post-injection was too late to assess any more rapid effects of the RNAi. A recent study by Yu at al. examined the effects of siRNA targeting ZO-1 at 24 hrs post-injection in a rat model of RP (Yu et al., 2016). In contrast to previously published reports (Pearson et al., 2010); Yu, Eom *et al.* did not observe any changes within the OLM after administration of 15 μM siRNA targeting ZO-1. A clear explanation for these discrepancies is not known, but RNAi technology has a number of limiting factors that could lead to different experimental results.

As the primary interest was in knowing whether it is possible to knockdown CRB1 in the mouse retina, an AAVShH10-Y445F vector was designed to deliver a shRNA sequence to Müller glial cells. Here, AAVShH10-Y445F vector was injected intravitrally into the eyes of P8 and P18 C57BL/6J mice and the retinae were assessed after 3 weeks and compared against uninjected and shCon injected controls. Preliminary findings showed that AAV.shCrb1 effectively ablated *Crb1* mRNA expression which then led to a reduction of CRB1 protein level as assessed by ICH analysis. It has been demonstrated that following delivery of AAV.shCrb1 at early time-point (P8), these reduced levels of CRB1 in Müller glia result in lamination defects giving rise to many retinal folds and rosettes suggesting a severe lack of adhesion between these cells and photoreceptor IS. The ONL undulations were present in both superior and interior regions of the retina, which is contrasts with the previously published reports on different mouse C*rb1* mutants (*Crb1*$^{-/-}$, *Crb1*$^{c249w/-}$ and *Crb1*$^{rd8/rd8}$), which suggested that the phenotype is restricted to the inferior quadrant of a retina (Mehalow et al., 2003; van de Pavert et al., 2004; van Rossum et al., 2006). This inferior phenotype has been explained in terms of differing levels of CRB1 between the superior and inferior areas;

however this study on the laser captured tissue showed no such difference. Recently, examination of the BN-J rat strain demonstrated that mislocalisation of CRB1 from the SAR of Müller glial cells leads to a retinopathy similar to that observed in *Crb1* mutant mice except that the observed phenotype manifests itself throughout the entire rat retina (Zhao et al., 2015). Given that the phenotypic severity of *Crb1* mutations depends upon the genetic background, different mutations may lead to various retinal phenotypes in different species, including humans (Bujakowska et al., 2011). The lack of a clear genotype–phenotype correlation suggests that either other Crumbs proteins like CRB2 are able to compensate for the loss of CRB1 function or that interactions between the members of the CRB complex vary between different species.

In a mouse retina, CRB1 and CRB2 display an intimate relationship (Alves et al., 2014b). A delivery of the shRNA vector and consequent downregulation of CRB1 had a negative impact upon *Crb2* expression, with levels being markedly decreased in comparison to AAV.shCon treated retinae. This decrease may have contributed to development of the severe phenotype, as CRB2 has roles in restricting proliferation of progenitor cells, the number of rod photoreceptor and Müller glia cells (Alves et al., 2012; 2014a). It has been shown that targeted ablation of CRB2 from retinal progenitor cells leads to abnormalities in retinal lamination, which results in a severe and progressive retinal degeneration with concomitant loss of retinal function (Alves et al., 2012; 2014a). Moreover, it has been demonstrated that in *Crb1Crb2* conditional knockout retinae, silencing of both CRB1 and CRB2 results in an abnormal and thickened retina without a proper and separated photoreceptor cell layer due to overproliferation of the retinal progenitor cells (Pellissier et al., 2013). Pelissier *et al.* also reported that the Crumbs proteins manifest a dose-dependent effect, as different levels of CRB proteins give rise to different phenotypes. *CRB1* retinal dystrophies have no clear genotype-phenotype correlation in humans (Bujakowska et al., 2011) nor is any such correlation apparent in different models of *Crb* knockout mice (Luhmann et al., 2015). This led some researchers to speculate that variation in CRB2 downregulation may be responsible for creating the range of different phenotypes observed in patients with CRB1 mutations such as CRB1-RP and CRB1- LCA (Alves et al., 2014a). In this study, the administration of AAVShH10-Y445F vector at P18 was demonstrated to lead to very sparse transduction of the mouse wild-type retina as assessed by RFP expression, in comparison to injection at P8. Following treatment with AAV.shCrb1 vector, only a small knockdown of CRB1 was observed with no significant change in *Crb2* mRNA levels. No observable pathological changes to retinal architecture including ONL undulations or any major breaks in OLM integrity were found at 3 weeks post-injection. These results are in line with previously published reports where it has been shown that short-term ablation of CRB2 using AAVShH10-

Y445F-shCrb2 vector in the adult retinae has no major consequences on the maintenance of the retinal structure. In contrast, ablation of CRB2 in early photoreceptors using the same vector is essential for proper retinal lamination and function (Alves et al., 2014a).

Recent studies of the AJs within the OLM demonstrate that there is emerging evidence for heterogeneity of junctional protein expression in different cell types. This heterogeneity could explain the appearance of focal disruptions to OLM integrity following the knockdown of junctional proteins (Omri et al., 2010). Indeed, retinal folds and rosettes were only formed following the loss of CRB2 from photoreceptor cells and not Müller glia, suggesting that CRB2 is critical for the maintenance of AJs between rods and cones (Alves et al., 2014a). This is of particular importance as in pathological conditions AJs undergo significant re-arrangements that may have a substantial impact upon retinal function or cell survival. As it was mentioned previously, numerous studies reported that some visual function can be reported following cell transplantation (Pearson et al., 2012; Santos-Ferreira et al., 2014). It has also been demonstrated that there is a significant increase in a number of observable GFP^+ cells in a recipient retina with a compromised OLM integrity (West et al., 2008; Pearson et al., 2010; Barber et al., 2013); although in mice this is mainly due to a novel phenomenon referred to as material transfer (Pearson et al., 2016) or cytoplasmic fusion (Singh et al., 2016). If OLM acts as a semipermeable barrier (Bunt-Milam et al., 1985), any discontinuity within it may help GFP particles to diffuse through the retina and be uptaken by the host cells making OLM a gate for macromolecule transport. If the underlying biological mechanisms of material transfer can be revealed, they may represent a new therapeutic strategy for a broad-spectrum of inherited retinal diseases by introducing functional proteins into otherwise diseased photoreceptors. Moreover, increased understanding of the changes to AJs and the expression of junctional proteins in different retinopathies may be crucial to developing successful therapeutic strategies as it is possible that these changes may influence the outcome of any medical intervention. Here, the reduction of CRB1 protein in Müller glia resulted in detrimental effects upon retinal structure. As demonstrated in previous chapters, Müller glia undergo significant changes in different retinal degenerations, having an important role in the remodelling of the retina following the death of photoreceptors. Upregulation of IF proteins in Müller cells allows for the extension of their glial processes to fill in the gaps left by photoreceptor loss and to create a gliotic seal at the outer edge of the neuroretina (Lee et al., 2011). These changes also result in alterations of the AJs, which has been illustrated very well in models such as the *Pde6b*$^{rd1/rd1}$, where during the course of degeneration the majority of the AJs were formed between Müller glial terminals (Hippert et al., 2015). Removal of the junctional proteins may then lead to

impairment in the formation of this glial seal and subsequent consequences upon the glial fibres and the retinal architecture itself. Indeed, in a recent study by Yu *et al.* it has been demonstrated that in the S334ter-line 3 rat model of RP, inhibition of ZO-1 expression results in a disruption of a distal glial seal as assessed by GFAP staining (Yu et al., 2016). This may create a potential risk of increasing the speed of retinal degeneration in models such as *Pde6b*$^{rd1/rd1}$, where glial scarring is perceived as an attempt to preserve the retinal architecture. Additionally, decreased expression of ZO-1 was also found in the all-cone retina of the *R91W;Nrl*$^{-/-}$ mutant where exposure to toxic levels of blue light led to vascular leakage, retinal swelling and the appearance of cystoid spaces in both INL and ONL indicating edema (Geiger et al., 2015). Together this could suggest that a retina with compromised levels of junctional proteins has a weaker OLM which as a result may be more prone to any retinal damage.

In summary, these results show that I have developed a tool for successful CRB1 knockdown, which may be prove to be useful in future when combined with potential therapeutic approaches. However, a thorough assessment of the long-term impact of CRB1 silencing upon the OLM function, especially in regard to permeability and the overall retinal structure must be done before proceeding with any such therapeutic strategy especially in severely degenerated models like *Rho*$^{-/-}$ mutant.

Chapter 8

Final conclusions

8.1 Summary

The degenerating retina is a complex and ever changing environment, which undergoes constant remodelling in order to adapt to the loss of photoreceptor cells. As in the CNS, upon a pathological stimuli, the glial cells become activated as a form of neuroprotective response (Sahel et al., 1990; Humphrey et al., 1993; Jones et al., 2003a)(Sahel et al., 1990; Humphrey et al., 1993). This activation leads to proliferation of Müller glia, changes in their morphology, alternations in ion transport and secretion of extracellular molecules, leading to the formation of a glial scar as the final outcome. Although gliosis has been extensively characterised, there is still no uniform view of its role and function and the field is beginning to recognise it as a complex system of interacting cells and biological processes. Moreover, rather than being a single process initiated by injury or disease, it is becoming increasingly clear that gliosis can present in many forms, depending upon the initiating insult (Seoane et al., 1999; Hippert et al., 2015; Martinez-De Luna et al., 2016); also reviewed in (Bringmann and Wiedemann, 2012)). The overarching aims of this thesis were firstly to characterise a number of different aspects of gliosis and provide a comprehensive spatio-temporal comparison of this process in different models of inherited retinal degenerations. Secondly, I sought to assess ways of modulating these factors with the aim of improving therapeutic outcomes, with particular reference to photoreceptor transplantation therapy. The results presented in Chapter 3 show marked variations both in the timing and the magnitude of the gliotic response in different mouse models of inherited retinal degeneration; these result in a unique, disease-specific pattern of alterations in the retinal microenvironment. Here, it has been demonstrated that the classic hallmarks of gliosis - the upregulation of intermediate filament (IF) proteins and increases in chondroitin sulphate proteoglycans (CSPGs) deposition – need not be positively correlated with disease severity. A prevailing hypothesis in the regeneration field is that the upregulation of IF proteins and the associated glial cell hypertrophy is inhibitory to therapeutic interventions, particularly those involving host-graft or host-device interactions. In Chapter 4, I sought to modulate this process by using RNAi to reduce the levels of GFAP and Vimentin in a mouse model of chronic. Levels of both GFAP and Vimentin in the *Rho*$^{-/-}$ mutant could be effectively reduced using AAV vectors and reducing Vimentin led to a marked decrease in degeneration-associated hypertrophy of the glial apical terminal processes. However, neither GFAP nor Vimentin downregulation had any significant effect on photoreceptor transplantation outcome, in contrast to previous reports (Kinouchi et al., 2003). A wide array of extracellular signalling molecules that variously support or inhibit neuronal regeneration are present at the site of CNS lesions, with CSPGs playing a major inhibitory role. In Chapter 3, I described the broad patterns of CSPG distribution in different models of retinal

degeneration and again found significant variations between models. In Chapter 5, the spatio-temporal expression of a specific CSPG, Aggrecan, together with the CSPG receptor LAR were assessed in two mouse models of RP. This showed that, despite the ability of exogenously applied Aggrecanase to reduce CSPGs deposited within the photoreceptor segment region of the retina, Aggrecan was only found in the inner retina. In contrast, a high abundance of LAR was found in the segment region. Although the role of LAR in the developing and mature normal and diseased retina are yet to be determined, its presence in the photoreceptor segment region offers a potential opportunity for future experimental work to manipulate the inhibitory role of CSPGs prior any therapeutic interventions.

Significant loss of photoreceptors and development of gliosis was predicted to have a significant impact on the integrity of the outer limiting membrane (OLM), a series of adherens junctions that have previously been shown to impair transplantation outcome (West et al., 2008; Pearson et al., 2010; Barber et al., 2013). A comprehensive examination of a number of different murine models of inherited retinal degenerations was performed; findings presented in Chapter 6 suggest that as the photoreceptors die, both the number and the nature of adherens junctions between the remaining cells undergo significant changes, with a shift in favour of junctions formed between two Müller glia cells, rather than between Müller glia and photoreceptor cells, as typically seen in the normal retina. These changes can probably be correlated with the rate of photoreceptor death and the extent of retinal remodelling, particularly glial hypertrophy (Omri et al., 2010; Hippert et al., 2015; Yu et al., 2016). As noted above, the OLM is often regarded as a barrier to therapeutic interventions. For this reason, a molecular tool to disrupt the connections between AJs was developed. Here, a AAV.ShH10.shCrb1 vector was designed and shown to effectively silence the expression of *Crb1* mRNA in a wild-type retina. Interestingly, findings from these study indicated that the removal of CRB1 from Müller glia cells, and the resulting disruption to OLM integrity in early postnatal retina, leads to defects in retinal lamination and the development of gliosis. In addition to underlying the importance of this protein in normal retinal development, it is of particular importance in considering the utility of targeted disruptions of the OLM in severely degenerated mutants; removing the remaining junctions may result in development of further pathological changes.

Overall, findings presented in this thesis increase our knowledge of the remodelling that happens within the diseased retina, but also challenge some of the commonly held views on the impact that these alterations may have on therapeutic strategies, including photoreceptor cell transplantation.

8.2 The glial scar and neuroregeneration

In the adult mammalian CNS, many damaged axons are unable to regrow across the site of injury. Potential mechanisms for this failure include: a reduction in the intrinsic growth capacity of mature neurons; absence of external growth promoting factors and the presence of external inhibitory factors associated with glial scarring. The last of these has received the greatest attention, with the common belief that the glial scar acts as the main impediment to regenerative strategies following CNS injury. However, there is increasing evidence, including a number of the findings presented in this study that challenge this prevailing dogma. As discussed in this thesis, one of the hallmarks of the glial scar in a retina is the upregulation of the IFs, particularly GFAP, and an increase in the hypertrophy of Müller glial cell (Jones et al., 2003a). Both factors have been argued to represent a major obstacle to retinal grafts and/or cell transplants and breaking down the scar has been viewed as a necessary requirement for good graft-host interactions (reviewed in (Seiler and Aramant, 2012; Veleri et al., 2015)). Here, no improvement in photoreceptor transplantation outcome was found following the removal of IF proteins. Moreover, removing of both GFAP and Vimentin resulted in exacerbated retinal degeneration including the ONL thinning and retinal detachment as well as other ocular complications in the model of chronic retinal degeneration, indicating that the diseased retina needs the glial hypertrophy to preserve its architecture. These findings are in line with a recent paper published by Anderson and colleagues who reported that ablation of scar-forming astrocytes or the removal of chronic astrocytic scars after severe spinal cord injury (SCI) in adult mice failed to result in spontaneous axonal regrowth (Anderson et al., 2016). So what is the role of this scar in the system? Previous reports demonstrated that immediately after injury reactive astrocytes seal the lesion site with their processes, which helps to modulate the immune response and protect the healthy tissue (Panickar and Norenberg, 2005; Pekny and Nilsson, 2005; Wilhelmsson, 2008; Anderson et al., 2016). Moreover, as also shown in the current study, in chronic diseases, the hypertrophied glial processes may be critical for sustaining tissue integrity as the removal of the IFs had detrimental effects on the retinal lamination in the *Rho*$^{-/-}$ mutant. In the damaged retina, activated Müller glia produce a number of neurotrophic growth factors (amongst others) including FGF, as well as several antioxidants, molecules that are not normally secreted in the healthy retina (reviewed in (Bringmann and Wiedemann, 2012)). To further support this argument, studies on transgenic *Gfap*$^{-/-}$*/Vim*$^{-/-}$ mice showed that removal of GFAP and Vimentin accelerates monocyte infiltration and faster degeneration of photoreceptors following retinal trauma (Lundkvist et al., 2004). In the genetic absence of both GFAP and Vimentin together, mortality rate drastically increased among *Gfap*$^{-/-}$*/Vim*$^{-/-}$ mice following a brain trauma, in comparison to controls (Lundkvist et al., 2004). Rather than

being the major impediment to axonal regrowth, as is often assumed, Anderson and colleagues reported that ablating chronic glial scars following SCI in mice does not help with axonal sprouting, and they argue that this scar is essential for preserving tissue integrity a(Anderson et al., 2016). Therefore, the development of the glial scar may be viewed as an attempt to restore homeostasis, which is needed for future axonal regrowth and re-establishing of the lost connections.

Further support for reactive glia acting as a 'sealing tape' is presented in this thesis, where removal of one of the junctional proteins, CRB1, led to disruption of OLM integrity and exacerbated gliosis. The OLM mainly forms between photoreceptor inner segments (IS) and the Müller glia apical processes, acts as a semipermeable diffusion barrier for extracellular components (Bunt-Milam et al., 1985). Removing CRB1 led to the activation of Müller glia cells, seen as an increase in the expression of the IFs and hypertrophy, possibly in an attempt to minimise the diffusion of extracellular proteins from the segment region. In the current study, the OLM was shown to significantly remodel over the course of degeneration, with many more junctions being formed among Müller glia apical processes. The heterogeneity of the junctions must be taken into account while considering any therapeutic strategy to reversibly disrupt OLM integrity. Conversely, it is possible that any intervention that inhibits the formation of the glial seal, including downregulation of the intermediate filament proteins, may lead to a disruption of the OLM remodelling and increased in OLM permeability to ECM molecules.

How is our understanding of the role of proteoglycans in retinal degeneration affected in the light of these changing roles for glial hypertrophy? Proteoglycans, especially CSPGs, are known for their immune-related activity as proteoglycans increase in order to target the immune response to the damaged area (Nandini and Sugahara, 2006). However, it has been suggested that the upregulation of CSPGs at the injury site may also help to create a diffusion barrier for molecules that are potentially harmful to the undamaged neurons (Roitbak and Syková, 1999). Although the digestion of CSPGs several weeks after the injury can be beneficial to axonal regeneration, their removal immediately after the lesion does not help axons to regrow. This could indicate that CSPG-mediated growth inhibition might be beneficial, as it can help to minimise the spread of neurotoxicity as well as stopping the neuronal death mediated by the immediate inflammatory response (Vorísek et al., 2002).

As it was already mentioned, any type of insult to the CNS leads to an immune response with macrophages and activated microglia starting to infiltrate the lesion site and secreting many different proinflammatory cytokine and chemokine molecules (Giulian et al., 1988; Balasingam et al., 1994; Liu et al., 2011; Shechter et al., 2011;

Smith et al., 2012). CNS-resident microglia cells are directly activated by CSPGs via the CD44 receptor (Rolls et al., 2008). Moreover, the elevated expression of cytokineses can stimulate the production of CSPGs including the expression of chondroitin 6-sulphate proteoglycan in neighbouring cells (Properzi et al., 2005). Recent studies demonstrated an important link between the microglia activation and the reactivity of astrocytes, where the two cell types are involved in a direct cross-talk with each other and modulates each other's activity and post-injury response (Liu et al., 2011; Schechter et al., 2011). For example, microglia can regulate the astrocytes expression of CSPGs such as Brevican, Neurocan, and Phosphacan which are believed to have a negative impact on axonal growth. Interestingly, macrophages themselves can also secrete CSPGs and may be a potentially significant source of CSPGs in the post-injury environment (Uhlin-Hansen et al., 1993). Overall, these studies indicate that different components of the glial scar are essential for regulating of the immune response and allowing the system to restore its homeostatic balance.

Despite the common acceptance of CSPGs being the 'bad guys', recent findings suggest that not all CSPGs are detrimental to neuronal growth. As already described in Chapter 5, there is some inconsistency in the evidence of CSPG-mediated inhibition. Although there is no doubt that removal of CSPGs a few weeks after the injury is beneficial to CNS regeneration, not all of these molecules may be detrimental to this process. For example, Versican, was found not to exhibit the same inhibitory effect, with axons not only being able to grow through deposits of Versican but also showed no signs of inhibition in the presence of the purified proteoglycan (Braunewell et al., 1995; Fidler et al., 1999). In a healthy retina, both Neurocan and Versican were reported to be expressed in the photoreceptor segment region (Singhal et al., 2008), which is a common site used for cell transplants and grafting of the retinal implants. Following cell transplantation, a robust number of donor-labelled cells are seen in the healthy recipient retina, despite the presence of CSPGs in the subretinal space (Singhal et al., 2008; Pearson et al., 2012; Barber et al., 2013; Santos-Ferreira et al., 2014). Although, the increase in a number of observable donor labelled cell was reported after ChABC treatment. Moreover, in non-mammalian species such as zebrafish, CSPGs were shown to guide rather than inhibit axon growth and regeneration following optic nerve injury (Becker and Becker, 2002). Wang and colleagues reported that CSPGs' receptor LAR helps to guide somatosensory nerves towards their location in the skin and its deletion leads to a disruption of the skin innervation (Wang et al., 2012).

The roles that glial scarring may have in the injured or damaged CNS are complex. However, despite some seeming contradictions in these roles, as shown in this thesis it is important remember that each disease is different and that the underlying

pathological mechanisms may result in a very different cellular response. With this in mind, only by understanding these changes and cellular processes can we expect to develop more effective and safer therapeutic strategies.

8.3 Future of cell transplantation

Cell transplantation has been viewed as a potentially powerful therapeutic strategy for tissue regeneration and a broad-spectrum treatment for many pathological eye conditions. A remarkable effort has been made in order to find the best method to replace lost photoreceptor and RPE cells, including transplantation of whole retinal sheets, microaggregates of developing neural retina and suspensions of stem cells and donor-derived progenitor cells (reviewed in (Pearson, 2014; Pearson et al., 2014). The past decade has seen the generation of retinal cells from renewable sources, including embryonic (ES) (Meyer et al., 2009) and induced pluripotent stem (IPS) cells (Lamba et al., 2006; Osakada et al., 2008). The use of 3*D* culture systems has further improved our ability to generate retinal neuroepithelial-like structures *in vitro* (Eiraku and Sasai, 2012; Zhong et al., 2014), and adaptations of these protocols has yielded transplantable populations of donor photoreceptor cells (Gonzalez-Cordero et al., 2013). Importantly, there are now many reports describing improvements in visual function following the transplantation of healthy photoreceptors into models of retinal degeneration (Lamba et al., 2006; 2009; Tucker et al., 2011; Pearson et al., 2012; Santos-Ferreira et al., 2014; Barnea-Cramer et al., 2016). Although undoubtedly exciting, recent work from our group (Pearson et al., 2016), the group of Marius Ader (Santos-Ferreira et al., 2016) and the lab of Robert MacLaren (Singh et al., 2016) has questioned our previously held assumptions about the ability of the transplanted cells to migrate into the correct places within the recipient retina from the injection site. Previously, it has been hypothesised that donor cells following transplantation extend a process towards the neuroretina in order to establish a contact with the host cells which then led to their migration from the subretinal space (Warre-Cornish et al., 2014). Recently, real-time imaging of explants of transplanted retina have confirmed these findings (Pearson et al., 2016). However, in the same study, Pearson and colleagues found that this process accounts for only a minority of apparently integrated cells within the host ONL.

The independent studies by Pearson and Ader ruled out the classic process of cell fusion, instead suggesting that, following transplantation, donor photoreceptor cells engage in the exchange of RNA and/or protein with host photoreceptor cells in a process they have termed ‘material transfer’. The precise cellular mechanism underlying this process remains unclear. What is known is that it does not involve uptake of free protein, RNA or DNA nor does it involve classic nuclear transfer.

Pearson *et al.* proposed that the transplanted cells release material in a form of microvesicles, which are subsequently taken up by host cells (and to a lesser extent vice versa). If true, this mechanism could explain why the number of reported donor-labelled cells was increased in the animals with a compromised OLM integrity (West et al., 2008; Pearson et al., 2010; Barber et al., 2013). If the OLM is a semipermeable barrier (Bunt-Milam et al., 1985), it may restrict the passage of microvesicles from donor to host and/or access to the uptake mechanisms. Another working hypothesis discusses the possibility of the cytoplasmic transfer similar to the one that occurs between photoreceptor outer discs and underlying RPE (Singh et al., 2016). Singh *et al.* argued that because host and donor cells are in a direct contact with each other, this could allow for the merger of the two lipid bilayer plasma membranes resulting in a cytoplasmic fusion. Interestingly, this novel biological phenomenon is specific to photoreceptor precursor donor cells, as previous studies reported rather poor outcomes of cell transplantation with more mature cells (MacLaren et al., 2006; Gonzalez-Cordero et al., 2013). Whatever the underlying process, material transfer is surprisingly robust, resulting in host cells be able to express a wide variety of photoreceptor specific proteins with high fidelity; for example, around 85% of GFP^+ cells in the ONL of *Gnat1*$^{-/-}$ hosts also express rod a-transducin, the protein missing from host photoreceptors (Pearson et al., 2016). Given that material transfer or cytoplasmic fusion appears to account for between 70-90% of the reporter-labelled cells seen in the host retina, it seems likely that this new mechanism is responsible for the observed improvements in visual function (Lamba et al., 2009; Tucker et al., 2011; Pearson et al., 2012; Santos-Ferreira et al., 2014). Thus, material transfer may still represent a potential therapeutic approach for the treatment of many retinopathies.

Whatever the mechanisms behind material transfer are, they must account for a number of intriguing observations. Previous studies indicated IFs as an obstacle to cell integration (Kinouchi et al., 2003), whereas in this study no increase in the observable donor cells was observed following the removal of GFAP or Vimentin. If Müller glia hypertrophy was a barrier to material transfer, one would have expected to see an improvement in the *Rho*$^{-/-}$ mutant after RNAi treatment. As discussed previously, CSPGs help to create a diffusion barrier for molecules (Roitbak and Syková, 1999). It is therefore interesting to ask whether material transfer is also impeded by it, and if so, which CSPGs are involved. Several studies have reported marked increases in the number of visible donor-labelled cells in the host retina after enzymatic treatment with ChABC, compared to controls, (Zhang et al., 2007; Singhal et al., 2008; Barber et al., 2013) which must now be considered likely arising from material transfer (although an improvement in true integration, again, cannot be ruled out at this time). At the same time, in a healthy recipient retina the number of donor-labelled cells is fairly high

despite the presence of CSPGs at the site of cell transplantation (Barber et al., 2013). Also, it will be important to determine whether material transfer is species-specific or whether it is a universal phenomenon and can be also observed in humans. Preliminary data from the group indicates that human photoreceptors can undergo true integration into the murine recipient retina, although some evidence of material transfer was also observed (Gonzalez-Cordero, personal communication). Despite this novel biological event, cell therapy is still of potential use especially when gene therapy is not possible and when all the photoreceptors are already being lost in severely degenerated retina.

References

Abe T, Sugano E, Saigo Y, Tamai M (2003) Interleukin-1beta and barrier function of retinal pigment epithelial cells (ARPE-19): aberrant expression of junctional complex molecules. Invest Ophthalmol Vis Sci 44:4097–4104.

Abrahan CE, Insua MF, Politi LE, German OL, Rotstein NP (2009) Oxidative stress promotes proliferation and dedifferentiation of retina glial cells in vitro. J Neurosci Res 87:964–977.

Acland GM, Aguirre GD, Ray J, Zhang Q, Aleman TS, Cideciyan AV, Pearce-Kelling SE, Anand V, Zeng Y, Maguire AM, Jacobson SG, Hauswirth WW, Bennett J (2001) Gene therapy restores vision in a canine model of childhood blindness. Nat Genet 28:92–95.

Adamis P, Miller JW, Bernal MT, D'Amico DJ, Folkman J,Yeo TK, Yeo KT (1995) Increased Vascular Endothelial Growth Factor Levels in the Vitreous of Eyes With Proliferative Diabetic Retinopathy. Am J Ophthalmol 118(4):445-50.

Afshari FT, Fawcett JW (2011) An In Vitro Assay to Examine Oligodendrocyte Precursor Cell Migration on Astrocytes. Methods in Molecular Biology, pp 393–399.

Afshari FT, Kwok JC, Andrews MR, Blits B, Martin KR, Faissner A, ffrench-Constant C, Fawcett JW (2010a) Integrin activation or alpha9 expression allows retinal pigmented epithelial cell adhesion on Bruch's membrane in wet age-related macular degeneration. Brain 133:448–464.

Afshari FT, Kwok JC, White L, Fawcett JW (2010b) Schwann cell migration is integrin-dependent and inhibited by astrocyte-produced aggrecan. Glia 58:857–869.

Agathocleous M, Harris WA (2009) From progenitors to differentiated cells in the vertebrate retina. Annu Rev Cell Dev Biol 25:45–69.

Akagi T, Mandai M, Ooto S, Hirami Y, Osakada F, Kageyama R, Yoshimura N, Takahashi M (2004) Otx2Homeobox Gene Induces Photoreceptor-Specific Phenotypes in Cells Derived from Adult Iris and Ciliary Tissue. Invest Ophthalmol Vis Sci 45:4570–4575.

Akimoto M, Cheng H, Zhu D, Brzezinski JA, Khanna R, Filippova E, Oh ECT, Jing Y, Linares J-L, Brooks M, Zareparsi S, Mears AJ, Hero A, Glaser T, Swaroop A (2006) Targeting of GFP to newborn rods by Nrl promoter and temporal expression

profiling of flow-sorted photoreceptors. Proc Natl Acad Sci 103:3890–3895.

Akita K, Toda M, Mizue I, Fushiki S, Oohira A, Okayama M, Yamashita YM, Nakada H (2004) Heparan sulphate proteoglycans interact with neurocan and promote neurite outgrowth from cerebellar granule cells. Biochem J 383:129–138.

Alexander JJ, Umino Y, Everhart D, Chang B, Min SH, Li Q, Timmers AM, Hawes NL, Pang J-J, Barlow RB, Hauswirth WW (2007) Restoration of cone vision in a mouse model of achromatopsia. Nat Med 13:685–687.

Ali MA (1971) Retinomotor response: characteristics and mechanisms. Vis Res 11:1225–1288.

Ali RR, Sarra GM, Stephens C, Alwis MD, Bainbridge JW, Munro PM, Fauser S, Reichel MB, Kinnon C, Hunt DM, Bhattacharya SS, Thrasher AJ (2000) Restoration of photoreceptor ultrastructure and function in retinal degeneration slow mice by gene therapy. Nat Genet 25:306–310.

Ali SAM, Hosaka YZ, Uehara M (2011) Spatiotemporal distribution of chondroitin sulfate proteoglycans in the developing mouse retina and optic nerve. J Vet Med Sci 73:13–18.

Allikmets R, Singh N, Sun H, Shroyer NF, Hutchinson A, Chidambaram A, Gerrard B, Baird L, Stauffer D, Peiffer A, Rattner A, Smallwood P, Li Y, Anderson KL, Lewis RA, Nathans J, Leppert M, Dean M, Lupski JR (1997) A photoreceptor cell-specific ATP-binding transporter gene (ABCR) is mutated in recessive Stargardt macular dystrophy. Nat Genet 15:236–246.

Alves CH, Pellissier LP, Vos RM, Garcia Garrido M, Sothilingam V, Seide C, Beck SC, Klooster J, Furukawa T, Flannery JG, Verhaagen J, Seeliger MW, Wijnholds J (2014a) Targeted ablation of Crb2 in photoreceptor cells induces retinitis pigmentosa. Hum Mol Genet 23:3384–3401.

Alves CH, Pellissier LP, Wijnholds J (2014b) The CRB1 and adherens junction complex proteins in retinal development and maintenance. Prog Retin Eye Res 40:35–52.

Alves CH, Sanz Sanz A, Park B, Pellissier LP, Tanimoto N, Beck SC, Huber G, Murtaza M, Richard F, Sridevi Gurubaran I, Garcia Garrido M, Levelt CN, Rashbass P, Le Bivic A, Seeliger MW, Wijnholds J (2012) Loss of CRB2 in the mouse retina mimics human retinitis pigmentosa due to mutations in the CRB1 gene. Hum Mol Genet 22:35–50.

Amin RH, Frank RN, Kennedy A, Eliott D, Puklin JE, Abrams GW (1997) Vascular endothelial growth factor is present in glial cells of the retina and optic nerve of human subjects with nonproliferative diabetic retinopathy. Invest Ophthalmol Vis Sci 38:36–47.

Anchan RM, Reh TA, Angello J, Balliet A, Walker M (1991) EGF and TGF-alpha stimulate retinal neuroepithelial cell proliferation in vitro. Neuron 6:923–936.

Anderson DH, Guérin CJ, Erickson PA, Stern WH, Fisher SK (1986) Morphological recovery in the reattached retina. Invest Ophthalmol Vis Sci 27:168–183.

Anderson MA, Burda JE, Ren Y, Ao Y, O'Shea TM, Kawaguchi R, Coppola G, Khakh BS, Deming TJ, Sofroniew MV (2016) Astrocyte scar formation aids central nervous system axon regeneration. Nat 532:195–200.

Applebury ML, Antoch MP, Baxter LC, Chun L (2000) The murine cone photoreceptor: a single cone type expresses both S and M opsins with retinal spatial patterning. Neuron 3:513-523.

Ardeljan D, Chan CC (2013) Aging is not a disease: distinguishing age-related macular degeneration from aging. Prog Retin Eye Res 37: 1-49.

Asher RA, Morgenstern DA, Fidler PS, Adcock KH, Oohira A, Braistead JE, Levine JM, Margolis RU, Rogers JH, Fawcett JW (2000) Neurocan is upregulated in injured brain and in cytokine-treated astrocytes. J Neurosci 20:2427–2438.

Assawachananont J, Mandai M, Okamoto S, Yamada C, Eiraku M, Yonemura S, Sasai Y, Takahashi M (2014) Transplantation of embryonic and induced pluripotent stem cell-derived 3D retinal sheets into retinal degenerative mice. Stem Cell Reports 2:662–674.

Assémat E, Crost E, Ponserre M, Wijnholds J, Le Bivic A, Massey-Harroche D (2013) The multi-PDZ domain protein-1 (MUPP-1) expression regulates cellular levels of the PALS-1/PATJ polarity complex. Exp Cell Res 319:2514–2525.

Aveleira CA, Lin CM, Abcouwer SF, Ambrósio AF, Antonetti DA (2010) TNF- Signals Through PKC /NF- B to Alter the Tight Junction Complex and Increase Retinal Endothelial Cell Permeability. Diabetes 59:2872–2882.

Baas D, Bumsted KM, Martinez JA, Vaccarino FM, Wikler KC, Barnstable CJ (2000) The subcellular localization of Otx2 is cell-type specific and developmentally regulated in the mouse retina. Brain Res Mol Brain Res 78:26–37.

Baden T, Euler T (2016) Retinal Physiology: Non-Bipolar-Cell Excitatory Drive in the Inner Retina. Curr Biol 26:R706–R708.

Baehr W, Karan S, Maeda T, Luo DG, Li S, Bronson JD, Watt CB, Yau KW, Frederick JM, Palczewski K (2007) The Function of Guanylate Cyclase 1 and Guanylate Cyclase 2 in Rod and Cone Photoreceptors. J Biol Chem 282:8837–8847.

Bainbridge JWB et al. (2015) Long-term effect of gene therapy on Leber's congenital amaurosis. N Engl J Med 372:1887–1897.

Bainbridge JWB, Smith AJ, Barker SS, Robbie S, Henderson R, Balaggan K, Viswanathan A, Holder GE, Stockman A, Tyler N, Petersen-Jones S, Bhattacharya SS, Thrasher AJ, Fitzke FW, Carter BJ, Rubin GS, Moore AT, Ali RR (2008) Effect of gene therapy on visual function in Leber's congenital amaurosis. N Engl J Med 358:2231–2239.

Banin E, Gootwine E, Obolensky A, Ezra-Elia R, Ejzenberg A, Zelinger L, Honig H, Rosov A, Yamin E, Sharon D, Averbukh E, Hauswirth WW, Ofri R (2015) Gene Augmentation Therapy Restores Retinal Function and Visual Behavior in a Sheep Model of CNGA3 Achromatopsia. Mol Ther 23:1423–1433.

Barber AC, Hippert C, Duran Y, West EL, Bainbridge JWB, Warre-Cornish K, Luhmann UFO, Lakowski J, Sowden JC, Ali RR, Pearson RA (2013b) Repair of the degenerate retina by photoreceptor transplantation. Proc Natl Acad Sci 110:354–359.

Bareil C, Hamel C, Delague V, Arnaud B, Demaille J (2001) Segregation of a mutation in CNGB1 encoding the β-subunit of the rod cGMP-gated channel in a family with autosomal recessive retinitis pigmentosa. Hum Genet 4:328-34.

Barhoum R, Martinez-Navarrete G, Corrochano S, Germain F, Fernandez-Sanchez L, la Rosa de EJ, la Villa de P, Cuenca N (2008) Functional and structural modifications during retinal degeneration in the rd10 mouse. Neurosci 155:698–713.

Barnea-Cramer AO, Wang W, Lu S-J, Singh MS, Luo C, Huo H, McClements ME, Barnard AR, MacLaren RE, Lanza R (2016) Function of human pluripotent stem cell-derived photoreceptor progenitors in blind mice. Sci Rep 6:29784.

Barnett NL, Pow DV (2000) Antisense knockdown of GLAST, a glial glutamate transporter, compromises retinal function. Invest Ophthalmol Vis Sci 41:585–591.

Barnett NL, Pow DV, Bull ND (2001) Differential perturbation of neuronal and glial glutamate transport systems in retinal ischaemia. Neurochem Int 39(4): 291–299.

Bartsch U, Oriyakhel W, Kenna PF, Linke S, Richard G, Petrowitz B, Humphries P, Farrar GJ, Ader M (2008) Retinal cells integrate into the outer nuclear layer and differentiate into mature photoreceptors after subretinal transplantation into adult mice. Exp Eye Res 86:691–700.

Baye LM, Link BA (2007) Interkinetic Nuclear Migration and the Selection of Neurogenic Cell Divisions during Vertebrate Retinogenesis. J Neurosci 27:10143–10152.

Beattie MS, Hermann GE, Rogers RC, Bresnahan JC (2002) Cell death in models of spinal cord injury. Prog Brain Res 137:37–47.

Becker CG, Becker T (2002) Repellent guidance of regenerating optic axons by chondroitin sulfate glycosaminoglycans in zebrafish. J Neurosci 22:842–853.

Berger W, Kloeckener-Gruissem B, Neidhardt J (2010) The molecular basis of human retinal and vitreoretinal diseases. Prog Retin Eye Res 29:335–375.

Bernardos RL, Barthel LK, Meyers JR, Raymond PA (2007) Late-Stage Neuronal Progenitors in the Retina Are Radial Muller Glia That Function as Retinal Stem Cells. J Neurosci 27:7028–7040.

Berta ÁI, Boesze-Battaglia K, Genini S, Goldstein O, O'Brien PJ, Szél Á, Acland GM, Beltran WA, Aguirre GD (2011) Photoreceptor cell death, proliferation and formation of hybrid rod/S-cone photoreceptors in the degenerating STK38L mutant retina. PLoS ONE 6:e24074.

Bicknese AR, Sheppard AM, O'Leary DD, Pearlman AL (1994) Thalamocortical axons extend along a chondroitin sulfate proteoglycan-enriched pathway coincident with the neocortical subplate and distinct from the efferent path. J Neurosci 14:3500–3510.

Biel M, Seeliger M, Pfeifer A, Kohler K, Gerstner A, Ludwig A, Jaissle G, Fauser S, Zrenner E, Hofmann F (1999) Selective loss of cone function in mice lacking the cyclic nucleotide-gated channel CNG3. Proc Natl Acad Sci 96:7553–7557.

Blackshaw S, Harpavat S, Trimarchi J, Cai L, Huang H, Kuo WP, Weber G, Lee K, Fraioli RE, Cho S-H, Yung R, Asch E, Ohno-Machado L, Wong WH, Cepko CL (2004) Genomic analysis of mouse retinal development. PLoS Biol 2:E247.

Blanquicett C, Johnson MR, Heslin M, Diasio RB (2002) Housekeeping gene variability in normal and carcinomatous colorectal and liver tissues: applications in pharmacogenomic gene expression studies. Anal Biochem 303:209–214.

Boon CJF, Hollander den AI, Hoyng CB, Cremers FPM, Klevering BJ, Keunen JEE (2008) The spectrum of retinal dystrophies caused by mutations in the peripherin/RDS gene. Prog Retin Eye Res 27:213–235.

Bovolenta P, Mallamaci A, Briata P, Corte G, Boncinelli E (1997) Implication of OTX2 in pigment epithelium determination and neural retina differentiation. J Neurosci 17:4243–4252.

Bradbury EJ, Carter LM (2011) Manipulating the glial scar: Chondroitinase ABC as a therapy for spinal cord injury. Brain Res Bull 84:306–316.

Bradbury EJ, Moon LDF, Popat RJ, King VR, Bennett GS, Patel PN, Fawcett JW, McMahon SB (2002) Chondroitinase ABC promotes functional recovery after spinal cord injury. Nat 416:636–640.

Braunewell KH, Pesheva P, McCarthy JB, Furcht LT, Schmitz B, Schachner M (1995) Functional Involvement of Sciatic Nerve-derived Versicanand Decorin-like Molecules and other Chondroitin Sulphate Proteoglycans in ECM-mediated Cell Adhesion and Neurite Outgrowth. Eur J Neurosci 7:805–814.

Brenner M (1994) Structure and transcriptional regulation of the GFAP gene. Brain Pathol 4:245–257.

Brenner M, Kisseberth WC, Su Y, Besnard F, Messing A (1994) GFAP promoter directs astrocyte-specific expression in transgenic mice. J Neurosci 14:1030–1037.

Bridges CD (1985) The interphotoreceptor matrix--functions and possible role in hereditary retinal degenerations. Prog Clin Biol Res 190:195–212.

Bringmann A, Iandiev I, Pannicke T, Wurm A, Hollborn M, Wiedemann P, Osborne NN, Reichenbach A (2009a) Cellular signaling and factors involved in Muller cell gliosis: Neuroprotective and detrimental effects. Prog Retin Eye Res 28:423–451.

Bringmann A, Pannicke T, Biedermann B, Francke M, Iandiev I, Grosche J, Wiedemann P, Albrecht J, Reichenbach A (2009b) Role of retinal glial cells in neurotransmitter uptake and metabolism. Neurochem Int 54:143–160.

Bringmann A, Pannicke T, Grosche J, Francke M, Wiedemann P, Skatchkov SN,

Osborne NN, Reichenbach A (2006) Müller cells in the healthy and diseased retina. Prog Retin Eye Res 25:397–424.

Bringmann A, Wiedemann P (2012) Müller Glial Cells in Retinal Disease. Ophthalmologica 227:1–19.

Brittis PA, Silver J (1994) Exogenous glycosaminoglycans induce complete inversion of retinal ganglion cell bodies and their axons within the retinal neuroepithelium. Proc Natl Acad Sci 91:7539–7542.

Brown DM, Kaiser PK, Michels M, Soubrane G, Heier JS, Kim RY, Sy JP, Schneider S (2006) Ranibizumab versus Verteporfin for Neovascular Age-Related Macular Degeneration. N Engl J Med 355:1432–1444.

Brückner G, GROSCHE J, Schmidt S, Härtig W, Margolis RU, Delpech B, Seidenbecher CI, Czaniera R, Schachner M (2000) Postnatal development of perineuronal nets in wild-type mice and in a mutant deficient in tenascin-R. J Comp Neurol 428:616–629.

Bujakowska K, Audo I, Mohand-Saïd S, Lancelot M-E, Antonio A, Germain A, Léveillard T, Letexier M, Saraiva J-P, Lonjou C, Carpentier W, Sahel J-A, Bhattacharya SS, Zeitz C (2011) CRB1 mutations in inherited retinal dystrophies. Hum Mutat 33:306–315.

Bulgakova NA, Kempkens O, Knust E (2008) Multiple domains of Stardust differentially mediate localisation of the Crumbs-Stardust complex during photoreceptor development in Drosophila. J Cell Sci 121:2018–2026.

Bull ND, Limb GA, Martin KR (2008) Human Muller Stem Cell (MIO-M1) Transplantation in a Rat Model of Glaucoma: Survival, Differentiation, and Integration. Invest Ophthalmol Vis Sci 49:3449–3456.

Bunt-Milam AHA, Saari JCJ, Klock IBI, Garwin GGG (1985) Zonulae adherentes pore size in the external limiting membrane of the rabbit retina. Invest Ophthalmol Vis Sci 26:1377–1380.

Burnside B (1978) Thin (actin) and thick (myosinlike) filaments in cone contraction in the teleost retina. J Cell Biol 78:227–246.

Burnside B, Nagle B (1983) Retinomotor movements of photoreceptors and retinal pigment epithelium: mechanisms and regulation. Prog Retin Res 2:67-109.

Busch SA, Silver J (2007) The role of extracellular matrix in CNS regeneration. Curr Opin Neurobiol 17:120–127.

Caggiano AO, Zimber MP, Ganguly A, Blight AR, Gruskin EA (2005) Chondroitinase ABCI Improves Locomotion and Bladder Function following Contusion Injury of the Rat Spinal Cord. J Neurotraum 22:226–239.

Cai X, McGinnis JF (2016) Diabetic Retinopathy: Animal Models, Therapies, and Perspectives. J Diabetes Res 2016:1–9.

Calame M, Cachafeiro M, Philippe S, Schouwey K, Tekaya M, Wanner D, Sarkis C, Kostic C, Arsenijevic Y (2011) Retinal Degeneration Progression Changes Lentiviral Vector Cell Targeting in the Retina Chédotal A, ed. PLoS ONE 6:e23782.

Caley DW, Johnson C, Liebelt RA (1972) The postnatal development of the retina in the normal and rodless CBA mouse: A light and electron microscopic study. Dev Dynam 133:179–211.

Calvert PD, Krasnoperova NV, Lyubarsky AL, Isayama T, Nicolò M, Kosaras B, Wong G, Gannon KS, Margolskee RF, Sidman RL, Pugh EN, Makino CL, Lem J (2000) Phototransduction in transgenic mice after targeted deletion of the rod transducin alpha -subunit. Proc Natl Acad Sci 97:13913–13918.

Campbell M, Humphries M, Kenna P, Humphries P, Brankin B (2007) Altered expression and interaction of adherens junction proteins in the developing OLM of the Rho(-/-) mouse. Exp Eye Res 85:714–720.

Campbell M, Humphries M, Kennan A, Kenna P, Humphries P, Brankin B (2006) Aberrant retinal tight junction and adherens junction protein expression in an animal model of autosomal dominant Retinitis pigmentosa: the Rho(-/-) mouse. Exp Eye Res 83:484–492.

Cao W, Li F, Steinberg RH, LaVail MM (2001) Development of normal and injury-induced gene expression of aFGF, bFGF, CNTF, BDNF, GFAP and IGF-I in the rat retina. Exp Eye Res 72:591–604.

Carter-Dawson L, Burroughs M (1992) Interphotoreceptor retinoid-binding protein in the cone matrix sheath. Electron microscopic immunocytochemical localization. Invest Ophthalmol Vis Sci 33:1584–1588.

Carter-Dawson LD, LaVail MM, Sidman RL (1978) Differential effect of the rd mutation on rods and cones in the mouse retina. Invest Ophthalmol Vis Sci 17:489–498.

Carulli D, Laabs T, Geller HM, Fawcett JW (2005) Chondroitin sulfate proteoglycans in neural development and regeneration. Curr Opin Neurobiol 15:252.

Centanin L, Hoeckendorf B, Wittbrodt J (2011) Fate Restriction and Multipotency in Retinal Stem Cells. Cell Stem Cell 9:553–562.

Chacon-Camacho OF, Zenteno JC (2015) Review and update on the molecular basis of Leber congenital amaurosis. World J Clin Cases 3:112–124.

Chaitin MH, Brun-Zinkernagel AM (1998) Immunolocalization of CD44 in the dystrophic rat retina. Exp Eye Res 67:283–292.

Challacombe JF, Snow DM, Letourneau PC (1997) Dynamic microtubule ends are required for growth cone turning to avoid an inhibitory guidance cue. J Neurosci 17:3085–3095.

Chang B, Hawes NL, Hurd RE, Davisson MT, Nusinowitz S, Heckenlively JR (2002) Retinal degeneration mutants in the mouse. Vis Res 42:517–525.

Chaum E (2002) Retinal neuroprotection by growth factors: A mechanistic perspective. J Cell Biochem 88:57–75.

Chen H, Weber AJ (2002) Expression of glial fibrillary acidic protein and glutamine synthetase by Müller cells after optic nerve damage and intravitreal application of brain-derived neurotrophic factor. Glia 38:115–125.

Chen H-J, Ma Z-Z (2007) N-cadherin expression in a rat model of retinal detachment and reattachment. Invest Ophthalmol Vis Sci 48:1832–1838.

Chen L-F, FitzGibbon T, He J-R, Yin ZQ (2012a) Localization and developmental expression patterns of CSPG-cs56 (aggrecan) in normal and dystrophic retinas in two rat strains. Exp Neuro 234:488–498.

Chen Y, Okano K, Maeda T, Chauhan V, Golczak M, Maeda A, Palczewski K (2012b) Mechanism of all-trans-retinal toxicity with implications for stargardt disease and age-related macular degeneration. J Biol Chem 287:5059–5069.

Chen Y, Palczewska G, Mustafi D, Golczak M, Dong Z, Sawada O, Maeda T, Maeda A, Palczewski K (2013) Systems pharmacology identifies drug targets for Stargardt disease-associated retinal degeneration. J Clin Invest 123:5119–5134.

Chen YJ, Tsai RK, Wu WC, He MS, Kao YH, Wu WS (2012c) Enhanced PKCδ and ERK signaling mediate cell migration of retinal pigment epithelial cells

synergistically induced by HGF and EGF. PLoS ONE 7(9): e44937.

Cheng H, Aleman TS, Cideciyan AV, Khanna R, Jacobson SG, Swaroop A (2006) In vivo function of the orphan nuclear receptor NR2E3 in establishing photoreceptor identity during mammalian retinal development. Hum Mol Genet 15:2588–2602.

Cho K-S, Yang L, Lu B, Feng Ma H, Huang X, Pekny M, Chen DF (2005) Re-establishing the regenerative potential of central nervous system axons in postnatal mice. J Cell Sci 118:863–872.

Cho NC, Poulsen GL, Ver Hoeve JN, Nork TM (2000) Selective loss of S-cones in diabetic retinopathy. Arch Ophthalmol 118:1393–1400.

Cho S-H, Cepko CL (2006) Wnt2b/beta-catenin-mediated canonical Wnt signaling determines the peripheral fates of the chick eye. Development 133:3167–3177.

Chrysostomou V, Rezania F, Trounce IA, Crowston JG (2013) Oxidative stress and mitochondrial dysfunction in glaucoma. Curr Opin Pharmacol 13:12–15.

Cideciyan AV (2010) Leber congenital amaurosis due to RPE65 mutations and its treatment with gene therapy. Prog Retin Eye Res 29:398–427.

Clark SJ (2006) His-384 Allotypic Variant of Factor H Associated with Age-related Macular Degeneration Has Different Heparin Binding Properties from the Non-disease-associated Form. J Biol Chem 281:24713–24720.

Clark SJ, Bishop PN, Day AJ (2010a) Complement factor H and age-related macular degeneration: the role of glycosaminoglycan recognition in disease pathology. Biochem Soc Trans 38:1342–1348.

Clark SJ, Perveen R, Hakobyan S, Morgan BP, Sim RB, Bishop PN, Day AJ (2010b) Impaired Binding of the Age-related Macular Degeneration-associated Complement Factor H 402H Allotype to Bruch's Membrane in Human Retina. J Biol Chem 285:30192–30202.

Close JL, Gumuscu B, Reh TA (2005) Retinal neurons regulate proliferation of postnatal progenitors and Müller glia in the rat retina via TGF beta signaling. Dev132:3015–3026.

Cobos E, Arias L, Ruiz-Moreno J, Rubio M, Garcia-Bru P, Caminal J, Catala-Mora J, Arruga J (2013) Preoperative study of the inner segment/outer segment junction of photoreceptors by spectral-domain optical coherence tomography as a prognostic

factor in patients with epiretinal membranes. Clin Ophthalmol 7:1467–1470.

Cochard P, Paulin D (1984) Initial expression of neurofilaments and vimentin in the central and peripheral nervous system of the mouse embryo in vivo. J Neurosci 4:2080–2094.

Colella P, Auricchio A (2012) Gene therapy of inherited retinopathies: a long and successful road from viral vectors to patients. Hum Gene Ther 23:796–807.

Cornish EE, Hendrickson AE, Provis JM (2004) Distribution of short-wavelength-sensitive cones in human fetal and postnatal retina: early development of spatial order and density profiles. Vis Res 44:2019–2026.

Coulombe PA, Wong P (2004) Cytoplasmic intermediate filaments revealed as dynamic and multipurpose scaffolds. Nat Cell Biol 6:699–706.

Crespo D, Asher RA, Lin R, Rhodes KE, Fawcett JW (2007) How does chondroitinase promote functional recovery in the damaged CNS? Exp Neuro 206:159–171.

Cuenca N, Fernández-Sánchez L, Campello L, Maneu V, la Villa De P, Lax P, Pinilla I (2014) Cellular responses following retinal injuries and therapeutic approaches for neurodegenerative diseases. Prog Retin Eye Res 43:17–75.

Cuenca N, Fernández-Sánchez L, McGill TJ, Lu B, Wang S, Lund R, Huhn S, Capela A (2013) Phagocytosis of photoreceptor outer segments by transplanted human neural stem cells as a neuroprotective mechanism in retinal degeneration. Invest Ophthalmol Vis Sci 54:6745–6756.

Cuenca N, Pinilla I, Sauvé Y, Lu B, Wang S, Lund RD (2004) Regressive and reactive changes in the connectivity patterns of rod and cone pathways of P23H transgenic rat retina. Neurosci127:301–317.

Cuenca N, Pinilla I, Sauvé Y, Lund R (2005) Early changes in synaptic connectivity following progressive photoreceptor degeneration in RCS rats. Eur J Neurosci 22:1057–1072.

Curcio CA, Sloan KR, Kalina RE, Hendrickson AE (1990) Human photoreceptor topography. J Comp Neurol 292:497–523.

da Cruz L, Chen FK, Ahmado A, Greenwood J, Coffey P (2007) RPE transplantation and its role in retinal disease. Prog Retin Eye Res 26:598–635.

Damiani D, Novelli E, Mazzoni F, Strettoi E (2012) Undersized dendritic arborizations

in retinal ganglion cells of the rd1 mutant mouse: A paradigm of early onset photoreceptor degeneration. J Comp Neurol 520:1406–1423.

Danciger M, Blaney J, Gao YQ, Zhao DY, Heckenlively JR, Jacobson SG, Farber DB (1995) Mutations in the PDE6B gene in autosomal recessive retinitis pigmentosa. Genomics 30:1–7.

Daniele LL, Adams RH, Durante DE, Pugh EN, Philp NJ (2007) Novel distribution of junctional adhesion molecule-C in the neural retina and retinal pigment epithelium. J Comp Neurol 505:166–176.

Daniele LL, Insinna C, Chance R, Wang J, Nikonov SS, Pugh EN Jr (2011) A mouse M-opsin monochromat: Retinal cone photoreceptors have increased M-opsin expression when S-opsin is knocked out. Vis Res 51:447–458.

Das AV, Mallya KB, Zhao X, Ahmad F, Bhattacharya S, Thoreson WB, Hegde GV, Ahmad I (2006) Neural stem cell properties of Müller glia in the mammalian retina: regulation by Notch and Wnt signaling. Dev Biol 299:283–302.

Davies SJ, Goucher DR, Doller C, Silver J (1999) Robust regeneration of adult sensory axons in degenerating white matter of the adult rat spinal cord. J Neurosci 19:5810–5822.

Day AJ, Clark SJ, Bishop PN (2011) Understanding the molecular basis of age-related macular degeneration and how the identification of new mechanisms may aid the development of novel therapies. Exper Rev Ophthalmol 6:123–128.

DeAngelis MM, Grimsby JL, Sandberg MA, Berson EL, Dryja TP (2002) Novel mutations in the NRL gene and associated clinical findings in patients with dominant retinitis pigmentosa. Arch Ophthalmol 120:369–375.

Desclaux M, Perrin FE, Do-Thi A, Prieto-Cappellini M, Gimenez Y Ribotta M, Mallet J, Privat A (2015) Lentiviral-mediated silencing of glial fibrillary acidic protein and vimentin promotes anatomical plasticity and functional recovery after spinal cord injury. J Neurosci Res 93:43–55.

Dickendesher TL, Baldwin KT, Mironova YA, Koriyama Y, Raiker SJ, Askew KL, Wood A, Geoffroy CG, Zheng B, Liepmann CD, Katagiri Y, Benowitz LI, Geller HM, Giger RJ (2012) NgR1 and NgR3 are receptors for chondroitin sulfate proteoglycans. Nat 15:703–712.

Dinet V, Bruban J, Chalour N, Maoui A, An N, Jonet L, Buret A, Behar-Cohen F, Klein

C, Tréton J, Mascarelli F (2012) Distinct effects of inflammation on gliosis, osmohomeostasis, and vascular integrity during amyloid beta-induced retinal degeneration. Aging Cell 11:683–693.

Domowicz MS, Sanders TA, Ragsdale CW, Schwartz NB (2008) Aggrecan is expressed by embryonic brain glia and regulates astrocyte development. Dev Biol 315:114–124.

Dou CL, Levine JM (1994) Inhibition of neurite growth by the NG2 chondroitin sulfate proteoglycan. J Neurosci 14:7616–7628.

Dowling JE, Boycott BB (1966) Organization of the Primate Retina: Electron Microscopy. Proc Biol Sci 166:80–111.

Dreher Z, Robinson SR, Distler C (1992) Müller cells in vascular and avascular retinae: a survey of seven mammals. J Comp Neurol 323:59–80.

Drenckhahn D, Wagner HJ (1985) Relation of retinomotor responses and contractile proteins in vertebrate retinas. Eur J Cell Biol 37:156–168.

Dryja TP, Finn JT, Peng YW, McGee TL, Berson EL, Yau KW (1995) Mutations in the gene encoding the alpha subunit of the rod cGMP-gated channel in autosomal recessive retinitis pigmentosa. Proc Natl Acad Sci 92:10177–10181.

Dryja TP, Hahn LB, Reboul T, Arnaud B (1996) Missense mutation in the gene encoding the alpha subunit of rod transducin in the Nougaret form of congenital stationary night blindness. Nat Genet 13:358–360.

Dryja TP, Rucinski DE, Chen SH, Berson EL (1999) Frequency of mutations in the gene encoding the alpha subunit of rod cGMP-phosphodiesterase in autosomal recessive retinitis pigmentosa. Invest Ophthalmol Vis Sci 40:1859–1865.

Du Y, Miller CM, Kern TS (2003) Hyperglycemia increases mitochondrial superoxide in retina and retinal cells. Free Radic Biol Med 35:1491–1499.

Dunah AW, Hueske E, Wyszynski M (2005) LAR receptor protein tyrosine phosphatases in the development and maintenance of excitatory synapses. Nat 4:458-67.

Eberle D, Kurth T, Santos-Ferreira T, Wilson J, Corbeil D, Ader M (2012) Outer segment formation of transplanted photoreceptor precursor cells. PLoS ONE 7:e46305.

Eckes B, Colucci-Guyon E, Smola H, Nodder S, Babinet C, Krieg T, Martin P (2000) Impaired wound healing in embryonic and adult mice lacking vimentin. J Cell Sci 113 (13):2455–2462.

Edwards MM, Lefebvre O (2013) Laminins and retinal vascular development. Cell Adh Migr 7:82–89.

Edwards TL, Jolly JK, Groppe M, Barnard AR, Cottriall CL, Tolmachova T, Black GC, Webster AR, Lotery AJ, Holder GE, Xue K, Downes SM, Simunovic MP, Seabra MC, MacLaren RE (2016) Visual Acuity after Retinal Gene Therapy for Choroideremia. N Engl J Med 374:1996–1998.

Eiraku M, Sasai Y (2012) Mouse embryonic stem cell culture for generation of three-dimensional retinal and cortical tissues. Nat Protoc 7:69–79.

Eiraku M, Takata N, Ishibashi H, Kawada M, Sakakura E, Okuda S, Sekiguchi K, Adachi T, Sasai Y (2011) Self-organizing optic-cup morphogenesis in three-dimensional culture. Nat 472:51–56.

Ekström P, Sanyal S, Narfström K, Chader GJ, VANVEEN T (1988) Accumulation of Glial Fibrillary Acidic Protein in Muller Radial Glia During Retinal Degeneration. Invest Ophthalmol Vis Sci 29:1363–1371.

El-Bab MF, Zaki NS, Mojaddidi MA, Al-Barry M, El-Beshbishy HA (2013) Diabetic retinopathy is associated with oxidative stress and mitigation of gene expression of antioxidant enzymes. Int J Gen Med 6:799–806.

Eliasson C, Sahlgren C, Berthold CH, Stakeberg J, Celis JE, Betsholtz C, Eriksson JE, Pekny M (1999) Intermediate filament protein partnership in astrocytes. J Biol Chem 274:23996–24006.

Emerling DE, Lander AD (1996) Inhibitors and Promoters of Thalamic Neuron Adhesion and Outgrowth in Embryonic Neocortex: Functional Association with Chondroitin Sulfate. Neuron 17:1089–1100.

Eng LF, Ghirnikar RS (1994) GFAP and astrogliosis. Brain Pathol 4:229–237.

Eng LF, Lee YL, Kwan H, Brenner M, Messing A (1998) Astrocytes cultured from transgenic mice carrying the added human glial fibrillary acidic protein gene contain Rosenthal fibers. J Neurosci Res 53:353–360.

Escher P, Cottet S, Aono S, Oohira A, Schorderet DF (2008) Differential neuroglycan C

expression during retinal degeneration in Rpe65(-/-) mice. Mol Vis 14:2126–2135.

Ethen CM, Reilly C, Feng X, Olsen TW, Ferrington DA (2006) The Proteome of Central and Peripheral Retina with Progression of Age-Related Macular Degeneration. Invest Ophthalmol Vis Sci 47:2280.

Faktorovich EG, Steinberg RH, Yasumura D, Matthes MT, LaVail MM (1990) Photoreceptor degeneration in inherited retinal dystrophy delayed by basic fibroblast growth factor. Nat 347:83–86.

Fan W, Lin N, Sheedlo HJ, Turner JE (1996) Müller and RPE cell response to photoreceptor cell degeneration in aging Fischer rats. Exp Eye Res 63:9–18.

Fanning AS, Ma TY, Anderson JM (2002) Isolation and functional characterization of the actin binding region in the tight junction protein ZO-1. FASEB J16:1835–1837.

Fariss RN, Li ZY, H MA (2000) Abnormalities in rod photoreceptors, amacrine cells, and horizontal cells in human retinas with retinitis pigmentosa. J Ophthalmol 129:215–223.

Fariss RN, Molday RS, Fisher SK, Matsumoto B (1997) Evidence from normal and degenerating photoreceptors that two outer segment integral membrane proteins have separate transport pathways. J Comp Neurol 387:148–156.

Faulkner JR (2004) Reactive Astrocytes Protect Tissue and Preserve Function after Spinal Cord Injury. J Neurosci 24:2143–2155.

Fawcett J (2009) Molecular control of brain plasticity and repair. Prog Brain Res 175:501–509.

Fawcett JW, Asher RA (1999) The glial scar and central nervous system repair. Brain Res Bull 49:377–391.

Feathers KL, Lyubarsky AL, Khan NW, Teofilo K, Swaroop A, Williams DS, Pugh EN, Thompson DA (2008) Nrl-knockout mice deficient in Rpe65 fail to synthesize 11-cis retinal and cone outer segments. Invest Ophthalmol Vis Sci 49:1126–1135.

Fei Y (2002) Cone neurite sprouting: an early onset abnormality of the cone photoreceptors in the retinal degeneration mouse. Mol Vis 8:306–314.

Ferguson RE, Carroll HP, Harris A, Maher ER, Selby PJ, Banks RE (2005) Housekeeping proteins: a preliminary study illustrating some limitations as useful references in protein expression studies. Proteomics 5:566–571.

Fernández-Sánchez L, Lax P, Campello L, Pinilla I, Cuenca N (2015) Astrocytes and Müller Cell Alterations During Retinal Degeneration in a Transgenic Rat Model of Retinitis Pigmentosa. Front Cell Neurosci 9:801.

Fernández-Sánchez L, Lax P, Pinilla I, Martín-Nieto J, Cuenca N (2011) Tauroursodeoxycholic acid prevents retinal degeneration in transgenic P23H rats. Invest Ophthalmol Vis Sci 52:4998–5008.

Ferrara N, Adamis AP (2016) Ten years of anti-vascular endothelial growth factor therapy. Nat Rev Drug Discov 15:385–403.

Fidler PS, Schuette K, Asher RA, Dobbertin A, Thornton SR, Calle-Patino Y, Muir E, Levine JM, Geller HM, Rogers JH, Faissner A, Fawcett JW (1999) Comparing astrocytic cell lines that are inhibitory or permissive for axon growth: the major axon-inhibitory proteoglycan is NG2. J Neurosci 19:8778–8788.

Fimbel SM, Montgomery JE, Burket CT, Hyde DR (2007) Regeneration of inner retinal neurons after intravitreal injection of ouabain in zebrafish. J Neurosci 27:1712–1724.

Fisher D, Xing B, Dill J, Li H, Hoang HH, Zhao Z, Yang X-L, Bachoo R, Cannon S, Longo FM, Sheng M, Silver J, Li S (2011) Leukocyte common antigen-related phosphatase is a functional receptor for chondroitin sulfate proteoglycan axon growth inhibitors. J Neurosci 31:14051–14066.

Fisher SK, Lewis GP (2003) Müller cell and neuronal remodeling in retinal detachment and reattachment and their potential consequences for visual recovery: a review and reconsideration of recent data. Vis Res 43:887–897.

Fisher SK, Lewis GP, Linberg KA, Verardo MR (2005) Cellular Effects of Detachment and Reattachment on the Neural Retina and the Retinal Pigment Epithelium. Prog Retin Eye Res 24:1991–2012.

Fitch MT, Doller C, Combs CK, Landreth GE, Silver J (1999) Cellular and molecular mechanisms of glial scarring and progressive cavitation: in vivo and in vitro analysis of inflammation-induced secondary injury after CNS trauma. J Neurosci 19:8182–8198.

Forrester JV (2003) Macrophages eyed in macular degeneration. Nat Med 9:1350–1351.

Friedlander DRD, Milev PP, Karthikeyan LL, Margolis RKR, Margolis RUR, Grumet MM

(1994) The neuronal chondroitin sulfate proteoglycan neurocan binds to the neural cell adhesion molecules Ng-CAM/L1/NILE and N-CAM, and inhibits neuronal adhesion and neurite outgrowth. J Cell Biol 125:669–680.

Fritsche LG, Fariss RN, Stambolian D, Abecasis GR, Curcio CA, Swaroop A (2014) Age-related macular degeneration: genetics and biology coming together. Annu Rev Genomics Hum Genet 15:151–171.

Fu X, Sun H, Klein WH, Mu X (2006) Beta-catenin is essential for lamination but not neurogenesis in mouse retinal development. Dev Biol 299:424–437.

Furukawa T, Morrow EM, Cepko CL (1997) Crx, a Novel otx-like Homeobox Gene, Shows Photoreceptor-Specific Expression and Regulates Photoreceptor Differentiation. Cell 91:531–541.

Furukawa T, Morrow EM, Li T, Davis FC, Cepko CL (1999) Retinopathy and attenuated circadian entrainment in Crx-deficient mice. Nat Genet 23:466–470.

Gal A, Orth U, Baehr W, Schwinger E, Rosenberg T (1994) Heterozygous missense mutation in the rod cGMP phosphodiesterase beta-subunit gene in autosomal dominant stationary night blindness. Nat Genet 7:551.

Galou M (1996) Disrupted glial fibrillary acidic protein network in astrocytes from vimentin knockout mice. J Cell Biol 133:853–863.

Galtrey CM, Fawcett JW (2007) The role of chondroitin sulfate proteoglycans in regeneration and plasticity in the central nervous system. Brain Res Rev 54:1–18.

Gao G-P, Lu F, Sanmiguel JC, Tran PT, Abbas Z, Lynd KS, Marsh J, Spinner NB, Wilson JM (2002) Rep/Cap gene amplification and high-yield production of AAV in an A549 cell line expressing Rep/Cap. Mol Ther 5:644–649.

García-Ayuso D, Ortín-Martínez A (2013) Changes in the Photoreceptor Mosaic of P23H-1 Rats During Retinal Degeneration: Implications for Rod-Cone Dependent Survival. Invest Ophthalmol Vis Sci 54(8): 5888-5900.

García-Fernández JM, Jimenez AJ, Foster RG (1995) The persistence of cone photoreceptors within the dorsal retina of aged retinally degenerate mice (rd/rd): implications for circadian organization. Neurosci Lett 187:33–36.

Gastinger MJ, Singh RSJ, Barber AJ (2006) Loss of Cholinergic and Dopaminergic Amacrine Cells in Streptozotocin-Diabetic Rat and Ins2 Akita-Diabetic Mouse

Retinas. Invest Ophthalmol Vis Sci 47:3143.

Geiger P, Barben M, Grimm C, Samardzija M (2015) Blue light-induced retinal lesions, intraretinal vascular leakage and edema formation in the all-cone mouse retina. Cell Death Dis 6:e1985.

Giamanco KA, Morawski M, Matthews RT (2010) Perineuronal net formation and structure in aggrecan knockout mice. Neurosci 170:1314–1327.

Giannelli SG, Demontis GC, Pertile G, Rama P, Broccoli V (2011) Adult human Müller glia cells are a highly efficient source of rod photoreceptors. Stem Cells 29:344–356.

Gilbert RJ, McKeon RJ, Darr A, Calabro A, Hascall VC, Bellamkonda RV (2005) CS-4,6 is differentially upregulated in glial scar and is a potent inhibitor of neurite extension. Mol Cell Neurosci 29:545–558.

Goel M, Dhingra NK (2012) Müller glia express rhodopsin in a mouse model of inherited retinal degeneration. Neurosci 225:152–161.

Goldman RD, Khuon S, Chou YH, Opal P, Steinert PM (1996) The function of intermediate filaments in cell shape and cytoskeletal integrity. J Cell Biol 134:971–983.

Gonzalez-Cordero A, West EL, Pearson RA, Duran Y, Carvalho LS, Chu CJ, Naeem A, Blackford SJI, Georgiadis A, Lakowski J, Hubank M, Smith AJ, Bainbridge JWB, Sowden JC, Ali RR (2013) Photoreceptor precursors derived from three-dimensional embryonic stem cell cultures integrate and mature within adult degenerate retina. Nat Biotechnol 31:741–747.

Goodman DS (1984) Vitamin A and Retinoids in Health and Disease. N Engl J Med 310:1023–1031.

Gosens I, Hollander den AI, Cremers FPM, Roepman R (2008) Composition and function of the Crumbs protein complex in the mammalian retina. Exp Eye Res 86:713–726.

Gouras P, Du J, Kjeldbye H, Yamamoto S, Zack DJ (1994) Long-term photoreceptor transplants in dystrophic and normal mouse retina. Invest Ophthalmol Vis Sci 35:3145–3153.

Gouras P, Tanabe T (2003) Survival and integration of neural retinal transplants in rd

mice. Graefes Arch Clin Exp Ophthalmol 241:403–409.

Greenfield B, Wang WC, Marquardt H, Piepkorn M, Wolff EA, Aruffo A, Bennett KL (1999) Characterization of the heparan sulfate and chondroitin sulfate assembly sites in CD44. J Biol Chem 274: 2511–2517.

Grimpe B, Pressman Y, Lupa MD, Horn KP, Bunge MB, Silver J (2005) The role of proteoglycans in Schwann cell/astrocyte interactions and in regeneration failure at PNS/CNS interfaces. Mol Cell Neurosci 28:18–29.

Grüter O, Kostic C, Crippa SV, Perez M-TR, Zografos L, Schorderet DF, Munier FL, Arsenijevic Y (2005) Lentiviral vector-mediated gene transfer in adult mouse photoreceptors is impaired by the presence of a physical barrier. Gene Ther 12:942–947.

Guérin CJ, Anderson DH, Fisher SK (1990) Changes in intermediate filament immunolabeling occur in response to retinal detachment and reattachment in primates. Invest Ophthalmol Vis Sci 31:1474–1482.

Gupta N, Brown KE, Milam AH (2003) Activated microglia in human retinitis pigmentosa, late-onset retinal degeneration, and age-related macular degeneration. Exp Eye Res 76:463–471.

H MA, Li ZY, Fariss RN (1998) Histopathology of the human retina in retinitis pigmentosa. Prog Retin Eye Res 17:175–205.

Haider NB, Mollema N, Gaule M, Yuan Y, Sachs AJ, Nystuen AM, Naggert JK, Nishina PM (2009) Nr2e3-directed transcriptional regulation of genes involved in photoreceptor development and cell-type specific phototransduction. Exp Eye Res 89:365–372.

Haider NB, Naggert JK, Nishina PM (2001) Excess cone cell proliferation due to lack of a functional NR2E3 causes retinal dysplasia and degeneration in rd7/rd7 mice. Hum Mol Genet 10:1619–1626.

Hamel CP (2007) Cone-Rod Dystrophies. Orphanet J Rare Dis 2:7.

Hanein S, Perrault I, Gerber S, Tanguy G, Rozet JM, Kaplan J (2004) Leber congenital amaurosis: comprehensive survey of the genetic heterogeneity, refinement of the clinical definition and phenotype–genotype correlations as a strategy for molecular diagnosis. Invest Ophthalmol Vis Sci 45:4729–4729.

Hayashi R, Ishikawa Y, Sasamoto Y, Katori R, Nomura N, Ichikawa T, Araki S, Soma T, Kawasaki S, Sekiguchi K, Quantock AJ, Tsujikawa M, Nishida K (2016) Co-ordinated ocular development from human iPS cells and recovery of corneal function. Nat 531:376–380.

Hicks D, Courtois Y (1990) The growth and behaviour of rat retinal Müller cells in vitro. 1. An improved method for isolation and culture. Exp Eye Res 51:119–129.

Himori N, Yamamoto K, Maruyama K, Ryu M, Taguchi K, Yamamoto M, Nakazawa T (2013) Critical role of Nrf2 in oxidative stress-induced retinal ganglion cell death. J Neurochem 127:669–680.

Hippert C, Graca AB, Barber AC, West EL, Smith AJ, Ali RR, Pearson RA (2015) Müller glia activation in response to inherited retinal degeneration is highly varied and disease-specific. PLoS ONE 10:e0120415.

Hippert C, Graca AB, Pearson RA (2016) Gliosis Can Impede Integration Following Photoreceptor Transplantation into the Diseased Retina. Adv Exp Med Biol 854:579–585.

Hirami Y, Osakada F, Takahashi K, Okita K, Yamanaka S, Ikeda H, Yoshimura N, Takahashi M (2009) Generation of retinal cells from mouse and human induced pluripotent stem cells. Neurosci Lett 458:126–131.

Ho AC et al. (2015) Long-Term Results from an Epiretinal Prosthesis to Restore Sight to the Blind. Ophthalmol 122:1547–1554.

Holcombe DJ, Lengefeld N, Gole GA, Barnett NL (2008) The effects of acute intraocular pressure elevation on rat retinal glutamate transport. Acta Ophthalmol 86:408–414.

Hollander den AI, Davis J, van der Velde-Visser SD, Zonneveld MN, Pierrottet CO, Koenekoop RK, Kellner U, van den Born LI, Heckenlively JR, Hoyng CB, Handford PA, Roepman R, Cremers FPM (2004) CRB1 mutation spectrum in inherited retinal dystrophies. Hum Mutat 24:355–369.

Hollander den AI, Ghiani M, de Kok Y (2002) Isolation of Crb1, a mouse homologue of Drosophila crumbs, and analysis of its expression pattern in eye and brain. Mech Dev 110(1-2):203-7.

Hollander den AIA, Brink ten JBJ, de Kok YJY, van Soest SS, van den Born LIL, van Driel MAM, van de Pol DJD, Payne AMA, Bhattacharya SSS, Kellner UU, Hoyng

CBC, Westerveld AA, Brunner HGH, Bleeker-Wagemakers EME, Deutman AFA, Heckenlively JRJ, Cremers FPF, Bergen AAA (1999) Mutations in a human homologue of Drosophila crumbs cause retinitis pigmentosa (RP12). Nat Genet 23:217–221.

Hollyfield JG, Rayborn ME, Midura RJ, Shadrach KG, Acharya S (1999) Chondroitin sulfate proteoglycan core proteins in the interphotoreceptor matrix: a comparative study using biochemical and immunohistochemical analysis. Exp Eye Res 69:311–322.

Holz FG, Tadayoni R, Beatty S, Berger AR, Cereda MG, Hykin P, Staurenghi G, Wittrup-Jensen K, Nilsson J, Kim K, Sivaprasad S (2016) Determinants of visual acuity outcomes in eyes with neovascular AMD treated with anti-VEGF agents: an instrumental variable analysis of the AURA study. Eye 30:1063–1071.

Huang L, Zhang Q, Li S, Guan L, Xiao X, Zhang J, Jia X, Sun W, Zhu Z, Gao Y, Yin Y, Wang P, Guo X, Wang J, Zhang Q (2013) Exome sequencing of 47 chinese families with cone-rod dystrophy: mutations in 25 known causative genes. PLoS ONE 8:e65546.

Humphrey MF, Chu Y, Mann K, Rakoczy P (1997) Retinal GFAP and bFGF expression after multiple argon laser photocoagulation injuries assessed by both immunoreactivity and mRNA levels. Exp Eye Res 64:361–369.

Humphrey MF, Constable IJ, Chu Y, Wiffen S (1993) A quantitative study of the lateral spread of Müller cell responses to retinal lesions in the rabbit. J Comp Neurol 334:545–558.

Humphries MM, Rancourt D, Farrar GJ, Kenna P, Hazel M, Bush RA, Sieving PA, Sheils DM, McNally N, Creighton P, Erven A, Boros A, Gulya K, Capecchi MR, Humphries P (1997) Retinopathy induced in mice by targeted disruption of the rhodopsin gene. Nat Genet 15:216–219.

Hüttl S, Michalakis S, Seeliger M, Luo D-G, Acar N, Geiger H, Hudl K, Mader R, Haverkamp S, Moser M, Pfeifer A, Gerstner A, Yau K-W, Biel M (2005) Impaired channel targeting and retinal degeneration in mice lacking the cyclic nucleotide-gated channel subunit CNGB1. J Neurosci 25:130–138.

Ichijo H (2004) Proteoglycans as cues for axonal guidance in formation of retinotectal or retinocollicular projections. Mol Neurobiol 30:23–33.

Iezzi R (2016) Regenerative ophthalmology: Technologic and pharmacologic

approaches to restoring sight via retinal prosthesis. Clin Pharmacol Ther 99:33–35.

Inatani M, Honjo M, Otori Y, Oohira A, Kido N, Tano Y, Honda Y, Tanihara H (2001) Inhibitory effects of neurocan and phosphacan on neurite outgrowth from retinal ganglion cells in culture. Invest Ophthalmol Vis Sci 42:1930–1938.

Inatani M, Tanihara H (2002) Proteoglycans in retina. Prog Retin Eye Res 21:429–447.

Inatani M, Tanihara H, Oohira A, Honjo M, Kido N, Honda Y (2000) Upregulated expression of neurocan, a nervous tissue specific proteoglycan, in transient retinal ischemia. Invest Ophthalmol Vis Sci 41:2748–2754.

Inman DM, Horner PJ (2007) Reactive nonproliferative gliosis predominates in a chronic mouse model of glaucoma. Glia 55:942–953.

Ishikawa M, Sawada Y, Yoshitomi T (2015) Structure and function of the interphotoreceptor matrix surrounding retinal photoreceptor cells. Exp Eye Res 133:3–18.

Ivaska J, Pallari H-M, Nevo J, Eriksson JE (2007) Novel functions of vimentin in cell adhesion, migration, and signaling. Exp Cell Res 313:2050–2062.

Jacobson SG (2012) Gene Therapy for Leber Congenital Amaurosis Caused by RPE65 Mutations. Arch Ophthalmol 130:9.

Jacobson SG, Cideciyan AV, Aleman TS, Pianta MJ, Sumaroka A, Schwartz SB, Smilko EE, Milam AH, Sheffield VC, Stone EM (2003) Crumbs homolog 1 (CRB1) mutations result in a thick human retina with abnormal lamination. Hum Mol Genet 12(9):1073-8.

Jacobson SG, Cideciyan AV, Regunath G, Rodriguez FJ, Vandenburgh K, Sheffield VC, Stone EM (1995) Night blindness in Sorsby's fundus dystrophy reversed by vitamin A. Nat Genet 11:27–32.

Jadhav AP, Mason HA, Cepko CL (2006) Notch 1 inhibits photoreceptor production in the developing mammalian retina. Development 133:913–923.

Jayakody SA, Gonzalez-Cordero A, Ali RR, Pearson RA (2015) Progress in Retinal and Eye Research. Prog Retin Eye Res 46:31–66.

Jayaram H, Jones MF, Eastlake K, Cottrill PB, Becker S, Wiseman J, Khaw PT, Limb GA (2014) Transplantation of photoreceptors derived from human Muller glia restore rod function in the P23H rat. Stem Cells Transl Med 3:323–333.

Jeon C-J, Strettoi E, Masland RH (1998). The major cell populations of the mouse retina. J Neurosci 18(21):8936-46.

Jing R, Wilhelmsson U, Goodwill W, Li L, Pan Y, Pekny M, Skalli O (2007) Synemin is expressed in reactive astrocytes in neurotrauma and interacts differentially with vimentin and GFAP intermediate filament networks. J Cell Sci 120:1267–1277.

Jobling AI, Vessey KA, Waugh M, Mills SA, Fletcher EL (2013) A Naturally Occurring Mouse Model of Achromatopsia: Characterization of the Mutation in Cone Transducin and Subsequent Retinal Phenotype. Invest Ophthalmol Vis Sci 54:3350.

John SK, Smith JE, Aguirre GD, H MA (2000) Loss of cone molecular markers in rhodopsin-mutant human retinas with retinitis pigmentosa. Mol Vis 6:204–215.

Johns PR (1977) Growth of the adult goldfish eye. III. Source of the new retinal cells. J Comp Neurol 176:343–357.

Johns PR, Fernald RD (1981) Genesis of rods in teleost fish retina. Nat 293:141–142.

Johnson TV, Bull ND, Martin KR (2010) Identification of barriers to retinal engraftment of transplanted stem cells. Invest Ophthalmol Vis Sci 51:960–970.

Jones BW, Kondo M, Terasaki H, Lin Y, McCall M, Marc RE (2012) Retinal remodeling. Jpn J Ophthalmol 56:289–306.

Jones BW, Marc RE (2005) Retinal remodeling during retinal degeneration. Exp Eye Res 81:123–137.

Jones BW, Watt CB, Frederick JM, Baehr W, Chen C-K, Levine EM, Milam AH, LaVail MM, Marc RE (2003a) Retinal remodeling triggered by photoreceptor degenerations. J Comp Neurol 464:1–16.

Jones LL, Margolis RU, Tuszynski MH (2003b) The chondroitin sulfate proteoglycans neurocan, brevican, phosphacan, and versican are differentially regulated following spinal cord injury. Exp Neuro 182 :399–411.

Jones LL, Yamaguchi Y, Stallcup WB, Tuszynski MH (2002) NG2 is a major chondroitin sulfate proteoglycan produced after spinal cord injury and is expressed by macrophages and oligodendrocyte progenitors. J Neurosci 22:2792–2803.

Jonnal RS, Besecker JR, Derby JC, Kocaoglu OP, Cense B, Gao W, Wang Q, Miller DT (2010) Imaging outer segment renewal in living human cone photoreceptors.

Opt Express 18:5257–5270.

Kamao H, Mandai M, Okamoto S, Sakai N, Suga A, Sugita S, Kiryu J, Takahashi M (2014) Characterization of human induced pluripotent stem cell-derived retinal pigment epithelium cell sheets aiming for clinical application. Stem Cell Rep 2:205–218.

Kaupp UB, Seifert R (2002) Cyclic nucleotide-gated ion channels. Physiol Rev 82:769–824.

Kaur C, Sivakumar V, Yong Z, Lu J, Foulds WS, Ling EA (2007) Blood-retinal barrier disruption and ultrastructural changes in the hypoxic retina in adult rats: the beneficial effect of melatonin administration. J Pathol 212:429–439.

Kedzierski W, Lloyd M, Birch DG, Bok D, Travis GH (1997) Generation and analysis of transgenic mice expressing P216L-substituted rds/peripherin in rod photoreceptors. Invest Ophthalmol Vis Sci 38:498–509.

Keen TJ, Inglehearn CF (1996) Mutations and polymorphisms in the human peripherin-RDS gene and their involvement in inherited retinal degeneration. Hum Mutat 8:297–303.

Keenan TDL, Clark SJ, Unwin RD, Ridge LA, Day AJ, Bishop PN (2012) Mapping the differential distribution of proteoglycan core proteins in the adult human retina, choroid, and sclera. Invest Ophthalmol Vis Sci 53:7528–7538.

Kevany BM, Palczewski K (2010) Phagocytosis of retinal rod and cone photoreceptors. Physiology (Bethesda) 25:8–15.

Khateb S, Hanany M, Khalaileh A, Beryozkin A, Meyer S, Abu-Diab A, Abu Turky F, Mizrahi-Meissonnier L, Lieberman S, Ben-Yosef T, Banin E, Sharon D (2016) Identification of genomic deletions causing inherited retinal degenerations by coverage analysis of whole exome sequencing data. J Med Genet 53:600–607.

Kim BG, Dai H-N, Lynskey JV, Mcatee M, Bregman BS (2006) Degradation of chondroitin sulfate proteoglycans potentiates transplant-mediated axonal remodeling and functional recovery after spinal cord injury in adult rats. J Comp Neurol 497:182–198.

Kim IB, Kim KY, Joo CK, Lee MY, Oh SJ, Chung JW, Chun MH (1998) Reaction of Müller cells after increased intraocular pressure in the rat retina. Exp Brain Res 121:419–424.

Kim K-Y, Ju W-K, Neufeld AH (2004) Neuronal susceptibility to damage: comparison of the retinas of young, old and old/caloric restricted rats before and after transient ischemia. Neurobiol Aging 25:491–500.

Kinouchi R, Takeda M, Yang L, Wilhelmsson U, Lundkvist A, Pekny M, Chen DF (2003) Robust neural integration from retinal transplants in mice deficient in GFAP and vimentin. Nat Neurosci 6:863–868.

Kiser PD, Golczak M, Maeda A, Palczewski K (2012) Key enzymes of the retinoid (visual) cycle in vertebrate retina. Biochim Biophys Acta 1821(1):137-51.

Kivelä T, Tarkkanen A, Virtanen I (1986) Intermediate filaments in the human retina and retinoblastoma. An immunohistochemical study of vimentin, glial fibrillary acidic protein, and neurofilaments. Invest Ophthalmol Vis Sci 27:1075–1084.

Klimczak RR, Koerber JT, Dalkara D, Flannery JG, Schaffer DV (2009) A novel adeno-associated viral variant for efficient and selective intravitreal transduction of rat Müller cells. PLoS ONE 4:e7467.

Kljavin IJ, Reh TA (1991) Müller cells are a preferred substrate for in vitro neurite extension by rod photoreceptor cells. J Neurosci 11:2985–2994.

Kohl S, Baumann B, Rosenberg T, Kellner U, Lorenz B, Vadalà M, Jacobson SG, Wissinger B (2002) Mutations in the Cone Photoreceptor G-Protein α-Subunit Gene GNAT2 in Patients with Achromatopsia. J Hum Genet 71:422–425.

Kohl S, Marx T, Giddings I, Jägle H, Jacobson SG, Apfelstedt-Sylla E, Zrenner E, Sharpe LT, Wissinger B (1998) Total colourblindness is caused by mutations in the gene encoding the alpha-subunit of the cone photoreceptor cGMP-gated cation channel. Nat Genet 19:257–259.

Koike C, Nishida A, Akimoto K, Nakaya M-A, Noda T, Ohno S, Furukawa T (2005) Function of atypical protein kinase C lambda in differentiating photoreceptors is required for proper lamination of mouse retina. J Neurosci 25:10290–10298.

Kolb H, Nelson R, Ahnelt P, Cuenca N (2001) Cellular organization of the vertebrate retina. Prog Brain Res.

Kostic C, Chiodini F, Salmon P, Wiznerowicz M, Deglon N, Hornfeld D, Trono D, Aebischer P, Schorderet DF, Munier FL, Arsenijevic Y (2003) Activity analysis of housekeeping promoters using self-inactivating lentiviral vector delivery into the mouse retina. Gene Ther 10:818–821.

Kowluru RA, Kanwar M (2007) Effects of curcumin on retinal oxidative stress and inflammation in diabetes. Nutr Metab (Lond) 4:8.

Krol J, Krol I, Alvarez CPP, Fiscella M, Hierlemann A, Roska B, Filipowicz W (2015) A network comprising short and long noncoding RNAs and RNA helicase controls mouse retina architecture. Nat Commun 6:7305.

Kuboyama T, Luo X, Park K, Blackmore MG, Tojima T, Tohda C, Bixby JL, Lemmon VP, Kamiguchi H (2010) Paxillin phosphorylation counteracts proteoglycan-mediated inhibition of axon regeneration.Exp Neuro 248:1–13.

Kvanta A, Algvere PV, Berglin L, Seregard S (1996) Subfoveal fibrovascular membranes in age-related macular degeneration express vascular endothelial growth factor. Invest Ophthalmol Vis Sci 37:1929–1934.

Kwan A, Wang S, Lund RD (1999) Photoreceptor layer reconstruction in a rodent model of retinal degeneration. Exp Neuro 159:21–33.

Laabs T, Carulli D, Geller HM, Fawcett JW (2005) Chondroitin sulfate proteoglycans in neural development and regeneration. Curr Opin Neurobiol 15:116–120.

Lai C-M, Shen W-Y, Brankov M, Lai YKY, Barnett NL, Lee S-Y, Yeo IYS, Mathur R, Ho JES, Pineda P, Barathi A, Ang C-L, Constable IJ, Rakoczy EP (2005) Long-term evaluation of AAV-mediated sFlt-1 gene therapy for ocular neovascularization in mice and monkeys. Mol Ther 12:659–668.

Lai CM, Estcourt MJ, Himbeck RP, Lee SY, Yew-San Yeo I, Luu C, Loh BK, Lee MW, Barathi A, Villano J, Ang C-L, van der Most RG, Constable IJ, Dismuke D, Samulski RJ, Degli-Esposti MA, Rakoczy EP (2011) Preclinical safety evaluation of subretinal AAV2.sFlt-1 in non-human primates. Gene Ther 19:999–1009.

Lakowski J, Baron M, Bainbridge J, Barber AC, Pearson RA, Ali RR, Sowden JC (2010) Cone and rod photoreceptor transplantation in models of the childhood retinopathy Leber congenital amaurosis using flow-sorted Crx-positive donor cells. Hum Mol Genet 19:4545–4559.

Lamba DA, Gust J, Reh TA (2009) Transplantation of human embryonic stem cell-derived photoreceptors restores some visual function in Crx-deficient mice. Stem Cell 4:73–79.

Lamba DA, Karl MO, Ware CB, Reh TA (2006) Efficient generation of retinal progenitor cells from human embryonic stem cells. Proc Natl Acad Sci 103:12769–12774.

Landers RA, Hollyfield JG (1992) Proteoglycans in the mouse interphotoreceptor matrix. VI. Evidence for photoreceptor synthesis of chondroitin sulfate proteoglycan using genetically fractionated retinas. Exp Eye Res 55:345–356.

Landschulz WH, Johnson PF, McKnight SL (1988) The leucine zipper: a hypothetical structure common to a new class of DNA binding proteins. Sci 240:1759–1764.

Lauritzen JS, Sigulinsky CL, Anderson JR, Kalloniatis M, Nelson NT, Emrich DP, Rapp C, McCarthy N, Kerzner E, Meyer M, Jones BW, Marc RE (2016) Rod-cone crossover connectome of mammalian bipolar cells. J Comp Neurol, cne.24084.

LaVail MM, Battelle BA (1975) Influence of eye pigmentation and light deprivation on inherited retinal dystrophy in the rat. Exp Eye Res 21:167–192.

LaVail MM, Matthes MT, Yasumura D, Steinberg RH (1997) Variability in rate of cone degeneration in the retinal degeneration (rd/rd) mouse. Exp Eye Res 65:45–50.

LaVail MM, Pinto LH, Yasumura D (1981) The interphotoreceptor matrix in rats with inherited retinal dystrophy. Invest Ophthalmol Vis Sci 21:658–668.

LaVail MM, Unoki K, Yasumura D, Matthes MT, Yancopoulos GD, Steinberg RH (1992) Multiple growth factors, cytokines, and neurotrophins rescue photoreceptors from the damaging effects of constant light. Proc Natl Acad Sci 89:11249–11253.

Lawrence JM, Singhal S, Bhatia B, Keegan DJ, Reh TA, Luthert PJ, Khaw PT, Limb GA (2007) MIO-M1 Cells and Similar Müller Glial Cell Lines Derived from Adult Human Retina Exhibit Neural Stem Cell Characteristics. Stem Cells 25:2033–2043.

Lebrun-Julien F, Duplan L, Pernet V, Osswald I, Sapieha P, Bourgeois P, Dickson K, Bowie D, Barker PA, Di Polo A (2009) Excitotoxic Death of Retinal Neurons In Vivo Occurs via a Non-Cell-Autonomous Mechanism. J Neurosci 29:5536–5545.

Lee E-J, Ji Y, Zhu CL, Grzywacz NM (2011) Role of Müller cells in cone mosaic rearrangement in a rat model of retinitis pigmentosa. Glia 59:1107–1117.

Lee H, McKeon RJ, Bellamkonda RV (2010) Sustained delivery of thermostabilized chABC enhances axonal sprouting and functional recovery after spinal cord injury. Proc Natl Acad Sci 107:3340–3345.

Lemke AK, Sandy JD, Voigt H, Dreier R, Lee JH, Grodzinsky AJ, Mentlein R, Fay J, Schünke M, Kurz B (2010) Interleukin-1alpha treatment of meniscal explants stimulates the production and release of aggrecanase-generated, GAG-substituted

aggrecan products and also the release of pre-formed, aggrecanase-generated G1 and m-calpain-generated G1-G2. Cell Tissue Res 340:179–188.

Lemons ML, Howland DR, Anderson DK (1999) Chondroitin sulfate proteoglycan immunoreactivity increases following spinal cord injury and transplantation.Exp Neuro 160:51–65.

Lemons ML, Sandy JD, Anderson DK, Howland DR (2003) Intact aggrecan and chondroitin sulfate-depleted aggrecan core glycoprotein inhibit axon growth in the adult rat spinal cord. Exp Neuro 184:981–990.

Letourneau PC, Condic ML, Snow DM (1994) Interactions of developing neurons with the extracellular matrix. J Neurosci 14:915–928.

Lewis G, Mervin K, Valter K, Maslim J, Kappel PJ, Stone J, Fisher S (1999) Limiting the proliferation and reactivity of retinal Müller cells during experimental retinal detachment: the value of oxygen supplementation. J Ophthalmol 128:165–172.

Lewis GP, Chapin EA, Luna G, Linberg KA, Fisher SK (2010) The fate of Müller's glia following experimental retinal detachment: nuclear migration, cell division, and subretinal glial scar formation. Mol Vis 16:1361–1372.

Lewis GP, Erickson PA, Guérin CJ, Anderson DH, Fisher SK (1989) Changes in the expression of specific Müller cell proteins during long-term retinal detachment. Exp Eye Res 49:93–111.

Lewis GP, Fisher SK (2000) Müller cell outgrowth after retinal detachment: association with cone photoreceptors. Invest Ophthalmol Vis Sci 41:1542–1545.

Lewis GP, Fisher SK (2003) Up-regulation of glial fibrillary acidic protein in response to retinal injury: its potential role in glial remodeling and a comparison to vimentin expression. Int Rev Cytol 230:263–290.

Lewis GP, Sethi CS, Carter KM, Charteris DG, Fisher SK (2005) Microglial cell activation following retinal detachment: a comparison between species. Mol Vis 11:491–500.

Lewis PM, Ackland HM, Lowery AJ, Rosenfeld JV (2015) Restoration of vision in blind individuals using bionic devices: a review with a focus on cortical visual prostheses. Brain Res 1595:51–73.

Léveillard T, Mohand-Saïd S, Lorentz O, Hicks D, Fintz A-C, Clérin E, Simonutti M,

Forster V, Cavusoglu N, Chalmel F, Dollé P, Poch O, Lambrou G, Sahel J-A (2004) Identification and characterization of rod-derived cone viability factor. Nat Genet 36:755–759.

Li H, Leung TC, Hoffman S, Balsamo J, Lilien J (2000) Coordinate regulation of cadherin and integrin function by the chondroitin sulfate proteoglycan neurocan. J Cell Biol 149:1275–1288.

Libby RT, Champliaud MF, Claudepierre T, Xu Y, Gibbons EP, Koch M, Burgeson RE, Hunter DD, Brunken WJ (2000) Laminin expression in adult and developing retinae: evidence of two novel CNS laminins. J Neurosci 20:6517–6528.

Lin B, Masland RH, Strettoi E (2009) Remodeling of cone photoreceptor cells after rod degeneration in rd mice. Exp Eye Res 88:589–599.

Lin H et al. (2016) Lens regeneration using endogenous stem cells with gain of visual function. Nat 531:323–328.

Linberg KA, Sakai T, Lewis GP, Fisher SK (2002) Experimental retinal detachment in the cone-dominant ground squirrel retina: morphology and basic immunocytochemistry. Vis Neurosci 19:603–619.

Logan CY, Nusse R (2004) The Wnt signaling pathway in development and disease. Annu Rev Cell Dev Biol 20:781–810.

Lu L, Nyalakonda K, Kam L, Bizios R, Göpferich A, Mikos AG (2001) Retinal pigment epithelial cell adhesion on novel micropatterned surfaces fabricated from synthetic biodegradable polymers. Biomaterials 22:291–297.

Lu Y-B, Franze K, Seifert G, Steinhäuser C, Kirchhoff F, Wolburg H, Guck J, Janmey P, Wei E-Q, Käs J, Reichenbach A (2006) Viscoelastic properties of individual glial cells and neurons in the CNS. Proc Natl Acad Sci 103:17759–17764.

Lu Y-B, Iandiev I, Hollborn M, Körber N, Ulbricht E, Hirrlinger PG, Pannicke T, Wei E-Q, Bringmann A, Wolburg H, Wilhelmsson U, Pekny M, Wiedemann P, Reichenbach A, Käs JA (2011) Reactive glial cells: increased stiffness correlates with increased intermediate filament expression. FASEB J 25:624–631.

Lu Y-B, Pannicke T, Wei E-Q, Bringmann A, Wiedemann P, Habermann G, Buse E, Käs JA, Reichenbach A (2013) Biomechanical properties of retinal glial cells: comparative and developmental data. Exp Eye Res 113:60–65.

Luhmann UFO, Carvalho LS, Holthaus S-MK, Cowing JA, Greenaway S, Chu CJ, Herrmann P, Smith AJ, Munro PMG, Potter P, Bainbridge JWB, Ali RR (2015) The severity of retinal pathology in homozygous Crb1rd8/rd8 mice is dependent on additional genetic factors. Hum Mol Genet 24:128–141.

Lui JH, Hansen DV, Kriegstein AR (2011) Development and Evolution of the Human Neocortex. Cell 146:18–36.

Luna G, Lewis GP, Banna CD, Skalli O, Fisher SK (2010) Expression profiles of nestin and synemin in reactive astrocytes and Müller cells following retinal injury: a comparison with glial fibrillar acidic protein and vimentin. Mol Vis 16:2511–2523.

Lundkvist A, Reichenbach A, Betsholtz C, Carmeliet P, Wolburg H, Pekny M (2004) Under stress, the absence of intermediate filaments from Müller cells in the retina has structural and functional consequences. J Cell Sci 117:3481–3488.

MacLaren RE, Pearson RA, MacNeil A, Douglas RH, Salt TE, Akimoto M, Swaroop A, Sowden JC, Ali RR (2006) Retinal repair by transplantation of photoreceptor precursors. Nat 444:203–207.

Maeda A, Maeda T, Golczak M, Chou S, Desai A, Hoppel CL, Matsuyama S, Palczewski K (2009) Involvement of all-trans-retinal in acute light-induced retinopathy of mice. J Biol Chem 284:15173–15183.

Maguire AM et al. (2008) Safety and efficacy of gene transfer for Leber's congenital amaurosis. N Engl J Med 358:2240–2248.

Mansergh FC, Carrigan M, Hokamp K, Farrar GJ (2015) Gene expression changes during retinal development and rod specification. Mol Vis 21:61–87.

Martin-Belmonte F, Perez-Moreno M (2012) Epithelial cell polarity, stem cells and cancer. Nat Rev Cancer 12:23–38.

Martinez-De Luna RI, Ku RY, Aruck AM, Santiago F, Viczian AS, San Mauro D, Zuber ME (2016) Müller glia reactivity follows retinal injury despite the absence of the glial fibrillary acidic protein gene in Xenopus. Dev Biol pii: S0012-1606(15)30360-2.

Martinez-Navarrete G, Seiler MJ, Aramant RB, Fernandez-Sanchez L, Pinilla I, Cuenca N (2011) Retinal degeneration in two lines of transgenic S334ter rats. Exp Eye Res 92:227–237.

Massey JM, Amps J, Viapiano MS, Matthews RT, Wagoner MR, Whitaker CM, Alilain

W, Yonkof AL, Khalyfa A, Cooper NGF, Silver J, Onifer SM (2008) Increased chondroitin sulfate proteoglycan expression in denervated brainstem targets following spinal cord injury creates a barrier to axonal regeneration overcome by chondroitinase ABC and neurotrophin-3.Exp Neuro 209:426–445.

Matsui F, Oohira A (2004) Proteoglycans and injury of the central nervous system. Congenit Anom 44:181–188.

Mazzoni F, Novelli E, Strettoi E (2008) Retinal Ganglion Cells Survive and Maintain Normal Dendritic Morphology in a Mouse Model of Inherited Photoreceptor Degeneration. J Neurosci 28:14282–14292.

McGraw J, Hiebert GW, Steeves JD (2001) Modulating astrogliosis after neurotrauma. J Neurosci Res 63:109–115.

McKeon RJ, Höke A, Silver J (1995) Injury-induced proteoglycans inhibit the potential for laminin-mediated axon growth on astrocytic scars. Exp Neuro 136:32–43.

McKeon RJ, Schreiber RC, Rudge JS, Silver J (1991) Reduction of neurite outgrowth in a model of glial scarring following CNS injury is correlated with the expression of inhibitory molecules on reactive astrocytes. J Neurosci 11:3398–3411.

McLaughlin ME, Sandberg MA, Berson EL, Dryja TP (1993) Recessive mutations in the gene encoding the beta-subunit of rod phosphodiesterase in patients with retinitis pigmentosa. Nat 4:130–134.

McNally N, Kenna PF, Rancourt D, Ahmed T, Stitt A, Colledge WH, Lloyd DG, Palfi A, O'Neill B, Humphries MM, Humphries P, Farrar GJ (2002) Murine model of autosomal dominant retinitis pigmentosa generated by targeted deletion at codon 307 of the rds-peripherin gene. Hum Mol Genet 11:1005–1016.

Mears AJ, Kondo M, Swain PK, Takada Y, Bush RA, Saunders TL, Sieving PA, Swaroop A (2001b) Nrl is required for rod photoreceptor development. Nat Genet 29:447–452.

Mehalow AK, Kameya S, Smith RS, Hawes NL, Denegre JM, Young JA, Bechtold L, Haider NB, Tepass U, Heckenlively JR, Chang B, Naggert JK, Nishina PM (2003) CRB1 is essential for external limiting membrane integrity and photoreceptor morphogenesis in the mammalian retina. Hum Mol Genet 12:2179–2189.

Mellough CB, Cui Q, Harvey AR (2007) Treatment of adult neural progenitor cells prior to transplantation affects graft survival and integration in a neonatal and adult rat

model of selective retinal ganglion cell depletion. Restor Neurol Neurosci 25:177–190.

Menet V, Prieto M, Privat A, Ribotta MGY (2011) Axonal plasticity and functional recovery after spinal cord injury in mice deficient in both glial fibrillary acidic protein and vimentin genes. Proc Natl Acad Sci 100:8999–9004.

Merriman DK, Sajdak BS, Li W, Jones BW (2016) Seasonal and post-trauma remodeling in cone-dominant ground squirrel retina. Exp Eye Res:1–16.

Mestrinerr ACD, Haddad A (1994) Serum albumin enters the posterior chamber of the eye permeating the blood-aqueous barrier. Graefes Arch Clin Exp Ophthalmol 232:242–251.

Meyer JS, Shearer RL, Capowski EE, Wright LS, Wallace KA, McMillan EL, Zhang S-C, Gamm DM (2009) Modeling early retinal development with human embryonic and induced pluripotent stem cells. Proc Natl Acad Sci 106:16698–16703.

Mieziewska K, van Veen T, Aguirre GD (1993) Structural changes of the interphotoreceptor matrix in an inherited retinal degeneration: a lectin cytochemical study of progressive rod-cone degeneration. Invest Ophthalmol Vis Sci 34:3056–3067.

Minassian DC, Reidy A, Lightstone A, Desai P (2011) Modelling the prevalence of age-related macular degeneration (2010-2020) in the UK: expected impact of anti-vascular endothelial growth factor (VEGF) therapy. Br J Ophthalmol 95:1433–1436.

Mitamura Y, Mitamura-Aizawa S, Katome T, Naito T, Hagiwara A, Kumagai K, Yamamoto S (2013) Photoreceptor impairment and restoration on optical coherence tomographic image. J Ophthalmol 2013:518170.

Mitashov VI (2001) Multipotential stem cells and progenitors in the vertebrate retina. Biol Bull Russ Acad Sci 28:606–615.

Miyoshi H, Takahashi M, Gage FH, Verma IM (1997) Stable and efficient gene transfer into the retina using an HIV-based lentiviral vector. Proc Natl Acad Sci 94:10319–10323.

Moiseyev G, Chen Y, Takahashi Y, Wu BX, Ma J-X (2005) RPE65 is the isomerohydrolase in the retinoid visual cycle. Proc Natl Acad Sci 102:12413–12418.

Montana CL, Lawrence KA, Williams NL, Tran NM, Peng G-H, Chen S, Corbo JC (2011) Transcriptional regulation of neural retina leucine zipper (Nrl), a photoreceptor cell fate determinant. J Biol Chem 286:36921–36931.

Mookherjee S, Hiriyanna S, Kaneshiro K, Li L, Li Y, Li W, Qian H, Li T, Khanna H, Colosi P, Swaroop A, Wu Z (2015) Long-term rescue of cone photoreceptor degeneration in retinitis pigmentosa 2 (RP2)-knockout mice by gene replacement therapy. Hum Mol Genet 24:6446–6458.

Moon LD, Asher RA, Rhodes KE, Fawcett JW (2001) Regeneration of CNS axons back to their target following treatment of adult rat brain with chondroitinase ABC. Nat Neurosci 4:465–466.

Morgenstern DA, Asher RA, Fawcett JW (2002) Chondroitin sulphate proteoglycans in the CNS injury response. Prog Brain Res 137:313–332.

Morris TA, Fong SL (1993) Characterization of the gene encoding human cone transducin alpha-subunit (GNAT2). Genomics 17:442–448.

Moussaif M, Rubin WW, Kerov V, Reh R, Chen D, Lem J, Chen C-K, Hurley JB, Burns ME, Artemyev NO (2006) Phototransduction in a transgenic mouse model of Nougaret night blindness. J Neurosci 26:6863–6872.

Muir D, Engvall E, Varon S, Manthorpe M (1989) Schwannoma cell-derived inhibitor of the neurite-promoting activity of laminin. J Cell Biol 109:2353–2362.

Myer DJ, Gurkoff GG, Lee SM, Hovda DA, Sofroniew MV (2006) Essential protective roles of reactive astrocytes in traumatic brain injury. Brain 129:2761–2772.

Naeem MA, Chavali VRM, Ali S, Iqbal M, Riazuddin S, Khan SN, Husnain T, Sieving PA, Ayyagari R, Riazuddin S, Hejtmancik JF, Riazuddin SA (2012) GNAT1 associated with autosomal recessive congenital stationary night blindness. Invest Ophthalmol Vis Sci 53:1353–1361.

Nakanishi K, Aono S, Hirano K, Kuroda Y, Ida M, Tokita Y, Matsui F, Oohira A (2006) Identification of neurite outgrowth-promoting domains of neuroglycan C, a brain-specific chondroitin sulfate proteoglycan, and involvement of phosphatidylinositol 3-kinase and protein kinase C signaling pathways in neuritogenesis. J Biol Chem 281:24970–24978.

Nakazawa M, Naoi N, Wada Y, Nakazaki S, Maruiwa F, Sawada A, Tamai M (1996) Autosomal dominant cone-rod dystrophy associated with a Val200Glu mutation of

the peripherin/RDS gene. Retin 16:405–410.

Nakazawa T, Takeda M, Lewis GP, Cho K-S, Jiao J, Wilhelmsson U, Fisher SK, Pekny M, Chen DF, Miller JW (2007) Attenuated glial reactions and photoreceptor degeneration after retinal detachment in mice deficient in glial fibrillary acidic protein and vimentin. Invest Ophthalmol Vis Sci 48:2760–2768.

Nandini CD, Sugahara K (2006) Role of the sulfation pattern of chondroitin sulfate in its biological activities and in the binding of growth factors. Adv Pharmacol 53:253–279.

Naskar R, Vorwerk CK, Dreyer EB (2000) Concurrent Downregulation of a Glutamate Transporter and Receptor in Glaucoma. Invest Ophthalmol Vis Sci 41:1940–1944.

Nishida A, Furukawa A, Koike C, Tano Y, Aizawa S, Matsuo I, Furukawa T (2003) Otx2 homeobox gene controls retinal photoreceptor cell fate and pineal gland development. Nat Neurosci 6:1255–1263.

Nishida A, Takahashi M, Tanihara H, Nakano I, Takahashi JB, Mizoguchi A, Ide C, Honda Y (2000) Incorporation and differentiation of hippocampus-derived neural stem cells transplanted in injured adult rat retina. Invest Ophthalmol Vis Sci 41:4268–4274.

Nishiguchi KM, Carvalho LS, Rizzi M, Powell K, Holthaus S-MK, Azam SA, Duran Y, Ribeiro J, Luhmann UFO, Bainbridge JWB, Smith AJ, Ali RR (2015) Gene therapy restores vision in rd1 mice after removal of a confounding mutation in Gpr179. Nat Commun 6:6006.

Nishiguchi KM, Sandberg MA, Kooijman AC, Martemyanov KA, Pott JWR, Hagstrom SA, Arshavsky VY, Berson EL, Dryja TP (2004) Defects in RGS9 or its anchor protein R9AP in patients with slow photoreceptor deactivation. Nat 427:75–78.

Nishimura T, Takeichi M (2009) Remodeling of the adherens junctions during morphogenesis. Curr Top Dev Biol 89:33–54.

Oakley RA, Tosney KW (1991) Peanut agglutinin and chondroitin-6-sulfate are molecular markers for tissues that act as barriers to axon advance in the avian embryo. Dev Biol 147:187–206.

Oh ECT, Cheng H, Hao H, Jia L, Khan NW, Swaroop A (2008) Rod differentiation factor NRL activates the expression of nuclear receptor NR2E3 to suppress the development of cone photoreceptors. Brain Res 1236:16–29.

Okada M, Matsumura M, Ogino N, Honda Y (1990) Muller Cells in Detached Human Retina Express Glial Fibrillary Acidic Protein and Vimentin. Graefes Arch Clin Exp Ophthalmol 228:467–474.

Omri S, Behar-Cohen F, Rothschild P-R, Gélizé E, Jonet L, Jeanny J-C, Omri B, Crisanti P (2013) PKCζ Mediates Breakdown of Outer Blood-Retinal Barriers in Diabetic Retinopathy. PLoS ONE 8:e81600.

Omri S, Omri B, Savoldelli M, Jonet L, Thillaye-Goldenberg B, Thuret G, Gain P, Jeanny JC, Crisanti P, Behar-Cohen F (2010) The outer limiting membrane (OLM) revisited: clinical implications. Clin Ophthalmol 4:183–195.

Ooto S, Akagi T, Kageyama R, Akita J, Mandai M, Honda Y, Takahashi M (2004) Potential for neural regeneration after neurotoxic injury in the adult mammalian retina. Proc Natl Acad Sci 101:13654–13659.

Osakada F, Ikeda H, Mandai M, Wataya T, Watanabe K, Yoshimura N, Akaike A, Sasai Y, Takahashi M (2008) Toward the generation of rod and cone photoreceptors from mouse, monkey and human embryonic stem cells. Nat Biotechnol 26:215–224.

Owen CG, Jarrar Z, Wormald R, Cook DG, Fletcher AE, Rudnicka AR (2012) The estimated prevalence and incidence of late stage age related macular degeneration in the UK. Br J Ophthalmol 96:752–756.

Palfi A, Millington-Ward S, Chadderton N, O'Reilly M, Goldmann T, Humphries MM, Li T, Wolfrum U, Humphries P, Kenna PF, Farrar GJ (2010) Adeno-Associated Virus-Mediated Rhodopsin Replacement Provides Therapeutic Benefit in Mice with a Targeted Disruption of the Rhodopsin Gene. Hum Gene Ther 21:311–323.

Pang J-J, Chang B, Hawes NL, Hurd RE, Davisson MT, Li J, Noorwez SM, Malhotra R, McDowell JH, Kaushal S, Hauswirth WW, Nusinowitz S, Thompson DA, Heckenlively JR (2005) Retinal degeneration 12 (rd12): a new, spontaneously arising mouse model for human Leber congenital amaurosis (LCA). Mol Vis 11:152–162.

Pang J-J, Chang B, Kumar A, Nusinowitz S, Noorwez SM, Li J, Rani A, Foster TC, Chiodo VA, Doyle T, Li H, Malhotra R, Teusner JT, McDowell JH, Min S-H, Li Q, Kaushal S, Hauswirth WW (2006) Gene therapy restores vision-dependent behavior as well as retinal structure and function in a mouse model of RPE65 Leber congenital amaurosis. Mol Ther 13:565–572.

Panickar KS, Norenberg MD (2005) Astrocytes in cerebral ischemic injury: Morphological and general considerations. Glia 50:287–298.

Pardue MT, Stubbs EB, Perlman JI, Narfström K, Chow AY, Peachey NS (2001) Immunohistochemical studies of the retina following long-term implantation with subretinal microphotodiode arrays. Exp Eye Res 73:333–343.

Parmeggiani F (2011) Clinics, epidemiology and genetics of retinitis pigmentosa. Curr Genomics 12:236–237.

Pearson RA (2014) Advances in repairing the degenerate retina by rod photoreceptor transplantation. Biotechnol Adv 32:485–491.

Pearson RA, Barber AC, Rizzi M, Hippert C, Xue T, West EL, Duran Y, Smith AJ, Chuang JZ, Azam SA, Luhmann UFO, Benucci A, Sung CH, Bainbridge JW, Carandini M, Yau KW, Sowden JC, Ali RR (2012) Restoration of vision after transplantation of photoreceptors. Nat 485:99–103.

Pearson RA, Barber AC, West EL, MacLaren RE, Duran Y, Bainbridge JW, Sowden JC, Ali RR (2010) Targeted disruption of outer limiting membrane junctional proteins (Crb1 and ZO-1) increases integration of transplanted photoreceptor precursors into the adult wild-type and degenerating retina. Cell Transplant 19:487–503.

Pearson RA, Hippert C, Graca AB, Barber AC (2014) Photoreceptor replacement therapy: challenges presented by the diseased recipient retinal environment. Vis Neurosci 31:333–344.

Pease ME, Zack DJ, Berlinicke C, Bloom K, Cone F, Wang Y, Klein RL, Hauswirth WW, Quigley HA (2009) Effect of CNTF on retinal ganglion cell survival in experimental glaucoma. Invest Ophthalmol Vis Sci 50:2194–2200.

Pekny M, Levéen P, Pekna M, Eliasson C, Berthold CH, Westermark B, Betsholtz C (1995) Mice lacking glial fibrillary acidic protein display astrocytes devoid of intermediate filaments but develop and reproduce normally. EMBO J 14:1590–1598.

Pekny M, Nilsson M (2005) Astrocyte activation and reactive gliosis. Glia 50:427–434.

Pellikka M, Tanentzapf G, Pinto M, Smith C, McGlade CJ, Ready DF, Tepass U (2002) Crumbs, the Drosophila homologue of human CRB1/RP12, is essential for photoreceptor morphogenesis. Nat 416:143–149.

Pellissier LP, Alves CH, Quinn PM, Vos RM (2013) Targeted ablation of crb1 and crb2 in retinal progenitor cells mimics leber congenital amaurosis. PLoS Genet 9(12):e1003976.

Pellissier LP, Lundvig DMS, Tanimoto N, Klooster J, Vos RM, Richard F, Sothilingam V, Garcia Garrido M, Le Bivic A, Seeliger MW, Wijnholds J (2014) CRB2 acts as a modifying factor of CRB1-related retinal dystrophies in mice. Hum Mol Genet 23:3759–3771.

Peng Y-W, Zallocchi M, Meehan DT, Delimont D, Chang B, Hawes N, Wang W, Cosgrove D (2008) Progressive morphological and functional defects in retinas from alpha1 integrin-null mice. Invest Ophthalmol Vis Sci 49:4647–4654.

Perez-Moreno M, Fuchs E (2006) Catenins: Keeping Cells from Getting Their Signals Crossed. Dev Cell 11(5): 1–612.

Perron M, Harris WA (2000) Retinal stem cells in vertebrates. Bioessays 22:685–688.

Petito CK, Morgello S, Felix JC, Lesser ML (1990) The two patterns of reactive astrocytosis in postischemic rat brain. J Cereb Blood Flow Metab 10:850–859.

Pokutta S, Weis WI (2007) Structure and Mechanism of Cadherins and Catenins in Cell-Cell Contacts. Annu Rev Cell Dev Biol 23:237–261.

Popp S, Maurel P, Andersen JS, Margolis RU (2004) Developmental changes of aggrecan, versican and neurocan in the retina and optic nerve. Exp Eye Res 79:351–356.

Properzi F, Asher RA, Fawcett JW (2003) Chondroitin sulphate proteoglycans in the central nervous system: changes and synthesis after injury. Biochem Soc Trans 31:335–336.

Pujic Z, Malicki J (2004) Retinal pattern and the genetic basis of its formation in zebrafish. Semin Cell Dev Biol 15:105–114.

Punzo C, Cepko C (2007) Cellular responses to photoreceptor death in the rd1 mouse model of retinal degeneration. Invest Ophthalmol Vis Sci 48:849–857.

Qiu G, Seiler MJ, Mui C, Arai S, Aramant RB (2005) Photoreceptor differentiation and integration of retinal progenitor cells transplanted into transgenic rats. Exp Eye Res 80:515–525.

Rachel RA, Li T, Swaroop A (2012) Photoreceptor sensory cilia and ciliopathies: focus

on CEP290, RPGR and their interacting proteins. Cilia 1:22.

Radtke ND, Aramant RB, Petry HM, Green PT, Pidwell DJ, Seiler MJ (2008) Vision Improvement in Retinal Degeneration Patients by Implantation of Retina Together with Retinal Pigment Epithelium. J Ophthalmol 146:172–182.e1.

Radtke ND, Aramant RB, Seiler M, Petry HM (1999) Preliminary report: indications of improved visual function after retinal sheet transplantation in retinitis pigmentosa patients. J Ophthalmol 128:384–387.

Ramachandran R, Fausett BV, Goldman D (2010) Ascl1a regulates Müller glia dedifferentiation and retinal regeneration through a Lin-28-dependent, let-7 microRNA signalling pathway. Nat Cell Biol 12:1101–1107.

Randlett O, Norden C, Harris WA (2011) The vertebrate retina: A model for neuronal polarization in vivo. Dev Neurobio 71:567–583.

Redmond TM, Poliakov E, Yu S, Tsai J-Y, Lu Z, Gentleman S (2005) Mutation of key residues of RPE65 abolishes its enzymatic role as isomerohydrolase in the visual cycle. Proc Natl Acad Sci 102:13658–13663.

Redmond TM, Yu S, Lee E, Bok D, Hamasaki D, Chen N, Goletz P, Ma J-X, Crouch RK, Pfeifer K (1998) Rpe65 is necessary for production of 11-cis-vitamin A in the retinal visual cycle. Nat Genet 20:344–350.

Reese BE (2011) Development of the retina and optic pathway. Vis Res 51:613–632.

Rehemtulla A, Warwar R, Kumar R, Ji X, Zack DJ, Swaroop A (1996) The basic motif-leucine zipper transcription factor Nrl can positively regulate rhodopsin gene expression. Proc Natl Acad Sci 93:191–195.

Reicher S, Seroussi E, Gootwine E (2010) A mutation in gene CNGA3 is associated with day blindness in sheep. Genomics 95:101–104.

Richard M, Roepman R, Aartsen WM, van Rossum AGSH, Hollander den AI, Knust E, Wijnholds J, Cremers FPM (2006) Towards understanding CRUMBS function in retinal dystrophies. Hum Mol Genet 15 Spec No 2:R235–R243.

Ridet JL, Malhotra SK, Privat A, Gage FH (1997) Reactive astrocytes: cellular and molecular cues to biological function. Trends Neurosci 20:570–577.

Roesch K, Jadhav AP, Trimarchi JM, Stadler MB, Roska B, Ben B Sun, Cepko CL (2008) The transcriptome of retinal Müller glial cells. J Comp Neurol 509:225–238.

Roesch K, Stadler MB, Cepko CL (2012) Gene expression changes within Müller glial cells in retinitis pigmentosa. Mol Vis 18:1197–1214.

Roitbak T, Syková E (1999) Diffusion barriers evoked in the rat cortex by reactive astrogliosis. Glia 28:40–48.

Roof DJ, Adamian M, Hayes A (1994) Rhodopsin accumulation at abnormal sites in retinas of mice with a human P23H rhodopsin transgene. Invest Ophthalmol Vis Sci 35:4049–4062.

Ruoslahti E (1989) Proteoglycans in cell regulation. J Biol Chem 264:13369–13372.

Sabel BA (2008) Plasticity and restoration of vision after visual system damage: an update. Restor Neurol Neurosci 26:243–247.

Sahel JA, Albert DM, Lessell S (1990) Proliferation of retinal glia and excitatory amino acids. Ophtalmologie 4:13–16.

Saint-Geniez M, Kurihara T, Sekiyama E, Maldonado AE, D'Amore PA (2009) An essential role for RPE-derived soluble VEGF in the maintenance of the choriocapillaris. Proc Natl Acad Sci 106:18751–18756.

Saint-Geniez M, Maharaj ASR, Walshe TE, Tucker BA, Sekiyama E, Kurihara T, Darland DC, Young MJ, D'Amore PA (2008) Endogenous VEGF Is Required for Visual Function: Evidence for a Survival Role on Müller Cells and Photoreceptors. PLoS ONE 3:e3554.

Sakaguchi DS, Van Hoffelen SJ, Grozdanic SD, Kwon YH, Kardon RH, Young MJ (2005) Neural progenitor cell transplants into the developing and mature central nervous system. Ann N Y Acad Sci 1049:118–134.

Sakaguchi DS, Van Hoffelen SJ, Theusch E, Parker E, Orasky J, Harper MM, Benediktsson A, Young MJ (2004) Transplantation of neural progenitor cells into the developing retina of the Brazilian opossum: an in vivo system for studying stem/progenitor cell plasticity. Dev Neurosci 26:336–345.

Samardzija M, Caprara C, Heynen SR, Willcox DeParis S, Meneau I, Traber G, Agca C, Lintig von J, Grimm C (2014) A mouse model for studying cone photoreceptor pathologies. Invest Ophthalmol Vis Sci 55:5304–5313.

Samardzija M, Lintig von J, Tanimoto N, Oberhauser V, Thiersch M, Reme CE, Seeliger M, Grimm C, Wenzel A (2007) R91W mutation in Rpe65 leads to milder

early-onset retinal dystrophy due to the generation of low levels of 11-cis-retinal. Hum Mol Genet 17:281–292.

Sanes JR, Masland RH (2015) The types of retinal ganglion cells: current status and implications for neuronal classification. Annu Rev Neurosci 38:221–246.

Santos-Ferreira T, Postel K, Stutzki H, Kurth T, Zeck G, Ader M (2014) Daylight Vision Repair by Cell Transplantation. Stem Cells 33:79–90.

Sanyal S, Bal AK (1973) Comparative light and electron microscopic study of retinal histogenesis in normal and rd mutant mice. Z Anat Entwicklungsgesch 142:219–238.

Sarra GM, Stephens C, de Alwis M, Bainbridge JW, Smith AJ, Thrasher AJ, Ali RR (2001) Gene replacement therapy in the retinal degeneration slow (rds) mouse: the effect on retinal degeneration following partial transduction of the retina. Hum Mol Genet 10:2353–2361.

Sarthy PV (1985) Establishment of Muller cell cultures from adult rat retina. Brain Res 337:138–141.

Sarthy V, Egal H (1995) Transient induction of the glial intermediate filament protein gene in Müller cells in the mouse retina. DNA Cell Biol 14:313–320.

Sato Y, Nakanishi K, Tokita Y, Kakizawa H, Ida M, Maeda H, Matsui F, Aono S, Saito A, Kuroda Y, Hayakawa M, Kojima S, Oohira A (2008) A highly sulfated chondroitin sulfate preparation, CS-E, prevents excitatory amino acid-induced neuronal cell death. J Neurochem 104:1565–1576.

Sawides L, de Castro A, Burns SA (2016) The organization of the cone photoreceptor mosaic measured in the living human retina. Vision Res pii: S0042-6989(16)30049-9.

Schmidt-Kastner R, Szymas J, Hossmann K-A (1990) Immunohistochemical study of glial reaction and serum-protein extravasation in relation to neuronal damage in rat hippocampus after ischemia. Neurosci 38:527–540.

Schumer RA, Podos SM (1994) The nerve of glaucoma! Arch Ophthalmol 112:37–44.

Schwartz NB, Domowicz M, Krueger RC, Li H, Mangoura D (1996) Brain aggrecan. Perspect Dev Neurobiol 3:291–306.

Schwartz SD, Hubschman J-P, Heilwell G, Franco-Cardenas V, Pan CK, Ostrick RM,

Mickunas E, Gay R, Klimanskaya I, Lanza R (2012) Embryonic stem cell trials for macular degeneration: a preliminary report. Lancet 379:713–720.

Seiler MJ, Aramant RB (2012) Cell replacement and visual restoration by retinal sheet transplants. Prog Retin Eye Res 31:661–687.

Seiler MJ, Aramant RB, Seeliger MW, Bragadottir R, Mahoney M, Narfstrom K (2009) Functional and structural assessment of retinal sheet allograft transplantation in feline hereditary retinal degeneration. Vet Ophthalmol 12:158–169.

Seoane A, Espejo M, Pallàs M, Rodríguez-Farré E, Ambrosio S, Llorens J (1999) Degeneration and gliosis in rat retina and central nervous system following 3,3'-iminodipropionitrile exposure. Brain Res 833:258–271.

Sernagor E (2005) Retinal development: second sight comes first. Curr Biol 15:R556–R559.

Sethi CS, Lewis GP, Fisher SK, Leitner WP, Mann DL, Luthert PJ, Charteris DG (2005) Glial remodeling and neural plasticity in human retinal detachment with proliferative vitreoretinopathy. Invest Ophthalmol Vis Sci 46:329–342.

Sharma K, Selzer ME, Li S (2012) Scar-mediated inhibition and CSPG receptors in the CNS.Exp Neuro 237:370–378.

Sheedlo HJ, Jaynes D, Bolan AL, Turner JE (1995) Mullerian glia in dystrophic rodent retinas: an immimocytochemical analysis. Brain Res Dev Brain Res 85:171–180.

Shen Y, Tenney AP, Busch SA, Horn KP, Cuascut FX, Liu K, He Z, Silver J, Flanagan JG (2009) PTPsigma is a receptor for chondroitin sulfate proteoglycan, an inhibitor of neural regeneration. Sci 326:592–596.

Siebert JR, Conta Steencken A, Osterhout DJ (2014) Chondroitin sulfate proteoglycans in the nervous system: inhibitors to repair. Biomed Res Int 2014:845323.

Siebert JR, Osterhout DJ (2011) The inhibitory effects of chondroitin sulfate proteoglycans on oligodendrocytes. J Neurochem 119:176–188.

Silver J, Miller JH (2004) Regeneration beyond the glial scar. Nat Rev Neurosci 5:146–156.

Simó R, Hernández C (2015) Novel approaches for treating diabetic retinopathy based on recent pathogenic evidence. Prog Retin Eye Res 48:160–180.

Singhal S, Bhatia B, Jayaram H, Becker S, Jones MF, Cottrill PB, Khaw PT, Salt TE, Limb GA (2012) Human Muller Glia with Stem Cell Characteristics Differentiate into Retinal Ganglion Cell (RGC) Precursors In Vitro and Partially Restore RGC Function In Vivo Following Transplantation. Stem Cells Transl Med 1:188–199.

Singhal S, Lawrence JM, Bhatia B, Ellis JS, Kwan AS, MacNeil A, Luthert PJ, Fawcett JW, Perez M-T, Khaw PT, Limb GA (2008) Chondroitin sulfate proteoglycans and microglia prevent migration and integration of grafted Müller stem cells into degenerating retina. Stem Cells 26:1074–1082.

Smith GM, Strunz C (2005) Growth factor and cytokine regulation of chondroitin sulfate proteoglycans by astrocytes. Glia 52:209–218.

Snow DM, Lemmon V, Carrino DA, Caplan AI, Silver J (1990) Sulfated proteoglycans in astroglial barriers inhibit neurite outgrowth in vitro. Exp Neuro 109:111–130.

Snow DM, Letourneau PC (1992) Neurite outgrowth on a step gradient of chondroitin sulfate proteoglycan (CS-PG). J Neurobiol 23:322–336.

Sobel RA, Ahmed AS (2001) White matter extracellular matrix chondroitin sulfate/dermatan sulfate proteoglycans in multiple sclerosis. J Neuropathol Exp Neurol 60:1198–1207.

Sofroniew MV (2005) Reactive astrocytes in neural repair and protection. The Neuroscientist 11:400–407.

Stacy RC (2005) Disruption and Recovery of Patterned Retinal Activity in the Absence of Acetylcholine. J Neurosci 25:9347–9357.

Stingl K, Bartz-Schmidt K-U, Gekeler F, Kusnyerik A, Sachs H, Zrenner E (2013) Functional outcome in subretinal electronic implants depends on foveal eccentricity. Invest Ophthalmol Vis Sci 54:7658–7665.

Stingl K, Zrenner E (2013) Electronic approaches to restitute vision in patients with neurodegenerative diseases of the retina. Ophthalmic Res 50:215–220.

Stone J, van Driel D, Valter K, Rees S, Provis J (2008) The locations of mitochondria in mammalian photoreceptors: relation to retinal vasculature. Brain Res 1189:58–69.

Strettoi E, Pignatelli V, Rossi C, Porciatti V, Falsini B (2003) Remodeling of second-order neurons in the retina of rd/rd mutant mice. Vis Res 43:867–877.

Strettoi E, Porciatti V, Falsini B, Pignatelli V, Rossi C (2002) Morphological and

functional abnormalities in the inner retina of the rd/rd mouse. J Neurosci 22:5492–5504.

Strom TM, Nyakatura G, Apfelstedt-Sylla E, Hellebrand H, Lorenz B, Weber BH, Wutz K, Gutwillinger N, Rüther K, Drescher B, Sauer C, Zrenner E, Meitinger T, Rosenthal A, Meindl A (1998) An L-type calcium-channel gene mutated in incomplete X-linked congenital stationary night blindness. Nat Genet 19:260–263.

Stuck MW, Conley SM, Naash MI (2012) Defects in the Outer Limiting Membrane Are Associated with Rosette Development in the Nrl−/− Retina Lewin A, ed. PLoS ONE 7:e32484.

Sullivan RKP, Woldemussie E, Pow DV (2007) Dendritic and synaptic plasticity of neurons in the human age-related macular degeneration retina. Invest Ophthalmol Vis Sci 48:2782–2791.

Suzuki T, Akimoto M, Imai H, Ueda Y, Mandai M, Yoshimura N, Swaroop A, Takahashi M (2007) Chondroitinase ABC treatment enhances synaptogenesis between transplant and host neurons in model of retinal degeneration. cell transplant 16:493–503.

Swaroop A, Kim D, Forrest D (2010) Transcriptional regulation of photoreceptor development and homeostasis in the mammalian retina. Nat Rev Neurosci 11:563–576.

Swaroop A, Xu JZ, Pawar H, Jackson A, Skolnick C, Agarwal N (1992) A conserved retina-specific gene encodes a basic motif/leucine zipper domain. Proc Natl Acad Sci USA 89:266–270.

Takahashi M, Miyoshi H, Verma IM, Gage FH (1999) Rescue from Photoreceptor Degeneration in therd Mouse by Human Immunodeficiency Virus Vector-Mediated Gene Transfer. J Virol 73:7812–7816.

Takeichi M (1991) Cadherin cell adhesion receptors as a morphogenetic regulator. Sci 251:1451–1455.

Tan CL, Andrews MR, Kwok JCF, Heintz TGP, Gumy LF, Fässler R, Fawcett JW (2012) Kindlin-1 Enhances Axon Growth on Inhibitory Chondroitin Sulfate Proteoglycans and Promotes Sensory Axon Regeneration. J Neurosci 32:7325–7335.

Tan CL, Kwok JCF, Patani R, ffrench-Constant C, Chandran S, Fawcett JW (2011)

Integrin Activation Promotes Axon Growth on Inhibitory Chondroitin Sulfate Proteoglycans by Enhancing Integrin Signaling. J Neurosci 31:6289–6295.

Tang BL (2001) ADAMTS: a novel family of extracellular matrix proteases. Int J Biochem Cell Biol 33:33–44.

Tang X, Davies JE, Davies SJA (2003) Changes in distribution, cell associations, and protein expression levels of NG2, neurocan, phosphacan, brevican, versican V2, and tenascin-C during acute to chronic maturation of spinal cord scar tissue. J Neurosci Res 71:427–444.

Tatzelt J, Maeda N, Pekny M, Yang SL, Betsholtz C, Eliasson C, Cayetano J, Camerino AP, DeArmond SJ, Prusiner SB (1996) Scrapie in mice deficient in apolipoprotein E or glial fibrillary acidic protein. Neurology 47:449–453.

Taylor KR (2006) Glycosaminoglycans and their proteoglycans: host-associated molecular patterns for initiation and modulation of inflammation. FASEB J 20:9–22.

Tepass U, Theres C, Knust E (1990) crumbsencodes an EGF-like protein expressed on apical membranes of Drosophila epithelial cells and required for organization of epithelia. Cell 61:787–799.

Testa F, Maguire AM, Rossi S, Pierce EA, Melillo P, Marshall K, Banfi S, Surace EM, Sun J, Acerra C, Wright JF, Wellman J, High KA, Auricchio A, Bennett J, Simonelli F (2013) Three-year follow-up after unilateral subretinal delivery of adeno-associated virus in patients with Leber congenital Amaurosis type 2. Ophthalmol 120:1283–1291.

Tortorella MD (1999) Purification and Cloning of Aggrecanase-1: A Member of the ADAMTS Family of Proteins. Sci 284:1664–1666.

Travis GH, Golczak M, Moise AR, Palczewski K (2007) Diseases Caused by Defects in the Visual Cycle: Retinoids as Potential Therapeutic Agents. Annu Rev Pharmacol Toxicol 47:469–512.

Travis GH, Sutcliffe JG, Bok D (1991) The retinal degeneration slow (rds) gene product is a photoreceptor disc membrane-associated glycoprotein. Neuron 6:61–70.

Tsang KY, Cheung MCH, Chan D, Cheah KSE (2009) The developmental roles of the extracellular matrix: beyond structure to regulation. Cell Tissue Res 339:93–110.

Tsukita S, Furuse M (1999) Occludin and claudins in tight-junction strands: leading or

supporting players? Trends Cell Biol 9:268–273.

Tsukita S, Furuse M, Itoh M (1999) Structural and signalling molecules come together at tight junctions. Curr Opin Cell Biol 11:628–633.

Tucker B, Klassen H, Yang L, Chen DF, Young MJ (2008) Elevated MMP Expression in the MRL Mouse Retina Creates a Permissive Environment for Retinal Regeneration. Invest Ophthalmol Vis Sci 49:1686–1695.

Tucker BA, Park I-H, Qi SD, Klassen HJ, Jiang C, Yao J, Redenti S, Daley GQ, Young MJ (2011) Transplantation of adult mouse iPS cell-derived photoreceptor precursors restores retinal structure and function in degenerative mice. PLoS ONE 6:e18992.

Turner DL, Cepko CL (1987) A common progenitor for neurons and glia persists in rat retina late in development. Nat 328:131–136.

Usuelli V, La Rocca E (2015) Novel therapeutic approaches for diabetic nephropathy and retinopathy. Pharmacol Res 98:39–44.

van de Pavert SA, Kantardzhieva A, Malysheva A, Meuleman J, Versteeg I, Levelt C, Klooster J, Geiger S, Seeliger MW, Rashbass P, Le Bivic A, Wijnholds J (2004) Crumbs homologue 1 is required for maintenance of photoreceptor cell polarization and adhesion during light exposure. J Cell Sci 117:4169–4177.

van de Pavert SA, Sanz AS, Aartsen WM, Vos RM, Versteeg I, Beck SC, Klooster J, Seeliger MW, Wijnholds J (2007) Crb1 is a determinant of retinal apical Müller glia cell features. Glia 55:1486–1497.

Van Itallie CM, Fanning AS, Bridges A, Anderson JM (2009) ZO-1 Stabilizes the Tight Junction Solute Barrier through Coupling to the Perijunctional Cytoskeleton. Mol Biol Cell 20:3930–3940.

van Rossum AGSH, Aartsen WM, Meuleman J, Klooster J, Malysheva A, Versteeg I, Arsanto J-P, Le Bivic A, Wijnholds J (2006) Pals1/Mpp5 is required for correct localization of Crb1 at the subapical region in polarized Muller glia cells. Hum Mol Genet 15:2659–2672.

Vázquez-Chona FR, Clark AM, Levine EM (2009) Rlbp1 promoter drives robust Müller glial GFP expression in transgenic mice. Invest Ophthalmol Vis Sci 50:3996–4003.

Vázquez-Chona FR, Swan A, Ferrell WD, Jiang L, Baehr W, Chien W-M, Fero M, Marc

RE, Levine EM (2011) Proliferative reactive gliosis is compatible with glial metabolic support and neuronal function. BMC Neurosci 12:98.

Vecino E, Rodriguez FD, Ruzafa N, Pereiro X, Sharma SC (2016) Glia-neuron interactions in the mammalian retina. Prog Retin Eye Res 51:1–40.

Veleri S, Lazar CH, Chang B, Sieving PA, Banin E, Swaroop A (2015) Biology and therapy of inherited retinal degenerative disease: insights from mouse models. Dis Model Mech 8:109–129.

Verardo MR, Lewis GP, Takeda M, Linberg KA, Byun J, Luna G, Wilhelmsson U, Pekny M, Chen DF, Fisher SK (2008) Abnormal reactivity of muller cells after retinal detachment in mice deficient in GFAP and vimentin. Invest Ophthalmol Vis Sci 49:3659–3665.

Verderber L, Johnson W, Mucke L, Sarthy V (1995) Differential regulation of a glial fibrillary acidic protein-LacZ transgene in retinal astrocytes and Müller cells. Invest Ophthalmol Vis Sci 36:1137–1143.

Villarroel M, García-Ramírez M, Corraliza L (2009) Effects of high glucose concentration on the barrier function and the expression of tight junction proteins in human retinal pigment epithelial cells. Exp Eye Res 89:913–920.

Vorísek I, Hájek M, Tintera J, Nicolay K, Syková E (2002) Water ADC, extracellular space volume, and tortuosity in the rat cortex after traumatic injury. Magn Reson Med 48:994–1003.

Vugler AA (2010) Progress toward the maintenance and repair of degenerating retinal circuitry. Retina 30:983–1001.

Wald G (1934) Carotenoids and the vitamin A cycle in vision. Nat 134.

Wang H, Katagiri Y, McCann TE, Unsworth E, Goldsmith P, Yu ZX, Tan F, Santiago L, Mills EM, Wang Y, Symes AJ, Geller HM (2008) Chondroitin-4-sulfation negatively regulates axonal guidance and growth. J Cell Sci 121:3083–3091.

Wang M, Ma W, Zhao L, Fariss RN, Wong WT (2011) Adaptive Müller cell responses to microglial activation mediate neuroprotection and coordinate inflammation in the retina. J Neuroinflammation 8:173.

Wanner IB, Anderson MA, Song B, Levine J, Fernandez A, Gray-Thompson Z, Ao Y, Sofroniew MV (2013) Glial scar borders are formed by newly proliferated,

elongated astrocytes that interact to corral inflammatory and fibrotic cells via STAT3-dependent mechanisms after spinal cord injury. J Neurosci 33:12870–12886.

Wehman AM, Staub W, Meyers JR, Raymond PA, Baier H (2005) Genetic dissection of the zebrafish retinal stem-cell compartment. Dev Biol 281:53–65.

Weil D, Levy G, Sahly I, Levi-Acobas F, Blanchard S, El-Amraoui A, Crozet F, Philippe H, Abitbol M, Petit C (1996) Human myosin VIIA responsible for the Usher 1B syndrome: a predicted membrane-associated motor protein expressed in developing sensory epithelia. Proc Natl Acad Sci 93:3232–3237.

West EL, Pearson RA, Barber A, Duran Y, Sowden JC, Ali RR (2010) Immune responses affect the survival of integrated photoreceptor precursors transplanted to the adult murine retina. Invest Ophthalmol Vis Sci 51:5242–5242.

West EL, Pearson RA, Tschernutter M, Sowden JC, MacLaren RE, Ali RR (2008) Pharmacological disruption of the outer limiting membrane leads to increased retinal integration of transplanted photoreceptor precursors. Exp Eye Res 86:601–611.

Westenskow PD, Kurihara T, Aguilar E, Scheppke EL, Moreno SK, Wittgrove C, Marchetti V, Michael IP, Anand S, Nagy A, Cheresh D, Friedlander M (2013) Ras pathway inhibition prevents neovascularization by repressing endothelial cell sprouting. J Clin Invest 123:4900–4908.

Wetts R, Fraser SE (1988) Multipotent precursors can give rise to all major cell types of the frog retina. Sci 239:1142–1145.

Wilhelmsson U1 (2008) Astrocytes, reactive gliosis and CNS regeneration.

Williams DS, Arikawa K, Paallysaho T (1990) Cytoskeletal components of the adherens junctions between the photoreceptors and the supportive Müller cells. J Comp Neurol 295:155–164.

Wittchen ES, Haskins J, Stevenson BR (1999) Protein interactions at the tight junction. Actin has multiple binding partners, and ZO-1 forms independent complexes with ZO-2 and ZO-3. J Biol Chem 274:35179–35185.

Wycisk KA, Budde B, Feil S, Skosyrski S, Buzzi F, Neidhardt J, Glaus E, Nürnberg P, Ruether K, Berger W (2006a) Structural and functional abnormalities of retinal ribbon synapses due to Cacna2d4 mutation. Invest Ophthalmol Vis Sci 47:3523–

3530.

Wycisk KA, Zeitz C, Feil S, Wittmer M, Forster U, Neidhardt J, Wissinger B, Zrenner E, Wilke R, Kohl S, Berger W (2006b) Mutation in the auxiliary calcium-channel subunit CACNA2D4 causes autosomal recessive cone dystrophy. Am J Hum Genet 79:973–977.

Xia X, Li Y, Huang D, Wang Z, Luo L, Song Y, Zhao L, Wen R (2011) Oncostatin M protects rod and cone photoreceptors and promotes regeneration of cone outer segment in a rat model of retinal degeneration. PLoS ONE 6:e18282.

Xu B, Park D, Ohtake Y, Li H, Hayat U, Liu J, Selzer ME, Longo FM, Li S (2015) Role of CSPG receptor LAR phosphatase in restricting axon regeneration after CNS injury. Neurobiol Dis 73:36–48.

Xu H-P, Tian N (2007) Retinal ganglion cell dendrites undergo a visual activity-dependent redistribution after eye opening. J Comp Neurol 503:244–259.

Xue LP, Lu J, Cao Q, Hu S, Ding P, Ling EA (2006) Müller glial cells express nestin coupled with glial fibrillary acidic protein in experimentally induced glaucoma in the rat retina. Neurosci 139:723–732.

Yang P, Seiler MJ, Aramant RB, Whittemore SR (2002) Differential lineage restriction of rat retinal progenitor cells in vitro and in vivo. J Neurosci Res 69:466–476.

Yao J, Ko CW, Baranov PY, Regatieri CV, Redenti S, Tucker BA, Mighty J, Tao SL, Young MJ (2015) Enhanced Differentiation and Delivery of Mouse Retinal Progenitor Cells Using a Micropatterned Biodegradable Thin-Film Polycaprolactone Scaffold. Tissue Eng 21:1247–1260.

Yaron O, Farhy C, Marquardt T, Applebury M, Ashery-Padan R (2006) Notch1 functions to suppress cone-photoreceptor fate specification in the developing mouse retina. Dev133:1367–1378.

Yiu G, He Z (2006) Glial inhibition of CNS axon regeneration. Nat Rev Neurosci 7:617–627.

Young M (2000) Neuronal Differentiation and Morphological Integration of Hippocampal Progenitor Cells Transplanted to the Retina of Immature and Mature Dystrophic Rats. Mol Cell Neurosci 16:197–205.

Young RW (1985) Cell differentiation in the retina of the mouse. Anat Rec 212:199–

205.

Young RW, Bok D (1969) Participation of the retinal pigment epithelium in the rod outer segment renewal process. J Cell Biol 42:392–403.

Yu W-Q, Eom YS, Shin J-A, Nair D, Grzywacz SXZ, Grzywacz NM, Craft CM, Lee E-J (2016) Reshaping the Cone-Mosaic in a Rat Model of Retinitis Pigmentosa: Modulatory Role of ZO-1 Expression in DL-Alpha-Aminoadipic Acid Reshaping. PLoS ONE 11:e0151668.

Zarbin M (2016) Cell-Based Therapy for Degenerative Retinal Disease. Trends Mol Med 22:115–134.

Zencak D, Schouwey K, Chen D, Ekström P, Tanger E, Bremner R, van Lohuizen M, Arsenijevic Y (2013) Retinal degeneration depends on Bmi1 function and reactivation of cell cycle proteins. Proc Natl Acad Sci 110:E593–E601.

Zhang Y, Caffé AR, Azadi S, van Veen T, Ehinger B, Perez M-TR (2003a) Neuronal integration in an abutting-retinas culture system. Invest Ophthalmol Vis Sci 44:4936–4946.

Zhang Y, Kardaszewska AK, van Veen T, Rauch U, Perez M-TR (2004) Integration between abutting retinas: role of glial structures and associated molecules at the interface. Invest Ophthalmol Vis Sci 45:4440–4449.

Zhang Y, Klassen HJ, Tucker BA, Perez M-TR, Young MJ (2007) CNS Progenitor Cells Promote a Permissive Environment for Neurite Outgrowth via a Matrix Metalloproteinase-2-Dependent Mechanism. J Neurosci 27:4499–4506.

Zhang Y, Rauch U, Perez M-TR (2003b) Accumulation of neurocan, a brain chondroitin sulfate proteoglycan, in association with the retinal vasculature in RCS rats. Invest Ophthalmol Vis Sci 44:1252–1261.

Zhao M et al. (2015) A new CRB1 rat mutation links Müller glial cells to retinal telangiectasia. J Neurosci 35:6093–6106.

Zhao X-F, Wan J, Powell C, Ramachandran R, Myers MG, Goldman D (2014) Leptin and IL-6 family cytokines synergize to stimulate Müller glia reprogramming and retina regeneration. Cell Rep 9:272–284.

Zhong X, Gutierrez C, Xue T, Hampton C, Vergara MN, Cao L-H, Peters A, Park TS, Zambidis ET, Meyer JS, Gamm DM, Yau K-W, Canto-Soler MV (2014) Generation

of three-dimensional retinal tissue with functional photoreceptors from human iPSCs. Nat Commun 5: 4047.

Zhou FQ (2006) Neurotrophins support regenerative axon assembly over CSPGs by an ECM-integrin-independent mechanism. J Cell Sci 119:2787–2796.

Zuo J, Neubauer D, Dyess K, Ferguson TA, Muir D (1998) Degradation of chondroitin sulfate proteoglycan enhances the neurite-promoting potential of spinal cord tissue.Exp Neuro 154:654–662.

Appendix

Appendix A. *Assessment of intermediate filament protein GFAP at early (6 weeks), middle (6 months) and late (12 months) time points in wild-type mice.* Cryosections were immunostained for glial cell marker GFAP (green) and counterstained with nuclei marker Hoechst 33342 (blue). Scale bar, 25 µm.

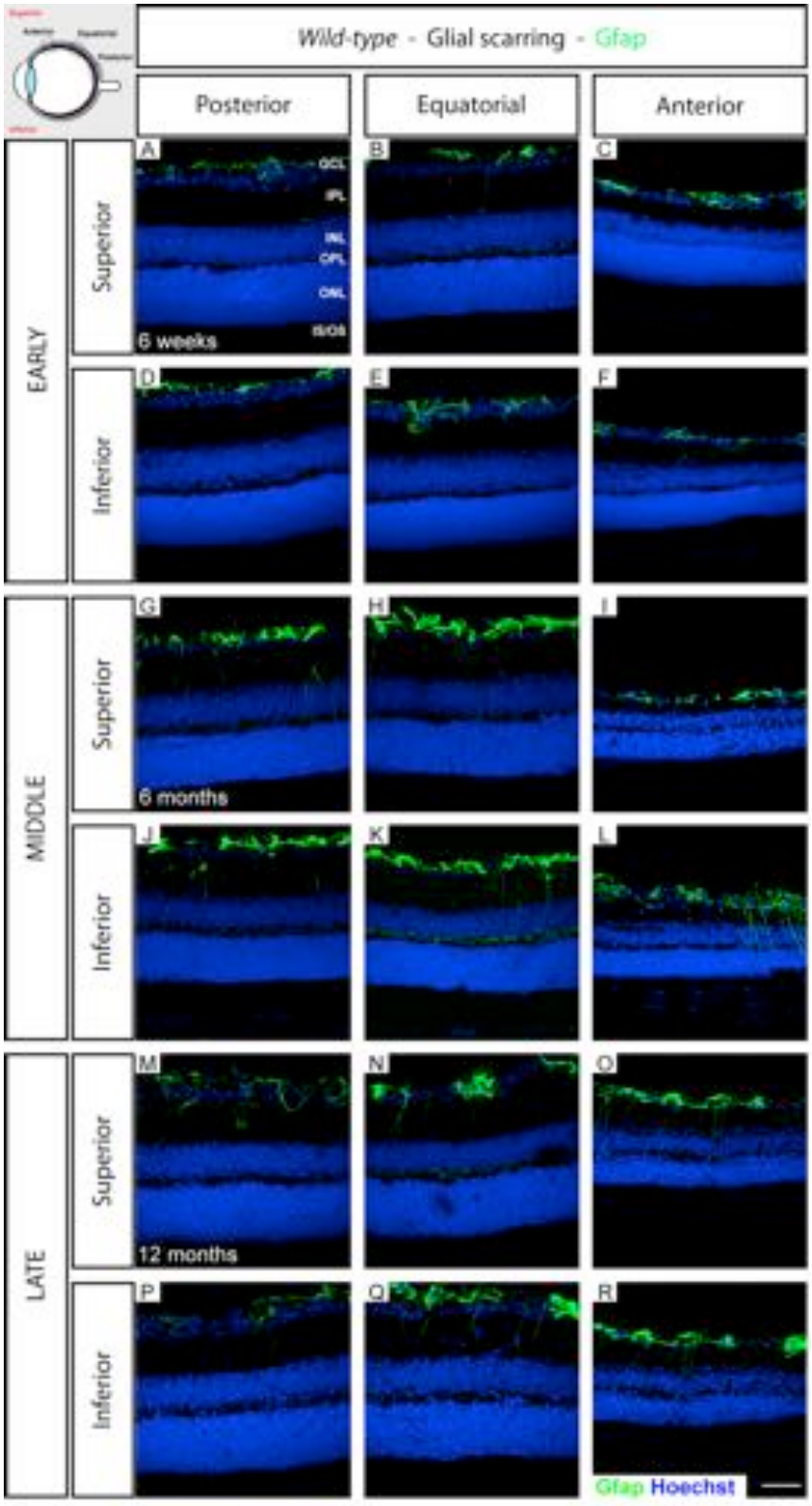

Appendix B. *Assessment of intermediate filament protein Vimentin at early (6 weeks), middle (6 months) and late (12 months) time points in wild-type mice.* Cryosections were immunostained for glial cell marker Vimentin (green) and counterstained with nuclei marker Hoechst 33342 (blue). Scale bar, 25 µm.

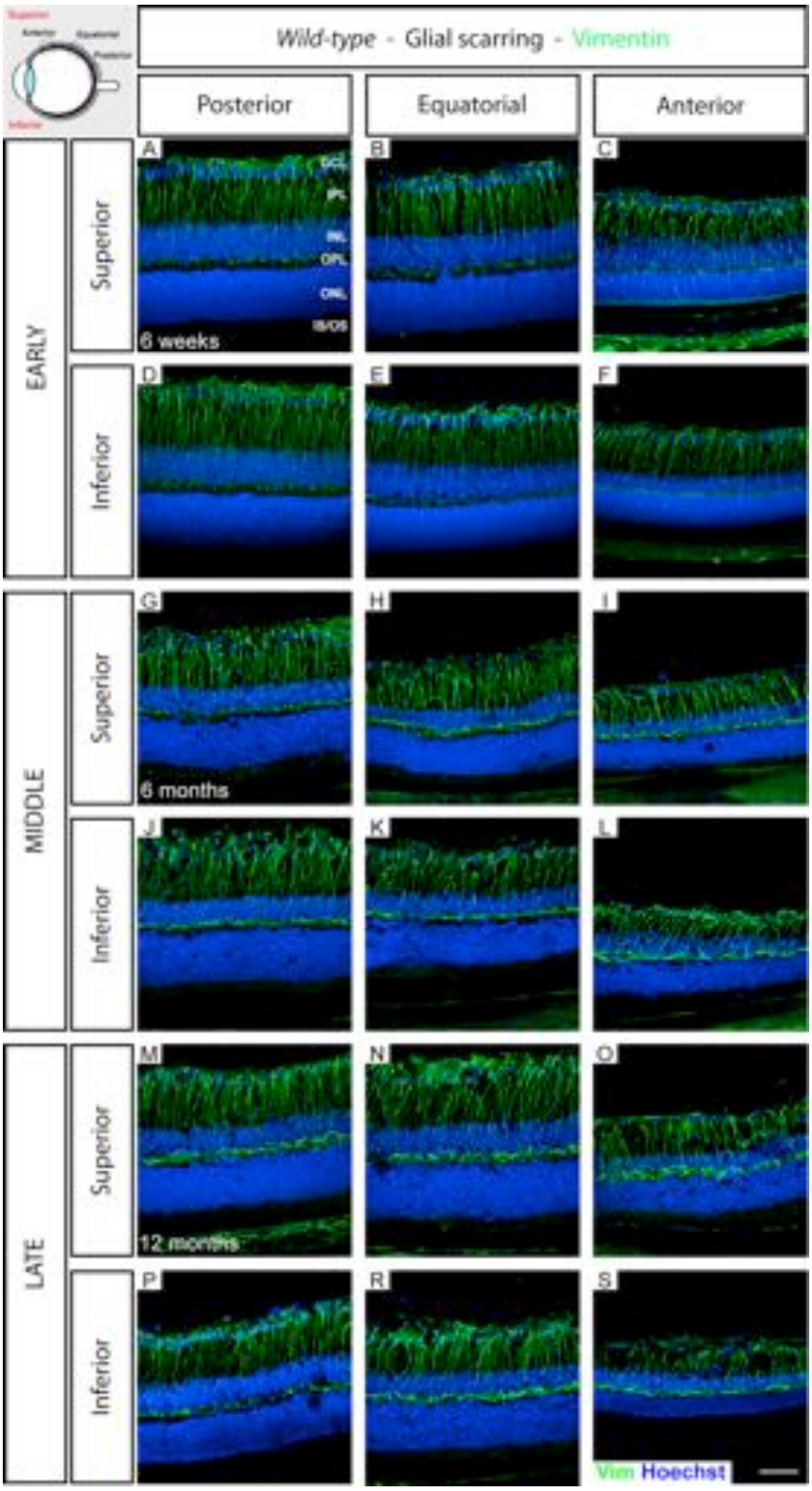

Appendix C. *Assessment of CSPGs deposition at early (6 weeks), middle (6 months) and late (12 months) time points in wild-type mice.* Cryosections were immunostained for CSPGs marker (CS-56; red) and counterstained with nuclei marker Hoechst 33342 (blue). Scale bar, 25 µm.

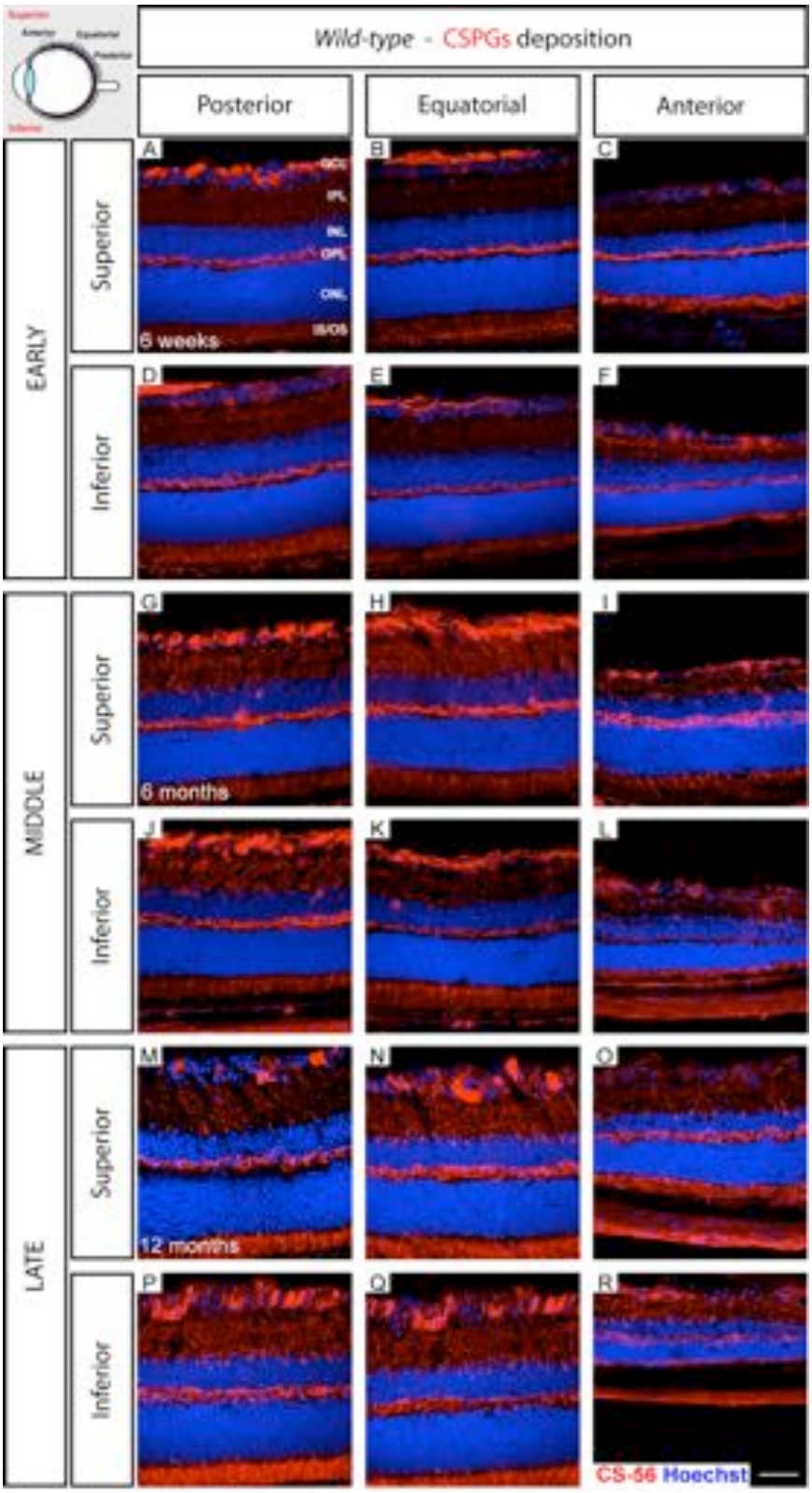

Appendix D. *Assessment of intermediate filament protein GFAP at early (3 weeks), middle (6 weeks) and late (12 weeks) time points in the Crb1$^{rd8/rd8}$ mice.* Cryosections were immunostained for glial cell marker GFAP (green) and counterstained with nuclei marker Hoechst 33342 (blue). Scale bar, 25 µm.

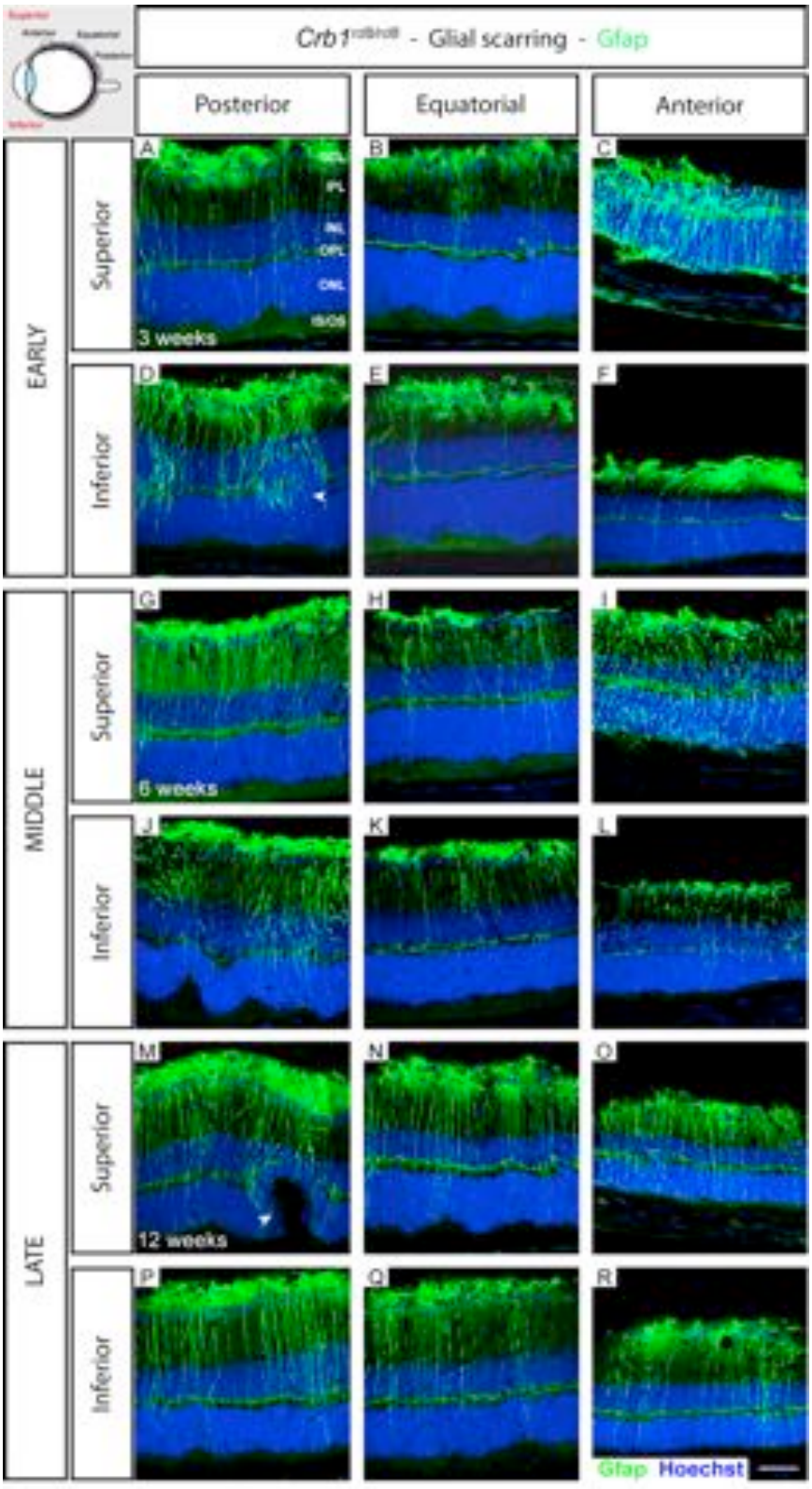

Appendix E. *Assessment of intermediate filament protein Vimentin at early (3 weeks), middle (6 weeks) and late (12 weeks) time points in the Crb1$^{rd8/rd8}$ mice.* Cryosections were immunostained for glial cell marker Vimentin (green) and counterstained with nuclei marker Hoechst 33342 (blue). Scale bar, 25 µm.

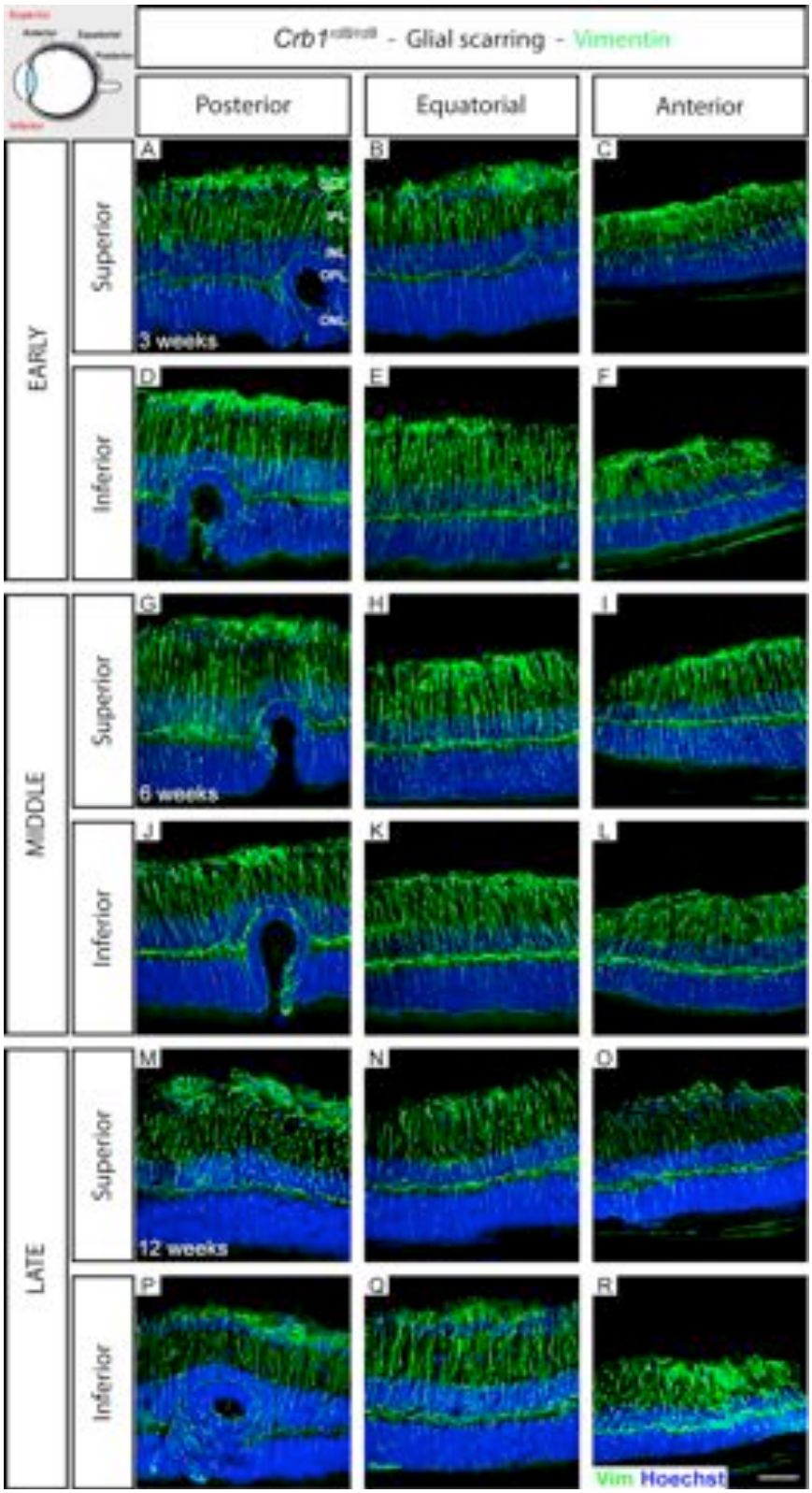

Appendix F. *Assessment of CSPGs deposition at early (3 weeks), middle (6 weeks) and late (12 weeks) time points in the Crb1$^{rd8/rd8}$ mice.* Cryosections were immunostained for CSPGs marker (CS-56; red) and counterstained with nuclei marker Hoechst 33342 (blue). Scale bar, 25 µm.

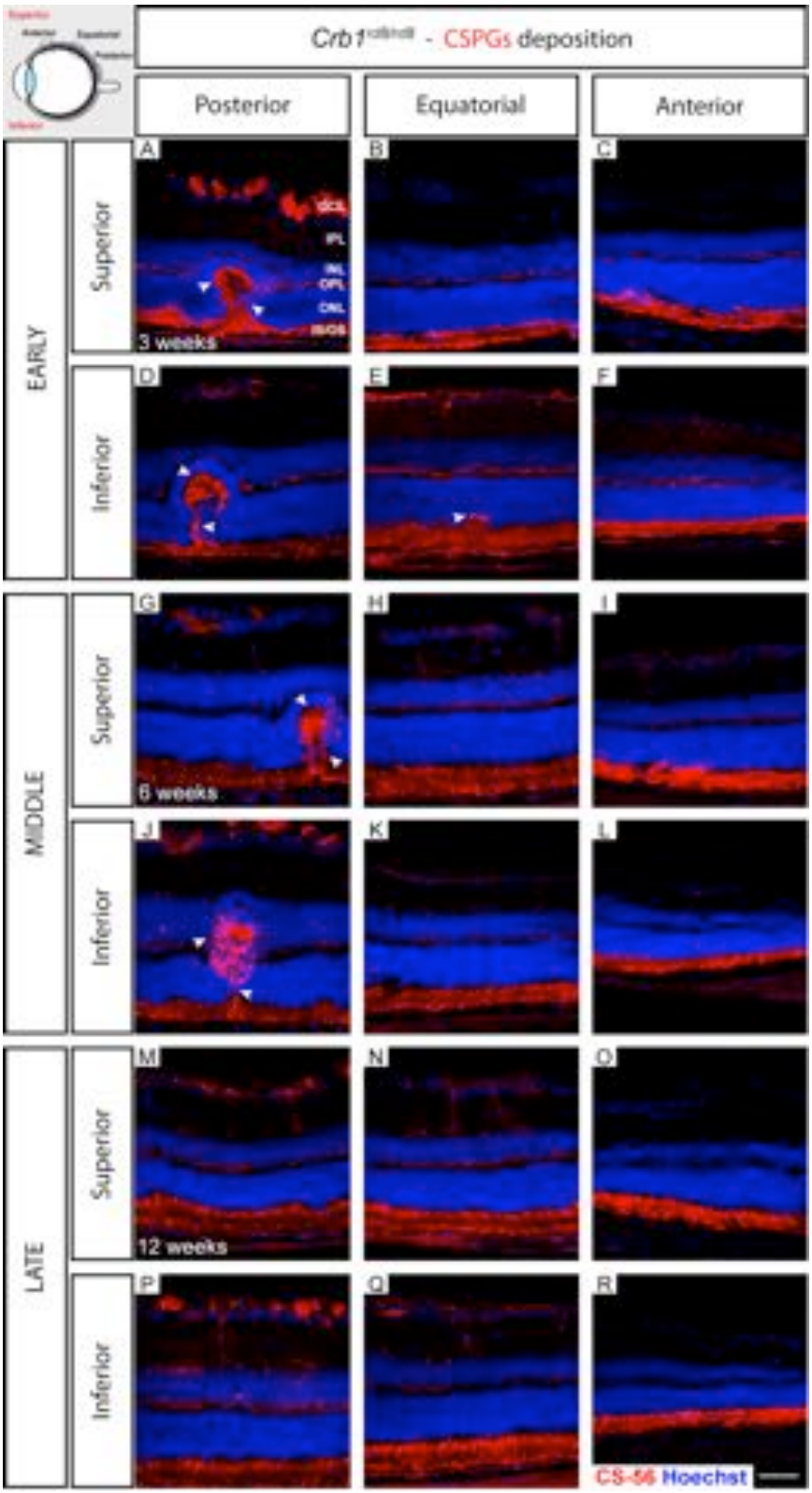

Appendix G. *Assessment of intermediate filament protein GFAP at early (4 weeks), middle (6 weeks) and late (12 weeks) time points in the Rds$^{rd1/rd1}$ mice.* Cryosections were immunostained for glial cell marker GFAP (green) and counterstained with nuclei marker Hoechst 33342 (blue). Scale bar, 25 µm.

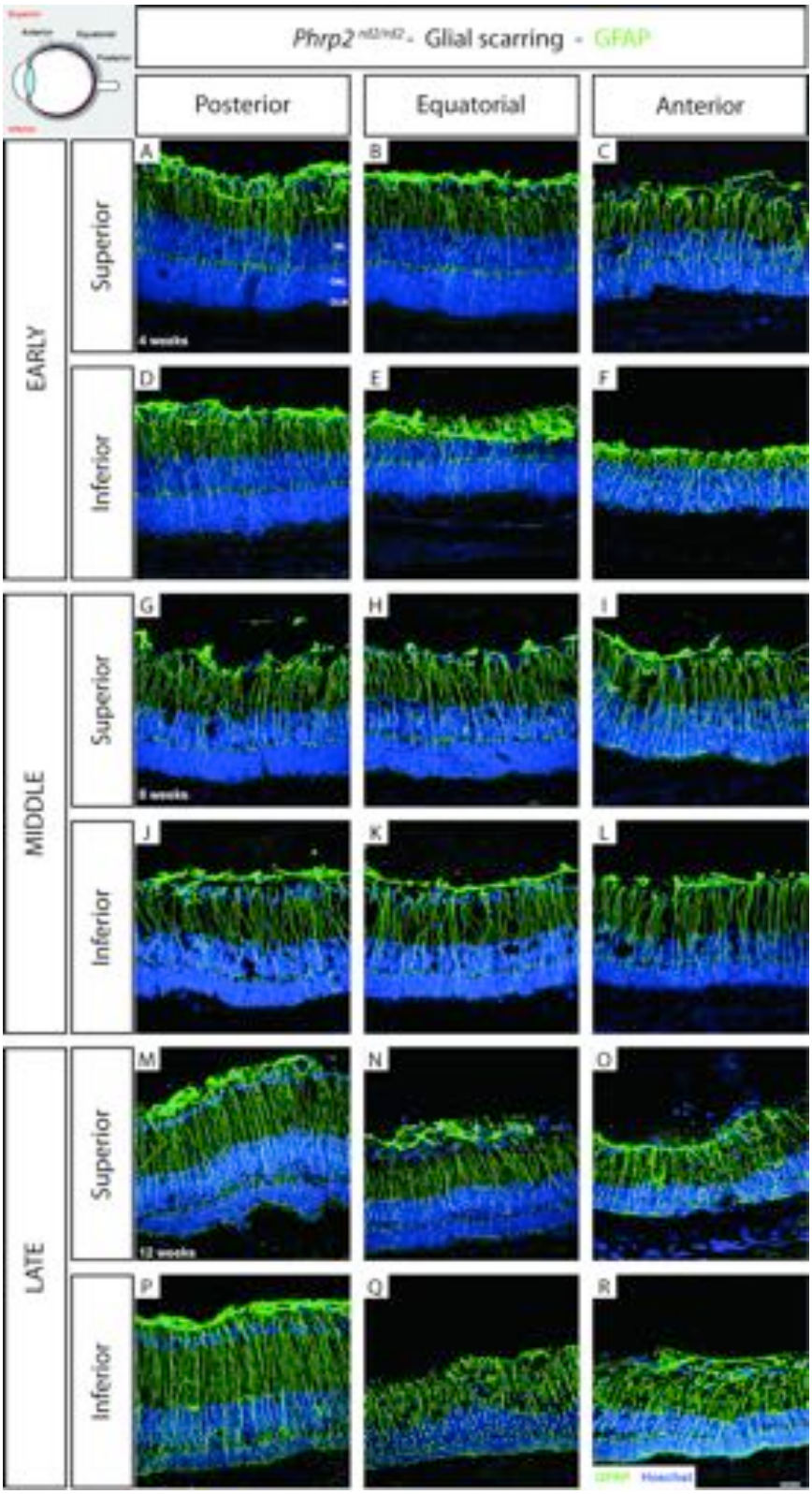

Appendix H. *Assessment of intermediate filament protein Vimentin at early (4 weeks), middle (6 weeks) and late (12 weeks) time points in the Rds$^{rd1/rd1}$ mice.* Cryosections were immunostained for glial cell marker Vimentin (green) and counterstained with nuclei marker Hoechst 33342 (blue). Scale bar, 25 µm.

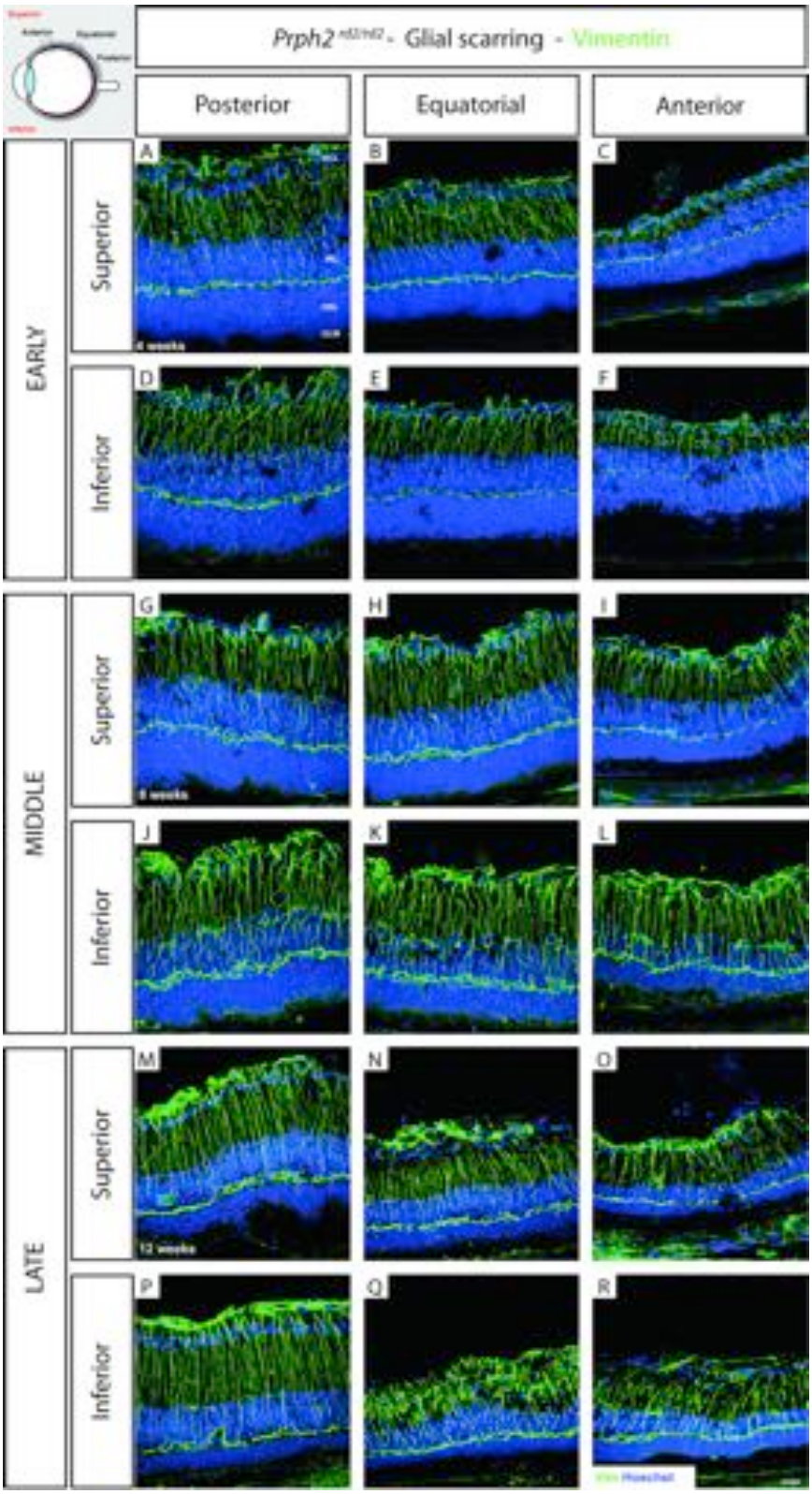

Appendix J. *Assessment of intermediate filament protein GFAP at early(P10), middle (3 weeks) and late (6-7 weeks) time points in the Pde6b*$^{rd1/rd}$ *mice.* Cryosections were immunostained for glial cell marker GFAP (green) and counterstained with nuclei marker Hoechst 33342 (blue). Scale bar, 25 µm.

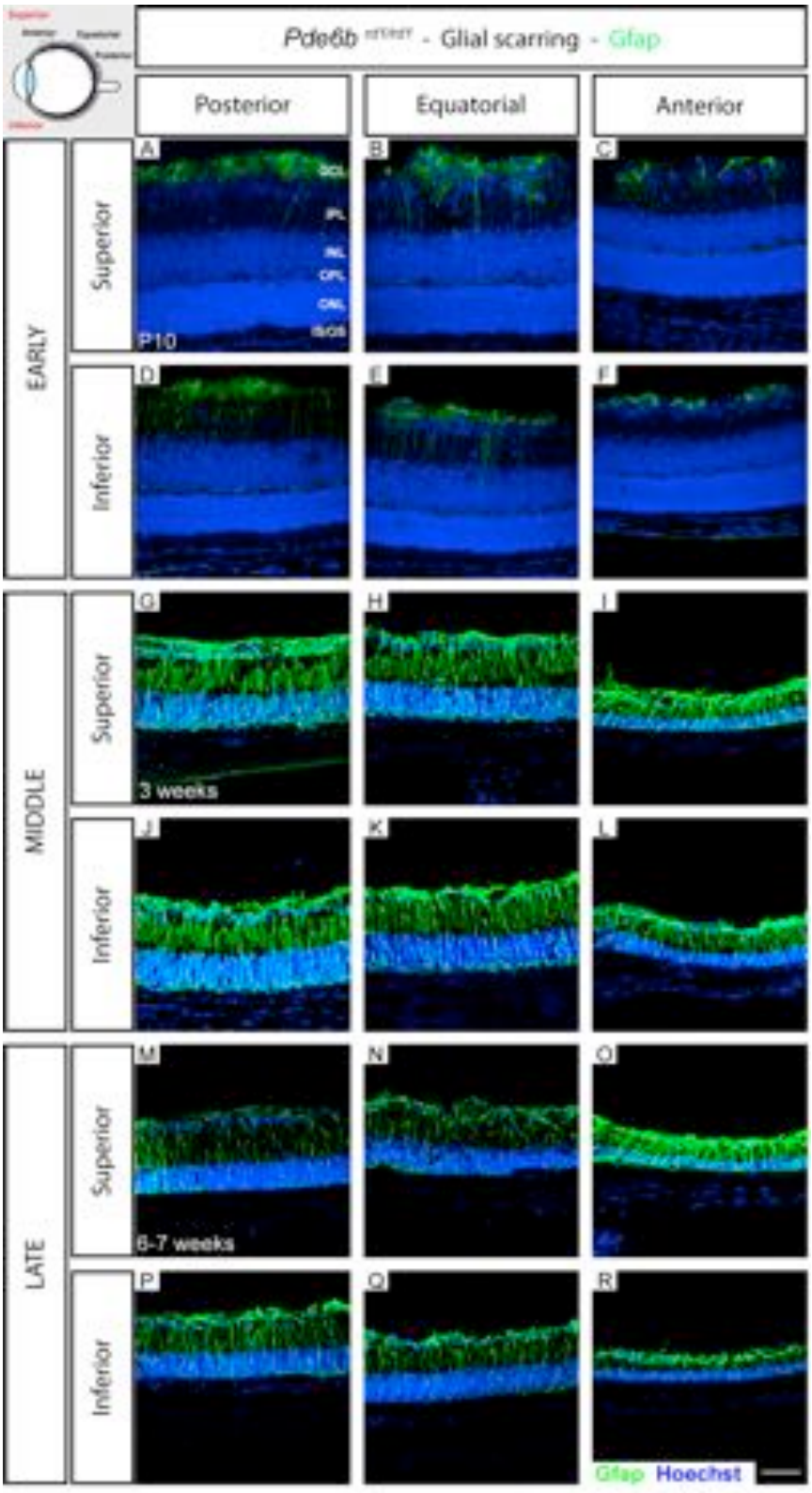

Appendix K. *Assessment of intermediate filament protein Vimentin at early(P10), middle (3 weeks) and late (6-7 weeks) time points in the Pde6b$^{rd1/rd}$ mice.* Cryosections were immunostained for glial cell marker Vimentin (green) and counterstained with nuclei marker Hoechst 33342 (blue). Scale bar, 25 µm.

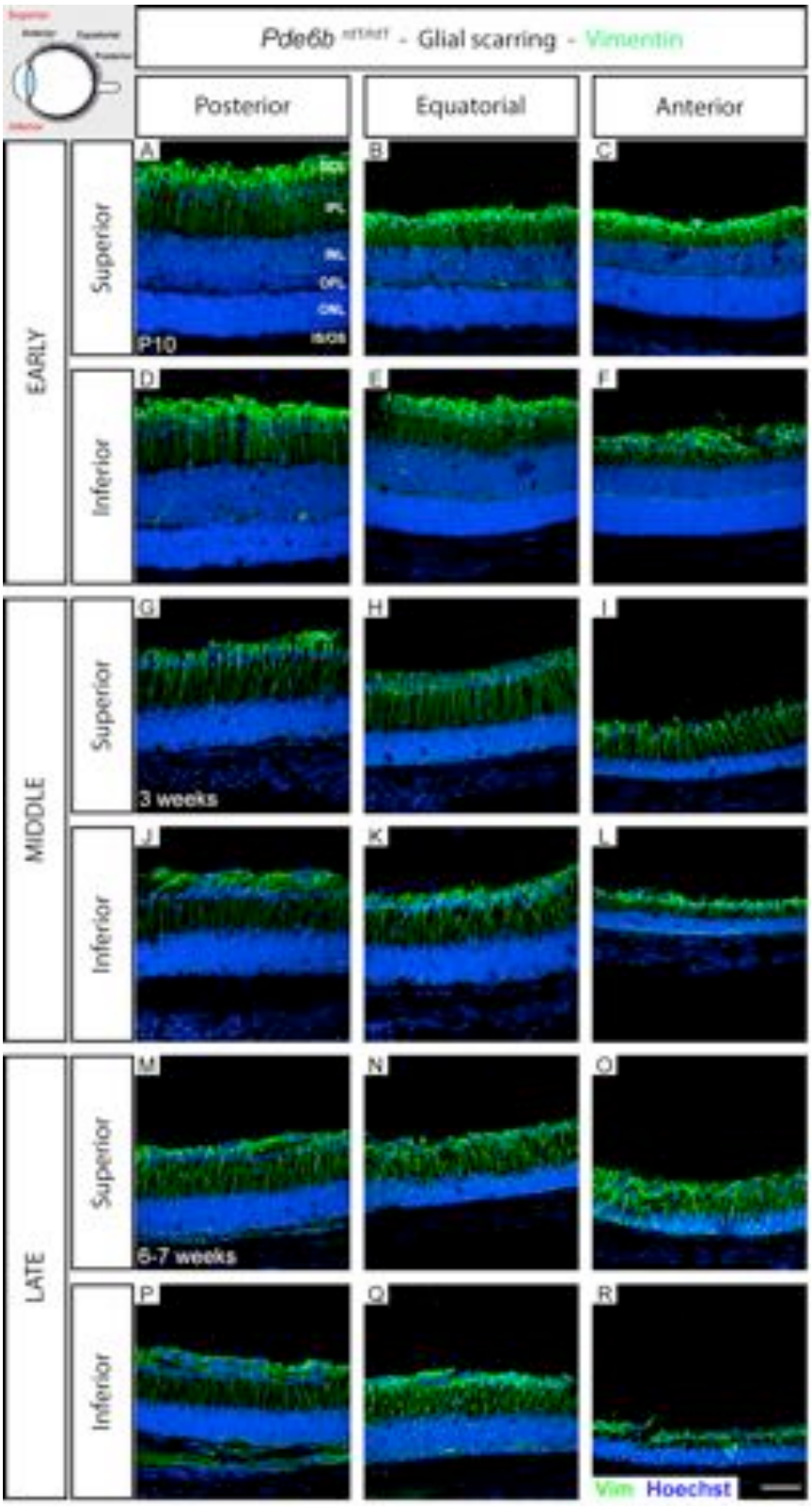

Appendix L. *Assessment of gliosis at P15 in the Pde6b$^{rd1/rd1}$ mice.* Cryosections were immunostained for glial cell marker GFAP (green) or Vimentin (green) or CSPGs (red) and co-stained with nuclei marker Hoechst 33342 (blue). Scale bar, 25 µm.

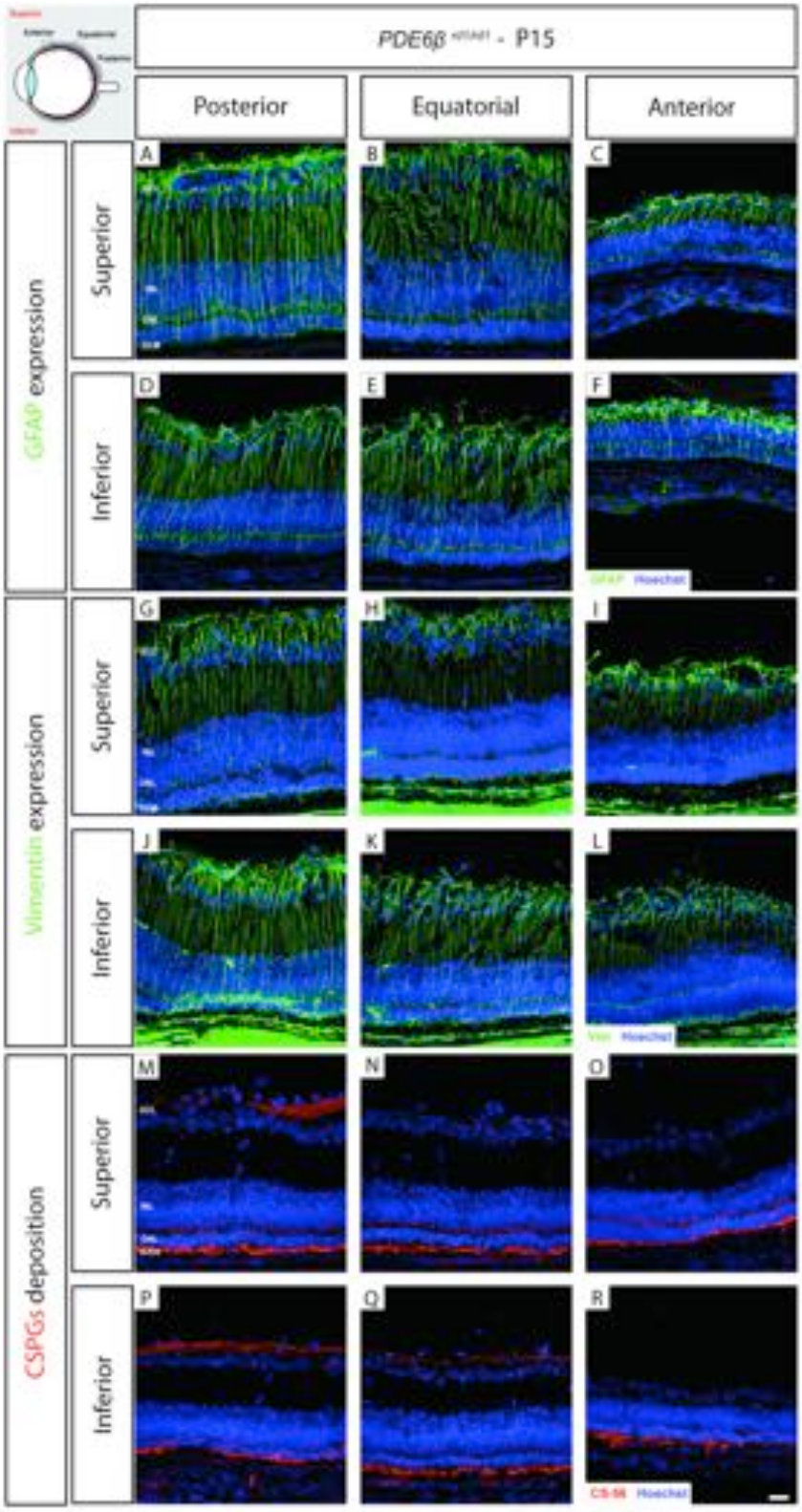

Appendix M. *Assessment of CSPGs deposition at early (P10), middle (3 weeks) and late (6-7 weeks) time points in the Pde6b$^{rd1/rd}$ mice.* Cryosections were immunostained for CSPGs marker (CS-56; red) and counterstained with nuclei marker Hoechst 33342 (blue). Scale bar, 25 µm.

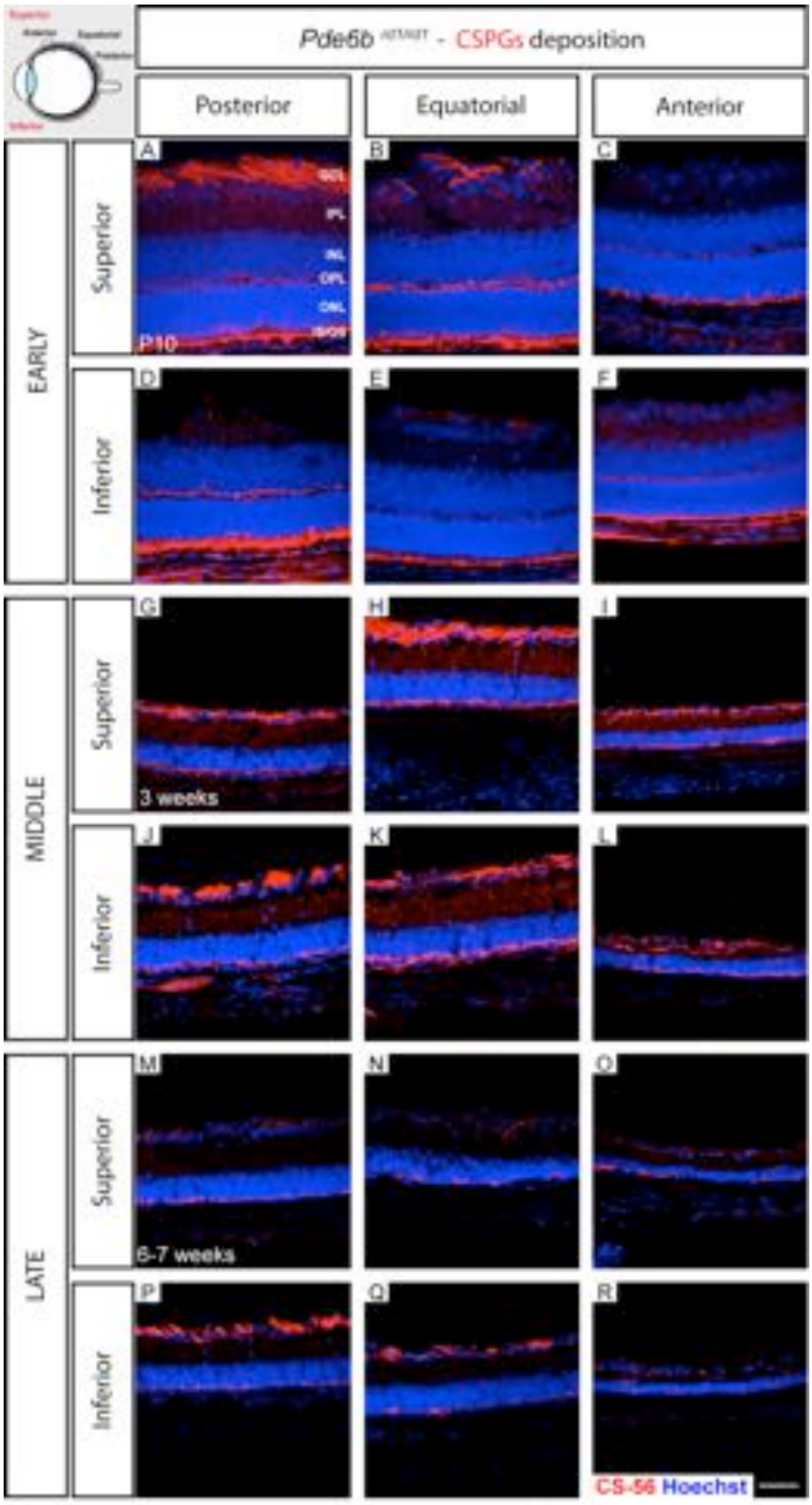

Appendix N. *Assessment of intermediate filament protein GFAP at early (4 weeks), middle (6 weeks) and late (10 weeks) time points in the Rho$^{-/-}$ mice.* Cryosections were immunostained for glial cell marker GFAP (green) and counterstained with nuclei marker Hoechst 33342 (blue). Scale bar, 25 µm.

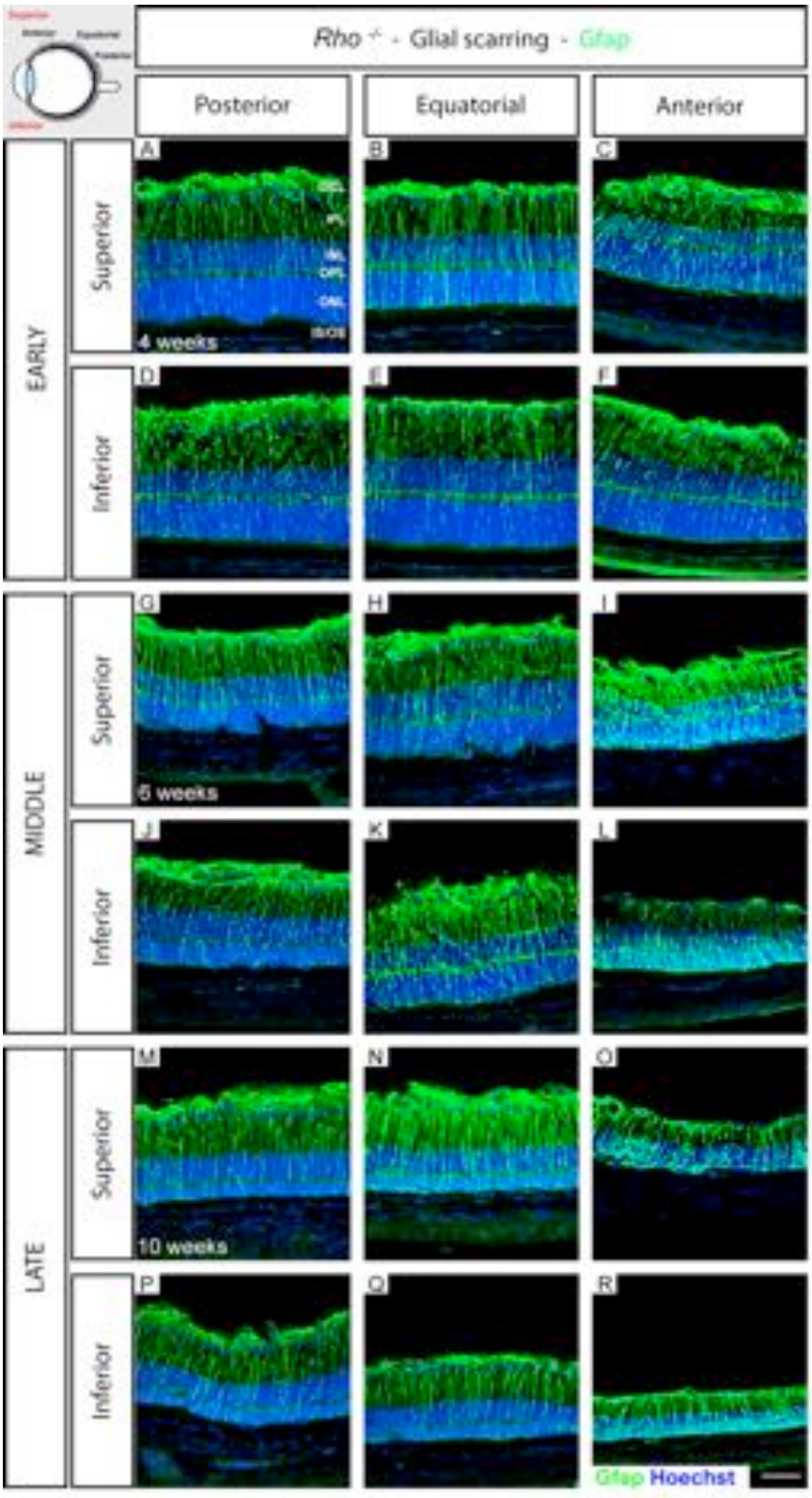

Appendix O. *Assessment of intermediate filament protein Vimentin at early (4 weeks), middle (6 weeks) and late (10 weeks) time points in the Rho$^{-/-}$ mice.* Cryosections were immunostained for glial cell marker Vimentin (green) and counterstained with nuclei marker Hoechst 33342 (blue). Scale bar, 25 µm.

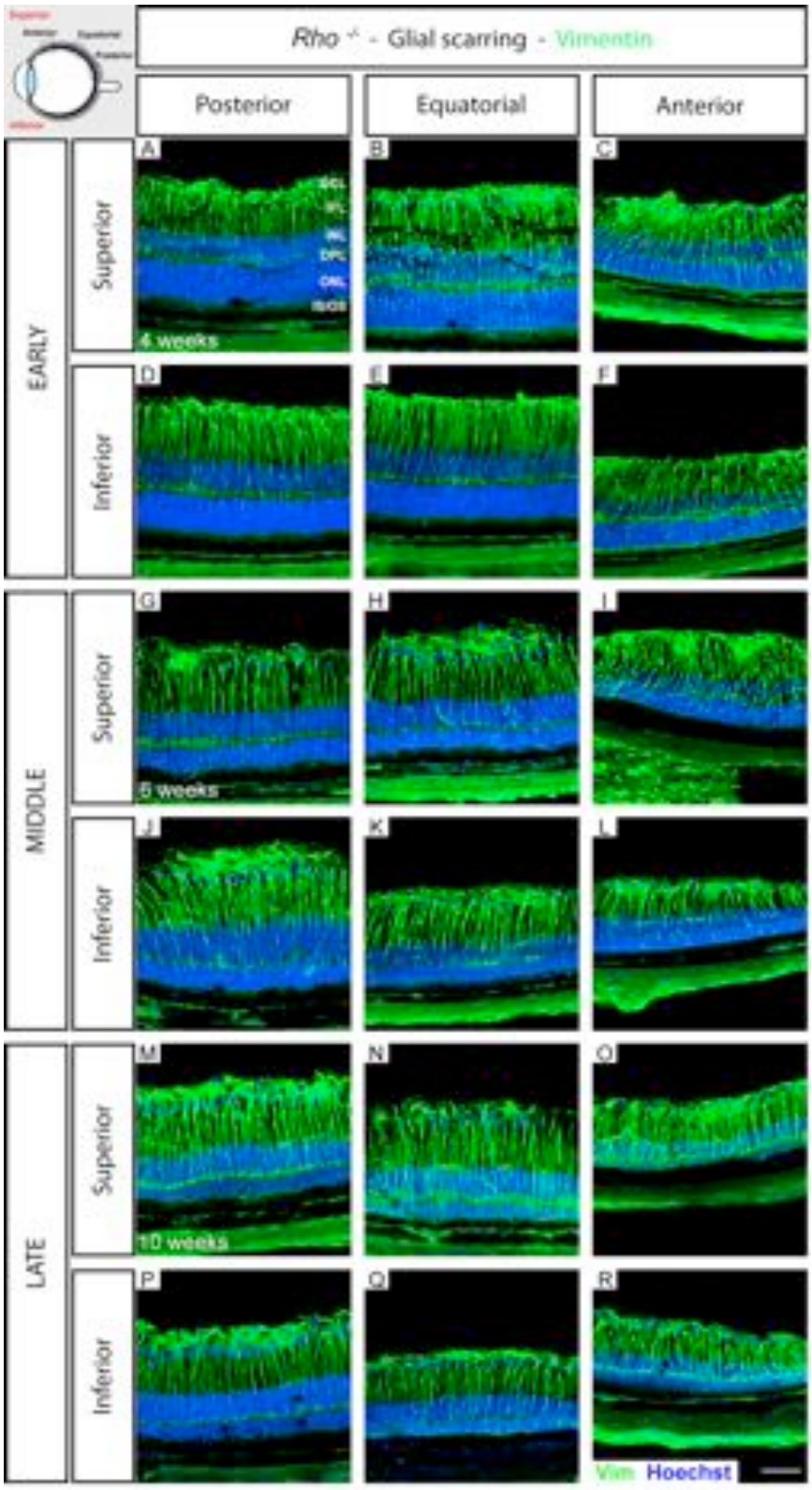

Appendix P. *Assessment of CSPGs deposition at early (4 weeks), middle (6 weeks) and late (10 weeks) time points in the Rho$^{-/-}$ mice.* Cryosections were immunostained for CSPGs marker (CS-56; red) and counterstained with nuclei marker Hoechst 33342 (blue). Scale bar, 25 µm.

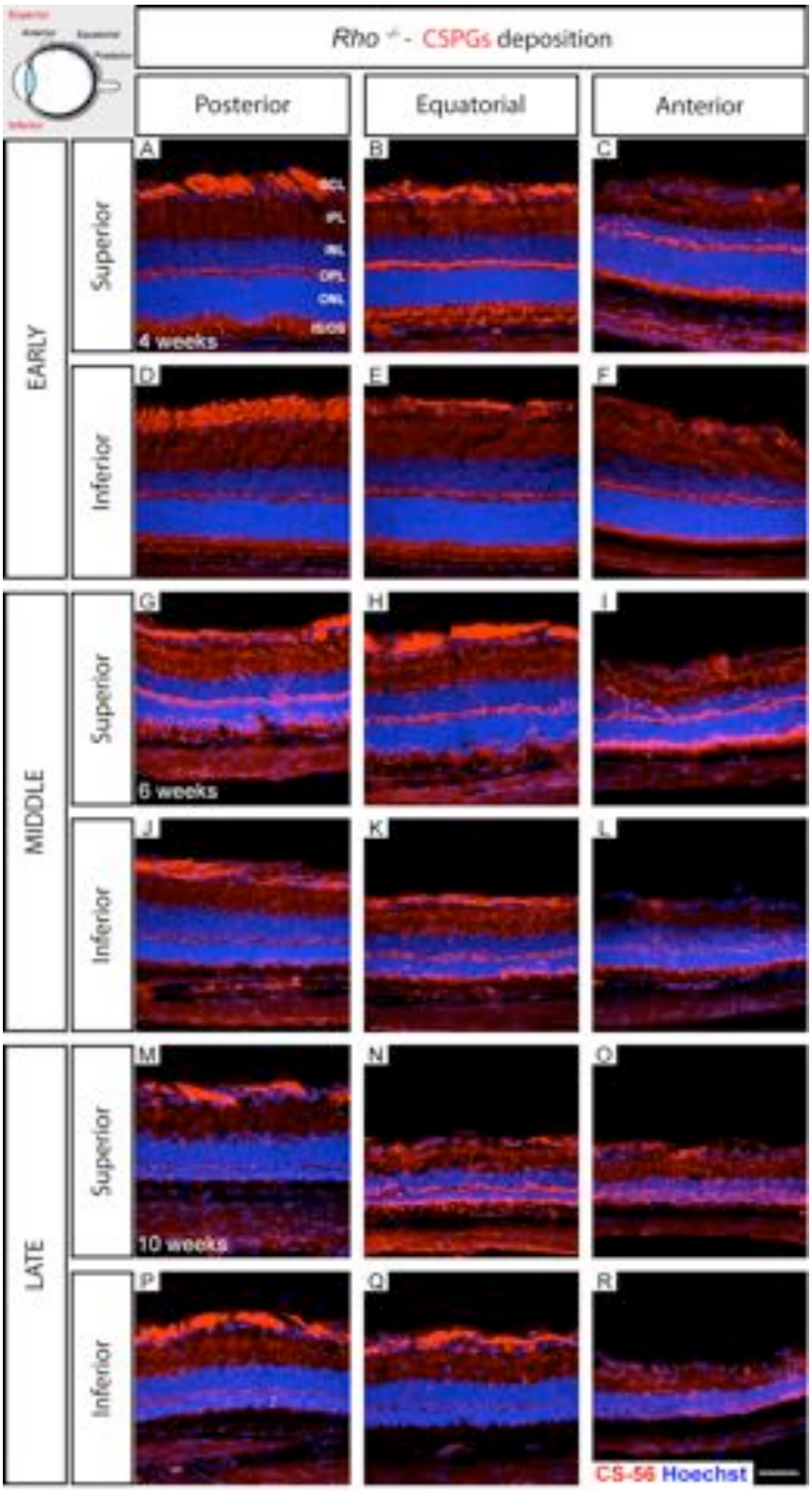

Appendix Q. *Assessment of intermediate filament protein GFAP at early (2 months), middle (4 months) and late (6 months) time points in the Prph2$^{+/\Delta 307}$ mice.* Cryosections were immunostained for glial cell marker GFAP (green) and counterstained with nuclei marker Hoechst 33342 (blue). Scale bar, 25 µm.

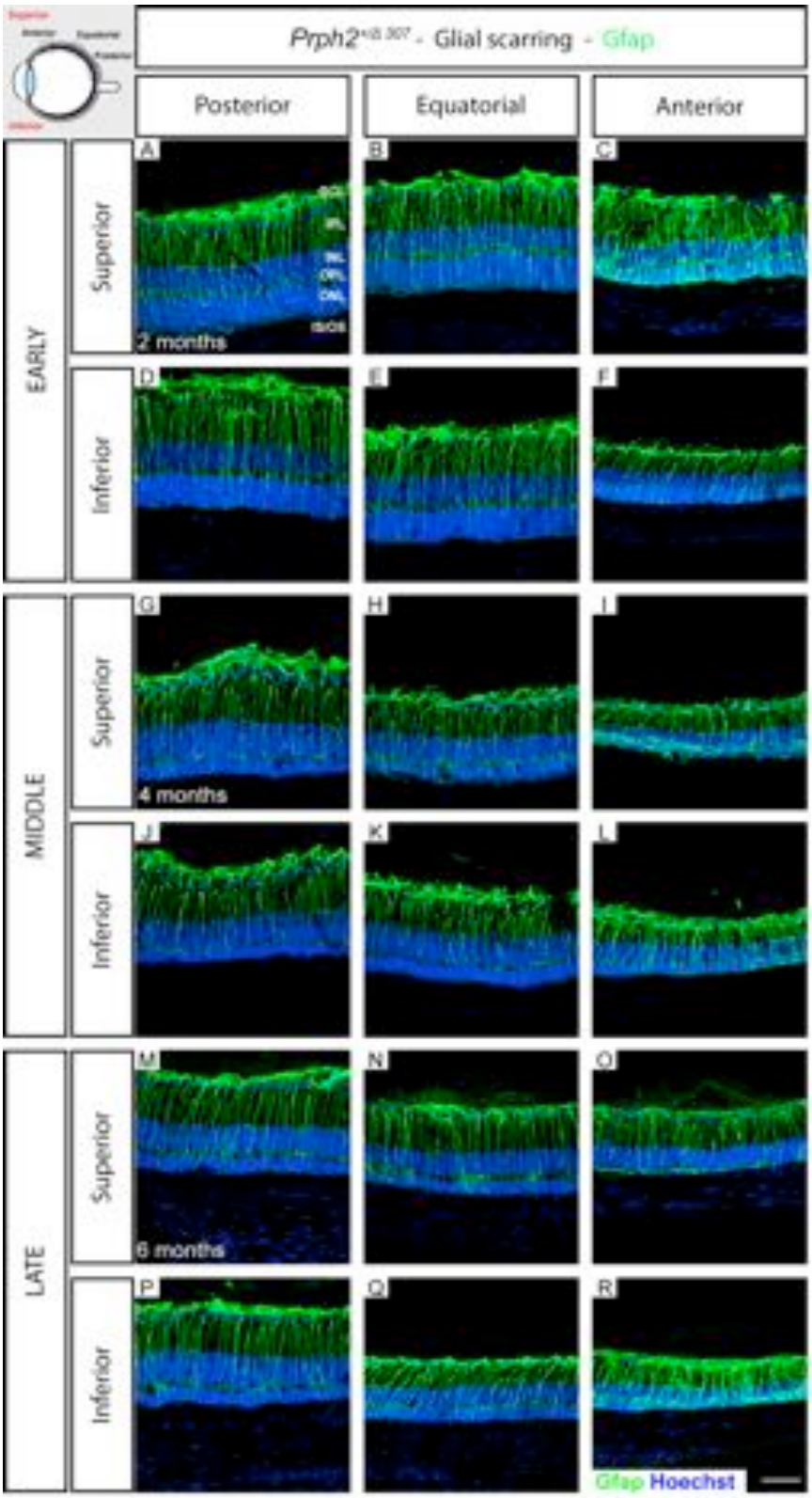

Appendix R. *Assessment of intermediate filament protein Vimentin at early (2 months), middle (4 months) and late (6 months) time points in the Prph2$^{+/\Delta 307}$ mice.* Cryosections were immunostained for glial cell marker Vimentin (green) and counterstained with nuclei marker Hoechst 33342 (blue). Scale bar, 25 µm.

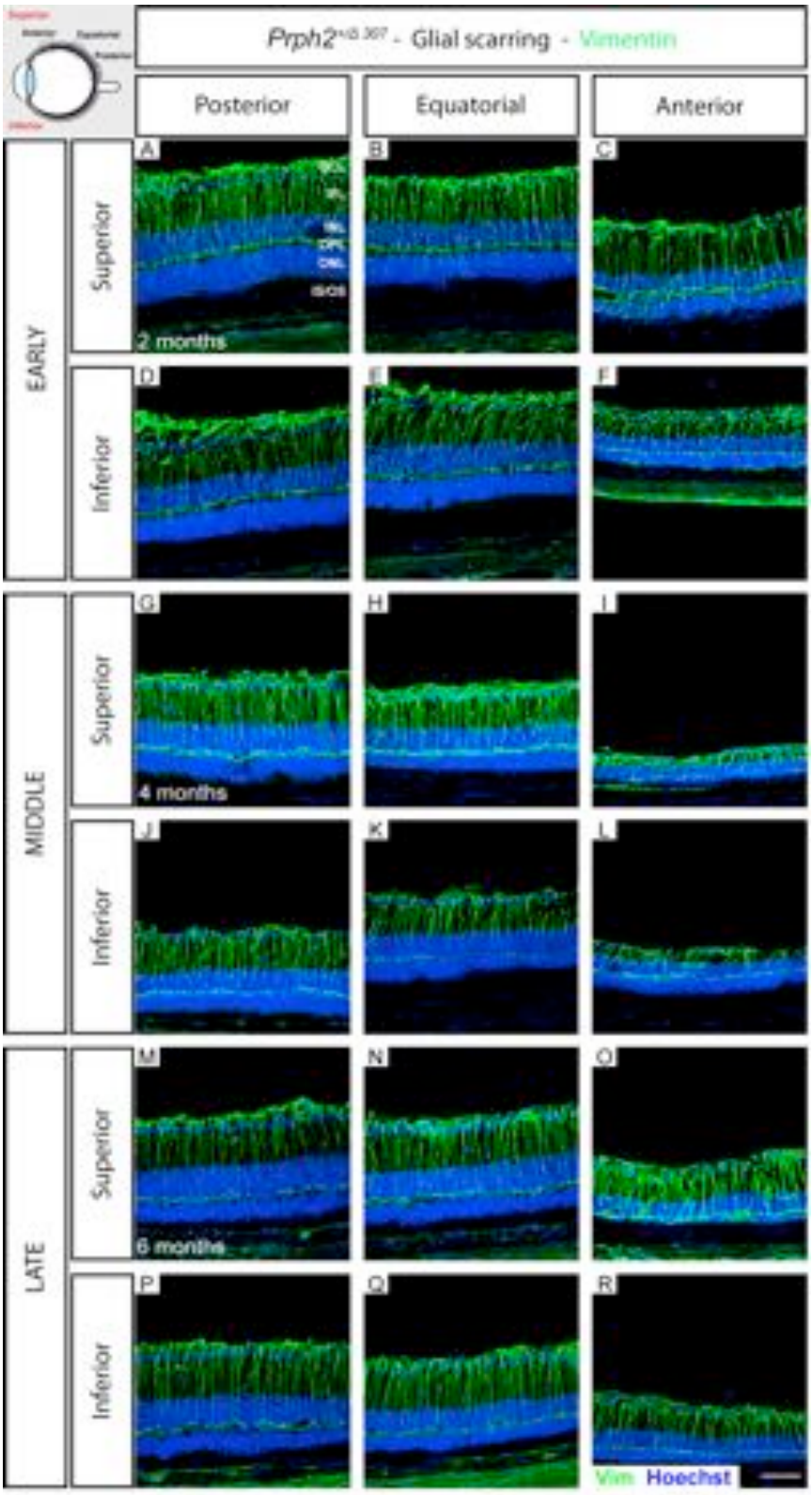

Appendix S. *Assessment of CSPGs deposition at early (2 months), middle (4 months) and late (6 months) time points in the Prph2$^{+/\Delta 307}$ mice.* Cryosections were immunostained for CSPGs marker (CS-56; red) and counterstained with nuclei marker Hoechst 33342 (blue). Scale bar, 25 µm.

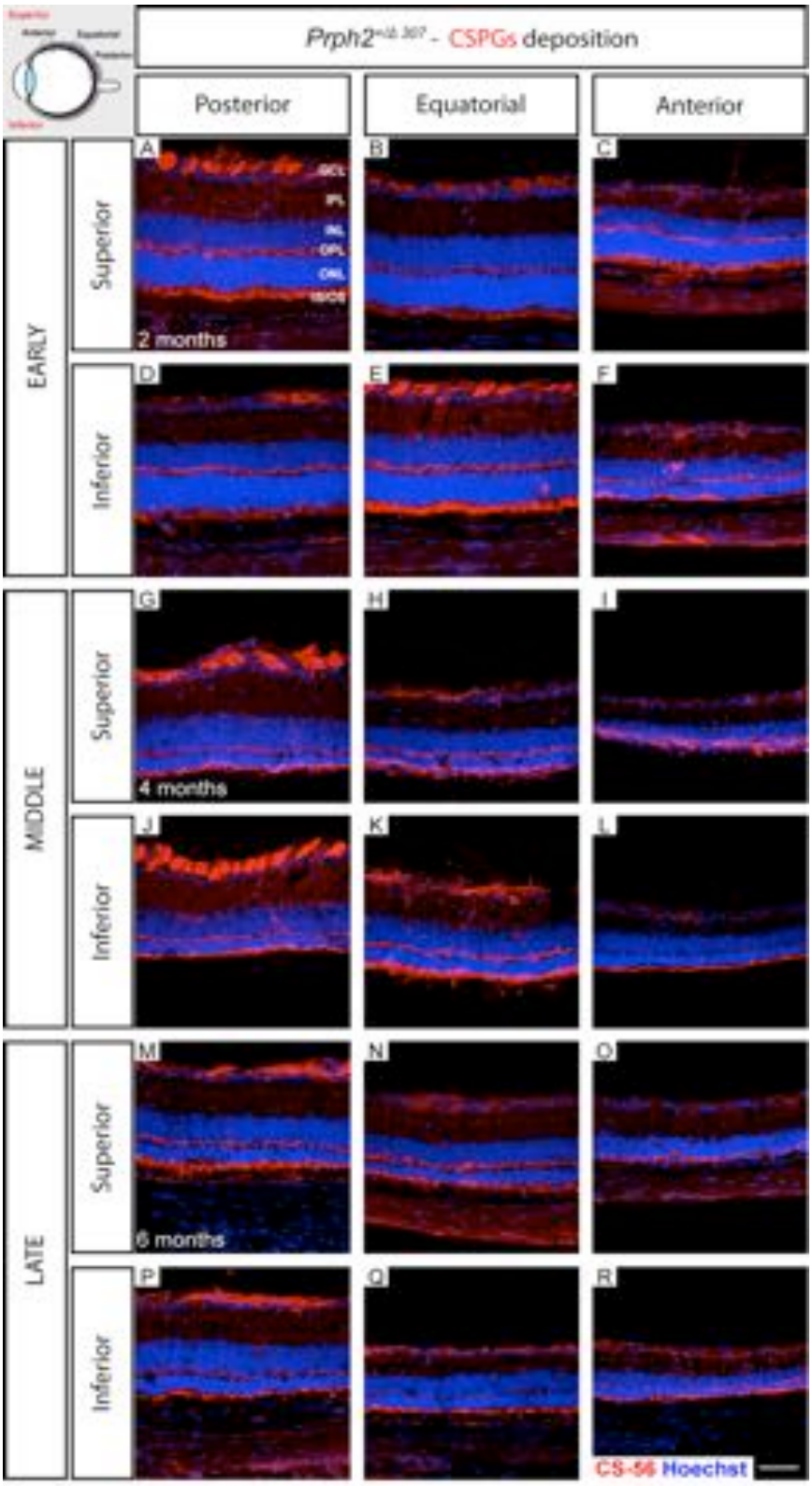

Appendix T. *Assessment of intermediate filament protein GFAP at early (3 weeks), middle (6 weeks) and late (12 weeks) time points in the Nrl$^{-/-}$ mice.* Cryosections were immunostained for glial cell marker GFAP (green) and counterstained with nuclei marker Hoechst 33342 (blue). Scale bar, 25 µm.

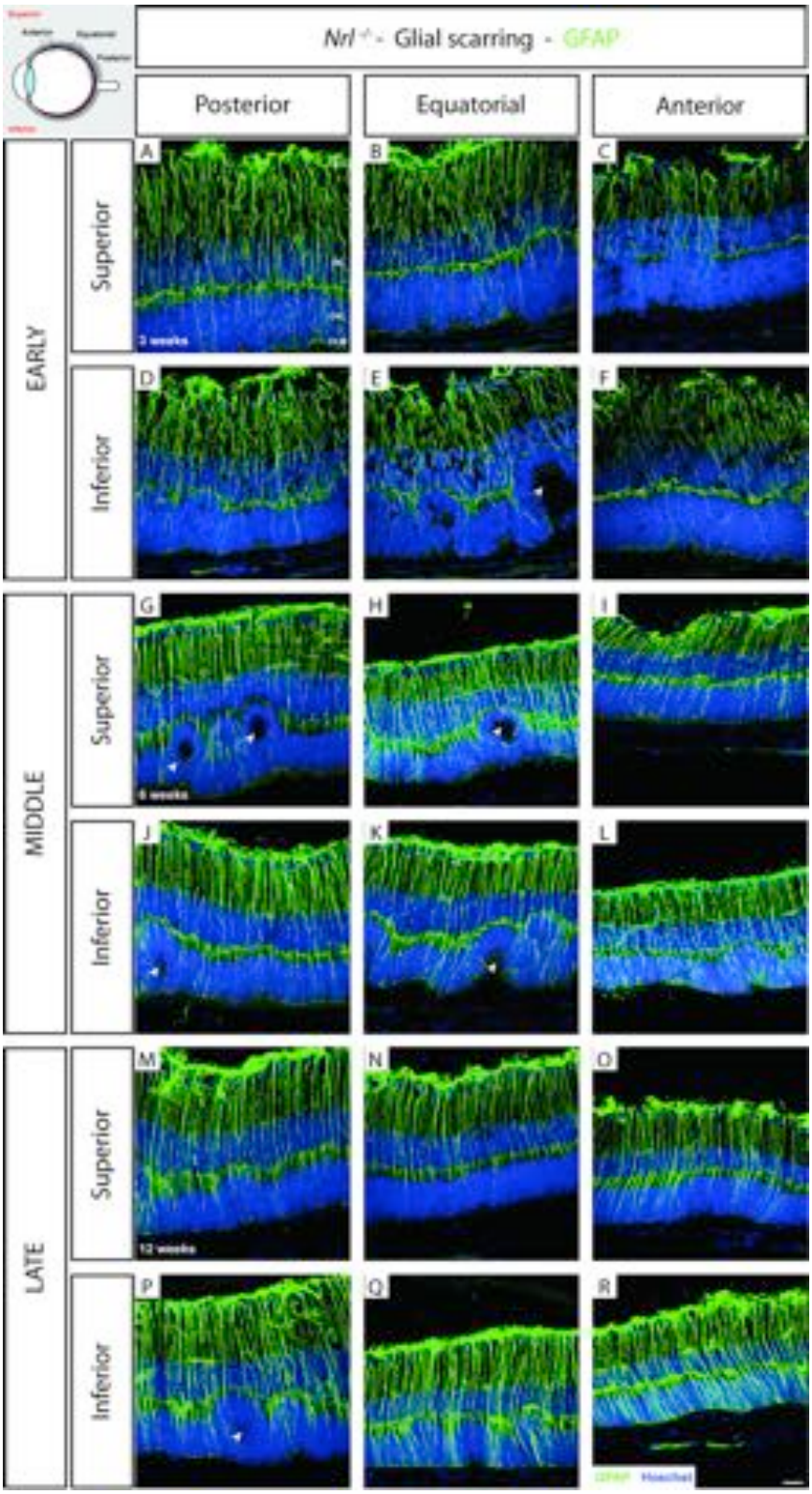

Appendix U. *Assessment of intermediate filament protein Vimentin at early (3 weeks), middle (6 weeks) and late (12 weeks) time points in the Nrl$^{-/-}$ mice.* Cryosections were immunostained for glial cell marker Vimentin (green) and counterstained with nuclei marker Hoechst 33342 (blue). Scale bar, 25 µm.

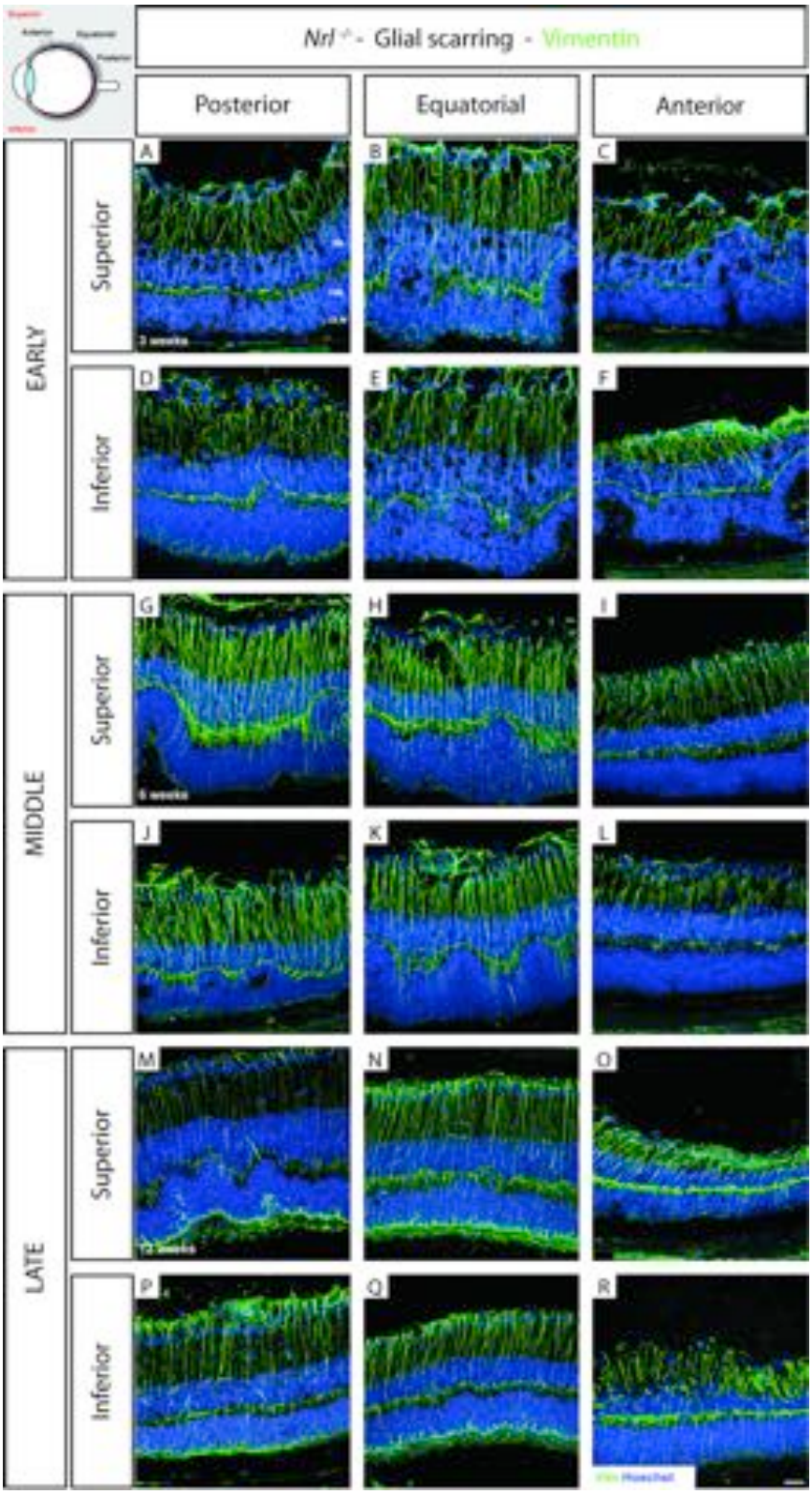

Appendix V. *Assessment of CSPGs deposition at early (3 weeks), middle (6 weeks) and late (12 weeks) time points in the Nrl$^{-/-}$ mice.* Cryosections were immunostained for CSPGs marker (CS-56; red) and counterstained with nuclei marker Hoechst 33342 (blue). Scale bar, 25 µm.

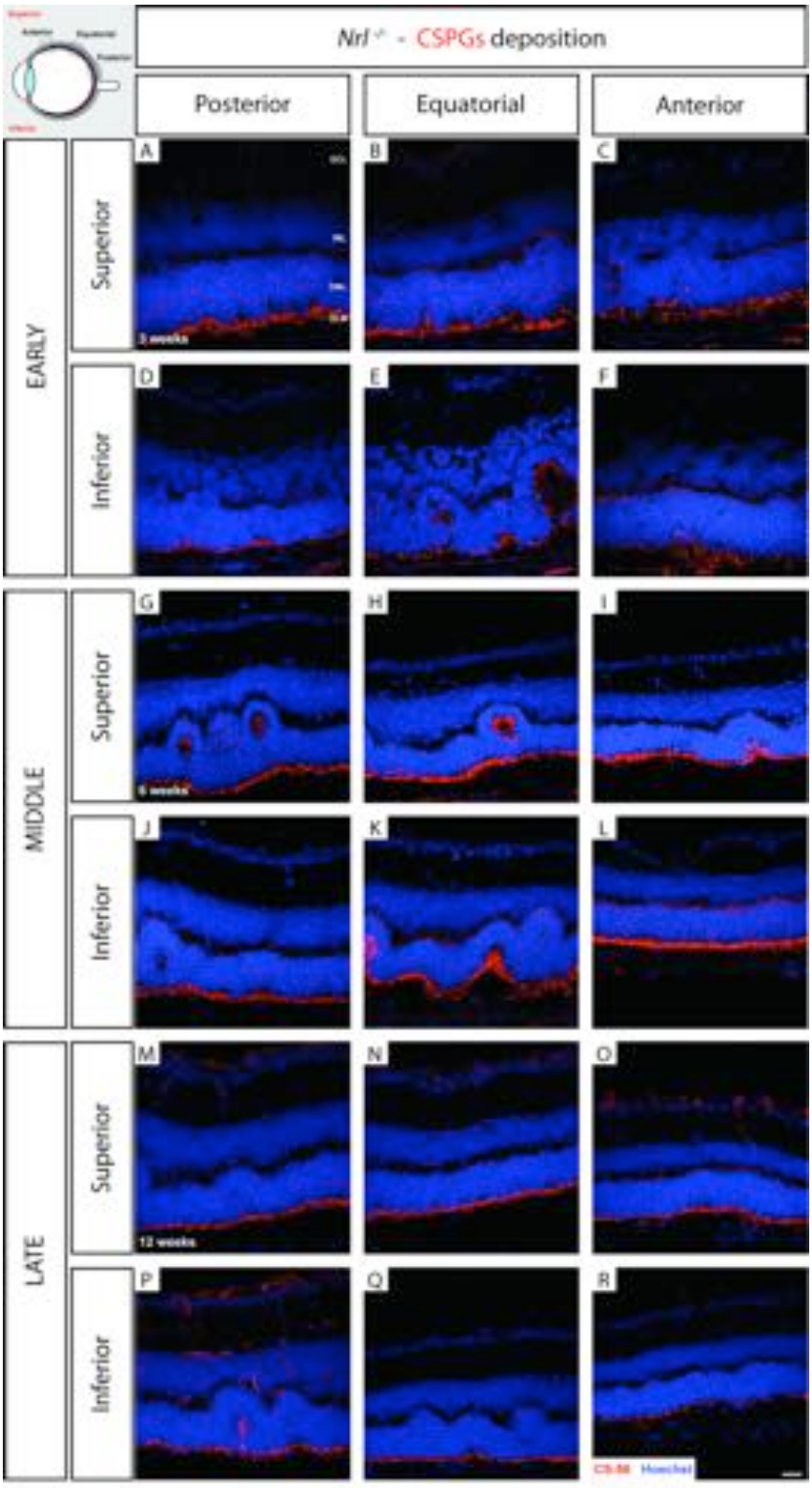

Appendix W. *Assessment of intermediate filament protein GFAP at early (3 weeks), middle (6 weeks) and late (12 weeks) time points in the RW1;Nrl$^{-/-}$ mice.* Cryosections were immunostained for glial cell marker GFAP (green) and counterstained with nuclei marker Hoechst 33342 (blue). Scale bar, 25 µm.

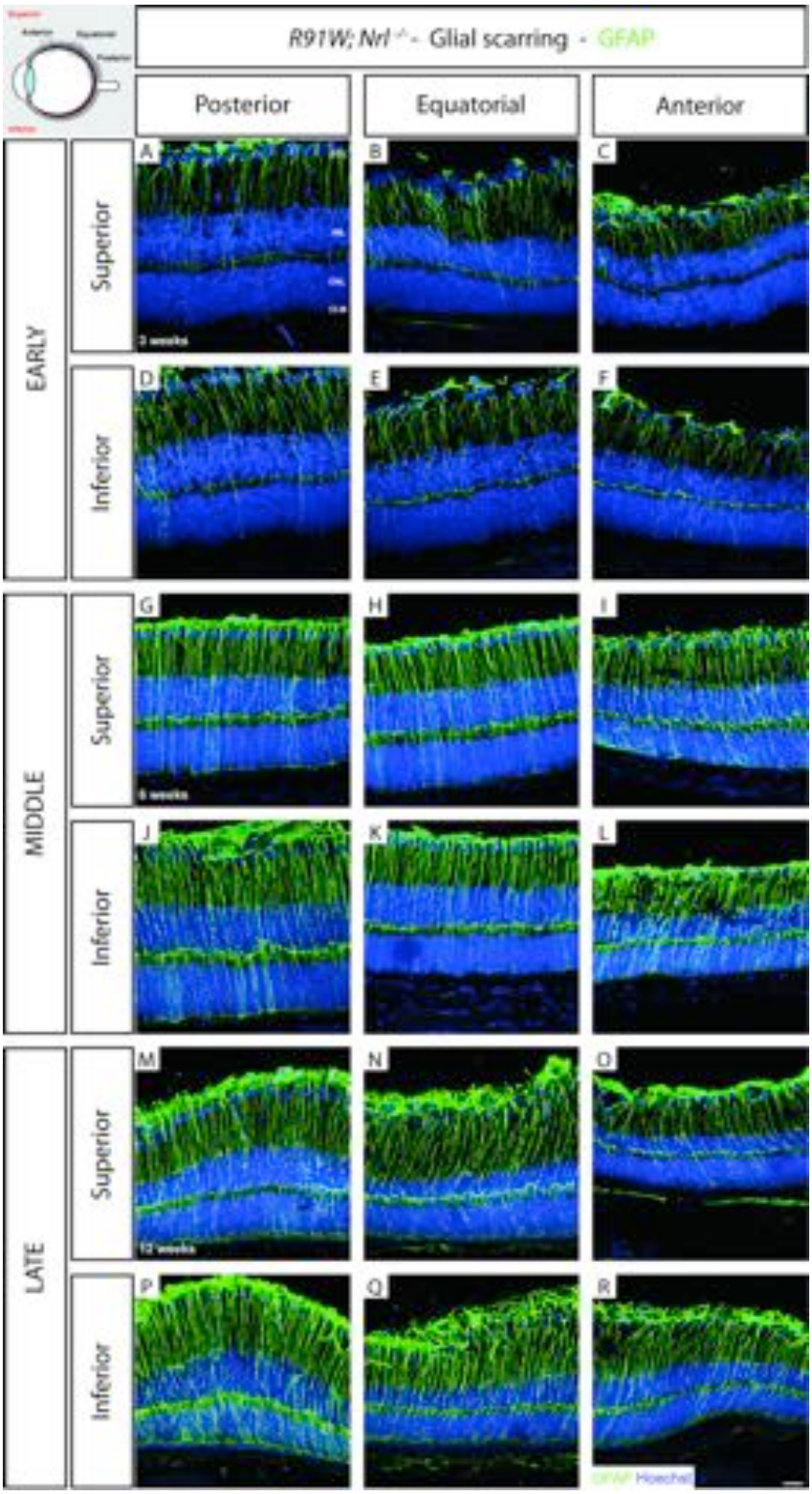

Appendix X. *Assessment of intermediate filament protein Vimentin at early (3 weeks), middle (6 weeks) and late (12 weeks) time points in the RW1;Nrl$^{-/-}$ mice.* Cryosections were immunostained for glial cell marker Vimentin (green) and counterstained with nuclei marker Hoechst 33342 (blue). Scale bar, 25 μm.

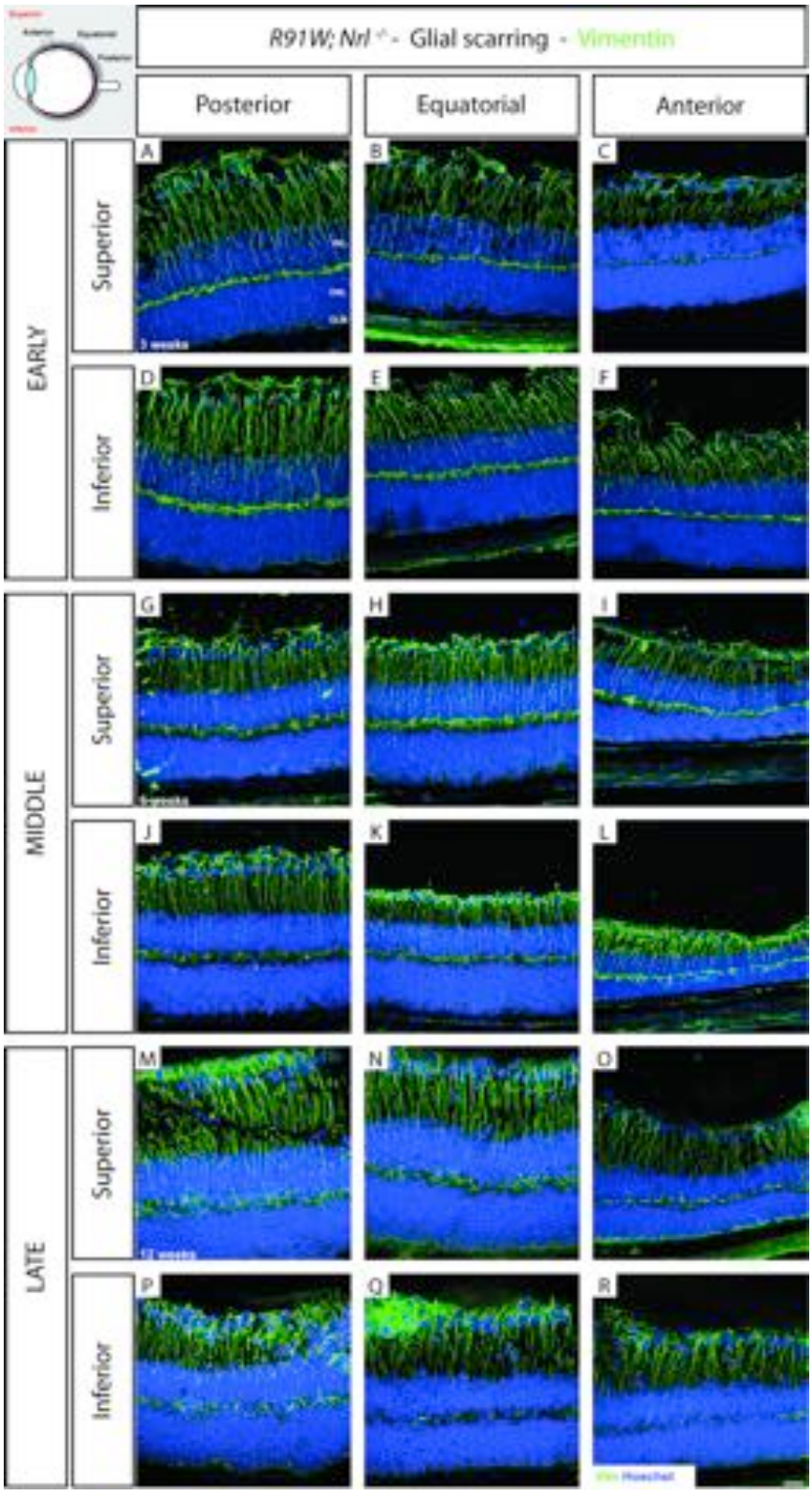

Appendix Y. *Assessment of CSPGs deposition at early (3 weeks), middle (6 weeks) and late (12 weeks) time points in the RW1;Nrl$^{-/-}$ mice.* Cryosections were immunostained for CSPGs marker (CS-56; red) and counterstained with nuclei marker Hoechst 33342 (blue). Scale bar, 25 µm.

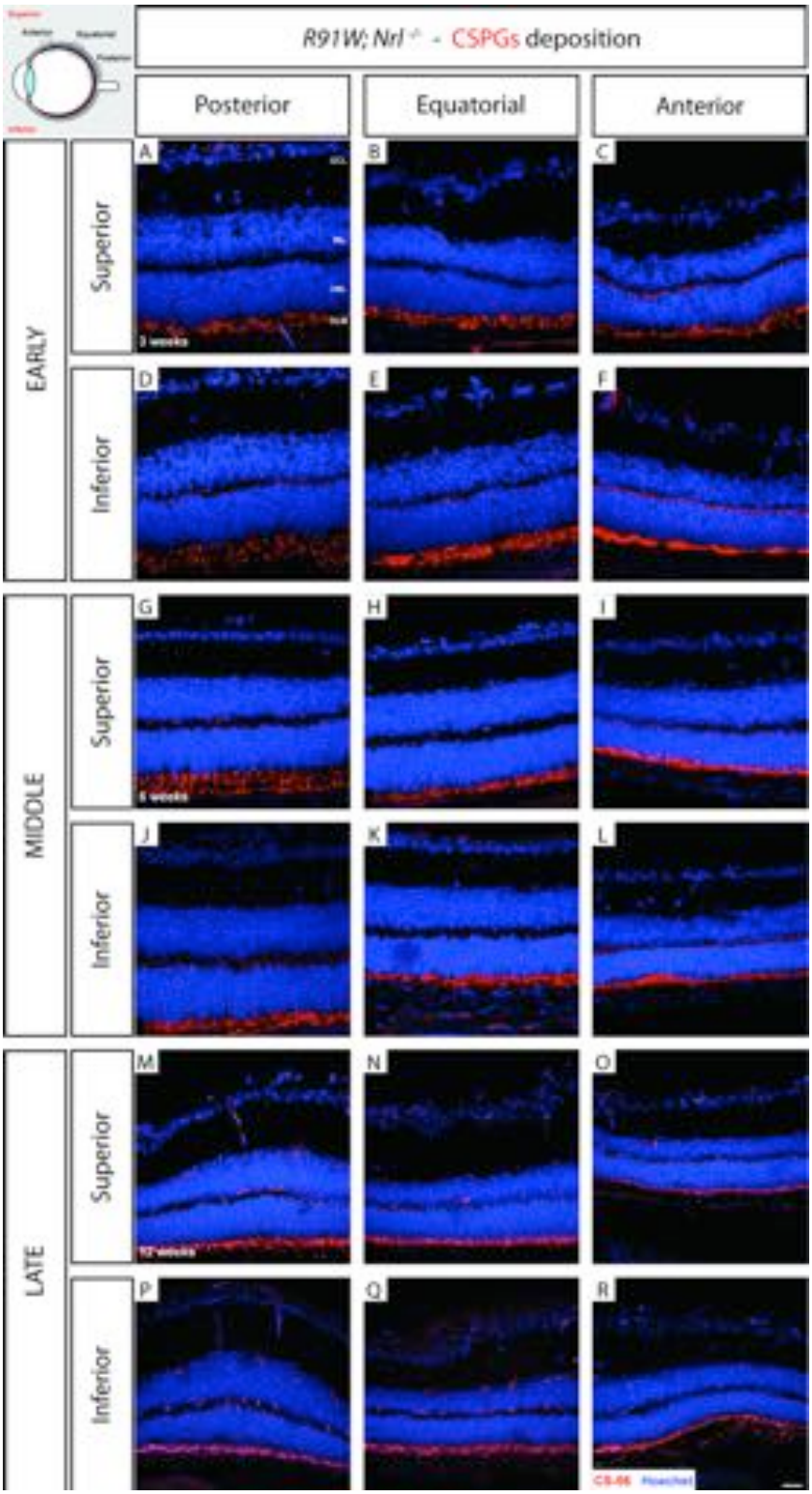

Appendix Z. *RNAi-mediated knockdown of Gfap and Vimentin mRNA in vitro.* (A, C) Histograms show RNA levels, assessed by qRT-PCR, for *Gfap* and (B, D) *Vimentin* following co-transfection of the respective expression cassettes, together with (A) pshGfap, (C) pshVimentin or (C, D) pLsh in 293T cells. Results are shown normalised against average values obtained following co-transfection with pshCont. **P* < 0.05, ***P* < 0.01 and ****P* < 0.001 with a one-way ANOVA (n=3 independent cultures). Error bars: SEM.

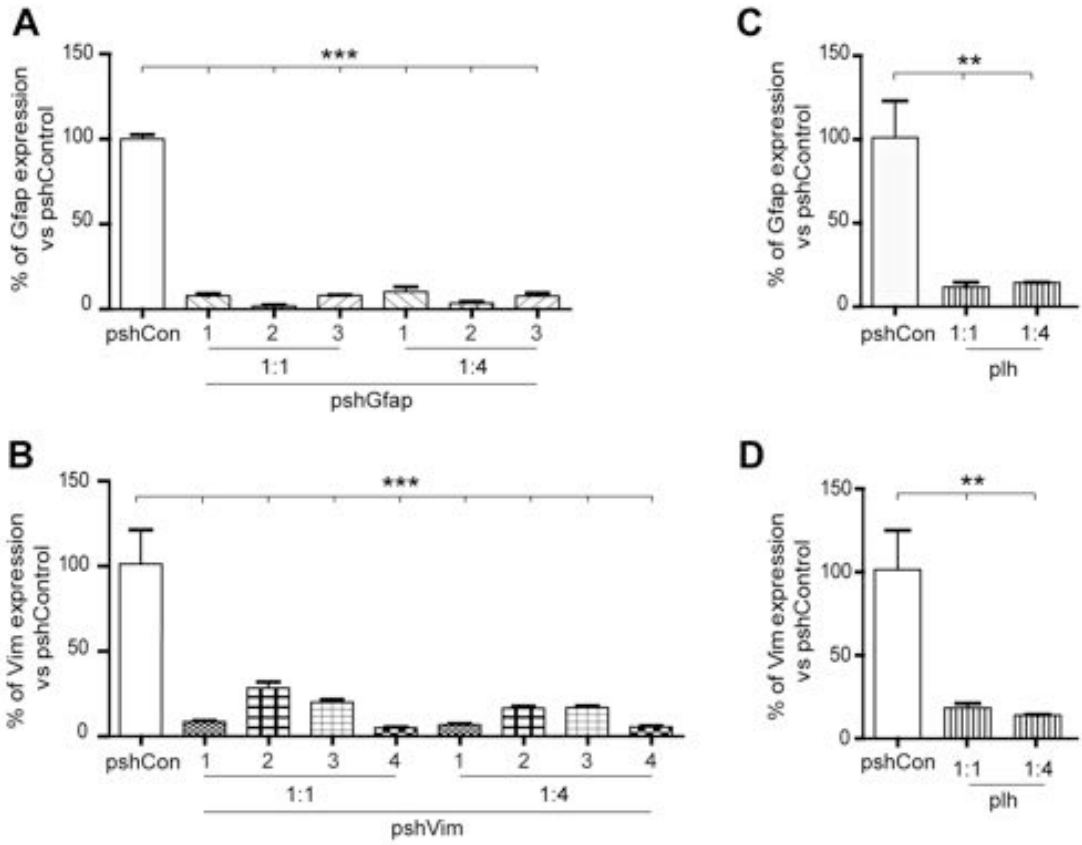

Appendix AA. *Assessment of OLM integrity at 22 weeks old in Rho$^{-/-}$.* Cryosections were immunostained for ZO-1 (red) and co-stained with nuclei marker Hoechst 33342 (blue). Scale bar, 50 µm.

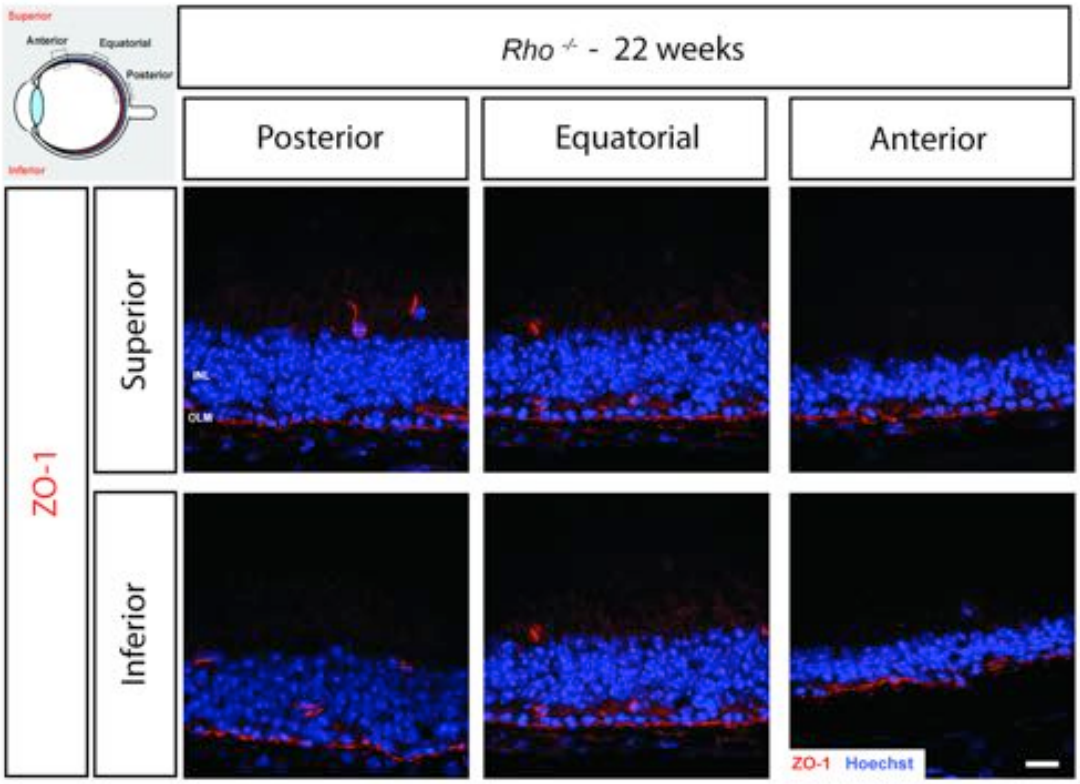

Appendix AB. *Transfection of HEK-293T cells with different concentrations (20, 40, and 100 pM) of a non-targeting RNAi control sequence with an attached AlexaFluor633.* Cells were co-stained with nuclei marker Hoechst 33342 (blue). Scale bar, 25 µm.